TRANSPORTATION RESEARCH RECORD 664

Bridge Engineering
Volume 1

Proceedings of a conference conducted by the Transportation Research Board, September 25-27, 1978

TRANSPORTATION RESEARCH BOARD

COMMISSION ON SOCIOTECHNICAL SYSTEMS
NATIONAL RESEARCH COUNCIL

NATIONAL ACADEMY OF SCIENCES
WASHINGTON, D.C. 1978

Transportation Research Record 664
Price $13.80

subject areas
03 rail transport
23 highway drainage
27 bridge design
33 construction
34 general materials
40 general maintenance
62 foundations
63 mechanics

Transportation Research Board publications are available by ordering directly from the board. They may also be obtained on a regular basis through organizational or individual supporting membership in the board; members or library subscribers are eligible for substantial discounts. For further information, write to the Transportation Research Board, National Academy of Sciences, 2101 Constitution Avenue, N.W., Washington, D.C. 20418.

ISBN 0-309-02696-2
Library of Congress Catalog Card No. 78-71939

Sponsorship of the Papers in This Transportation Research Record

GROUP 2--DESIGN AND CONSTRUCTION OF TRANSPORTATION FACILITIES
Eldon J. Yoder, Purdue University, chairman

Contents

Preface

During the past several decades, an impressive amount of research has been conducted in the development of new materials and technology to design, construct, and maintain vehicular bridges. Much has been learned about these complex problems and should be conveyed to a user community that represents such varied interests as state, federal, and local governments; private transportation agencies; consulting engineering firms; industry; planners; scientists; and engineers. Much remains to be learned, and this user community should be involved in guiding future research programs.

A continuing trend toward heavier loads and increasing traffic volumes, combined with adverse environmental conditions, has resulted in a reduction in the life expectancy of bridges and more rapid deterioration of existing bridges. A comprehensive review of the national bridge inventory by the U.S. Department of Transportation concluded that approximately 40 000 bridges on the Interstate highway system alone are structurally deficient and functionally obsolete. Similar bridge problems are faced by railroad and transit agencies.

The problem is widely recognized; both federal and state appropriations and operating agency appropriations are continually increasing for bridge construction and maintenance. An even larger effort must be made if the nation's surface transportation system is to function efficiently. Because funds are limited for bridge construction and for the repair, rehabilitation, and strengthening of existing bridges, a careful evaluation should be made of all available technology and needed research to ensure the optimum use of resources.

The Bridge Engineering Conference was organized to facilitate an interchange of information on all aspects of design, construction, rehabilitation, and maintenance of vehicular bridges and to have specific emphasis on problems and solutions of interest to highway, railroad, and transit bridge engineers, administrators, and managers. The papers in Transportation Research Records 664 and 665 constitute the proceedings of the conference held September 25-27, 1978, at the Chase-Park Plaza Hotel, St. Louis, Missouri. These two records contain all of the papers prepared in advance of the conference as well as several that were not included in the program due to limitations of time and space.

Organization and direction of the conference were the responsibilities of the Conference Steering Committee, whose members are listed on the reverse side of the title page of this Record.

The Bridge Engineering Conference was partially funded by the Federal Highway Administration and Federal Railroad Administration. The following organizations cooperated to make the conference possible:

COSPONSORS
Federal Highway Administration
Federal Railroad Administration
PARTICIPATING AGENCIES
American Association of State Highway and Transportation Officials
American Railway Engineering Association
American Road and Transportation Builders Association
American Society of Civil Engineers
International Association for Bridge and Structural Engineering
Missouri Pacific Railroad Company
Missouri State Highway Commission
National Association of County Engineers

The Eads Bridge, St. Louis, Missouri, 1874. Designer and builder, Capt. James Buchanan Eads. Designated National Civil Engineering Landmark.

DEVELOPMENT OF A COMPUTERISED BRIDGE INVENTORY FOR A STATE ROAD AUTHORITY

B.L. Richards, B. Tech., M.I.E. Aust., Highways Department, South Australia

The Highways Department of South Australia is currently developing a computerised bridge inventory system which will be used by the Bridge Inspection Section to rationalise the approach to the inspection of bridges. It will also be used by the Planning Branch to provide a basis for economic comparison of alternatives in the replacement and strengthening of bridges, by the Construction Branch for the rational allocation of maintenance funds and to provide information to the National Association of Australian State Road Authorities (NAASRA) proposed data bank. One of the most important functions of a bridge inventory is to provide a complete and accurate record of each bridge on a highway system. Maintenance of bridges requires complete records in usable form including history of the structure, all repairs, widening, strengthening or reconstruction, or other actions which have been taken, subsequent to inspections. Information should be easily accessible and readily updated; factors which today are made possible by computerisation. However, conflicting requirements must be dealt with. On the one hand data handling facilities should be large enough to provide sufficient information for managing inspection, maintenance but flexible enough to be used for planning functions both at the regional and national level; yet the system developed should not become cumbersome and difficult to use.

The purpose of this paper is to explain the experience that the Highways Department of South Australia has had in relation to the design, implementation and operation of a bridge inventory system.

With the exception of a relatively low mountain range, 500 kilometres long by 80 kilometres wide, extending through the centre of South Australia, most of the settled areas of the State consist of flat alluvial plains crossed by wide shallow creeks and rivers. South Australia has a low average rainfall and is the driest State in one of the driest continents in the world, making it devoid of extensive natural forests thus forcing early bridge builders to use durable but relatively expensive concrete, steel and masonry as raw materials. There is an almost total absence of timber structures; most of those built have long since succumbed to the ravages of fire, termites or dry rot. These environmental conditions suited bridges of beam and slab design of moderate span lengths - usually less than 30 metres

South Australia was founded in 1836 and, consequently, there are few bridges of historic interest. Some of the more interesting structures are wrought iron bridges fully imported from the United Kingdom and erected on site. This practice lasted until the early 1900's when local technical expertise reached a sufficiently high level for these types of bridges to be built using local resources.

Design Loads for Bridges

Although State Road Authorities were formed in each of the Australian States during the late 1920's no comprehensive bridge design standard or codes were used in Australia until 1947. (1) Until that time design loads varied considerably between the States and were generally comparable to the HS10 to about HS15. However, since 1947 all Australian States adopted the HS20 loading or heavier, the latter being restricted to particular routes. Increased pressure from the Transport Industry to raise both legal weight limits and those allowed under permit led to a more substantial design loading being adopted in 1977. (2) This loading retains the concept of the AASHTO type vehicle but is approximately 33 percent heavier. Therefore, a situation exists where the design loading for bridges generally decreases with increasing age. In South Australia approximately 60% of bridges have design loadings less than HS20 standard.

Requirements of a Bridge Inventory System

Bridges represent a sizeable capital outlay requiring regular and rational inspections to preserve the initial investment. The main purpose of a bridge inventory is to catalogue all the information gathered from inspections and other sources so that it may be used for:-

. Setting priorities for the maintenance of bridges.

. Setting priorities for the strengthening or replacement of bridges.

. Planning for a rational bridge inspection programme.

. Route selection for vehicles carrying abnormal loads.

. National data banks for planning purposes on a national scale.

Records must be in usable form and should include information on the history of the structure, all repairs, widening, strengthening or other actions which have been taken subsequent to inspections. Information should be readily accessible and capable of easy updating.

However, the problem of conflicting requirements must be solved. On the one hand the data stored must be comprehensive enough to provide information for the decision making process on engineering, economic and planning aspects, but flexible enough to meet changing conditions and requirements, yet the system used should not be cumbersome and difficult to use.

Several systems have been used for the collection, storage and retrieval of bridge inventory data ranging from relatively simple card systems used in earlier times to extensive computerised data banks made possible by modern technology. A perusal of systems used by numerous authorities reveal that in many cases a considerable effort is expended to collect very detailed information about each bridge in a region, presumably because electronic data processing facilities have made it possible to store and process such information. (3, 4) This leads to a large data bank which contains much irrelevant information, is difficult to manipulate and it is hard to see how such information can be used. An analogous situation is the spare room or attic where items that "may come in handy one day" are kept. The philosophy adopted was to begin with a simple system and aim for an inventory file which would be sufficiently flexible to allow for the later integration of additional information to meet new needs which may arise.

Development of the Bridge Inventory System

Bridges in this State were inspected only spasmodically, usually resulting from reports of signs of distress, until 1972 when Departmental policy was formulated requiring the regular inspection of all bridges within its jurisdiction. A small team of professional engineers and technicians was formed to undertake this task.

The road network in the State is maintained on a two tier system. The main arterial network is administered by the Highways Department through District Offices. All other roads are maintained by local government authorities (County Councils) and financed partly from local taxes and subsidised from Government grants through the Highways Department. The first priority was to register all bridges maintained by the Department.

Initially, a manual reporting system was used but the files generated were soon found to occupy a large amount of space, were awkward to access and difficult to retrieve information from, particularly in regard to the planning functions and re-inspection schedules. During this period computer facilities were expanded, more sophisticated software became available and the advantages of computerising inspection records became more apparent. A Cyber 73 computer with online facilities including visual display units had become available to the Department in 1973 and a decision was made to use these facilities for compilation of the bridge inventory system.

Development of a computerised Bridge Inventory began late in 1976 and was initially aimed at converting and updating about 1200 records of maintained bridges filed in the manual recording system. A relatively simple computerised catalogue system, based on files of punched cards, with three 80 column cards storing the data was used. Using software packages only the system was used to manipulate basic data (mainly concerning bridge identification, location, dimensions, load rating and other administrative data). Development of the system was gradual and generally proceeded from this simple system to a stage where, from the knowledge and experience gained, objectives became more clearly defined and a consolidation of previous work became necessary. During this phase a great deal of consideration was given to deciding on the amount and type of information which should be retained in the inventory, keeping in mind its source, form and the use to which it was likely to be put, together with the most suitable system to maintain it within the constraints of the available computer facilities.

Description of the System

A Control Data Corporation (CDC) data base management system (DMS-170) was available and judged to be appropriate for the implementation of a Bridge Inventory. This system maintains the inventory on mass storage devices which may be accessed either by DMS-170 software or by application programs prepared by or for the user, or a Data Base Administrator who is responsible for preparing and managing the data base. Briefly, the system is a software package based on the concept of a centrally controlled data base, independent of the applications accessing it. Inherent to the system are the means to:-

. Create a common-user data base in which files can be used jointly or joined in relationships.

. Provide and maintain a variety of data on structures for specific users.

. Control, monitor and interpret requests from application programs to access one file or several related files at a time.

The system is being used to form an interelated data bank for the whole Department of which the Bridge Inventory forms one segment.

Records relating to bridge structures and retained on computer files consist of:-

. Bridge Inventory File detailing the location, principal dimensions, material and rating of each structure.

. Inspection Ratings File storing the rating of each structural element. This file also includes in code form necessary repairs or other required action, posting of load limits and target dates for remedial action and reinspection.

. Comments File storing comments qualifying the ratings, other general comments and recommendations.

The Inspection Rating and Comments Files contain data from all inspections of each bridge thus providing a complete historical inspection record. Other files required for operating the system are:-

. Dictionary File containing information common to other files e.g. titles of main roads, map names, district areas, report headings, etc.

. Description File containing information peculiar to particular bridges, e.g. river names, local bridge titles.

. Enquiry Program File storing each application program for future use.

Figure 1. Schematic diagram of the Bridge Inventory System

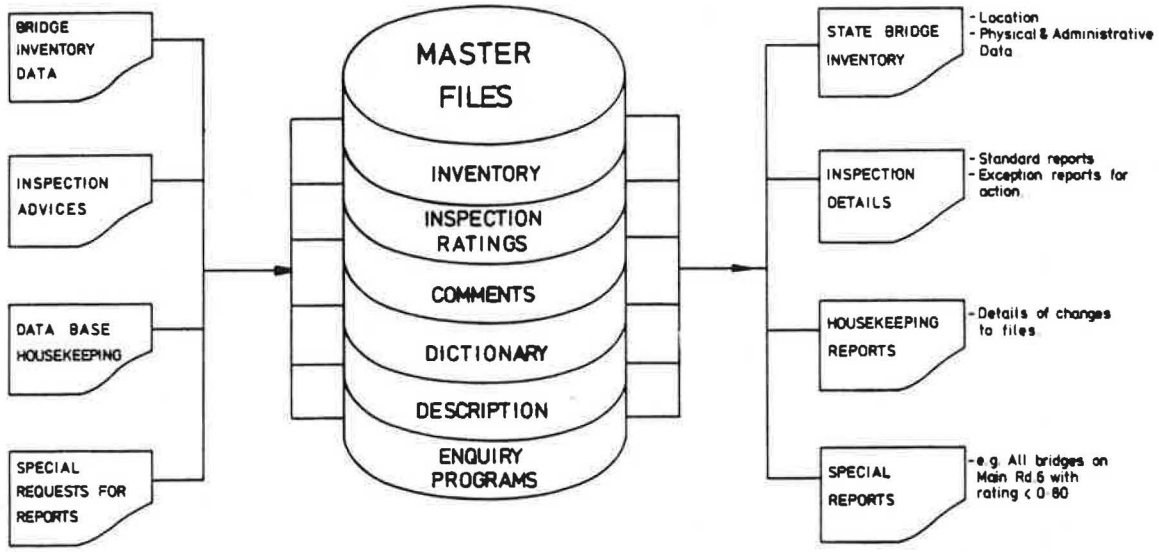

The system has inbuilt protection to prevent inadvertant corruption of existing files but for correction of data the Data Base Housekeeping routine, with its own validation procedures is used. Although the Bridge Inventory system will ultimately be a complete Data Base it is being developed on traditional lines using batch processing to facilitate the transition, from the user's viewpoint, from the existing system to the new. The interaction between the various files and relationship between the input of data and generation of reports is schematically shown in Figure 1.

Information concerning existing bridges can be broadly divided into two areas:-

1. Information obtained from original plans, design calculations and other records.
2. Information gained from detailed inspections of structures.

Standard coding sheets have been designed and consist of two types viz., a Bridge Inventory sheet and Field Inspection sheets, which are shown in Figures 2 to 4. The Bridge Inventory file includes information describing the structure in terms of location, reference number, principal dimensions and other administrative data. The Field Inspection sheets have been specifically designed for use by experienced engineers familiar with bridge design and likely problem areas. All sheets have been designed so that each inspection is carried out thoroughly and is supported by careful observation and appropriate comments without resorting to copious field notes. These comments are linked with the rating of each element of the bridge and recorded for every inspection carried out. The rating is the subjective evaluation by the engineer of the condition of the particular structural element and is given a value between 1 and 5 (chosen as being a practical range without attempting to be too definitive). The Field Inspection report is finalised by completion of the Recommendation Sheet where each recommendation will be coded for follow-up and costed in man-days work at the site and an estimated cost where warranted.

On completion of a bridge inspection a standardised computer output report is forwarded to the relevant District Engineer who is responsible for the construction and maintenance of Departmentally maintained roads and bridges in that District. Format of the computer print-out is:-

Fixed Data:
Location of structure; type, dimensions, material.

Inspection Report:
Ratings and comments from inspection, Live Load capacity rating.

Recommendations:
Load Limit; Monitoring required by District Staff; Repairs required - Desirable (within 3 years), Necessary (within 1 year), Urgent (within 3 months).

It is envisaged that the standard report will be sufficient for the majority of bridges inspected. However, in special circumstances, the report would be supported by plans for remedial work or a more detailed report.

In the near future it is intended to extend the reporting of the field inspection reports to include a "Repairs Action Report" which will be compiled by the District Staff, returned to the Bridge Inspection Group, coded and included in the computer file for future reference and easy retrieval. The inspection report outlined above is intended to maximise the efforts of all concerned in the process, in so far as record keeping and information processing is concerned.

Data: Too Much or Not Enough?

Careful consideration was given to deciding on the level of information to be retained. The prime objective being to store only that data which was likely to be used. For instance, the volume of traffic using particular structures may be useful in certain circumstances, but in this State where traffic volumes are relatively low it is not an

Figure 2. Bridge Inventory Coding Sheet

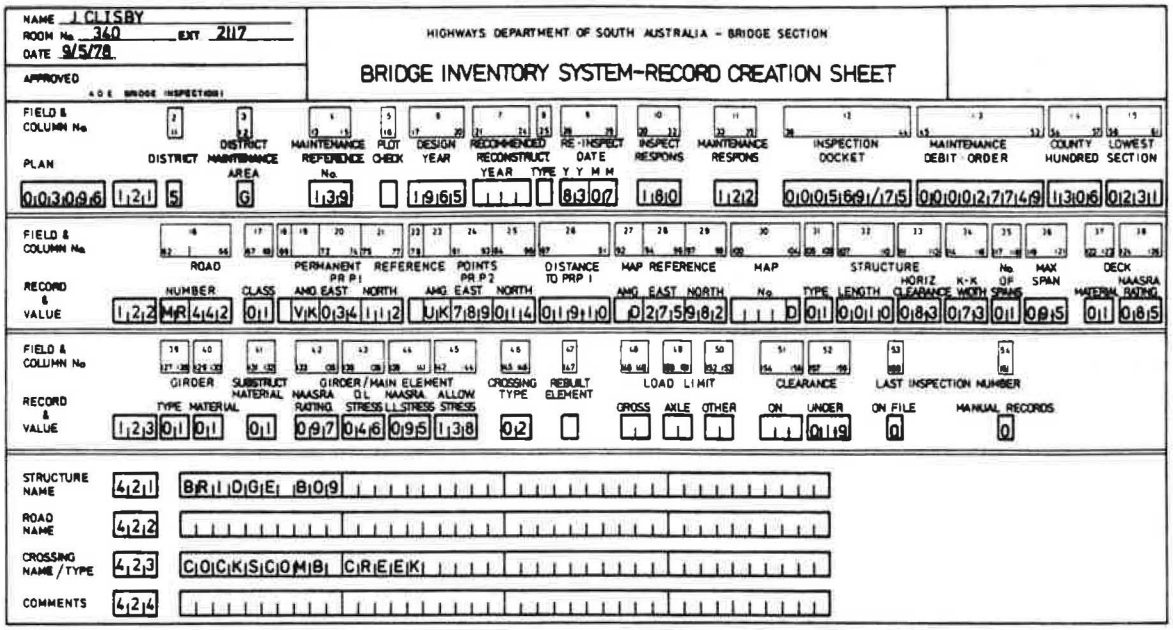

Figure 3. Field Inspection Coding Sheets

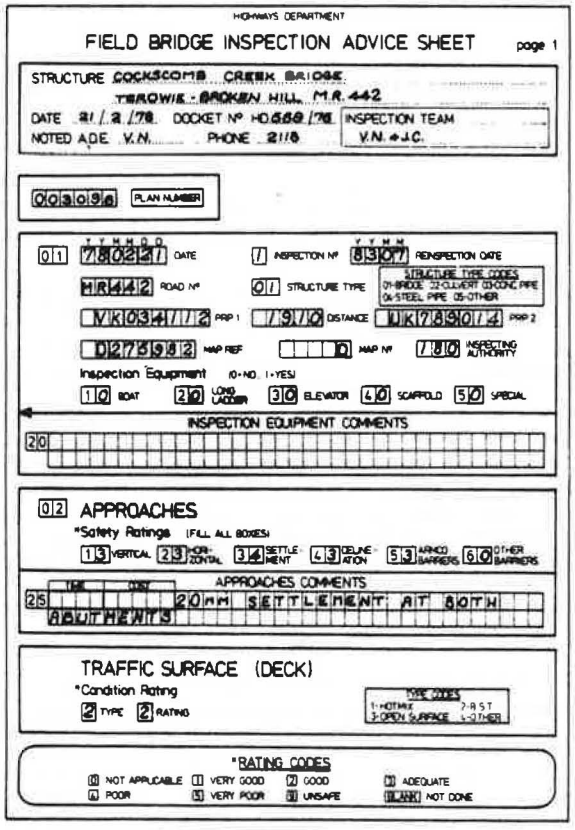

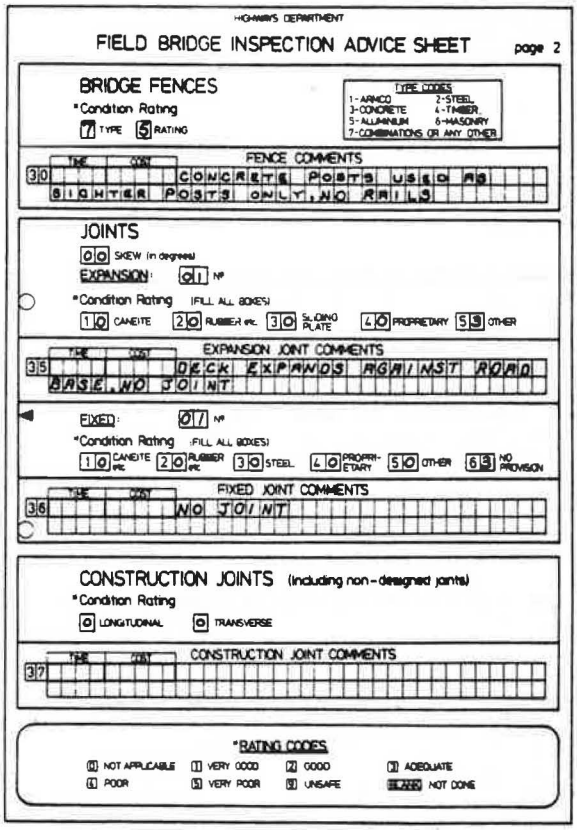

Figure 4. Field Inspection Coding Sheets

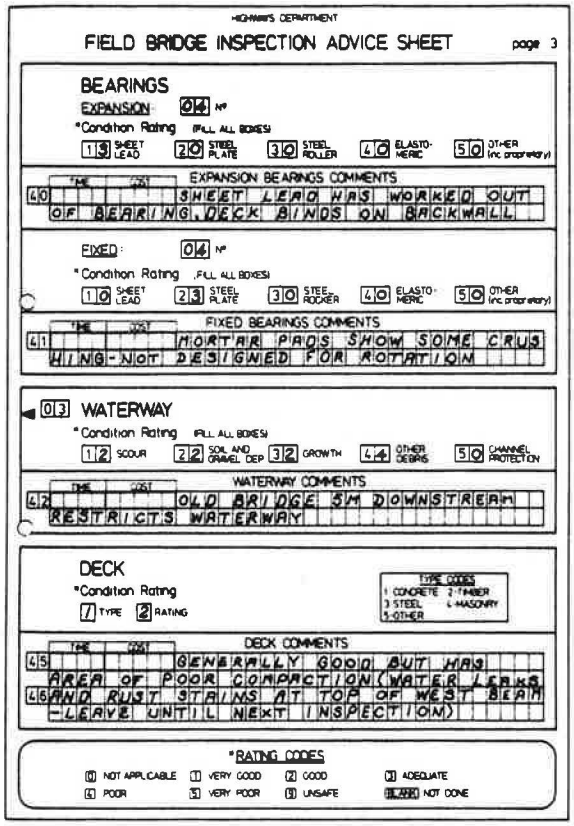

HIGHWAYS DEPARTMENT

FIELD BRIDGE INSPECTION ADVICE SHEET page 3

BEARINGS

EXPANSION: 04 Nº

*Condition Rating (FILL ALL BOXES)

1 SHEET LEAD | 2 STEEL PLATE | 3 STEEL ROLLER | 4 ELASTOMERIC | 5 OTHER (inc proprietary)

EXPANSION BEARINGS COMMENTS

40 SHEET LEAD WAS WORKED OUT OF BEARING. DECK BINDS ON BACKWALL

FIXED: 04 Nº

*Condition Rating (FILL ALL BOXES)

1 SHEET LEAD | 2 STEEL PLATE | 3 STEEL ROCKER | 4 ELASTOMERIC | 5 OTHER (inc proprietary)

FIXED BEARINGS COMMENTS

41 MORTAR PADS SHOW SOME CRUSHING - NOT DESIGNED FOR ROTATION

03 WATERWAY

*Condition Rating (FILL ALL BOXES)

1 SCOUR | 2 SOIL AND GRAVEL DEP | 3 GROWTH | 4 OTHER DEBRIS | 5 CHANNEL PROTECTION

WATERWAY COMMENTS

42 OLD BRIDGE 5M DOWNSTREAM RESTRICTS WATERWAY

DECK

*Condition Rating

1 TYPE | 2 RATING

TYPE CODES: 1 CONCRETE 2 TIMBER 3 STEEL 4 MASONRY 5 OTHER

DECK COMMENTS

45 GENERALLY GOOD BUT HAS AREA OF POOR COMPACTION (WATER LEAKS

46 AND RUST STAINS AT TOP OF WEST BEAM - LEAVE UNTIL NEXT INSPECTION)

*RATING CODES

0 NOT APPLICABLE | 1 VERY GOOD | 2 GOOD | 3 ADEQUATE | 4 POOR | 5 VERY POOR | 9 UNSAFE | BLANK NOT DONE

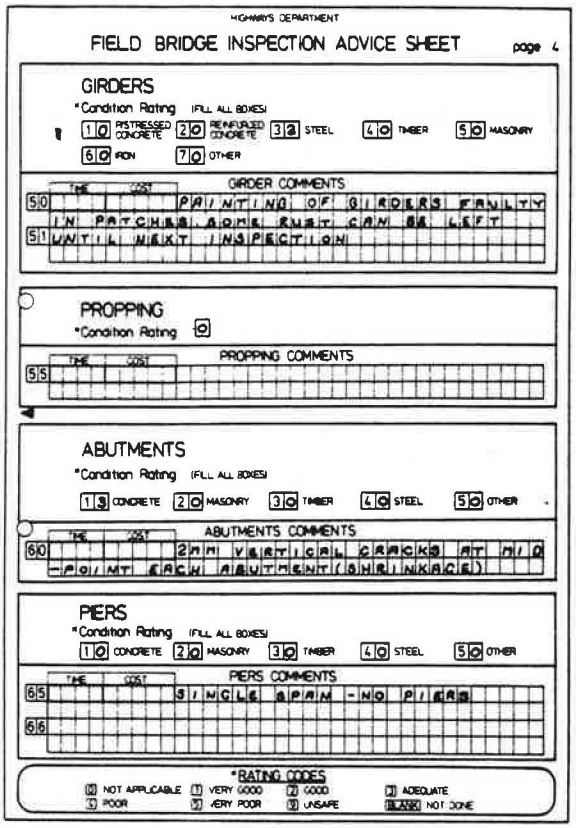

HIGHWAYS DEPARTMENT

FIELD BRIDGE INSPECTION ADVICE SHEET page 4

GIRDERS

*Condition Rating (FILL ALL BOXES)

1 PRESTRESSED CONCRETE | 2 REINFORCED CONCRETE | 3 STEEL | 4 TIMBER | 5 MASONRY | 6 IRON | 7 OTHER

GIRDER COMMENTS

50 PAINTING OF GIRDERS FAULTY

51 IN PATCHES. SOME RUST CAN BE LEFT UNTIL NEXT INSPECTION

PROPPING

*Condition Rating 0

PROPPING COMMENTS

55

ABUTMENTS

*Condition Rating (FILL ALL BOXES)

1 CONCRETE | 2 MASONRY | 3 TIMBER | 4 STEEL | 5 OTHER

ABUTMENTS COMMENTS

60 2MM VERTICAL CRACKS AT MID-POINT EACH ABUTMENT (SHRINKAGE)

PIERS

*Condition Rating (FILL ALL BOXES)

1 CONCRETE | 2 MASONRY | 3 TIMBER | 4 STEEL | 5 OTHER

PIERS COMMENTS

65 SINGLE SPAN - NO PIERS

66

*RATING CODES

0 NOT APPLICABLE | 1 VERY GOOD | 2 GOOD | 3 ADEQUATE | 5 POOR | 7 VERY POOR | 9 UNSAFE | BLANK NOT DONE

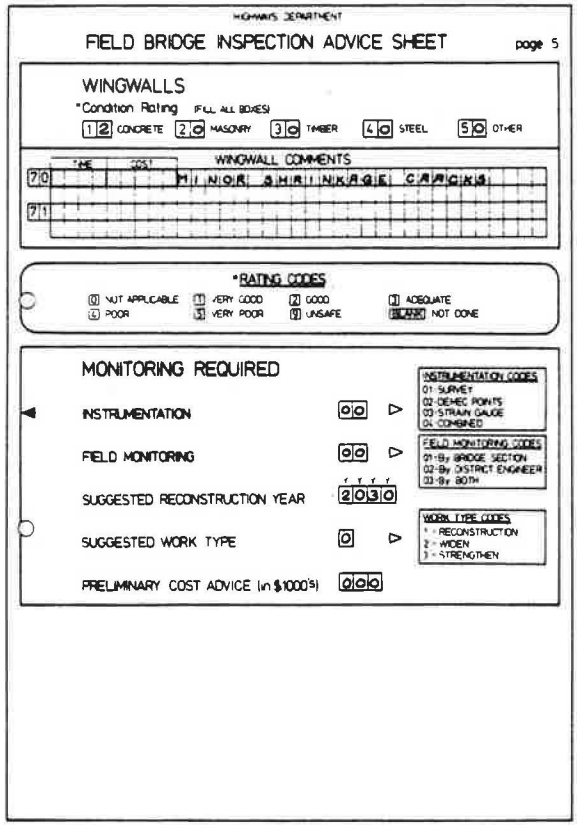

HIGHWAYS DEPARTMENT

FIELD BRIDGE INSPECTION ADVICE SHEET page 5

WINGWALLS

*Condition Rating (FILL ALL BOXES)

1 CONCRETE | 2 MASONRY | 3 TIMBER | 4 STEEL | 5 OTHER

WINGWALL COMMENTS

70 MINOR SHRINKAGE CRACKS

71

*RATING CODES

0 NOT APPLICABLE | 1 VERY GOOD | 2 GOOD | 3 ADEQUATE | 4 POOR | 5 VERY POOR | 9 UNSAFE | BLANK NOT DONE

MONITORING REQUIRED

INSTRUMENTATION CODES: 01-SURVEY; 02-DEMEC POINTS; 03-STRAIN GAUGE; 04-COMBINED

INSTRUMENTATION 00 ▷

FIELD MONITORING CODES: 01-By BRIDGE SECTION; 02-By DISTRICT ENGINEER; 03-By BOTH

FIELD MONITORING 00 ▷

SUGGESTED RECONSTRUCTION YEAR (Y Y Y Y) 2030

WORK TYPE CODES: 1 - RECONSTRUCTION; 2 - WIDEN; 3 - STRENGTHEN

SUGGESTED WORK TYPE 0 ▷

PRELIMINARY COST ADVICE (in $1000's) 000

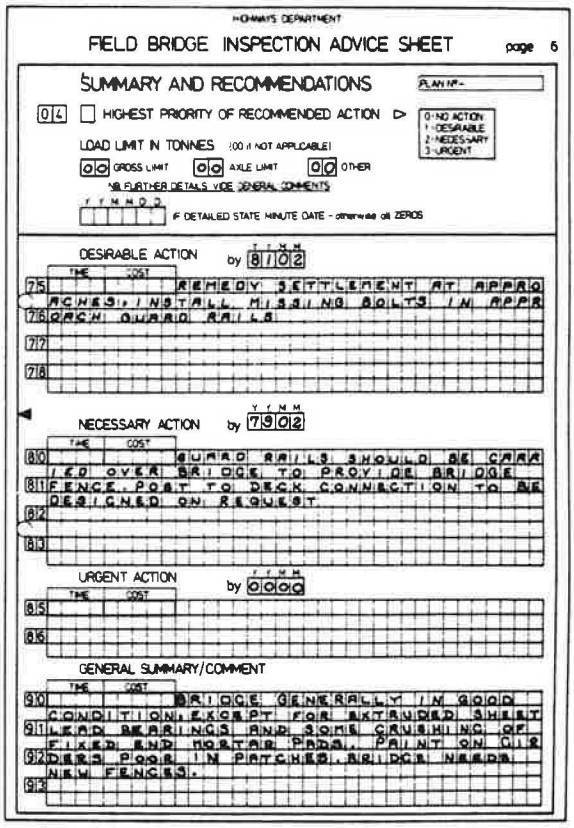

HIGHWAYS DEPARTMENT

FIELD BRIDGE INSPECTION ADVICE SHEET page 6

SUMMARY AND RECOMMENDATIONS PLAN Nº-

04 ☐ HIGHEST PRIORITY OF RECOMMENDED ACTION ▷

0 NO ACTION; 1 DESIRABLE; 2 NECESSARY; 3 URGENT

LOAD LIMIT IN TONNES (00 = NOT APPLICABLE)

00 GROSS LIMIT | 00 AXLE LIMIT | 00 OTHER

*IN FURTHER DETAILS VIDE GENERAL COMMENTS

(Y Y M M D D) IF DETAILED STATE MINUTE DATE - otherwise all ZEROS

DESIRABLE ACTION by 8102

75 REMEDY SETTLEMENT AT APPROACHES; INSTALL MISSING BOLTS IN APPR

76 ORCH GUARD RAILS

77

78

NECESSARY ACTION by 7902

80 GUARD RAILS SHOULD BE CARRIED OVER BRIDGE TO PROVIDE BRIDGE

81 FENCE POST TO DECK CONNECTION TO BE DESIGNED ON REQUEST

82

83

URGENT ACTION by 0000

85

86

GENERAL SUMMARY/COMMENT

90 BRIDGE GENERALLY IN GOOD

91 CONDITION EXCEPT FOR EXTENDED SHEET LEAD BEARINGS AND SOME CRUSHING OF

92 FIXED AND MORTAR PADS. PAINT ON GIRDERS POOR IN PATCHES. BRIDGE NEEDS

93 NEW FENCES.

important factor and, therefore, not included in the Bridge Inventory. Omitted for similar reasons are reports or ratings of the minor non-structural elements of a bridge, e.g. kerbs, median strips, lighting standards, etc. which tend to clutter inventory records. If, on inspection, these elements are found to be requiring attention they are referred to in the general Comments File. More important are the major structural elements viz. Deck, beams, bearings, expansion joints, abutments and piers including foundations where accessible.

One of the most important pieces of information, if not the most important retained in a bridge inventory is the load rating of a structure assessed after a thorough inspection. The load rating is usually expressed as the ratio of the live load capacity of the bridge to a standard loading, usually the design loading currently used. In this way the load rating of a structure is a convenient measure of the overall condition of a structure and forms the basis of setting priorities for a bridge replacement or strengthening program.

One serious drawback to bridges rated in this manner is that it does not accurately express the over-load capacity of structures. Most of the existing bridges have been designed on the allowable stress philosophy which result in varying actual factors of safety (i.e. safety factors related to live load only) for different bridge elements. (5) This actual factor of safety for the various bridge elements usually becomes larger as the ratio of dead load to live load increases. Therefore, bridge elements designed on the basis of allowable stresses with high dead load percentages have greater reserve capacities for carrying abnormal heavy vehicles than those where the dead load percentage is small. In the system under development the stresses induced by the dead and live loads are recorded so that the real capacity of each bridge to carry heavy vehicles travelling under permit, can be assessed. Since the majority of structures in South Australia have substantial sub-structures with high dead load to live load ratios, the load rating is confined to the deck slab and/or beams. Massive deterioration of the sub-structure would be required to significantly affect the capacity of the structure or overall load rating.

Almost as significant as the rating, for setting priorities for bridge replacement, are the width of structures and the adequacy of the approach roads for alignment, delineation and sight distance. With increased traffic speeds the width between kerbs for bridges has progressively widened so that some of the bridges built comparatively recently are now virtually sub-standard and considered to be relatively hazardous to traffic. Policy decisions have been made for a long term replacement program for bridges below certain acceptable widths depending on the road classification. Road approaches are an integral part of a bridge and its condition from a road safety aspect is subjectively assessed and recorded and used for determining priorities in a similar way as for width of structures.

Current and Future Developments

Using a computerised data bank of the type described, information can easily be re-grouped logically and globally as a function of the needs of the Department which range from data required for statistical purposes, as for example in the grouping of common problems, cost of common repairs, inspection costs to those providing information required to make decisions on relative priorities for bridge strengthening, widening or replacement.

The Bridge Inventory is used by the Bridge Inspection Team for planning a rational inspection program. South Australia covers an area of 980 000 square kilometres and although over half of this area if of little economic or topographical significance, a large area remains to be covered by a centrally located inspection team. A large proportion of the team's time is occupied in travelling and, therefore, a properly planned itinerary for inspecting bridges grouped according to their location and priority is of paramount importance.

The Bridge Inventory system adopted and described in this paper has been developed with flexibility in mind. It permits extension to and changes to be made to the type of information stored without affecting the usefulness of previously created files. It can also be used by other sections of the Department for their own particular needs by simple extension of recorded information.

Future development of the system will be in the areas of devising methods of optimising heavy load routes, and in combining programs with the digital mapping services for the automatic plotting of bridge locations and selected strategic routes.

Acknowledgements

The author would like to thank Mr A.K. Johinke, Commissioner of Highways, for permission to present this paper and my colleague, Mr V. Nechvoglod for his assistance in its preparation. The views in this paper are those of the author and do not necessarily reflect the views of the Highways Department.

References

1. J.R. Webber, Economics of Road Vehicles Limits Study, Technical Report T3, March 1976. Page 21 National Association of Australian State Road Authorities.
2. National Association of Australian State Road Authorities. NAASRA Bridge Design Specification 1976. Section 2.
3. American Association of State Highway and Transportation Officials. Manual for Maintenance Inspection of Bridges 1974.
4. OECD Research Group. Road Research. Bridge Inspection. Organisation for Economic Co-operation and Development. Paris 1976.
5. C.S. Matloch and F.C. Bundy. The Buffalo Bayou Bridge and Future Long Span Possibilities. Welding Journal Vol 38, 1959 p.g. 665-671.

THE NEW MEXICO BRIDGE INSPECTION PROGRAM

Kenneth White and John Minor, New Mexico State University

The New Mexico bridge inspection program is reviewed for its uniqueness as well as the use of the resulting data. Annual training sessions and field work with college professors has kept the program viable and continuing. Close cooperation with the Civil Engineering Department, New Mexico State University, has led to utilization of bridge capacity data developed within the program into a statewide overload routing and permit system. The system takes an overload wheel configuration and load distribution and computes an equivalent HS loading which is compared to the capacity of each bridge along a given route.

Congress in the 1968 Federal Highway Act called for national bridge inspections. National standards based generally upon the contents of the "Manual of Maintenance Inspection of Bridges 1970" (2) were issued in 1971 (1).

This paper describes how New Mexico not only established a viable bridge inspection program meeting all Federal requirements but utilizes the accumulated data in routine checks resulting from requests for permits for overweight vehicles. New Mexico has 3,000 bridges on the federal-aid highway system, with about 2,000 over geographical barriers and the remainder being over highways and railroads. All of these bridges had received their initial inspection and inventory by July of 1973.

History of the Inspection Program

The New Mexico State Highway Department initially established its bridge inspection program in November 1970. Bridge inspection crews were selected in each of the five districts. The Assistant District Highway Engineer of Maintenance, under the general direction of the District Engineer, was placed in direct charge of the district bridge inspection crews and made responsible for the prompt and proper reporting of information gathered. The District Bridge Inspection Crews were directed to make the required inspections and to place the information in reports so that it could be checked and forwarded to the general office. Consultation and general guidance was available to the districts on all technical data regarding the inspections from the Bridge Maintenance Engineer and the Bridge Engineer in the general office.

It was realized early that such a bridge inspection program would be only as good as its field inspectors - i.e. the District Bridge Inspection Crew. Although it would have been desirable to place an experienced professional engineer in each field crew and staff the crews with experienced bridge inspectors, this was not possible. However, a registered engineer was placed in charge of each crew.

In order to have trained, qualified inspectors for the program, the New Mexico State Highway Department in conjunction with the Federal Highway Administration, conducted a three week training program in January 1971. In the program the need for the importance of bridge inspection was emphasized along with inspection techniques and proper use of newly printed forms. It was decided that as much of the capacity ratings and computer coding as possible would be done at the district level. Since most bridges in New Mexico are of relatively simple design, much of the load computation could be accomplished at the district level with guidelines furnished from the general office.

A booklet, "New Mexico Bridge Inspection and Evaluation Guide," (3) was published by the Maintenance Division which covered all aspects of the Program. This booklet plus the AASHO "Manual for Maintenance Inspection of Bridges, 1970" and the FHWA "Bridge Inspectors Training Manual, 1970" (4) provided written guidance for the inspection teams. Guidance for coding data was provided by "Bridge Maintenance Inventory System" (5) published by the Engineering Computer Unit of the general office.

Implementation of Present Program

Due to the turnover of personnel and the introduction of new techniques and requirements, plus a better understanding of the scope of the project, additional training at periodic intervals was considered necessary. A staff member of the Civil Engineering Department of New Mexico State University was employed at the time with the New Mexico State Highway Department. Upon discussion of the problem, it was felt that the Department of Civil Engineering, with assistance from the experienced general office state highway department

personnel, was well qualified to do the additional training. The University had the necessary facilities in terms of classrooms, training aids, and laboratory space for the efficient and economical instruction of bridge inspectors. The faculty was uniquely qualified to instruct the trainees because they were experienced professional engineers as well as professionals in the instruction of students.

In January 1972 a bridge inspection short course was initiated at New Mexico State University sponsored jointly by NMSU and the New Mexico State Highway Department. Instructors included staff members from both NMSU and NMSHD. The Federal Highway Administration also furnished assistance. Participants in the course included the highway department bridge crews, the assistant district engineers of maintenance, representatives from the general office and, as guests of the highway department, several members of the Bureau of Indian Affairs. In all, thirty-two people attended the two week course and received certificates of completion of the course. The course was based on the "Training Manual for Bridge Inspectors, 1970;" however, only sections pertinent to New Mexico were covered.

The first week curriculum was primarily basic mechanics such as strength of materials and statics, nomenclature, and laboratory demonstrations. Laboratory demonstrations included the destructive testing of materials and some structural elements. Also included were demonstrations of the proper use of equipment such as torque wrenches and the corrosion detector.

The second week leaned more toward application of techniques which included the proper description of bridges and defects. Field trips were conducted to various types of bridges common to New Mexico. The local bridges had sufficient defects to promote many lively discussions about how to best describe and assign a rating. The question of load reduction and posting was also extensively discussed. A complete inspection was conducted of a bridge with known defects. Color slides of the bridges and defects were available for the post field trip discussions. In all, much information was gained and exchanged during and after the trips--thus complementing the classroom instruction.

Although the school was well received, it was apparent that much improvement could be accomplished in several areas for future short courses. Areas of improvement included the following. First, additional visual aids could be related directly to New Mexico's needs. For instance, the attention of the trainees could have been greater with discussion of a particular structure native to New Mexico. Secondly, the instructors felt a need to be better acquainted with the New Mexico inspection techniques and problems. These improvements could be accomplished only by working closely with the inspection teams in the field and with the general office in Santa Fe.

Consequently, an annual training school for bridge inspectors was proposed with the recommendation that two instructors from the university work with the Highway Department and its inspectors for the summer. The Highway Department and the University agreed on an annual program plus a summer background study for the program. The background study called for a research team consisting of two staff members of NMSU to spend seven weeks in the field with the inspectors, one week in the general office and two weeks for course preparation.

The research team divided the seven week period with the various NMSHD districts. During this time various phases of the program were reviewed with the bridge inspection crews. Filing systems and data storage techniques were checked. Field inspections with crews were undertaken. Field reports were taken, placed into final form, and coded for the data bank at the general office. Special inspection equipment such as the snooper, torque wrench, and corrosion detector were utilized during the inspections.

Many color slides for later use in the short course were taken. These pictures included all phases of inspection including proper use of safety cones, utilization of flagmen, and proper use of equipment. All types of bridges were photographed including many unique and unusual bridges. Close up, detailed photographs were made of both the usual and the unusual defects. Common type of defects included salt deterioration of concrete, hazardous approaches, outdated bridge railing and inadequate deck geometry.

A general survey of "interesting" bridges gave the research inspectors much insight into the problems of a bridge and how to inspect it. A rapport was established with all of the inspection crews which helped immeasurably in training and updating.

Particular subjects and ideas suggested by the inspectors were put into the course. A more detailed explanation of the appraisal and condition rating evaluation was requested. Careful review was necessary to establish exactly what was meant by such things as minimum tolerable condition or present minimum criteria. How to incorporate certain defects into capacity ratings was a common question. In New Mexico capacity ratings were initially computed by the actual inspector, if at all possible, and reviewed by the district office and the general office.

A week in the general office was of great benefit to the NMSU group. Coordination in establishing guidelines with the FHWA was discussed. Much of the criteria for ratings was clarified. Coordination with other sections, particularly the roles of the bridge design and engineering computer section were discussed and evaluated.

An overall understanding was developed by the NMSU team in how bridge inspection data was collected, where it went and for what purpose. The fact that actual field operation is only an initial step in bridge inspection was made evident. Reports, computer code forms, filing and capacity ratings take an appreciable amount of time and effort. This understanding helped immensely with course preparation and evaluation for the annual training program.

New Mexico now has a viable and continuing program for bridge inspection. The inventory has been completed for several years and a process has been established for reinspection of bridges as required. Also, a continuing training program for inspectors has been established.

Uniqueness of the New Mexico Program

The fact that NMSHD and NMSU have put together a cooperative annual training program is probably not unique. However, the manner in which the course directors from the university involved themselves with the program probably is unique. These professors not only worked with the field inspectors in establishing a training program, but have continued to assist in various ways. The Rio Grande Gorge bridge, a 366m (1200 ft) deck truss with a 183m (600 ft) main span and 200m (650 ft) clearance, has been inspected three times since the New Mexico bridge inspection program began. Each time the NMSU professors were two of the members of the inspection crew. Techniques and procedures

were developed which were unique to this size and type structure. A similar case involves the 122m (400 ft) steel arch at Los Alamos. In both situations the college professors worked hand in hand with the field crews providing training and experience for both groups. A continuing rapport has been established.

These professors have also worked in the NMSHD bridge design section in evaluating capacities of existing bridges. This opportunity gave not only insight to evaluating defects as reported from the field but also a working knowledge of establishing inventory and operating capacity ratings.

This unusual position of the engineering professors of not only observing but also participating in inspection, capacity evaluation, and data recording has yielded some unique benefits to the NMSHD. Among these benefits was the coupling of the data on bridge capacities from the inspection to the reoccurring problem of overweight or "permit" vehicles. This coupling which is discussed in some detail below has made the New Mexico bridge inspection program unique. In addition this data base provided by the bridge inspection program is utilized to establish posted capacity limits. Height and width restrictions are also evaluated along any particular route with this data.

Coupling Bridge Inspection and Overload Permits

In New Mexico a permit is necessary if, among other criteria such as length and width, the gross weight of any vehicle exceeds 384kN (86,400 lbs). Any truck requiring a permit because of gross weight is referred to the New Mexico State Highway Department for evaluation of the effects on the highway and bridge structures. Permits for overweight vehicles have been requested for vehicles with gross weights over 3.56MN (800,000 lbs). Unexpected requests to check the adequacy of structures for a particular route for an overweight truck with odd axle spacing were becoming more and more numerous. Previously these requests required engineers to be removed from their normal duties to pinpoint potential problem bridges and reanalyze them for the particular overload vehicle. The procedure was not only time consuming with valuable engineering man hours, but the potential for serious error existed.

First, it was possible that a potentially dangerous structure could be overlooked. Second, there was a chance for error in a rush analysis. Also, the data available in the bridge section did not always reflect the current condition of a bridge. The problem seemed to be becoming worse as more heavy industry was being located in areas where no railhead existed.

To alleviate the problem the New Mexico State Highway Department considered a more automated method of operation. Two facts stood out. First, a computerized technique of locating bridges along a proposed route as well as performing a structural analysis of the bridges would certainly speed up the operation and allow the bridge engineer to make a decision on each new overload configuration. Second, the latest information concerning any modifications and structural conditions of all bridges within the State was already available through the bridge maintenance inspection program.

The inventory and operating ratings, as well as other pertinent data such as bridge type and location, were stored on magnetic tape (4). Since the Civil Engineering Department, New Mexico State University, had helped in creating the data by assisting in the training of the inspectors and in some cases actually inspecting bridges and calculating the load ratings, they were not only aware of the data tapes but also the quantity and quality of the data. Computer programs to check capacities of bridges had been proposed by consultants and agencies but no one before had proposed utilizing directly the data accumulated by the bridge maintenance program.

In a cooperative agreement the Civil Engineering Department, New Mexico State University, was charged with developing a computer system that would meet the criteria of the NMSHD to streamline the operation and use the bridge maintenance inspection information already collected and stored on magnetic tapes. This data bank included the results of a complete analysis of every bridge in New Mexico. The load capacity rating was recorded as a HS loading for both the inventory and operating rating.

A new analysis of each structure along each route was rejected as impractical. First, too much input data for each structure would be required to perform such an analysis. Second, this detailed structural data was not available from the bridge inspection inventory system. Also, large quantities of computer time would be required to check out a proposed route, and finally, a detailed analysis would be repetitious. Each bridge was already analyzed and given a safe load capacity rating as a part of the bridge inspection program and this rating was stored as a part of the bridge inspection inventory data. With this in mind, the following approach was used to develop ØVLØAD, a computer program to automatically check bridge structure capacity with a given overweight vehicle.

Method of Equivalent Loading

For several years the New Mexico State Highway Department has been determining the overload capacity of bridges by comparing the moments used by the overloading vehicle to the designed moments produced by the standard AASHTO truck. Therefore, the operating capacity of bridges was designated the standard HS truck configuration which produced the over-stresses permitted in the Manual for Maintenance Inspection of Bridges published by the American Association of State Highway Officials. (2)

Within ØVLØAD a method of equivalent loads is established which simulates the actual overload truck passing over each and every bridge on the proposed route. The overload truck is converted into an equivalent HS truck for each particular bridge based on maximum bending moments or other criteria. This equivalent HS truck is then compared with either the operating rating or inventory rating as stored within the computer. Any time the equivalent HS load exceeds the stored value, the computer program automatically prints out the bridge number, location, equivalent load capacity required, and the rated safe load capacity. This printout is available for evaluation by the bridge engineer. The engineer may, at his option, prohibit the overload, reroute the overload, or do a more detailed analysis of the particular bridge or bridges.

Description of Program

The program, ØVLØAD, consists of the main program and three subroutines. The main program receives input data, reads stored data on bridges, determines whether or not a bridge is on the requested route, makes a comparison between safe load capacity and the required capacity, and prints information on inadequate bridges. The subroutines

compute the required capacity for a given overload vehicle on each particular bridge. A simplified flow chart of the program is shown in Figure 1.

The process is initiated by the input of the route numbers and Department of Defense, DOD, section numbers over which the proposed overloaded truck is to take. The axle spacings and axle loads of the truck are inputted for use in the computation of an equivalent HS truck. Finally, whether the comparison will be with inventory rating or operating rating is entered.

All bridge data are stored in numerical order by bridge number on a magnetic tape or disk. All data for a particular bridge are read and evaluated and any bridges not on the route are rejected before any equivalent load computations are made. If the bridge is on the desired route and within the desired DOD sections, the structure is classified into one of four types and an equivalent loading determined.

The structures in New Mexico can be divided into four general categories: Simple span bridges, continuous span bridges, truss type bridges, and concrete box culverts. Although other types of bridges exist, such as rigid frame structures, each can be classified into one of the above categories for determination of the equivalent HS truck rating of an overweight vehicle.

For structures classified as simple span bridges, the subroutine SIMSP is called. The SIMSP subroutine utilizes the span lengths of the bridge to be checked and the axle spacing and axle loads of the overloaded vehicle. The first axle of the vehicle is placed at mid span of the first span and the criticial bending moments are determined by a standard matrix method of structural analysis. This moment is retained for later comparison. The next axle is moved to mid span and a new bending moment is calculated. The bending moment is compared to the previous bending moment and the larger value is retained. This procedure is continued until bending moments for all positions of the vehicle have been compared. The bending moments produced by a standard HS 20 truck is computed in a similar manner for the same span. An equivalent HS rating is assigned to the overloaded truck by the ratio of bending moments produced by the two trucks times twenty. This equivalent HS value is stored for later comparison. The overloaded vehicle is then moved to the next span. The entire procedure is repeated for this span. The new equivalent HS rating is compared to the old rating and the larger value retained. This procedure is continued until all spans have been checked. The largest equivalent HS rating is then returned to the main program for comparison with either the operating or inventory rating as requested.

For structures classified as continuous span bridges, the subroutine CØNTU is called. The CØNTU subroutine has a general procedure similar to that of SIMSP. The computation of bending moments by matrix methods is made on the basis of a continuous prismatic structure with actual span lengths. Both positive and negative bending moments are determined. The maximum values for each span is saved and the equivalent HS ratings are returned to the main program.

Structures classified as trusses are subjected to the computations of the subroutine TRBM. The subroutine TRBM proceeds in a manner similar to SIMSP except that three equivalent HS ratings are computed. These three equivalent HS ratings are necessary because the data bank does not indicate in what manner an excess load would cause the truss to fail. The overload vehicle is moved across the truss and the maximum equivalent HS ratings are computed based on stringer moments, floor beam reactions, and span length moments. All three HS ratings are returned to the main program and if any exceed the safe capacity, the bridge is considered inadequate.

Once a structure has been classified and the equivalent HS rating has been assigned for the overload vehicle by one of the three subroutines, the equivalent HS rating is compared to the safe loading capacity that has been previously determined for that structure by a complete analysis. If the equivalent HS rating is less than the safe load capacity assigned the bridge, the program goes to the next bridge. If the equivalent HS rating is greater than the stored operating capacity, the bridge is considered inadequate and pertinent information about the bridge is printed. The information gives the user a quick identification of the critical bridges, possible need for reanalysis or whether detours might be necessary and available. This procedure is repeated until every bridge on the designated route has been checked and every inadequate bridge listed.

Output Information

Figure 2 is a typical output which lists all inadequate bridges on the route. Each bridge number, route, and DOD section is listed. This information is followed by the type of bridge, a description of the location of the bridge, the critical span length, the equivalent HS load capacity required and the rated HS load capacity. The equivalent load is divided by the rated operating load to give a ratio to assist in evaluating the bridge. Trusses have three equivalent HS truck printouts. The first indicates an equivalent truck based on floorbeam reaction loadings, the second indicates the stringer moments and the third indicates an equivalent truck based on overall moment.

This output pinpoints all potentially critical bridges and prints a comparison of the capacity based on allowable criteria set by AASHTO (4) as analyzed in the bridge inspection program and the equivalent capacity computed by the program. These critical bridges, capacities, and required equivalent capacities are reviewed by an engineer before any decision is made on the issuance of a permit.

In some cases a requirement for adjustment of axles or axle spacing, restrictions on speed, or re-evaluation of bridge capacity is all that is required to approve a permit. In other cases the vehicle may not be allowed to use one or more structures and the construction of a detour may be necessary. In all cases the engineer has the confidence that all bridges on a route have been considered and critical bridges with essential data have been referred to him.

Present Operation

The program ØVLØAD has the capability to pick out all bridges which do not meet the equivalent load criteria along a proposed route and print the pertinent data within minutes. In New Mexico an engineering technician inputs the necessary information via a remote terminal and the results are available within minutes. If the proposed route is inadequate, an engineer can either choose an alternate route which can be checked by the same system

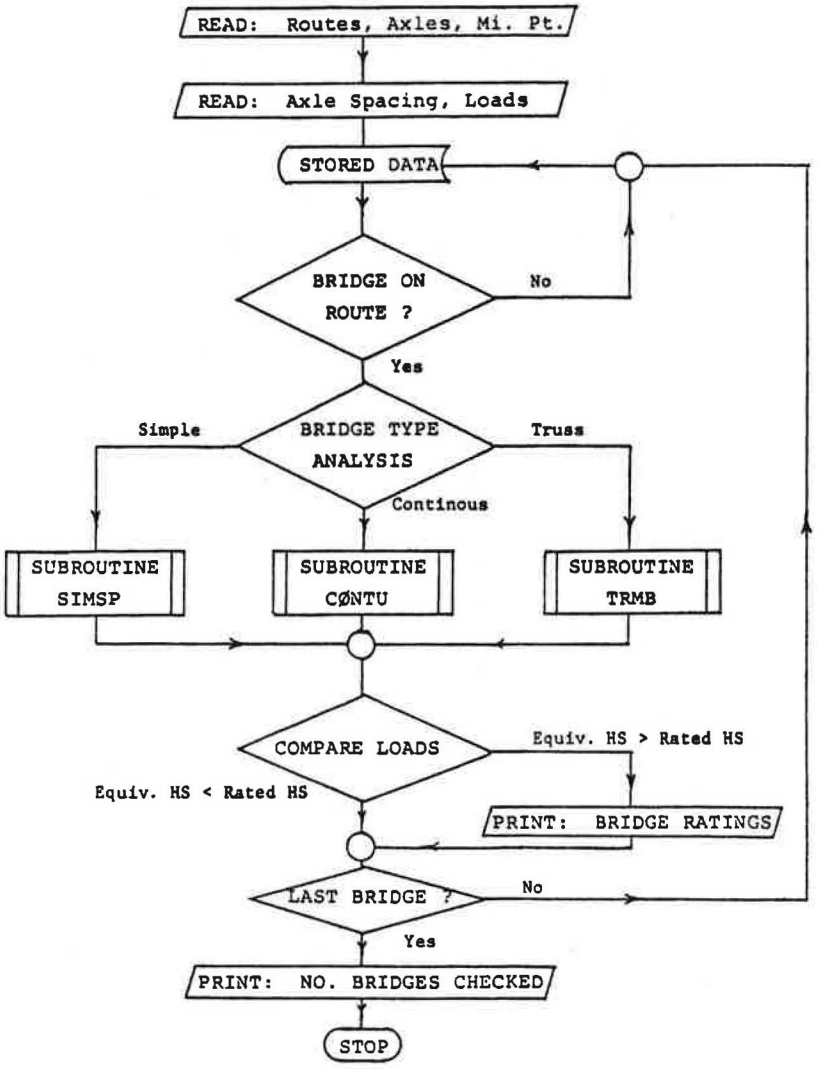

Figure 1. MAIN PROGRAM ØVLØAD

```
OUTPUT DATA

THE BRIDGE OVERLOAD PROGRAM DEVELOPED BY
WHITE-MINOR, NMSU 1973-74 AND SPONSORED BY THE NEW MEXICO STATE
HIGHWAY DEPT. LATEST UPDATE AUGUST, 1977.
ROUTE DIRECTION CODE EXPLAINED IN NMSHD BRIDGE INSPECTION MANUAL, ARTICLE 14.10.8
NOTE:  THE FOLLOWING IS COMPARED WITH OPERATING RATING

BRIDGE NO.1744 ROUTE NO. 44 DOD SECT NO. 430 ROUTE DIRECTION 1
DOD MILEPOINT IS 21.15
TIMBER SIMPLE SPAN BRIDGE
21.1NM W OF JCT SR126&44
SPAN LENGTHS   25.00
EQ HS =102.0 RATED HS = 19.0 RATIO =5.4

BRIDGE NO. 1780 ROUTE NO. 44 DOD SECT NO. 425 ROUTE DIRECTION 1
DOD MILEPOINT IS .23
STEEL CONTINUOUS BRIDGE
STRINGER TYPE
0.4ME OF US 85, BERNALILLO
SPAN LENGTHS 28.00   42.00   28.00
POS HS = 99.5 RATED HS = 30.0 RATIO = 3.3

BRIDGE NO. 3107 ROUTE NO. 44 DOD SECT NO. 425 ROUTE DIRECTION 0
DOD MILEPOINT IS 18.10
17.7 M NW JCT I-25 & SR 44
SPAN LENGTHS     10.00
CONCRETE BOX CULVERT RATED CAPACITY = 23.0

BRIDGE NO. 6946 ROUTE NO. 44 DOD SECTION NO. 425 ROUTE DIRECTION 1
DOD MILEPOINT IS 9.08
PRESTRESSED CONCRETE SIMPLE SPAN BRIDGE
8.7 M NWEST JCT I-25 & SR 44
SPAN LENGTHS    51.00
EQU HS = 101.8 RATED HS = 45.0 RATIO = 2.3

BRIDGE NO. 1521 ROUTE NO. 90 DOD SECT NO. 999 ROUTE DIRECTION 1
DOD MILEPOINT IS 0
92.3 MI NE OF US70/SR90
TRUSS LENGTH = 100.00 SPAN LENGTHS = 17.00
EQ DECK HS = 31.3 EQ FLBM HS = 32.2 EQ TRUSS HS = 38.5 RATED HS = 22.0
RATIO-1 = 1.4 RATIO-2 = 1.5 RATIO-3 = 1.7

57 BRIDGES HAVE BEEN CHECKED
```

Figure 2. SAMPLE OUTPUT FROM ØVLØAD

or take a detailed look at the inadequate structures.

Although the analytical procedures used are relatively simple and contain approximations such as assuming prismatic members and no lateral distribution of load, these simplifications and assumptions were essential to the successful mating of ØVLØAD to the bridge inspection program data. This was accomplished only through thorough understanding of the field operation, data collection, safe load rating techniques, and data record keeping of the bridge inspection program.

Many requests each week for permits based on weight are received by the New Mexico State Highway Department. All such requests are evaluated with the system. The majority of the requests are evaluated with the system. The majority of the requests indicate no inadequate bridges along their proposed route. Only those overloads indicating inadequate bridges are referred to engineers for further evaluation. The system has reduced engineering manpower requirements for checking structures for an overweight vehicle permit, yet has reduced the potential for error without sacrificing engineering evaluation.

A similar computer program has simplified the posting of inadequate bridges. The specified legal loads are passed over all bridges within the state via the computer and compared with the inventory capacity. Those bridges where the equivalent legal load exceeds the inventory rating were posted at the inventory capacity. The system also provides a quick method for listing posted bridges.

Conclusions

The New Mexico State Highway Department has a viable and continuing program for bridge inspection. This program was developed in close cooperation with New Mexico State University. Data developed within the program is utilized on a continuing basis in a statewide overload routing and permit system as well as in other routing operations.

References

1. Federal Register. Vol. 36, No. 71, p. 7851, Tuesday, April 27, 1971.
2. Manual for Maintenance Inspection of Bridges, 1970. American Association of State Highway Officials, Washington, D. C. 2004, (1970).
3. New Mexico Bridge Inspection and Evaluation Guide. Intra-agency publication, Maintenance Division, New Mexico State Highway Department, October 1971.
4. Bridge Inspectors Training Manual, 1970. Department of Transportation, U. S. Government Printing Office, Washington, D. C. 20402, (1970).
5. Bridge Maintenance Inventory System, 1971. Intra-agency publication, Engineering Computer Unit, New Mexico State Highway Department (1971).

PRECEPTS OF THE EVALUATION OF FACILITIES FOR HUMAN USE AND THE APPLICATION TO BRIDGE REPLACEMENT PRIORITIES

James C. Porter, Louisiana Department of Transportation and Development

Over the years, highway departments have inventoried and appraised their highway systems. One of the concepts that evolved is the sufficiency expressed as a percentage. This concept can be formalized as an inventory and appraisal process for general application. The concept has been applied intuitively to specific inventory needs such as the "Recording and Coding Guide for the Structure Inventory and Appraisal of the Nation's Bridges" and the sufficiency rating formula for bridges developed by the Federal Highway Administration. A generalized process which concisely defines terms required to develop precepts is presented. The methodology is a synthesis developed around the recognition that facilities subject to evaluation are directly or indirectly intended for human use. The process is then applied to a bridge replacement priority process through use of the sufficiency in an abridged example. Other uses are also discussed.

Precepts of the Evaluation of Facilities

The precepts of the evaluation of facilities for human use are a generalization of concepts narrowly applied only to highway facilities in the past. The concept of sufficiency or sufficiency rating which is the net results of the evaluation presented is not new. The context in which it has been traditionally used is the highway sufficiency rating used for planning purposes or more specifically ordering priorities or determining needs for upgrading highway facilities. The origin of the sufficiency concept is documented as early as 1946 and its use and the development of inventory data seem to be a somewhat arbitrary practice which relies on intuition.(9) The precepts advance the concept of systematically developing evaluation goals, facility functions and the required inventory data to evaluate them. This ultimately involves establishing a glossary of terms to describe the evaluation process, generalizing and enhancing the evaluation process and presenting a systematic approach to the selection of strategic inventory data necessary to the evaluation process.

Emphasis should be placed on inventory data which is measured and not subject to judgement which may introduce bias.(3) Subjective evaluations, when included in the inventory data, should be in a uniform reporting approach to minimize bias in the site observations.

The need for this generalized approach became evident when the Federal Highway Administration developed a sufficiency formula around its bridge inventory data (10) which was required to be collected by the States and supplied to a national base it maintains. On occasion this inventory data has been questioned as to its value or need as inventory data. Justification for this data led to the review of the sufficiency formula to determine what was needed to evaluate a bridge. It logically follows that initial development of inventory data sets can be arrived at systematically and thereby justified through analysis of predetermined evaluation goals and facility functions.

The engineer is often called upon to investigate the feasibility of developed alternatives for capital outlay programs to maximize profits as well as optimize other benefits to his organization or client. The investigation of existing facilities which are directly or indirectly intended for human use can be accomplished by evaluating their sufficiency in the context of current standards of technology and practice. Several common precepts defined for the sufficiency evaluation presented herein are, in part, independent of a facility's specific function(s). The relative independence of function should be most valuable in a multi-discipline, team environment. Each team member can independently develop the function assessment in his specialty and together they must agree on the relative importance of each function. Another use of the sufficiency is the comparison of several similar facilities of different ages, states of repair and levels of usage. It provides a common denominator for input with other considerations in a retirement, maintenance, and replacement planning program.

Basic terminology is necessary to develop the sufficiency concepts. A glossary of terms follows to define the several terms which will be used herein:

Capacity - a data assessment standard representing a standard of capacity of the function to serve the elements in the environment of the facility.

Data Assessment Standards - a defined range of inventory data values defining levels of service.

Efficiency - the assessment of an inventory data

item which is used in a composite to evaluate the function assessment. An inventory data item can be an assessment requiring no further evaluation.

Element - the human element or a vehicle, machine or other device operated or utilized directly or indirectly by the human element for production purposes, comfort or other need. An element may also be defined as a function.

Essentiality - an evaluation of the inventory data with respect to its relative importance to the function and to the elements served by the function.

Facility - a distinct operational unit that may be independently evaluated relative to the elements it serves or affects in its environment.

Function - a service or product a facility provides or an effect it produces on one or more elements in its environment.

Function Assessment Standard - The evaluation of a function considering the vital and the nonvital data assessment results.

Inventory Data - information which is qualitatively descriptive of a function. Data best suited is that used in current practice to design or develop similar functions for new facilities and site observations, measurements, and evaluations.

Nonvital Data Assessment Standards - evaluation of inventory data items not relative to human health in terms of their essentiality to the function they describe and in terms of the efficiency expressed by the interactive effects of performance and capacity of the function.

Performance - a data assessment standard representing a standard of observed or measured service the function provides to the elements in the environment of the facility.

Relative Importance Factor - a relative importance to the human element is assigned to each function. The sum of the relative importance factors for all functions in the facility will equal unity.

Safety - a data assessment standard representing a standard of health and safety of the human element in contact with the function.

Serviceability - the function assessment based on the evaluation of its composite vital and nonvital data assessments.

Sufficiency Rating - the facility assessment based on the sum of the products of the serviceability of each function and its respective relative importance factor.

Utilization - a data assessment standard representing a standard of observed or measured service provided the human element served by the function.

Vital Data Assessment Standards - evaluation of inventory data items relative to human health in terms of their essentiality to the function they describe and in terms of the efficiency expressed by the interactive effects of utilization and safety on the human element.

First the facility must be clearly defined and so must its functions. A facility can be defined as a bridge or a segment of highway, an office unit or an office building, or a production unit or a production plant. A facility's functions can be divided into two somewhat related categories; the facility's objective(s) and its interaction with the human element. Facility objectives for example would be to convey automobile and truck traffic, provide office rental space or produce gasoline. Interaction of a facility with elements in its environment is inevitable. Environmental safety and comfort of the elements in contact with or affected by the facility and its contribution to their general welfare are the usual interactions to be sought to identify functions.

Once the several functions have been defined, an inventory data set is defined to adequately describe each function in terms of vital and nonvital assessments. The best source of data for a function's assessment is the parameters currently used to design the same function for a new facility. Another source of data is a systematic process of on-site observations, measurements, and evaluations. An example of standardized reporting for on-site measurements, observations, and evaluations is the following condition ratings in a convenient numerical form which are particularly valuable for multi-facility evaluations:

9 New condition - no maintenance recommended
8 Good condition - no maintenance recommended
7 Fair condition - recommend maintenance on minor items
6 Fair condition - recommend maintenance on major items
5 Poor condition - recommend major rehabilitation
4 Poor condition - minimally adequate to operate with current use
3 Poor condition - inadequate to operate with current use - recommend restricted operation
2 Critical condition - inadequate to operate with current use - recommend minimum restricted operation
1 Critical condition - inadequate to operate with current use - recommend ceased operation until rehabilitated
0 Critical condition - inadequate to operate with current use - recommend ceased operation until replaced

Note: Condition Ratings 4, 3, and 2 will generally require the major rehabilitation recommended in Condition Rating 5, but prevailing conditions make the immediate concern, restricting operations, more important. If a facility or facility function is planned for another use, substitute the word "planned" for "current".

Each function identified will require evaluation of its importance relative to the importance of the other facility functions. The evaluation assigns a total importance of unity to the (n) facility functions. The relative importance (I_i) of each facility function will be identified by its assigned portion of unity as demonstrated in Equation 1.

$$\sum_{i=1}^{n} I_i = 1 \qquad (1)$$

After the inventory data for a function has been selected, it is necessary to develop data assessment standards to evaluate the function described. It is convenient to divide the inventory data into two (2) distinct groups, vital and nonvital data. Vital data is descriptive of a function operation which directly affects element safety relative to utilization such as a structure's integrity versus the applied live load. Nonvital data is descriptive of a function operation in terms of performance relative to capacity and does not directly relate to element safety or utilization. Nonvital data might be considered those items associated with creature comforts such as heating, ventilation, and air conditioning and lighting. The data assessment standards are mathematical functions or data ranges which define standards of service.

Each function is assessed independently as a direct result of its associated inventory data assessments. The function assessment standards can be defined in common generic terms. The function may be appraised as being in either desirable, adequate, tolerable, or inoperative condition. A useful numerical evaluation for a facility function assessment

is in the form of appraisal ratings such as:

9 Better than desirable standards
8 Equal to desirable standards
7 Better than adequate standards
6 Equal to adequate standards
5 Tolerable conditions
4 Tolerable conditions - recommend rehabilitation
3 Intolerable conditions - recommend rehabilitation
2 Inoperative - recommend rehabilitation
1 Intolerable conditions - recommend replacement
0 Inoperative - recommend replacement

The appraisal ratings are directly applicable to establishing data assessment standards because of the direct contribution of the data assessment to the function assessment. The efficiency of the vital and nonvital data, (V_{ij}) and (E_{ij}) respectively, is the percent effectiveness of the function operation the data describes. The efficiency can be numerically related to the appraisal ratings if they are used. Each item of data must also be evaluated for its essentiality to its related function. The essentiality (K_{ij}) is the proportion of unity assigned each of the (m) items of data demonstrated by Equation 2.

$$\sum_{j=1}^{m} K_{ij} = 1, \quad i = 1,2,3,\ldots,n \qquad (2)$$

The serviceability (S_i) of a facility function is computed by summing the products of the efficiency and essentiality of its related data. The serviceability is the percent effectiveness of the function as determined by its assessment results demonstrated in Equation 3.

$$S_i = \sum_{j=1}^{m} (E_{ij} + V_{ij})K_{ij}, \quad i = 1,2,3,\ldots,n \qquad (3)$$

where (E_{ij}) or (V_{ij}) is zero when it is a vital or nonvital data assessment respectively.

The sufficiency rating (S_T) for the total facility is computed by summing the products of the serviceability and the relative importance of the facility function as demonstrated by Equation 4. The sufficiency rating is then a composite of the serviceability modified by the relative importance of each function resulting in a percent sufficiency for the facility.

$$S_T = \sum_{i=1}^{n} S_i I_i \qquad (4)$$

In retrospect the process for evaluation of facilities for human use as presented provides a guideline which will aid the engineer or other specialists in communicating complex technological evaluations. This is accomplished by reducing the evaluation results into layman's terms such that the input and output can be easily comprehended by all parties involved. Facilitating effective input into the evaluation process and reducing its results to layman's terms makes it attractive as a communication tool. An equally important feature is that the evaluation implementation process leads to a strategic selection of inventory data (D_{ij}) which best describe and thereby evaluate a facility. The facility function serviceability provides easy access to the magnitude of functional problems affecting the sufficiency evaluation. The complete evaluation process is demonstrated by the flow chart in Figure 1.

Figure 1. Sufficiency evaluation flow chart.

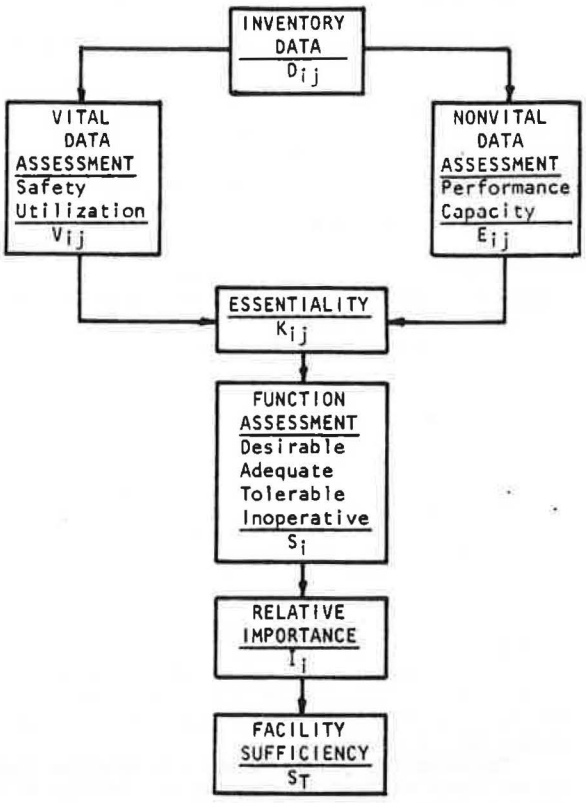

Bridge Replacement Priorities

The facility for human use shall be defined as a highway bridge. The facility functions normally provided for through the design process for bridges are structural and geometric. Structurally the bridge design provides the required strength to routinely accommodate legal weight vehicles and the reserve strength to accommodate occasional overweight vehicles. Geometrically the bridge design provides for a high probability of success in negotiating the bridge site for the motorist. Geometrics account for the psycological and physical limitations of the driver and also for the performance, dimensions, speed, and volume of the vehicle expected to use the facility.

Another function which the highway bridge design must provide for, is adequacy of opening or underclearances for the facility or geographic barrier bridged over. The underclearances for underpassing highways, railways, or navigable waterways and the adequacy of opening for drainage through the bridge site must be included in the assessments when applicable. The regional significance of the bridge is also a facility function to be assessed. Regional significance is measured by the regional importance of the route the bridge is on, the detour distance which would be necessary to by-pass the bridge if it were lost from service and the volume or traffic served by the bridge.

With the facility functions for a highway bridge thus defined, it is now necessary to determine what inventory data sets would be most suited to evaluate each of them. The functions were identified from the design process. Most of the inventory data can also be selected from the design process.

The design strategy is to determine the structural and geometric standards which are desirable for a planned bridge. Consideration is given to the

planned and actual significance of the highway and bridge as a transportation link. This provides the standards of highway traffic expected in terms of speed, volume, size, and weight. The bridge is fitted to its site for the required underclearances and other site requirements while meeting the necessary geometric and structural standards for highway traffic.

The evaluation strategy is to assess the structural and geometric capabilities of an existing bridge using assessment standards compared with the actual traffic characteristics and also assess the underclearance needs with respect to those provided. The difference between design and evaluation is simply the difference between prescription and appraisal respectively.

Facility Function Considerations

Structural Evaluation. The AASHTO Standard Specifications for Highway Bridges(11) provides for hypothetical trucks and lane loads in terms of the designations H20-44 and HS20-44 for example. These design loads simulate actual traffic loads for structurally proportioning bridges in the design process. The AASHTO Manual for Maintenance Inspection of Bridges(8) provides for the evaluation of bridge components by specifying stress carrying capacity in terms of the "inventory" load producing the design stress and the "operating" load producing an infrequently allowed stress such as that for a permitted overweight vehicle. The "operating" load stress is allowed on a more frequent basis provided that the rate of surveillance is greater than that for structurally adequate bridges.

The inverse of the design process is applied. The structural capacity of a component is computed and the dead load stress effects are applied. The resulting stress available for live load is consumed by an H, HS or other vehicle configuration with axle weights in the same proportion as provided for in the specifications. A direct comparison between current design load and the evaluated load is then possible. A common denominator is provided for by this method comparing the results and the evaluation processes for bridges.

Geometric Evaluation. The geometric evaluation of a bridge and its site is concerned primarily with those parameters which affect the ability of a vehicle and its driver to successfully traverse them. Under clearances will be taken as a geometric evaluation based on the specific needs of the underpassing functions. These parameters can be obtained from field measurements or from original plans when available.

The stopping sight distance as defined in A Policy on Geometric Design of Rural Highways(2) is the distance at which a vehicle driver can detect an object of a given size in the roadway. This distance is associated with vehicle speed and the time required for the driver to react and physically stop the vehicle before passing the object. A direct evaluation between the measured stopping sight distance and the speed limit is possible.

The approach roadway width compared to the clear roadway width of the bridge deck is another significant parameter affecting safety. There is a direct correlation between the two and the traffic accident rate. The most serious of these conditions is when the bridge roadway width is narrower than the width of the approach roadway. The accident rate dramatically increases for this condition.(7) Some other geometric considerations which require evaluation are the number of highway lanes provided by the structure, presence of one-way or two-way traffic and vertical clearance provided by through structures with elements over the roadway. The under clearance requirement is evaluated from the specific underpassing function need.

Condition Rating. The structural and geometric information can be obtained from direct field measurements and sampling or from plans and specifications when available. Another form of evaluation which plays a significant part in the overall evaluation is the condition rating. It represents a relatively subjective view based on field observations of individuals trained and experienced in such observations.

The condition rating is an analysis of observed site conditions and resulting recommendations which may stipulate corrective actions to improve or repair observed deficiencies. The condition rating as previously presented in a standardized format is suitable for multiple facility evaluation where hundreds or even thousands of facilities are to be compared to established repair and/or replacement priorities. This approach lends itself well to numerical evaluation. It is also helpful to divide the site and the bridge into components or inspection items and rate each one by a performance criteria as an aid to making the condition rating judgement. These ratings will be of great value in determining specific maintenance needs and repair priorities for large multiple facility systems. Performance ratings may take the following form:

9 The item is in new condition with no repairs necessary.
8 The item is in good condition with no repairs necessary.
7 The item is in good condition, but is in need of minor repairs.
6 The item is performing the function for which it was intended, but is in need of minor repairs.
5 The item is still performing the function for which it was intended at a minimum level, but is in need of minor repairs.
4 The item is still performing the function for which it was intended at a minimum level, but is in need of major repairs.
3 The item is still performing the function for which it was intended at a minimum level, but is in need of replacement.
2 The item is not performing the function for which it was intended and is in need of minor repairs.
1 The item is not performing the function for which it was intended and is in need of major repairs.
0 The item is not performing the function for which it was intended and is in need of replacement.

Regional Significance Evaluation. The regional significance of a bridge can be accounted for through the functional classification of the route the bridge is on and the net by-pass detour length. The net by-pass detour length is the extra distance which would be required to route the through traffic on a comparable facility which could accommodate the volume and character of the traffic currently using the bridge. These parameters should be used to independently evaluate regional significance of the bridge. The regional significance is incorporated into the selection of several data assessment standards such as volume of traffic to select the appropriate data assessment standards for the roadway width or number of lanes provided by the bridge. Regional significance is therefore not entirely an independent function.

Why have an independently evaluated regional significance? The subtle effect of regional significance

Table 1. Inventory data and related functions.

Structural Function	Geometric Function	Regional Significance Function
Inventory rating	Stopping sight distance	Average daily traffic
Operating rating	Bridge roadway width	Net by-pass length
Condition rating	Approach roadway width	Functional classification
	Vertical clearance over roadway	
	Underclearances	
	Condition ratings	

cannot be controlled or measured by its effects on the data assessment standards. By providing a separate function, the effect can be controlled and recognized in the total evaluation.

Inventory Data. The inventory data established thus far for the evaluation of a highway bridge facility is summarized in Table 1. There will be obvious questions raised about the choice of inventory data. As an example, some would question why the accident records are not included in the data as geometric inventory data. The answer is that the accident rate at a given bridge site would have a high correlation with geometric problems already described and therefore it would not be independent data. Also, raw accident data does not provide the cause of a series of recurring accidents unless uniform reporting procedures of traffic accidents are sufficient enough that review of the individual reports can determine the cause.

The functions chosen were arbitrary. Another approach would have been to combine some of the functions into "provide safe transit through bridge site". This would include all the inventory data items under structural and geometric functions except underclearances. Any valid choice of function and complete analysis should lead to an appropriate and valid inventory data set. A limitation of selecting an all encompassing function is the lost opportunity to review the results at the more detailed function definitions. An example of further expanding the functions would be to separate underclearance, bridge geometry, and approach geometry as separate functions.

Relative Importance of Functions

The obvious need for structural integrity should require that the structural function receive a substantial part of the relative importance. The safety aspects involved in the potential for collapse are onerous relative to structurally deficient bridges. However, it should not be overlooked that nine out of ten highway deaths associated with bridges are those related to geometric deficiencies.(12) The regional significance of a bridge should also play a role in determining priorities.

The goals of a replacement program should be reviewed in determining the relative importance assigned to the various functions. If the goal is to replace structurally deficient bridges, regardless of other operational characteristics or regional significance, the choice of relative importance factors is trivial. The relative importance would be unity for the structural function and zero for all others. If the goal is to replace structurally deficient bridges of regional importance, the regional importance function would share some relative importance with the structural function for example 0.2 and 0.8 for the regional importance and structural functions respectively.

The factors which affect the need for replacement are considered for each defined function in proportion to its contribution to the goals of the program when selecting the relative importance value. Values representing the goals of three replacement programs are shown in Table 2. Policy I gives the structural function the prime consideration with slight modification by the geometric and regional significance functions. Policy II gives a strong significance to the geometric and regional importance functions coupled with the structural function. This may be more in line with the real needs for consideration of highway bridge replacements. Policy III places heavy emphasis on the regional importance function especially in the view that items in its inventory data set will be used in setting data assessment standards for other functions. The benefits that may be derived from a replacement program based on Policy II compared with Policy I is a greater reduction in fatal traffic accidents associated with the replaced bridges at a slightly higher risk of collapse from those structures not replaced as soon with Policy II as they would have been with Policy I. The benefits associated with Policy III might be improved capacity of bridges on principal arterials at the sacrifice of higher risk of collapse of structures on secondary roads which would have been replaced sooner by Policies I or II. However, the exposure to the dangers of collapse may actually be reduced for the total motoring population by Policy III. It is possible that there may be significantly more traffic and therefore more exposure to collapse of bridges on the principal arterials which would remain by following Policies I and II. For the purpose of this example, Policy III will be used.

Table 2. Relative importance assignments to functions.

Function	Policy I	Policy II	Policy III
Structural	.60	.50	.50
Geometric	.30	.40	.30
Regional significance	.10	.10	.20

Serviceability of a Function

The serviceability of each function may be derived from a direct relationship established between the previously presented appraisal ratings which are a numerical approach to the function assessment. The serviceability is associated with a percent effectiveness a function has, based on its assessment. The serviceability could be arbitrarily assigned as

Table 3. Assigned serviceability percentages for appraisal rating values.

Appraisal Rating	Serviceability Percentage	Appraisal Rating	Serviceability Percentage
9	100	4	84
8	100	3	64
7	100	2	36
6	100	1	0
5	96	0	0

Table 4. Structural appraisal limits.

ADT[a]	Desirable	Adequate	Tolerable	Inoperative	Rating
Over 1,500[b]	HS20	HS20	HS15	-	Inventory
	-	-	HS20	HS2	Operating
750-1,500	HS20	HS15	-	-	Inventory
	-	HS20	HS20	HS2	Operating
Less than 750	HS15	-	-	-	Inventory
	HS20	HS20	HS20	HS2	Operating
-	9,8	7,6	5,4	1,0	Condition[c]

[a]ADT is not applicable with condition ratings.
[b]All principal arterials.
[c]Condition Ratings of 3 and 2 are in the intolerable range.

demonstrated in Table 3.

The boundary conditions selected are the appraisal ratings 9, 8, 7, and 6 will have a serviceability of 100 percent and the appraisal ratings 1 and 0 will have a serviceability of 0 percent. The remaining task is to select a reasonable declining scale between 6 and 1 based on the relative need for replacement of the facility stated in appraisal ratings 5 through 2. An estimate of these values is represented by a second degree parabolic function with zero slope at the appraisal rating of 6 as a third boundary condition.

The serviceability is ordinarily determined directly from the inventory data assessment using the efficiency and essentiality. This is a particularly valuable alternative when several data assessments are involved for a function. In this alternative, the efficiency will be determined in the same way as described here for serviceability.

Data Assessment Standards

The data assessment standards convert the inventory data into an efficiency through mathematical functions or ranges of data. The efficiency is described in terms of appraisals which are either desirable, adequate, tolerable or inoperative. For highway facilities, there is a wealth of information available for assessing some of the inventory data. (1,2,4,5,6,7,8,11)

Structural Function Inventory Data. The structural evaluation is accomplished by developing a table of inventory and operating loads and condition ratings which are characterized as one of the four stated appraisals describing the function. Table 4 is a policy for the efficiency evaluation of the data for the structural function.

Though Table 4 is presented using all HS type loads, it can be converted for other load types. The condition rating used in the evaluation would be the lowest of those associated with the bridge structure exclusively. The efficiency of the structural rating and the condition rating are expressed with the same values used for serviceability and the essentiality is expressed as .75 and .25 of their efficiencies respectively.

Geometric Function Inventory Data. The geometric function for this example is divided into two functions to provide more detailed significance at the function level. These functions will be bridge geometry with an assigned relative importance of .20 and approach geometry and underclearances with an assigned relative importance of .10.

The stopping sight distance limited by the approaches to the bridge ends and limited by the bridge itself is applied in part to the appraisal ratings of the approach geometry and the bridge geometry respectively. The data assessment standards for evaluating the desireable criteria for the stopping sight distance (SSD) are common to both applications and a policy is demonstrated in Table 5. The adequate criteria is represented by the posted speed limit or advisory speed for the location equated to its corresponding wet pavement stopping sight distance. The tolerable criteria is represented by the posted speed limit or advisory speed for the location equated to its corresponding dry pavement stopping sight distance. The condition ratings for the bridge roadway and the approach roadway are included in the assessment with the same appraisal limits demonstrated in Table 4. The inoperative criteria is not considered applicable to geometric function assessments.

The bridge roadway evaluation policy demonstrated in Table 6 and Table 7 is a component of the bridge geometry function evaluation which will also include the stopping sight distance, condition rating and the vertical clearance. The essentiality of the inventory data are expressed by allocating .50 of the lowest

Table 5. Desirable criteria for Stopping Sight Distance

Functional Classification	Average Daily Traffic	Speed (Km/h)	Wet Pavement SSD(m)
Principal arterial	Over 3,000	110	210
Principal arterial	3,000 or less	95	150
Minor arterial	750 or less	70	95
Other	400 or less	65	80

Note: 1 Km/h = 0.62 mph; 1 m = 3.28 feet.

Table 6. Desirable criteria for bridge roadway width.

Functional Classification	Average Daily Traffic	Roadway Width (meters)
Principal arterials	Over 12,000	15.2[a]
	12,000-3,000	11.6[a]
	Less than 3,000	12.2
Minor arterials	1,500-751	12.2
	750-400	8.5
	Less than 400	8.5

Note: 1 meter = 3.28 feet
[a]Twin structures are required.

Table 7. Adequate and tolerable criteria for bridge roadway width.

Average Daily Traffic	Adequate Roadway Width (meters)	Tolerable Roadway Width[a] (meters)
Over 1,500	11.0	9.1
1,500-751	9.8	7.3
750-401	8.5	6.7
400-250	8.5	6.7
Less than 250	7.9	6.1

Note: 1 meter = 3.28 feet
[a]Roadway width shall not be less than the approach roadway width.

efficiency value between the roadway width or vertical clearance and .25 of the efficiency of the stopping sight distance and condition rating each.

The vertical clearance evaluation through a bridge structure is not as complex in application. For example; a vertical clearance policy of 4.9 meters can be taken as the desirable criterion, 4.6 meters as the adequate criterion and 4.3 meters as the tolerable criterion.

The underclearance and approach geometry are also components of the bridge geometry function. The approach geometry is evaluated as previously shown by the least stopping sight distance from the bridge ends and the condition rating. The essentiality of these inventory data items are expressed as .60 and .20 of their respective efficiencies.

The underclearance evaluation can not be assessed in a uniform manner. The vertical and horizontal underclearances and other dimensional requirements will be dependent on the unique services under the bridge or the hydrological characteristics of a stream. This evaluation must be done independently for each bridge. An essentiality of .20 is assigned to this inventory data assessment.

Regional Significance Function Inventory Data. The regional significance evaluation is a measure of the impact of the increased costs to transportation if the bridge were suddenly lost from service. Additional data is collected to compare the cost of the replacement structure to the increased cost of transportation. The increased cost for transportation is due to the detour distance added per vehicle over the time required to restore bridge service. The approximate replacement cost and time required before bridge service could be restored can be estimated from the physical size of the existing bridge. The cost per mile for operation of the average vehicle can also be estimated.

An appraisal rating for regional importance would have no significant meaning. A mathematical function (Equation 5) is developed which directly computes the function's serviceability. The regional significance of a bridge can be thought of as independent of its condition. In this instance it is the regional significance of the bridge relative to its current adequacy which is of interest. This will require that the regional significance appraisal be performed last such that the results of the remaining function serviceabilities can be used.

$$S = \left[1 - F \frac{C_t}{C_b} \left(\frac{\sin \pi \left(\frac{20 + S_T}{80} \right) + 1}{2} \right)^{1/a} \right] 100 \qquad (5)$$

The variables in this equation are the regional significance function serviceability (S), the functional classification factor (F), the total increase in transportation cost (C_t), the bridge replacement cost or a base cost (C_b), the sufficiency if the regional significance function serviceability were 100 percent (S_T), and an arbitrary constant (a). The arbitrary constant (see figure 2.) is taken as 2 and the functional classification factor is taken as 1.00 for principal arterials, 0.95 for minor arterials and 0.90 for other roads. The value of ($F\ C_t/C_b$) should not exceed unity. The total increase in transportation cost is the product of the average daily traffic, the estimated time required to restore the bridge to service in days, the net bypass detour length and the cost per unit length traveled per vehicle.

Sufficiency of a Facility

As previously presented, the sufficiency of a facility is a percentage determined from multiplying the serviceabilities by the relative importance and summing the resulting products. Depending upon the goals of the replacement programs as previously discussed the bridge with the lowest sufficiency percentage should have the highest replacement priority. In order to calibrate the algorithm to obtain the desired goals of a replacement program, substitute several different sets of relative importance values and review the priority sequence of bridges obtained. Continue this process until the desired results are obtained. It should be realized that the desired results are obtained only in a general sense because there are no absolutes in the comparison of deficient bridges requiring replacement.(9)

Ordering priorities

The established goals represent benefits expected from a facility. They provide the scale to measure the sufficiency or a percent of the benefit provided by a facility. The benefit of replacing or repairing a facility can be directly measured by the percent

increase in a facility's sufficiency once an action is complete.(3) With the inclusion of the cost of the action in the inventory data, the cost-benefit ratio can be compared and priorities can be reassessed to maximize benefits at the least cost.

References

1. A Policy on Design Standards for Stopping Sight Distances. American Society of State Highway Officials, Washington, D.C., 1971.
2. A Policy on Geometric Design of Rural Highways. American Associaton of State Highway Officials, Washington, D.C., 1965.
3. C. E. Fritts. Relation of Sufficiency Ratings, Tolerable Standards, and Priorities. Highway Research Board Bulletin, No. 53, Highway Sufficiency Ratings, Washington, D. C., 1952.
4. Geometric Design Standards for Highways Other than Freeways. American Association of State Highway and Transportation Officials, Washington, D. C., 1969.
5. Geometric Design Guide for Local Roads and Streets, Part 1. American Association of State Highway and Transportation Officials, Washington, D. C., 1971.
6. Highway Design and Operational Practices Related to Highway Safety, Second Edition. American Association of State Highway and Transportation Officials, Washington, D. C., 1974.
7. Highway Safety, Design and Operation, Narrow Bridges - Drivers' Dilemmas. Hearings before the Subcommittee on Investigations and Review of the Committee on Public Works - House of Representatives, Ninety-third Congress, First Session, June 12-14, 1973, U. S. Government Printing Office, Washington, D. C., 1973.
8. Manual for Maintenance Inspection of Bridges, Second Edition. American Association of State Highway and Transportation Officials, Washington, D. C., 1974.
9. Karl Moskowitz. Numerical Ratings for Highway Sections as a Basis for Construction Programs. Highway Research Board Bulletin, No. 17, Highway Planning, Washington, D. C., 1948.
10. Recording and Coding Guide for the Structural Inventory and Appraisal of the Nation's Bridges. U.S. Department of Transportation/Federal Highway Administration, Washington, D. C., July, 1972.
11. Standard Specifications for Highway Bridges, Eleventh Edition. American Association of State Highway and Transportation Officials, Washington, D. C., 1973.
12. Weak Bridges: Growing Hazard on the Highways. U. S. News and World Report, Vol. 84, No. 1, January 9, 1978.

Figure 2. Effect of the arbitrary constant (a) on the regional significance function serviceability (Equation 5).

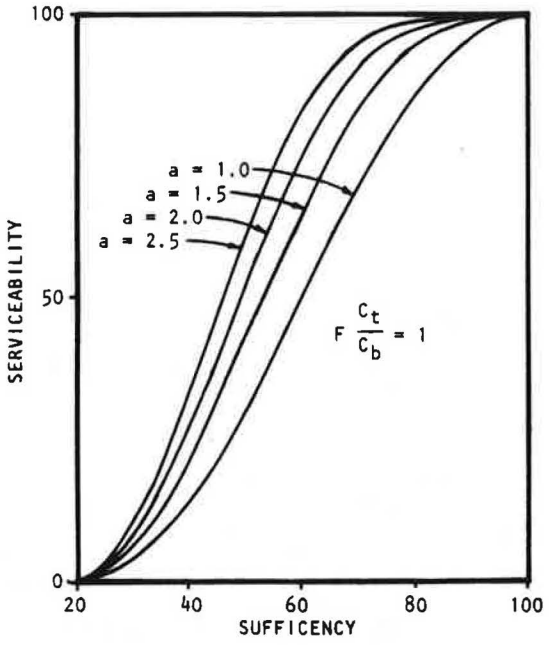

SYSTEMS APPROACH TO BRIDGE STRUCTURE REHABILITATION OR REPLACEMENT DECISION-MAKING

Arunprakash M. Shirole', P.E., City of Minneapolis
James J. Hill, P.E., Minnesota Department of Transportation

This paper presents a systems approach to the difficult bridge structure rehabilitation or replacement decision-making. Essential elements of the data base, or structure information system, supporting this decision-making process are indicated. Adequacy for future use and economic criteria for a rational appraisal of alternates are developed and their application is indicated. Constraints; like available and projected flow of funds and of local or legal nature are identified and their impact on the decisions is analyzed. Analytical decision methods, such as pay-off matrix and decision tree, for evaluation of alternate proposals are presented and illustrated in a systematic, step-by-step procedure. Guidelines are also presented to assist the decision-maker in the selection of a method suitable for individual situations.

For a decision-maker, the decision to rehabilitate or to replace a deficient bridge structure and its subsequent justification have not always been easy. One principal cause for this has been the approach of piecemeal synthesis in the existing decision-making that has, in general, been oriented toward emphasizing certain advantages of one alternate and underestimating its disadvantages. Need exists, therefore, to accomplish the decision-making process through a complete, integrated and logical analysis. The systems approach provides such a coordinated step-by-step analysis which, when applied to bridge structure rehabilitation or replacement decision-making, offers several advantages. It integrates essential elements of reliable information, well defined criteria, clearly perceived constraints and uniform evaluation of all available alternatives. Further, it allows for and encourages the use of experience, judgment, and analysis of the impact of uncertainty and of possible future decisions. Thus, the decision-making, based upon systems approach, can take place in a logical and orderly manner, which can facilitate rationally sound decisions and ensure the optimal or near optimal use of the limited public funds.

Systems Approach

The system for decision-making can be described as a logical, clearly defined and step-by-step procedure operating to accomplish the decision-making process. A comprehensive formulation of the decision process; characterizing various technical, economic and other aspects; which is needed before a realistic operating system can be developed is described by the following: objectives, data-base, criteria, constraints, and methodology for evaluation.

Objectives

Objectives of the systems approach are to bring out all possible alternatives, evaluate them on the basis of clearly defined criteria and constraints, and arrive at an optimal or near optimal decision. The ultimate aim of systems logic is to discover and take into account those aspects that truly influence the outcome of an optimal or near optimal (i.e., the best and the second best) decision.

Data-base

A user oriented, up to date, complete and orderly structured data-base is presented in Tables 1, 2, and 3. To facilitate its efficient retrieval, use and ease of updating, this data-base has been divided into the following sections:

Structure Inventory and Traffic. Physical characteristics of the existing structure and traffic related information are presented in this section. Estimates for rehabilitation, relative importance of the bridge to traffic and physical requirements of future replacement structure can be determined from this information.

Structure Inspection and Appraisal. Inspection of the existing bridge structure reveals condition of its superstructure (i.e., deck, stringers, etc.) and substructure (i.e., abutments, piers, footings, etc.). It also reveals unsafe conditions, serviceability considerations, estimated remaining life and the extent of repairs needed.

Table 1. Data-base: Part I

STRUCTURE INVENTORY AND TRAFFIC (SECTION A): (Dated . . . . . .; Updated . . . . .)

1. Structure Number . . . . . .; Built in . . . . . .; Remodeled in . . . . .; Owner . . . . . .
2. Inventory Route. . . . . .; Over/Under . . . . . .; Location . . . . . .
3. Alternate Length . . . . . .; Impact on Travel Time. . . . .min.; kmh (mph). . . . . .
4. Lanes/R.R. Tracks (over) . . . . . .; (under) . . . . . .; One/Two Way . . . . . .
5. Av. Daily Traffic (ADT) on Structure . . . . . .; Peak Hour Traffic . . . . . .; Year. . . . . .
6. Projected ADT . . . . . .; For Year . . . . .; Heavy Commercial ADT . . . . . .
7. Design Load . . . . . .; Present Structural Capacity . . . . . .; Posted Load Limit . . . . . .
8. Approach Width: Roadway. . . . . .; With Shoulder . . . . . .
9. Angle Skew . . . . . .; Is Structure Flared?. . . . . .; Width: Max . . . . .; Min. . . . . .
10. Minimum Clearances: Vertical: Over. . . . . .; Under . . . . . .
    Horizontal: Over . . . . . (North/West); . . . . . (South/East) . . . . . .
    Under. . . . . (North/West); . . . . . (South/East) . . . . . .
11. Navigation Control: Yes/No; Vertical . . . . . .; Horizontal . . . . . .
12. Structure Type: Main Span . . . . . .; Approach Spans . . . . . .
13. Number of Spans: Main . . . . . .; Approach . . . . . .
14. Structure Length: Total . . . . . .; Max. Span . . . . . .; Approach Spans. . . . . .
15. Widths: Roadway (curb to curb). . . . . .; Deck (out to out). . . . . .
    Sidewalks: . . . . . (North/West) . . . . . (South/East). . . . . .
16. Wearing Course and Overburden: Type(s). . . . . .; Thickness(es) . . . . . .
17. Guardrail: Type . . . . . Length; Other Railings: Type . . . . . .; Length. . . . . .
18. Utilities Carried, Location. . . . . .
19. Joints on the Bridge: Type . . . . . .; Length. . . . . .
20. Lighting System . . . . . .
21. Painted in . . . . . .; Type of Paint . . . . . .
22. Material Inventory: Roadway . . . . . .; Sidewalk . . . . . .; Superstructure. . . . . .
    Substructure. . . . . .
23. Other Features (such as safety lights):. . . . . .

STRUCTURE INSPECTION AND APPRAISAL (SECTION B): (Dated . . . . . .)

1. Deck: Overall Condition . . . . . .
   Type and Extent of Deterioration. . . . . .
   Repairs Needed and When . . . . . .
2. Superstructure: Overall Condition . . . . . .
   (Other than Deck) Type and Extent of Deterioration. . . . . .
   Repairs Needed and When . . . . . .
3. Substructure: Overall Condition . . . . . .
   Type and Extent of Deterioration. . . . . .
   Repairs Needed and When . . . . . .
4. Safety Considerations: Unsafe or Hazardous Conditions . . . . . .
   (Width, alignment, load-limits, steep grades, railings, clearances, etc.)
5. Serviceability: Drainage. . . . . .
   Rideability (Roughness Coefficient) . . . . . .
   Lighting. . . . . .
6. Condition of Paint . . . . . .
7. Estimate of Remaining Life: Without (with) major repairs. . . . . (. . . .) Years
8. Description and Estimated Cost of Major Repairs Needed and When. . . . . .

STRUCTURAL CAPACITY AND FUNCTIONAL ADEQUACY (SECTION C): (Dated . . . . . .)

1. Load Carrying Capacity . . . . . .
   (Based on: Current Legal Loads. . . . . ., Estimate of Deterioration. . . . .)
2. Minimum Clearances: Vertical. . . . . .; Horizontal . . . . . .
3. Adequacy for Present and Projected Traffic . . . . . .
4. Waterway Adequacy and Protection (e.g., Pier or Scour Protection). . . . . .
5. Limits for Special Permit Loads. . . . . .; Wheel-Load Configuration Used. . . . . .

Structural Capacity and Functional Adequacy. Load carrying capacity of the structure and functional adequacy are indicated in this section. This information is helpful in appraising rehabilitation alternates.

Maintenance History and Projected Future Needs. This section provides information on the major, or recurrent minor, maintenance and repair work done in the past and projected future maintenance. This information is valuable in appraising the rehabilitation alternates.

Environmental and Other Factors. Information on aesthetic considerations, developmental plans and projected needs of the area served, and major items of information for environmental impact statements are provided in this section.

Relevant Details for Rehabilitation and Replacement. Details relevant to all available rehabilitation and replacement alternatives such as cost estimates, are presented in this section.

Table 2. Data-base: Part II

MAINTENANCE HISTORY AND PROJECTED FUTURE NEEDS (SECTION D): (Dated . . . . .)
1. Chronology and a Brief Description of Major Repairs Done: . . . . .
(When, what, at what cost and who made them, improvement in life expectancy). . . . .
. . . . .
2. Brief Description of Minor Repairs in the Past Five Years . . . . .
. . . . .
3. Projected Future Maintenance Needs: (e.g., New Overlay). . . . .
ENVIRONMENTAL AND OTHER FACTORS (SECTION E): (Dated . . . . .)
1. Aesthetical Considerations (e.g., Paint, etc.). . . . .
2. Developmental Plans and Projected Needs of the Area Served. . . . .
. . . . .

Table 3. Relevant Details for Rehabilitation and Replacement.

RELEVANT DETAILS FOR REHABILITATION (SECTION F)
1. Data-base Sections "A" through "D"
2. Alternate Proposals for Rehabilitation: Details, Cost Estimates, and Improvement in Life Expectancy
RELEVANT DETAILS FOR REPLACEMENT (SECTION G)
1. Data-base Sections "A", "C" and "E"
2. Physical Requirements of Proposed Structure:
Roadway width (curb to curb): . . . . . .; Sidewalk widths: . . . . .
Minimum Clearances: Over: Vertical. . . . . .; Horizontal . . . . .
Under: Vertical . . . . . .; Horizontal . . . . .
Traffic Capacity (Peak Hour): . . . . . .; Design Loads . . . . .
Alignment: . . . . . .; Related Structures, needed. . . . .
Approaches:. . . . . .; Utilities, to be carried. . . . .
Other: . . . . .
3. Special Features of the Site (e.g., subsurface data). . . . .
4. When is New Bridge Needed?. . . . .
5. Alternate Replacement Proposals: Details, Life Expectancy and Estimates of Initial, Maintenance and Other Costs. . . . .

The information provided in Tables 1, 2, and 3 has been so structured and organized that it can easily be maintained manually or on computer. Further, the information from this data-base can be utilized to reinforce an agency's decision-making process.

Criteria for Decision-Making

One of the major reasons for difficulties experienced in rehabilitation or replacement decision-making is the lack of appropriate and clearly defined criteria for a comparative appraisal of available alternates. Further, major investment decisions like bridge structure rehabilitation or replacement must be consistent with the agency objectives and policies.

The first important criterion is adequacy, for projected future use, of the rehabilitated or replacement structure. This adequacy must be determined to establish a rehabilitation or replacement proposal as a realistic alternate. Developmental plans and projected future needs of the area served influence the functional adequacy of the rehabilitated bridge. These plans can change traffic patterns, thus influencing the type and frequency of traffic at a bridge-crossing. Inadequacy to sustain the projected traffic may eliminate a simple and economical rehabilitation alternate, thereby requiring selection of an acceptable replacement alternate. In addition to adequacy for present and projected traffic, the rehabilitated or replacement structure shall also need to meet the minimum requirements of horizontal and vertical clearances, roadway width, waterway opening, and safety.

Analysis of highway improvements on the basis of engineering economics, which is the second group of criteria, began over 100 years ago. The illusory nature of initial costs as decision criteria was recognized by Gillespie, in his book on road-making, published in 1853 (2, 9), who recommended use of estimated total costs and benefits in the selection of highway improvements. This principle of estimated total costs as a decision criterion still underlies all rational economic analyses in highway engineering. Three most commonly used criteria for comparing total costs of alternate investment proposals are: present value, annualized costs, and prospective rate of return. In economic evaluations, comparative estimated values of future series of benefits and costs, such as maintenance costs, are arrived at through present value conversion. Where comparisons are for a limited number of years, present value of the cost of the same number of years of service is calculated for each alternative. The second method of economic evalu-

ation is to compare alternates on the basis of equivalent uniform cost using a suitable interest or discount rate. Annualized cost comparisons are convenient to use when many of the estimated costs are essentially the same year after year. The basic data for such comparisons consists of estimated costs associated with the alternatives being compared. Conversions into equivalent annual cost require the use of appropriate factors, obtained from compound interest tables or computed using compound interest formulas. The third criterion, prospective rate of return, provides another way of considering the time value of investments. A comparison between alternatives involving costs and quantified benefits of different amounts at different dates may be expressed by an interest rate that makes the two alternatives equivalent. When one alternative involves a higher present investment and higher future net benefits, possibly as a result of lower future disbursements, the interest rate is called the prospective rate of return on extra investment.

There are many difficulties in applying any of these three criteria to engineering economic analysis of alternate bridge rehabilitation and replacement proposals. Although initial costs can be arrived at with reasonable accuracy, problems emerge while estimating future series of maintenance costs. One way of estimating these costs is by using past experience with similar structures. Such projections tend to be quite subjective and considerable care needs to be exercised in analyzing the past experience. To arrive at a reasonably close estimate, from a range of estimates of future series of maintenance costs, statistical techniques such as expected monetary value (EMV) are utilized. Another difficulty arises in estimating the life of an improvement because in many long-lived projects, such as bridge structures, analyses are made and costs are computed as if the economic life were fifty years. However, life expectancy of a rehabilitated structure is difficult to estimate, although past experience with similar improvements is helpful. Levels of future use and sound engineering judgments based upon performance characteristics of the method and materials used in rehabilitating structure will be valuable. Further, the selection of a suitable interest rate or discount rate to determine time value of money is particularly difficult for the decision-maker. For longer time spans, one could estimate a range of such rates; and with the help of economists, use probabilistic methods to select the most probable interest rate. Quantification of benefits is another difficult proposition. However, it is not likely to be a critical factor in the bridge structure rehabilitation or replacement decision-making.

Constraints of Decision-Making

Lack of a clear perception of all constraints on decision-making has been another major reason for difficulties experienced by a decision-maker. The most important group of constraints are those pertaining to the available and projected flow of funds. No agency ever seems to have enough funds to follow through what it considers to be the most desirable capital improvements. Grants of different kinds, bond and general revenue funds are used to carry out what are considered to be high priority projects. A decision-maker has to take into account not only the availability of funds for initial investment, but also the requirements of future flow of funds that the investment is expected to create. This future investment is particularly difficult for the decision-maker, because of the element of uncertainty associated with it. Statistical techniques, which deal with the element of uncertainty, can provide a clearer perception of this constraint.

Local and legal constraints constitute another group that can substantially influence the decision-making process. In recent years, local groups have increasingly managed to change what a decision-maker had determined to be the best decision. The decisions to rehabilitate or replace bridge structures are no exception to this process. Involvement of local groups and consideration of their concerns, during the decision-making, has become necessary. Where major rehabilitation is intended, some state laws require compliance with minimum clearances, and these legal constraints may render a major rehabilitation proposal totally uneconomical. Recent Uniform Relocation Act requires extensive environmental reviews and complex acquisition procedures even on small bridge rehabilitation projects. Peculiar site conditions, historical value of a bridge, technological limitations, local availability of specialized labor, materials or equipment, etc., also influence a rehabilitation or replacement decision.

Methodology for Decision-Making

Decisions to rehabilitate or replace a structurally deficient or functionally inadequate bridge generally involve outlay of large amounts of money, have long-lasting effects and often require judgmental estimates about future events. In this respect, they are important and generally difficult investment decisions. If the evaluation of such an investment decision is based only on a single estimate--the "best guess"--of the cost of each factor affecting the outcome, the resulting evaluation will be incomplete and possibly wrong. In recent years, increasingly sophisticated methods have become available for analyzing investment decisions. The most widely known of these new developments are the analytical methods that take into account time value of money. However, there have been two troublesome aspects of investment decision-making that need adequate treatment. One problem is handling the uncertainty that exists in virtually all investment decisions. Another problem is analyzing separate but related investment decisions, such as stage construction, that must be made at different points in time. The decision theory approach indicated in the payoff matrix and opportunity loss tables (Tables 4 and 5) provides a basis for reaching objective decisions under uncertainty. Another method, called "decision tree" method (5,6,7,8), is particularly applicable to investments under uncertainty and require a sequence of related decisions to be made over a period of time.

Payoff and Opportunity Loss Tables. These tables illustrate the various dimensions involved in any decision problem. A payoff table indicates all alternatives available to the decision-maker, events that can happen, probability distribution of these events, and monetary payoff (+ sign: benefits, - sign: costs) that result from each alternate/event combination. The formulation of a payoff table is probably the most difficult step in analysis of decision problems under uncertainty. It can also be the most beneficial, because in some decision problems the creation of new alternatives can have a great benefit. Some of the consequences that result from the specified alternate/event

combination are not initially in monetary terms, and this causes difficulties in the construction of a payoff table. Although it is not easy, it is necessary to convert non-economic consequences into their monetary equivalent before the decision analysis process can continue. A very useful decision criterion for many decision problems under uncertainty is expected monetary value (EMV). In order to compute the EMV for a given alternate, the payoff is simply multiplied by the probability of that event's occurring, and products for each event are added (see step 1, Table 4). The expected value of a chance event or random variable X, which can take on any one of n values, is defined to be:

$$\text{Expected Value of } X = E(X) = \sum_{i=1}^{n} X_i P(X_i)$$

Where X is the monetary outcome of a decision problem under uncertainty, the expected value of X is usually called Expected Monetary Value, or EMV. The optimal alternative in the payoff table is indicated by the highest EMV.

Another way of analyzing decision problems under uncertainty is to construct an opportunity loss table (see Table 5). The opportunity loss for an alternate/event combination is the difference between payoff for that combination and the best payoff for that event. To construct an opportunity loss table, each event is considered one at a time. All rows of the opportunity loss table are thus completed (see step 1, Table 5). The bottom row shows the Expected Opportunity Loss, EOL, for each of the alternates. The EOL is calculated from the opportunity loss table (see step 2, Table 5), in the same way as EMV is calculated from the payoff table. An alternative which has the lowest expected opportunity loss is the optimal alternative. This optimal alternative will also have the best expected monetary value. In many decision problems, it is quite easy to construct the opportunity loss table directly without going through the payoff table. One principal reason for considering opportunity losses is that it helps a decision-maker understand the cost-structure of difficult investment problems.

Decision Trees. The decision tree approach, a technique very similar to dynamic programming, is a convenient method for representing and analyzing a sequence of related decisions to be made over a period of time (5, 6, 7, 8). Each decision point is represented by a numbered square at a fork or node in the decision tree (Figure 1). Each branch extending from a fork represents one of the alternatives that can be chosen at this decision point. In addition to representing decision points, decision trees represent chance events. The forks in the tree where chance events influence the outcome are indicated by circles. A node representing a chance event generally has a probability associated with each of the branches emanating from that node. This probability is the likelihood that the chance event will assume the value assigned to the particular branch. The total of such probabilities leading from a node must equal one. Each combination of decisions and chance events has some outcome, in terms of Net Present Value (see NPV calculation in Figure 1), associated with it. The key steps in building and using a decision tree for investment project analysis are:

Identification of the problem and alternatives. It is important to identify all alternatives, freedom of action, and present and future uncertainties; and also to estimate costs and probabilities of uncertain events. All future possibilities cannot be identified, but a reasonable job can be done. Those engaged in this analysis should be encouraged to express doubts and uncertainties and to bring out facts about cost estimates, engineering feasibility and forecasts of future conditions in terms of ranges or probabilities.

Layout of the Decision Tree. This formulates the structure of alternatives underlying the decision. The time span over which the analysis must extend will vary for particular decisions. Roughly, the practical time span to consider should extend at least to the point where the distinguishing effect of the initial alternative with the longest life is liquidated, or where, as a practical matter, the differences between the initial alternates can be assumed to remain fixed (see Illustrative Example). Outlining major choices, breaking the problem into two to four decision stages, and thinking out the decision at least through a second decision stage enriches the analysis considerably over a conventional single-stage consideration (see "Discussion of Illustrative Example).

Obtaining the Data Needed. The data needed are: a. probabilities of each uncertain outcome, b. cost estimates associated with each combination of decision alternative and chance outcome, and c. an estimate of discount rate to be applied to future costs and benefits. The estimation of elemental probabilities permits review of the basis for conclusions. It also permits the decision-maker to make use of the intuitions and skills of his staff without abdicating his position as the decision-maker. Further, it permits analysis of the impact of variations in the estimate--that is called sensitivity analysis (see Discussion of Illustrative Example).

Evaluation of Alternatives. A good evaluation test which alternatives appear desirable in light of standards used. It shows whether apparent conclusions are sensitive to changes in doubtful or controversial estimates. It examines the effect of choosing alternate standards, which in turn may lead to revision of standards, further analysis, or reformulation. The optimal sequence of decisions in a decision tree is found by starting at the right-hand side and "rolling backward". At each node, an expected Net Present Value, NPV, is calculated. If the node is a chance event node, the expected NPV is calculated for all of the branches emanating from that node. If the node is a decision point, the expected NPV is calculated for each branch emanating from that node, and the highest is selected. In either case, the expected NPV is carried back to the next chance event or decision point by multiplying it by the probabilities associated with branches that it travels over. The preferred alternative shall be one with greatest net present value (see Typical Calculation, Figure 1).

One modification of a decision tree is stochastic decision tree which is similar to the conventional decision tree approach, except that it uses continuous, instead of discrete, empirical probabilities, and provides results in a probabilistic form.

Use of the decision tree concept, as a basis for capital improvement analysis, evaluation and decision, is a means for making explicit the process which must be at least intuitively present in good

decision-making. It brings out the impact of both uncertainty and of possible future decisions, conditioned on future developments. It allows for and encourages use of analysis, experience and judgment. It helps force out into the open those differences in assumptions or standards of value that underlie differences in judgment or choice. A decision tree need be only as complex as the decision itself. If the decision is a simple choice among alternatives, then the decision tree reduces to a single stage analysis, i.e., the use of present value technique applied to alternative benefits and costs. Where the situation is more complicated, more stages and alternatives are necessary. Explicit use of the decision tree concept helps force a consideration of all alternatives, definition of problems for investigation, and clarification for the decision-maker of the nature of the uncertainties present and the estimates that must be made. Thus, the decision tree concept contributes to the quality of the decision a decision-maker must make.

Operational System for Decision-Making

An operational system for bridge structure rehabilitation or replacement decision-making is indicated by the flow chart, in Figure 2. The development of this working system can be described by the following: System Inputs, Constraints and Alternatives, Decision Criteria, Evaluation of Alternatives, and System Output.

System Inputs

System inputs are dictated by various generated alternatives and by methods of evaluation used by the system. These system inputs can be described in the following general groups:

Information from the Data Base. Information from Tables 1, 2 and 3 is used to generate possible alternatives and to provide the basis for evaluation of options or alternatives available to the decision maker.

Probability Estimates. A certain amount of uncertainty underlies all estimates, whether they are estimates of initial and subsequent costs or estimates of life expectancies. The cost of some types of work, such as replacing stringers, are easier to estimate with a reasonable amount of accuracy than others like gunite repair of deteriorated concrete arches. Further, it is possible for any experienced decision-maker to reasonably estimate a probability for each probable state. These probabilities may be objective or subjective. Objective probabilities are derived from actual data. Subjective probabilities are derived by judgment, and reflect the engineer's estimation of the relative likelihood that a particular state would occur. For a decision-maker, expressing professional judgments over a range of values as probabilities is more accurate than simply using a single best estimate value.

Cost Inputs. The criterion of total overall cost in terms of present value is used in this working system to indicate the preference for one option over others. The total overall cost is the sum of the present values of design, construction, future expected maintenance and indirect costs. A number of cost inputs are, therefore, used by the working system for evaluation of different available alternatives. In some cases, these inputs may include quantified estimates of economic, social or environmental losses that may result. For a rational economic analysis, a discount rate or interest rate needs to be used to properly evaluate future benefits and costs. If necessary, statistical techniques can be used to arrive at a reasonable rate.

Constraints and Alternatives

The overall number of feasible alternatives is controlled or limited by a set of specified constraints. These constraints can be located at various stages in the working system. All possible alternatives are analyzed and checked against these constraints. Alternatives are either accepted or rejected at these checks. In general, system constraints and options are part of the decision-maker's decisions to generate a reasonable type and number of alternate solutions. But at certain times, these constraints can be actual physical limitations advocated by conditions of site, design, and construction.

Decision Criteria

The total overall cost, in terms of expected monetary value, expected opportunity loss or net present value, is chosen as the prime decision criterion for the selection of the optimal or near optimal decision strategies. Provisions for additional future structural capacity and functional adequacy, safety and serviceability, and maintenance economics are some of the other criteria which may be relevant in some cases.

Evaluation of Alternatives

Any one of the methods, namely payoff matrix, opportunity loss table or decision tree, may be used by the decision-maker in the evaluation of alternatives. In some simple choice situations, the mental exercise in assessing each of the dimensions is sufficient to give the decision-maker insight into the problem so that the desired course of action will become obvious without further analysis. In general, the payoff matrix or opportunity loss table methods can be used in nearly all situations. Where sequential decisions are to be considered, the decision tree method should be used.

Output

The decision criteria included in the present operating system are not comprehensive enough to make final judgments. It is difficult to quantify the relative importance a decision-maker will ascribe to various economic, social, environmental and experience values. Universally acceptable methods for quantifying such values are not available at the present time. The output for decision, therefore, is arranged in a way that would assist the judgment of the decision-maker. An orderly structured set of alternatives and conclusions of the evaluation process for each of the alternatives are produced in the form of a summary table. This is based on increasing order of the expected present value of total costs (see "Discussion of Illustrative Example).

Illustrative Example

A 4-lane, 456 m. (1500 feet) long, steel girder type river bridge is structurally deficient and in need of rehabilitation or replacement. Future projections indicate the need of 2 additional lanes for mass transit, 25 years later.

Available Alternatives: (all costs are in terms of present values)

Alternative I. Immediate Limited Rehabilitation (Restrict Traffic) . . . . . $ 250,000
(Deck repair; replace railings, few stringers, etc.)

Major Rehabilitation, 5 years later. . . 3,500,000
(New deck; replace other stringers, floor beams, joints; sidewalks; repair pier caps, beam seats, etc.)

Widen the Bridge, 25 years later 2,500,000
(Add 2 more lanes, reconstruct portions of piers and abutments, etc.)

Maintenance and Other Costs: 0-5 years @ $30,000/year 150,000
6-25 years 150,000
26-50 years 450,000
Present Value of Total Costs for Alternative I $7,000,000

Alternative II. Immediate Major Repair. $3,750,000
(New deck, sidewalks, railings, stringers, floor beams, joints, repair pier caps, beam seats, etc.)

Widen the Bridge, 25 years later. . . . 2,500,000
(Add 2 more lanes, reconstruct portions of piers and abutments, etc.)

Maintenance and Other Costs: 0-25 years 225,000
26-50 years 450,000
Present Value of Total Costs for Alternative II $6,925,000

Alternative III. Immediate Removal of Existing Bridge and Replacement with Steel Plate Girder (CORTEN-Weathering Steel) Type Bridge and Substructure Provision for Future Widening. 5,750,000

Widen the Bridge for 2 additional Lanes at the end of 25 years 1,100,000

Maintenance and Other Costs: 0-25 years 150,000
26-50 years 250,000
Present Value of Total Costs of Alternative III $7,250,000

Alternative IV. Immediate Removal of Existing Bridge and Replacement with Segmental Post-tensioned Box Girder and Substructure Provision for Future Widening 5,500,000

Widen the Bridge for 2 additional Lanes at the end of 25 years 1,100,000

Maintenance and Other Costs: 0-25 years 100,000
26-50 years 200,000
Present Value of Total Costs of Alternative IV $6,900,000

Additional Information

Beyond 50 years, costs for all alternatives are approximately equal.

Cost overruns in rehabilitation projects are very common.

Estimates for replacement projects could be prepared with a high degree of accuracy.

The two additional lanes of mass transit are not to be constructed at the present time.

All cost estimates are in terms of present values, which have been arrived at by multiplying future costs with discount factors, for inflation and interest rates.

Table 4. Pay-off Table (Time Span = 50 Years)

Events	Rehab. Alternatives (in Dollars)			Replace. Alternatives (in Dollars)		
	Alt. I	Alt. II	Probability of Occurrence	Alt. III	Alt. IV	Probability of Occurrence
Actual Costs 10% Below Estimated	-$6,300,000	-$6,232,500	0.05	-$6,525,000	-$6,210,000	0.05
Actual Costs = Estimated	- 7,000,000	- 6,925,000	0.50	- 7,250,000	- 6,900,000	0.80
Actual Costs 10% Above Estimated	- 7,700,000	- 7,617,500	0.23	- 7,975,000	- 7,590,000	0.10
Actual Costs 20% Above Estimated	- 8,400,000	- 8,310,000	0.22	- 8,700,000	- 8,280,000	0.05
Expected Monetary Value (EMV)	- 7,434,000	- 7,354,350		- 7,358,750	- 7,003,500	

Step 1: Alt. I: (-$6,300,000 x 0.05) + (-$7,000,000 x 0.50) + (-$7,700,000 x 0.23) + (-$8,400,000 x 0.22) = $7,434,000

Step 2: Best expected monetary value (EMV) = lowest expected total cost, i.e., $7,003,500 or Alternative IV.

Table 5. Opportunity Loss Table (Time Span = 50 Years)

Events	Rehab. Alternatives (in Dollars)			Replace. Alternatives (in Dollars)		
	Alt. I	Alt. II	Probability of Occurrence	Alt. III	Alt. IV	Probability of Occurrence
Actual Costs 10% Below Estimated	$ 90,000	$ 22,500	0.05	$315,000	-0-	0.05
Actual Costs = Estimated	100,000	25,000	0.50	350,000	-0-	0.80
Actual Costs 10% Above Estimated	110,000	27,000	0.23	385,000	-0-	0.10
Actual Costs 20% Above Estimated	120,000	30,000	0.22	420,000	-0-	0.05
Expected Opportunity Loss (EOL)	$106,000	$ 26,435		$355,250	-0-	

Step 1: Consider in the event that actual costs are 10% below estimate: The best alternative is Alt. IV.

Opportunity loss in selecting:
Alt. I = (-$6,210,000) - (-$6,300,000) = $ 90,000.
Alt. II = (-$6,210,000) - (-$6,232,500) = $ 22,500.
Alt. III = (-$6,210,000) - (-$6,525,000) = $315,000.
Alt. IV = (-$6,210,000) - (-$6,210,000) = 0.

Step 2: Alt. I - EOL = ($90,000) (0.05) + ($100,000) (0.5) + ($110,000) (0.23) + ($120,000) (0.22) = $106,200.

Step 3: Best Expected Opportunity Loss (EOL) = lowest expected opportunity loss, i.e., $0 or Alt. IV.

Negative signs indicate costs.

Figure 1. Decision Tree

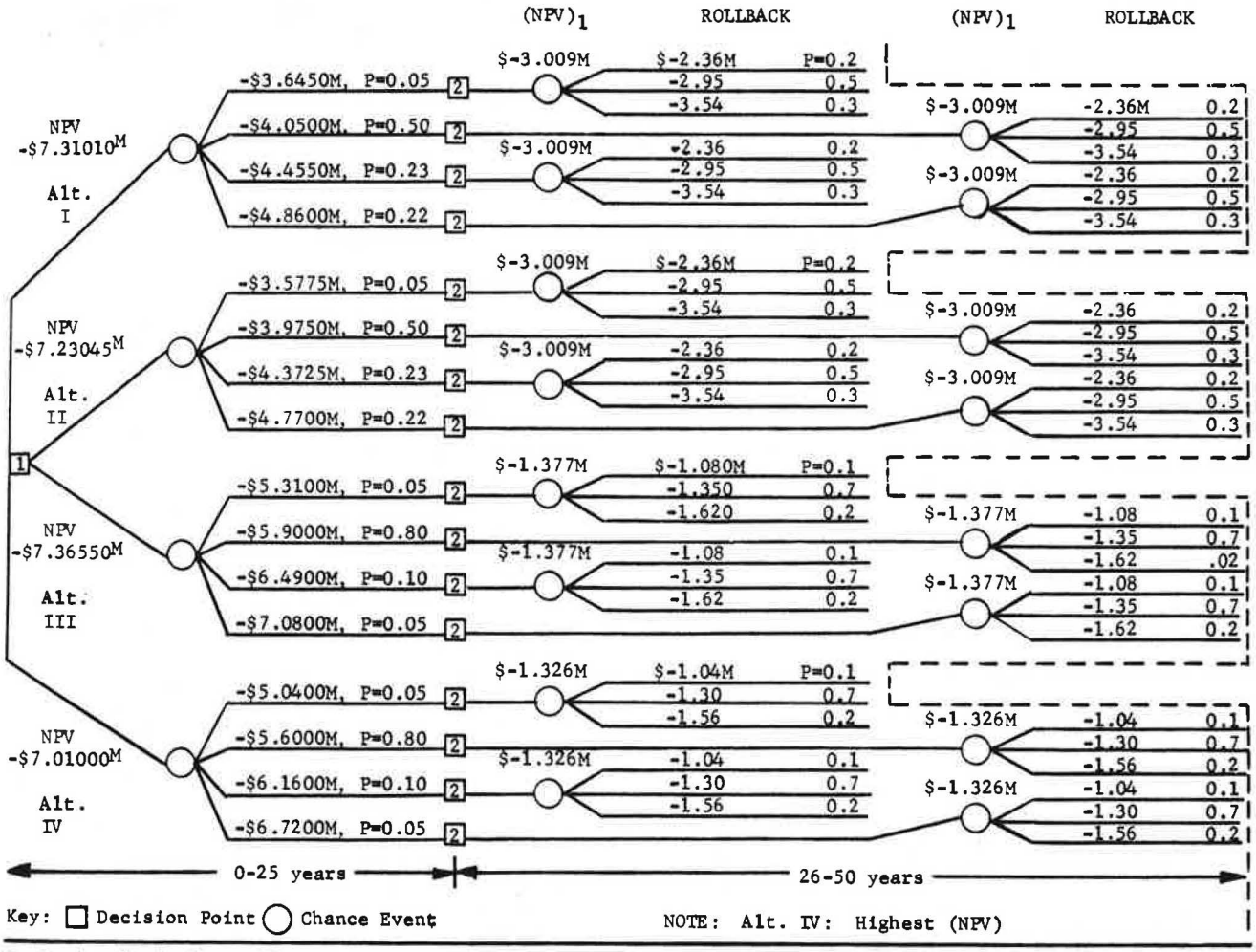

Typical calculation: Alt. II: $(NPV)_1 = -[(2.36 \times 0.2) + (2.95 \times 0.5) + (3.54 \times 0.3)]\,M = \$3.009M$

$(NPV) = -[(3.5775 + 3.009)(0.05) + (3.975 + 3.009)(0.50) + (4.3725 + 3.009)(0.23) + (4.77 + 3.009)(0.22)]\,M$ = $7.23045 million.

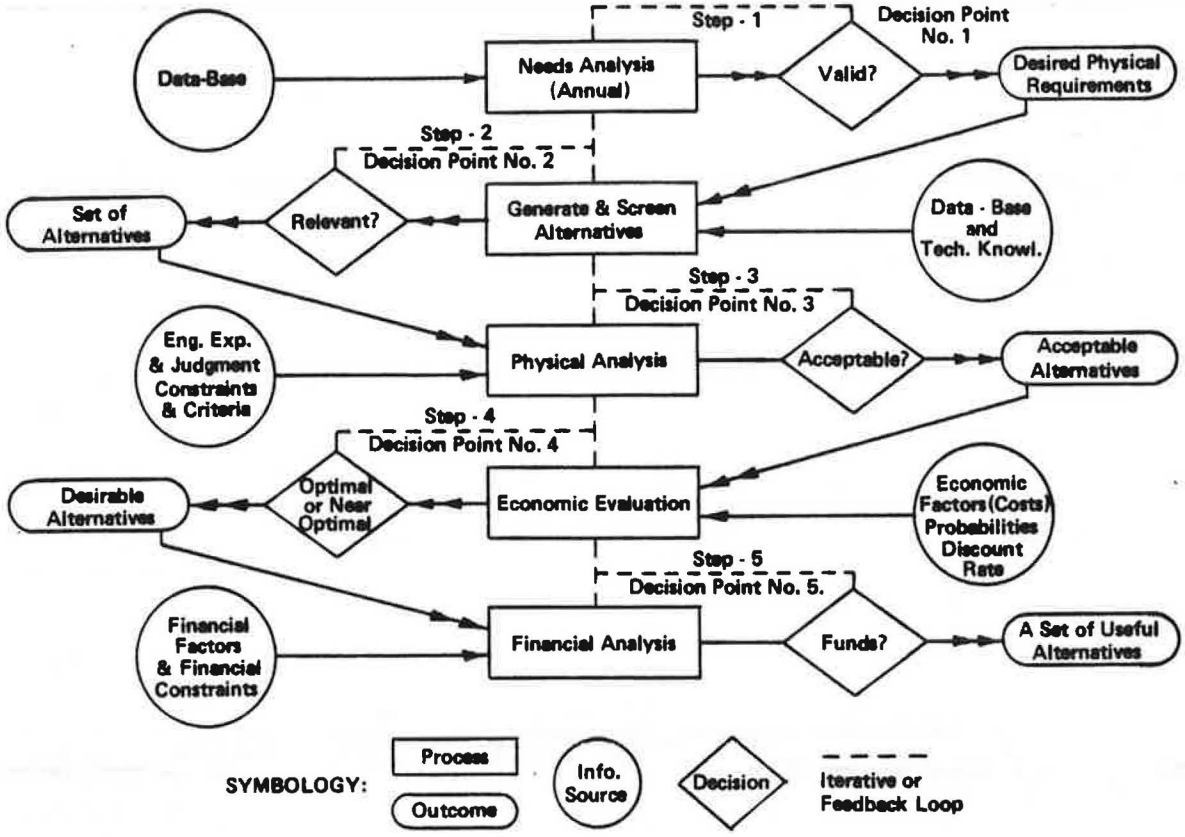

Figure 2: FLOW CHART OF DECISION-MAKING SYSTEM

Discussion of Illustrative Example

Tables 4 and 5, as well as Figure 2, indicate Alt. IV as the optimal or best alternative. Further, all alternatives can be tabulated in increasing order of present value of the total costs. The decision tree brings out two-stage nature of the decision. It uses two separate sets of probability values to reflect increased uncertainty of future costs. Further, it helps a decision-maker match available alternatives with present and future sources of funds. For example, an agency with extremely limited present funds may wish to select Alternative I and defer major capital outlay to a future date. When financing costs are expected to remain high for more than five years, an agency may wish to select Alternative II. When funds are available and present financing costs are reasonable but expected to rise sharply, an agency may wish to select Alternative IV.

Events: Experience indicates the general range of actual costs of bridge projects to be 10% below to 20% above the estimated costs. For simplicity of illustration, indicated events were selected.

Probabilities: 10% or 20% cost-overruns for rehabilitation projects are considered equally likely, but about half as likely as event of no overruns. Accuracy of replacement estimates is considered high. Probabilities of occurrence have been set accordingly. For decision-tree, probabilities of events associated with the second decision are adjusted for increased uncertainties of the future. In case of genuine differences of opinion about selected probabilities, sensitivity analysis with different sets of probabilities can be used to examine the optimality of the decision.

Expected Opportunity Losses are also costs one could incur to obtain perfect information. It indicates the maximum amount of money that could be spent to predict an outcome with absolute certainty (8). For example, a decision-maker could determine the amount he could spend in ultrasonic or other testing to make estimates of rehabilitation with certainty.

Conclusion

This paper has presented a systems approach to the difficult bridge structure rehabilitation or replacement decision-making. The decision-maker can select a suitable method for evaluation of different alternates based upon special requirements of individual situations and future implications of decisions. This system is simple, adaptive, and the decision process is easy to control. The decision-making process based on systems approach can be utilized manually for smaller and simpler investment decisions or can be computer based for large and complex investment decisions. It can be easily adapted to the needs and desires of the decision-maker, and can be no more difficult or involved than the decision itself.

References

1. Churchman, C. West. The Systems Approach. Delacarte Press, New York, N.Y., 1968.
2. Gillespie, W. M.. Road Making. 6th Edition, A. S. Barnes and Co., 1853.
3. Grant, Eugene L. and W. Grant Ireson. Principles of Engineering Economy. The Ronald Press Company, New York, 1964.
4. Hespos, R. and P. A. Strassmon. Stochastic Decision Trees for Analysis of Investment Decisions. Management Science, Volume 11 #10, August, 1965, pp. B-244 - B-259.
5. Magee, John F.. Decision Trees for Decision Making. Harvard Business Review, July-August, 1964.
6. Magee, John F.. How to Use Decision Trees in Capital Investment. Harvard Business Review, September-October, 1964.
7. Manheim, Marvin L.. Decision Theories in Transportation Planning. Special Report 108, Highway Research Board, 1970, pp. 17-25.
8. Plane, Donald R., and Gary A. Kochenberger. Operations Research for Mangerial Decisions. Richard D. Irwin, Inc., Homewood, Illinois, 60403, 1972.
9. Winfrey, Robley. Highway Engineering Economy Analysis. Special Report 108, Highway Research Board, 1970.

SYSTEMS APPROACH TO BRIDGE STRUCTURE REPLACEMENT-PRIORITY PLANNING

Arunprakash M. Shirole', P.E., City of Minneapolis
James J. Hill, P.E., Minnesota Department of Transportation

This paper presents a systems approach to the bridge structure replacement-priority planning. Structural condition and functional adequacy; safety; essentiality to traffic and other criteria for setting replacement priority are developed and evaluated. Budgetary, environmental, developmental, policy and other constraints on the replacement priority are identified and analyzed for their possible impact. A quantitative methodology is developed, based upon assignment of weights to the rated criteria and is illustrated step by step through a flow chart. Guidelines are provided to easily adapt use of this methodology to meet the needs of an individual area or policy, for a rational determination of long-range programming.

In recent years, the number of structurally deficient and functionally inadequate bridges has increased at an alarming rate. This increased number has made it imperative for agencies responsible for bridges to include bridge-replacement, in a major way, in their planning and programming process. A logical, consistent and comprehensive evaluation of an agency's bridge-replacement needs thus becomes necessary, not only to accomplish a rational and equitable distribution of limited public funds but also to ensure public safety. The systems approach, based upon use of factual data, can facilitate such a logical, consistent and comprehensive evaluation.

Systems Approach

The system for replacement-priority planning can be described as a step-by-step procedure following clearly defined guidelines to accomplish the priority planning process (see Fig. 1: Flow-chart). A comprehensive formulation of the priority planning process; characterizing various structural, functional, safety, traffic-related, economic and other aspects; is described by the following: Objectives, system inputs, criteria, constraints, evaluation and system output.

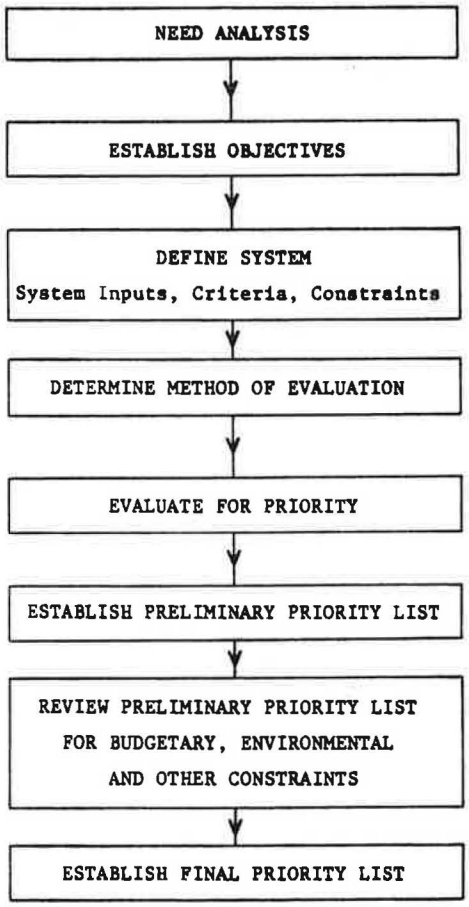

Figure 1. System flow chart for bridge replacement priority planning.

Table 1. Bridge replacement-priority rating.

Item	Number of Points: Individual Sub-category	Number of Points: Range for Category
I. Structural Condition and Functional Adequacy: (from Table 2):		0-40
a. Estimated Remaining Life	0-5	
b. Structural Condition Appraisal	0-15	
c. Deck Width	0-5	
d. Approaches and Alignment	0-5	
e. Overclearances	0-5	
f. Underclearances or Waterway Adequacy	0-5	
II. Safety: (from Table 3):		0-25
a. Safe Load Capacity	0-16	
b. Safety Appraisal (Frequency and Type of Accidents, % Correctible, User Complaints, Potential Hazards)	0-9	
III. Essentiality to Traffic: (from Table 4)		0-35
a. Traffic Demand (Present & Projected A.D.T., Peak Hour Traffic, Volume/Capacity ratio)	0-16	
b. Area Served (Planned or Projected Development)	0-8	
c. Alternate Route (Length @ Average speed...., Access to Metro-scale or similar facility, Link in Commercial and Industrial network of Out-state Significance)	0-8	
d. Road System	0-3	
RATING		0-100

Objectives

Objectives of this systems approach are to evaluate and rate the relative importance of all bridge structure replacement needs on the basis of clearly defined criteria and constraints, and arrive at a bridge-replacement priority list. The ultimate aim of this systems logic is to take into account all those aspects that truly influence the optimal or near optimal use of public funds.

System-inputs

An up to date and complete data-base (Tables 1, 2, 3 and 4) shall provide inputs for a rational replacement-priority planning. These system inputs, which utilize basic inventory and inspection data, are divided into the following sections:

Structural Condition and Functional Adequacy. Annual physical inspection reports by qualified staff provide information about estimated remaining life of the existing structure, condition of its superstructure (i.e., deck, stringers, etc.) and substructure (i.e., abutments, piers, and footings). Further, these reports indicate the type, extent, estimated costs of needed improvements, and replacement cost; as well as data for appraisal of deck-width, approaches, alignment, clearances and waterway adequacy.

Safety. The safe load carrying capacity (@ 0.75 of yield stress) and safety appraisal of the existing structure is given in this section. It provides information about frequency and type of accidents related to the structure, potential hazards, percentage of hazards and causes of accidents that are correctible, as well as user complaints.

Essentiality to Traffic. This section provides information about the present and projected Average Daily Traffic, Peak-hour traffic, and volume/capacity ratios. Further, it provides information about area served by the existing bridge, which is determined by using origin-destination studies (i.e., planned or projected development of the area and effect on its tax-base); alternate route (i.e., its length and impact on travel time or energy use); and the road-system (i.e., relative importance in overall transportation network).

Criteria

Criteria for developing a bridge replacement-priority list are factors or types of considerations that go into comparison of existing bridge structures. The first group of criteria relate to structural condition and functional adequacy of bridges. Estimated remaining life sets the time limit within which the bridge replacement is desired. Structural condition is compared on the basis of the ability of a structure to perform according to present acceptable standards. Comparison of deck-widths is based on the latest AASHTO (or equivalent) recommendations (1,2,3,5,6). Criteria for acceptable approaches and alignment relate to their effect on traffic flow and may influence early structure replacement. Overclearances, underclearances and waterway adequacy are judged against the current minimum AASHTO (or equivalent) recommendations (1,2,3,6). The second group of criteria relates to safety aspect of bridge structures. Criteria for safe load capacity are based upon legal vehicle loads. Safety of a structure is appraised on the basis of frequency and type of accidents as well as hazardous conditions and

their extent of correctibility. The third group of criteria pertains to essentiality to traffic. Structures are compared on the basis of their ability to meet traffic demand in terms of present and projected average daily (as well as peak-hour) traffic and traffic volume/capacity ratios. Planned or projected development of the area served by the bridge in terms of projected increase in its tax-base is used as a criteria for comparison. Alternate routes are compared on the basis of their lengths. Finally, the road systems are evaluated on the basis of their importance in the overall transportation network.

Table 2. Structural condition and functional adequacy.

	Rating
a. Estimated Remaining Life ("L" in years):	0-5 points
L > 20 years :	0 point
16 years ≤ L ≤ 20 years :	1 point
11 years ≤ L ≤ 15 years :	2 points
6 years ≤ L ≤ 10 years :	4 points
L ≤ 5 years :	5 points
b. Structural Condition Appraisal:	0-15 points
Good: Meets present requirements :	0 point
Fair: Needs minor improvements (@ costs 5% of replacement cost) to meet present requirements :	5 points
Fair to Poor: Does not meet present requirements, needs major improvements (@ costs 5% but 25% of replacement cost) to maintain in full service :	10 points
Poor: Does not meet present requirements, needs major improvements (@ costs 25% of replacement cost) to maintain in limited service :	15 points
c. Deck-width:	0-5 points
- Meets present desirable (i.e., better than AASHTO recommended or equivalent) requirements :	0 point
- Meets minimum (AASHTO recommended or equivalent) requirements :	1 point
- Does not meet minimum (AASHTO recommended or equivalent) requirements, but can be brought up to meet these requirements :	3 points
- Does not meet and cannot be rehabilitated to meet the minimum (AASHTO recommended or equivalent) requirements :	5 points
Note: Stable traffic flow with operating design speeds >65 kmh (40 mph): Desirable: 3.66 m.(12')/lane + 1.83 m. (6') distance from outside traffic lane edge to obstruction. Minimum: 3.66 m.(12')/lane + 0.61 m. (2') distance from outside traffic lane edge to obstruction. (not less than 9.75 m. (32 ft.) for 2 lane undivided roadway) Unstable traffic flow with operating speeds <65 kmh (40 mph): Desirable: 3.66 m.(12')/lane + 0.61 m. (2') distance from outside traffic lane edge. Minimum: 3.35 m.(11')/lane + 0.61 m. (2') distance from outside traffic lane edge to obstruction.	
Note: Sidewalk Widths: Desirable - 1.83 m.(6 ft.), Minimum - 1.22 m.(4 ft.)	
d. Approaches and Alignment:	0-5 points
- Do not adversely affect traffic flow :	0 point
- Slow down peak-hour traffic :	1 point
- Slow down traffic flow and affect Average Daily Traffic (ADT) :	3 points
- Slow down traffic flow, affect ADT and create traffic hazards which lead to accidents :	5 points
e. Overclearances (vertical and horizontal):	0-5 points
- Meet desirable (i.e., better than AASHTO minimum, or equivalent) requirements :	0 point
- Meet minimum (AASHTO or equivalent) requirements :	1 point
- Does not meet, but can be brought up to, minimum (AASHTO or equivalent) requirements :	3 points
- Do not and cannot be brought up to meet minimum (AASHTO or equivalent) requirements :	5 points
f. Underclearances (vertical and horizontal) or Waterway Adequacy:	0-5 points
- Meet desirable (i.e., better than AASHTO minimum underclearances or 100-year flood capacity plus 0.30 m.(1 ft.) freeboard) requirements :	0 point
- Meet minimum (AASHTO underclearances or 50-year flood capacity with 0.30 m.(1 ft.) freeboard) requirements :	1 point
- Do not meet, but can be brought up to above minimum requirements :	3 points
- Do not and cannot be brought up to meet above minimum requirements :	5 points

Table 3. Safety.

				Rating
a.	Safe Load Capacity (in W_L, gross weight):			0-16 points
	Closed to Traffic:		:	16 points
	Two Axle Vehicles	Three Axle Vehicles	Four or More Axle Vehicles	
	3 tons $\leq W_L <$ 8 tons	$W_L <$ 12 tons	$W_L <$ 12 tons	: 12 to 14 points
	8 tons $\leq W_L <$ 15 tons	12 tons $\leq W_L <$ 18 tons	12 tons $\leq W_L <$ 27 tons	: 8 to 11 points
	15 tons $\leq W_L <$ Legal	18 tons $\leq W_L <$ Legal	27 tons $\leq W_L <$ Legal	: 4 to 7 points
	Legal $\leq W_L$	Legal $\leq W_L$	Legal $\leq W_L$	: 0 to 3 points
b.	Safety Appraisal:			0-9 points
	- No recorded accidents/no obvious hazards noticed or reported			: 0 point
	- Accidents with minor vehicle damage reported/some hazards noticed and reported; hazards and causes completely correctible			: 2 points
	- Accidents with vehicle and structure damage, and bodily injury reported/ some hazards noticed and reported; hazards and causes completely correctible			: 4 points
	- Accidents with vehicle and structure damage, and bodily injury reported/ some hazards noticed and reported; hazards and causes partially (i.e., 50% or less) correctible			: 6 points
	- Accidents with vehicle and structure damage, and bodily injury reported/ some hazards noticed and reported; correction of hazards and causes economically not feasible, warrants replacement			: 9 points

1. AASHTO H-15 and H-20 Trucks[4].
2. AASHTO HS-15 and HS-20 Trucks[4].
3. AASHTO 3S2 and 3-3[4].
4. Use equivalent legal vehicle weights, if different.

Constraints

Various types of constraints or limitations generally control the bridge replacement priority planning process. The first group of constraints is of economic or financial type. Present and projected future available funds for a certain category of bridges can influence an early replacement of a lower rather than a higher priority bridge. A second group of constraints is environmental and local political factors, which have become prominent in recent years. Legitimate concerns of neighborhood groups can effectively prevent a bridge-replacement. The third group of constraints pertains to the consistency of the replacement priorities with local plans, civil defense needs and policies of the agency responsible for bridge replacement. Requirements of unusual length of construction periods that would unfavorably affect the economy of the area can influence priority. Finally, emergency situations, like accidents and failures as they develop can influence and change the replacement priorities. Experience has indicated that any of these constraints can move a bridge up or down on the replacement-priority list.

Evaluation

The method of evaluation devised for arriving at priorities for bridge replacement are based upon a form of numerical evaluation of factors that influence bridge-replacement. Such rating procedures have been proved to be the most satisfactory, realistic and factual means of evaluating highway needs and programming improvements (7). The factors pertinent to bridge replacement are grouped into Structural Condition and Functional Adequacy, Safety and Essentiality to Traffic. Points are assigned to these groups in the order of their importance. Table-1 indicates assignment of these points.

In assigning points to factors in the first group, structural condition and estimated remaining life are given fifty percent of weight of the group. The structural condition appraisal is based upon maintenance-economics. Deck-width, approaches and alignment, overclearances, underclearances and waterway adequacy are weighed equally. Table-2 indicates assignment of these points. In the second group, Safety, about two-thirds of the weight in assigning points was given to the safe load carrying capacity, since it is the single most important factor in bridge replacement. Table-3 indicates assignment of points for this group. The traffic demand is considered the most important factor in the Essentiality to Traffic group and is assigned about fifty percent of the weight. Minor weight was given to the Road System while area served and alternate route were weighed equally. Table-4 indicates assignment of points for this group.

A preliminary list according replacement priority is the outcome of this stage of evaluation process. The preliminary list is then reviewed for budgetary, environmental and other constraints, discussed earlier. This review process will result in the final list of bridge replacement priority. The weights assigned in Table-1 can be changed to adapt to an individual agency's policies, such as policies to upgrade all bridge crossings to meet minimum legal requirements. Further, this system can be adapted to prepare separate replacement-priority lists for bridges on certain classified routes in order to utilize specific sources of funds.

Table 4. Essentiality to traffic.

	Rating
a. Traffic Demand:	0-16 points
Present Bridge:	
- Will satisfy projected (10-year) Average Daily Traffic (ADT) and peak-hour traffic, with no adverse effect on traffic flow	0 point
- Will satisfy projected (10-year) ADT and present peak-hour traffic, with no adverse effect on traffic flow	3 points
- Satisfies present peak-hour traffic and ADT, (Present peak-hour traffic volume/capacity = 1 or less)	7 points
- Satisfies present ADT, (Present ADT volume/capacity = 1 or less)	12 points
- Does not satisfy present ADT of the route and has adverse effect on traffic flow, (Route ADT volume/capacity>1)	16 points
b. Area Served:	0-8 points
- No appreciable area tax-base increase (< 10% of present tax base, in real values) projected in 10 years	0 point
- Moderate area tax-base increase (10% - 50% of present tax-base, in real values) projected in 10 years	4 points
- Considerable area tax-base increase (> 50% of present tax-base, in real values) projected in 10 years	8 points
c. Available Alternate Route:	0-8 points
- Alternate newer or better direct access to metro-scale or similar facility is available, and/or better alternate link(s) to commercial and industrial network of out-state significance is available. (Alternate route length < 1.6 km @ 32 kmh (1 mile @ 20 mph) average, or < 4 km @ 80 kmh (2.5 miles @ 50 mph) average or equivalent)	0 point
- Alternate access to metro-scale or similar facility is available, and/or alternate link to commercial and industrial network of out-state significance is available. (Alternate Route length < 8 km @ 32 kmh (5 miles @ 20 mph) average, or < 20 km @ 80 kmh (12.5 miles @ 50 mph) average or equivalent)	4 points
- No direct access to metro-scale or similar facility, and/or no alternate link to commercial and industrial network or out-state significance is available. (Alternate Route length < 8 km @ 32 kmh (5 miles @ 20 mph) average, or < 20 km @ 80 kmh (12.5 miles @ 50 mph) average or equivalent).	8 points
d. Road System:	0-3 points
- Non-municipal and non-county State-Aid Roads	1 point
- Municipal or County State-Aid Roads	2 points
- Interstate or State Highways and Federal Aid Urban Roads	3 points

System-Output

This consists of a preliminary and the final bridge replacement-priority list in decreasing order of final rating points. The agency responsible for bridge replacement can utilize this priority list in its planning and programming process.

Conclusion

This paper has presented a systems approach to the difficult bridge structure replacement-priority planning. The approach is comprehensive in that it goes beyond the structural sufficiency to include consideration of all relevant factors. The numerical rating system devised makes an objective evaluation possible. This system is simple, uses linear interpolation, and is easy to understand. Further, it is adaptable and its results are easy to communicate.

References

1. American Association of State Highway and Transportation Officials. A Policy on Design of Urban Highways and Arterial Streets. Washington, D.C., 1973.
2. American Association of State and Highway Officials, A Policy on Geometric Design of Rural Highways. Washington, D.C., 1965.
3. American Association of State Highway and Transportation Officials. Standard Specifications for Highway Bridges. Twelfth Edition, Washington, D.C., 1977.
4. American Association of State Highway and Transportation Officials. Manual for Maintenance Inspection of Bridges. Washington, D.C., 1974.
5. American Public Works Association. A Survey of Urban Arterial Design Standards. Chicago, Illinois, 1969.
6. Highway Research Board. Highway Capacity Manual. Special Report 87, Washington, D.C., 1965.
7. Moskowitz, Karl. Numerical Ratings for Highway Sections as a Basis for Construction Program. U.S. Public Roads Administration, Phoenix, Arizona, 1939, Rev. 1947.

WHAT HAS BEEN LEARNED FROM THE FIRST PRESTRESSED CONC. BRIDGES-REPAIR OF SUCH BRIDGES

Heinz P. Koretzky, Pennsylvania Department of Transportation

Engineers often wonder to what extent prototype structures have lived up to their expectations. As examples, old construction of the Walnut Lane Bridge, Amdeck section, and one other structure which showed signs of distress over the years will be illustrated. The speaker will discuss the apparent background and reasons for such a distress plus the improvements which may be made to make such effects less severe. Also, methods of repair and what has been learned from these old designs will be described. The lecture is supported with many color slides and viewgraphs which depict old construction details and the increasing severity of distress. Accidental damages caused by vehicles on three different types of prestressed bridge superstructures are also illustrated.

History

Modern use of commercial prestressed concrete was introduced by E. Freyssinet of France, who in the late 1920's started using high strength steel wires for prestressing. (1) Although others before him worked on, designed, or received patents on prestressing systems, it was Freyssinet who identified the conditions and established the parameters under which it is possible to assess strains in concrete, and clarified methods to apply a prestress force which give the predicted strains. (2)

Use of Prestressed Concrete in North America started at the beginning of the 1950's. The structure most often mentioned in magazine articles and in text books is the Walnut Lane Bridge in Philadelphia which was conceived in the late 1940's.

There are several claims for the position of "first" in prestressed concrete bridges. According to the Engineering News Record, (3) the first prestressed bridge was completed in October 1950 in Madison County, Tennessee. On the other hand, PennDOT records reserve this distinction for a bridge near Hershey in Pennsylvania, and also for the Walnut Lane Bridge in Philadelphia, Pennsylvania.

However, these claims to fame can be divided into different phases, i.e.: being first in prestressed concrete bridge design, start of construction, completion of construction, and opening to traffic. When examing the facts closer, each of these claims is bona fide and can be supported for the following technical reasons:

Walnut Lane Bridge

Located in Philadelphia, Pennsylvania. This is the first prestressed (post tensioned) bridge in the USA using site cast I girders (bulb T type, with wide top-flange).

Main span girders 48.8 m (160 ft.) long, 2 m (6 ft. - 7 in.) deep and weighing 122 mg (135 tons) each were cast on top of 15.2 m (50 ft. high) falsework and piers. The center span girders are prestressed by 4 parallel wire cables, each cable consisting of 64 wires, each wire .7 mm (.276 inch) in diameter and stressed to 862 kPa (125,000 psi).

Two cables were parabolic and two straight. The girders have 8 web stiffeners (7) and are assembled to form a superstructure which would now resemble an adjacent AASHTO, Type VI Beam Superstructure.

An interesting sound movie had been prepared by the Portland Cement Association, a copy of which was still available from the PCA a few years ago.

Construction of the first main span girder, which was test loaded under the supervision of Professor Gustave Magnel (7) to destruction under a force of ten times the design live load, began in the fall of 1949. After the successful load test of this girder, construction of other girders started and continued through the winter. The deck was completed in the fall of 1950. The bridge was opened to traffic in February 1951. (5) Fig. 1.

Madison County Bridge

Located in Tennessee, this structure used beams assembled from precast concrete blocks compressed to form a monolithic unit by tensioning 7 wire galvanized strands.

"This pioneering structure consists of a cast-in-place concrete deck carried on 6.1 m (20 ft.) and 9.1 m (30 ft.) beams placed side by side. (4) The beams were built up of 20.3 x 40.6 x 30.5 cm (8 x 16 by 12 inches) deep, machine made hollow concrete blocks, which were battered on opposite sides with mortar and threaded on tensioning cable." (This tensioning work for the multiple span bridge

was done by the county highway maintenance crews.)

"Cable are 7 wire bridge strands with anchor fittings made by John Roebling's Sons Co. at both ends. Tensioning was done with hydraulic jacks. The first day, an initial tension of 4536 kg (10,000 lb.) per strand was applied and the mortar allowed to set overnight. The next day, a final prestress of 11793 kg (26,000 lb.) was applied, giving the strands a prestress of about 862 kPa (125,000 psi).

Fabricated in the field by the county maintenance crew in three days, the beams were erected and the bridge opened to traffic in less then two weeks after construction began." (4)

Designed by Ross H. Bryan and Culver B. Dozier and built in October 1950, this bridge was heralded as opening up a new market. (Fig. 2)

Figure 1. Walnut Lane Bridge, Philadelphia.

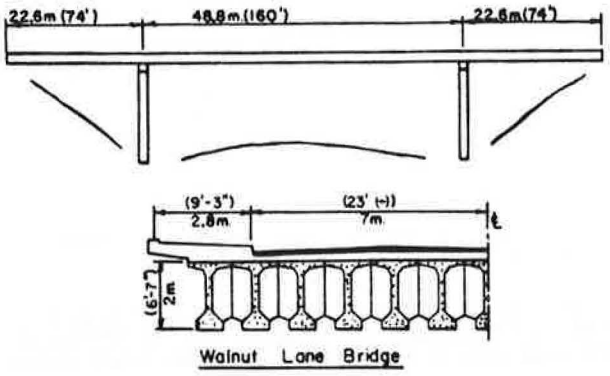

Figure 2. Madison County Bridge, Tennessee.

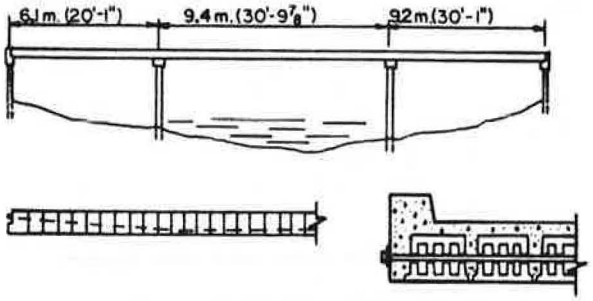

Hershey Bridge

Located in Pennsylvania, "In December, 1951, pretensioning took a bow in the United States, when a 7.3 m (24 ft.) span-consisting of rectangular beams laid side by side to form a 6.7 m (22 ft.) roadway-was erected near Hershey, Pennsylvania."(8) (9)

One of the pretensioned prestressed concrete bridge members was test-loaded to destruction May 20, 1950 at the Pottstown Plant of Concrete Products of America (which was the longest continuously operating prestressing plant in the USA until it changed ownerships; first to American-Marietta Co. (Martin Marietta Co. then to Pottstown Newcrete). Another beam was fatigue-loaded at Lehigh University, July 1951. (10)

It is interesting that, since May 1947, this plant had fabricated Precast Reinforced Concrete Channel beams for Pennsylvania, and then switched over to prestressed concrete bridge beams in 1950.

According to PennDOT records this first bridge had a clear span of 7.9 m (26 ft.) and is 7.3 m (24 ft.) wide. (Fig. 3)

Figure 3. Hershey Bridge, Pennsylvania.

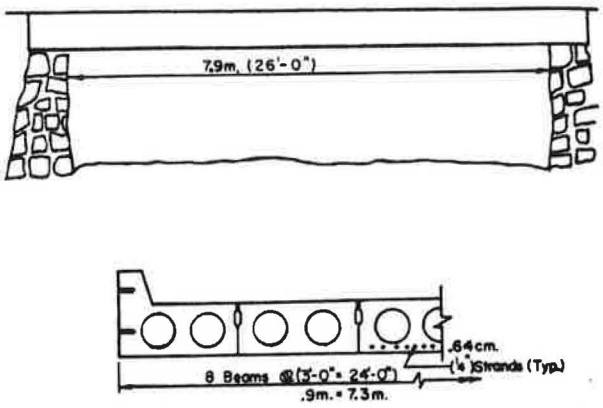

What does a short selective history of USA prestressing tell us? It says that when a good idea such as prestressing comes along and the time is right, many will have similar ideas.

In summary, the Walnut Lane Bridge was the first cast-in-place post tensioned concrete bridge, completed in the Fall of 1950 and opened to traffic, February 1951. First beam was load tested, Fall of 1949.

The Madison County Bridge was the first segmental precast post tensioned concrete block bridge, completed Fall of 1950, and opened to traffic, October 28, 1950.

The Hershey Bridge was the first precast pretensioned concrete box beam bridge, and was completed December 1951, and a test beam was load tested May 20, 1950.

I think that it really does not matter who was first in designing a prestressed bridge, or who was first in building a prestressed bridge beam, or who was first in test loading such a bridge beam, or first in completing a prestressed bridge or who first had traffic on it; what matters is that each bridge of the three precedent-setting bridge types represent a pioneering effort in bridge construction. Such effort was only possible by the pooling of the efforts of many talented engineers, contractors, material suppliers, and government officials, who added to and converted European

Similar Ideas

Such bridges remain a monument to progress. We now know in which direction the technology established by these pioneers developed, and what use is still being made today of the bridge systems developed by them, as well as new direction the prestressed bridge technology has taken.

Design-Construction-Fabrication

It should be understood that only two of the 3 bridge types which received early prominence withstood the test of time. Repeated use of those systems was made after their initial introduction.

Early standards began developing in the early

50's, soon after engineers thought they had a viable product.

It is interesting to note, that of the two surviving bridge types, the I-beam Walnut Lane Bridge consisted of large heavy field-cast bridge members, which were field post tensioned, while the box beam Hershey Bridge was plant-fabricated, and pretensioned, and was, in comparison, much lighter in weight.

Design

The first standards were developed by the box beam fabricator, the Concrete Products Company of America. Standards dated November 16, 1951 and August 19, 1952 were distributed showing adjacent box beams with circular voids for clear spans from 5.5 m (18 ft.) to 11 m (36 ft.) in .6 m (2 ft.) increments; and Standards dated December 17, 1951 and subsequent revision showed 83.8 cm (33 in.) deep beams with spans from 11.6 m (38 ft.) to 15.2 m (50 ft.), also with circular voids.

This plant was purchased by the American-Marietta Company, which expanded upon those Standards and issued their famous Amdek Standards, dated December 30, 1955, which had wide distribution at the time. Standards showed all necessary details to build the beams including the number of .95 cm (3/8 in.) strands. These Amdek Standards were further expanded in 1957 and 1959 by American-Marietta Company.

I-beam standards were proposed by the Prestressed Concrete Institute for acceptance under the auspices of the "Joint Committee, American Association of State Highway Officials Committee on Bridges and Structures, and Prestressed Concrete Institute". (printed in 1963, with standards enclosed which were dated 1961)

During the period from 1958 thru 1962, efforts to establish Industry, Statewide or Regional standards proliferated.

As a typical example, I show the national development of Standards by the U.S. Bureau of Public Roads.

Issues were 1956 (11), June 1962 (12), August 1968 (13), and January 1976 (14).

The Federal Standards are in some aspects different from the various State Standards. The difference is generally in the section/wall thickness in box beams, webs or flange configuration in I-beams, or different minimum reinforcement. This difference is readily explained because some Regional State Standards were developed earlier then Federal Standards and took precedence in their respective regions since fabricators had already invested in forms and turned out successful products.

Construction

The most frequently used prestressed bridge stringer systems for prestressed concrete bridges are the I-systems (Walnut Lane Bridge) and the box beam system (Hershey Bridge).

It must be remembered that both systems were properly designed with a more than adequate factor of safety when they were initially conceived and that, as an additional safe guard they were subjected to test loadings. They were only used on an actual structure after they successfully passed the tests.

In the early stages of prestressed concrete development in the United States, the prevailing design philosophy was that "because the concrete was prestressed" it will remain crack free. This philosophy was also expressed in some literature circulating at that time. Because of this, the effects of temperature (temperature reinforcing) and shrinkage were often neglected. Furthermore, there may have been less attention given to prestressed losses than would be given today and in addition, the assumption that net compression could be maintained throughout the section was overly optimistic, since the determination of the effect of force reduction caused by losses was not as sophisticated as today's methods, therefore, resulting in an over estimation of the remaining prestressed forces.

Also, we must recall that at the time of construction (1950) as well as through the following decade, concrete placement was a problem. This was obviously the case with the Walnut Lane Bridge.

If you look at the various construction slides, you receive an overall view of the conditions prevailing at that time.

Slide 1. Shows general view of midspan of Walnut Lane Bridge.

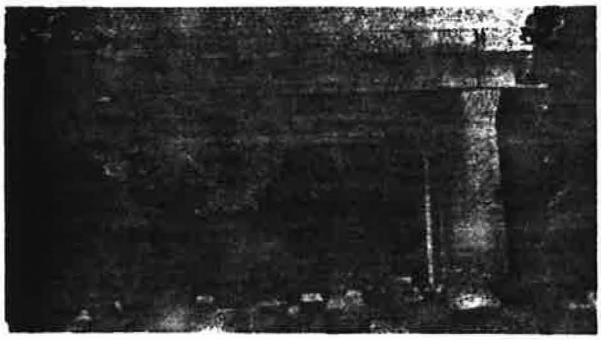

Slide 2. Depicts bottom view of Walnut Lane Bridge showing close intermediate diaphragm spacing.

Slide 3. Illustrating closeup of intermediate diaphragms showing weight reducing holes in endspans of Walnut Lane Bridge.

It should be noted that the bridge was being constructed for the City of Philadelphia and now is owned by the Pennsylvania Department of Transportation.

Slide 4. Shows portions of the original falsework of the Walnut Lane Bridge including maintenance of traffic.

Slide 5. Shows a different view of the same falsework.

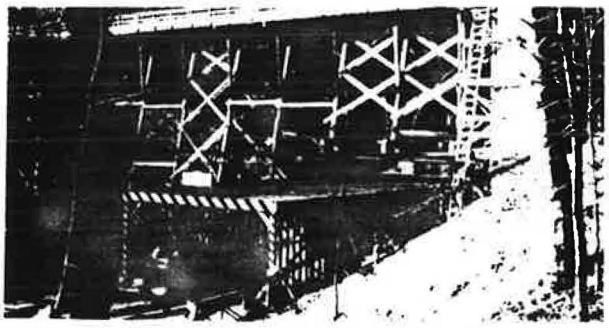

Slide 6. General view of Walnut Lane Bridge, girder on falsework.

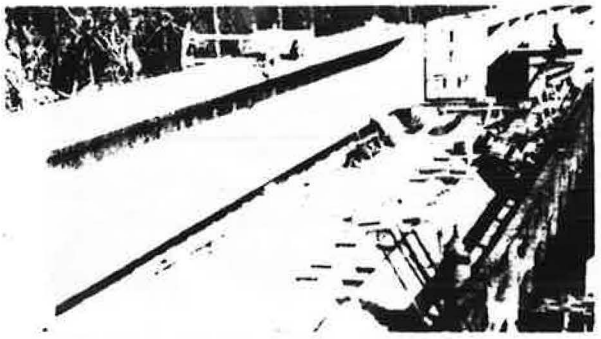

Slide 7. End view of girder with tendons and tendon voids.

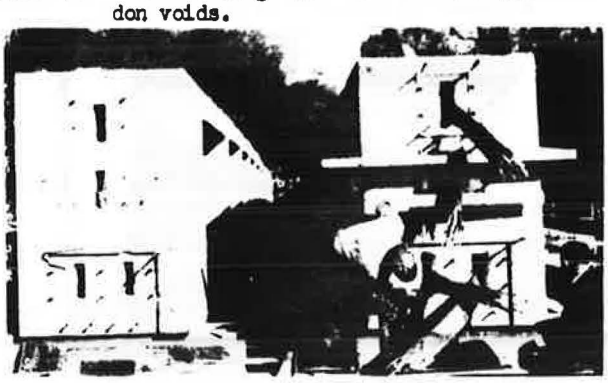

Slide 8. Closeup of tendons and end anchorages.

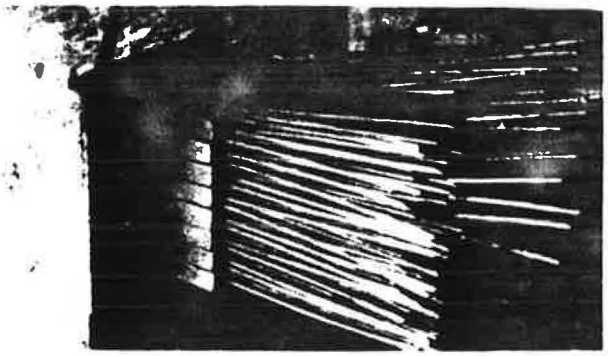

Please keep in mind that all the photographs except for slides 1, 2, and 3 were taken in February, 1948 prior to the load test which I previously mentioned.

After the first field cast beam was cured and test loaded, the regular production casting started. But something went wrong in the fabrication of the first production girder - the south fascia girder.

Slide 9 documents this and shows what was wrong with some of the old construction. It is obvious that with thin webs and the large percentage of duct space and the use of wooden forms, low slump concrete could not satisfactorily be placed everywhere.

Fig. 4 shows the Walnut Lane Bridge fascia beam cross section. This should be compared with slide 9.

This bridge had been closely observed by its owner, the City, which found problems. The City retained Zollman Associates early in 1968 as a consultant. The consultant inspected the bridge and reported his findings and recommendations to the City on June 24, 1968.

The report makes interesting reading. Some excerpts follow:

"In November, 1957, a routine inspection made by members of the Maintenance Division of the City's Department of Streets, revealed the existence of longitudinal cracks in the fascia girders of the main span. In addition, there were a number of very localized, fine cracks, hardly visible when observed through binoculars from the floor of the valley some 60 feet below the bridge. There was no pattern to these localized cracks since they occurred erratically throughout the bridge.

The strong discoloration of the concrete in the vicinity of the cracks indicated that they had been present for some time. It also appeared that the cracks had been pointed with grout at some previous time, even though there is apparently no record of this procedure having been carried out. In any event, it was determined that none of the cracks would endanger the structural integrity of the bridge. After the size, type and location of the cracks had been recorded, the City then decided to apply a cement coating to the exposed areas of the girders for the sake of appearances.

Over the next ten years, the cement coating weathered to a point where the cracks again became visible. During a routine inspection made in November of 1967, it was observed that the longitudinal cracks in the South Fascia Girder of the main span seemed to have lengthened and widened. In view of this situation, representatives of the Department decided to inspect all of the girders at close range, and to make and record their observations as accurately as possible."

Slide 9. Construction problem in 1st cast girder.

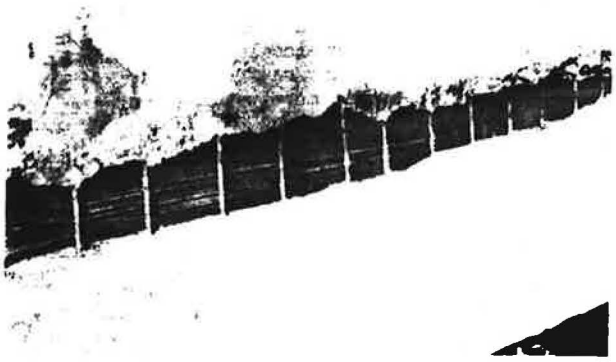

Figure 4. Typical reinforcing in Walnut Lane Bridge girder - also typical cracks shown in large scale detail.

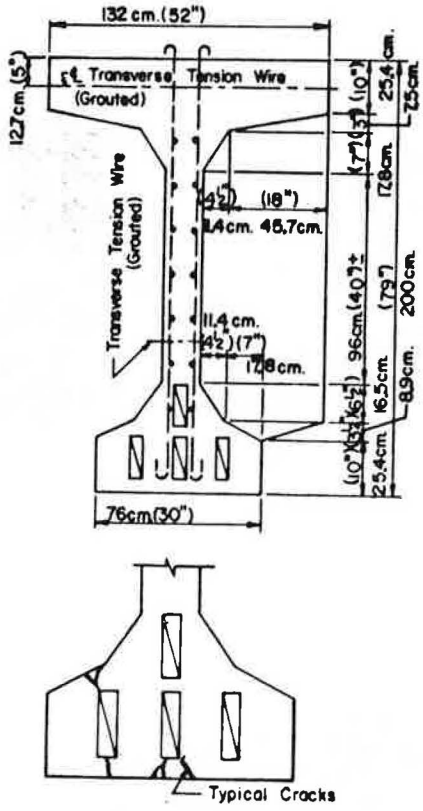

This report also casually mentions the design and construction philosophy prevailing at the early stage of U.S. Prestressed development.

Looking at slide 9, it is obvious what we would do today with such a girder, but at that time, such thoughts were different. I am quoting from the report which indicates that in spite of poor concrete surfaces, honeycombs, exposed reinforcing steel bars, cold joints in bay 4, displacement of vertical web reinforcing steel and displacement of tendon cavities, it was decided that they should proceed with prestressing. The thought at that time was, "if the girder was structurally deficient, the high prestressing forces later to be applied to it would cause the girder to fail." The prestressing was carried out without difficulty, leading to the conclusion that the observed imperfections were of less significance than originally thought. Therefore, the girder was repaired for appearances sake and incorporated into the bridge.

The report gives the following additional observations which are of interest: rectangular duct spaces created an area reduction of 18% of bottom flange and a plane of weakness which was aggravated by possible misalignment of ducts during construction.

Early in load testing, the first cast girder, horizontal cracks unexpectedly appeared near the junction of web and bottom flange on one face. The cracking was not considered to be of any particular consequence, but nevertheless was reported by Gustave Magnel. (7)

In accordance with what was then common practice in prestressed concrete construction, no stirrups were placed in either the top or bottom flange.

Shortly after this report was given to the City, the Pennsylvania Department of Highways became the owner of the bridge.

My office, in cooperation with the office of the Philadelphia District Bridge Engineer, made its own inspection of the bridge, and prepared new repair plans for letting, which relied heavily on the epoxy pressure injection process to seal cracks. The repair/seal work was done by contract during 68/69 and cost about $140,000. (16)

Now it is prudent to look again at a series of slides which depict defects.

Slide 10. Typical cracks found at bottom of fascia beam.

Slide 11. Same crack with some concrete pried out.

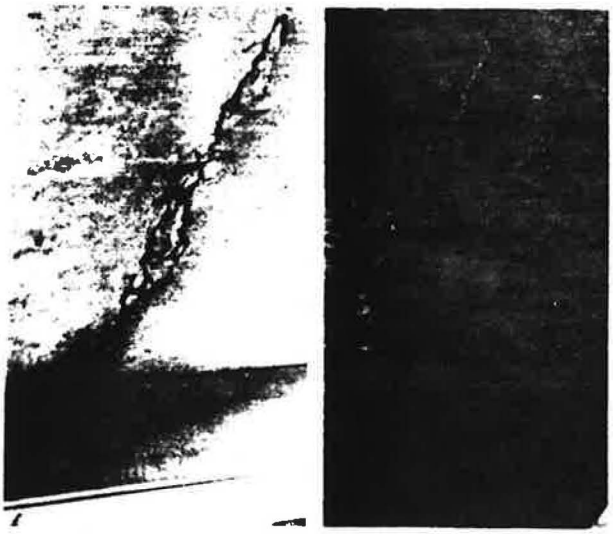

Some of the effects of the built-in latent defects previously discussed in connection with Slide 9 are shown in Fig. 5. This figure shows a composite of the cracks and defects selectively copied from construction plans dated October 4, 1968, and shows cracks observed by the Department, and supplemented by cracks recorded on plans prepared by the repair contractor, and dated January and February 1969. The contractor's plans showed cracks found through close visual inspection and listed observations made during the injection process.

Fabrication

Now to the other old structures which, instead of being field cast like the Walnut Lane Bridge, were plant fabricated.

Slide 12. Space between cracks exposing duct space.

Slide 13. Crack in the top of bottom flange.

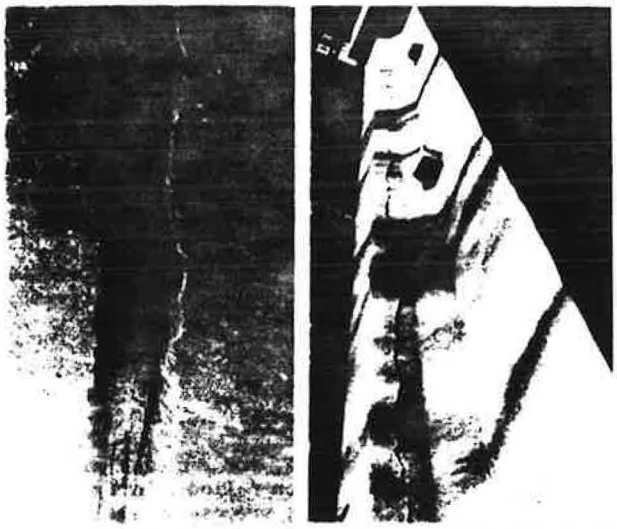

Figure 5. Composite of cracks in a selected area found on Walnut Lane Bridge.

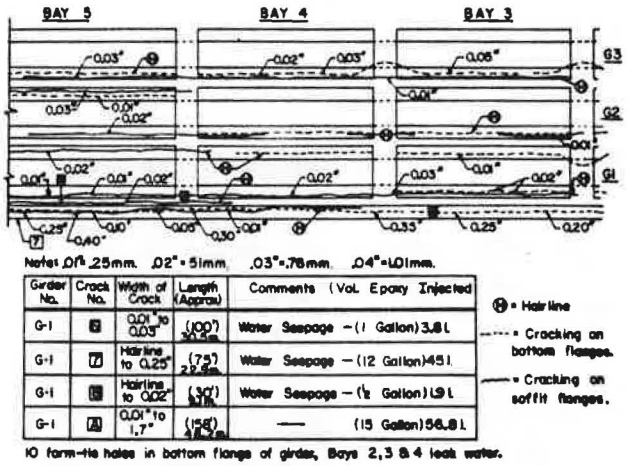

Notes: .01" = .25mm. .02" = .51mm. .03" = .76mm. .04" = 1.01mm.

Girder No.	Crack No.	Width of Crack	Length (Approx)	Comments (Vol. Epoxy Injected
G-1	6	0.01" to 0.03"	(100") 2.54m	Water Seepage — (1 Gallon) 3.8 L
G-1	7	Hairline to 0.25"	(75") 2.29m	Water Seepage — (12 Gallon) 45 L
G-1	8	Hairline to 0.02"	(30") 0.76m	Water Seepage — (½ Gallon) 1.9 L
G-1	A	0.01" to 1.7"	(156") 4.88m	— (15 Gallon) 56.8 L

⊕ = Hairline
---- = Cracking on bottom flanges.
—— = Cracking on soffit flanges.

10 form-tie holes in bottom flange of girder, Bays 2, 3 & 4 leak water.

Slide 14 shows the predecessor of Prestressed Box Beam Bridges used in Pennsylvania between 1947 and 1951, namely the Precast Channel Section. Anything which is now a problem with this bridge will show up in the future on older Prestressed Concrete Boxes; it is just a matter of time.

Slide 14. Precast channel bridge built in 1947-51 predecessor of prestressed box beam bridges.

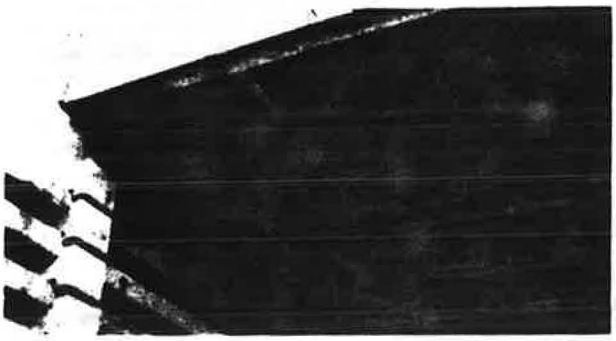

The bridge spans a creek and the deterioration is caused by the moisture-condensation effect on inadequate concrete cover for this exposure condition. The worst damages are visible on the inside leg of the fascia beam/outside leg of interior beam since condensation of moisture from the stream and the environment generates more wetting cycles at those locations than elsewhere.

Slide 15 shows the bottom of the Hershey Bridge Beam and clearly shows the imprint left by the vacuum curing process used for this beam and for all beams produced in Pennsylvania from 1951 thru 1955, and for some bridge beams produced by a certain plant to 1959.

While the placing of concrete for some girders on the Walnut Lane Bridge was a problem, the precaster at that time bypassed this problem by using high slump concrete for placement, and the vacuum process for removal of excess water, in order to gain high early strength for speedy release of prestressed force, therefore avoiding the problems of frequent honey combing.

Slide 15. Hershey Bridge with vacuum cured surfaces.

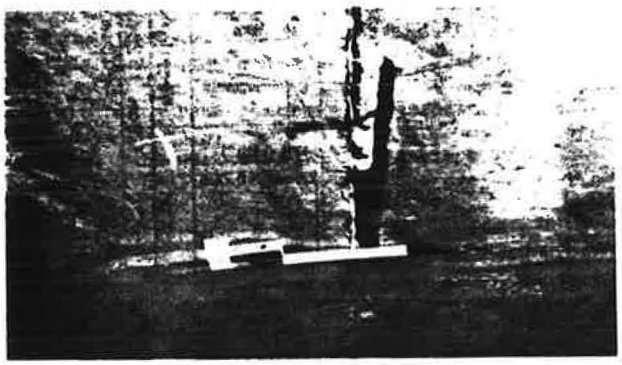

Slide 16. Outside surface of Hershey Bridge fascia beam in distress.

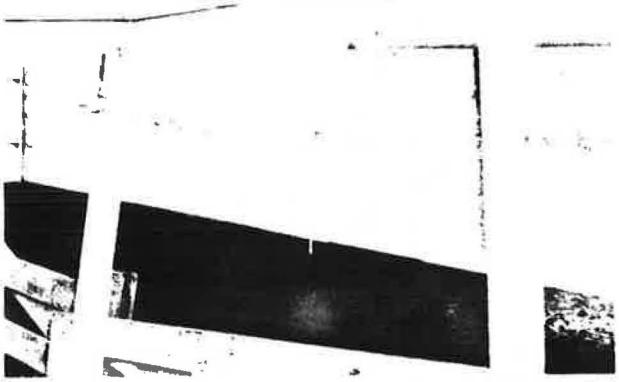

Figure 6. Typical cross section, Hershey bridge beam.

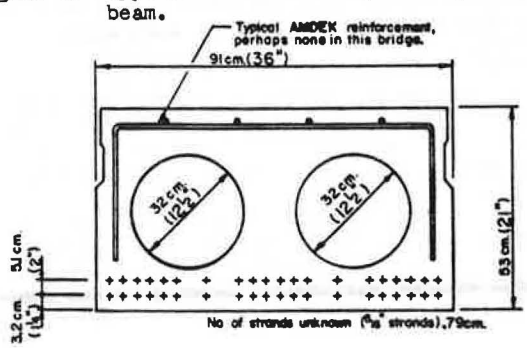

Slide 17. Fascia beam in distress.

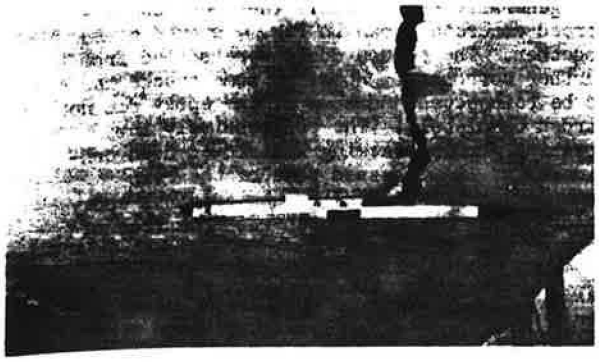

Slide 18. A 1956 adjacent box beam bridge but photographed in 1962

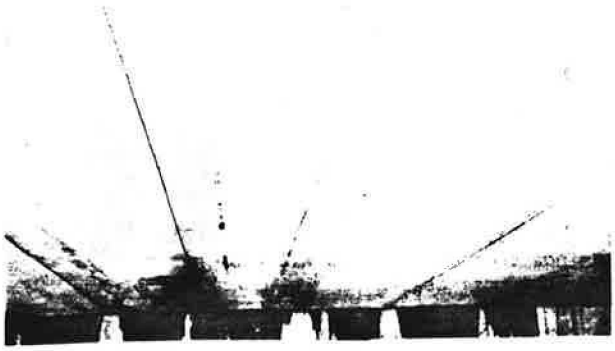

Slide 19. View of further deterioration in 1977.

Slide 17 shows the outside surface of one fascia beam showing some surface distress.

Fig. 7 shows the beam cross section as restructured from existing documents. Slide 17 shows the cause for the surface distress in the fascia beam shown in slide 16, namely the damage caused by free water freezing in the beam void and rupturing it.

This type of damage, even though noted on about 10 more bridges, was only observed on fasica beams. This damage was avoided since 1959/60 with the introduction of bottom drains in all voided Prestressed Box Beam Girders.

Slide 18 taken in 1962 shows an early adjacent box beam bridge, approximately 1956 vintage, which shows progressive corrosion due to insufficient concrete cover over the bottom strands of a bridge over a stream. I recall a .63 cm ($\frac{1}{4}$ in.) clearance in some locations while plans specified 3.18 cm ($1\frac{1}{4}$ in.) clear.

Repair/Maintenance of Prestressed Bridges

There are some governing but apparently conflicting observations and suggestions:

As is demonstrated by these slides, which show defects in the oldest (Historical) prestressed bridges, these bridges appear to have a great deal of excess strength. They are not going to collapse soon; they are in no immediate danger.

Since the strength of prestressed bridges depends on prestressing forces, it appears to be of overriding importance to protect the tendons, through which prestressed forces are applied, from any progressive corrosion. If corrosion is suspected, it would require immediate action to protect the tendons.

Since tendons are generally inaccessible, except where exposed by defects, it is very difficult to detect corrosion or damage to the tendons in areas not exposed. Such damage in all probability is present but covered up by concrete. Often it is assumed that sound concrete will hide corrosion defects which however are probably less severe than the corrosion defects visible in an exposed area.

This removes the urgency of immediate action to arrest further corrosion and allows time for study to find the most cost effective way of arresting the condition since repair/restoration in most instances becomes impractical.

What should be done?

My recommendation is that distressed structures be reanalyzed using various assumptions of deficiences of tendons including an assumed rate of deterioration. In order to compensate for the occasionally obsolete practices used, allowances must then be made for construction practices, design philosophies, acceptance practices, and materials fabrication techniques used at the time the bridge was designed and fabricated.

This forces the engineer into the unaccustomed position of being a bridge historian and also to be a detective skilled in ferreting out old reports, standards, practices and documents, and into discovering the unpleasant ommissions or to define the reasons which led to distress. Such ommissions if in existance at the time of design, fabrication or construction, would rather be forgotten by the principals especially if they did not clearly report those ommissions at the time when they occured.

All of this has to be considered when making a final decision as to what should be done to provide an answer to some of the basic questions:

Is the bridge adequate for the current design load?

If not adequate, should the bridge be posted?

If in need of posting, for how much?

If inadequate, shall the bridge be closed or dismantled and how soon?

For the Walnut Lane Bridge, this question was answered at that time by Stress Analysis, Installation of deflection/camber "tattle tales" (deflection indicators), Simple Load Test, and the application of repair methods which extended the life of the structure.

Such a method is shown in the following slides:

A follow-up inspection in 1970 (16) showed no new cracks. Subsequent inspections and two additional inspections made by myself in cooperation with the District Bridge Engineer's Office as late as 1977 showed some small new cracks and opening of some old cracks.

Slide 20. Enclosure for epoxy sealing - Walnut Lane Bridge.

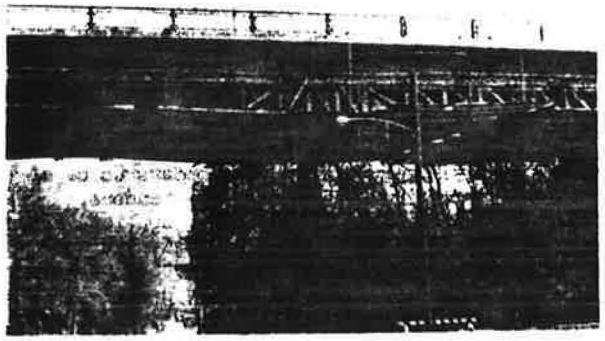

Slide 21. Inside enclosure - view of outside face of fascia beam

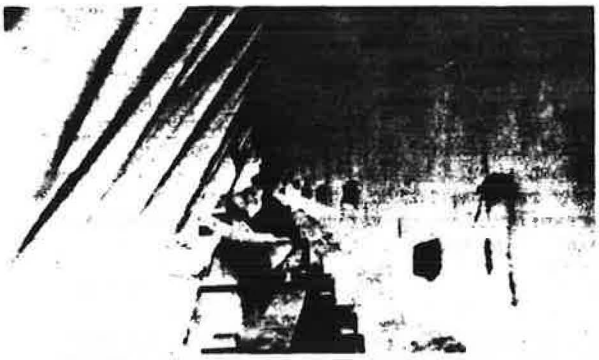

Slide 22. Pressure injection of epoxy.

For the Walnut Lane Bridge, the injection was generally successful. The loose unreinforced concrete shown in Fig. 4 stayed glued together. The tendon ducts were sealed from further corrosion. However, some cracks had to be reinjected and some of the epoxy did not harden completely. The progressively increasing girder cracking was slowed down considerably. I witnessed some of the reinjection of those cracks by the original epoxy injection contractor, which was done free of charge.

When inspecting the bridge, the writer recalls that it was virtually impossible to properly inspect the strands even at some areas where the bottom of a wire tendon was exposed. Some corrosion was apparent. Rust was dark with some scaling evident. Also the epoxy injectors, and the repair contractor's engineer observed and reported some water seepage present in cracks apparently leading to the ducts. It appeared that water seeped through the superstructure joints and was then running along the end face of the beam. It is this writer's hypothesis that some of the deck expansion joints leaked water onto the end face of the beam. This water then penetrated through the end anchorage grout patches and leaked into the duct. This is an assumption, since close visual inspection of the end face, including probing beyond the sound concrete surfaces, was impossible.

The Hershey Bridge Beam (slides 15 to 17) has not been repaired at all and this writer did note progressive corrosion in the strands exposed by the wide cracks but feels that mortar or epoxy sealing in this instance would be a cosmetic procedure and would not protect the tendons properly unless the beam is pressure-injected with epoxy through-out and the voids are packed with epoxy mortar.

For other box beams showing damages similar to slides 18 through 20, a surface coating of sealer for all exposed surfaces of undamaged beams plus epoxy coating for the exposed strands (after sand blasting or - power brush cleaning) is recommended, preceded by a stress analysis of the defective bridge to determine if damaged member is not overstressed under current design criteria. The result of such a stress analysis should be favorable and therefore generally supporting a decision to determine if the sealing is cost effective. When compared with the estimated remaining life of the sealed member as compared with replacement cost.

Cosmetic patching is generally not recommended since it may hide further progressive deterioration.

There is a word of caution, however. Increasingly in the literature, there are reports about bridge restoration through epoxy injection.

This writer feels that all that can be done is to treat such a structure to slow down its deterioration. The structure cannot be strengthened by cosmetic patching no matter what "wonder" compound may be used. Pressure injection (one system can inject cracks down to .0076 cm (.003 in.) width) is a good method to seal cracks and perhaps to glue some pieces together, but this process is limited by one's ability to properly clean and surface-prepare narrow existing cracks and is, to some extent limited by the care with which the materials have to be field mixed and injected; and further, restricted by the constraints of weather, humidity and temperature.

It is very encouraging that only very few examples of distress in old bridges can be found. These distresses currently are overshadowed by vehicle-caused defects. Typical examples are shown in the following slides.

After appropriate stress analysis it was determined that for the box beam bridges cosmetic repairs were all that was required. Cracks were sealed, exposed strands received protective coating and holes were patched.

Similar damage to a prestressed I-beam bridge are shown on the following three slides.

The same procedure was deemed acceptable for the I-beam bridge. Cosmetic repair for the fascia beam was not considered feasible and therefore it was determined to replace the fascia beam in its entirety.

Slide 23. General view of traffice damage to a prestressed concrete adjacent box beam superstructure.

Slide 24. Closer view of the traffic caused damage.

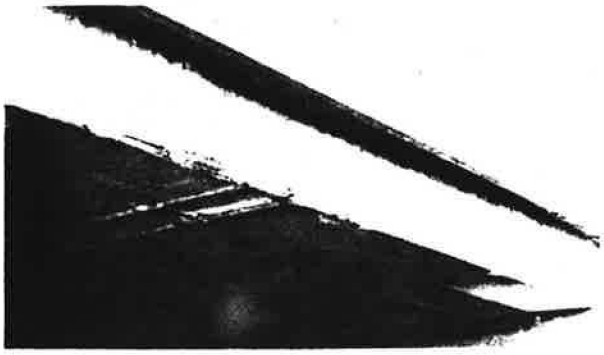

Slide 25. Closeup of the shattered concrete and exposed strands caused by traffic impact.

Slide 26. General view of traffic damage to a prestressed concrete spread box beam superstructure.

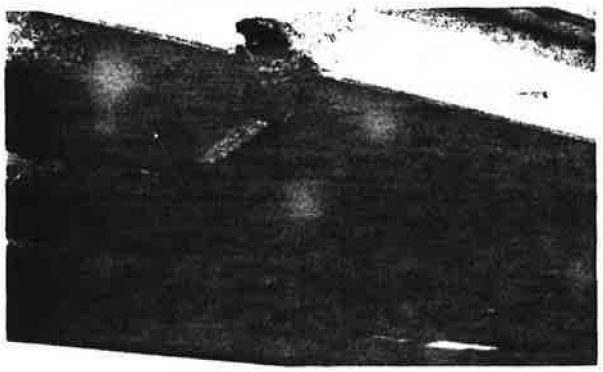

Slide 27. Closeup of damage and ruptured strands.

Slide 28. Detailed closeup showing also the cardboard void inside the box beam.

Slide 29. General view of repeated traffic damage to a prestressed I-beam superstructure.

Slide 30. Inside view of the same damage, showing exposed strands and shattered concrete.

Slide 31. Closeup of the damage, showing ruptured strands, exposed stirrups, and complete loss of concrete in web area.

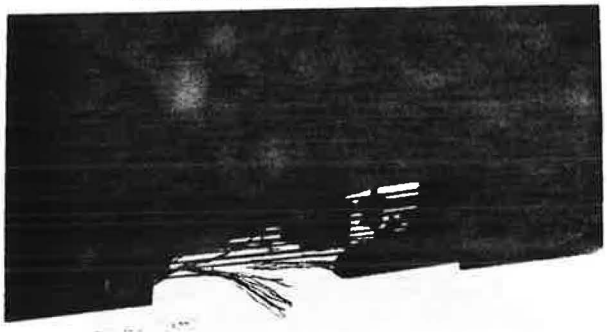

Conclusions - Recommendations

Design

Designs originally were very conservative and further backed up by successful load testing of full scale bridge members. New bridge systems must be very conservatively designed since effect of wear and tear on structure caused by loads, environment and unanticipated factors cannot be readily envisioned at time of initial design.

Construction

Construction techniques must be completely assessed and compatible with the intent of the design. Any aspects of construction procedures which could in one way or another affect the durability of a structure should be identified and replaced with more compatible procedures.

Repair-Maintenance

It must be recognized that prestressed bridges are difficult to repair. The best repair method would require a complete "unloading" of the bridge utilizing jacking or other methods which introduce a reversal of camber (unloading of prestressed moment).

Replacement of tendons is virtually impossible. However, effects of "Lost" tendons can be compensated for, in some cases, by the application of sophisticated external post tensioning.

Considering the inherent difficulty in applying any effective structural repair, cosmetic repairs are often applied but they should be identified as such.

This then leaves maintenance as the only effective means to protect prestressed bridges. However because of the difficulty to repair such bridges properly the maintenance must be really preventive maintenance. In order to avoid wasting maintenance money, preventive maintenance should be applied selectively with regard to type and extent of work on areas of prestressed bridges which can be identified by an engineer thoroughly familiar with past and current prestressed bridge design and fabrication practices.

Bibliography

1. T. Y. Lin, Design of Prestressed Concrete Structures, John Wiley and Sons Incorporated, New York.
2. Prestressed Concrete, Guyon, John Wiley and Sons, Incorporated, New York.
3. Engineering News Record, March 20, 1952, page 52.
4. Engineering News Record, January 18, 1951, page 39.
5. Civil Engineering - ASCE March, 71, page 39
6. Civil Engineering - ASCE July 69, page 37.
7. Journal of the American Concrete Institute, December 1950, page 301 and 302.
8. Preprint, 1957 Concrete Industries Yearbook, Part III, Pitt and Quarry-Publications, Incorporated, Chicago, page 12.
9. Pretensioned-Prestressed Concrete Bridge Members, by M. W. Loving, Cons. Eng., Glenview, Illinois, page 1 and page 2.
10. Progress Report No. 2, Prestressed Concrete Bridge Members, by Richard Myo, Lehigh University Institute of Research.
11. Standard Plans for Highway Bridge Superstructures, Revised 1956, U.S. Dept. of Commerce, Bureau of Public Roads.
12. Standard Plans for Highway Bridges, Volume I Concrete Superstructures, June 1962, U.S. Dept. of Commerce, Bureau of Public Roads.
13. Standard Plans for Highway Bridges, Volume I Concrete Structures, August 1968, U.S. Dept. of Transportation, Federal Highway Administration, Bureau of Public Roads.
14. Standard Plans for Highway Bridges, Volume I Concrete Superstructures, January 1976, U.S. Department of Transportation, Federal Highway Administration, Bureau of Public Roads.
15. Walnut Lane Bridge, June 1968, Report and Recommendations to City of Philadelphia by Zollman Associates.
16. ASCE March 71, Epoxy injections repairs historic prestressed concrete bridge, H. G. Garfield.

EXTENDING THE SERVICE LIFE OF EXISTING BRIDGES

R. H. Berger, Byrd, Tallamy, MacDonald and Lewis
Stanley Gordon, Federal Highway Administration

This paper briefly discusses background material and statistical data regarding the nation's current bridge problems and the research presently underway that will aid in resolving this problem. Bridge deficiencies as uncovered in the inspection of over 140 bridges located in five states are outlined. These deficiencies are categorized as Structural, Mechanical, Geometric, and Safety and are discussed as they apply to various bridge types and bridge materials. A catalog of deficiencies is included which lists the deficiencies in the order of frequency of occurrence. Bridge rehabilitation techniques presently in use are outlined and some unique techniques discussed. These include techniques to increase live load capacity, correct mechanical deficiencies, and to improve geometrics. Improvements to rideability, to safety, drainage and other miscellaneous repairs are also discussed. Sketches are included depicting the concepts of some of these rehabilitation techniques. "Improvement Factor" curves are developed for various techniques that can be utilized to increase live load capacity. This factor is an indication of the percentage of increase in flexural strength that can be achieved by a particular technique. Cost information for each of these techniques is also provided so that a "Cost Effectiveness Factor" can be computed for each. This provides a convenient means of comparison of various techniques from both a cost and an improvement standpoint.

CHAPTER I

INTRODUCTION

The United States highway network, recognized by many as being the world's finest, is quietly and even more quickly being threatened by the condition of our bridges. This has become one of our Nation's greatest problems. It is difficult to understand why, in an era where we have developed enough technical knowledge and expertise to put a man on the moon, we have not had and maybe still do not have the proper foresight to provide the necessary maintenance for our Nation's bridges. As a result of this neglect, we have seriously jeopardized not only our surface transportation system, but our lives as well.

All of our problems, of course, are not due to neglect. Many of our Nation's bridges have become functionally obsolete because of heavier vehicle usage, inadequate roadway width and antiquated alignment.

Status of National Bridge Inventory

Currently, it is estimated that there are 564,000 bridges in the United States of which approximately 105,500 are either considered structurally deficient or functionally obsolete. A structurally deficient bridge is one that has been restricted to light loads or closed. A functionally obsolete bridge is one whose deck geometry, clearances, approach roadway alignment and load restrictions can no longer satisfactorily service the system of which it is an integral part. The inventory and inspection of all bridges on the Federal-aid highway system, encompassing 234,000 structures, is substantially complete. This inventory has uncovered approximately 33,500 deficient bridges.(1) The remaining 72,000 deficient bridges are not on any Federal-aid system and are the sole responsibility of the state and local governments. Each year, for various reasons, an estimated 125 to 150 of these deficient bridges sag, buckle or collapse--sometimes tragically.

In an attempt to alleviate this problem, several bills regarding funding for a Special Bridge Replacement Program have been introduced in Congress and have generated a great deal of discussion. While there is a general feeling that more Federal money will become available for bridge inspection, replacement and/or rehabilitation, it is not realistic to expect that all of the deficient bridges can be attended to in a short period of time. Consequently, our direction and purpose at this time should be to initiate and develop procedures for extending the service life of existing bridges until such time as we have the money, time and manpower to replace those deficient structures in an orderly manner.

Current Research

With this endeavor in mind, the Federal Highway Administration, in an effort to respond to the bridge problem, has sponsored a research project entitled "Extending the Service Life of Existing Bridges by Increasing Their Load Carrying Capacity."(2) Another project, sponsored by the National Cooperative Highway Research Board is entitled "Bridges on Secondary Highways and Local Roads - Rehabilitation and Replacement."(3) While these research projects do have different objectives, both are studying bridge deficiencies and various rehabilitation techniques that are currently being utilized by several different state highway departments. The results of these studies should prove invaluable to the practicing bridge engineer.

While many deficiencies are caused by normal traffic, weather and deterioration, some deficiencies are the direct result of cracks appearing in the steel. These occur in both old and new metal and in old and new designs. In an effort to detect cracks, two instruments using nondestructive test principles were developed specifically for field inspection. The Acoustic Crack Detector and the Magnetic Crack Definer were used respectively for detecting cracks in metal and for defining the limits of the cracks. Cracks have also been detected with tests involving dye penetrants, radiography, magnetic particle inspection and acoustic emission. Ongoing research in this area includes the development of equipment to identify fractures in prestressing bars used in concrete structures, the determination of stress corrosion fatigue characteristics of new steels and continued research into the touchness of weld materials.

Additional research is underway regarding bridge deck protective systems. These include studies of various membrane waterproofing systems, reinforcing bar coatings, cathodic protection, latex and low slump overlays, wax beads in the concrete and systems for heating bridge decks.

Intent of Paper

The total bridge problem which we must resolve is obviously quite broad and has many facets. This paper will deal only with a few of these involving deficiencies and rehabilitation techniques. Certain aspects such as fatigue cracking, deck protection systems and cosmetic repairs will be touched only briefly.

CHAPTER II

BRIDGE DEFICIENCIES

Bridge deficiencies evolve from a variety of situations and conditions. Basic design criteria, traffic usage, environmental factors, and other site conditions are all involved to some extent and are responsible for specific deficiencies. An additional, and perhaps the most important, contributor to bridge deficiencies is the level of maintenance employed.

Deficiency causes can be categorized into two broad areas: (1) those which result from the design of the facility and are thus inherent deficiencies, and (2) those which result from the use of the facility and are essentially the result of wear. Deficiencies from either cause are subdivided into four areas: Structural, Mechanical, Geometric and Safety.

Structural

Structural deficiencies are defined as those which affect the structure's ability to carry imposed loads. These are caused most frequently by lack of proper maintenance, poor design details and light original designs.

Steel Structures. In steel structures, paint system breakdown permits corrosion of the base metal to begin. Once started, the process accelerates as larger areas become exposed. Eventually the metal corrosion can result in section loss serious enough to have an impact on the load-carrying capacity of the member. If left uncorrected, the process will continue, resulting in the ultimate collapse of the bridge.

The corrosion process is accelerated when snow laden with chemical de-icing agents comes in contact with the primary structural elements either as splash or storage. This is particularly true in through girders and trusses.

Webs of through girders become "paper thin" and bearing stiffeners are known to have been totally lost. Truss members likewise become severely corroded in critical areas.

Concrete Members. Concrete members also deteriorate at a rapid rate when exposed to adverse environmental conditions. Penetration of brine solution through the unprotected concrete surface causes the reinforcing steel to oxidize and expand, ultimately leading to spalling and cracking of the concrete cover. Once the process begins, it accelerates at a rapid pace as more of the corrosive materials reach the reinforcing steel.

This process, which is very common in bridge decks, also occurs in primary structural members. Prestressed girders and mild steel reinforced concrete members deteriorate when conditions permit penetration by a corrosion conducive solution. Observations of bridges in a number of areas have shown that this condition occurs as a result of salt water splash where low level bridges cross bodies of water with a high saline level or where roadway joints and drainage details permit runoff to come in contact with concrete beams and girders for prolonged periods of time.

Timber Members. Timber members, too, deteriorate as a result of general weathering when unprotected. Wet-dry cycles that occur frequently accelerate the process.

Light Designs. Many of the structures currently an integral part of our highway system were not designed initially to carry the loads being imposed on them by modern traffic. These "light designs" were based on vehicle weights much less than those in present use and on load frequency rates that are only a small percentage of those now utilizing the crossings. Some of these older structures were designed for 3 or 4 lanes of H15 traffic and now carry heavier vehicle loads by restricting the traffic to one or two lanes. It is a credit to the designers of these antiquated structures that many of them remain serviceable today in spite of the heavy use by modern traffic loads.

These deficiencies apply to sub-structure members as well as to superstructure members. In addition, substructure elements can be structurally deficient because of foundation conditions. Pile deterioration, scour, and deep failures in underlying soil strata can cause significant reduction in the load-carrying capability of the bridge.

Mechanical

These deficiencies are defined as those which prohibit the structure from reacting in a controlled manner to environmental factors. These are primarily caused by corrosion of metal elements, the accumulation of debris and silt around bearings and joints, lateral movement of substructure units, and poor design details.

Build-up of debris around bearing areas often completely covers metal bearings. This debris is composed of bird droppings, nesting materials and other deposits that are highly corrosive. When this material is saturated with a salt solution from roadway runoff it becomes even more corrosive. The bearings freeze as a result of this corrosion and prevent the bridge from functioning as intended.

Pavement "shove" pressures often add to this problem. This is the result of temperature expansion and contraction in the approach roadway combined with traffic generated pavement movements. Stub abutments move longitudinally as a result of these forces and backwalls deflect and eventually crack. As a result, it is no longer possible for the bridge to function as intended without exerting loads on the structure beyond those considered by the designers.

Settlement as well as lateral movements in piers can cause a similar situation. Pier rotation causes roadway joints to close and bearings to exhaust their capability to accommodate movement. Ensuing temperature changes can then result in serious overstress in other elements of the bridge.

Geometric

These deficiencies are those that relate to the geometrics of the roadway as it approaches and traverses the bridge. Vertical and horizontal alignment, roadway width, vehicle sight distance, and traffic capacity are included. In almost every instance these are inherent deficiencies that were built in as a result of the initial design.

Safety

Deficiencies relating to the safety of the motorist include those that jeopardize the safety of the vehicle as it passes over the structure. Many of these are geometric in nature (roadway width, clearance, etc.). Others pertain to the roadway appurtenances such as a bridge railing, approach guardrail protection, and traffic control devices.

Rideability deficiencies are those that impact on the riding quality of the crossing and are included in the safety category. Bridge deck deficiencies are the most common involving rideability. They can impair the load carrying capability of the bridge if the deck is designed as an integral part of the primary structural member such as in concrete T-beams and composite designs. Even with these designs the roadway becomes virtually impassable due to potholes and general deterioration of the deck before failure occurs.

Approach slab settlement can impair the structural integrity of the abutments and cause an increase in live load impact but usually has a greater effect on the safety of vehicles utilizing the facility since severe bumps and dips are created by the settlement.

Other safety deficiencies are those which occur because structure members are located in a position where they become a hazard to the motorist. End posts on through trusses, ends of through girders, pier and abutment pylons placed close to travelled lanes are examples.

Bridge Deficiency Catalog

A catalog of bridge deficiencies is included. This is based on inspection of approximately 140 deficient bridges located in five states which was part of a research project done for the Federal Highway Administration.(2)

Photos and descriptive information on these and other deficiencies can be obtained in the USDOT Training Manual 70(4), AASHTO Manual for Bridge Maintenance (5) and other publications.

CHAPTER III

REHABILITATION PROCEDURES

The process of rehabilitating a deficient bridge can vary extensively depending on the degree and the severity of the problems needing correction. The work can include a deck replacement and minor repair or can be an involved procedure including strengthening of critical members, correcting settlement problems, replacing bearings and others.

For bridges of the types discussed in this paper, rehabilitation procedures are included in six general categories:

1. Increase live load carrying capacity
2. Improve geometrics
3. Correct mechanical deficiencies
4. Correct drainage problems
5. Improve rideability
6. Miscellaneous repairs

Increase Live Load Carrying Capacity

There are many ways in which the live load carrying capacity of a bridge can be increased. These can be divided into four general categories. First, strengthen critical members by adding additional material to the member itself or replace with a new member; second, add supplemental supports or members to assist in carrying loads; third, reduce the dead load on the bridge and thereby provide additional capacity for live loads; and fourth, change the structural system in a manner that will provide additional live load capacity.

Strengthen Critical Members

The routine procedures for strengthening steel bridges followed by most agencies is to add cover plates to steel beams or girders or to add plates to steel truss members to increase the available section. Many of these details have been developed utilizing welding to attach the new material. In some cases, the welding operation on the existing steel, because of the location and the particular detail employed has had an adverse effect on the structural capacity of the member. Stress raisers that are susceptible to fatigue failures have unwittingly been incorporated in the structure through lack of attention to detail or to state-of-the-art knowledge of welding procedures.

Material can be added successfully by welding to existing primary members providing that the design and details are developed in accordance

with current specifications, including those dealing with fatigue characteristics. (6) The other obvious requirement is the weldability of the material used in the existing member.

Concrete Members. Reinforced concrete primary members pose a different problem. Designs have been successfully developed wherein external steel reinforcing is attached to the member by connections utilizing bolts extending through the member (see Figure 1). Reinforcing can be post tensioned as necessary.

Figure 1. External Concrete Reinforcing

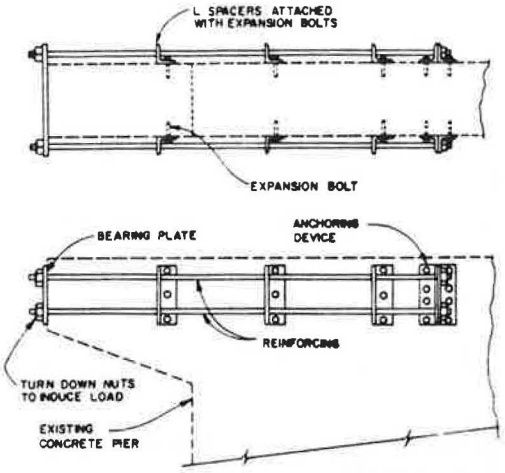

Other designs have been developed for post-tensioning concrete girders, anchoring the tendons with attachments at the bearings. The tensioning strands are then placed in a concrete section added to the beams or are confined in a protective metal conduit which is left exposed.

A method has been developed and implemented in England and in South Africa for strengthening concrete beams by adding steel plates that are "glued" to the concrete.(7) This has proven to be a very simple and effective method. Plates are added to the underside of simply supported concrete beams to increase flexural capacity and to the sides of the beams near the bearings, to increase shear capacity.

Provide Supplemental Members

Adding additional members is a technique used routinely in strengthening bridges. Structurally inadequate floor systems on truss and girder bridges can be rehabilitated by erecting additional members between the existing stringers to provide necessary overall capacity. On girder bridges, additional floor beams can be added to provide added strength.

Concrete beam and girder bridges can be strengthened by adding steel beams or precast concrete beams between or adjacent to the existing concrete sections. Timber bridges likewise can be strengthened by adding additional primary steel members.

Critical members that are defective can be replaced. This is frequently done in situations where collision damage to a key member has weakened the bridge. End posts of through or pony type trusses are recurring examples. Concrete or steel fascia stringers in overpass structures are often damaged by oversized vehicles and must be replaced.

Truss member replacement requires careful analysis and development of step-by-step procedures. Shoring must be developed to insure the integrity of the structure during the replacement operation. If this is not feasible then an alternate support system must be developed utilizing post-tensioned cables or other such devices to carry temporary loads.

Adding new stringer or floor beam members will often require the removal and replacement of at least a portion of the bridge deck. Procedures have been developed, however, to eliminate the need to remove any of the bridge deck. These procedures utilize supplemental supports jacked into place from below the structure. By drilling through the deck and pressure grouting, any void that exists between the top of the supplemental support and the underside of the deck can be filled. Lifting cables threaded through the same holes drilled through the deck can also be utilized for lifting the supplemental supports into place.

The addition of crutch bents and/or pony bents to pick up the load of a defective pile or pile bent is commonly used and is an effective rehabilitation technique. Likewise, the addition of supplemental cap beams laced to the existing cap beam provides an efficient means of strengthening a deteriorated bent. The transfer of load from the strengthened member to the vertical supports must be carefully considered and proper details developed.

Reduce Dead Load

Dead load reduction can most easily be effected by removing the existing deck and providing a lighter weight substitute. In some instances, removal of asphalt wearing surface buildup can provide significant reduction in dead loads.

A number of deck systems have been developed to provide a lightweight yet structurally adequate system. The most familiar of these are:

1. Open steel grid deck.
2. Concrete filled steel grid.
3. Corrugated metal with asphalt wearing surface.
4. Laminated timber with asphalt wearing surface.
5. Metal plate (Orthotropic) with asphalt wearing surface.

Improvement Factor. Employing each of these concepts,(8) flexural requirements were determined for a 15 m (50 feet) and a 27 m (90 feet) simple span using stringers spaced at 2.1 m (7 feet) center to center. Requirements for a comparable span and stringer spacing using a conventionally reinforced concrete deck were also made. A comparison of these two values provides an indication of the merits of each concept. This comparison figure is termed the "Span Improvement Factor." A graphical presentation of these values is shown in Figure 2.

It should be noted that the requirements calculated reflect not only a change in dead load associated with each concept, but also a change in live load distribution developed in accordance with AASHTO specifications. The combined effect can produce a negative factor as evidenced by the shorter spans utilizing a laminated timber deck. Also an increase in live load stress due to distribution factor changes can also cause changes in stress range effecting the fatigue life of the member. This is not considered in the development of the improvement factor.

Figure 2. Span-Improvement Factor. Dead Load Reduction Systems.

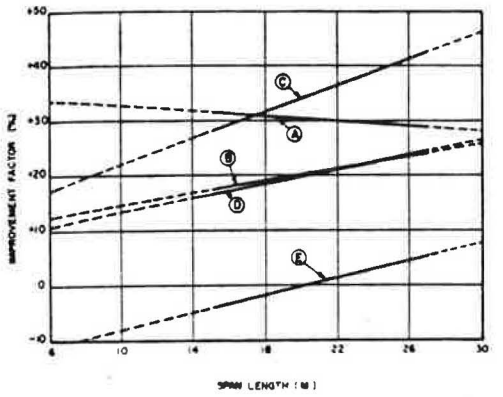

COST PER SQ. M.	
A	$ 410
B	$ 270
C	$ 290
D	$ 310
E	$ 310

CONVERSION FACTOR 1M = 3.28FT

A. STEEL PLATE W/ASPHALT WEARING SURFACE SUPPLEMENTAL DECK SUPPORT SYSTEM.
B. CORRUGATED METAL W/ASPHALT WEARING SURFACE SUPPLEMENTAL DECK SUPPORT SYSTEM.
C. OPEN STEEL GRID.
D. CONCRETE FILLED STEEL GRID.
E. LAMINATED TIMBER

NOTE: DASHED LINES REPRESENT EXTRAPOLATED VALUES OF THE CURVES

Cost Effectiveness Factor. By dividing the improvement factor by the estimated cost per square foot (shown in Figure 2 for the Washington, D. C. area) a "Cost Effectiveness Factor" can be determined. The higher the value of this factor the greater the cost effectiveness for a given situation. For example, comparing the cost effectiveness of modifying a 25 m (82 feet) span by utilizing either an open grid deck or a corrugated metal deck with an asphalt wearing surface, indicates that the open grid deck provides a factor of 0.138 (40 ÷ 290) and the corrugated metal deck provides 0.085(23 ÷ 270). Therefore, the open grid deck will provide the most cost effective technique.

Each of the concepts for which data was developed have other factors that must be considered in addition to initial cost. These include both maintenance and operational considerations.

Steel Grid. The open grid flooring can become slippery when wet or ice-covered. Serrated top bars or welded studs can significantly reduce this problem. The open grid has the advantage of permitting snow and rain to pass through the structure, thereby eliminating the need for bridge drainage and the use of snow and ice control chemicals on the bridge. Details should be developed that eliminate pockets over the main support members that will collect debris and cause corrosion in these members. Care should also be taken in selecting the proper grating design. Welded details often fail due to impact and fatigue. Riveted grates can provide a more reliable deck.

Concrete filled floor grating has the advantage of improving skid resistance and reducing the impact and fatigue failures in the internal connections. The disadvantage is the added weight as compared to the open grid and subsequent reduction in live load capacity of the bridge. Also, it is necessary to provide and maintain an adequate deck drainage system and to employ chemicals for snow and ice control.

Corrugated Metal. The use of corrugated metal plate deck with an asphalt wearing surface is a recent development. Installations have shown that the system can be designed to withstand modern design loading. Length of service can be increased by properly designing the drainage system to remove surface runoff and by providing adequate protection for the metal sheets against corrosion.

When replacing a concrete deck with this system, it will usually be necessary to add lightweight supplemental support beams between the existing stringers in order to reduce the effective deck span. On multiple stringer bridges, these can be framed to floor beams placed between existing stringers or to existing diaphrams. On truss bridges and other structures with similar floor systems, these beams can be framed to existing floor beams. The "Improvement Factor" curve developed in Figure 2 is based on framing the supplemental stringers to new floor beams spanning between existing stringers.

Timber. Laminated timber bridge decking is also a relatively new concept. This provides some reduction in dead load but live load distribution factors increase resulting in little or no betterment for the shorter spans. It does provide advantages from a maintenance point of view since it is less susceptible to chemicals used in snow and ice control. It is important to provide details for fastening the panels to stringer supports that will not be conducive to insect infestation and resulting deterioration. The joint between panels must also be carefully detailed to provide shear transfer and to provide a proper seal. Clamping devices that do not require drilling or nailing are preferred to drilling and bolting.

Metal Decking. Steel plate decking as a replacement for deteriorated concrete provides significant weight reduction. This can also provide additional carrying capacity for the primary members if properly designed. Ribs or supplemental lightweight flooring must be included with the decking to provide adequate roadway support. Adhesion between the steel plate and asphalt wearing surface is a potential maintenance problem, but through careful attention to specifications and with proper construction techniques, this problem can be greatly reduced.

Modify Structural System

The structural system in a bridge can be modified in a number of ways to provide additional capacity to support live loads. Three such concepts are composite action, beam continuity and kingpost truss.

For each of these concepts, "Improvement Factor" curves have been developed in a manner similar to that already described for procedures used to reduce dead load. Cost factors have also been developed and are included with the "Improvement Factor curves in Figure 3.

Composite Action. This procedure changes an existing steel beam or girder system to a composite system so that the steel support and the concrete slab act together in resisting live loads. Composite action is provided through suitable shear connection between the beam and concrete slab. The most practical device used to accomplish this is the welded stud.

The rehabilitation procedure includes removing the deteriorated concrete deck, welding shear connectors to the top flanges of the steel beam, and casting a new deck slab. In situations where the

Figure 3. Span-Improvement Factor. Structural Modification Systems.

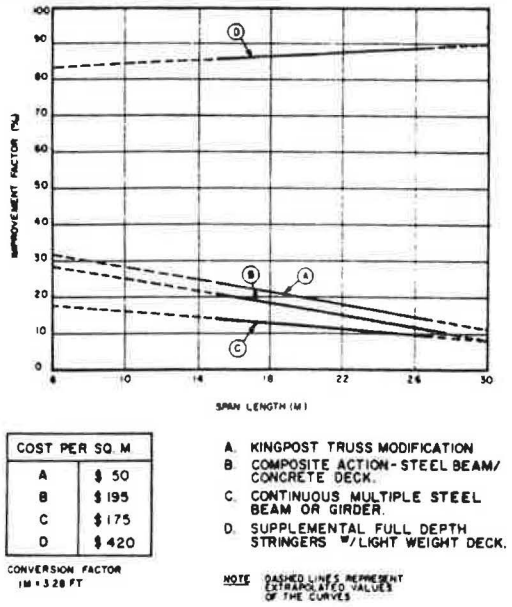

COST PER SQ. M	
A	$ 50
B	$ 195
C	$ 175
D	$ 420

CONVERSION FACTOR 1M = 3.28 FT

A. KINGPOST TRUSS MODIFICATION
B. COMPOSITE ACTION-STEEL BEAM/ CONCRETE DECK.
C. CONTINUOUS MULTIPLE STEEL BEAM OR GIRDER.
D. SUPPLEMENTAL FULL DEPTH STRINGERS W/LIGHT WEIGHT DECK.

NOTE DASHED LINES REPRESENT EXTRAPOLATED VALUES OF THE CURVES

deck slab is sound and does not have to be replaced, holes can be drilled through the slab from the roadway to the steel support for welding the studs. Epoxy grout is then placed in the void between the slab and the stud. Another process now in the experimental stage, provides shear resistance by pressure injecting epoxy adhesive into the void between the steel flange and the underside of the concrete slab.(9) This is injected through drilled holes in the deck. Early test data indicates that this can become an effective and economical method for developing shear resistance. Construction specifications and testing procedures must be further developed, however, before this method can be used with the necessary reliability.

Steel Beam Continuity. This procedure is employed to change a series of simple steel beam spans to a continuous system. Through the interaction between spans, additional load-carrying capacity can be obtained.

The procedure utilized in this modification includes first, the removing of a portion of the deck and the deck joint over the pier. Next, a splice is installed between the adjacent beams. The existing bearings are removed and a single bearing is installed. Bearing stiffeners are added as necessary. The deck slab is then replaced, completing the installation. A conceptual detail of this is shown in Figure 4.

In addition to providing greater live load capacity and reducing live load deflections, this system also reduces future maintenance requirements since it eliminates a roadway joint and one set of bearings, both of which cause constant maintenance problems.

Kingpost Truss. In situations where underclearance permits, the modification of either a stringer or a floor beam to a kingpost truss (trussed-beam) system provides an excellent means to increase live load capacity. The procedure requires the installation of a "kingpost" truss to the bottom flange of the member. Threaded end connections are provided so that proper tension can be induced into the system. A conceptual detail of this is shown in Figure 5.

Figure 4. Conceptual Details. Simple Span Steel Beam to Continuous

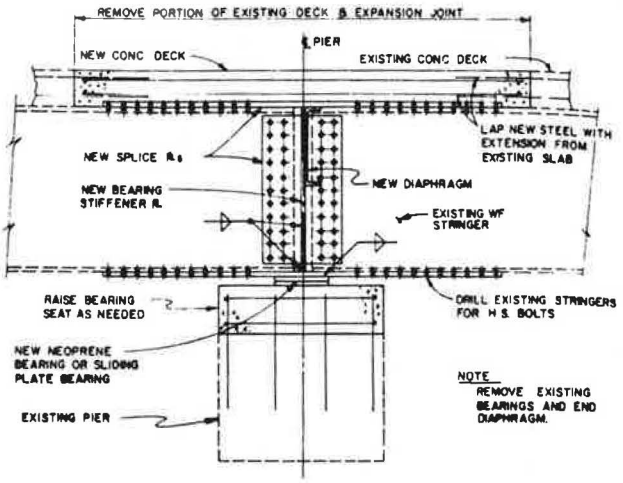

Figure 5. Kingpost Truss Beam Reinforcement.

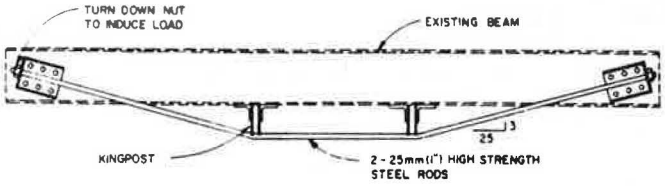

The "Improvement Factor" surve as shown in Figure 3 is based on a single post system with a 3:25 bevel on the struts. Struts are stressed to 11.2 kN (25 kips). This predetermined force must be induced in the system by tightening at the end connections. The installation must be carefully monitored by measuring the number of turns as well as resulting deflections in the original member. Other geometric configurations and induced loads will produce different "Improvement Factors."

Improve Geometrics

Rehabilitating a deficient bridge to improve geometrics includes increasing vertical clearance, widening usable roadway and improving approach horizontal and vertical alignment.

Vertical Clearance

Inadequate vertical clearance is a common geometric deficiency found in through truss type bridges. Additional clearance can be provided by reducing the depth of portal and sway frames. The resulting bracing system must be properly designed to transmit imposed loads.

In certain cases it may be possible to lower the floor system on through truss bridges and thereby increase vertical clearance. Where stringers ride over floor beams the roadway can be lowered by

framing the stringers into the floor beams, keeping the top of the stringers and the top of the floor beam in the same plane. Another possibility is to lower the floor beam connection to the truss itself thereby increasing vertical clearance.

As discussed under structural rehabilitation techniques, it is often desirable to replace an existing concrete deck with a lighter roadway support system to increase live load capacity. In most instances on through truss type bridges this will also provide additional vertical clearance due to the thinner deck system.

Improved vertical clearance on grade-separation structures can be most economically achieved by lowering the bottom roadway providing this can be done without undermining or otherwise jeopardizing pier or abutment footings. It is possible, although usually more costly, to raise the superstructure and adjust the vertical alignment of the overpass roadway. This requires adding to the height of the abutments and piers. These elements must be carefully analyzed to insure that they are capable of absorbing the increased loads imposed by the added height. If not adequate, structural modifications must be included with the rehabilitation plans.

Roadway Widening

On multiple girder or multiple beam bridges of either concrete or steel construction, it is a straightforward and fairly routine process to widen the roadway. Parapets and sidewalks must be removed, piers and abutments extended, new stringers added and a new deck and curb installed. Control of traffic during construction of the new deck is necessary to insure that excessive deflection and vibration from heavy vehicles are controlled.

Through systems are more difficult to widen. Short of removing the entire superstructure and replacing with a new one, it is impracticable to consider widening a through truss and in most instances a pony truss. Providing site conditions will permit adjustments in grade of several feet, it can be practical to widen a through girder bridge by moving the floor system to the top flange of the girder and constructing a wider deck. The main girders may require strengthening. However, this can be minimized by utilizing a lightweight deck in conjunction with the rehabilitation. A conceptual cross section of this is shown in Figure 6.

Correct Mechanical Deficiencies

These repairs are those associated with bridge bearings, expansion joints, hangers, wind tongues, and similar devices that permit the structure to expand and contract. Such devices often freeze as a result of corrosion thereby losing all capability of reacting to movement. The usual rehabilitation technique is to replace the defective item or to clean the existing device and adjust it to the proper position. Vertical and longitudinal jacking of the superstructure is an integral part of this work. With careful planning, this work can be done without traffic interruption.

In situations where pavement shove, rotation of supports or other movements have caused the expansion devices to become jammed, it may be necessary to rebuild the abutment backwall or to remove a portion of the longitudinal member adjacent to the backwall in order to provide sufficient gap for movement.

Figure 6. Conceptual Details. Thru Girder Deck Widening.

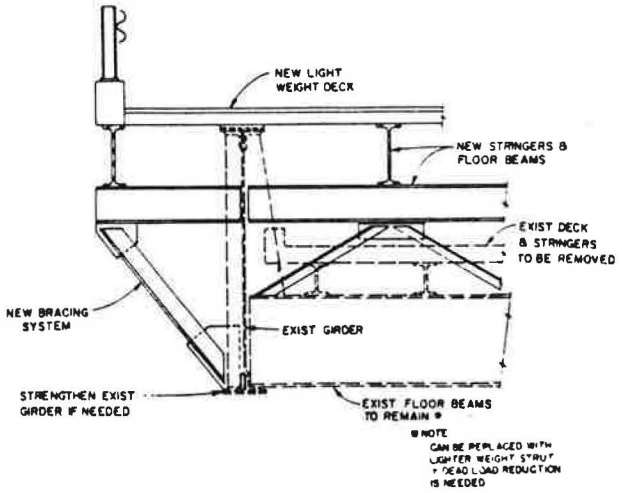

Replacement of roadway expansion joints is often required when rehabilitating the structure to correct mechanical deficiencies. Replacement joints should be watertight if possible. When open joints must be used, provision for drainage collection should be included to prevent pavement wash from reaching bearings or hangers beneath the joint. Scuppers located as close as practical to the open joint with drainage troughs under the joint provide an effective method for controlling runoff in these areas. The steel components of replacement joints should be galvanized or constructed of weathering steel to control corrosion.

Correct Drainage Problems

An ineffective bridge deck drainage system is a major cause of bridge deterioration. Rehabilitation should include replacement with an adequate drainage system. Special attention should be given to details that will prevent deck wash from reaching bearings, superstructure members, piers, and abutments. Scuppers must be properly spaced and should be large enough to minimize clogging from roadway deposits. Proper provision must be included for maintenance cleaning of downspouts and collection pipes. Discharge points should be detailed to prevent erosion. Consideration should be given to galvanizing all parts of the drainage system or using weathering steel.

Improve Safety and Rideability

Safety

Replacement of inadequate bridge railing, alteration of parapet and railing ends where these face oncoming traffic, protection with attenuators at ends of through girders or through trusses, in gore areas on structures, or in front of piers within the recovery zone (9 m, 30 feet from pavement edge) are all measures that should be considered in bridge rehabilitation plans.

Adequate protection for pedestrian traffic should also be provided. Redirectional barriers provided between the sidewalk or bikeway and the roadway can be effective in providing safety for pedestrians as well as for vehicles.

Approach roadway alignment improvements can have substantial impact on improving safety at the bridge site. This is often more difficult to achieve due to right-of-way requirements and other local restrictions than from an engineering standpoint.

Rideability

Bridge rehabilitation to improve riding quality includes repairs to approach roadway for settlement and to the bridge deck. Deck repairs vary from full deck replacement to patching of isolated areas. Deck replacement should include adequate protection of reinforcing steel to prevent corrosion and subsequent concrete deterioration. State-of-the-art indicates that this can best be provided by coating the rebars with an epoxy sealant or by constructing a high density concrete overlay on the structural slab. Cathodic protection systems are under development and appear to be promising.

On existing decks that require repair but not replacement, the rehabilitation should include a sealing system which will prevent or at least reduce the further buildup of chlorides in the deck. A procedure to reduce the chloride content in the existing deck should be considered with the rehabilitation program.

Miscellaneous Repairs

Many other repair techniques are available to correct deficiencies in bridge components but have not been discussed in this paper. These include cosmetic repairs as well as repairs needed to increase capacity and improve the structural integrity of the bridge.

CHAPTER IV

SUMMARY

The results of research and practical experience in the bridge maintenance area have shown that bridge rehabilitation can be done in a cost effective manner. When proper attention is given to current rehabilitation practices, additional years of service can be obtained from existing structures.

Current techniques employed to renovate deficient bridges include increasing the live load capacity of the bridge by decreasing the dead load, strengthening critical members, providing supplemental members and modifying the original structural system. In addition, substructure stabilization, proper cleaning of bearing and roadway joints, improved geometrics and safety improvements such as new or modified bridge railing systems have also played a significant role in improving the serviceability and extending the life of existing structures.

While each bridge rehabilitation project has unique features, there are general concepts that can be compared and evaluated to determine the most practical technique to be used. Because of these unique features, there is always a need for creative thinking and the development of innovative procedures in bridge rehabilitation projects. New products and techniques are constantly being developed that provide more efficient and longer lasting repairs to be made.

The deficiencies outlined and discussed in this paper include many that are encountered in fixed spans ranging in length from short to medium. The discussion of rehabilitation procedures has covered many of these deficiencies, although in many instances has been cursory and conceptual only. The ideas and suggestions as presented are intended to provide the basis for further development for application to a specific situation.

As we are in a time period where many bridge departments have little maintenance money and must make the most of what they have, we should, through creative engineering, utilize our talents to the utmost to attack our nationwide bridge problems. The concepts for increasing the load carrying capacity presented herein are a start. However, much additional work needs to be done. More research is needed and new rehabilitation concepts must be developed. We must do our homework thoroughly in order to eventually resolve our current bridge crisis.

REFERENCES

1. Seventh Annual Report to Congress, Federal Highway Administration, 1977.
2. Berger, R. H. "Extending the Service Life of Existing Bridges by Increasing Their Load Carrying Capacity." FHWA Research Report, 1978.
3. "Bridges on Secondary Highways and Local Roads-Rehabilitation and Replacement." Virginia Highway and Transportation Research Council. NCHRP 20-5. Not complete.
4. "Bridge Inspector's Training Manual 70." U.S. Department of Transportation, Federal Highway Administration, Bureau of Public Roads, 1971.
5. "AASHTO Manual for Bridge Maintenance." American Association of State Highway and Transportation Officials, 1976.
6. Fisher, John W. "Bridge Fatigue Guide, Design and Details." American Institute of Steel Construction, 1977.
7. Sommerard, T. "Swanley's Steel-Plate Patchup." New Civil Engineer, June 16, 1977, London.
8. "Standard Specifications for Highway Bridges," Twelfth Edition. American Association of State Highway Officials, 1977.
9. Kahn, Larry. "Strengthening of Existing Bridges by Epoxy Injection." School of Civil Engineering, Georgia Institute of Technology.

BRIDGE TYPE AND DEFICIENCY CATALOGUE

SUPERSTRUCTURE

I. PRIMARY SUPPORT SYSTEM

A. Steel

1. Multiple Beam or Girder (Simple or Continuous Span).

   Paint deterioration
   Flange and/or web corrosion
   Bearings inoperable
   Collision damage fascia stringers
   Stiffener and other detail corrosion
   Brittle fracture.

2. Thru Girder or Twin Deck Girder (Simple or Continuous Span).

   Paint Deterioration
   Flange and/or web corrosion
   Bearings inoperable
   Connections, stiffener and miscellaneous detail corrosion
   Bracing member corrosion and damage
   Collision damage - Girder, kneebraces

3. Deck Truss, Thru Truss, Pony Truss (Simple Span).
   - Paint deterioration
   - Flange and/or web corrosion - Stringers and floor beams
   - Bearings inoperable
   - Truss member corrosion.
   - Collision damage - Portal, truss member, sway frame
   - Bracing member corrosion, failure
   - Connection corrosion
   - Inadequate design

B. Concrete
1. Slab (Simple or Continuous Span).
   - Surface delamination
   - Surface spall--Rebar exposure and corrosion.

2. Multiple Beam and T Beam (Simple or Continuous Spans).
   - Web cracks
   - Surface spall - Rebar exposure and corrosion
   - Collision damage
   - Bearings inoperable

3. Prestressed or Post Tensioned Beams (Simple or Continuous Spans)
   - Surface spall - Tendon exposure
   - Web and Flange cracks
   - Bearings inoperable

C. Timber
1. Multiple Stringer (Simple or Continuous Spans).
   - Timber rot, surface weathering and splits
   - Bearings inoperable

II. DECKS
A. Reinforced Concrete
   - Wearing Surface Breakdown
   - Delamination
   - Surface Spall and Cracks
   - Joint Inoperable

B. Open Grid Steel
   - Connection Failure
   - Corrosion

C. Corrugated Metal
   - Wearing Surface Breakdown
   - Protective Coating Deterioration
   - Corrosion

D. Timber
   - Wearing Surface Breakdown
   - Weathering - splits, cracks and rot
   - Failure of Connections to Support Members

SUBSTRUCTURE

I. ABUTMENTS
A. Masonry
   - Mortar Deterioration
   - Bearing Seat Deterioration
   - Scour

B. Concrete, Stub/Spill Thru
   - Cracking and Surface Spall
   - Bearing Seat Deterioration
   - Settlement and/or Rotation
   - Back wall failure
   - Erosion - Scour

C. Concrete, Full Height
   - Cracking and Surface Spall
   - Bearing Seat Deterioration
   - Settlement and/or Rotation
   - Back wall failure
   - Erosion - Scour

D. Timber - Bulkhead
   - Decay - Rot
   - Insect infestation

II. PIERS
A. Reinforced Concrete - Hammerhead/Solid Wall
   - Cracks
   - Bearing seat deterioration
   - Pier nose deterioration
   - Settlement and/or tilting
   - Scour

B. Reinforced Concrete - Rigid Frame
   - Cap Bm. Spall - Rebar exposure and corrosion
   - Cracking in Cap
   - Bearing seat deterioration
   - Column Concrete deterioration
   - Settlement and/or tilting

C. Masonry
   - Mortar deterioration.
   - Erosion/scour

III. BENTS
A. Timber Piles and Cap
   - Pile Decay - Rot
   - Cap weathering - splits, cracks
   - Insect infestation - marine borers
   - Scour

B. Concrete Pile & Cap
   - Longitudinal Cracks in pile
   - Bearing seat deterioration
   - Pile spall - rebar exposure & corrosion
   - Cap spall - Rebar exposure and corrosion
   - Collision damage
   - Scour

C. Steel H Pile - Concrete Cap
   - Pile corrosion - Section loss
   - Cap Spall - rebar exposure and corrosion
   - Bearing seat deterioration
   - Scour

MISCELLANEOUS

A. Drainage
   - Inadequate deck drainage (Number and/or size of Scuppers).
   - Drainage discharge on primary members
   - Snow and Ice storage in contact with primary members
   - Leaking deck joints
   - Ground erosion at discharge point.

B. Geometrics
   - Inadequate roadway width
   - Inadequate vertical clearance
   - Approach alignment poor

C. Safety
   - Narrow roadway
   - Inadequate railing
   - Alignment - site distance
   - Roadway surface deterioration

SOME CONSIDERATIONS IN WIDENING AND REHABILITATION OF BRIDGES

M. H. Soto, Chief Bridge Engineer, Gannett Fleming Corddry and Carpenter, Inc.

Bridge rehabilitation, whether required for repairs, strengthening, or widening, requires an insight into unique structural problems. These problems are compounded if modifications must be accomplished while maintaining traffic and if modifications alter the structural characteristics of the existing structure. This paper deals with solutions employed on two widening and rehabilitation projects. Widening the Hackensack River Bridge on the New Jersey Turnpike required integrating the superstructure with the existing superstructure. Techniques of jacking the widening main members against the existing system, inducing compatible cambers and ensuring proper load distribution, are described. This paper describes foundation additions to main river piers which were integrated by temporarily leaving a gap between the foundations. This permitted elastic shortening of new piles under pier dead load, and prevented overloading the existing piles. A classic example of fatigue failure is illustrated. Welding of fills caused a geometrical notch at the toe of welds, producing a crack through the main members of brackets and floorbeams. Widening the I-83 bridge over the Susquehanna River in Harrisburg required an inspection which revealed rivet failures at bracket tie plates. These failures appear to correlate with findings by researchers at Lehigh University (1). Unfastening the bracket tie plates from the main girders is discussed as well as other design considerations resulting from unfastening tie plates near the girder supports.

Bridge rehabilitation, whether required for repairs, strengthening, or widening as part of a safety update program, provides an insight into unique structural problems---some quite unexpected. These problems are often compounded if modifications must be accomplished under traffic and more particularly if such modifications alter the characteristics of the existing structure. Quite apart from the ricochet effect of details when modifications are made to a member or members, there is much insight to be gained about how the various structures and their components actually function. Such matters as fatigue, corrosion, and joint details relate to an understanding of actual structural action. This paper addresses several design and construction features in the widening and rehabilitation of some conventional bridge structures.

In the widening or rehabilitation of a structure, certain obvious constraints will often dictate the overall plan, design scheme and construction methods. Alignment may be predicated on right of way, physical features or proximity of interchanges. The volume and type of traffic will materially affect the modification should it be necessary to maintain traffic on the structure. Run-arounds, detours, or temporary structures permit modifications without the inconvenience and hazards of traffic, but only under rare and fortunate circumstances are these devices found both feasible and cost effective.

Widening the Hackensack River Bridge

Widening the Hackensack River Bridge carrying the New Jersey Turnpike is an example of maintaining the center-line alignment and widening the structure symmetrically. See Figures 1 & 2.

Figure 1.

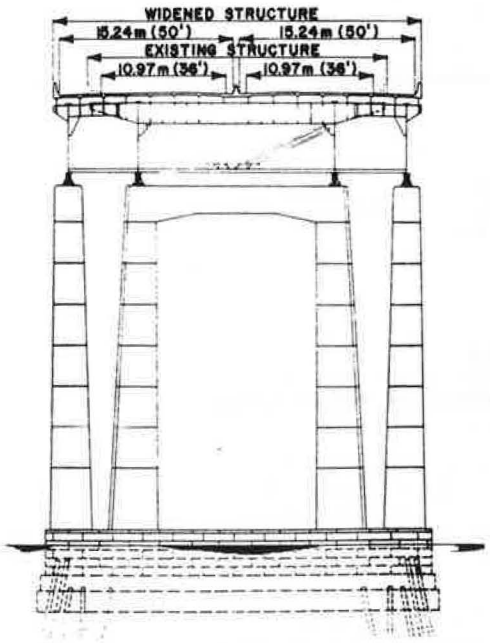

Figure 2.

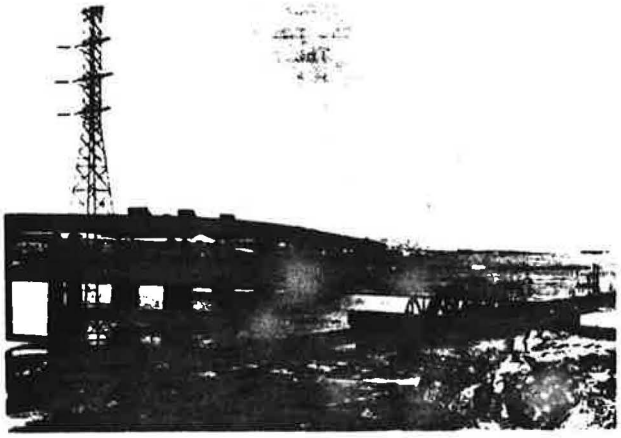

Figure 4.

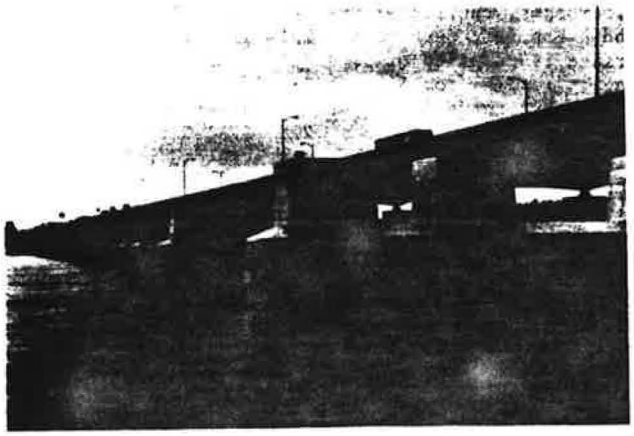

Widening the John Harris Bridge, which carries I-83 over the Susquehanna River in Harrisburg, PA, is an example of a realignment and widening all on one side. See Figures 3 & 4. These two widening schemes and their associated structural design considerations will be discussed.

The New Jersey Turnpike Authority's General Engineering Consultant (2) studied several schemes for the proposed symmetrical widening before selecting the adopted scheme. This scheme proposed new pier shafts constructed adjacent to the existing piers with new longitudinal steel welded girders paralleling the existing girders. Floorbeams between the new and existing girders were to be constructed by splicing a segment onto modified existing cantilever brackets. New cantilever brackets were proposed on the outside of the new main girders. These floorbeams and brackets would then support the additional stringers and extended concrete deck and barrier parapet. All new steel members were to be of welded construction using ASTM 588 weathering steel with high strength bolted field connections.

Figure 3.

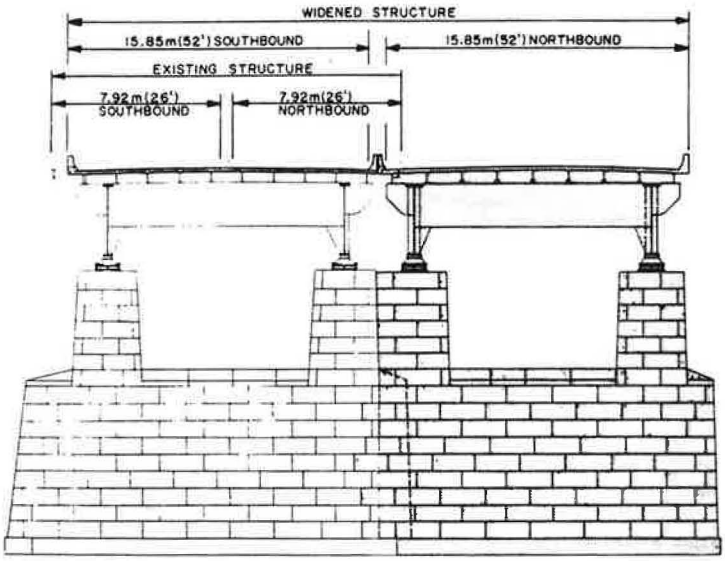

Given the structural scheme to be employed and the requirements for maintaining traffic, the superstructure design called for construction in two phases. The first phase consisted of modifying the median. The added width of roadway would later be very important when undertaking the shoulder widening. Space for temporary barriers and for the two lanes of traffic were at a premium. Moreover, of considerable importance was the lighting placed along the median when the outside lights were removed for the shoulder widening. The median lighting consisted of double bracket poles mounted at deck level and within the width of the median.

Structure Integration

For the shoulder widening, the integration of the new superstructure elements with the existing bridge required construction procedures that would insure the desired load distribution to both the new and existing main members.

The Hackensack River Bridge, constructed in 1951, is an all-riveted plate girder deck type bridge with floorbeams, cantilever brackets, a stringer system and a concrete deck slab. This 1707-m (5600-ft) bridge is composed of 35 simple approach spans varying in length from 32 m (105') to 52 m (170') and three continuous spans over the river measuring 68.6 m - 114.3 m - 68.6 m (225'-375'-225'). At the time of construction, this was a record main span for a plate girder bridge. The concrete deck provided a 11-m (36-ft) roadway curb to curb for each direction, thus accommodating two directional lanes of traffic with 3.66-m (12-ft) shoulder.

In 1956, the northern portion of the turnpike was converted to three lanes in each direction. The bridge was also converted to three lanes on the 11-m (36-ft) deck. Obviously, as traffic increased, there was no provision whatsoever for breakdowns, and the potential for a catastrophe was ever-present.

Figure 5.

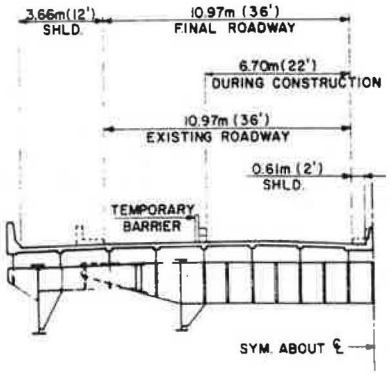

The 1971 widening program focused on providing a 3.66-m (12-ft) shoulder on the right and a 0.61-m (2-ft) additional space adjacent to the high speed lane by replacing the raised median with a New Jersey-type barrier. The primary constraint for construction was that two lanes of traffic in each direction were to be maintained at all times. (See Figure 5). Alternates A & B were proposed in the contract plans for integrating the new members with the existing structural system.

Under Alternate A, the plans called for preloading the new main girder by jacking against the new floorbeam to remove the dead load camber of the girder. The procedure called for a full strength splice between the new segment of floorbeam and the modified cantilever bracket. The floorbeam was to be erected in its final position with slotted guide holes for a temporary connection to the main girder. This temporary connection provided stability to the girder during erection and jacking. Once the girder was erected, the erector had merely to jack until the mating holes were in alignment. Figure 6 illustrates the magnitude of displacements at the center of the middle span of the three continuous spans. In this figure, (A) is the upward deflection of the existing main girder upon removal of steel and concrete beyond the adjacent stringer; (B) is the deflection of the new steel due to its dead load; (C) is the upward deflection of the floorbeam due to the jacking force [155688 N (17.5 tons);] (D) is the deflection of the new girder due to the jacking force; (E) is the upward deflection of the existing girder due to the jacking force. The summation of these equals the total dead load camber (F) of the new girder without increasing the loading on the existing girder.

Figure 6.

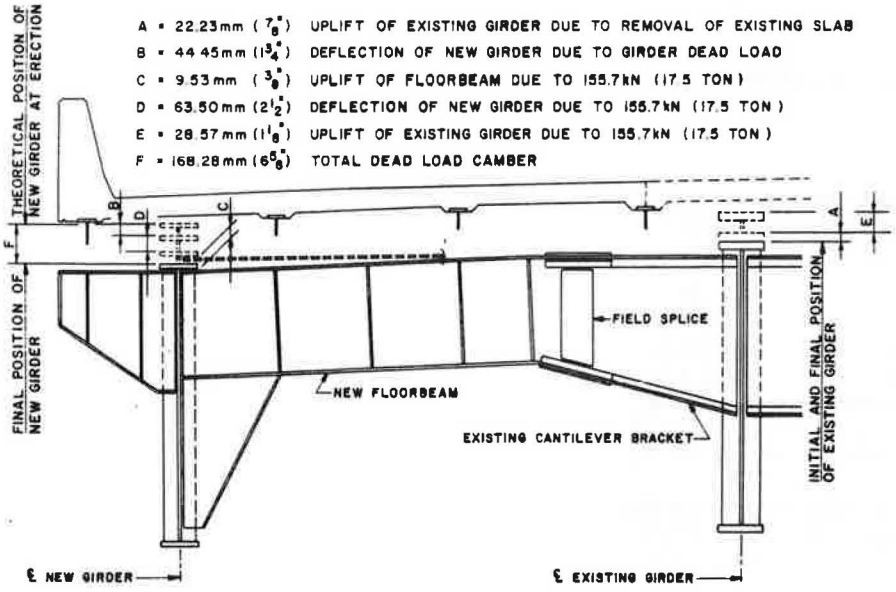

Under Alternate B, the plans called for placing a temporary pin at the splice between the new floorbeam segment and the modified existing bracket. (See Figure 7). In stage 1, the new girder and floorbeam are erected and the temporary pin connection is made. In the second stage, the stringers are erected and the deck slab and parapet are placed on the three outboard stringers, leaving a gap in the slab between the third and fourth stringers. This distributes the appropriate loading to the two girders. In stage three, the full section splice is completed and the last segment of slab is placed.

Figure 7.

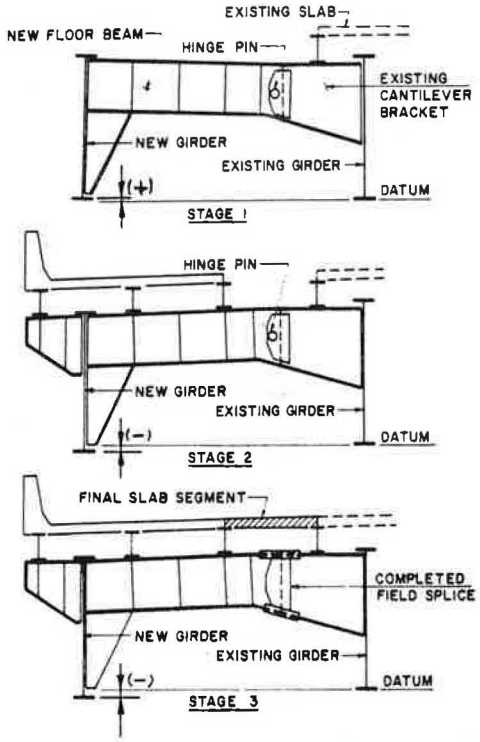

Alternate A has the advantage of having each trade complete its work at one time. In Alternate B, the ironworkers are interrupted and must return to complete the splice, erect diaphragms between the third and fourth stringers and erect the lateral bracing. Similarly, the concrete crew must return to form and place the last segment of slab.

The contract documents required the contractors to bid both alternates. The successful bidder bid Alternate A for less than Alternate B; thus Alternate A was employed. The contractor used a jacking set-up as shown on Figures 8 & 9. A simple yoke arrangement could have also been employed. This method of integrating a new member with an existing system, where proper distribution of load is essential, is not only simple, but direct and inexpensive.

Figure 8.

Figure 9.

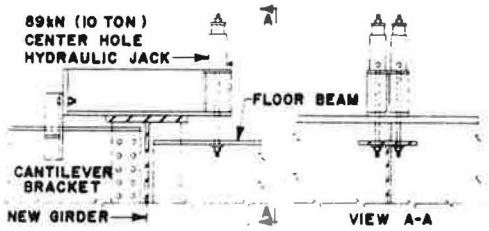

Fatigue Failures on the Hackensack Bridge

During the initial stages of construction, cracks were discovered in the top flange of the cantilever brackets. The cracks started from the toe of a continuous fillet weld between a fill plate and the flange angle, with the crack propagating through the outstanding leg of the angle. These cracks were, we believe, just beginning to occur. It was considered unlikely that they would have been missed in a recent bridge inspection or by the painters who had also recently painted the structure. (See Figures 10 & 11).

The cause of these cracks became readily apparent when it was discovered that for several of the approach spans, the fill plate between the flange and tie plate had been inadvertently welded for its full length along the sides by an 8-mm (5/16-inch) fillet weld instead of by intermittent welds as was intended. At other locations where the intermittent welds had been used, these had failed and the stress transfer from flange to tie plate was through the rivets as intended.

At the locations where the continuous weld was employed, the welds were probably carrying the total load. This was the tension flange and the stresses were not excessive, but the stress ranges induced in the welds were obviously high enough to initiate fatigue failure. Where failures had occurred, these were repaired with splice angles (Figure 12). At all other locations, the weld was removed and the material ground smooth. The

Figure 10.

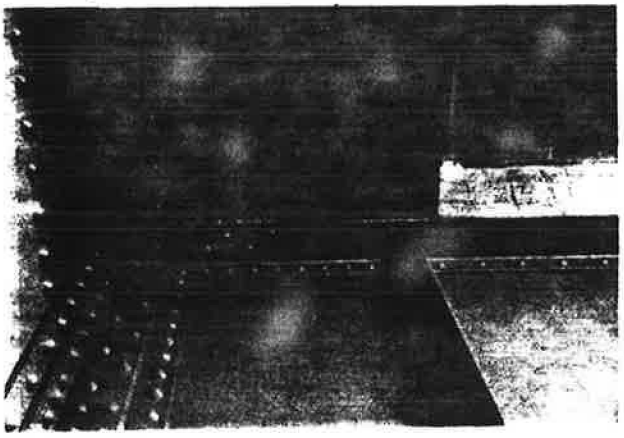

Figure 11.

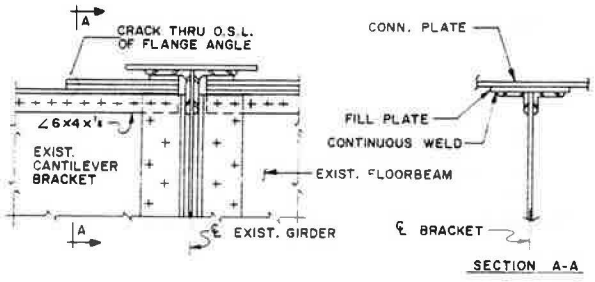

Figure 12.

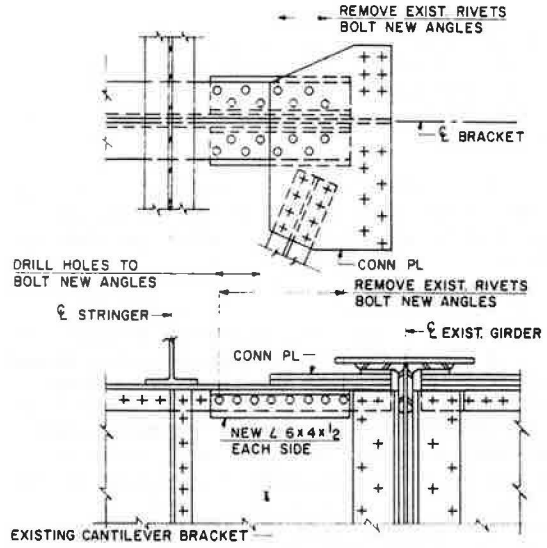

conversion of the cantilever bracket to a floorbeam materially reduced the tensile stresses at this location and no further remedies were considered.

Foundations for the Hackensack Bridge

Generally, all new pier shafts and foundations were constructed separately from the existing piers and foundations except for the river pier foundations. Because of space limitations and the desirability of a continuous footing, the new river pier foundations were integrated with the existing foundations. The existing pier was founded on 14 HP89 piles 15.25-m (50-ft) to 30.5-m (100-ft) long driven to rock. To preclude overloading the existing piles, the new foundations were constructed free of the existing footing, leaving a gap between the stems until the elastic shortening of the new piles induced by the DL of the new pier had occurred. (See Figures 13 & 14).

Figure 13.

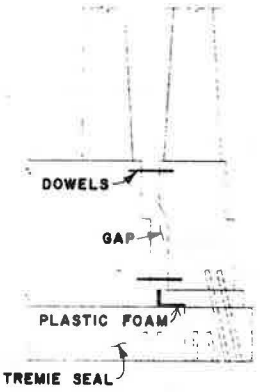

The bottom and face of the new footing where it overlapped the existing tremie seal was placed on a plastic foam to prevent a load transfer. Dowels were placed between the two footings; however, these would not offer much resistance in bending but were required for the final pier integration. When the pier shaft was completed, the gap was filled with concrete, forming a composite foundation to sustain the superstructure dead and live loads.

Figure 15 shows the completed widening.

John Harris Bridge (I-83) over the Susquehanna River

The Safety Update for the John Harris Memorial Bridge carrying Interstate 83 over the Susquehanna River at Harrisburg, Pennsylvania will convert the existing four-lane two-direction crossing to a three-lane plus shoulder southbound crossing. An all-new separated superstructure, roughly a twin to the existing one, will accommodate northbound traffic lanes and shoulders. See Figure 3.

Although this method of widening does not normally present many complex structural problems, there are features worthy of note in this type of structure.

The existing John Harris Memorial Bridge was constructed in 1959. It includes an all-riveted deck plate girder portion of 19 spans. Lengths are

Figure 14.

Figure 15.

1 @ 43.2 m, 17 @ 51.82 m, 1 @ 45.3 m (1 @ 141'-8", 17 @ 170'-0", 1 @ 148'-7") for a total length of 969.4 m (3,180' - 2 3/4"). Of these 19 spans, four of them include hangers at a one-sixth point. This permits the advantages of continuity with a reasonable limit on the expansion dam movements.

Steel in the girders is High Strength Low Alloy steel with a minimum yield point of 345 MPa (50 ksi). Steel in the floorbeams, stringers, and bracing is carbon steel with a minimum yield point of 228 MPa (33 ksi).

The main bridge has two girders spaced 12.8 m (42 feet) apart. The girders are 2440 m (8 feet) deep at the center of each 51.82 m (170-foot) span. A circular arc for the bottom flange results in a depth of 3660 mm (12 feet) at each intermediate pier. Girder flanges are 203 x 203-mm (8 x 8-in) angles with multiple covers 508 mm (20 inches) wide.

In the typical region of the main bridge, there are 10 stringers spaced 1700 mm (5'-7") apart, except 1625 mm (5'-4") for the center space. The first interior roadway stringers are located only 480 mm (1'-7") inboard from the girders. All the stringers are rolled shapes---W21x68 sections except for W18x50 fascias. Stringer splices are located at floorbeams.

The typical floorbeam is riveted member with a web plate 1725 mm (68 inches) deep at the bridge centerline. Flanges are 152 x 152-mm (6 x 6-in) angles with 355-mm (14-inch) cover plates. The floorbeams at all the intermediate piers have 2340-mm (92-inch) webs, 152 x 152-mm (6 x 6-in) flange angles and 355-mm (14-inch) cover plates. All floorbeams have kneebraces to the bottom flanges of the girders.

In the typical section of the main bridge, floorbeams are spaced 8.64 m (28'-4") apart. Each has cantilever brackets on each side of the bridge 3125 mm (10'-3") long. These brackets support exterior roadway stringers and fascia stringers. A strap-plate over the top of the girder---and attached to the girder---transmits top flange tension from the bracket to the floorbeam.

The typical tension strap is cut from a steel plate 13 mm (1/2 inch) by 406 mm (16") by 1725 mm (5'-8"). The connection to the top flange of the bracket uses 14 rivets; to the girder, 8 rivets; to the floorbeam, 14 rivets. Four of the latter group also pass through the bottom flange of the first interior roadway stringer.

Prior to designing the widening details for the existing bridge, an inspection of the structural metalwork was conducted. It revealed a large number of broken and loose rivets in the connection of the first stringer inboard from the girder where the stringer is attached to the strap plate for the floorbeam out-rigger bracket and to the floorbeam top flange. The failed rivets were most often found at the floorbeams directly over the piers and in diminishing numbers the farther from a pier. See Figure 16.

Figure 16.

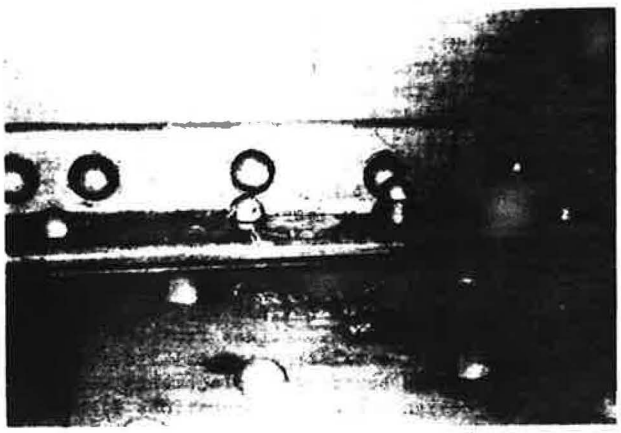

At the time of our inspection, we had been informed that several bridges in Pennsylvania had experienced floorbeam bracket tension strap plate cracking. We searched diligently for evidence of similar cracks, but found none. Our inspectors did find a number of defective rivets---predominantly in the stringer-to-strap-plate connection. The superstructure contains 117 floorbeams, so there are 234 strap plates and 936 rivets connecting stringers to strap plates. Of these, 124 were found loose or altogether missing. The failure rate---in excess of 13 percent---demanded an explanation and possibly remedial action.

The location of defective rivets was marked in the field on a set of 48 inspection sheets. A compilation revealed that the incidence of defective rivets favored the floorbeams directly over the piers, where approximately 40 percent of the defective rivets were found. Another 40 percent were found at the floorbeams immediately adjacent to the piers.

Severe rusting was observed at 29 locations on the line of the edge of the first interior roadway stringer, indicating relative motion with respect to the supporting strap plate. At 59 other such locations, light rust was observed. This makes a total of 88 out of 234 such locations, nearly 38 percent, at which evidence of distress existed. Floorbeams directly over piers had 32 percent of the rust locations. Another 40 percent were at floorbeams immediately adjacent to the piers.

Analytical and field studies of tie-plate stresses were conducted at about the time of these inspection findings. (3) Those studies resulted in a recommendation that designers should avoid connecting tie-plates to the girders, in bridges of this type. Our office, with the approval of PennDOT and FHWA, adopted that policy both for the new portion of the I-83 bridge and for modifications to the existing bridge.

The plans for modification require removal of the existing rivets connecting the tie plates to the girder top flanges. The rivets will be replaced with high strength bolts which will not pass through the tie plates. Omission of existing fill plates leaves room for the bolt heads in many locations, so the existing tie plates may be reused. Elsewhere, special tie plate narrow enough to fit between the bolt heads in the existing pattern, with a welded-on stem (upstanding) to preserve the tension area, will be installed. Special surface protection will be provided to avoid corrosion on the resulting unconnected faces or in the resulting narrow spaces. The feature of special surface protection will apply both to the modified existing bridge and to the new bridge with strap plates unconnected where they pass over girder flanges.

The design of the tie plates was carried one step further. It was recognized that there existed the possibility of out-of-plane flexure of the web of the floorbeam near its connection to the girder due to the relative longitudinal motion of the girder top flange and the deck system.

An analysis, using a finite element procedure and the program RIPL1 (4) was undertaken. The mathematical model consisted of 704 plate elements and 68 beam elements, with a finer mesh in the region of greater interest. It was representative of the geometry of the existing typical floorbeam connection. Imposed boundary displacements were based on HS20 design vehicles at locations likely to be repeated 2 million times or more and, therefore, deemed significant fatigue loadings.

From the voluminous results obtained, maximum principal stresses were determined. The contours for those stresses have been plotted and are shown on Figure 17. Near point A, the level is 57 MPa (8.2 ksi). By extrapolation, it has been determined that for an HS20 vehicle located in the left-hand passing lane, at the near girder to floorbeam connection, the floorbeam web distortion stress level would be 69 MPa (10.0 ksi) which is well below that tolerable for fatigue at 2,000,000 cycles. Similarly, an HS20 vehicle located in the right-hand traffic lane (not the shoulder) would cause a floorbeam web distortion stress at the exterior girder to floorbeam connection of 54 MPa (7.9 ksi) which is well below that considered tolerable for fatigue at "over 2,000,000 cycles".

Figure 17.

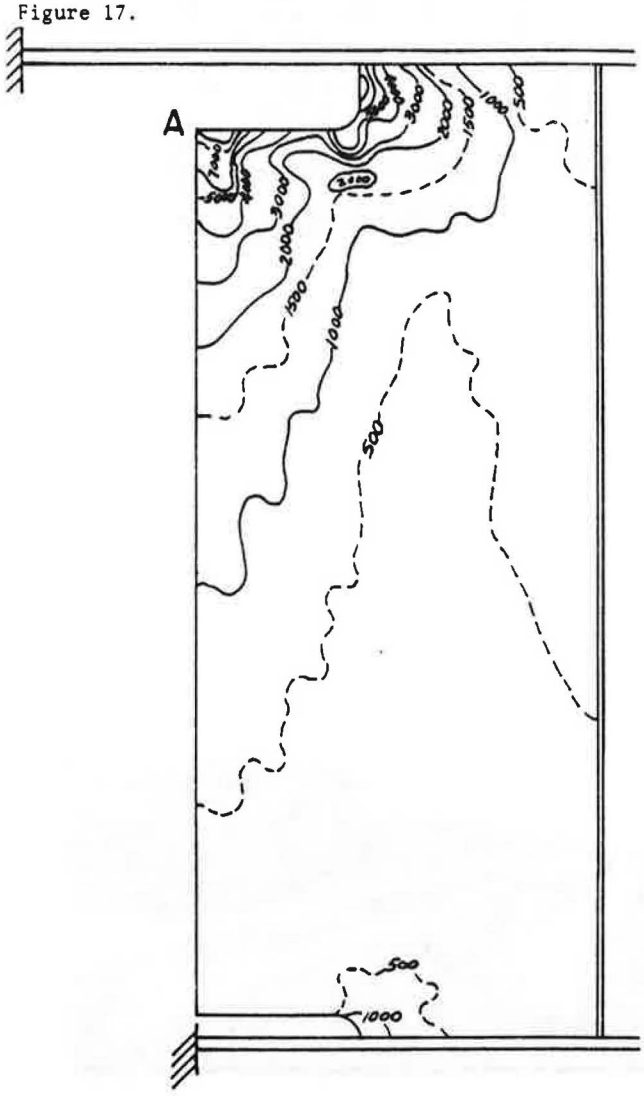

Stress is shown in Pounds per Square Inch

It was concluded that cyclical web stresses generated in the floorbeam associated with elimination of the connection of the strap plates to the girders are low enough to create no difficulty in fatigue. However, it was requested that the details for the new structure be such that the displacement-induced secondary stresses (5) in the floorbeam web will not exceed the "threshold" 28 MPa (4.0 ksi), a value identified for the Lehigh Canal Bridge.

To accomplish this reduction, a study was made, again using the finite element procedure, in which the depth of the cope which clears the girder flange was varied. Three cope depths were used: 114 mm (4.5 inches), 165 mm (6.5 inches), and 203 mm (8 inches). As a result of this study, the 114-mm (4.5-inch) cope was modified, which is the least that will accommodate the girder flanges, to 165 mm (6.5 inches). This change reduced the "gage location" stress level from 45.6 MPa (6.61 ksi) to 22.9 MPa (3.32 ksi) which is well below the limiting "threshold".

The existing bridge does not permit this solution in any practicable way. Hence, it has been proposed to omit connectors from the two top outer locations in the connection angle and to place substitute bolts elsewhere in the pattern. Subsequently, PennDOT decided to apply these modifications to the bracket side of the girder as well as to the floorbeam side. They have also proposed to monitor the strains that occur in the floorbeam and bracket connection plates to ensure that the modified structure performs as intended.

Table of Stresses at the "Gage Location", MPa

Location	Web Thickness	Code Depth, mm 114	165	203
Girder G-3 at Piers	9.5 mm	45.6	22.9	9.9
Girder G-3 at Int. Fl. Bms.	11.1 mm	38.3	19.2	8.3
Girder G-4 at Piers	4.5 mm	36.1	18.2	7.9
Girder G-4 at Int. Fl. Bms.	11.1 mm	30.5	15.3	6.6

Note: 1 MPa = 145 lbf/in^2 = 0.145 ksi

Summary

Two illustrations have been presented of widening similar and conventional structures. Widening of the Hackensack River Bridge, because of alignment constraints, required symmetrical widening and the integration of new structure with existing. This widening was accomplished under traffic and although this complicated construction. the methods of integrating the new elements were simple and effective. The widening of the John Harris Bridge (I-83 over the Susquehanna River, now under construction, is being accomplished by adjacent construction. This does not involve any superstructure interaction between new and existing, or the same degree of impact on traffic. Several structural problems and their solutions common to this type of structure, were identified.

Acknowledgements

Gannett Fleming Corddry and Carpenter, Inc. was the design engineer and performed Technical Inspection for the Hackensack River Bridge project for the New Jersey Turnpike Authority. Howard Needles Tammen and Bergendoff was the General Engineering Consultant to the Authority, as well as designer of the original structure.

Widening design of the John Harris Bridge was by Gannett Fleming Corddry and Carpenter, Inc. for the Pennsylvania Department of Transportation.

References

1. John W. Fisher, et al: Transportation Research Record 607, pp. 56-62.
2. Howard Needles Tammen and Bergendoff, also the Engineers for the original structure.
3. Fisher, Yen, Daniels. "Fatigue Damage in the Lehigh Canal Bridge from Displacement-Induced Secondary Stresses". Transportation Research Record 607, pp 56-62.
4. Developed by Sandia Corporation.
5. At the gage location corresponding to that of a strain gage used on the Lehigh Canal Bridge.

EXTENSION OF LIFE FOR PERLEY BRIDGE

H. Vaidyanathan, M.M. Dillon Limited, Consulting Engineers & Planners, Ottawa
M.S. Cheung, and J.C. Beauchamp, Public Works Canada

This paper describes a comprehensive evaluation procedure undertaken to decide the future of the 45-year old Perley Bridge, a multi-span, 696.16 m (2284 foot) steel structure, traversing the Ottawa River between Hawkesbury, Ontario and Grenville, Quebec. The bridge was originally designed for approximately H-15 live load and this was to be increased substantially. The bridge consists of an assortment of trestle, deck-truss, through-truss and bowstring-truss spans. The evaluation procedure included a number of phases, such as a review of past performance records and field inspections, theoretical analyses, field and laboratory tests etc. which resulted in recommendations for repairs and/or replacements of deficient members of the bridge. Each phase of the study is discussed in detail, in the hope that it might prove useful as a guide in the evaluation and upgrading of other existing bridge structures. Special attention is drawn to the need for field and laboratory tests to complement the theoretical analyses in assessing the validity of the original design assumptions and procedures in order to develop more realistic analytical models. The load factor design method was employed to assess the theoretical capacity of the bridge. Strengthening measures proposed would extend the life of the bridge at the current traffic level (up to 722.80 kN (162,500 pounds)), while allowing for increases in the future.

The Perley Interprovincial Bridge is a two lane high-level structure spanning the Ottawa River between Hawkesbury, Ontario and Grenville, Quebec. The only crossing from Ottawa to Montreal Island, it links Highway 148 in the Province of Quebec to Highways 17 and 34 in the Province of Ontario (Fig. 1a). Considerable industrial traffic uses the bridge, usually to and from the paper mill in Hawkesbury. A petition initiated by Sir George Perley, M.P., in 1909, first stressed the need for a road link across the Ottawa River at Hawkesbury. Though the design of Perley Bridge was done prior to 1919, the actual construction was completed in 1931.

History

Structural

From the scant records [1] it appears that the original structure remained untouched, except for some routine painting and minor alignment improvements to the approach roadway, until 1961, when the Carillon Dam development necessitated raising the structure to provide a navigational clearance of 12.802 m (42 feet). A section of about 548.64 m (1800 feet) was raised, to heights varying from 2.44 m (8 feet) to 3.05 m (10 feet), and a new through-truss replaced one of the original deck trusses for navigational purposes.

The steel superstructure, as it stands today, is 696.16 m (2,284 feet) long between abutments, and is made up of an assortment of 27 trestle spans, 5 deck-truss spans, 1 through-truss span and 1 bowstring-truss span (Fig. 1b). The deck is an exposed concrete slab, carrying a clear roadway with a width of 7.315 m (24 feet) between curbs, and a 1.524 m (5 feet) sidewalk on the west side only, resting on supporting steelwork with no shear connectors. The deck over the relatively new through-truss span (1961) is of corrugated metal planks tack welded to the supporting steel work and filled with asphalt to form the riding surface.

Most of the superstructure is of open-hearth steel and assembled together by power driven shop and field rivets. The substructure piers and pedestals are 20.648 MPa (3,000 psi) concrete founded on solid rock.

More than 300 contract, shop and erection drawings prepared during the period 1914-1961 were obtained from various sources, and from them it was determined that the structure was built according to C.E.S.A. standard A6-1929 [2,3,4,5]. The design live-load was specified as U-100 (4.79 kN/m^2 (100 psf) for spans up to 30.48 m (100 feet), dropping linearly to 3.822 kN/m^2 (80 psf) for spans 60.96 m (200 feet) and greater), or one 177.9 kN (20-ton) road roller or two H-15 trucks side-by-side. The through-truss span was

designed for two lanes of HS-20 loading in 1961.

Maintenance

Improvements to the south approaches were made in 1965-66 and the superstructure was painted in 1963 and 1972-73.

Performance

During the winter of 1972-73, a header angle (Fig. 2) on one of the south trestle spans failed, causing one corner of the span to fall several inches. Repairs were rapidly carried out and the structure was put back in service. This failure prompted serious considerations about the ability of the structure to carry modern traffic, and a program to assess the safety of the structure was begun in May 1973.

Figure 1a. Perley Bridge.

Investigation Program

A flow chart indicates the sequence of operations conducted under this investigation (Fig. 3).

The three main groups (apart from various individual specialists) involved in the safety assessment program were Public Works Canada, M.M. Dillon Ltd., Consulting Engineers, Ottawa and the Ministry of Transportation & Communications, Ontario. Each phase of activity undertaken by the various groups would form a chapter by itself, and hence it is suggested that reference be made to the individual reports of each of these groups [6, 7, 8, 9, 10 and 11].

The investigation program was conducted in several stages; field inspection (underwater, visual and non-destructive), collection of traffic data, theoretical estimates of the carrying capacity of the existing structure based on the 1970 and 1974 AASHTO manual for maintenance inspection of bridges [12, 13], field tests to supplement the theoretical work, laboratory tests to determine the various properties of materials in the structure and determination of the various strengthening measures needed to accommodate the more realistically observed Ontario loads [14, 15]. This paper briefly reviews the salient features of this program.

Program Description

Field Inspection

Underwater Inspection. The piers and foundations under water were inspected visually for major structural damage such as ice damage, cracking, scouring and shifting of foundations. Noted were small cracks or concrete honeycombing that might indicate causes for possible failure in the future. Depth soundings were taken at the four faces of each pier and the existing river bottom around the footings was inspected for erosion or undermining. Underwater photography was not required.

Generally, the substructure below the waterline appeared to be in good condition. The approximate velocity of the current varied from 0.5 m/sec to 3 m/sec (1 to 6 knots) and no cause for concern of erosion was noted. Minor damage in the form of cracks or honeycombed areas were observed.

Figure 1b. General arrangement (existing).

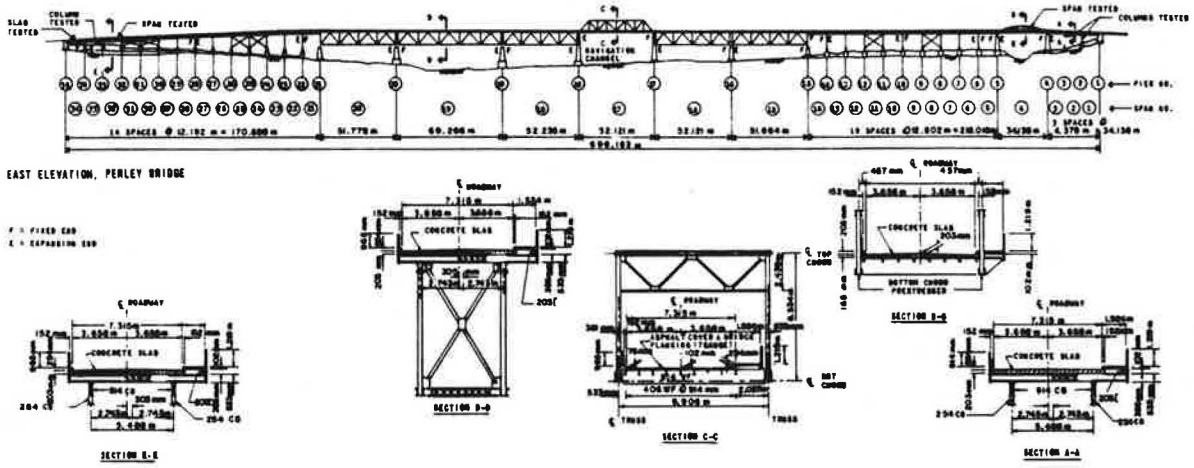

Figure 2. Header angle connection.

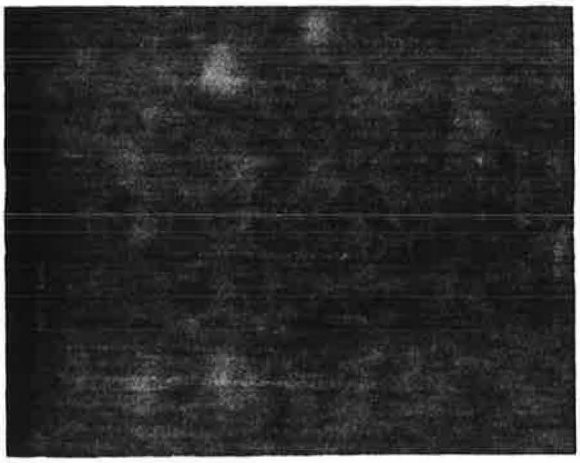

Figure 3. Perley Bridge investigation program (Flow Chart).

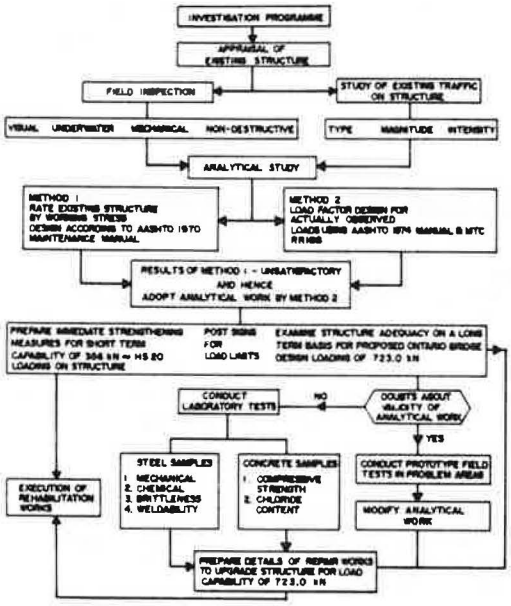

Above Water and Superstructure Inspection. A visual inspection of all members and connections in the steel superstructure was supplemented by mechanical testing and magnetic particle testing. In general, the following deficiencies were observed:

1. A visual inspection was carried out at all piers and abutments above water or ground level. Apart from some minor cracks, spalls and honeycombed areas, the substructure appeared generally sound (Fig. 4a).
2. Bearings varied from good to severely corroded or completely frozen (Fig. 4b).
3. Some header angles connecting girders to columns appeared to be undergoing possible fatigue problems. While no apparent evidence of surface cracking was observed, the heavy magnetic particle equipment detected possible fatigue problems at the top of the heel of some header angles.
4. Severe corrosion on floor beams was observed adjacent to the open expansion joints, and where curb drain holes discharged directly over floor beams. Some end floor beams appeared to have lost 50 per cent of their web thickness locally (Fig. 4c).
5. The steel decking of the relatively new through-truss was flexible, and as a result the asphalt surfacing had been deteriorating badly. Neither surfacing nor decking were watertight, and this caused corrosion of the decking and floor system.
6. Expansion joints in the various spans had not been functioning properly and they appeared to suffer from poor detailing, poor installation and bad corrosion (Fig. 4d).
7. Concrete deck and sidewalk, from a visual inspection and the chain-drag method, showed localized areas of spalling and delamination over 5 per cent of the deck. The spalls were mainly confined to the top of deck slab, but also occurred on the underside of the slab (Fig. 4e).
8. The railing generally appeared to be in poor to fair condition, and did not meet current traffic rail standards (Fig. 4f).
9. Clearance, speed limit and load limit signs were illegible, faint and badly weathered.

Traffic Study

It was considered prudent to obtain and collect information on the traffic using the bridge before settling down to any theorizing. Based on the traffic data gathered in 1972 and a series of one-hour and half-hour counts in October 1973, the SAWDT (Summer Average Weekday Traffic) was estimated to be about 11,000 to 12,000 vehicles per day, 20 to 30 per cent being trucks. Apart from logging trucks bound for the Canadian International Paper mill (C.I.P.), other heavy vehicles using the bridge included liquid and solid bulk carriers, floats with heavy earth-moving equipment, and flat-beds with loads of concrete blocks or concrete pipe (Figs. 5a, 5b). The following information was extracted from C.I.P. weight records in 1973 (Fig. 6).

Clearly, the bridge structure had been subjected to loads much heavier than those for which it was designed.

Theoretical Estimate of Structural Capacity - Analysis and Design

An elastic analysis with assumptions consistent with common practices according to existing standards [12, 13, 16] had been made as a first step in the evaluation procedure. These assumptions have been summarized below.

1. Deck slab continuous over transverse floor beams, considered non-deflecting.
2. Floor beams simply supported on longitudinal girders and act without any composite action from the deck slab. In estimating loads on floor beams, no wheel load distribution has been allowed for in the lateral direction, while in the longitudinal direction, distribution has been determined based on the deck slab acting as continuous span, all wheel loads being considered as point loads.
3. Longitudinal girders span between the trestle columns as simple spans. Note the absence of any connection between the flanges of girders and the columns.
4. Columns fixed in position and direction

Figure 4a. Local spall areas in pier.

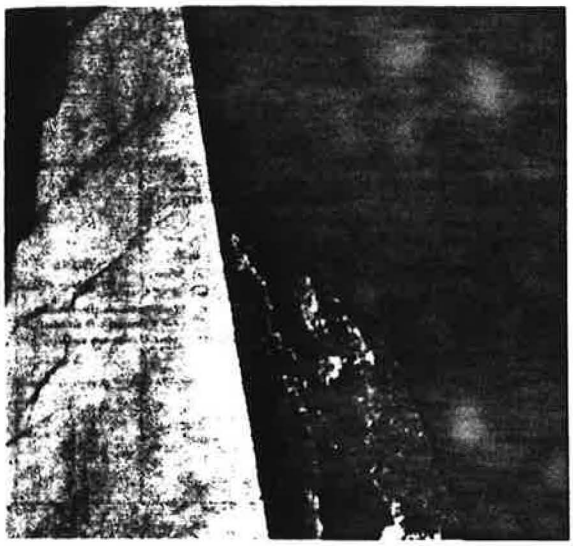

Figure 4b. Bearing assembly.

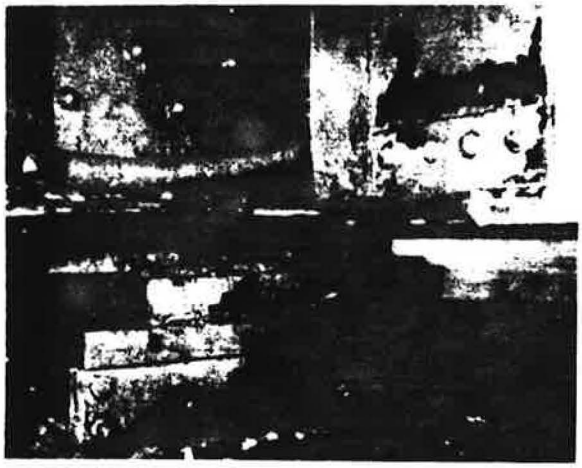

Figure 4c. Severe corrosion of floor beam.

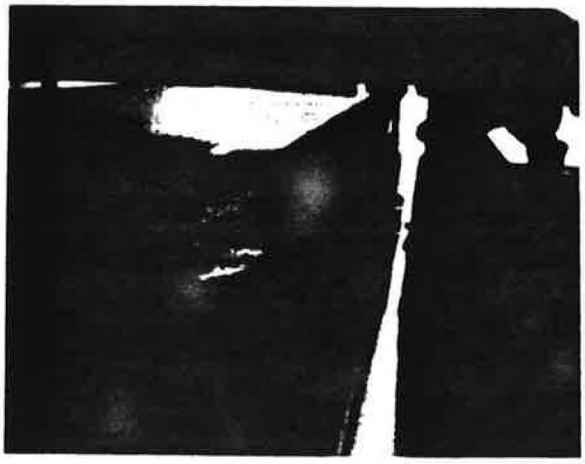

Figure 4d. A typical expansion joint.

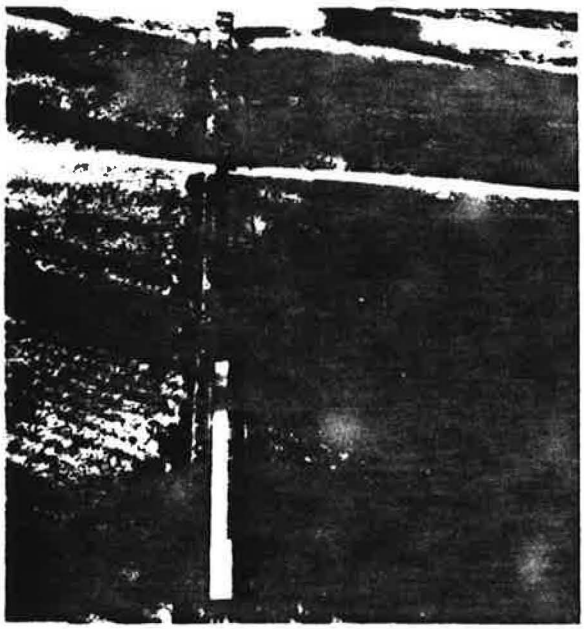

Figure 4e. Spall areas (underside of the deck)

Figure 4f. Inadequate railing.

Figure 5a. Floats with construction equipment.

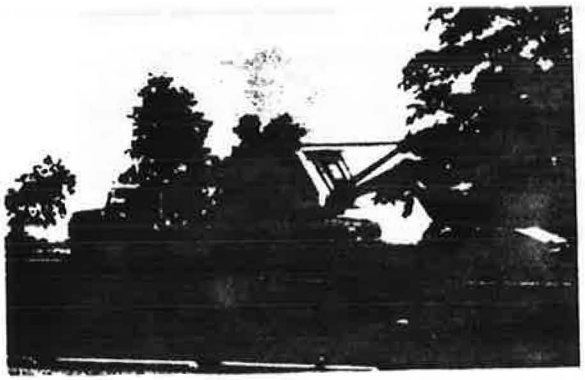

Figure 5b. Flat-beds with concrete blocks.

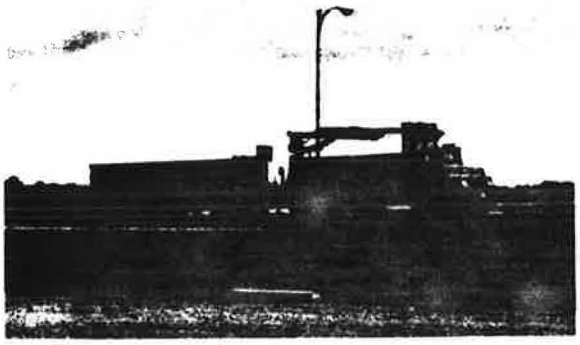

at the base, and held in position at the top by restraints provided by bracings in the longitudinal direction.

5. Trusses analysed as both pinned and rigid jointed plane frames.

Design Methods. The theoretical capacity for design employed two methods; Method I - Working Stress Design (WSD) and Method II - Load Factor Design (LFD).

Working Stress Design. This is based on "AASHTO Manual for Maintenance Inspection of Bridges - 1970" [12].

1. Allowable stresses specified in [12] were used for both operating and inventory load rating. These are summarized in Table 1 for the inventory rating.

2. The Secant formula, as in [12], was used to deal with cases of axial compression and bending.

3. Load capacities of the various elements of the structure were computed as fractions of AASHTO loadings. For example, a member capable of carrying 65 per cent of H-20 loading was rated at H-13, and so on. Table 2 provides a summary of ratings of some of the items in the structure. It is clear from the table that some structural elements rated in the order of AASHTO H-12 (60 per cent of AASHTO loading H-20). According to the 1931 specifications the structure was designed for a loading similar to AASHTO H-15 (75 per cent

Figure 6. Status of traffic on bridge at time of inspection (May, 1973) - abstract from C.I.P. weight records.

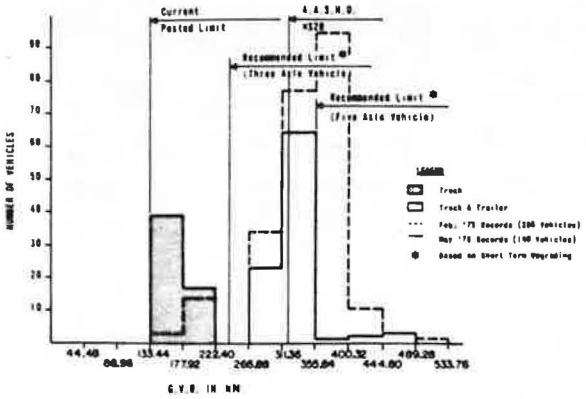

Table 1. Allowable stresses used for inventory rating.

Type of Stress	Allowable stresses
Tension in Structural steel (0.55 times yield point)	113.76 MPa (16.6 ksi) - 1931 steel 125.49 MPa (18.2 ksi) - 1961 steel
Tension in reinforcing steel	125.49 MPa (18.2 ksi)
Shear in rivets	91.01 MPa (13.2 ksi)
Compression in Concrete	12.41 MPa (1.8 ksi)
Safety factor in Compression member	1.48

Table 2. Summary of load rating.

Members	Load rating using AASHTO (Manual 1970) (Inventory Level)			
	HS - Trucks		H - Trucks	
Columns	7-9[a]	(55%)[b]	11-13	(45%)
	9-11	(45%)	13-16	(55%)
Deck Trusses	8-16	(52%)	12-16	(40%)
	16-20	(24%)	16-19	(12%)
	20-25	(24%)	>19	(48%)
Bowstring Truss	13-15	(48%)	17	(34%)
	15-20	(52%)	19	(14%)
			>19	(52%)
Girders	10		13	
Floorbeams	13			
Deckslab	20			

Note: Through-truss not evaluated. Design according to AASHTO HS-20 loading.

[a]Indicate rating of HS7-HS9.
[b]Indicate percentage of rated members.

of AASHTO H-20 loading). The discrepancy between the rating and the original design loading can likely be attributed to differences in design criteria and methods, or higher allowable working stresses in the original specifications (that is, the allowable tensile stress in 1931 specifications was 124.1 MPa (18.0 ksi) as compared to

Figure 7. Proposed Ontario bridge design load - RR186 (modified since this project to form the basis of the forthcoming Ontario Highway Bridge Code).

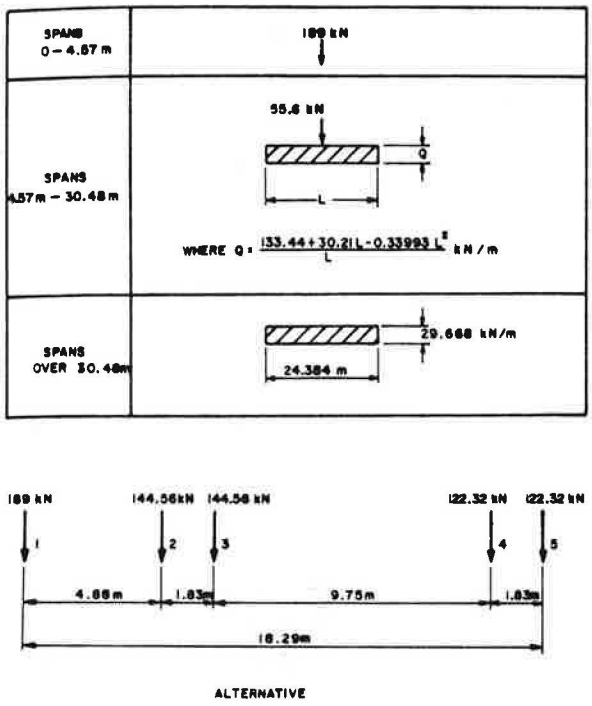

the allowable rating stress of 113.76 MPa (16.5 ksi)).

Load Factor Design. This is according to the most recent edition of the AASHTO Maintenance Manual (1974) [13] and partial load factors criteria [14].

1. To allow for the type of heavy traffic using the bridge, a hybrid concept was developed from AASHTO Codes [13, 16] and MTC Research Report No. RR186 [14]. Because it was economically impossible to restrict traffic for even a short period of time, a two-stage approach was taken. The first stage called for an immediate short-term upgrading/remedial works to carry loads of gross vehicle weight (GVW) less than 355.84 kN (80,000 pounds) and gross axle weight (GAW) less than 88.96 kN (20,000 pounds) [17]. The second stage called for long-term remedial work that would enable the bridge to carry the maximum proposed Ontario Bridge Design load. (GVW and GAW not to exceed 722.80 kN (162,500 pounds) and 189.04 kN (42,500 pounds) respectively) (Fig. 7). The short-term solution depended on implementation of all recommendations regarding traffic, weight and speed control on the structure [16]. Whenever guidance was not available from RR186, AASHTO Codes were used.

2. The structure capacity evaluated by the introduction of partial-load factors [14] satisfied the following general equation:

$$[(1-\mu)\ \phi \times \text{Capacity}] \geq [D \times FD + (1+i)\ m \times A \times FL]$$

where:

μ - deterioration factor
= 0.10 (members immediately below deck and existing fasteners)
= 0.05 (all other members)

ϕ - capacity reduction factor
= 0.80 (truss members)
= 0.85 (remaining steel members and reinforced concrete in shear)
= 0.90 (reinforced concrete in flexure)

Capacity (moment, Shear or reaction)
= Fy x flexure modulus etc., as per AASHTO

D - dead load (moment, shear or reaction)

FD - dead load variation factor
= 1.10 (steel)
= 1.15 (concrete)
= 1.33 (asphalt)

i - impact factor
= as per AASHTO

m - multiple presence indicator representing various possible combinations of simultaneous presence of more than one vehicle on the bridge (m = 1 for two loaded lanes)

A - maximum allowable live-load (moment, shear or reaction)

FL - Live-load variation factor
= 1.10 for short-term
1.20 for long-term (Based on MTC's projected study of traffic growth for the period of 15 years.)

Safe load capacities of members with axial compression and bending were determined according to the load factor design method given by the AASHTO 1974 Maintenance Manual.

3. The types of vehicular loadings investigated were; proposed Ontario Bridge Design Load (Fig. 7) and axle combinations permissible by the Ontario Bridge formula [17].

Short-term Upgrading. The structure was strengthened to carry loads up to 355.84 kN (80,000 pounds) on a short-term basis and sign posted for load limits. The extent of major repairs was confined to the following:

1. Seating brackets under girders of trestle spans.
2. Prestressing to the bottom chord of bowstring truss and to the tension diagonal of 68.28 m (224 feet) decktruss.
3. Bracing members to increase the capacity of some diagonals in deck trusses.
4. Armouring of all joints in the deck.

Long-term Upgrading. While the short-term solution was arrived at hastily, on the basis of theoretical findings only, the target of achieving a load capacity of 722.80 kN (162,500 pounds) on a long-term basis (a phenomenal increase from the present day AASHTO standards), required a careful and efficient assessment of the full capabilities of the structure. Considering the question of total reliability of the various assumptions in a theoretical exercise, a combination of analytical and experimental procedure in the form of load tests on the actual structure was pursued. The main thrust of the testing program, details of which are described below was to verify or suitably influence the analytical method in its theoretical assessment. Apart from that, the test would provide, with a reasonable degree of confidence, ultimate proof of the load-carrying capacity of the structural units corresponding

to the application of selected loads. In view of the expected increase in the life of the structure and possible variations of traffic types during this period, some changes were made to the design and analysis criteria adopted earlier. The changes introduced also reflected the findings of the test program and were as follows:

1. Trusses were to be analysed as rigid-jointed plane frames.
2. Partial continuity of longitudinal girders in trestle spans were to be considered.
3. Flexural effects in the columns were to be suitably accounted for due to 2 above.
4. Thermal stress in the structure was to be relieved by repair or replacement of expansion bearings.
5. Floor beams were to carry loads without the help of composite action from the deck slab.
6. Impact factors were to be modified to 50 per cent (columns) and 30 per cent (trestle spans and trusses).
7. Refined methods of analysis considering the interaction of the various elements of the bridge were to be used, where felt necessary, to draw upon the more realistic load distributing properties of the structure than assumed by simple methods. This approach appeared to be reasonable from the capability of the existing bridge to carry the test loads without signs of distress.

Figure 8. Trestle span (typical).

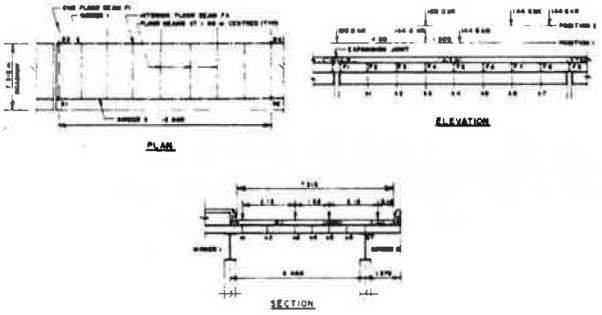

Numerical Example. An example shown in Figure 8 and Table 3 illustrates the differing results obtained depending on the type of analysis employed; Analysis I - simplified method according to AASHTO code Section 3 (13, 16); Analysis II - Finite Element Analysis Using "STRUDL" Program.

The following procedure was adopted for Analysis I:

1. Proportion of axle load 'P' for the design of floor beams is (S/6)xP (Table 1.3.1 c).
2. No lateral distribution is considered (1.3.1 c) for calculating a) bending moments on floorbeams and b) proportion of load on girders.
3. Longitudinal distribution of load on girder is obtained as reactions on floor beams based on continuous slab analysis.
4. Using reactions determined from 2 & 3 above, bending moments in girders are calculated.

In Analysis II, the structure was modelled into an assemblage of beam and plate elements and the following assumptions were made:

1. Linear elastic analysis
2. Isotropic slab resting on floor beams without composite action; sidewalk slab ignored.
3. Concentrated wheel loads assigned to nodal points.

Table 3. Vehicular load distribution effects

Bending moment in floor beam (kN - m)

Floorbeam	Load Position	Location a1	a2	a3	a4	a5	a6	a7
F1 (adjacent to Exp. joint)	1	41.9 (17.2[c])[a] 17.0	100.1 (60.9[c]) 61.7	158.4 (112.3[c]) 114.9	137.0 (92.5[c]) 94.6	105.9 (80.1[c]) 80.5	21.9 (7.2[c]) 6.8	-63.3 (-68.3[c]) -69.3
F4 (typical interior beam)	2	41.9 (7.5[c]) 8.0	100.1 (22.4[c]) 25.0	158.4 (56.7[c]) 69.2	137.0 (41.8[c]) 43.7	105.9 (43.5[c]) 45.0	21.4 (-1.0[b,c]) 4.1	-63.3 (-43.4[c]) -47.6

Bending moment in Girders (kN-m)

Girder	Load Position	Location b1	b2	b3	b4	b5	b6	b7
1	1	212.6 (207.1[c]) 205.2	425.6 (406.9[c]) 406.0	637.9 (597.0[c]) 612.5	658.3 (626.6[c]) 644.1	514.1 (494.9[c]) 494.0	342.5 (328.7[c]) 327.7	171.5 (163.5[c]) 163.1
2	1	299.7 (283.8[c]) 281.0	599.4 (547.6[c]) 550.3	899.0 (793.8[c]) 818.8	928.0 (832.0[c]) 858.6	724.6 (654.8[c]) 657.0	482.9 (433.0[c]) 433.9	241.8 (216.6[c]) 217.0
1	2	225.5 (216.0[c]) 221.0	451.1 (435.8[c]) 438.4	676.6 (631.6[c]) 648.0	651.0 (627.2[c]) 640.3	625.4 (601.3[c]) 599.9	599.9 (561.5[c]) 560.8	382.3 (361.8[c]) 361.5
2	2	318.0 (285.8[c]) 289.2	635.8 (574.8[c]) 581.2	953.8 (830.3[c]) 856.3	917.7 (827.3[c]) 854.4	881.7 (796.1[c]) 797.1	845.6 (745.8[c]) 746.6	538.7 (487.6[c]) 488.2

[a] Figures in ( ) indicate Analysis II
[b] -ve indicates hogging moments
[c] Indicates results obtained by Analysis II, considering random slab elements with negligible thickness to represent scattered spalls in bridge deck.

4. External restraints in the direction of loads only at column supports.
5. Poisson's ratio in concrete = 0.15, in steel = 0.30.

Comparative study of the two methods indicated that simplified methods could lead to overestimation of capacity requirements as noted below:

1. Maximum bending moments in floor beams obtained from Analysis I are far in excess of those obtained from Analysis II (41% for Load Position 1 and 279% for Load Position 2).
2. Maximum bending moments in girders determined by Analysis I are slightly in excess of those obtained from Analysis II (5 to 15%); the aspect ratio (span/width = 2.33) of this grid reflects its predominant behaviour in the longitudinal direction.
3. Random spalls in bridge deck do not have any significant effect on the load distribution characteristics of the grid.

Field Tests

These tests involved experimental stress analysis by monitoring parts of the structure mainly through strain readings taken with the aid of electrical resistance strain guages [8] and simultaneous complemental monitoring of these components by acoustic emission [11], as loads were applied in increments up to a predetermined proof load.

Briefly, the two systems differ in the sense that while electrical resistance strain guages are quantitative, the acoustic emission is only qualitative. The latter provides an indication of the integrity of the structure at the selected points of interest by projecting warnings of incipient failures during test loading.

Objectives. The load testing program was confined to specific and representative areas of the structure evaluated as deficient by the theoretical work. The main objectives of the test were to determine the actual behaviour and the load distributing properties of the various components of the structure in its true three-dimensional state, a factor not accounted for adequately in the analytical evaluation of the capacity of the structure. The main areas of investigation were:

1. For trestle spans, the possibility of longitudinal girders possessing more stiffness and capacity than could be predicted by the analytical assumptions of simply-supported spans between columns.
2. The effect of deck slab on the composite action of floor beams in flexure and on the webs of the floor beams directly over the longitudinal girders.
3. The load-moment transfer into the supporting columns from live load and the study of more realistic boundary conditions for the columns than the assumed end conditions (these effects were monitored for both static and dynamic loading).
4. The load distribution characteristics from decking system to main load-carrying members in trestle spans.
5. For trusses, the end conditions of the various members forming the truss were investigated, and the effects of thermal variations in the truss members caused by malfunctioning of existing expansion devices.
6. The study of impact factors based on dynamic tests.
7. The strength capacity of randomly deteriorated deck slab subjected to heavy axle loads.

Procedure. Two remote-controlled test vehicles (Fig. 9), capable of providing load lifts of about 765.06 kN (172 kips) each, were loaded incrementally using concrete blocks for the load. Dynamic effects were simulated by running the vehicles at various speeds over bumps created by laying plywood planks over the deck.

Conclusions. The following observations and conclusions were drawn from the above mentioned field tests.

1. For the floor beam and deck slab, the bare steel section of the floor beam has neutral axis (NA) at 267 mm (10.5 inches) from the soffit, while with full composite action with deck slab (without any shear lag), the theoretical NA should have been at 484 mm (19.07 inches). Table 4 shows

Figure 9. Two testing vehicles.

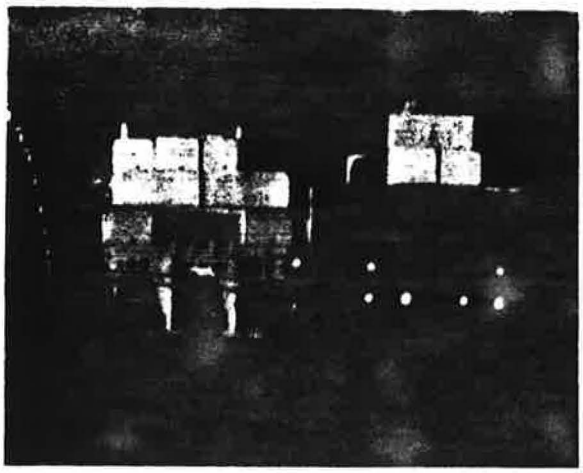

Table 4. Measured neutral axis (floor beam).

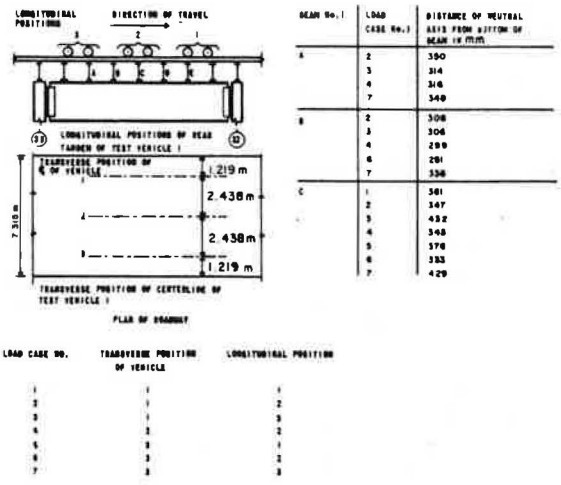

Figure 10. Test and analytical results (Trestle span).

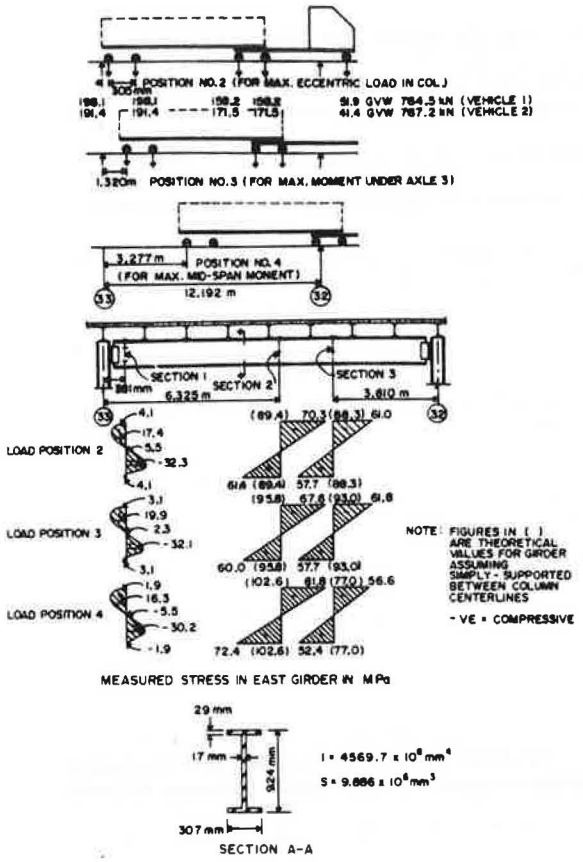

scattered results indicating no fixed pattern. Thus there was a failure to predict the degree of composite action with any certainty.

2. Figure 10 indicates a comparison of test and analytical stresses in the longitudinal girder of the trestle span. The theoretical figures are consistently higher than the corresponding measured ones. This is explained by the existence of partial continuity of the girders through columns and non-functioning expansion joints restraining joint rotations over the supports. Measurement of thermal stresses in the girder suggested the desirability of reducing these by functioning expansion devices. Though the existing header angle connection between girder and column is theoretically a flexible one transferring pure shear only, field tests revealed the presence of some restraining moments at the junction.

3. Table 5 reveals that good correlation exists between the test and the analytical results of a rigid-jointed truss.

4. Impact factor derived as a ratio of maximum increase in static load stresses to maximum static load stress at any time is tabulated in Table 6 for various speeds and bump heights. A reasonable interpretation of the results suggests an estimate of impact factors higher than AASHTO criteria.

5. Acoustic emission monitoring detected no active cracks in the members tested. Minor reversible emissions noted in some members were attributed to normal relaxation of the structure in response to application and removal of the load. Joints monitored on the bowstring truss showed emissions corresponding to discreet movements but this activity did not increase systematically

Table 5. Comparison of field & analytical results (Bowstring truss).

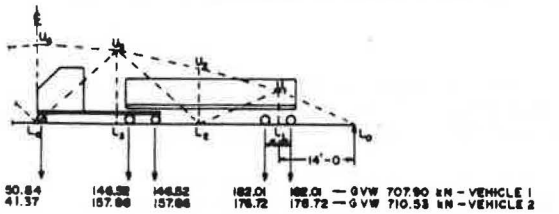

Member P - kN M_1, M_2 - kN-m		Test[a] (Total load = 1414.46 kN)	Analytical[b] (Total load = 1445.6 kN)
L_0U_1	P	1063.07	1214.30
	M_1	-15.73	8.27
	M_2	49.49	72.94
U_1U_2	P	1169.82	1240.99
	M_1	22.78	42.57
	M_2	12.47	20.47
L_0L_1	P	791.74	1112.0
	M_1	-24.27	-8.13
	M_2	62.64	96.67
L_1L_2	P	809.54	1116.45
	M_1	63.54	91.92
	M_2	4.75	7.19

[a] Moment values obtained outside of gusset plates
[b] Moment values obtained at junction of members

Table 6. Impact factors computed from data of dynamic load test on span 2.

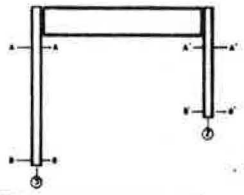

IMPACT FACTOR = (MAXIMUM INCREASE IN STATIC LOAD STRESSES AT ANY TIME / MAXIMUM STATIC LOAD STRESS AT ANY TIME) x 100

VEHICLE SPEED* in km/hr	HEIGHT OF BUMP(mm)	IMPACT FACTOR: COLUMN 3 SECTION AA	COLUMN 3 SECTION BB	COLUMN 2 SECTION A'A'	COLUMN 2 SECTION B'B'	VIBRATING FREQUENCIES c.p.s.: UNDER MAX. STRESS AA	UNDER MAX. STRESS BB	AFTER VEHICLE OFF THE SPAN A'A'	AFTER VEHICLE OFF THE SPAN B'B'
4.8	0	21%	12	5	8%	3.5	3.0		
16.0	0	32%	25	11	7	2.7	1.0	8.0	8.0
16.0	19	50%	33%	15	36%	3.5	3.5	8.0	7.5
48.3	19	39%	39%	25	40	8.0	8.0	8.0	8.0
48.3	38	52%	46%	32	38%	8.0	8.0	8.0	8.0

* vehicle brought to a sudden stop on the span

with the load, suggesting no active cracks but only possible slipping in the joint.

Laboratory Tests

Laboratory tests were grouped into the following categories:

Steel in Superstructure (chemical, mechanical, weldability, brittleness). Test coupons were taken from columns, floor beams and some truss members. Samples chosen for analysis were considered fairly representative of the bridge considering that almost all steel was fabricated by the open-hearth process according to C.E.S.A. specifications for steel highway bridges No. A6-1929.

Table 7. Properties of steel.

Mechanical

Sample Number	Yield point MPa	Tensile strength MPa	% Elongation (203 mm gauge length)
1M	235.8	384.0	30
2M	281.3	386.1	24
3M	266.8	409.6	32
4M	228.9	355.1	23
5M	279.2	386.8	27
6M	266.8	386.8	20
7M	279.2	376.5	29

Chemical

Sample Number	Carbon (C)%	Manganese (Mn)%	Phosphorus (P)%	Sulphur (S)%	Silicon (Si)%
1C	0.18	0.60	0.016	0.011	0.02
2C	0.14	0.49	0.018	0.014	0.04
3C	0.10	0.43	0.013	0.012	0.02
4C	0.13	0.44	0.012	0.015	0.06

Charpy V-notch

Sample Number	Test temperature (C°)	Charpy Energy (N-m)	Average Energy (N-m)
1V		14.9	
2V	-17.5°	13.6	15.1
3V		16.9	
4V		18.3	
5V		20.3	
6V	- 6.6°	29.2	22.8
7V		24.4	
8V		21.7	

Note: 1 MPa = 0.145 ksi, 1 N-m = 0.738 ft-lb.

Table 8. Properties of concrete.

Compressive strength

Core Number	Diameter mm	Height mm	Unit Weight kg/m^3	Compressive Strength MPa
1C	94	184	83.7	32.27
2C	94	140	86.6	45.16
3C	94	117	89.6	50.33
4C	94	165	81.9	42.95
5C	94	152	87.2	39.85
6C	94	156	86.6	51.30
7C	94	133	86.0	56.68
8C	94	156	87.8	50.54
9C	94	165	84.8	47.78
10C	94	171	85.4	36.61

Chloride Content

Core Number	Slide number[a]	p.H value	Chloride content kg (chloride)/m^3
1CH	1	11.6	4.56
	2	11.7	3.79
	3	11.7	1.94
2CH	1	12.0	5.47
	2	12.0	2.22
	3	12.1	0.33
3CH	1		10.06
	2		5.84
	3		4.91
4CH	1		7.95
	2		4.44
	3		1.64

[a]Slide number 1 represented the wearing surface slide number 2 represented concrete to a depth of approximately 1-1/2 inches below surface and slide number 3 represented concrete approximately 2-1/4 inches below surface.

Carbon equivalent obtained from the chemical analysis based on the formulation Ceq = C + Mn/3 (a "worst case" formulation) rates the steel to be highly weldable. Weld tests performed on the samples indicated hardness of the heat affected zones not exceeding Vickers 223 with 300 being the practical limit, and suggested no problems of crack formations [19]. However, in view of the possibilities of high restraint and variations in the chemistry of material in the actual structure, a low strength, low hydrogen electrode E 7016 as specified in CSA code W59.1 - 1970 was adopted.

Charpy V-notch testing of specimens was conducted at two different temperatures. Considering, in bridges, the expected maximum rate of loading to be 1/10,000 times the strain rate in a Charpy Impact test [20], the fracture toughness obtained was considered satisfactory. Table 7 shows the results of analysis on some of the samples.

Concrete in the Deck. Concrete cores obtained from various locations in the deck were subjected to compression tests and chemical analysis to determine the level of soluble chloride ions. Table 8 shows consistently high compressive strengths and a remarkably high chloride ion content than present day researches on bridge deck deterioration would accept. Reasons for such high concentration remain unclear though possibilities of chloride admixtures in the concrete could not be ruled out.

Fatigue Life

Complexity of factors attending the determination of the remaining fatigue life of an existing structure needs no special emphasis. Considering only the sketchy history of traffic available in the present case, attempted theoretical study did not seem satisfactory. However, it has been decided to replace the existing rivets by high strength bolts on all members subjected to tension and reversals as a measure to prolong the fatigue life of the structure [21]. Welded details for member strengthening have been kept to a minimum and totally avoided on members subjected to tension and stress reversals.

Details of some Strengthening Measures

At the time of writing this paper, the project is in various stages of design and construction. Some repair techniques are discussed briefly here. Strengthening in general, has been done by the addition of materials using both bolted and welded arrangements. Welded details have been avoided on tensile members and members subjected to reversals. This is to ensure lesser burden on future inspection and maintenance. Some compression members have been upgraded by bracing them against buckling (Fig. 11a). A combination of knee braces between columns & girders and cross braces between the webs of floor beams at the trestle spans

Figure 11a. Bracing details.

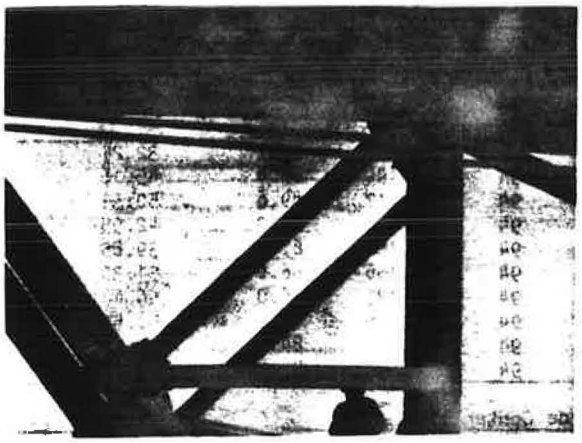

Figure 11b. Kneebraces.

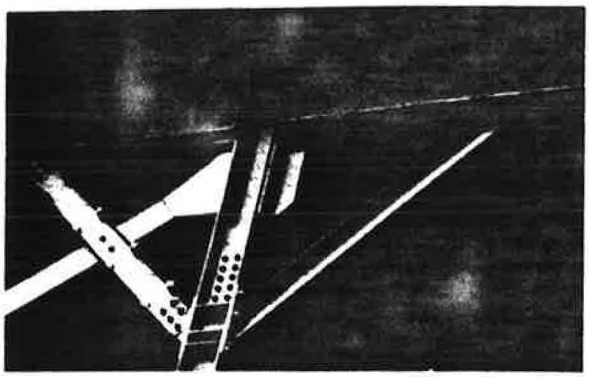

Figure 11c. Expansion bearing.

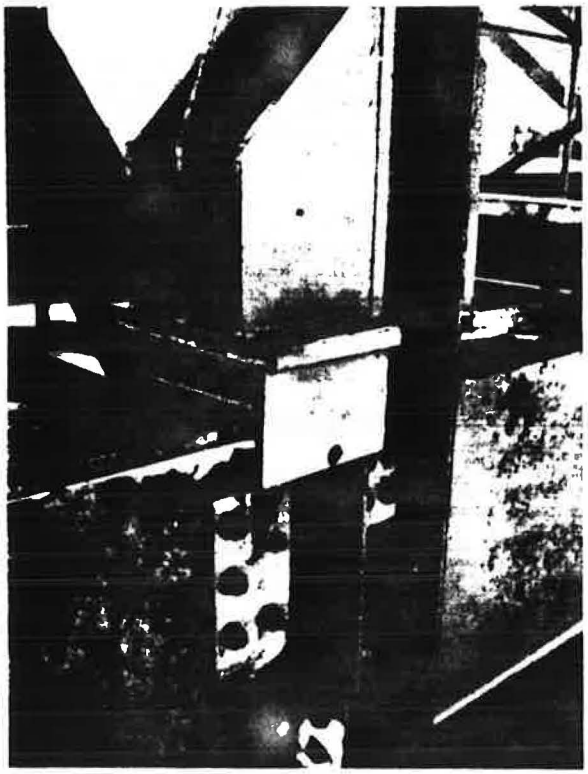

(Fig. 11b) reduces the possibility of failure of floor beam webs, improves the capacity of longitudinal girders by providing continuity over spans, strengthens the supporting columns against buckling and relieves partly the load on the header angle connections between girders and columns by sharing in the joint effects. Existing cast-steel bearing assemblies under expansion ends of trusses have been replaced by elastomeric type bearings. Trestle span expansion devices have been modified as shown in (Fig. 11c). Figs 12a, 12b, show details of some strengthening items.

Strengthening details have been proportioned according to load factor design such that;

1. Totally new members and compression members are stressed to yield limits.
2. New materials added to the original members (tension and reversals only) are stressed to a limit of (Fy-Fo), where Fy is yield stress of original members and Fo is stress in original member from dead load only.

Cost of Repairs

Before deciding on a programme of long term upgrading, studies were made on the relative economics of (i) retaining the existing bridge for auto traffic only with minimal maintenance works and an adjacent new bridge for heavy truck traffic only and (ii) strengthening the existing bridge for one lane auto and one lane truck traffic and an adjacent new bridge for similar traffic. The total replacement of the bridge on the same location was not studied in detail considering the good salvage value of majority of the bridge components and the serious consequences of major shutdown of the crossing on the local industries.

The total estimated cost of repairs is about $1.7 million. Repair works are being done in various phases to accommodate the availability of funds and the urgency of repair items. All major structural repairs are expected to be completed by September, 1979. Two contracts amounting to $540,000 (about $300,000 for short term upgrading) have already been completed and the next one amounting to $744,000 is to begin in July 1978. Breakdown of repair costs is as follows:

Trestle Spans	-	$ 348,000
Deck Truss (68.28 m)	-	$ 54,000
Deck Trusses (51.82 m)	-	$ 116,000
Bowstring Truss	-	$ 51,000
Through Truss	-	$ 62,000
Miscellaneous	-	$1,000,000
(Deck Patching, Pier Spalls Expansion bearings, seals, approaches, replacing rivets by bolts, etc.)		

Conclusions

Superstructure

Generally, the safe load capacity of existing bridge components based on simplified methods of analysis and working stress design can be underestimated. Load factor design using refined methods of analysis to account for the complete interaction of the various elements of the bridge results in better assessment, as noted in the case of Perley Bridge. This approach appears to be satisfactory considering the ability of the existing bridge to carry the test loads without signs of

Figure 12a. Top and bottom chord strengthening details (Bowstring truss).

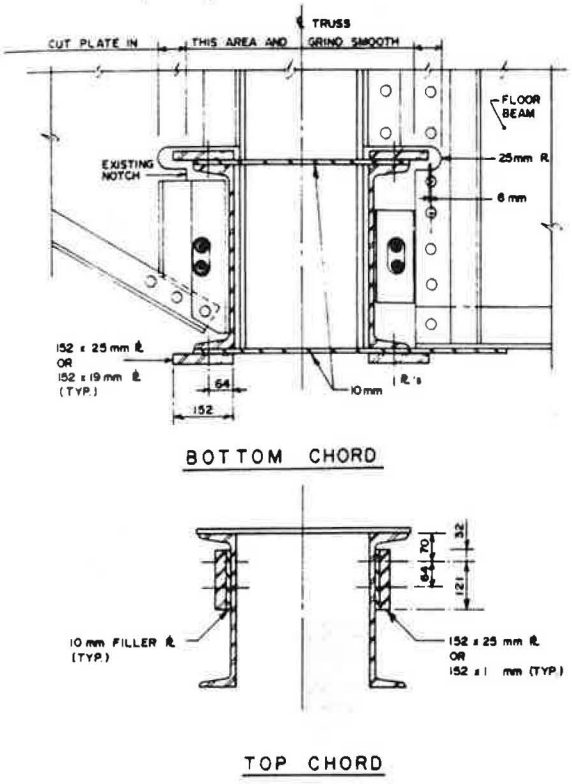

Figure 12b. Tension diagonal (U_1L_2) strengthening details (Through truss).

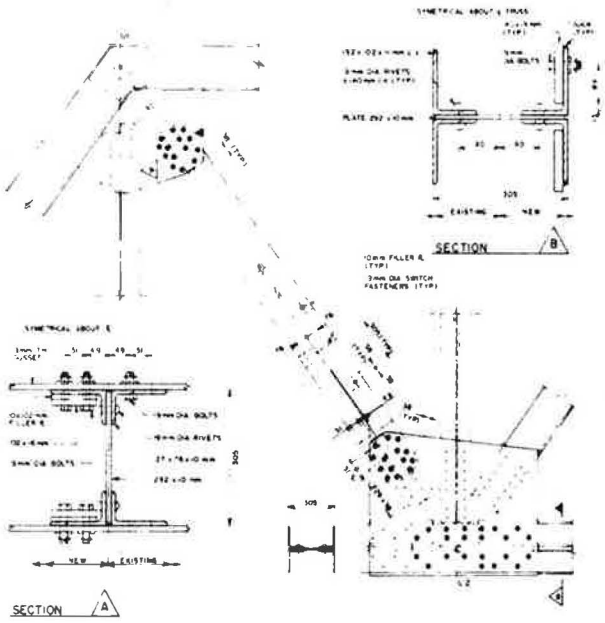

distress. Needless to say, the extent of the sophistification that can be employed in the analysis must reflect the high probability of non-homogenity of materials due to decay and other causes, variations of dimensional tolerance, damage to existing members, if any present in an aging structure.

Perley Bridge, evaluated originally to be grossly deficient according to WSD, has now been upgraded to the desired level with minimum remedial measures by employing the many - faceted approach described in this paper. Deviations from the normally accepted AASHTO standards have been made to reflect the prevailing conditions in Ontario and Quebec and the prototype field tests conducted on the bridge, with regard to loading and load factors, impact factors, distribution of vehicular loads, actual joint condition at ends of truss members, column-girder connections and slab capacity.

Substructure

Foundations resting on solid rock were not considered to be problematic in accommodating the increased loads. Analytical checks on pier and abutment sections, based on load factor design, indicated no cause for concern provided the integrity of substructure was carefully monitored by periodic inspections.

Deck

Despite the alarming presence of chlorides, the deck appeared generally sound. The long-term requirement of a durable deck raises the debate about the choice between total replacement or maintaining the existing deck by frequent programs to patch stray areas of scaling and spalling as they develop. Considerable work on the economics and workability of these two choices finally led to an interim decision to continue the current maintenance program, and defer any major replacement until absolutely necessary. In the meantime, the state of the deck is being carefully monitored. However, it has been planned to repair the deficient metal pan deck of the through truss with concrete filling using the pans as forms.

Handrails

The nature of work in upgrading the handrails to modern day standards is directly tied in with the possible future deck slab replacement (anchorages etc.).

Acknowledgements

A variety of organizations have been involved in this undertaking, and the authors' appreciation is expressed for their efforts to renew the life of an aging structure.

References

1. International Bridge Report. Development Engineering Branch, Public Works Canada, Ottawa, April 1965.
2. Perley Interprovincial Highway Bridge. The Canadian Engineering (A weekly paper for Civil Engineers & Contractors). Feb. 9, 1932.
3. Specification for the Steel Superstructure including latticed fence and lamp-posts on approaches of the Interprovincial Highway Bridge across the Ottawa River between Hawkesbury, Ontario and Grenville, Quebec. Public Works Canada, 1930. (1914, 1931, 1961).
4. Design Drawings on Perley Bridge. Public Works Canada & Hydro Quebec (1931, 1961).
5. Shop and Erection Drawings (1931, 1961). Canadian Bridge and Dominion Bridge.

6. Perley Bridge Investigation. M.M. Dillon Ltd., Consulting Engineers & Planners, May 1974.
7. Load Limits on Perley Bridge. Public Works Canada, Ottawa, Project No. 4344, July 1974.
8. B. Bakht & P.F. Csagoly. Testing of Perley Bridge. RR 207 Research & Devleopment Division, Ministry of Transportation and Communications, Ontario, January 1977.
9. Underwater Inspection of the Perley Bridge. A.W. Huffy, Consulting Engineers Ltd., Cornwall. Sept. 28, 1973.
10. Laboratory Testing of Concrete Cores and Steel Samples. Research & Development Laboratories. Public Works Canada, Ottawa,May 1976.
11. M.N. Bassim & D.R. Hay. Acoustic Emission Monitoring of the Perley Bridge. Failure Control International, Division of Tekrend International Ltd., Sept. 29, 1975.
12. Manual for Maintenance Inspection of Bridges. American Association of State Highway Officials, 1970.
13. Manual for Maintenance Inspection of Bridges. American Association of State Highway and Transportation Officials, 1974.
14. P.F. Csagoly & R.A. Dorton. Proposed Ontario Bridge Design Load. RR 186, Research & Development Division, Ministry of Transport & Communications, Ontario, Nov. 1973.
15. K.G. Tamberg & P. Smith. A System for the Strength Evaluation of Concrete Bridges. IR 25, Research & Transportation Systems Branch, Department of Highway, Downsview, Ontario. June 1970.
16. Standard Specifications for Highway Bridges, 1973 including Interim Specifications -1974 & 1975. American Association of State Highway Officials.
17. Axle Weight Legislation Made Under the Highway Traffic Act and Regulations. Department of Transport, Ontario, March 1971.
18. H.W. Ferris. Historical Record. Dimensions & Properties of Rolled Shapes, Steel & Wrought Iron Beams & Columns (as Rolled in U.S.A., Period 1873-1952). American Institute of Steel Construction. Fifth Printing 1968.
19. M. Bibby. Consultation of the Perley Bridge Steel. A report submitted to Public Works Canada, 1975.
20. R.G. Keen. Bridging '75 -Design Considerations. Steel Company of Canada, Feb. 1975.
21. H.S. Reemsnyder. Fatigue Life Extension of Riveted Connections. ASCE Journal of Structural Division, Vol. 101, No. ST12, Dec. 1975.

RENOVATION OF LIONS' GATE BRIDGE NORTH VIADUCT

Peter R. Taylor, Buckland & Taylor Ltd., Consulting Structural Engineers, Vancouver, Canada

This paper is concerned with the deck replacement of the 670 m (2200 ft) long approach viaduct to Lions' Gate Suspension Bridge in Vancouver, Canada, which was carried out during night closures without affecting peak daytime commuter traffic flows. The structure was built in 1938 and comprised a series of steel plate girder spans supported on steel bents and with a 0.18 m (7 in.) reinforced concrete deck without wearing surface. Under the cumulative effects of road salt and traffic for 35 years, the deck was cracked through in places and the rebar was heavily corroded, resulting in surface spalling and potholes. The support steel had suffered some section loss from corrosion and also corrosion buckling in thin cover plates over long rivet spacings. A solution was required which would reduce the load in the support steel, cut down the corrosion rate, permit wider lanes and a wearing surface, all under the constraint of maintaining the bridge open for daily commuter traffic. This paper discusses the unusual design concepts adopted to satisfy these requirements and explains how they were realized in practice by careful attention to detail in every aspect of the job. Methods used to alert the bridge users to closures and estimated opening times are discussed together with emergency plans in the event of failure to complete a section on time.

Original Structure

Lions' Gate Bridge was built in 1937-8 to the design of Monsarrat and Pratley of Montreal. The structure is divided into two parts, the 670 m (2200 ft.) North Viaduct, and the suspension bridge itself. This project was concerned with renovation of the former structure. This comprised a 8.8 m (29') wide by 178 mm (7 in.) thick concrete road slab plus two 1.2 m (4') wide sidewalks supported by steel WF crossbeams resting on rivetted plate girders. The girder flanges were built up from 8 mm (5/16") plate with rivet spacings considerably in excess of sealing pitch. The concrete deck had no wearing surface and run off drained directly onto the support steel below. The application of deicing salts, coupled with the use of studded tires by most of the bridge traffic, had caused severe distress in the concrete deck. Wear in places was below the top steel and cores showed micro-cracks extending through full slab depth. The deck was essentially failed and breaking up at an increasing rate. The exposed support girders and bents beneath the deck also suffered corrosion losses from deicing salts. The accumulation of corrosion products under the flange cover plates caused buckling of up to 12 mm (1/2 in.) between the widely spaced rivets.

Requirements for Renovation

By 1972 the deterioration of the North Viaduct deck had reached the point where the B.C. Department of Highways felt it was essential to commence planning of renovations. The problems, in order of importance, appeared to be the break-up of the viaduct deck and the continuing corrosion of the support steelwork, also the traffic lanes at 2.9 m (9'8") were too narrow and should be widened if possible. In July 1972 Buckland and Taylor Ltd. were commissioned to study the problem. A detailed examination of the bridge was carried out and it was concluded further that the bridge lighting and electrical system was in need of renewal and that the heavy traffic density made a high grade replaceable wearing surface essential.

Neither the nature of the renovation work, nor the pattern of daily traffic were suited to progressive lane by lane renovation. Therefore, short total bridge closures were planned for the major work. Daytime traffic flows could not tolerate more than a single lane closure and peak rush hour traffic must have use of all three lanes. This meant that the portion of the work requiring total closures of the bridge would have to be carried out between midnight and 6 a.m. with single lane closures at other off peak times.

Constraints on the Design

The requirements to remove a section of bridge and replace it with a new one ready for traffic in six hours was the largest constraint on the scheme and the one which provided much of its difficulty and fascination. The structural constraints were a little more complex. Heavier modern traffic loads on a wider deck, acting at larger eccentricities

from the girders and riding on a wearing surface which didn't previously exist, all tended to increase the forces on the existing support steel. Conversely, corrosion losses in the existing steel required that the total effective load be reduced for safety. These opposing structural constraints had to be constantly borne in mind as the design of structural renovations evolved.

Evolution of the Design

Consideration of the constraints led to two conclusions. Firstly, the new deck must have a much lower dead weight than the original and secondly, a very high degree of prefabrication was necessary in order to permit installation within the limited time available. Several materials and many schemes were examined and compared. A 14.3 m (47') wide orthotropic steel deck with a 38 mm (1.5") wearing surface of epoxy asphalt was finally selected because it best met all the demands and constraints and when connected by shear diaphragms to the existing weakened girders, provided increased strength by composite action under live load.

Corrosion of Support Steelwork

Many approaches were considered for inhibiting the corrosion attack on the viaduct support steel. These ranged from encasing the structure in concrete to the use of sophisticated non corrosive deicing compounds. A study was made of the extent of existing corrosion and then three future section loss curves were projected, see Figure 1. Curve 1 shows a continuation of the existing corrosion rate, Curve 2 shows a reduced rate and Curve 3 an intermediate situation.

Figure 1. Estimated cumulative section losses due to corrosion.

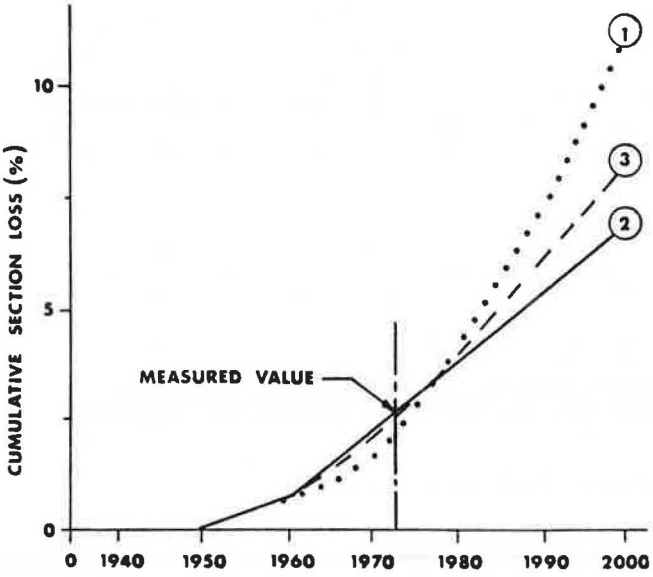

It was concluded that a moderate reduction in the existing corrosion rate would leave adequate structural reserves for four or five more decades of bridge life at present live load levels. It was therefore decided to seal the deck and to take steps to duct the deicing solutions down to ground level away from the support steelwork and to carry out blast cleaning and repainting of this steelwork to bring it to a common level of protective coating. It was considered impractical to attempt to seal all existing corrosion cells in the bridge.

Traffic Loading

In order to arrive at a rational design load for the viaduct and suspension bridge, a traffic study was carried out using stop frame cine cameras to record the size and spacing of vehicles. Statistical methods were used to derive load probability curves for the bridge. This work was later extended to the general situation of traffic loading on long span bridges, culminating in a paper on the subject presented to this Conference. The traffic studies indicated that some control of loads was necessary and a permanent 12,684 kg (28,000 lb) G.V.W. load limit was instituted.

Details of Design

One key to success in this project was the careful design of the numerous new deck to existing girder connections. They were required to be of adequate strength and stiffness, but also simple to connect and tolerant of misalignments in any planar or rotational direction. In order to provide realistic tolerances for the connection of new steel to existing, the new cross beams are attached by field welding to oversize shims which in turn are connected by countersunk bolts through existing rivet holes in the main girders. As mentioned earlier, extra reserve strength was attained by making the new deck composite for live load. The necessary shear connections at the end of each span were obtained by inserting 3 or 4 panels of plate diaphragms between the cross beams and aligned over the main girders. The steel orthotropic deck used was the conventional arrangement of U troughs. Concresive ® epoxy asphalt was selected after testing due to its outstanding abrasion resistance under studded tires. Other improvements incorporated in the new deck scheme included traffic barriers protecting the widened sidewalks, maintenance catwalks and gantries, telephone trunk cable trays, and a new electrical power distribution system, lighting system, overhead traffic sign bridges and stand-by generator. Half sections of the original and new design are shown in Figure 2.

Figure 2. Half sections of original and new structure.

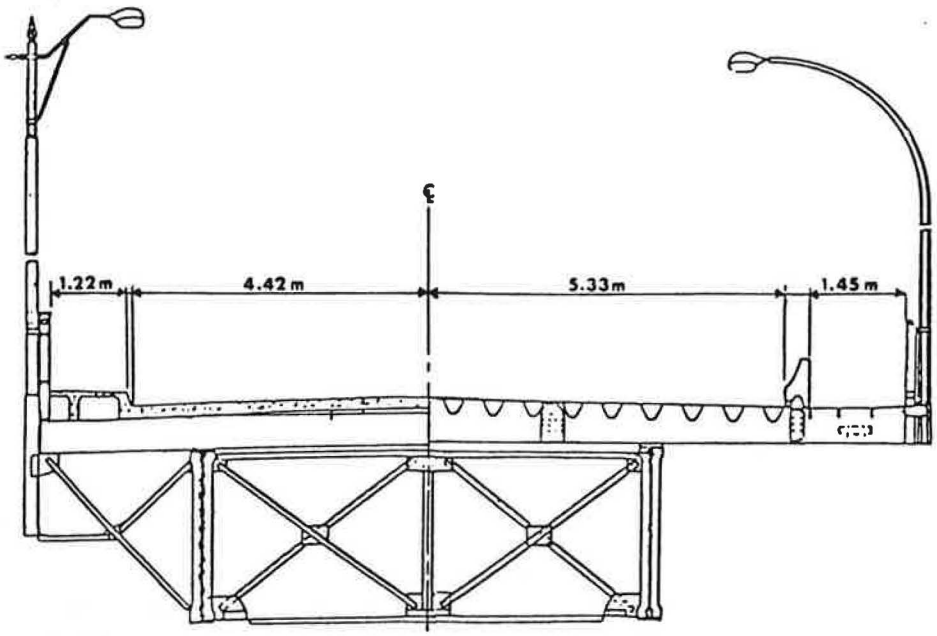

Construction

Due to the critical structural nature and time restraints on the work, all aspects of construction were under 24 hour supervision by the Consulting Engineer. Prior to erection, the deck units were spliced on a carefully prepared paving site and paved. Then they were taken apart and transported to the bridge. Preliminary work on the bridge involved successively removing all the floorbeam connection rivets and replacing them with HS bolts for speedy dismantling. The thin girder cover plates were subject to local buckling failure after removal of the rivets and precautionary stabilization by welding was required by specification. Removal of the original deck and installation of the new was handled by a Manitowoc Ringer crane.

Emergency Precautions and Public Information

One major concern during renovation was the possibility of equipment breakdown occurring while a gap existed in the roadway. Therefore, the Contractor was required to hold light emergency deck components on trucks at each end of the bridge. By careful planning and co-ordination, the 58 new deck sections were installed with delay to the public by late opening on only 4 occasions.

The need for public information and confidence was recognized early by both ourselves and the client and a most successful three pronged information system was set up. This consisted firstly of media advertisements giving a full explanation of what was going to be done and defining the extent of traffic closures. This was followed up by mailings to local businesses containing calendars of bridge closures. Finally, morning bulletins were supplied to local radio stations at 15 minute intervals until the bridge was open to traffic.

Suspended Spans

The next task to be tackled is the renovation of the suspension bridge part of the crossing. After investigation, it was discovered that the main cables had stretched, causing the centre of the bridge to drop 1 m (3.3 ft) and the towers to move out of plumb. Aerodynamically, the bridge was found to be stable only if reliance was placed on the natural turbulence of the wind. Accordingly, full model tests were conducted in turbulent wind in the N.R.C. 9 m (30 ft) wind tunnel in Ottawa.

Tenders will be called shortly for the replacement of the entire suspended structure - stiffening trusses and deck - to be replaced with a wider, lighter orthotropic deck with welded rectangular tubular stiffening trusses. It is believed that this is the first time that the entire suspended structure of a bridge has been replaced. Reconstruction will take place one section at a time during weekend closures and the bridge will remain open 24 hours per day Monday to Friday.

ORTHOTROPIC BRIDGE SAVES OLD COVERED BRIDGE

Robert F. Victor, P.E., Connecticut Department of Transportation

When inspection of the Old Covered Bridge at West Cornwall, Connecticut revealed extensive deterioration of its floor system and trusses, a new bridge was proposed to be built just upstream. The old bridge, dating from 1841, would have been left open to pedestrians only. This proposal angered local residents who wanted the old bridge restored. Because of tight vertical clearance restrictions, structure depth was severely limited. Preliminary computer analyses showed that a slender orthotropic steel deck bridge could be independently built within the old bridge and designed for AASHTO HS20 and alternative loadings. The construction consisted of building a parallel temporary bridge, raising the old structure 61 cm (2-ft.) higher to clear future floodwaters, painting, reshingling and whitewashing the interior and, erecting the steel deck bridge within. A timber floor was bolted to the steel deck plate. The total project cost $360,000 which is a savings of more than $1,500,000 over the cost of the proposed upstream bridge. More importantly, a historic nineteenth century structure was preserved as a heritage for the twenty-first century.

When inspection revealed deterioration of the floor system and trusses of the Old Covered Bridge at West Cornwall, Connecticut (Figs. 1 & 2), a new modern two-lane bridge was proposed to be built just upstream, bypassing the village of West Cornwall. The old bridge, dating from 1841, would have been left open to pedestrians only. This proposal angered local residents, who insisted that some way be found to strengthen the old structure without changing its appearance in any way!

Since any new floor had to remain at the existing grade to hold the existing vertical clearance of 3.35 m (11'-0") and since reconstruction would have to include a strong bottom lateral bracing system, only 76 cm (30 inches) was available for structure depth and vertical deflections. An orthotropic steel deck bridge, which is only possible through the use of extensive arc welding, can be made the most slender of all bridges. Preliminary computer analyses showed that a lightweight, economical, orthotropic bridge could be built within the covered bridge (Fig. 3).

To thoroughly analyze this highly redundant structure, a curved girder matrix grid analysis computer program (1) was modified to more easily handle the many members and loading conditions. The AASHTO (2) HS20 and alternative loadings were used to load the structure and design the various members.

Description

The deck plate of the bridge is 9.5 mm (3/8-in.) thick (based on L/300 deflection criteria between rib walls for an HS20 wheel) (3) and 4.27 m (14 ft.) wide (Fig. 4). Five trapezoidal ribs are 61 cm (2 feet) o.c. Brake press formed, the ribs are 23 cm (9-in.) deep, 8 mm (5/16-in.) thick, 31 cm (12-in.) and 17 cm (6½-in.) wide at the top and bottom respectively. The ribs are hermetically sealed between field splices and the end floorbeams. Since tests have shown that fillet welds would develop fatigue cracking (4), due to the transverse bending of the deck plate, the ribs were joined to the deck plate by 80 percent partial penetration groove welds.

The two main girders are 3.35 m (11 ft.) apart and each consists of 32 mm x 457 mm (1¼" x 18") bottom flange plate and 9.5 mm x 559 mm (3/8" x 22") web, fillet welded to the deck plate. Two edge plates 9.5 mm x 152 mm (3/8" x 6") are welded to each edge of the deck by partial penetration groove welds.

The steel bridge is two-span continuous (28.35 m - 22.86 m spans) (93' - 75') with each end cantilevered out from the bearings to form a total deck length of 52.61 m (172.55 ft.). In the longer span, floorbeams are 4.73 m (15.5 ft.) o.c.; in the shorter span 4.57 m (15 ft.) o.c.

A 13 mm x 152 mm (½" x 6") bottom flange and a 9.5 mm x 559 mm (3/8" x 22") web (castellated to fit tightly around the ribs) form the floorbeams which are fillet welded to the deck plate and ribs. The floorbeam web is fillet welded directly to the girder webs and the bottom flange is butt welded to the girder bottom flange. Trapezoidal plates 9.5 mm x 559 mm deep (3/8" x 22") stiffen the deck plate outside the floorbeams.

At each end of the bridge, the ribs are seal welded to the last floorbeam. Trapezoidal plates 9.5 mm x 559 mm (3/8" x 22") support the end of the deck plate. An edge plate is welded to the end of the deck plate. All steel conforms to ASTM A588 (Weathering Steel).

Design Data

Since the bridge is so lightweight (2.1 kPa-(44 psf) steel dead load, 2.5 kPa-(52 psf) total dead load) the live load stresses and deflections are large. The maximum computed live load deflection is 95 mm (3.75-in.) or L/300. This deflection was viewed as satisfactory since speeds are low and the largest vehicles using the bridge regularly would be school buses, fire trucks and other two-axle trucks.

In the actual bridge, the deflections, with the passage of a heavy vehicle are noticeable but not disturbing, since deck accelerations are small and vibration frequencies high (5). This is due to high stiffness-to-weight ratio and the mounting of the bridge on elastomeric bearings.

With the overall section determined by deflection criteria (as in most orthotropic bridges) (6), the meeting of fatigue criteria was easily accomplished. Most of the AASHTO fatigue categories (2) are present in this structure. Stress ratios and ranges vary considerably, depending upon the member and its location in the structure. At the section of maximum positive moment in the 28.35 m (93 ft.) span, the stress range in the bottom flange is 138 MPa (20 ksi) (from 159 MPa (23 ksi) max. to 21 MPa (3 ksi) min.) Dead load stress is 41 MPa (6 ksi). Thus live load stress plus impact is nearly three times greater than dead load stress. The deck plate, with its threaded welded studs for the timber decking, has a fatigue allowable stress of 114 MPa (16.5 ksi). Its maximum design stress is 105 MPa (15.3 ksi).

Construction

The construction started with the building of a 61 m (200-ft.) one-way temporary bridge adjacent to the covered bridge (Fig. 5). It was constructed from salvaged steel beams supplied by the Department and timber decking supplied by the contractor. This arrangement yielded a bid price of about $107 per sq. meter ($10/s.f.) which is very economical considering that the price included hauling, erecting and dismantling the three span (@ 20.4 m - (67 ft.) each) structure. It also included two river piers and two abutments.

With traffic thus diverted, the floor system of the covered bridge, consisting of steel floorbeams and a two-layer wood decking, was removed. The covered bridge was then jacked to an elevation 61 cm (two feet) higher in order to clear possible debris from design floods. New stone rubble masonry was added to the abutments and concrete to the pier (matching the existing appearance as much as possible). At the same time, new abutments consisting of a crossbeam, column and footing were built and buried inside the old abutments. The old abutments are thus relieved of much dead weight and all live load.

Fabrication

While construction proceeded apace in the field, the fabrication of the three full width orthotropic bridge sections was well underway (Figs. 6 & 7) in the shop. The specifications required that the fabricator, as part of the shop plan submission, submit a list showing the shop fabrication sequence. The designer was then able to review the proposed welding procedures in conjunction with overall fabrication methods with the view of minimizing distortion and shrinkage stresses.

The fabrication procedure evolved was as follows: (1) the top surface of the deck plates was sandblasted near-white and a weldable inorganic zinc-filled primer was sprayed on to provide a dry film thickness of 25 microns (one mil). This was done for environmental considerations at the bridge site. A clean surface was needed for stud welding and the high-build primer. Field sandblasting would have raised clouds of dust and a large quantity of debris which could be lethal to the trout in the stream. (2) Placed upside down (the entire bridge was fabricated upside down), half the square-edged longitudinal butt weld was made between the 1.83 and 2.44 mm (six and eight foot) wide deck plates. (3) All plates were then assembled and tacked (the floorbeam and girder web-to-flange fillet welds having previously been made). (4) The ribs were then welded to the deck plate. The fabricator had previously requested and received approval for a change in the partial penetration weld in which the ribs now would be supported on 2.4 mm (3/32") weld wire at 1.5 m (5 ft.)± intervals and rib edges left square-edged (giving a 17° root angle). Macroetch tests required by the qualification procedure showed that 100 percent penetration was achieved. (5) Upon completion of the underside welding, the bridge sections were turned over, the deck plate and ribs cut to length, and the longitudinal butt weld completed. Turned over again, the girder web and flange were cut to length. The bridge was then completely assembled and the holes for the bolted field splices drilled in the ribs and girders to assure proper assembly in the field.

Steel Erection

The three sections (measuring 18.6, 18.6, and 15.4-m; 61, 61, and 50.5-ft.) were trucked to the bridge site where they were assembled on the east bank of the river. The contractor had previously erected skid beams spanning from the abutments to the pier, over which the steel bridge would be pulled to the west abutment. Heavy duty machinery skates were attached to the bottom flange at the west end of the west section and another pair were set upside down at the east abutment. After each splice was completed, the steel bridge was pulled by a bulldozer winch on and over the skates (Fig. 8). Another set of skates were positioned at the pier while making the second splice in order to keep stresses within allowables during erection.

The two transverse field splices consisted of high-strength bolted ribs and girders (Fig. 9) and a welded deck splice and edge plates (Fig. 10). The welded deck gave a smooth surface for the deck planking. The sections were first aligned and the bolts placed without tightening. After fillet welding the backup strips to one side, the transverse groove weld was made. With this procedure, weld stresses were minimized. The transverse welds were inspected by the ultrasonic method (as were all butt welds in this bridge). This bridge required 1229 m (4030 feet) of welded joints, only 9.1 m (30 ft.) of which were required in the field.

A strong lateral bracing system composed of W6x20's was attached to the bottom chord of the old wooden trusses to complete the steel erection (Fig. 11). This bracing, made of weathering steel, required that nearly all of the fillet welds be made in the overhead position.

Other Operations

Each of the 625 cadmium plated threaded studs which hold the diagonal timber plank decking in place, had to be welded in exactly the right loca-

tion in order that the pre-drilled holes in the planks fit over them. The planks had been pre-cut and drilled in order that they be properly preservative treated.

The contractor first positioned all the planks on the deck plate. Then the location of each hole was marked on the steel plate with a felt-tipped marker. The planks were consecutively numbered and removed from the bridge. The studs then were welded at the marked locations. After the deck was painted, the planks were brought back and bolted in position.

After stud welding, a self-curing inorganic zinc-filled coating was applied to a dry film thickness of 76 microns (three mils) (threads of studs were taped). Two coats of a high-build low-temperature curing epoxy-polyamide topcoated the zinc-filled coating. Total thickness of all coatings is 305 microns (12 mils). Although the deck is A588 weathering steel, it was felt that pitting corrosion on the bare steel could take place, under the planking, with road salt solution brought in by vehicles.

To put finishing touches on the bridge, timber curbing was installed and the interior whitewashed (Fig. 12). Outside, the roof was reshingled with white cedar shingles and the siding painted barn red (Fig. 13). Temporary approaches were constructed and the bridge reopened with appropriate, colorful ceremonies. Later the temporary bridge was removed, new approaches built and the area restored to its former condition.

Total construction cost for the project was $360,000 which is a savings of more then $1,500,000 over the cost of a new bridge, originally proposed to be built upstream. Total cost of all steel was $101,750 ($1.91 per kg., $0.87 per lb.). More importantly, it is now possible to enjoy an old covered bridge well into the twenty-first century.

Acknowledgments

Photography: Joseph Rummel, Louis Sugland

Drawings: Ronald Gessay

Typist: Judith Gilistro

References

1. J. G. Bouwkamp and G. H. Powell. Structural Behavior of an Orthotropic Steel Deck Bridge. Department of Civil Engineering, University of California, Berkeley, Rept. SESM 67-27, 1967.
2. Standard Specifications for Highway Bridges. American Association of State Highway and Transportation Officials, Washington, D.C., 1977.
3. American Institute of Steel Construction. Design Manual for Orthotropic Steel Plate Deck Bridges, New York, 1963.
4. H. L. Davis and A. A. Toprac. Fatigue Testing of Ribbed Orthotropic Plate Bridge Elements. Center for Highway Research. University of Texas, Austin, Research Report No. 77-1, May 1965.
5. R. N. Wright and W. H. Walker. Vibration and Deflections of Steel Bridges. Engineering Journal, American Institute of Steel Construction, Volume 9, No. 1, New York, January 1972, pp. 20-31.
6. M. S. Troitsky. Orthotropic Bridges Theory and Design. James F. Lincoln Arc Welding Foundation, Cleveland, Ohio, 1967.

Figure 1. Bridge Before Restoration

Figure 2. Floor System Before Restoration

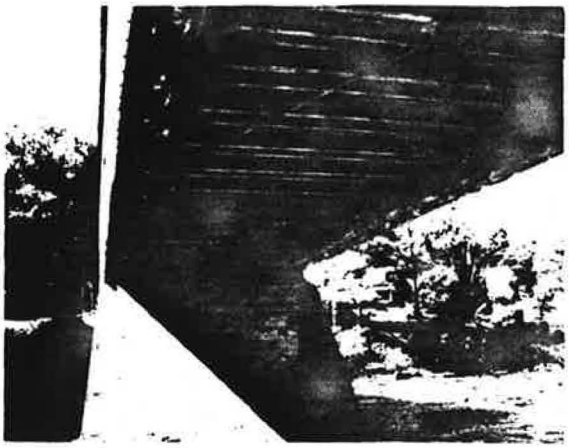

Figure 3. Bridge Elevation

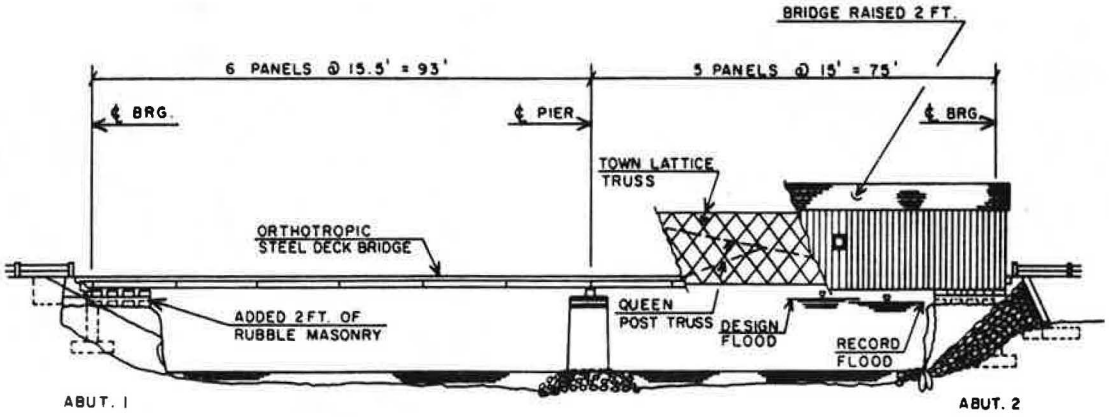

Figure 4. Bridge Cross-Section

Note: 1 ft. = 0.3 m

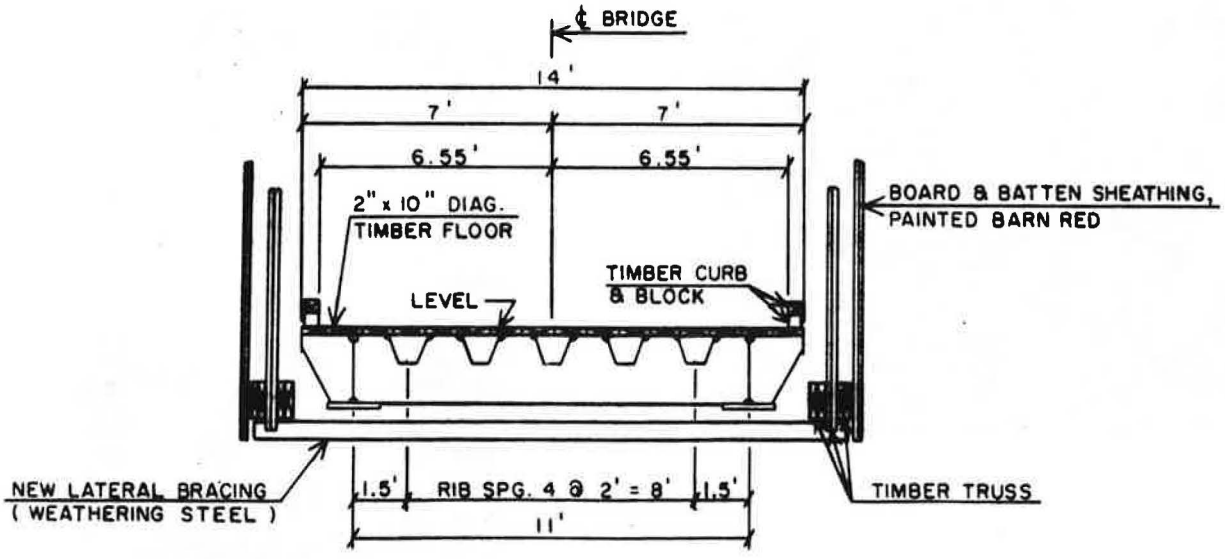

Figure 5. Temporary Bridge

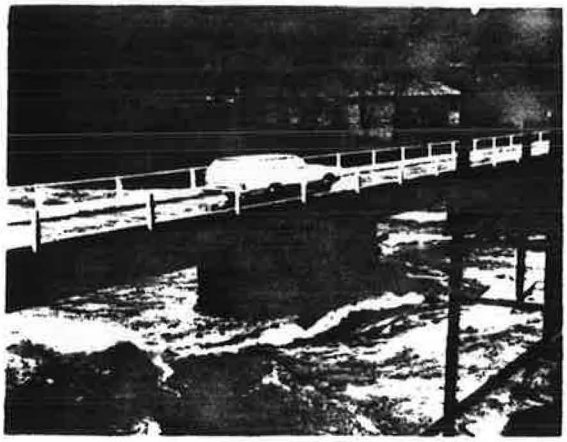

Figure 6. Orthotropic Bridge Fabrication

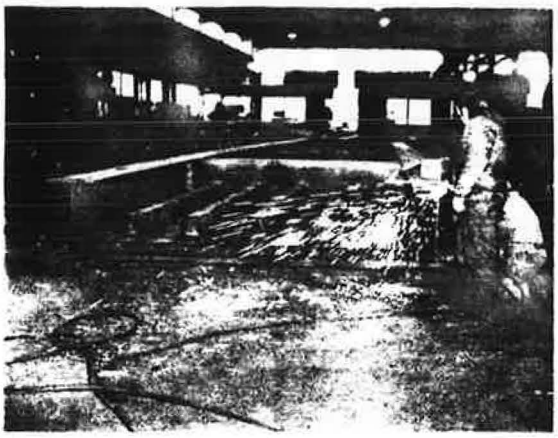

Figure 7. Completed End Section

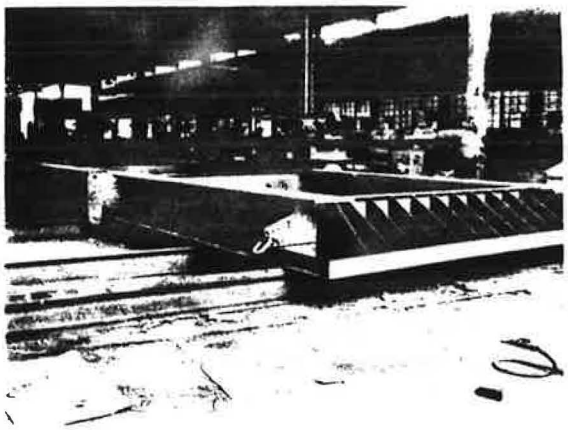

Figure 8. Bridge Site (Bulldozer Foreground)

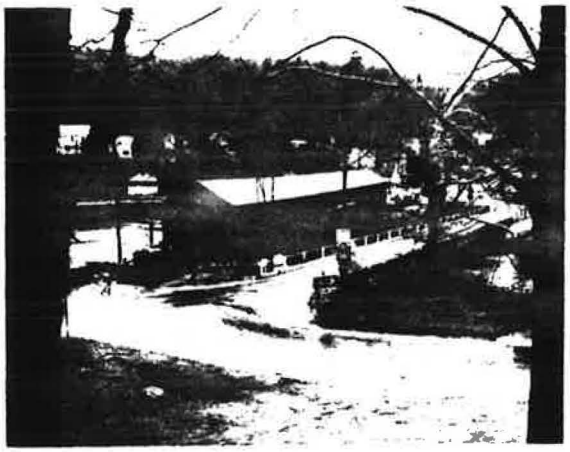

Figure 9. Bolted Girder Splice

Figure 10. Deck Plate Weld

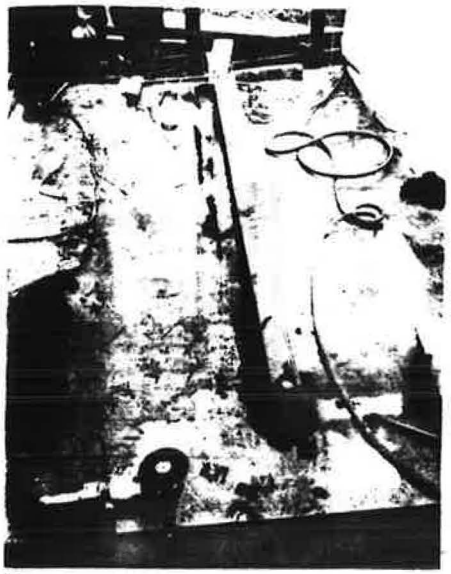

Figure 11. Completed Orthotropic Bridge and Lateral Bracing

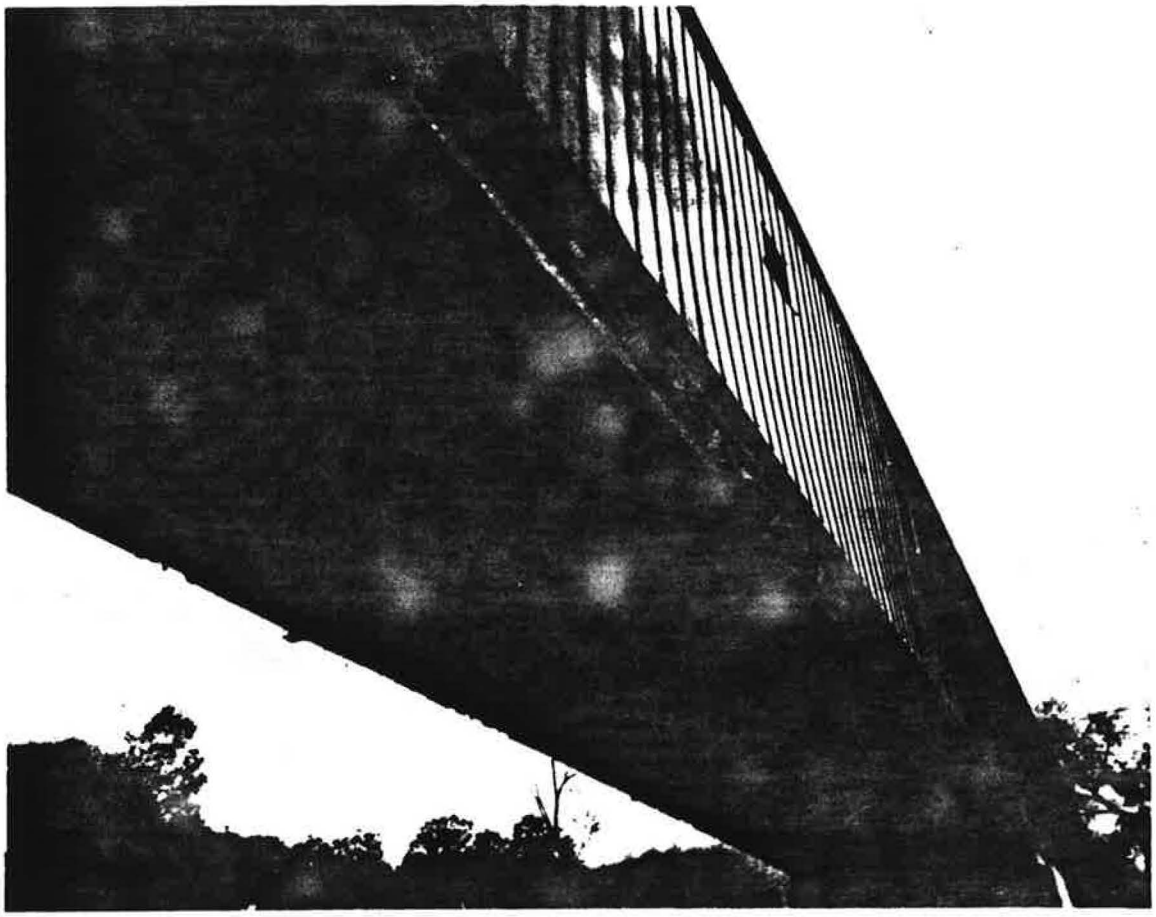

Figure 12. Restored Interior

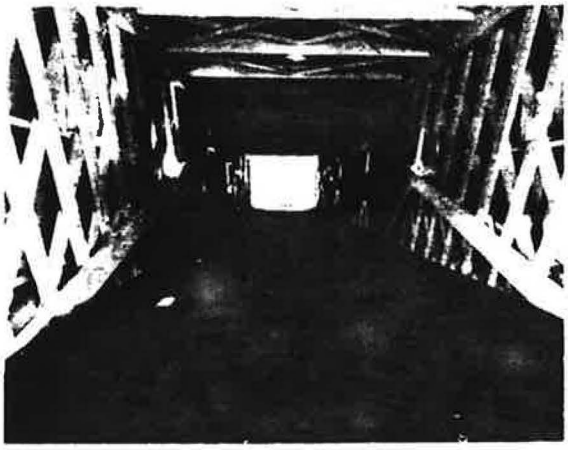

Figure 13. Bridge After Restoration

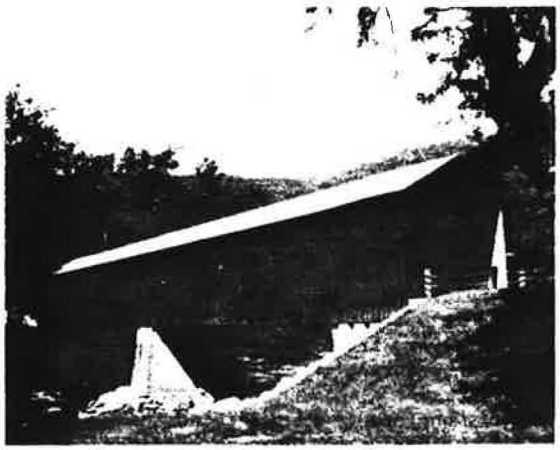

FATIGUE CONSIDERATIONS FOR THE DESIGN OF RAILROAD BRIDGES

Manfred A. Hirt, Swiss Federal Institute of Technology,
Lausanne, Switzerland

This paper describes a concept for the fatigue evaluation and design of railroad bridges. The primary objective is to account for the number of stress cycles per train, the corresponding stress ranges, and the total number of trains in the lifetime of the structure. Stress recordings from various structural elements of existing bridges were used as input for fatigue tests on beams. The test results are evaluated using the rainflow counting method and Miner's cumulative damage law. These results show good correspondence with constant amplitude test data. The assessment of traffic is based on theoretical traffic models and on measurements of axle loads and axle spacings. The fatigue effect of the traffic models is simulated by computer programs in terms of span length and compared to field measurements. It is shown that a correction factor may be applied to the design live load when used for fatigue considerations. In addition, the fatigue design concept enables to account for the total number of trains in the lifetime of the bridge. Also, a different safety factor may be applied for redundant and non-redundant load path structures.

Introduction

The collapse of a given structure due to fatigue depends on the fatigue behaviour of its different structural elements. The governing stresses causing fatigue damage in these elements are due to actual traffic conditions. For railroad bridges, the actual traffic may be described by axle loads and axle spacings for every train, and by the total number of train crossings during the lifetime of the bridge (Figure 1).

However, one has to bear in mind that it is impossible for a design engineer to consider actual traffic conditions except for the average number of trains per day. It is therefore important to adjust the design live load in such a way that the corrected live load may account for the actual traffic.

It is obvious that a brittle material may considerably shorten the lifetime of a structure. Hence, fatigue and brittle fracture are not independent (1, 2). It is therefore important that a sudden failure without preceding large deformations should be excluded either by using a sufficiently ductile material (3), or by adopting a highly redundant structural system. For the following discussion it is assumed that brittle fracture is not the governing mode of collapse.

Figure 1. Passenger train and a typical short span steel bridge.

Constant Amplitude Fatigue Strength

An extremely large amount of experimental test data on steel beams has been obtained since 1967 from a study sponsored by the National Cooperative Highway Research Program and carried out at the Fritz Engineering Laboratory of Lehigh University. These studies have shown that the most important factors which govern the fatigue strength are the stress range and the type of details, regardless of the type of steel (4, 5). Comprehensive specifications based on the stress range concept have been developed in the USA and are actually proposed in different countries in Europe.

Figure 2 shows the design categories proposed for the Swiss specifications for steel structures (6). An additional category A1 has been added for bolted connections, and the 95 % survival limits have been adjusted to a slope of m = 3 in the double-

Figure 2. Allowable fatigue stress ranges according to Swiss specifications for steel construction.

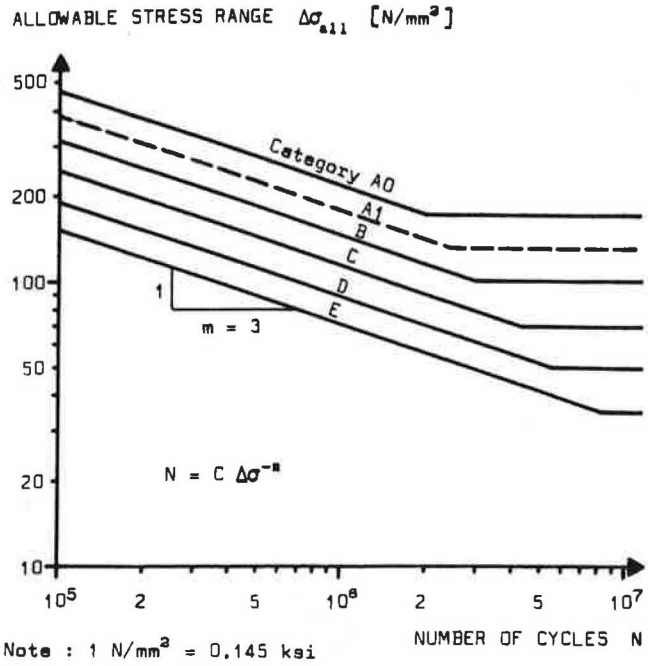

Note : 1 N/mm² = 0.145 ksi

logarithmic representation.

$$N = C\ \Delta\sigma^{-m} \qquad (1)$$

It will be shown that the parallel lines enable to consider the cumulative damage due to traffic stresses independently of design categories. This may not be true when the fatigue limit becomes important since the cut-off points are not always located at the same number of cycles.

The proposed fatigue strength categories had to be confirmed for typical design details and fabrication procedures used in Switzerland and Europe. The test results (7, 8) show good correspondence with previous results and the proposed categories appear to give a conservative estimate for all details tested.

Variable Amplitude Fatigue Strength

Figure 3 shows actual live load stresses in three different structural elements of the riveted bridges shown in Figure 1. Each bridge is built up of two riveted plate girders of 19.5 m (64 ft) span length and of floorbeams every 2.44 m (8 ft). The stringers, located under the rails and connected to the webs of the floorbeams support the wooden ties.

Figure 3. Typical live load stresses in three different structural elements and for two types of trains.

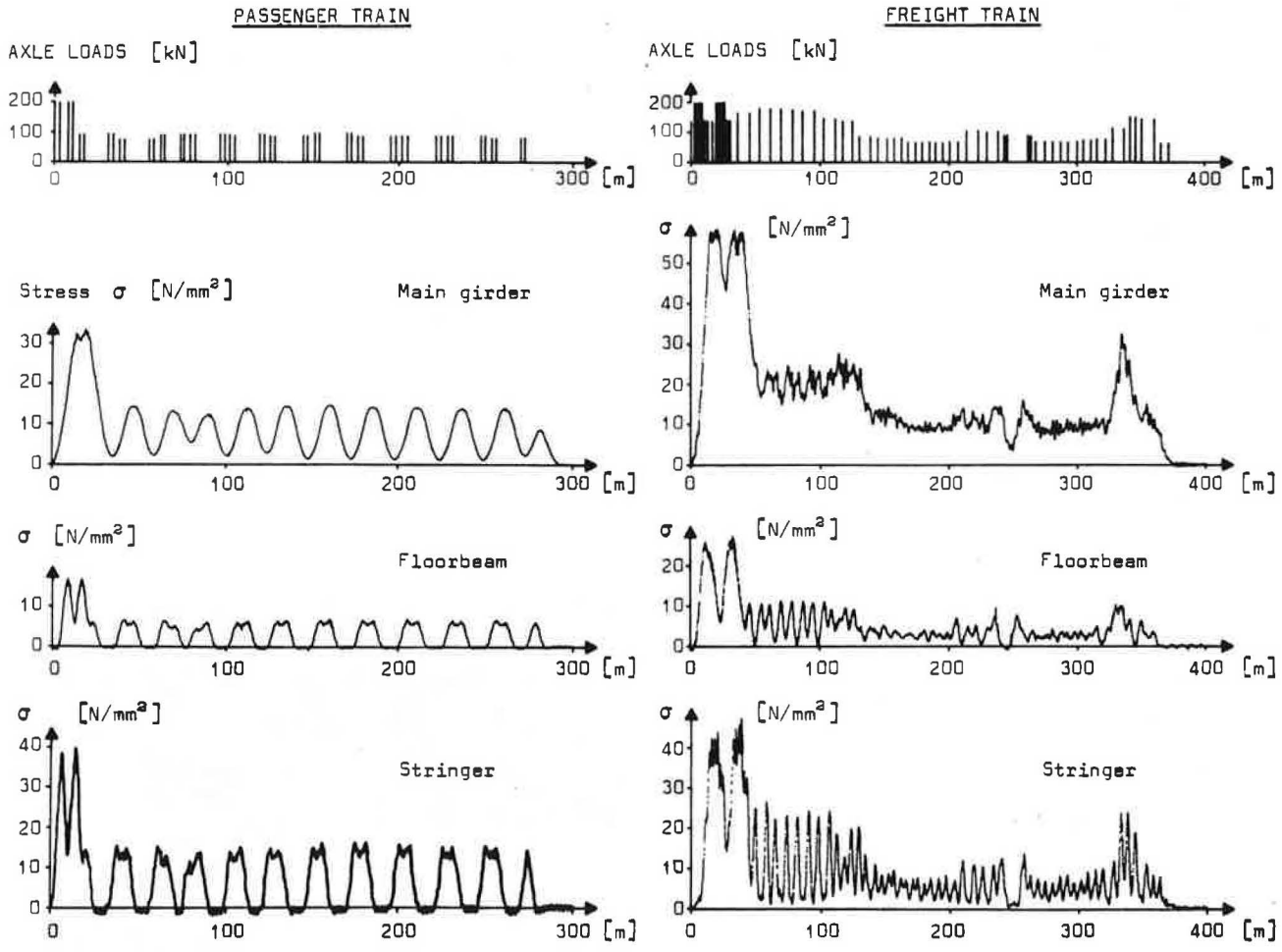

Note : 1 kN = 0.225 kip , 1 N/mm² = 0.145 ksi , 1 m = 3.28 ft

The recordings show quite regular stress fluctuations under the passage of the passenger train, they are much more random under the freight train. The locomotives of both train types cause predominant stress peaks.

The question arises as to how to treat (statistically and theoretically) such recordings in order to assess the cumulative fatigue damage of the stress fluctuations.

Figure 4. Comparaison of three different categories of stress-time diagrams.

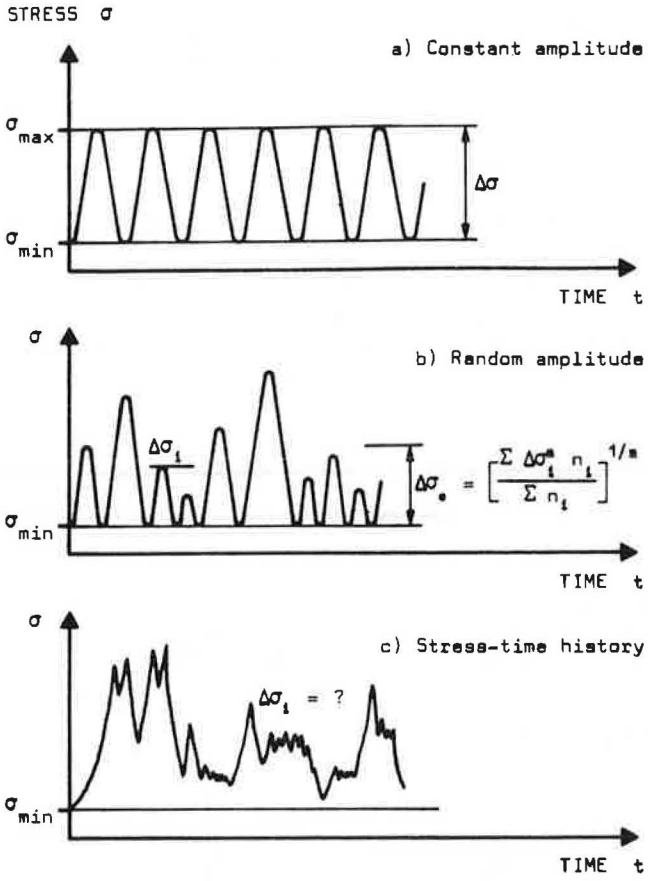

Figure 5. Schematic representation of the rainflow counting method.

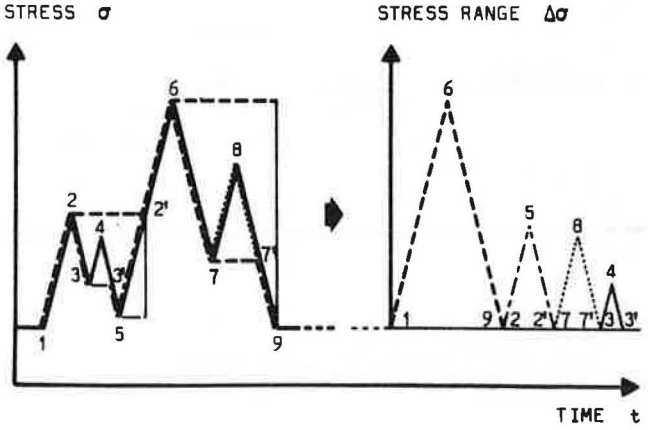

Equivalent Stress Range

General stress-time histories (Figure 4 c) have to be correlated to constant amplitude data (Figure 4 a). This may be done in two steps :

1. The first step consists in defining and counting the individual stress ranges $\Delta\sigma_i$ of a given stress-time history. This procedure assumes a priori the validity of the stress range concept. Hence, of the many counting methods available (9) only those can be used that adequatly define stress ranges. The European railroad convention (UIC : Union Internationale de Chemins de fer) has proposed to apply the rainflow counting method (10) of which a graphical representation is shown in Figure 5. It can be shown that the results of the rainflow count correspond well to those given by the range pair count. However, the rainflow method presents the advantage that the cut-off level for small stress cycles does not have to be fixed in advance.

2. The second step relates the fatigue effect of the above defined stress ranges $\Delta\sigma_i$ to an equivalent constant amplitude stress range $\Delta\sigma_e$ (11). Based on the cumulative damage law of Palmgren-Miner and the fatigue strength lines according to equation 1, the equivalent stress range $\Delta\sigma_e$ becomes

$$\Delta\sigma_e = \left[\frac{\Sigma\, \Delta\sigma_i^m\, n_i}{\Sigma\, n_i}\right]^{1/m} \qquad (2)$$

where m is the slope of the lines without consideration of the fatigue limits.

This second step had been shown to be a conservative approach to account for the cumulative damage of random stress cycles (12). However, it is important to note that the assumptions for the first and second steps are not necessarily independent. Only test results can confirm the validity of the hypotheses.

Stress History Fatigue Tests

Stress recordings from passages of different types of trains were used for fatigue tests at the Swiss Federal Institute of Technology. The test set-up of Figure 6 shows two 500 kN (110 tons) hydraulic jacks, two load cells, and a test beam as well as the electronic control panels. This closed loop system with a capacity of 250 litres of oil per minute (65 gpm) was designed and fabricated by F + W Emmen, Switzerland.

Figure 6. Fatigue test simulator.

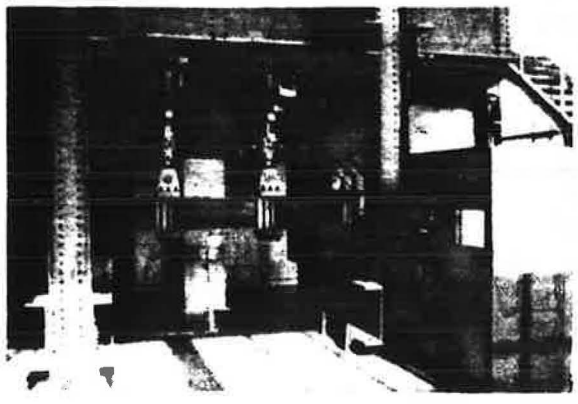

One set of test results of cover-plated beams is shown in Figure 7. The number of stress cycles corresponds to the total number of cycles counted, and the equivalent stress range is calculated using equation 2 with m = 3. Also included are five results from constant amplitude tests. It can be seen that the tests using stress-time histories give results comparable to constant amplitude data.

However, it should be noted that a slightly better correlation between test results might be obtained using an exponent m greater than 3. Additional tests on beams with gusset plates welded to the tension flange (13) yield similar results. More tests are under way to further investigate the correlation between actual stress histories and constant amplitude test data.

Considering the many influencing parameters of actual traffic, it shall be assumed that equation 2 is sufficiently accurate. The next question is therefore, how to obtain the number of stress cycles and the corresponding equivalent stress ranges for every structural element.

Figure 7. Fatigue test results of cover-plated beams subjected to real stress-time histories.

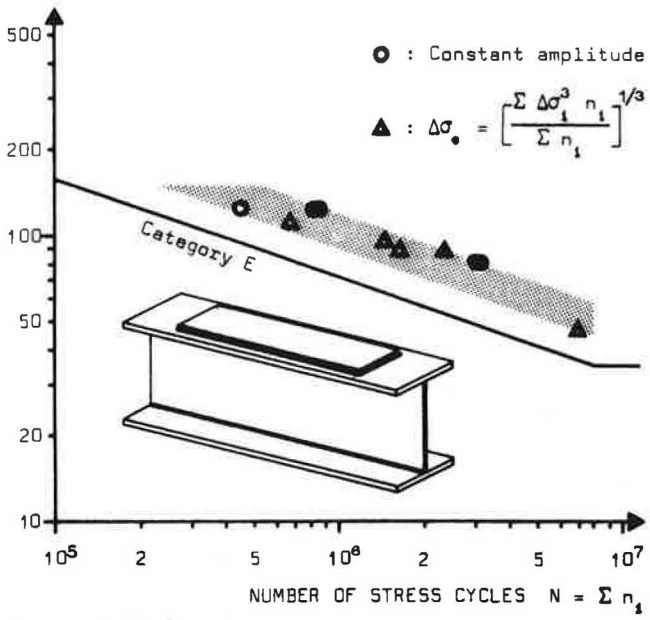

Note : 1 N/mm² = 0.145 ksi

Effect of Traffic Loads

Traffic Models

One of the traffic models used for computer simulation is shown in Figure 8. It is representative of the rolling stock and assumes a certain number of passenger trains, differently loaded freight trains, and some block trains. Up to a total number of 150 trains per day in each direction have already been recorded on a double track line in Switzerland.

The above defined traffic is used to compute the number of stress cycles and the equivalent stress ranges. This can be done for different shapes of influence lines, such as for a simple span bridge,

Figure 8. Traffic model (Swiss Federal Railroads) used for a computer analysis of the effect of actual traffic on railroad bridges.

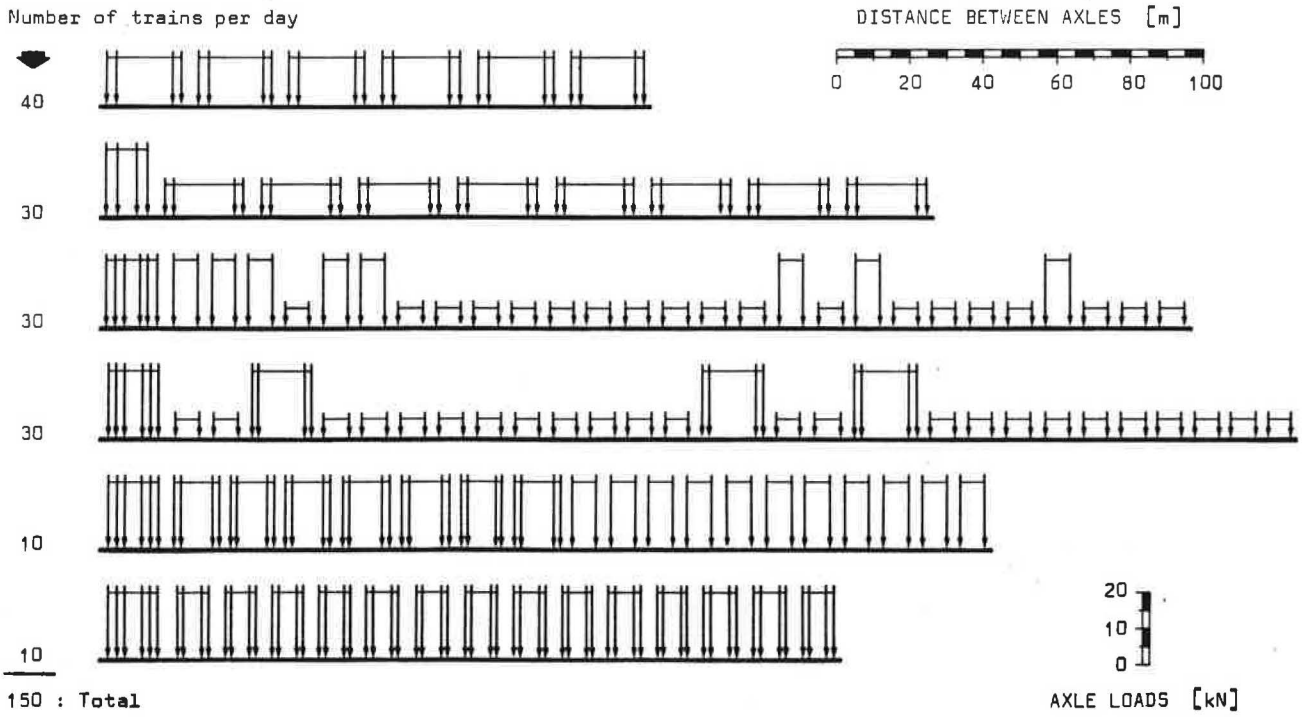

Note : 1 kN = 0.225 kip , 1 m = 3.28 ft

continuous bridge or a stringer on spring supports. However, in order to avoid computing stresses, the effect of the traffic is directly compared to the effect of the UIC design live load, shown in Figure 9.

The equivalent stress range $\Delta\sigma_e$ and the maximum stress range $\Delta\sigma_{max}$ of the traffic model are compared in Figure 10 to the stress range due to the UIC live load. The corresponding number of stress cycles in terms of span length are shown in Figure 11. The following observations can be made from these two figures :

1. The maximum stress range remains generally below 70 % of the UIC design stress range. This value shall be used later on when the effect of the fatigue limits are discussed.
2. The equivalent stress range $\Delta\sigma_e$ amounts to approximately 40 % of the UIC design stress range, depending only slightly on span length.
3. The corresponding number of stress cycles, given as an average number of cycles per train greatly depends on span length. For very short spans, almost every axle causes a major stress cycle, then for spans up to 20 m (65 ft) approximately one cycle per car occurs, and for longer spans only one cycle per train is observed. It should be noted that all stress ranges smaller than 10 % of the UIC design stress range have been neglected.

The two parameters, equivalent stress range $\Delta\sigma_e$ and average number of cycles per train N_{av}, can now be used to assess the fatigue life of a given structure. Also, their fatigue damage can be compared to the theoretical damage due to the UIC design stress range.

Correction Factor

The fatigue life, expressed in number of trains N_t for a given structural element is

$$N_t = \frac{C\ \Delta\sigma_e^{-m}}{N_{av}} \qquad (3)$$

when $\Delta\sigma$ in equation 1 is replaced by the equivalent stress range $\Delta\sigma_e$ for the traffic model, and the corresponding number of stress cycles per train N_{av} is accounted for. Conversely, the design stress range $\Delta\sigma_{UIC}$ can be adjusted by a correction factor κ in such a way that the same number of theoretical load applications results :

$$N = N_t = C\ (\kappa\ \Delta\sigma_{UIC})^{-m} \qquad (4)$$

The comparison of the right hand sides of equations 3 and 4 yield the correction factor

$$\kappa = \frac{\Delta\sigma_e}{\Delta\sigma_{UIC}}\ N_{av}^{1/m} \qquad (5)$$

Both terms of equation 5 ($\Delta\sigma_e/\Delta\sigma_{UIC}$ and N_{av}) have already been given in Figures 10 and 11. Hence, the correction factor can be computed. This can be done regardless of design categories provided the slope m of the fatigue strength lines (Figure 2) is the same.

The heavy line in Figure 12 shows the resulting correction factor for the traffic model used. A strong influence of span length is apparent ; the values increase rapidly with decreasing span length (14). This obviously reflects the greater number of

Figure 9. UIC design live load (UIC : Union Internationale des Chemins de fer).

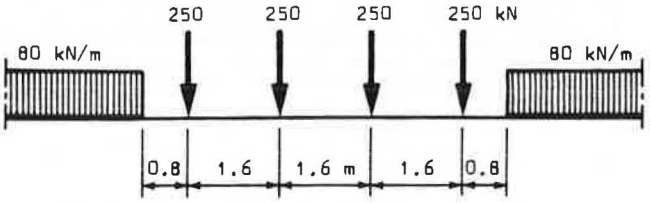

Note : 1 kN = 0.225 kip , 1 kN/m = 68.6 pounds per foot

Figure 10. Comparison of the maximum and equivalent stress ranges due to the traffic model with the stress range due to the UIC design load.

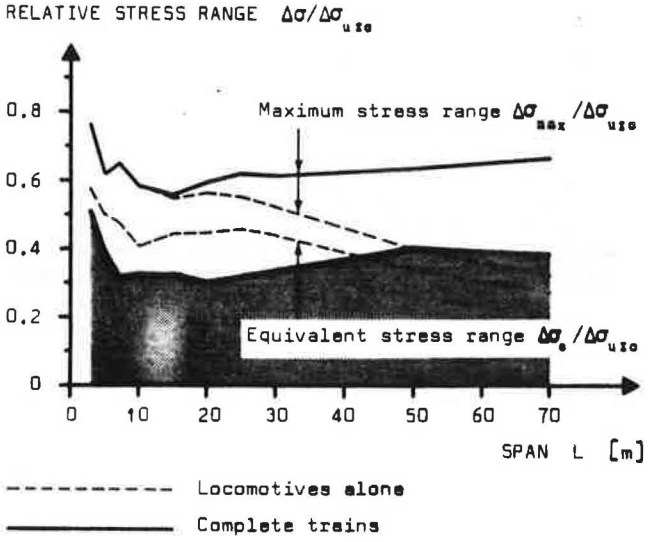

Figure 11. Average number of major stress cycles per train depending on span length.

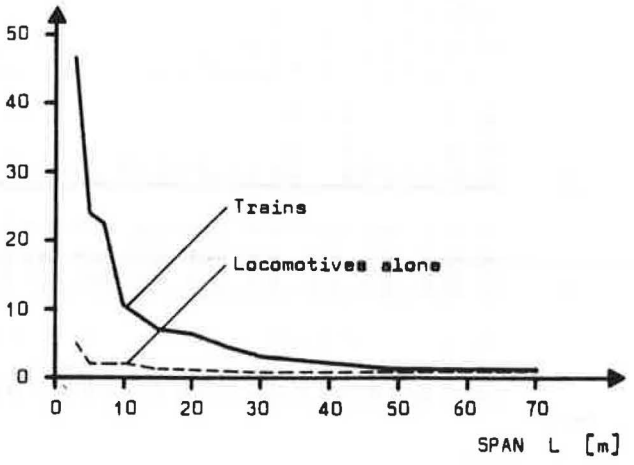

stress cycles per train for shorter spans. Similar curves have been obtained for different European countries representing various traffic models.

Comparison with Actual Traffic

Equation 5 gives a correction factor based on a traffic model and on theoretical influence lines. It is of interest to compare these values with values derived from stress recordings ; a few results (14, 15) are shown in Figure 12. It can be seen that the measured values for the main girder correspond well to the theoretical value, but the values for the floorbeam and stringer are substantially below the calculated values. This might be explained as follows :

Figure 12. Correction factor applied to the UIC design load in order to account for the cumulative fatigue damage of actual service traffic.

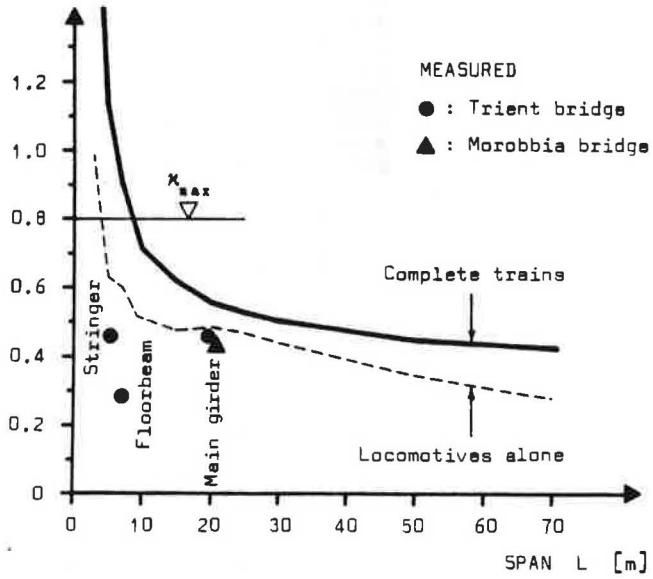

1. The actual axle loads measured were generally smaller than those used for the traffic model, in particular a smaller percentage of heavy freight trains and trains with two locomotives were observed.
2. The design stress range $\Delta\sigma_{u\,ic}$ includes an impact factor to account for dynamic effects. This impact factor is quite important for short spans, typically about 50 % for a span of 5 metres (15 ft). However, stress recordings showed much smaller impact values.
3. The statical behaviour of bridges is generally more favorable than assumed in structural analysis due to load distribution effects and greater redundacy of the structural elements.
4. The design of short elements, like floorbeams and stringers, is often based on stiffness because of deflection limitations. Hence, actual traffic stresses are quite small.

The comparison between measured and theoretical reduction factors (which is not affected by the actual number of trains) indicates a certain margin of safety. However, the few experimental results available to date do not enable to attribute numerical values to this margin of safety. Studies are under way in different European countries to obtain more data.

Fatigue Design Concept

Based on the preceding results and conclusions, the following fatigue design rule is proposed :

$$\kappa\ \Delta\sigma_{u\,ic} \leq \frac{1}{\gamma}\ \Delta\sigma_{all}\ (N_t\ ;\ \text{Category}) \qquad (6)$$

1. The left hand side (load side) considers the design stress range $\Delta\sigma_{u\,ic}$ based on the static design live load, including impact, but adjusted by a correction factor κ (Figure 12) such as to account for the cumulative fatigue damage of actual traffic.
2. The right hand side (strength side) defines the allowable fatigue strength $\Delta\sigma_{all}$ in terms of the total number of trains N_t in the lifetime of the structure, and according to the design category of a given detail (Figure 2).
3. The safety factor can be adjusted to differentiate between redundant and non-redundant load path structures.

The design engineer simply uses the regular design live load to compute the design stress range at a given point in the structure. This value is then corrected to account for the cumulative fatigue damage of actual traffic, where the correction factor is defined in terms of span length for a simple span element, or in terms of the influence length for redundant elements. The fatigue strength for the given structural detail is obtained in terms of the predicted number of trains in the lifetime of the structure.

The same concept may be applied to evaluate the remaining fatigue life of existing bridges. A different correction factor may be used respectively for past, present and future traffic.

Influence of the Fatigue Limit

It is obvious that for a great daily traffic, for example 150 trains, and design lifetime of the structure, for example 100 years, the total number of trains becomes very large ; for the values cited about 5.5 million. For most design categories, this number is greater than the number of cycles N_f of the fatigue limit. Hence, equation 6 could be replaced by

$$\kappa\ \Delta\sigma_{u\,ic} \leq \frac{1}{\gamma}\ \Delta\sigma_f\ (\text{Category}) \qquad (7)$$

This is still too conservative, in particular for small spans, since the reduction factor is obtained without consideration of the fatigue limit. In fact, one must only assure that every stress range $\Delta\sigma_i$, in particular the largest stress range $\Delta\sigma_{max}$, remains below the fatigue limit σ_f ; or analytically

$$\Delta\sigma_{max} \leq \frac{1}{\gamma}\ \Delta\sigma_f \qquad (8)$$

Comparing the left hand sides of equations 7 and 8, a limit for κ can be defined,

$$\kappa_{max} = \frac{\Delta\sigma_{max}}{\Delta\sigma_{uic}} \qquad (9)$$

which amounts to approximately 0.7 according to the values shown in Figure 10.

Small Number of Trains

The general equation 6 is valid, but the limiting value κ_{max} has to be adjusted :

$$\kappa_{max} = \frac{\Delta\sigma_{max}}{\Delta\sigma_{uic}} \left[\frac{N_f}{N_t}\right]^{1/m} \qquad (10)$$

N_f is again the number of cycles at the cut-off point for the fatigue limit, and $N_t \leq N_f$ corresponds to the total number of trains in the lifetime of the structure. It is seen that the numerical values of κ_{max} depend on the design category since the fatigue limits do not intersect the fatigue strength lines at the same number of cycles N_f (Figure 2).

Conclusion

The primary objective of this paper is to account for the fatigue effects of actual traffic on railroad bridges. Based on the stress range concept for the fatigue strength, the fatigue damage of stress-time histories are related to constant amplitude test data using the rainflow counting method and Miner's cumulative damage law. The design stress range is then related to the effects of actual traffic or traffic models by a correction factor. As a result, it is shown that design engineers may use the usual design live load and adjust the resulting stress range by this correction factor. The only additional information needed for design is the number of trains in the lifetime of the structure. This number, based on actual or predicted traffic volumes, has to be fixed by the railroad administration.

Acknowledgments

Much of the research discussed in this paper was carried out at the Federal Institute of Technology, Lausanne, Switzerland, under the sponsorship of the Swiss Federal Railroad Administration, the Swiss Federal Department of Transport and the Swiss National Science Foundation. Appreciation is also expressed to the staff at the Institute for Steel Construction.

References

1. Scheffey, C.F. Point Pleasant Bridge Collapse - Conclusion of the Federal Study. ASCE Civil Engineering, 7, 1971, pp. 41-45.
2. Madison, R.B. and Irwin, G.R. Fracture Analysis of King's Bridge, Melbourne. ASCE Journal of the Structural Division, ST9, 1971, pp. 2229-2244.
3. Roberts, R. and Irwin, G.R. Fatigue and Fracture of Bridge Steels. ASCE Journal of the Structural Division, ST2, 1976, pp. 337-353.
4. Fisher, J.W., Frank, K.H., Hirt, M.A. and McNamee, B.M. Effect of Weldments on the Fatigue Strength of Steel Beams. NCHRP Report 102, Highway Research Board, Washington D.C., 1970.
5. Fisher, J.W. et al. : Fatigue Strength of Steel Beams with Transverse Stiffeners and Attachments. NCHRP Report 147, Highway Research Board, Washington D.C., 1974.
6. Schweizerischer Ingenieur- und Architekten-Verein. Steel Structures, SIA Norm 161-E, Zürich, 1978.
7. Hirt, M.A. and Crisinel, M. La résistance à la fatigue des poutres en âme pleine composées-soudées, - Effet des plaquettes et goussets soudés à l'aile. Ecole Polytechnique Fédérale de Lausanne, ICOM 017, 1975.
8. Hirt, M.A. and Crisinel, M. La résistance à la fatigue des poutres en âme pleine composées-soudées, - Effet des détails constructifs et comparaison avec la norme. Ecole Polytechnique Fédérale de Lausanne, ICOM (en préparation).
9. Buxbaum, O. Statistische Zählverfahren als Bindeglied zwischen Beanspruchungsmessung und Betriebsfestigkeitsversuch. Laboratorium für Betriebsfestigkeit, TB-65, Darmstadt, 1966.
10. International Union of Railways. Statistical Distribution of Axle Loads and Stresses in Railway Bridges - Introduction and Definitions. ORE Report D 128/RP1, Utrecht, 1973.
11. Swanson, S.R. Random Load Fatigue : State of the Art Survey. Materials Research and Standards, April, 1968, pp. 10-44.
12. Schilling, C.G., Klippstein, K.H., Barsom, J.M. and Blake, G.T. Fatigue of Welded Steel Bridge Members under Variable-Amplitude Loadings. Final Report NCHRP Project 12-12, Transportation Research Board, Washington D.C., 1975.
13. Hirt, M.A. and Jacquemoud, J. Analyse des essais préliminaires sous charges aléatoires par la méthode de la différence de contraintes équivalente. Ecole Polytechnique Fédérale de Lausanne, ICOM (en préparation).
14. Wolchuk, R. and Mayrbaurl, R.M. Stress Cycles for Fatigue Design of Railroad Bridges. ASCE Journal of the Structural Division, ST1, 1976, pp. 203-213.
15. Jaccard, A. Comportement à la fatigue des ponts-rails. Travail de diplôme, Ecole Polytechnique Fédérale de Lausanne, ICOM, 1976.
16. Hirt, M.A. and Hausammann, H. Betriebsfestigkeit von Eisenbahnbrücken in Verbundbauweise am Beispiel der Morobbia-Brücke. Ecole Polytechnique Fédérale de Lausanne, ICOM 027, 1976.

FATIGUE PROBLEMS IN HIGHWAY BRIDGES

G P Tilly, Transport and Road Research Laboratory

Abstract

During the past few years there has been an increasing incidence of fatigue cracking in the welded joints of modern steel bridges. Many examples have occurred in welds on main girders of short or medium span highway bridges having concrete decks, and in welded joints in orthotropic steel decks of temporary bridges and long span bridges. Design of British bridges is checked for lives of 120 years involving up to 7.10^8 cycles of stress. Calculations to assess fatigue require a realistic loading spectrum, reliable methods to obtain local stresses, and relevant S/N relationships between stresses and numbers of cycles to failure. This paper briefly describes some of the recent research to improve the background to these three steps for design of bridges, particularly those having orthotropic steel decks. The research includes investigation of the influence of surfacing, type of stress cycle, residual stress, plate thickness, cyclic frequency, rest-periods, weathering and consideration of programmed loading.

Highway bridges in Britain are checked for a fatigue life of 120 years during which time up to 7.10^8 potentially damaging major stress cycles may be produced by the passage of commercial vehicles. Until recent years, fatigue was not considered to be an important feature of design because there were comparatively few cases of reported damage. The picture has changed with the build up of information about the performance of welded joints. Such joints involve stress concentrations due to their geometry and contain incipient flaws so that the crack initiation phase of fatigue is almost entirely eliminated. This causes a drastic reduction in fatigue life as compared with plain unwelded components.

For highway bridges, fatigue problems tend to fall into three classes; those concerned with attachments welded to steel girders of structures having intermediate length spans, those concerned with the welded joints in orthotropic steel decks, and components subjected to resonant vibration. The problems can, of course, be exacerbated by poor design detailing and workmanship. For main girders, the stress ranges are due to gross vehicle weight rather than axle weight. There have been a number of reported cases of fatigue cracks of this type in North American bridges (1 to 4) and it has been shown that the lives can be correlated with calculated figures derived from traffic data and measured laboratory performance. Much of this success is due to the work of Fisher and his colleagues at Lehigh University. There have also been several cases in Europe of fatigue cracking in composite bridges having steel girders and concrete decks. There have been instances of fatigue cracking in the welded joints of orthotropic steel decks. This form of construction involves weld details that have relatively poor fatigue resistance and are subject to high stresses due to the local effects of wheel loads at trough-stiffener to cross-beam welds and at trough-stiffener to deck-plate welds. The latter stresses are influenced by the presence of the asphalt wearing surface (5). The earliest recorded cracks occurred in one of two experimental deck panels installed in a busy road at Denham, England (6). One panel was surfaced with 38mm thick mastic asphalt, the other with 9mm thick resin based material. After 4 years, cracks developed in three of the trough-stiffener to cross-beam welds on the panel having the thinner surfacing. After 9 years, additional cracks had developed but there were none in the panel having thicker surfacing. Cracks have developed in orthotropic decks of temporary bridges. Such bridges, although designed for full traffic loading usually have relatively thin surfacing so that high stresses are developed close to the deck plate. In a Swedish temporary bridge, several cracks were found in the trough-stiffener to cross-beam joints. In a German temporary bridge, cracks and failures were found in a number of the trough-stiffener to deck plate joints.

There have also been several instances of cracks in steel orthotropic decks of permanent bridges having normal thickness of surfacings. In all cases the faults have been repaired to a good standard. An interesting situation arose in the Severn Bridge, England, where temporary bulkheads were welded to the ends of the box sections so that they could be floated down river to the construction site. The bulk heads were welded to the underside of the trapezoidal trough-stiffener giving a connection with a low fatigue resistance. In addition, the bulkhead formed a "hard spot" under trafficking so that relatively high cyclic stresses developed

cracks in the welded joints between the bulkhead plate and the lower flanges of the stiffeners. Effective repairs were made by cutting away the bulkhead plate beneath the stiffener and bolting cover plates on each side of the bottom flange of the trough-stiffener. Later, cracks developed in intermittent fillet welds in a splice joint between "stub" plates and "main" plates, in about thirty diaphragms (7). In this case it was not necessary to remove any material and the overlapping plates were bolted together. About 24 cracks were found in the trough-stiffener to deck plate joints in 1977 (8). None exceeded 1m and the average length was 500mm. The cracked material was removed and the joints rewelded to give sound and effective repairs.

In order to improve the trough-stiffener to cross-beam detail in orthotropic decks, many designs have taken the troughs through a cut-out in the cross beam. This scheme improves the detail at the cross-beam but transfers the problem to the trough connections. Special attention was given to design of joints in trapezoidal stiffeners in the bridge at Ewijk across the River Waal in Holland. Laboratory fatigue tests were made on three types of joint and it was found that the best performance was given by having a 300mm long intermediate stiffener of the same thickness and butt welded on to backing strips (9). A different detail was designed for the Rio Niteroi bridge, the joints having splice plates which were welded to the sides and bottom of the trapezoidal stiffeners. Soon after construction, measurements were made under normal traffic which showed that cyclic stresses occurred whose ranges exceed the fatigue cut-off. It was calculated that visible fatigue cracking could develop after 30 to 40 years service (10).

Fatigue can also occur through resonant stresses as opposed to direct traffic induced stresses. In a bridge in England, traffic induced vibrations produced almost continual resonance of lightweight cross-bracing which eventually caused fatigue fractures to occur at welded nodal connections. Fortunately these were readily accessible so that the welds could be repaired cheaply and effectively. The bracing was bolted to a cross-beam to eliminate the vertical vibrations. There have been several instances of failures due to wind induced vibration of bridge components. Examples have been reported of damage to hangers of Japanese bridges (11); there were cracks in the Shitoku-Oshashi bridge which vibrated at 3.45Hz and in the Maroroshi bridge which vibrated at 7.7Hz. Vibrations occurred in the inclined hangers of the Severn Bridge, England, and it was necessary to fit modified Stockbridge dampers to avoid potential problems. Wind and traffic induced vibrations are, however, not normally found to produce significant cyclic stresses in bridge superstructures and reported problems have been confined to lightweight attachments that can vibrate at a resonant frequency.

This paper is mainly concerned with the appraisal of fatigue caused by traffic induced stresses in orthotropic steel decks.

1. Traffic Loading

Considerable attention has been given to collecting axle load and vehicle load data for use in design of pavements as well as bridges. Several types of dynamic weighbridges, for weighing moving traffic without interruption to flow, have been devised (12 to 16). The system developed for British work is composed of three 0.6m square modules made from aluminium castings each having four load cells (12). When used with inductive loop detectors and an axle detector, data can be collected for vehicle speed, length, wheel base, headway and axle weight. It is essential for installations to be in smooth road surfaces free from ruts or undulations which could cause dynamic effects in the vehicle suspension system. Measurements made using different vehicles driven across a specially constructed test track, showed that the range of variations in the measured axle load can exceed 15% of the static value (17). In practice the pavement surfaces adjacent to and across bridges tend to have irregularities associated with features such as expansion joints. Soil compacted behind abutments can settle so that there is a pronounced step in the approach to the bridge. Such irregularities generate extra variations in dynamic loads so that high peak values can occur. In order to assess these effects, a 160kN test vehicle was fitted with instrumentation to its back axle to enable dynamic loads to be measured. The vehicle was driven across thirty motorway and over-motorway bridges (18). It was found that peak values of impact factors (ratio of dynamic to static wheel load) ranged from 1.09 to 1.75. In an extreme case of a bridge which carried an unclassified road over a motorway a peak value of 2.77 was recorded. Measurements were also made on two long span bridges having orthotropic steel decks. Peak values of impact factor were up to 1.7 and the RMS value of the dynamic component of wheel load was 5.8kN for the two bridges (the static wheel load was 50 kN). The impact effects are dominant for the first cycle and rapidly decay. The biggest effects are for unladen vehicles so that the heavy loads which are potentially the most damaging develop smaller dynamic components.

Figure 1. Transverse section of orthotropic deck showing distribution of nearside wheels.

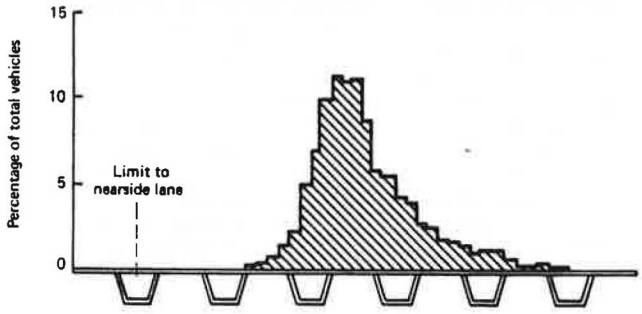

Assessment of the fatigue lives of orthotropic steel decks presents special problems because stresses are very sensitive to the lateral position of the vehicle. Measurements made of transverse positions, using a photographic technique, showed that 71% of all wheels passed with ± 300mm of the centre line of the lane, figure 1. For multi-lane dual carriageways, the heavy vehicles tend to be concentrated in the near-side (right hand) lanes. Measurements of the distributions of vehicles exceeding 15 kN between lanes of dual carriageways, for flows Q ranging from 300 to 850 vehicles per hour, have shown that the proportion of vehicles in the nearside lane is given by the empirical expression $\frac{1200}{1200+Q}$. Thus, for a flow of 500 vehicles per hour, 70% of the heavy vehicles occupied the near side lane (19).

During the trials of orthotropic steel deck panels at Denham continuous measurements were made of axle and vehicle loads, 24 hours a day for three weeks, ie for a total time of 504 hours (20). Axle loads between 1.14 and 272 kN were recorded and classified in 9.1 kN increments. A total of 71,299

axles and 33,619 vehicles was recorded. Of these, 612 axles exceeded the legal limit plus a 10% allowance for impact and 57 vehicles exceeded the gross weight limit. Assuming that fatigue damage is proportional to $\sigma 3$ and neglecting cut-off, the overloaded axles have a damage potential of 24%, (σ is stress range). Using these and more recent data, consultants on behalf of Department of Transport have recommended a loading spectrum for the new British Standard for design of bridges. A 25 band spectrum of commercial vehicles (those vehicles having gross weights exceeding 15 kN) has been derived. Numbers of occurrences per million commercial vehicles were given and the damaging effect calculated. From these figures a standard fatigue vehicle was derived, figure 2.

Figure 2. Dimensions and spectrum of standard fatigue vehicle (not factored).

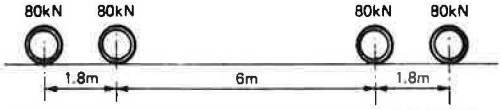

A) AXLE ARRANGEMENT OF STANDARD FATIGUE VEHICLE

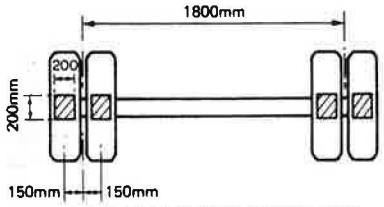

B) PLAN VIEW OF STANDARD AXLE

Axle weight kN	Vehicle weight kN	Proportion of vehicles
720	2880	0.00001
402	1608	0.00002
327	1308	0.00003
168	672	0.00044
84.8	339.2	0.1045
65.6	262.4	0.105
57.6	230.4	0.09
29.6	118.4	0.7

C) DESIGN LOAD SPECTRUM FOR MAIN MEMBERS

This has an axle arrangement similar to the type of vehicle responsible for half the damage in the 25 band spectrum. It has other advantages including the fact that it has the same axle arrangement as the notional HB design vehicle, so that results of static elastic analysis can be scaled and used for some of the fatigue checks. An equivalent spectrum of these standard fatigue vehicles is given in figure 2.

2. Stress Spectra

The determination of local stresses may be required for assessing the strength of an existing bridge or for determining a new design. Calculation of stresses in orthotropic decks presents problems due to the sharp stress gradients that develop at the joints and the difficulty in assessing effects of the asphalt wearing surface. The asphalt influences stresses due to its contribution to bending stiffness. Measurements of this composite action have shown that stresses close to the deck plate can be reduced to about 10 per cent of the values without asphalt, depending on features such as the deck temperature, speed of the vehicles, and grade of asphalt (5). A second series of tests on a different grade of asphalt showed that behaviour is influenced by time dependent mechanisms; when the vehicle is stationary the material directly beneath the wheels creeps so that stresses close to the deck plate reduce with time (21). After removal of the vehicle, periods of up to 20 minutes elapsed before the strains returned to the no-load condition. It was found that stresses in the lower surface of the deck plate were reduced by about 30 per cent when vehicle speeds were increased from crawl to 30 km/h, most of the effect occurring between crawl and 5 km/h. The stresses were increased by up to 100% for an increase in asphalt temperature from 20°C to 37°C.

For existing decks, it is more satisfactory to measure stresses produced by a vehicle, preferably under dynamic conditions. The fatigue life can either be calculated by relating measured influence lines to assumed vehicle spectra, or by measuring stress spectra at the detail in question. Measurement of influence lines requires both longitudinal and transverse directions so that it is really influence surfaces that are required. Because stresses are so sensitive to lateral wheel position, the measurements are most conveniently made with the vehicle stationary. For transverse influence lines, measurements should be at intervals not exceeding 75mm and for longitudinal influence lines they should be 38 to 100mm. Measurements have been made at TRRL with two types of deck having V-stiffeners and trapezoidal stiffeners (22,23). Loading was applied through a 900 x 20 wheel which could be accurately positioned on the panels. Transverse and longitudinal influence lines were produced, see for example figure 3.

Figure 3. Transverse stresses adjacent to the stiffener to deck plate weld.

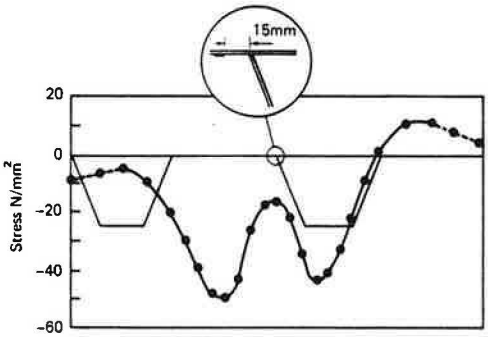

(a) TRANSVERSE INFLUENCE LINE, MID-WAY BETWEEN CROSSBEAMS

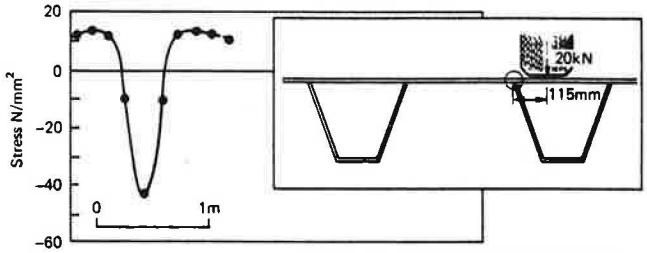

(b) LONGITUDINAL INFLUENCE LINE, WHEEL ABOVE STIFFENER

The data for unsurfaced panels tested in the laboratory are suitable for comparison with calculated stresses, partly because the questionable effect of the asphalt is eliminated and partly because the stresses are produced by more accurately controlled positioning of the wheel. Values of the stresses in the stiffener to deck plate joint have been calculated by a method using finite strip analysis. Comparisons between calculated and measured stresses, in figure 4, show good agreement.

Figure 4. Comparison of measured and calculated stresses adjacent to stiffener to deckplate weld.

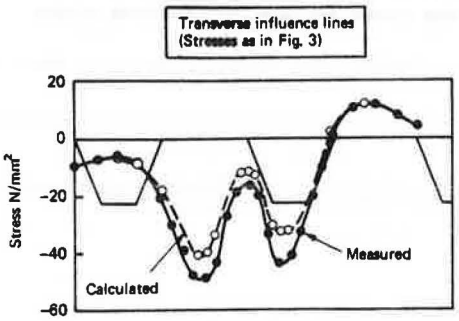

Measurements have been made of the traffic induced stresses in the panels installed at Denham (24). Strain gauges were fixed at different positions on the underside of the panels. The outputs were recorded on analogue magnetic tape and analysed in the laboratory. The shapes of stress cycles were irregular as shown by the examples in figure 5.

Figure 5. Typical traffic induced stress cycles.

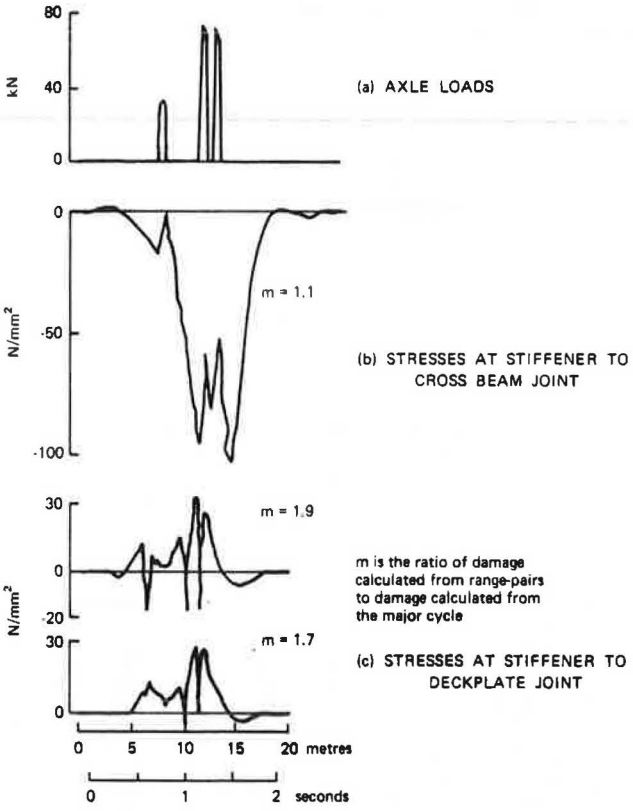

For the cycles considered, it was insufficient to record the peak to peak range and a program was written to count range-pairs and to classify occurrences in increments of 7.72 N/mm^2. In this method, counts are made of constituent cycles within a major cycle caused by one vehicle. Damage estimated from range-pairs for the cycles shown in figure 5, is up to 1.9 times more than that derived from the major cycles alone (the ratio is expressed as m). Histograms of results for 12 hours a day for 6 days are shown in figure 6.

Figure 6. Load and stress spectra measured at Denham.

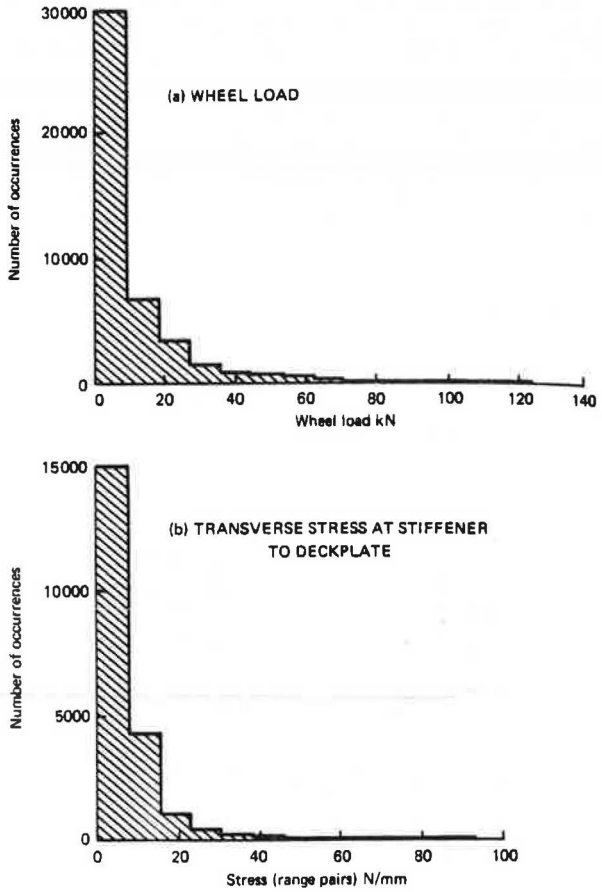

During the time that has elapsed since the stress data were collected at Denham, there have been changes to the vehicle regulations in Britain as well as differing trends in the distribution of types of vehicle. In addition a new generation of equipment has been developed so that data can be processed more quickly and a wider range of information obtained. It is therefore timely to update the state of the art and work is being done as part of a collaborative project sponsored by the European Coal and Steel Community. The first phase of the programme, which is currently under way, involves collection of 120 hours of data during two visits to each of three steel bridges, ie there will be a total of 360 hours data collected during six sessions at the bridges. Stresses are recorded on eleven channels. Axle loads, axle spacings, vehicle headways and speeds are also recorded (25).

3. Fatigue Relationships

The relevant S/N relationship between stress range and number of cycles to failure, for the component in question, can be selected by reference to a standard classification which gives curves based on conventional laboratory data for common types of welded joint. There is, however, the question of how realistically laboratory testing can simulate service conditions. For traffic loading of highway bridges it is necessary to have S/N data in the range 10^6 to 10^8 cycles, longer lives being too time consuming to produce. Many investigations have stopped at 10^7 cycles and missed the

more relevant longer endurances. For some cases this may not matter because there is a 'knee' in the S/N curve of many joints, at about 2.10^7 cycles, beyond which constant amplitude tests remain unbroken. Under variable amplitude loading however, failures can occur at lower mean stresses and longer endurances.

For investigations related to full scale behaviour it is necessary to use test pieces big enough to hold residual welding stresses which are typically up to yield stress. This is important because residual stresses play a significant role in the fatigue mechanisms of welded joints in bridges, particularly for pulsating - compression.

3.1 Residual Stresses

Most of the current understanding of effects of residual stress is due to the work of Gurney (26) who tested axial specimens having longitudinal non-load-carrying connections. In a co-ordinated series of tests at Welding Institute and TRRL, the main effects due to residual stresses were shown to be as follows:

1. For loading varying from pulsating-tension to fully reversed push-pull, the fatigue life is dependent upon stress range and is almost independent of mean stress and stress ratio, R. For pulsating-compression, lives are a little longer than those for pulsating-tension at the same range of stress, see figure 7.
2. The slope of the S/N relationship is steep-ended and the fatigue strength (the stress to produce a given life) is reduced significantly at longer lives, see figure 8.

Figure 7. Effect of tensile and compressive stress ratio on fatigue.

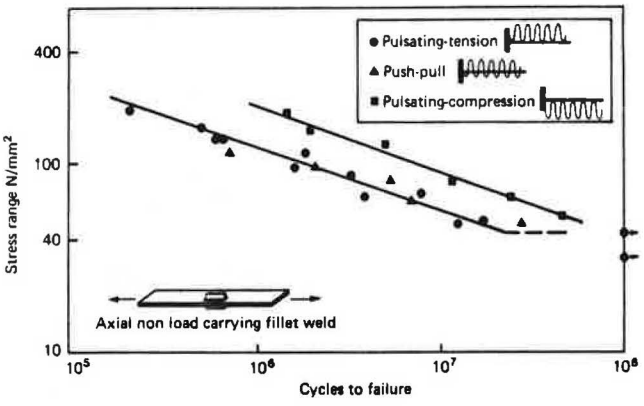

Figure 8. Effect of residual stresses on fatigue.

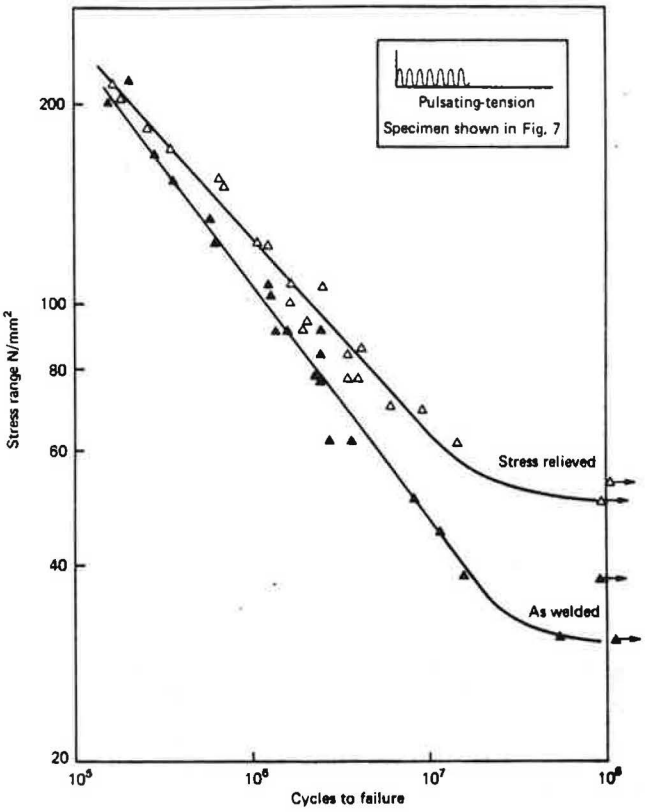

These effects can be explained from consideration of the stress/strain relationship for structural steel. This has a prolonged flat portion beyond yield stress and prior to the onset of work hardening. For applied stress ranges of yield stress magnitude, the surrounding elastic material is plastically deformed so that regions of high residual stress are relieved and fatigue life is unaffected. For lower stress ranges, the residual stresses are unaffected and lives are reduced due to the higher value of true (as opposed to nominal) stress ratio. For stress relieved specimens the true and nominal stress ranges are the same.

Pulsating-compression can be shown to be effectively the same as pulsating-tension because tension merely produces a small plastic excursion along the stress/strain curve which work hardens to the same stress range. However, it has been shown that pulsating-compression continues to propagate cracks beyond the zones of residual tensile stress and through the zone of compressive stress. In fact it is possible to fracture a welded test piece under the action of pulsating-compression. Such behaviour is almost certainly due to the fact that a crack has a plastic enclave at its tip, which is subject to strain-cycling due to the presence of the surrounding elastic material. Once initiated, the material ahead of the crack continues to experience the same value of strain range irrespective of whether it is in the zone originally containing residual tension.

Figure 9. Effect of plate thickness on fatigue of longitudinal non load carrying fillet weld.

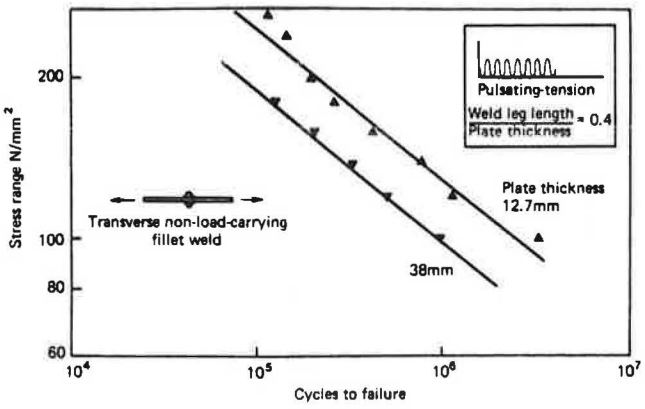

3.2 Plate Thickness

When relating laboratory data to bridge performance, it is necessary to consider size effect in relation to plate thickness. Analysis shows that the size of an initial defect at the weld toe which just allows crack propagation, decreases with increase in plate thickness. Tests have been done at the Welding Institute to confirm the extent of these effects for an axial specimen having a transverse non-load-carrying fillet weld. These show that there is indeed a comparatively big effect for a ratio of weld-leg-length to plate thickness of 0,4, figure 9. The difference in strength at 2.10^6 cycles for plate thicknesses of 12.7 and 38mm, can be seen to be approximately 24 per cent.

3.3 Test Time

The production of fatigue data for endurances of around 10^8 cycles is essentially the simulation of 120 years design life by laboratory tests lasting for up to about 12 weeks. Such acceleration involves assumption that there are no significant effects due to increased frequency, reduction of exposure time and elimination of rest-periods between heavy vehicles and during off-peak hours. In the past there have been numerous investigations of the effect of frequency. At ambient temperatures and a high ratio of frequencies, there is commonly a small effect whereby number of cycles to failure increases with frequency, eg tests on butt welded specimens exhibited a 20 per cent increase in fatigue strength for frequencies of 8 to 116 Hz (27). In tests on stainless steel at 0.0013 Hz, 2 Hz and 120 Hz, and endurances of up to 10^8 cycles, it was found that in the regions where the respective curves overlapped a sixty fold increase in frequency raised the strength at the longer endurance by a similar factor, figure 10. In practice, commercial vehicles travelling in convoy are likely to cross a given detail at a rate corresponding to a frequency of about 1 Hz. For the types of influence line shown in figure 3, constituent cycles are developed at frequencies of about 30 Hz. The highest frequency that laboratory tests can be run, about 120 Hz depending on the stiffness of the test piece, is unlikely therefore to increase endurance by a significant factor.

Figure 10. Effect of frequency on fatigue life.

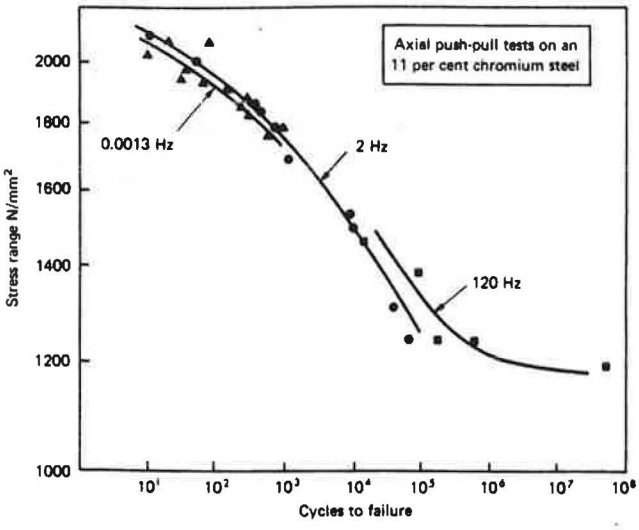

There have been a number of investigations into effects of rest-periods. The most notable work was by Whitman (28) who tested mild steel cantilever specimens for durations of up to 23,000 hours. Holes were drilled to lower the fatigue strength and simulate a welded joint. When compared with continuous cycling, it was found that the rest-periods caused increases in endurance of about 18 per cent and raised the cut-off stress by 17 per cent. More recently it was considered necessary to re-examine the effect of rest-periods to check whether behaviour is similar for a welded joint. Tests were conducted at TRRL on a non-load-carrying fillet welded specimen. Different combinations of rest-periods to cycling phases were used but the main part of the programme was for equal times cycling and resting, and with static stress during the rest-period, figure 11. It was found that at the lower stress and longer rest-periods, there may be a very small increase in life. The presence of differing levels of stress during the rest-period had no effect. It seems clear that although rest-periods can cause an increase in cyclic life, the effect is too small to be a significant factor in design. Moreover the effect is opposite to that of frequency so that high frequency continuous cycling should not introduce significant net errors in fatigue assessment.

Figure 11. Effects of rest-periods on fatigue life.

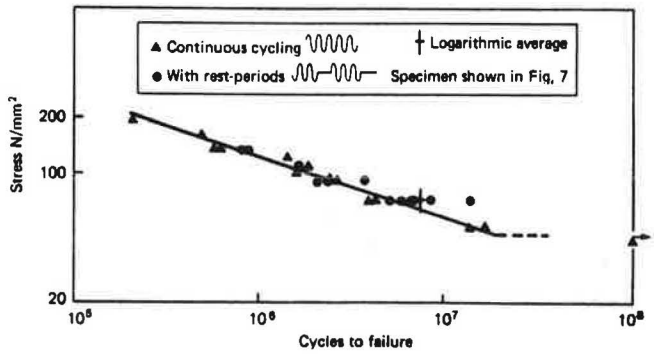

In considering other errors due to accelerating the cycling, the most worrying effect is due to the reduction of real time exposure by a factor of 500, possibly more. Fatigue tests in normal ambient conditions involve a mild form of corrosion considered by some to be the mechanism responsible for frequency effects. This process involves real time and it is not possible to simulate it satisfactorily with the present level of understanding of corrosion over long periods of time. There have been numerous investigations of corrosion and the consensus show that fatigue strength can be reduced by about 50 per cent. Endurances under corrosion fatigue are strongly dependent upon applied frequency, low frequencies giving the shortest lives. The literature on corrosion fatigue has been surveyed by Knight (29) who noted that there is an interaction between corrosion and fatigue so that when the two are simultaneous the strength is lower than for the sum of the individual effects. Laboratory corrosion tests are of necessity accelerated and there is insufficient knowledge about longer term behaviour, for periods of several years and more. The most common type of laboratory test involves cycling a specimen which is immersed in a salt water bath. Whilst such tests give conservative data it is arguably more realistic to consider fatigue of materials exposed in a natural environment for longer times. Tests specifically related to bridges have been conducted on specimens exposed to marine environments for periods of up to two years. It was found that fatigue strengths at 2.10^6 cycles were reduced by between 20 and 40 per cent (30). Tests on reinforcement bars embedded in concrete beams which were loaded in flexure till cracking developed, involved exposures of up to one year. It was found that the fatigue strength at 2.10^6 cycles was reduced by about 37 per cent (31). In the current research programme of the TRRL, specimens are being exposed in a natural marine environment for periods of up to ten years. The first assessment will be in 1980.

3.4 Programmed Loading

The term programmed loading refers to cycles of varying amplitude, whether random or non-random. Although fatigue testing is usually conducted at a constant amplitude of stress, bridges experience a spectrum of stresses which must be interpreted in relation to the available data. There has been a very considerable volume of research into crack propagation and rupture life under programmed loading and it has been found that summation of linear cumulative damage* can be used successfully in a variety of situations. (*The Palmgren-Miner hypothesis (32,33) first proposed in 1924 in a study of the durability of ball bearings.) It has subsequently been shown that a fracture mechanics analysis of crack propagation gives the same results as the linear summation of cumulative damage. The hypothesis is currently very widely used and is embodied in the new British Standard for bridge design.

For analysis of crack propagation under programmed loading, Barsom (34) showed that the RMS value of the spectrum can be correlated with constant amplitude loading. This gave very good results for different spectra. Overbeeke (35) conducted an unusually comprehensive programme of tests on spot welded lap joints. This work is notable because it involved endurances of up to 10^8 cycles and the tests included narrow-band Rayleigh and broad-band Gaussian spectra. The rupture data correlated using RMS values of stress. This work is very significant because there is a dearth of data for broad-band spectra relevant to fatigue of joints in orthotropic bridge decks. Yamada and Albrecht (36) tested I-beams with welded cover plates and butt jointed plates, using a stress spectrum recorded on a relevant bridge detail. In analysis of the data the programmed loading was expressed in terms of RMC (Root Mean Cube) rather than RMS because summation of crack propagation using fracture mechanics involves an exponent of 3. It was confirmed that RMC stresses correlate with constant amplitude fatigue. Schilling and Klippstein (37) tested similar specimens using a Rayleigh distribution which was shown to represent a measured spectrum of stresses. It was found that the equivalent stresses, whether calculated from cumulative damage or RMS values, correlated with constant amplitude data.

Clearly a large proportion of traffic induced stresses are below the fatigue limit (cut-off stress). The fatigue limit is the lowest stress that will propagate cracks from a representative size of defect and is therefore influenced by the initial state of the specimens. Once a crack has propagated a finite distance, lower stresses become damaging. Gurney (38) calculated the extent of this effect for several conditions and in a typical case found that a joint having a cut-off of 56.6 N/mm^2 for constant amplitude fatigue has an effective cut-off of 42 N/mm^2 under programmed loading. This work is currently being extended to the spectrum given in the proposed British Standard.

4. Conclusions

There have been a number of cases of fatigue cracks developing in steel bridges under normal traffic. These may be loosely classified as being associated with welded attachments to main steel girders, welded connections in orthotropic steel decks, and components subjected to resonant vibration. In design of welded connections it is necessary to assess fatigue performance using the best current procedures. In this paper special attention is given to orthotropic steel decks and the following points emerged:-

1. Vehicle induced stresses in unsurfaced orthotropic deck details may be calculated with adequate accuracy using methods such as finite strip analysis. The composite action of asphalt surfacing reduces stresses close to the deck plate by factors of up to 10 to 1. Current practice is to ignore this composite action in design calculation and regard it as a hidden factor of safety.
2. For the types of traffic induced stress cycle in orthotropic decks, it is necessary to count constituent cycles within the major cycle produced by a vehicle. Damage assessed from range-pairs can be about twice that assessed from major cycles alone.
3. In laboratory tests to simulate fatigue of highway bridges it is necessary to use large specimens that can retain residual welding stresses and have realistic plate thicknesses. Applied stresses should be selected so that cyclic endurances exceed 10^7 cycles and should preferably run to 10^8 cycles using relevant programmed loading.
4. Residual stresses play a significant role in fatigue processes. The slope of the S/N curve is steepened and the stress range is the dominant factor for pulsating-tension and push-pull loading. Pulsating-compression has the same logarithmic S/N slope as pulsating-tension but exhibits longer endurances.
5. Accelerated testing at high frequency and

continuous cycling is unlikely to introduce serious errors in estimation of lives up to about 10^7 cycles. Effects may be more significant at lower stresses associated with cut-off.

Acknowledgements

The work described in this paper forms part of the programme of the Transport and Road Research Laboratory and is published by permission of the Director. Much of the internal work has been carried out by Mr D. E. Nunn over a number of years. The contribution of Dr. T. R. Gurney who has worked under contract and made many suggestions is acknowledged.

References

1. D. G. Bowers. Loading History of Span 10 on Yellow Mill Pond Viaduct. Highway Research Record No. 428, 1973, pp. 64-71.
2. J. W. Fisher, B. T. Yen and J. Hartley Daniels. Fatigue Damage in the Lehigh Canal Bridge from Displacement Induced Secondary Stresses. Transport Research Record No. 607, Washington 1976, pp. 56-62.
3. J. P. C. King, P. C. Csagoly and J. W. Fisher. Field Testing of Aguasabon River Bridge in Ontario. Transport Research Record No. 579, Washington, 1976.
4. J. W. Fisher, A. W. Pense and R. Roberts. Evaluation of Fracture of Lafayette Street Bridge. Proc. ASCE Vol. 103, No. ST 7, July 1977, pp. 1338-1357.
5. D. E. Nunn and S. A. H. Morris. Trials of Experimental Orthotropic Bridge Deck Panels under Traffic Loading. TRRL Report LR. 219, Crowthorne, 1974.
6. D. E. Nunn. An Investigation into the Fatigue of Welds in an Experimental Orthotropic Bridge Deck Panel. TRRL Report LR. 629, Crowthorne, 1974.
7. Anon. Weld Cracks led to Severn Checks. New Civil Engineer, 26 June 1975, pp. 14.
8. G. Barstow. Fairfield Mabey on Last Leg of the Severn Bridge Sector Replacement. Construction News, 10 November 1977, pp. 28-29.
9. T. Schaaf and J. S. Spoelstra. Cable-stayed Bridge over the Waal near Ewijk, Netherlands. Acier Stahl Steel, vol. 41, January 1976, pp. 10-21.
10. J. Hartley Daniels, B. T.Yen and J. W. Fisher. Stresses in Orthotropic Deck of Rio Niteroi Bridge under Traffic. Transport Research Record No. 607, Washington, 1976, pp. 31-36.
11. T. Okubo. Wind Induced Oscillation of Bridge Members. Third Meeting of US Japan Panel on Wind and Seismic Effects UJNR, Tokyo, May 10-12, 1971.
12. J. J. Trott and J. W. Grainger. Design of Dynamic Weighbridge for Recording Vehicle Wheel Loads. TRRL Report LR. 219, Crowthorne, 1968.
13. H. Kalish. Installation and Operation of 146 Instruments for Axle Weight and Counting in a Long Term Research Project. Strasse Und Autobahn (27), November 1976, pp. 431-438.
14. P. Christiansson and B. Goteson. Mobile Weighing Station for Registration of Axle Loads, Axle Speeds and Lateral Tracks in Real Time. Report 63, Div. Build. Tech., Lund Inst. of Tech., Lund, Sweden, 1976.
15. M. Siffert. L'exploitation des Bascules Dynamiques. Bull Liaison Laboratory, Ponts et Chaussees, 70, March/April, 1974.
16. E. Murakami, T. Kunihiro, M. Ohta and H. Asakura. Actual Traffic Loadings on Highway Bridges and Stress Levels in Bridge Members. Tech. Memo. No. 1023, Part I, 1975, Public Works Res. Inst., Tokyo, Japan, pp. 25-34.
17. D. R. Leonard, J. W. Grainger and R. Eyre. Loads and Vibrations caused by Eight Commercial Vehicles with Gross Weights exceeding 32 tons (32.5 Mg). TRRL Report LR. 582, Crowthorne, 1974.
18. J. Page. Dynamic Wheel Load Measurements on Motorway Bridges. TRRL Report LR. 722, Crowthorne, 1976.
19. E. Hollis and R. Evans. Motorway Traffic Patterns. TRRL Report LR. 705, Crowthorne, 1976.
20. D. E. Nunn. A Method of Recording Axle Load Sequences and Groupings. TRRL Report LR. 568, Crowthorne, 1973.
21. S. A. H. Morris. Stresses under Dynamic Wheel Loading in a Surfaced Steel Orthotropic Deck with V-stiffeners. TRRL Report SR. 237UC, Crowthorne, 1976.
22. D. E. Nunn and J. R. Cunninghame. Stresses under Wheel Loading in Steel Orthotropic Decks with Trapezoidal Stiffeners. TRRL Report SR. 53UC, Crowthorne, 1974.
23. D. E. Nunn and J. R. Cunninghame. Stresses under Wheel Loading in a Steel Orthotropic Deck with V-stiffeners. TRRL Report SR. 59UC, Crowthorne, 1974.
24. S. A. H. Morris and H. Howells. Derivation of Stress Spectra from Measurements on Orthotropic Bridge Decks during Normal Trafficking. TRRL Report SR. 44UC, Crowthorne, 1974.
25. J. Page, J. G. Dennis and H. Howells. Analysis of Measured Traffic Induced Stresses in Bridges. Society of Environmental Engineers. Conference on Applications of Computers in Fatigue, Warwick, April 1978.
26. T. R. Gurney. Some Recent Work Relating to the Influence of Residual Stresses on Fatigue Strength. International Conference on Residual Stresses in Welded Construction and their Effects, The Welding Institute, London, November 1977.
27. F. Gyorgyi. Influence of Loading Frequency and Other Factors on Fatigue Test Results of Butt Welded Joints. IIW Doct. XIII, 383, 1965.
28. J. G. Whitman. Repeated Rest Periods in the Fatigue of a Mild Steel Bar. The Engineer, 30 June 1961, pp. 1074-1076.
29. J. W. Knight. Corrosion Fatigue Related to Welded Steel Structures - A Literature Survey, Weld Res. Inst., Vol. 7, 1977, No. 3 pp. 195-240.
30. T. Okuda. Corrosion Fatigue Strength of Steel for Railway Bridges. Quarterly Reports, Railway Tech., R9, Inst., Japan, Vol. 15, No. 3, 1974, pp. 168.
31. T. Nishi, Y. Hisamatsu, J. Murata, K. Kobayashi and H. Okamura. Investigation on Mechanical Behaviour of Galvanized Steel Reinforcement in Concrete. Japan Testing Centre for Construction Materials. Final Report ILZRO Project ZE-170, 1974.
32. A. G. Palmgren. Die Lebensdauer von Kugellargern (The Durability of Ball Bearings). VDI-Zeitschrift des Vereines Deutscher Ingenieure, Vol. 68, No. 14, April 1924, pp. 339-341.

33. M. A. Miner. Cumulative Damage in Fatigue. Transactions of the American Society of Mechanical Engineers, Vol. 67, 1945, pp. A159-A164.
34. J. M. Barsom. Fatigue Crack Growth under Variable - Amplitude Loading in ASTM A 514 - B Steel. ASTM-STP 536, 1973, 147-167.
35. J. L. Overbeeke. The Fatigue Behaviour of Heavy Duty Spot Welded Lap Joints under Random Loading Conditions. Welding Research International, Vol. 7, No. 3, 1977, 254-275.
36. K. Yamada and P. Albrecht. Fatigue Design of Welded Bridge Details for Service Stresses. Transport Research Record No. 607, Washington, 1976, pp. 25-30.
37. C. G. Schilling and K. H. Klippstein. Fatigue of Steel Beams by Simulated Bridge Traffic. J of Struc. Div. Proc. ASCE Vol. 103, No. ST8, 1977, pp. 1561-1575.
38. T. R. Gurney. Cumulative Damage Calculations Taking Account of Low Stresses in the Spectrum. Welding Research International, Vol. 6, No. 2, 1976.

RETROFITTING FATIGUE DAMAGED BRIDGES

John W. Fisher, Alan W. Pense, Robert E. Slockbower, and Hans Hausammann, Lehigh University

This paper examines continuing laboratory and field studies on ways to retrofit fatigue damaged members. Results of a pilot field study on two bridge structures with known fatigue cracks at the ends of cover plates are reviewed. Fatigue damaged members were retrofitted by peening and gas tungsten arc remelting the weld toe. The initial retrofit is summarized and the results of subsequent inspection after 1½ years is reviewed. Also discussed is the retrofitting of several more bridges by peening weld toes on a more extensive scale. In recent years many highway and bridge structures have experienced fatigue damage from out-of-plane displacements. This has resulted in web cracking at the ends of transverse stiffeners and floor beam connection plates which were not welded to tension flanges. Cracking as a result of out-of-plane movement is reviewed and several examples of cracking in a number of bridges is discussed. Nearly all of these fatigue damaged members have been repaired and retrofitted by drilling holes in the web plate at the ends of the horizontal cracks. A series of laboratory studies have been carried out to evaluate the fatigue behavior of stiffeners due to out-of-plane displacement. After fatigue cracking from out-of-plane movement these test beams are retrofitted by drilling holes in the web plate. Subsequently the fatigue damaged girder has been cycled to confirm the adequacy of the retrofitting procedures. These results will be summarized and related to bridges with comparable conditions.

Laboratory Studies on Cover-Plated Beams

Fatigue studies on beams with welded cover plates and long attachments have demonstrated that large reductions in fatigue strength occur when fatigue crack growth occurs at the micro-sized discontinuities that exist at the weld periphery.

In addition, fatigue cracking has been observed in the field at cover-plated beam bridges that carried an unusually high volume of heavy truck traffic causing large numbers of stress cycles(1).

The formation of these cracks showed the desirability of examining methods for improving (upgrading) the fatigue strength of welded joints without changing the design details. In addition, methods are needed for arresting the progress of fatigue damage that occurs at the weld toes of severe notch-producing details where the probability of failure is greatest.

An experimental program was carried out on sixty steel cover-plated beams in either the as-welded or precracked condition, to determine the fatigue strength of these details when treated by techniques intended to extend their fatigue life. Three of the most successful methods reported in the literature for as-welded details were utilized(2,3,4,5). They included: (1) grinding the weld toe to remove the slag intrusions and reduce the stress concentration, (2) air hammer peening the weld toe to introduce compression residual stresses, and (3) remelting the weld toe using the Gas Tungsten Arc process.

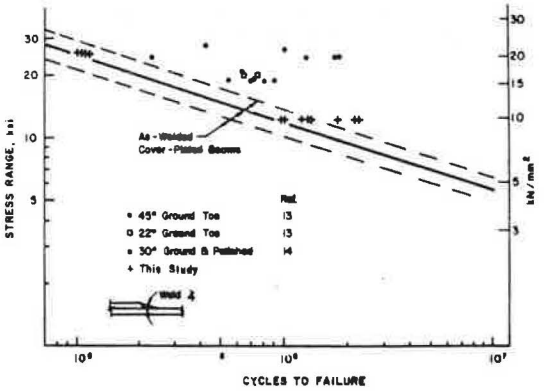

Figure 1. Effect of grinding weld toe on fatigue strength

Grinding the weld toe with a burr to provide a smooth transition and minimize the size of the initial discontinuities was the least reliable method. Some improvement was noted at the lower stress range levels as illustrated in Figure 1, but none at all

at the highest level of stress range. Similar results were obtained in earlier studies on as-welded details which indicated that erratic results could be expected.

Peening the weld toe was observed to be most effective when the minimum stress was low. This was true for as-welded and precracked details. This appeared to be directly related to the effectiveness of the compressive residual stresses introduced by the peening process. When peening was carried out on unloaded beams, the application of a high minimum stress and/or high stress range decreased the effectiveness of the residual compressive stresses that were introduced. Several tests were carried out on beams which were peened under a simulated dead load condition. Under these conditions about the same improvement was noted at both high [68.9 MPa (10 ksi)] and low [13.8 MPa (2 ksi)] minimum stress levels and at higher stress range levels as well.

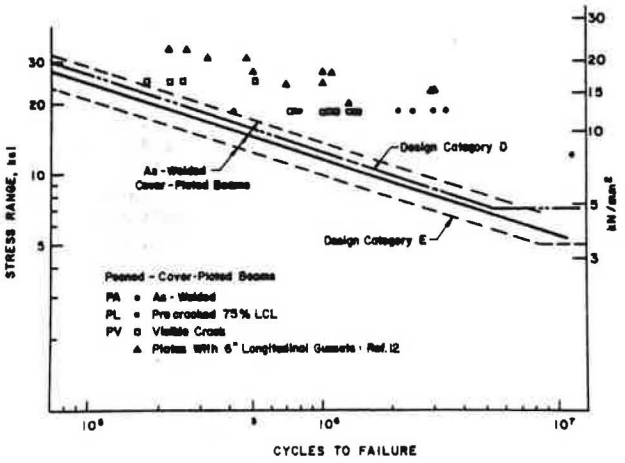

Figure 2. Effect of Peening on Fatigue Strength

The results of all beams with peened details that were tested under a low minimum stress level [13.8 MPa (2 ksi)] or that were peened under their minimum load, are summarized in Figure 2. Those details that were peened in the absence of dead load are not plotted in Figure 2. When the 68.9 MPa (10 ksi) minimum stress was applied to these beams it eliminated most of the beneficial effects of the peening treatment.

The test points designated as PA were as-welded beams treated prior to any fatigue testing. The test points designated as PL were for beams that were first precycled to 75% of the lower confidence limit of as-welded-untreated beams. After precycling these beams were then treated. They had fatigue cracks of various sizes. Two series of precracked beams (PL and PV) and one series of as-welded beams (PA) were tested to determine the effectiveness of peening. Cracks as large as 19 mm (0.75 in.) length and between 1.3 and 3.8 mm (0.05 and 0.15 in.) deep were observed prior to peening. After peening the precycled cracks were no longer visible. Inspection of the fracture surfaces indicate that movement occurred between the crack surfaces to a depth of 3.8 mm (0.15 in.). The precracked details usually failed from continued crack growth from the original crack, but at a slower rate. In a few cases failure was observed from the weld root. It is readily apparent that substantial increases in life were achieved for as-welded and precracked beams after peening, when peening was applied in the presence of dead load. The fatigue strength was increased by at least one design category(6)

Also shown in Figure 2 are test results on small plate specimens with 152 mm (6 in.) longitudinal gussets welded to their surface. These tests were reported by Gurney and were made on as-welded specimens(5). The studies on welded attachments reported in NCHRP Report 147 have demonstrated that the attachment length has a significant effect upon fatigue strength. Hence, these 152 mm (6 in.) longitudinal gusset plates were expected to exhibit slightly more life than those provided by cover-plated beams. This was confirmed by the test data. All of the peened plate specimens fell near the upper limit provided by peened cover-plated beams. This suggests that other details can be expected to exhibit a similar increase in fatigue strength when subjected to peening at the weld toe.

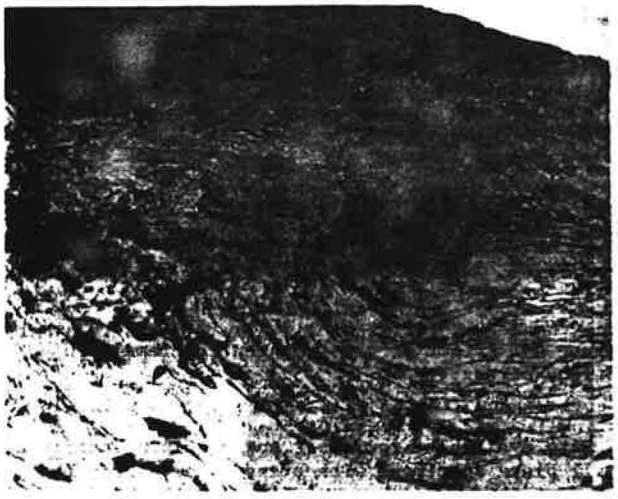

Figure 3. Lap-type defect in a peened weld toe

Transverse sections through several peened weld toes, revealed numerous lap-type defects which were the result of extensive surface deformation. An example of this deformation is shown in Figure 3. The depth of these laps was in the order of 0.05 mm (0.002 in.) to 0.25 mm (0.010 in.) which was approximately the same depth as the original slag intrusions. These defects are believed to be typical of the whole weld toe since they were found on all transverse sections.

Gas tungsten arc remelting at the weld toe termination was observed to provide the most reliable and consistent method of improving the fatigue strength in the as-welded or previously precracked condition. In a few instances the initial crack was not removed. Application of the gas tungsten arc remelt process did not succeed in completely fusing the fatigue crack in these specimens and no improvement was observed. These cases were encountered before suitable procedures were developed to obtain a desired depth of penetration.

The results of all three test series are summarized in Figure 4. The test points plotted as as-welded beams were treated prior to applying cyclic loading. The test points identified as precracked to 75% LCL were all precycled to 75% of the lower confidence limit for untreated details. At that time the "fatigue-damaged" detail was treated with the gas tungsten arc remelt. In some cases no

visible crack existed. Those points indicated as visible precracked all had clearly visible cracks prior to treatment. Except for those failures in precracked beams that occurred because of failure to incorporate the complete crack into the gas tungsten arc remelt (see Figure 4), approximately the same increases in life were achieved by all specimens. None of the test series exhibited an influence of minimum stress. Stress range was observed to account for nearly all of the variation in fatigue strengh.

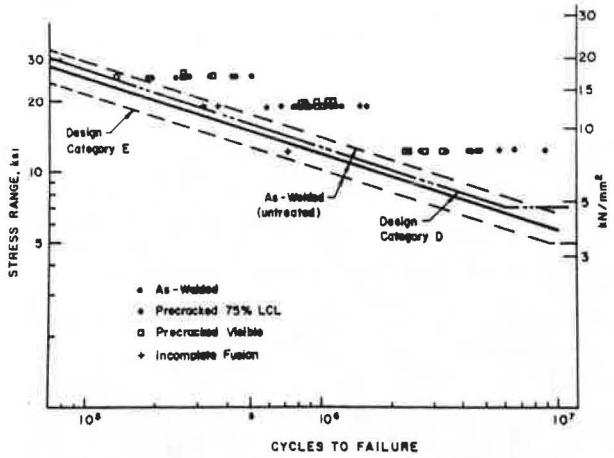

Figure 4. Effect of gas tungsten arc remelt on fatigue strengh

Data available from other sources is primarily on small plate specimens with transverse gussets that provide a non-load carrying joint(3,4). The studies on NCHRP Project 12-7 have indicated that this type of specimen provides fatigue behavior that is similar to stiffener type details(6). No data was available on cover-plated beam details that had been subjected to gas tungsten arc remelting at fillet weld toes.

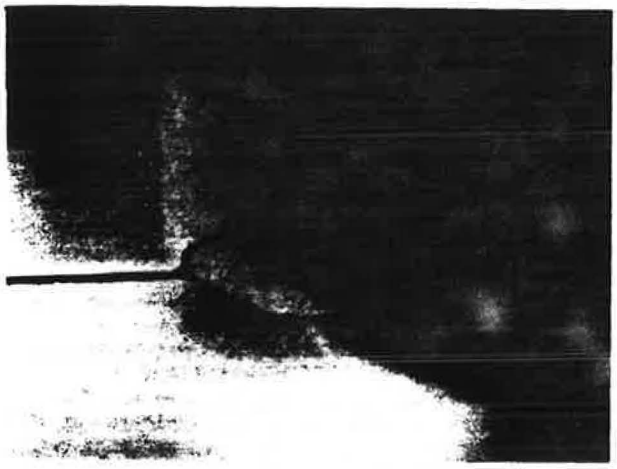

Figure 5. Cross-section of cover plate end weld

An etched cross-section of the transverse end weld is shown in Figure 5. The remelt penetration is visually evident at the weld toe. It was possible to provide up to 5 mm (0.2 in.) penetration in the gas tungsten arc remelt. Figure 5 also demonstrates the reason that an upper bound to fatigue strength was observed for welded cover-plated beams. Improvements in the condition at the weld toe could not affect the growth of cracks from the weld root. Most of the details treated by gas tungsten arc remelt passes had their life governed by failure from the weld root. Treatment at the weld toe forced the failure to the less severe weld root and resulted in greater life. Tests currently underway on full size beams have yielded comparable behavior.

Fatigue Damage in Cover-Plated Beam Bridges

In October-November 1970, during cleaning and repainting of the Yellow Mill Pond Bridge, one of the cover-plated steel beams on the eastbound bridge on span 11 was found to have a large crack(1). The crack had developed at the west end of the primary cover plate on Beam 4. It had grown from the toe of the cover plate transverse fillet weld into the tension flange and up 406 mm (16 in.) into the web.

A visual inspection (10X magnification) showed that Beams 3 and 5 in span 11 of the eastbound roadway which were adjacent to the casualty girder had cracks along the cover plate end. These cracks were subsequently verified by ultrasonic testing and a depth of penetration equal to 16 mm (0.625 in.) was measured. They were about half the flange thickness in depth and were found to have a semielliptical shape. An indication of possible fatigue cracking was also observed at five other details on span 10 and two on span 11. No ultrasonic confirmation could be obtained at the other possible crack locations.

In December 1970, after the detailed inspection, a section of the fractured girder was removed and all three damaged girders were subsequently repaired with bolted web and flange splices. The section of fractured girder was taken to Lehigh University for the purpose of investigating the fracture surface and determining the material characterization.

In November 1973, the east end of Beams 2 and 3 in the eastbound roadway of span 10 were inspected again by J. W. Fisher for fatigue damage. This was the first inspection at Beam 2. An indication of possible cracking was observed at Beam 3 in 1970. Cracks were detected visually in both girders at the toe of the primary cover plate transverse weld. A magnetic crack definer(7) indicated that the crack in Beam 2 was approximately 9.5 mm (0.375 in.) deep at one point. The magnetic crack definer could not verify the presence of a crack in Beam 3.

In June 1976, forty cover plate details in the east and westbound span 10 bridges were inspected for fatigue cracking using visual, magnetic particle, dye penetrant, and ultrasonic procedures prior to retrofitting these girders during Phase I of NCHRP Project 12-15(2). Twenty-two of these details were found to be cracked by visual inspection. The smallest visual crack indication was 6.4 mm (0.25 in.) long. Fifteen of these cracks had propagated deep enough to be detected by ultrasonic inspection.

To inspect for cracks it was first necessary to blast clean and remove paint, dirt and oxide which had accumulated in the weld toe region. The visual (10X magnification), magnetic particle and dye penetrant inspection provided data regarding the length of the surface cracks. The magnetic particle

inspection was discontinued after examining several cover plates due to difficulty in working with the probe in the overhand position.

The ultrasonic inspection provided data regarding both the length and depth of cracks. Cracks at the weld toe smaller than approximately 2.5 mm (0.1 in.) deep could not be reliably detected by the ultrasonic probe. The deepest crack depth indications of 13 mm (0.5 in.) were found at the west end of the eastbound span 10 bridge in Beams 3 and 7. Comparisons of estimated crack depths from ultrasonic inspection and actual measured crack depths after a fracture surface was exposed indicate that deviations of 1.6 mm (± 0.06 in.) are possible.

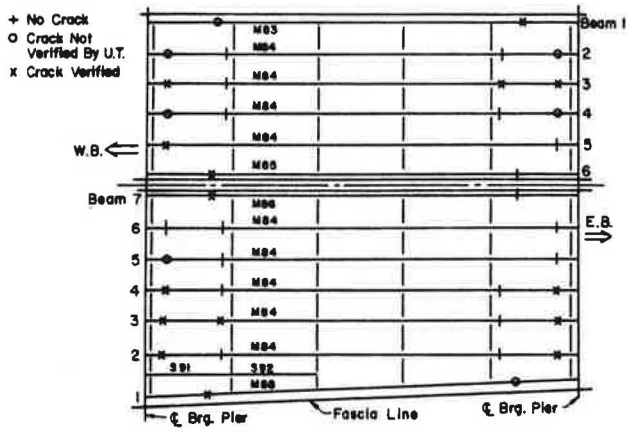

Figure 6. Plan of inspected details in span 10 Yellow Mill Pond Bridge

Figure 6 shows the approximate location of the details which were inspected in span 10 and summarizes the findings. Nine details in span 11 were also visually inspected. Indications of cracking were found at seven details. Very large cracks were observed at the east end of Beam 5 of the eastbound bridge and Beam 4 of the westbound bridge - span 11.

In November 1976, a brief inspection was made by J. W. Fisher at span 13. Four large cracks were detected without removing the paint. These cracks were first observed with field glasses from the ground. It is believed that these cracks must be approximately 150 to 250 mm (6 to 10 in.) long and about 13 mm (0.5 in.) deep for the crack to break the paint film at the weld toe. This condition is probably also related to the ambient temperature. Decreasing temperatures cause a more brittle paint coat and increase the likelihood of the paint to crack.

In September 1977, a brief inspection was made by J. W. Fisher and A. W. Pense and three additional beams in the eastbound structure had cracks at the ends of secondary cover plates. These cracks were observed to be about 6 mm (0.25 in.) long and occurred at several points along the transverse weld toes.

Retrofitting Fatigue Damaged Bridge Members in Span 10 - Yellow Mill Pond

Peening and gas tungsten arc remelting procedures were used to retrofit the cover-plated beams in span 10 of the Yellow Mill Pond Bridge which were found to have fatigue damage.

Grinding of the weld toe to reduce the size of the initial discontinuities and severity of the stress concentration had shown little or no improvement of fatigue strength of fatigue damaged members. Hence no attempt was made to employ this procedure at Yellow Mill Pond.

Peening of the weld toe introduces compressive residual stresses. The weld toe was mechanically air-hammer peened until it was plastically deformed.

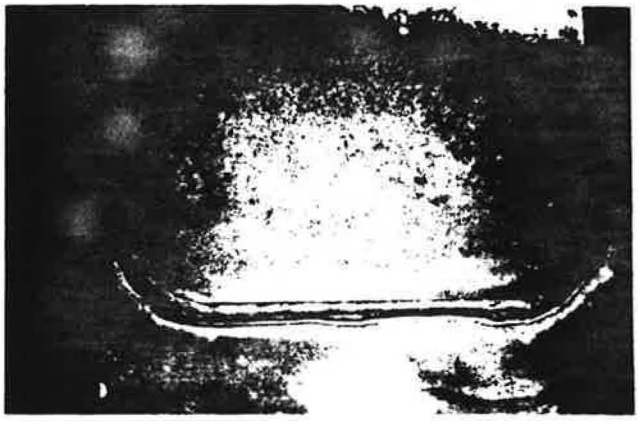

Figure 7. Peened weld toe on Yellow Mill Pond Road

Peening was performed with a small pneumatic air hammer operated at 0.17 N/mm^2 (25 psi) air pressure. The end of the peening tool was radiused with a 19 mm (3/4 in.) radius about one axis and a 3 mm (1/8 in.) radius about the other axis. All sharp edges were ground smooth. Several minutes were required to peen the weld toe. Peening was continued until the weld toe became smooth. A peened weld toe at Yellow Mill Pond is shown in Figure 7. The depth of indentation due to peening was approximately 0.8 mm (0.03 in.).

The Gas Tungsten Arc Process (GTA) removes the nonmetallic instrusions at the weld toe and reduces the magnitude of the stress concentration by smoothing the weld termination. The tungsten electrode was manually moved along the toe of the fillet weld. This melted a small amount of the fillet weld and base metal. Provided that the cracks are not too deep, the metal around the cracks can be sufficiently melted so that after solidification, the cracks will have been removed.

The welding equipment used was a 200 amp DC power source with drooping V-I characteristics. A high frequency source was used to start the arc. The electrode was 4.0 mm (0.156 in.) in diameter with a 4.8 mm (0.188 in.) stick out. The composition of the electrode was 2 percent thoriated tungsten. A Linde HW-18 water-cooled torch was used. The entire welding unit was mounted on a Bernard portable carriage which also contained the water supply and a recirculating pump to cool the torch. The portable carriage was mounted on the rear of a truck with the portable gasoline power supply. A 15 m (50 ft.) line from the welding unit to the torch permitted the welded access to the girder.

A series of preliminary tests were conducted in Reference 6 to find the effect of welding variables

on GTA remelt penetration. The results of this study indicate that maximum penetration is obtained by the use of helium shielding gas and a cathode vertex angle between 30 and 60 degrees.

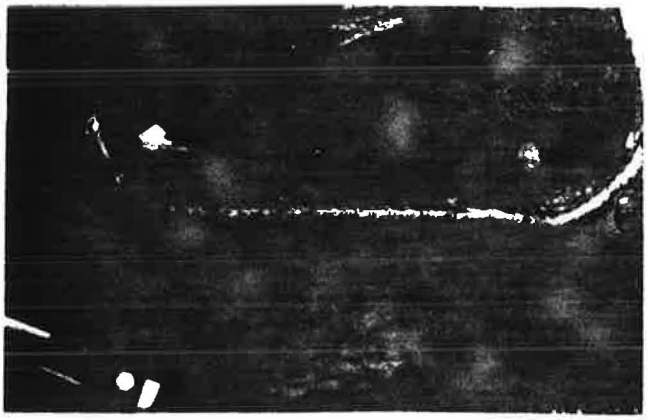

Figure 8. Transverse fillet weld after gas tungsten arc remelt

All retrofit welds on span 10 were performed in the overhead position. The areas to be welded were sandblasted to remove the mill scale that promotes undercutting. A helium and argon mixture shielding gas and a cathode vertex angle between 30 and 60 degrees were used as the mixture provided about the same penetration as helium alone. Travel speed was approximately 1.3 mm/sec. (3 in/min.). The retrofit weld was started on the longitudinal weld toe and continued along the transverse weld toe. The weld finally terminated at the opposite longitudinal weld toe. Intermediate terminations were made at approximately 100 mm (4 in.) intervals because of the duty cycle of the portable welding unit. Each of these terminations were carried up to the weld face to prevent cratering at the weld toe. Figure 8 shows a transverse fillet weld after the gas tungsten arc retrofit.

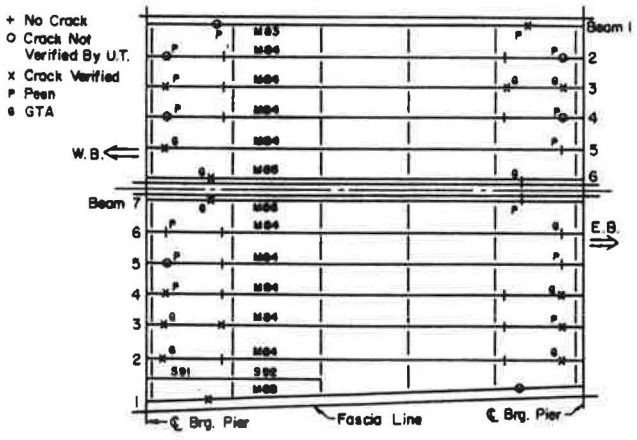

Figure 9. Repair methods on span 10, Yellow Mill Pond Bridge

Twenty-five of the cover plate details in span 10 were repaired after being inspected. Fourteen were peened and eleven were gas tungsten arc remelted. Figure 9 summarizes the type of repair which was made at each cover plate weld toe.

Seven of the remelted details which had cracks detectable by ultrasonic examination were reinspected after the repairs were completed. The east primary details on Beams 2 and 4 (eastbound bridge) both produced a spot indication at a depth of 3.2 mm (0.125 in.). The ultrasonic examination of the west primary details on Beams 3 and 7 (eastbound bridge) which had cracks about 13 mm (0.5 in.) deep, indicated a large embedded crack. The remelt at these details did not change the crack depth. The depth of remelt penetration was approximately 6.4 mm (0.25 in.) (see Figure 10). These cracks were purposely treated without gouging and rewelding by conventional means in order to evaluate the effectiveness of the treated details. The length of time required for the crack to penetrate back through the weldment could be compared with theoretical estimates of life extension. No crack indications were found at the west primary detail of Beam 2 (eastbound bridge) or at the east primary and secondary details of Beam 3 (westbound bridge).

Residual Fatigue Life after Retrofitting

Since the field repair of the Yellow Mill Pond Bridge members was only recently completed, the effectiveness of this repair must be judged on the basis of available laboratory studies on similar members. Fortunately both experimental data and analytical techniques exist to make this assessment. Peening was most effective in the laboratory when the initial cracks were very small. For this reason, peening was selected for retrofitting all beams where ultrasonic inspection was unable to confirm a visual indication of cracking or where neither inspection technique detected cracking. All cracks greater than 3.2 mm (0.125 in.) deep were gas tungsten arc remelted.

No cracks were indicated by ultrasonic inspection at ten of the cover plate ends which were peened in span 10. Four cover plates which were peened had a maximum depth indication of approximately 3.2 mm (0.125 in.). Therefore, the effectiveness of peening at Yellow Mill Pond should be comparable to the results plotted in Figure 2.

The laboratory studies on fatigue damaged details that were retrofitted by peening indicated a greater tendency for improvement at the lowest level of stress range tested [82.7 MPa (12 ksi)]. The details yielded fatigue lives up to 10^7 cycles. Since the stress range experienced at Yellow Mill Pond seldom exceeds 41.4 MPa (6 ksi), this procedure should be even more successful in prolonging life. The lower level of applied stress range will make the peened detail more effective because the induced compressive residual stresses at the crack tip are not likely to be overcome. As a result the details should be subjected to cyclic stresses that are well below the effective crack growth threshold. Tests currently underway have verified the expected behavior. Beams subjected to 41.4 MPa (6 ksi) or 55.2 MPa (8 ksi) stress range have been retrofitted after developing small fatigue cracks at the weld toe. These details have been retrofitted by peening and have not experienced any further crack growth after being subjected to 30 million stress cycles.

The increased fatigue strength developed by the retrofitted (gas tungsten arc remelted) precracked beams also suggested that substantial increases in fatigue strength could be expected at the lower

stress ranges to which the Yellow Mill Pond Bridge beams were subjected. The crack growth threshold of Category D appears to be about 58.4 MPa (7 ksi), which is substantially above the stress ranges experienced at Yellow Mill Pond (see Figure 4). Hence, retrofitting by the gas tungsten arc remelt procedure should eliminate the possibility of subsequent cracking.

The probability of a root failure occurring is dependent on the relative size of the weld with respect to the thickness of the cover plate. As the ratio between weld throat width and cover plate thickness increases, the probability of root failure decreases. For the W14x30 cover-plated beams the ratio of throat width to cover plate thickness is 0.31. This ratio at the primary and secondary cover plate details of the interior beams (W36x230) at Yellow Mill Pond is 0.28 and 0.32, respectively. Therefore, comparable results should result at Yellow Mill Pond. The scatter in the fatigue lives of remelted details is due primarily to the effectiveness of melting the material surrounding the fatigue cracks. The maximum crack depth closed in the remelting test beams was approximately 3.8 mm (0.15 in.). Ultrasonic inspection of the large fatigue cracks at the west end of Beams 3 and 7 (eastbound roadway) after remelting indicate that the depth of penetration was approximately 6.4 mm (0.25 in.). A sample plate was cleaned and gas tungsten arc remelted at the Yellow Mill Pond. The specimen was then sectioned, polished and etched. The depth of penetration was measured between 3.5 mm (0.14 in.) and 5.8 mm (0.23 in.).

After the remelt retrofit was completed, the details that had provided indications of cracking were ultrasonically inspected. No indications of residual cracks were found at the primary or secondary details of Beam 3 (east end, westbound roadway) and at the primary detail of Beam 2 (west end, eastbound roadway). This indicated that the gas tungsten arc remelt procedure had effectively eliminated the small fatigue cracks that were detected at those details.

The increased fatigue life as a result of peening or remelting should increase the crack growth threshold stress range, $\Delta\sigma_{TH}$. If the peening operation is capable of embedding the crack initiation sites in a compressive residual stress field a significant increase in the threshold stress range will be observed. The gas tungsten arc remelt procedure reduces the stress concentration by smoothing the transition at the weld toe and also minimizes the embedded discontinuities and fatigue cracks. Therefore, $\Delta\sigma_{TH}$ will also be increased.

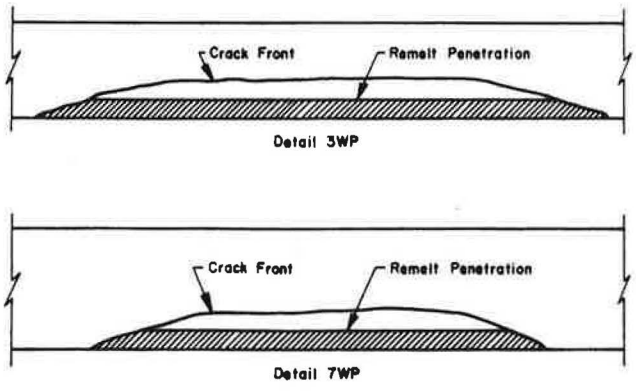

Figure 10. Crack shape for Beams 3 and 7 (1976)

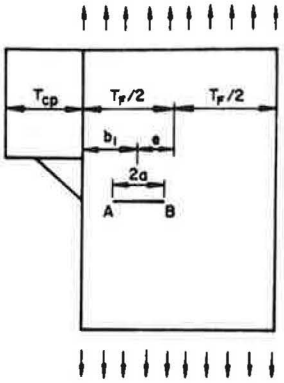

$$K_{I,A} = \sigma\sqrt{\pi a}\; F_A\left[\frac{a}{T_F/2 - e}, \frac{e}{T_F/2}\right] F_G\left[\frac{b_1 - e}{T_F}, SCF\right]$$

$$K_{I,B} = \sigma\sqrt{\pi a}\; F_B\left[\frac{a}{T_F/2 - e}, \frac{e}{T_F/2}\right] F_G\left[\frac{b_1 + e}{T_F}, SCF\right]$$

F_A, F_B from Ref. 8

$$F_G = \frac{SCF}{1 + \frac{1}{0.1473}\left(\frac{a}{T_F}\right)^{0.4343}}$$

Figure 11. Stress intensity model for embedded cracks

The shape of the large embedded cracks at the west primary detail of Beam 3 (eastbound bridge) and at the west detail of Beam 7 (eastbound bridge) are shown in Figure 10. The stress intensity model for these embedded cracks is shown in Figure 11. This approximate model combines the solution for an eccentric crack(8) with the stress gradient correction factor, F_G, defined in Ref. 9. Utilizing this model and the crack growth rate $da/dN = 3.8\times10^{-9}\,\Delta K^3$ (ΔK in units of MPa$\sqrt{mm}$, da/dN in units of mm/cycle), the number of cycles necessary for the crack to propagate through the retrofit weld toward the weld toe was estimated. It was assumed that when the embedded crack penetrated the exterior flange face it would quickly become an elliptical surface crack with the major semidiameter axis being defined by the crack shape ratio prior to retrofitting.

For this study the retrofit weld penetration was assumed to be 4.8 mm (3/16 in.). The estimated number of cycles necessary to propagate the embedded cracks through the retrofit weld at a stress range of 13.1 MPa (1.9 ksi) for Beams 3 and 7 were 7.0 and 6.7 million cycles, respectively. The elliptical surface cracks for both beams were approximately 13.5 mm (0.53 in.) deep at the beginning of the final stage of crack growth. An additional 1.0 and 2.7 million cycles would be necessary for the cracks to grow through the flange thickness for Beams 3 and 7, respectively.

The stress intensity model for the growth of embedded cracks probably overestimates the fatigue life since it does not account for crack growth which is occurring simultaneously from the weld toe. Nevertheless, substantial improvement in fatigue strength can be expected even if the entire crack has not been completely remelted, if the crack initiation sites along the weld toe have been effectively reduced.

Ultrasonic inspection of the primary detail of Beam 2 (east end, eastbound roadway) and the secondary detail of Beam 3 (east end, eastbound roadway) produced a spot indication at a depth of 3.2 mm

(0.12 in.). These embedded discontinuities may be below the crack growth threshold. Since their size and shape is nearly impossible to estimate, an exact evaluation is not possible.

The beams with the large embedded cracks were inspected again during September 1977 and showed no evidence of further crack growth. The tungsten inert gas remelt pass was still intact. Approximately 1 million stress range cycles had been experienced since the original treatment.

Retrofitting Web Cracks at the Ends of Stiffener and Floor Beam Connection Plates

Web cracking has been observed in welded girders at the ends of transverse stiffeners and floor beam connection plates(10). These cracks are caused by out-of-plane movement at the web. Out-of-plane movement as shown schematically in Figure 12 is introduced from the end rotation and displacement of floor beams which frame into the web of the main longitudinal built-up girders and by horizontal deflections of bracing members connected with stiffeners. It can also be introduced by bending during handling and shipping. Out-of-plane movement causes large bending stresses in the short gap at the end of the stiffeners.

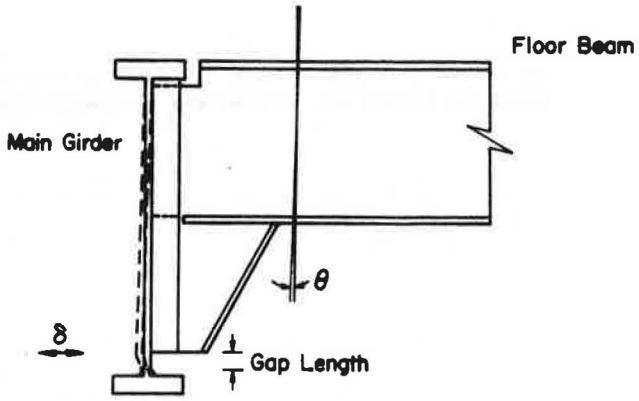

Figure 12. Schematic of deformation at end of floor beam connection plate

At the present time fatigue tests are being conducted at Lehigh University to evaluate the fatigue strength of comparable details. In these tests web cracking is introduced by simulating the out-of-plane moment that occurs at interior floor beams where the tension flange is restrained. The experimental test program includes various gap (distance between the end of the transverse stiffener and the flange) and the magnitude of out-of-plane deflection. Gap lengths equal to 2.5, 5, 10 and 20 times the web thickness are being examined when the out-of-plane deflection varies between 0.13 mm (0.005 in.) and 2.5 mm (0.1 in.).

The tests have shown that the specimens crack either immediately at the end of the transverse stiffener or at the end of the stiffener weld. No cracking occurred at the longitudinal weld between the web and the flange. In Figure 13 the preliminary results for several gaps under different deflections are shown.

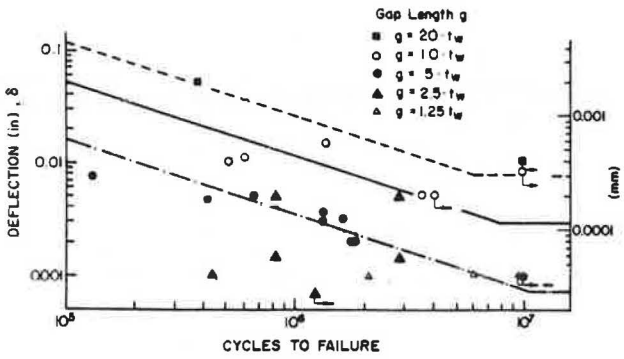

Figure 13. Experimental relationship between web gap length and out-of-plane displacement

The experimental data suggest that increasing the gap by a factor of two results in an order of magnitude increase in the cyclic life. If the stress range at the gap were only proportional to the deflection, i.e.

$$\sigma_r \propto A\,\delta\,\frac{EI}{g^2} \tag{1}$$

Then the cyclic life could be estimated from the relationship

$$N = \frac{1}{C}\int_{a_i}^{a_f}\frac{da}{\Delta k^3} \tag{2}$$

Since $\Delta K \cong \sigma_r F \sqrt{\pi a}$, this would result in

$$\Delta K \propto \bar{A}\,\frac{\delta}{g^2} \tag{3}$$

Substitution into Equation 2 yields

$$N \propto \bar{\bar{A}}\,\frac{g^6}{\delta^3}\left(\frac{1}{\sqrt{a_i}} - \frac{1}{\sqrt{a_f}}\right) = B\,\frac{g^6}{\delta^3} \tag{4}$$

The ratio of life for a given level of deflection can be estimated for this lower bound condition as

$$\frac{N_{g_1}}{N_{g_2}} = \frac{Bg_1^6/\delta^3}{Bg_2^6/\delta^3} = \frac{g_1^6}{g_2^6} \tag{5}$$

Considering the ratio of life for a gap length of 5 t_w and 10 t_w results in

$$\frac{N_{g_1}}{N_{g_2}} = \frac{(5\,t_w)^6}{(10\,t_w)^6} = 0.015 \tag{6}$$

The test data indicate that a ratio of 0.15 exists. This difference appears to be due to rotation of the flange and variance from the assumed model. This evaluation has indicated that increasing the gap does not increase resistance to fatigue cracking at as fast a rate as implied by Equation 1. However, the results also suggest that careful consideration should be given to details that will result in out-of-plane movement in gap regions.

Figure 14. Holes drilled at ends of crack

After each transverse stiffener on the test girder was fatigue cracked by the out-of-plane movement, holes were drilled at the crack tip. Figure 14 shows a typical retrofitted stiffener end. After retrofitting by drilling holes, the girder was subsequently subjected to cyclic loading at a stress range corresponding to category C [i.e. 96.5 MPa (14 ksi) at the stiffener end].

All cracked stiffener ends sustained cyclic loading until the test exceeded the lower confidence limit corresponding to Category C. No cracks were detected in the drilled holes perpendicular to the bending stress in the girder. Fortunately the cracks from out-of-plane movement are mainly parallel to the cyclic stresses. Hence the drilled holes were very effective in preventing further cracking and provided a detail comparable to the fatigue design condition.

Summary and Conclusions

Extensive laboratory experimental work on welded details has demonstrated that fatigue damaged details can be retrofitted and their fatigue life extended. Three repair or improvement methods were studied experimentally and observed to be effective to varying degrees in extending the fatigue life of welded details. Grinding was not as effective as peening under dead load and the gas tungsten arc remelt pass.

Peening was observed to produce good results with both uncracked as-welded details and fatigue damaged details with surface cracks less than 3 mm (1/8 in.) deep. The application of a high minimum stress after peening caused a reduction in the effectiveness of peening as it caused a decrease in the compression residual stress. As a result of the laboratory results on cover-plated beams which had experienced fatigue damage, peening was used to retrofit fatigue damaged bridge details that showed no significant crack growth.

The gas tungsten arc remelt pass was the most effective method examined in the laboratory and was also effective in repairing fatigue damaged details with surface cracks less than 5 mm (3/16 in.) deep. The procedure was used to retrofit bridge beams with cracks up to 12 mm (1/2 in.) deep. This did not permit the fusion of all of the crack surface. However, it was predicted that the embedded crack would provide several years additional life. Bridge beams with cracks at cover-plated weld toes that were 5 mm (3/16 in.) or less deep could be retrofitted and the fatigue crack removed by the remelt procedure. This was confirmed in the field.

Acknowledgments

This paper is based on research conducted under the National Cooperative Highway Research Program under Projects 12-15(1) and 12-15(2), Transportation Research Board, National Academy of Sciences and sponsored by the American Association of State Highway and Transportation Officials, in cooperation with the Federal Highway Administration.

The study was conducted at Fritz Engineering Laboratory, Lehigh University, Bethlehem, PA. Appreciation is expressed to the staff at Fritz Labortory, in particular, Robert Dales and Hugh Sutherland for experimental work, Richard Sopko for photography, John Gera for drafting and Ruth Grimes for preparation of the manuscript.

References

1. D. G. Bowers. Loading History Span 10 Yellow Mill Pond Bridge I-95, Bridgeport, Connecticut. Highway Research Record No. 428, TRB, 1973.
2. E. E. Brine et al. A Note on the Effect of Shot Peening on the Fatigue Properties of Plain Plate and Welded Joints in 18% Ni Maraging Steel and Al-Zn-Mg Alloy. Technical Note No. 5/68, Military Engineering Experimental Establishment, Christchurch, New Zealand, May 1968.
3. D. Millington, TIG Dressing to Improve Fatigue Properties in Welded High-Strength Steels. Metal Construction and British Welding Journal, Vol. 5, No. 4, April 1973.
4. F. Watkinson et al. The Fatigue Strength of Welded Joints and Methods for its Improvement. Proceedings of Conference on Fatigue of Welded Structures, The Welding Institute, 1971, pp. 97-113.
5. T. R. Gurney. Effect of Peening and Grinding on the Fatigue Strength of Fillet Welded Joints. British Welding Journal, Vol. 15, No. 12, 1968.
6. J. W. Fisher et al. Improving Fatigue Strength and Repairing Fatigue Damage. Fritz Engineering Laboratory Report No. 385.3, Lehigh University, Bethlehem, PA, December 1974.
7. A. Leone et al. A New System for Inspecting Steel Bridges for Fatigue Cracks. Public Roads, Vol. 37, No. 8, March 1974.
8. H. Tada et al. The Stress Analysis of Cracks Handbook. Del Research Corporation, Hellertown, PA, 1973.
9. N. Zettlemoyer. Stress Concentration and Fatigue of Welded Details, Ph.D. Dissertation, Lehigh University, Bethlehem, PA, 1976.
10. J. W. Fisher. Bridge Fatigue Guide - Design and Details. AISC, 1977.

REPAIR OF POPLAR STREET COMPLEX BRIDGES IN EAST ST. LOUIS

Wei Hsiong, Illinois Department of Transportation

The web cracks found in the Poplar Street Complex Bridges were located at the top of the web-to-bottom flange fillet weld near the end floor beams. The buckled web was observed at the end of the girders behind the bearing stiffener. This report summarizes the results of the study which intends to determine the proper causes of the distress. It is believed that the main cause of the web crack was due to the out-of-plane movement of the web; and that the cause of the web buckling was from the eccentric reaction induced by the seized bearing pin. The repair method was developed mainly to stiffen the section and to carry the secondary stress induced from the out-of-plane movement of the web and to resist the distortion of the girder due to differential deflection of the main girders. Suggested details for future design are also included.

Introduction

The Poplar Street Complex, located on the east bank of the Mississippi River in East St. Louis, Illinois, is a focal point where Interstate Highways I-55, I-70 and U.S. Route 40 join to cross the Mississippi River. The system was built in stages with the first stage opened to traffic in 1967.

The Complex is one of the largest and busiest interchange system in the State of Illinois (see Fig. 1). It extends from the Poplar Street Bridge over the Mississippi River on the west, northeast to Broadway in East St. Louis for the main line routes with additional ramps to the south and southeast to connect with State routes and East St. Louis Street. It consists of many vaiducts with series of three and four span continuous two girder type bridges.

The majority of the two girder type bridges are on horizontal curves with radii of approximately 550 meters (1800 feet). The torsional rigidity of the open frame system is provided by the closely spaced floor beams which are rigidly connected to the main girders. The floor beams support the stringers and the reinforced concrete deck which carry the traffic loads. The floor beams, then, transfer the loads from the stringers to the main griders.

In late 1973, the Bridge Inspection Team of the Illinois Department of Transportation made their first in-depth field inspection of this bridge. They discovered many structural problems in the main supporting members of the bridges. These problems consisted of web cracking, web buckling and separation between the bottom flange of the girder and the top bearing plate. The major areas of distress were predominantly located at the ends of the continuous girders.

This report summarizes the findings from a series of studies. These studies were intended to determine the causes of the distress. From these studies, corrective measures to restore the structural integrity have been developed. Recommendations for future design are also presented.

Description of Structural Problems

The distressed areas found in these bridges can be categorically divided into three groups.

Web Cracking

Web cracks were first observed at the end of the girder under the end floor beam connecting plate which is positioned 18 cm. (7 inches) toward the center of the span from the center line of the bearing stiffeners. Most of these cracks started near the lower end of the vertical connecting plate and extended in both directions in the girder web as shown in Fig. 2. The longest crack observed was 48 cm. (19 inches) long. Some had two cracks at the same location, one was immediately under the lower end of connecting plate; the other, just above the web-to-flange weld toe. The former was shorter in length. In a later inspection, it was found that the web cracks had also developed at the upper end of the connecting plate in the negative moment region.

Web Buckling

Web buckling was observed at the end of the girder. This buckling of the web occurred a few inches above the bottom flange as shown in Fig. 3 and was often associated with the separation of the top bearing plate from the bottom flange of the girder (see Fig. 4). In some cases, web cracking above the web-to-bottom-flange weld toe was also observed. This crack started at the end of the girder and progressed horizontally toward the bearing stiffeners.

Separation Between Bottom Flange and Bearing Plate

The front part (span side) of the top bearing plate separated from the bottom flange of the girder. In some locations the separation started at the front edge of bearing plate and extended horizontally to a point below the end bearing stiffeners. In other locations, the separation was wider at the outside edge of the flange than on the inside edge of the flange. Figure 4 shows a general view of the separation.

Analytical Study

Analytical Study was initiated in December 1973 by the Bridge and Traffic Structures Section of the Illinois State Department of Transportation to determine the probable causes of the structural problems. The following is a discussion of the study:

Web Cracking

These cracks were found near the end of the girders. As shown in Figure 5, the end floor beam is rigidly connected to a connecting plate on the inside face of the girder web. The connecting plate located 18 cm. (7 inches) from the centerline of the end bearing stiffeners was welded to the top flange and the web of the girder, but had a tight fit at the bottom flange of the girder. Since the end floor beam is rigidly connected to the connecting plate, the rigid connection transmits the rotation of the floor beam to the supporting girder. The rotation tends to pull the top half of the main girder inwards and push the bottom half outwards. The girder flanges at this location are restrained from movement by the concrete slab at the top and by the bearing assembly at the bottom. This restraint induces a moment at the junction of the girder web and the girder flange. The moment at bottom of the girder web produces tension stress on the inside face of the girder web and compression stress on the outside face of the girder web. The unconnected but tight fitted lower end of the connecting plate cannot resist this tensile stress and this additional force is transmitted into the web. The stress produced by this force on the web approaches the yield strength of the material every time when the end floor beam is subject to the designed live load. The fatigue resistance of the web at the end of the welded connection plate is classified as categoty C in AASHTO Specifications. It is apparent that the high cyclic tensile stress in the web will initiate the fatigue crack.

If the connecting plates had been welded to the flanges, the additional strength of the T-section formed by the connecting plate and the web would have reduced the stress in the web due to moment to within the allowable stress range. It appears to us that this is the reason why there were no cracks in the web where the connection plates were welded to the flange. Cracking did not occur in the lower web of the girder at the piers or at end of the girder where the floor beams were connected to the bearing stiffeners. Since the bearing stiffeners were milled to bear on the bottom flange and were placed on both sides of web, the compression stress in the stiffeners due to reaction at the bearing can offset the tensile stress produced by the movement of the web as mentioned previously; besides, the frictional restraint at the contact surfaces between mill-to-bearing end of the stiffeners and the top face of the bottom flange can prevent the web from moving.

The floor beams located in the positive moment regions which are connected to a single connecting plate as previously discussed showed no distress because the bottom flange of the girder was free to displace and rotate. The freedom to move released the stress in the web and prevented the cracks in the web near the bottom flange from developing.

Buckling of Web Behind End Bearing Stiffener

The cause of the web buckling was due to the eccentricity of the reaction between the bearing shoe and the bearing stiffener. This eccentricity of the reaction resulted from the following two existing conditions: (a) Misalignment of the centerline of the bearing stiffener with the centerline of bearing assembly during construction of the structure (b) The transverse separation of the bottom flange of the girder from the top plate of the bearing due to a seized bearing pin in the bearing assembly.

The misalignment of the bearing was apparently the result of the substructure being built out of alignment and/or incorrect fabrication of the curved girders. It was noted that some of the bearing shoes (see Figs. 3 and 4) were not bolted to the bottom flange as specified in the plans, but were welded to the bottom flange in the field.

The seized bearing pin forced the girder to bend in order to accommodate the thermal movement and rotation. This additional bending pulled the bottom flange and top bearing shoe apart and resulted in the eccentricity of reaction between the effected area of the bearing shoe and the bearing stiffener.

The eccentric position of the bearing shifted part of the load from the bearing stiffener to the web behind the stiffener and can cause the web to buckle. It should be kept in mind that since the reactions are very large, a small eccentricity of the reaction from the bearing will result in a very high stress on the end of the web plates.

Separation Between Bottom Flange and Bearings

The separation of the bottom flange from the top bearing plate occurred at locations where the bearing pin seized and ceased to rotate. It appears from the unscraped painted surface on the pin that many of the bearing pins have never functioned properly. This painted surface referred to is between the center support plates of the top and the bottom bearing shoes on the bearing pin. Since these support plates are in contact with the painted surface on the pin, any movement of the bearing will scrape paint from the pin.

At several locations, separation between the bottom flange and the bearing shoe along the outside edge of the flange was observed. In some cases, this longitudinal separation was associated with the broken connecting bolts. These bolts held the bottom flange to the bearing shoe. The cause for this type of separation seems to be due to the moment at the floor beam connection which has a tendency to push the bottom of the girder outwards and the additional bending of the girder from the seized bearing pin as discussed previously. The twist of the bottom flange induced a tension force in the bolt. This is a tensile fatigue loading. After enough cycles, fatigue cracks in the bolt will result.

Field Tests

It had been reported from visual field inspection that most of the expansion bearings were seized. In order to verify the visual observation, field tests

were planned and carried out by the Research Team of the Department of Transportation, State of Illinois, from December, 1973 through February, 1974.

Two sets of measuring devices were developed and installed at six different locations (Fig. 6). One measuring device consisted of two steel bars attached to the top and the bottom shoes of the pin supported type bearing assemblies to measure the rotation. Another measuring device consisted of a scale fastened to the bottom flange of the girder and a point indicator attached to the substructure to measure the relative movement. Test readings indicated no movement on half of the bearings tested, and less movement than expected on the other half.

The seized bearings at the east abutment of ramp B were removed and replaced with elastomeric bearings reinforced by steel laminas (see Fig. 7). These elastomeric bearings were set tangent to the radius at the center line of the bearing. An instrument was installed on the bottom of the girder flange to measure the thermal movement of the girder. Theoretically, the thermal movement of a curved girder is along the chord line between the fixed bearing and the expansion bearing. The measured direction of the movement at the east abutment of ramp B for the temperature differential of 28° C(50° F) was about 4° shown on Fig. 8. The angle between the tangent at center line of bearing and the chord line through the fixed bearing is about 1° 30' according to plan dimensions. The measure angle was approximately 2.7 times the theoretical angle. The discrepancy may be due to the following reasons:

1. The rotation of the end floor beam pushed the girder outward.
2. The distortion of the structure by restraining force developed within the system of steel bearings used.
3. The substructure was built out of alignment and/or incorrect fabrication of the curved girder.

This field test supported the visual observation reported by the Inspection Team that a majority of the expansion bearings were seized. The seized bearing pin forced the girder to bend in order to accommodate the expansion and rotation. The bending of the girder had contributed to the separation between the bottom flange and the top bearing plate. The separation created an eccentric load on the bearing stiffeners. A small eccentricity of the reaction from the bearing results in a very large stress on the end of the web plate. When this stress is larger than the critical stress of the web plate, the web will buckle.

A second field test was planned and performed by Professor John Fisher in the Summer of 1975. The purpose of the test was to ascertain what caused the web cracking.

Strain gauges were installed on the web at the pre-selected locations for strain measurement. The complete results were presented in Professor Fisher's Report (3).

Following is a discussion relative to the test results:

At the End Floor Beams

Most of the end floor beams are set near the top of the girder and are rigidly connected to a vertical connecting plate. This plate was welded to the top flange and the web of the girder, but had a tight fit at the bottom flange. This plate is located 18 cm. (7 inches) from the centerline of the end bearing stiffeners. The connecting plate was clipped 25x25 mm. (1x1 inches) top and bottom at the inside corners to clear the web-to-flange weld. The gap between the clipped edge of the plate and the web-to-flange weld was created in the web. See Fig. 5.

Two strain gauges were installed in the lower gap region at the northwest bearing of pier 26, ramp C, identified as C-26NW. See Fig. 9. Gauge readings indicated very little out-of-plane movement of the web at this location. This was due to the fact that the gap in the web is very small, about 2.5 mm (0.1 in.), and the tight fit joint may provide enough friction to reduce the movement. No web cracking was observed.

A few of the end floor beams are connected to the bearing stiffeners. The bearing stiffeners had a tight fit end at the top and mill-to-bear end at the bottom. Four strain gauges were installed, two at the top and two at the bottom at location B-27 NW. See Fig. 10 and Fig. 11. It was found while installing the strain gauges that the tight fit end of the bearing stiffeners had a larger gap between stiffeners and the top flange than was anticipated. The top gauge readings, shown in Fig. 12, clearly indicated that the web was pushed out-of-plane by the rotation of the end floor beam. The stress in the web as computed from strain gauge readings is shown in Fig. 13. The web is subject to this high stress every time there is a live load on the floor beam. After many occurrences, web cracking due to fatigue is inevitable and a crack was observed. The measurement at the bottom indicated that the stress in the web was smaller. See Figs. 14 and 15.

Interior Floor Beam - Positive Moment Regions

The interior floor beams in positive moment regions were connected to the girders in the same manner as discussed above except the top of the floor beam is set near the mid-depth of the girder. In addition, a stiffener was welded to the outside web and the stiffener was undercut by 16 mm (5/8") at the tension flange.

Strain gauges were installed at location B-27FBI-W, the first interior floor beam west of pier 27, ramp B. See Fig. 16. Some of the gauge readings are shown in Fig. 17, others are shown in Fig. 12. There was very little movement in the web at this location. This is due to the inability of the flange to resist lateral movement because of lack of torsional stiffness, thereby relieving substantially the strain which might be introduced in the web gap. No crack was observed. None will likely develop in the future.

Interior Floor Beams - Negative Moment Regions

The connecting plates in the negative moment region were welded to the bottom flange and had a tight fit at the top. Web cracks at the top were observed at several locations. The strain gauges installed at location B-26FBI-W (see Fig. 18), showed some movement in the web. The stress in the web induced by the movement is shown in Fig. 19. The stress is less than the fatigue limit of category C. However, since web cracking at the upper end of the connecting plate was observed on the inside face of the web, it was apparent that the large web bending stress, which was even larger than measured by strain gauge, had been present at some time.

It is interesting to note that two types of deformations at the web gap region are possible. One is translation which creates double curvature bending; the other, single curvature bending as shown in Figure 20. This variance is not clearly understood from the limited test data. A tentative explanation

may be:

1. When the floor beam is set close to the web gap region, the connection plate becomes very stiff and could not be bent due to the shorter distance between the floor beam connection and the web gap. Hence, the translation type deformation results.
2. When the floor beam is set at some distance away from the web gap region, the bending of the connection plate is possible.

However, it can be concluded that the out-of-plane movement of the web was the only cause producing the web crack.

LABORATORY TESTS

Laboratory test were carried out by the Research Team of the Illinois State Department of Transportation in order to determine the cause of the bearing seizure. A pilot test was made on a one-third size model. Loads were applied in increments up to a maximum load which produced a unit bearing pressure of 228 Mpa (33 Ksi) on the contact surface of the bearing pin. Examination of the pin after testing had revealed evidence of galling on both the pin and the saddle as shown in Figs. 21 and 22. The galling had produced a build-up of hard, solid material which could lock the pin to the saddle.

A series of four tests were performed under the same loading pressure, 70 Mpa (10 Ksi), and the same 2000 cycles of movement. The bearing pins were made of the same material with different surface treatments.

A mild steel pin without surface treatment was tested first. Galling appeared on the surface of the pin as shown in Fig. 23, specimen T-1. A second specimen was of the same mild steel pin but was case hardened. The amount of wear experienced was not significant as can been seen in Fig. 23, specimen T-2. A third specimen was of a mild steel pin with no surface treatment but lubricated with a heavy duty grease. Galling to some extent was evident as shown in Fig. 23, specimen T-3. The last specimen was a case hardened pin with a dry film lubricant. The result of this test showed little benefit in the use of dry lubricant. See Fig. 23, specimen T-4.

It was interesting to learn that the coefficient of friction for specimen T-1, T-2 and T-4 increased with increases in the number of cycles of movement and gradually tapered off after 200 to 300 cycles. However, the coefficient of friction for specimen T-3 which had the heavy grease lubricant was constant throughout the test and about one-half of the value obtained for pins without grease lubricant. See Figs. 24 and 25.

A conclusion can be drawn from these tests that use of the pin with a case hardened surface and lubricated with a heavy duty grease would be highly beneficial as a means of improving the behavior and life expectancy of a pin supported bearing.

Two steel bearings were removed from the east abutment of ramp B as mentioned before. These bearings were cut open to inspect the contact surface of the pin and the saddles. See Figs. 26, 27 and 28. A layer of highly compacted rust was found on the contact surfaces of the pin and the saddles. After approximately 95 percent of the rust material was removed by a rust solvent, the contact surface of the pin was inspected again and the visual inspection did not reveal any severe sign of galling as observed on the laboratory specimens. The absence of galling indicates that the formation of compacted rust was probably the primary factor contributing to the seizure of the bearings.

REPAIR

The repair plans were prepared in late 1974, and the contract was let in early 1975. The corrective measures were developed based on our initial study. The method of repair was to stiffen the ends of the girders so as to carry the secondary stresses induced from the out-of-plane movement of the web or from the eccentric reaction.

Web Cracking

The web cracks were due to the out-of-plane movement of the web. The method of repair was to stop the movement or to minimize the damage. The repair procedure was as follows:

At Grider End.

a. Drill a 13 mm. (1/2") hole in the web at the end of the crack.
b. Clean and prepare the edge of the crack for a full penetration butt weld.
c. Weld the connecting plate to the bottom flange by continuous fillet weld.
d. Weld a new plate 203x13 mm. (8"x1/2") on the outside face of the girder opposite to the inside connecting plate as shown in Fig. 29.

At Negative Moment Regions.

The web cracks at the top of the web in the negative moment regions were repaired by a different technique. Due to the stress range in the tension flanges, to weld the connecting plate to the flange would create a fatigue problem in the flanges. The repair was done as follows:

a. If there was no crack in the web, a 13 mm. (1/2") hole was drilled just below the web-to-flange weld at 102 mm. (4") on each side of the connection plate and a 13 mm. (1/2") hole was also drilled on each side of the top end of the connecting plate.
b. If there were cracks in the web, 13 mm. (1/2") holes were drilled at each end of the cracks. See Fig. 30

Web Buckling

It was concluded that the buckling of the web at the girder end was due to the eccentric reaction created by the seized bearing pin. The repair procedure was:

a. Split the girder web a few inches above the buckled web.
b. Place clamping plates on both sides of the web.
c. Apply force on the clamping plates to straighten the web.
d. The cut portion, then, shall be welded together.
e. After the web is straightened, weld a stiffening plate on each side of the web as shown in Fig. 31.

Frozen Bearing Pin

Most of the expansion bearings at the girder end were seized. This resulted in the separation between the bottom flange and the top bearing plate, therefore causing the web to buckle. In order to provide uniform bearing area and to allow freedom of thermal

movement, bearings at the girder ends were replaced with elastomeric bearings as shown in Fig. 7. Steel bolsters were provided to make up the difference in height between the elastomeric bearing and the original bearing.

RECOMMENDATION FOR FUTURE DESIGN

To prevent similar problems from developing in future designs, the following are recommended:

1. The connection plates for the floor beams or the cross frames shall be welded to both flanges. In this case, the stress range in the tension flange shall be limited to the category C fatigue allowable range. An alternate is to provide a sufficient gap between the end of the connection plate and the inner face of the tension flanges. A large gap can provide the web a "breathing" room and then a higher stress will not be introduced in the web. Stiffeners should not run the full depth of the web on the opposite side of the connection plate if this plate is cut short. See Fig. 32.
2. When pin supported type bearings are used, double bearing stiffeners shall be detailed to prevent the end of the web from buckling if the bearing is misaligned or seized. The surface of the bearing pin shall be treated for case hardening. Grease inserts shall be also provided and the pin shall be lubricated upon installation and at regular intervals thereafter in order to reduce the friction and extend the life expectancy of the pin.

SUMMARY AND CONCLUSION

The most important conclusion of the study reported here is that the web cracks at the gap between the end of the floor beam connection plates and the girder flanges are all fatigue related. The cracking has resulted from cyclic web bending stresses in the gap region. Field tests confirmed that the rotation of the floor beam which was rigidly connected to the main girder pushed the web out-of-plane. Since the connection plate with the strong axis perpendicular to the web acts like a rigid bar, the out-of-plane movement is forced into the web gap between the end of the connection plate and the girder flanges due to the lack of resistance to this movement in this gap region. The severity of this movement is greater at the places where the flanges are restrained from movement. In the middle of the span, the inability of the flange to resist the lateral movement relieves substantially the strain which might otherwise be introduced in the web gap.

In addition to the above, the study also yielded the following conclusions:

1. The seizure of the pin supported bearing was related to the presence of packed rust between the contact surfaces of the pin and the supporting saddles.
2. The seized bearing pin forced the girder to bend in order to accommodate the thermal movement and rotation. The bending of the girder lifted the bottom flange up from the bearing shoe, and shifted the reaction from the bearing shoe to behind the bearing stiffeners, therefore causing the web to buckle.

REFERENCES

1. Investigation Report on Poplar Street Complex Bridge. East St. Louis, St. Clair County, Illinois -- By Illinois Department of Transportation, Bureau of Design, Bridge and Traffic Structures Section, June, 1974.
2. Investigation of Bridge Approach Spans to Poplar Street Bridge. East St. Louis, Illinois -- By Illinois Department of Transportation, Bureau of Materials and Physical Research, May, 1975.
3. Report on Investigation of the Girder Web Cracking at Floor Beam Connection Plates of the Poplar Street Complex -- By John W. Fisher, October, 1975.

Figure 1. Vicinity map.

Figure 2. Web cracking.

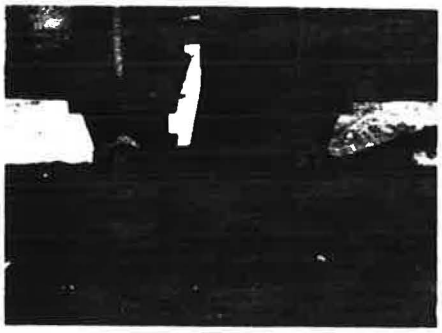

Figure 3. Web buckling.

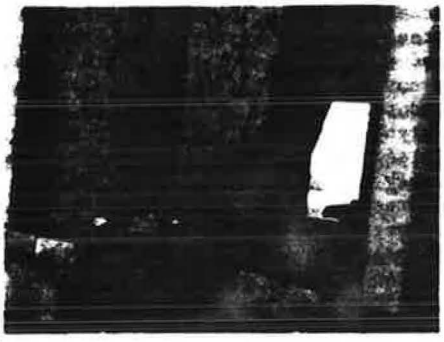

Figure 4. Separation between bottom flange and bearing shoe.

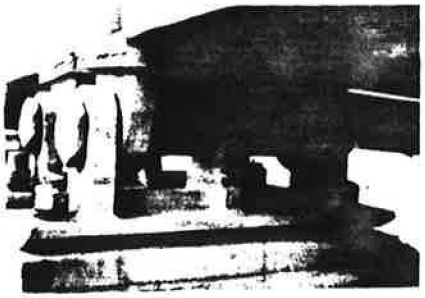

Figure 6. Instrumentation at seized bearing.

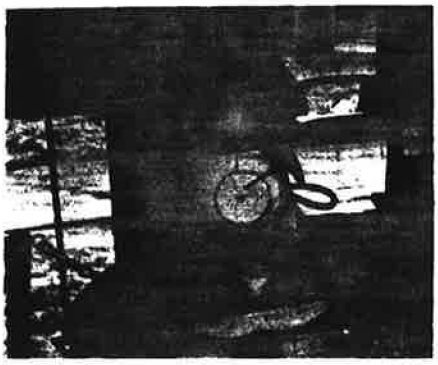

Figure 7. Elastomeric bearing.

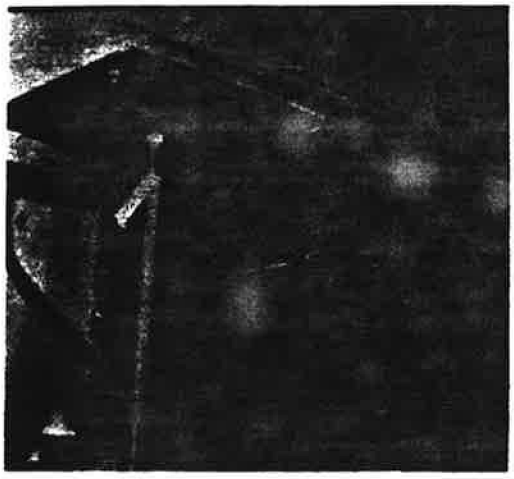

Figure 9. Strain gages at Pier C-26NW.

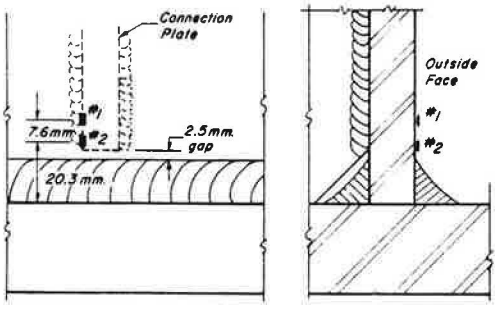

Figure 5. End floor beam connection.

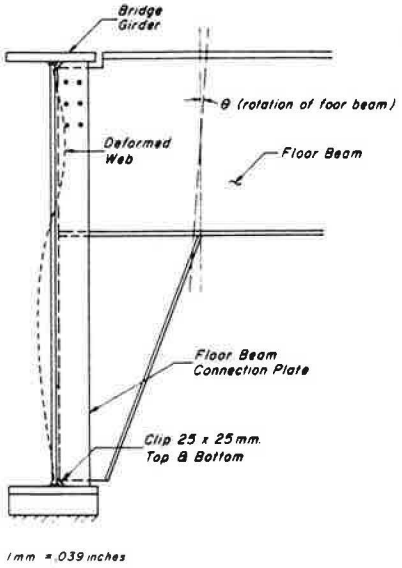

Figure 8. Thermal movement at elastomeric bearing.

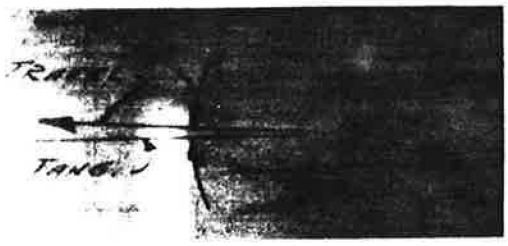

Figure 10. Strain gages at gap near top flange at Pier B-27 NW inside face.

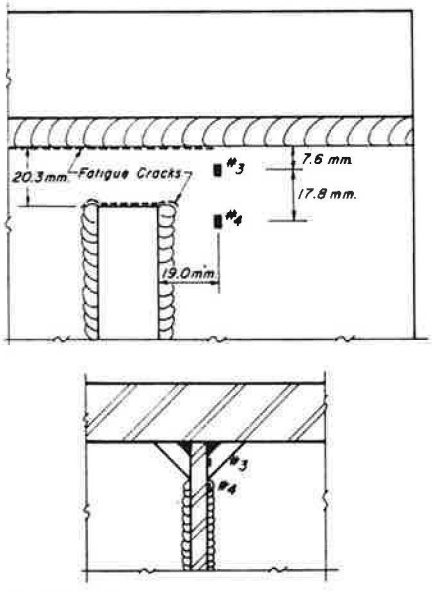

Figure 11. Strain gages near bottom flange gap at Pier B-27 NW.

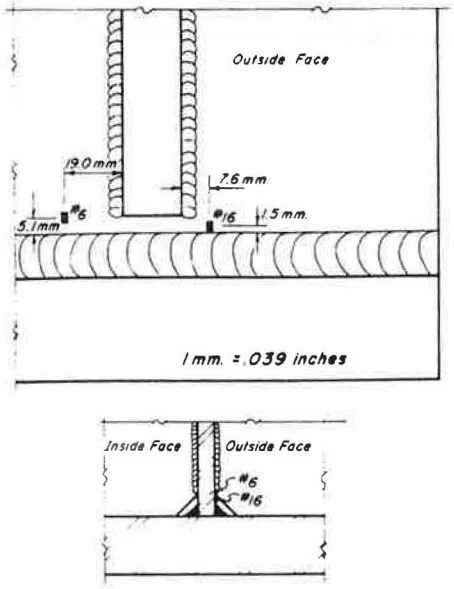

Figure 12. Typical strain response at B-27 NW, B-27 FBI-W.

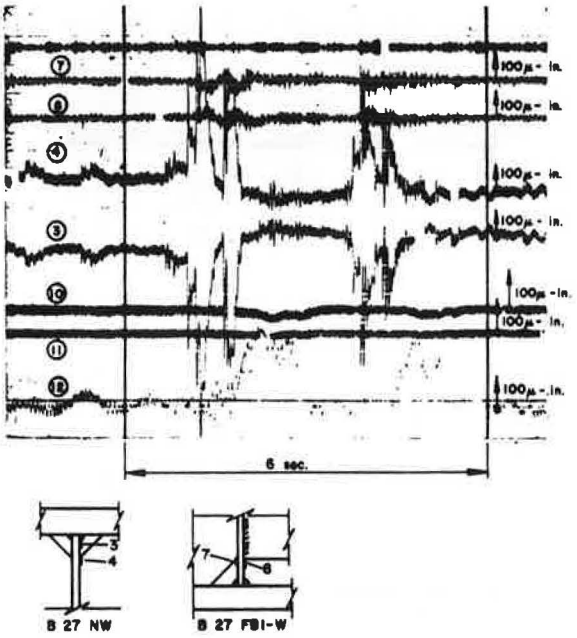

Figure 13. Stress gradient at top gap B-27 NW.

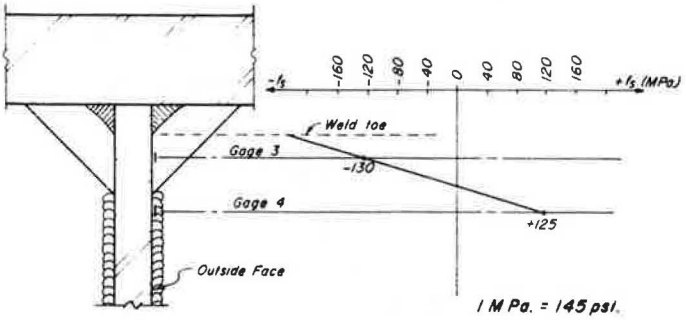

Figure 14. Typical strain response at B-27 NW, C-26 NW.

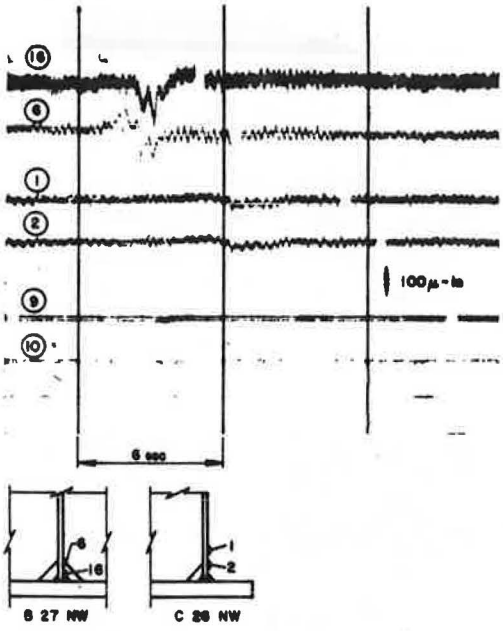

Figure 15. Stress gradient at bottom gap B-27 NW.

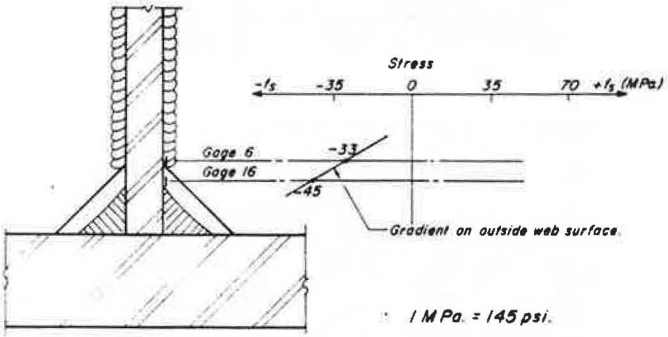

Figure 16. Strain gages near bottom flange gap at floor beam B-27 FBI-W.

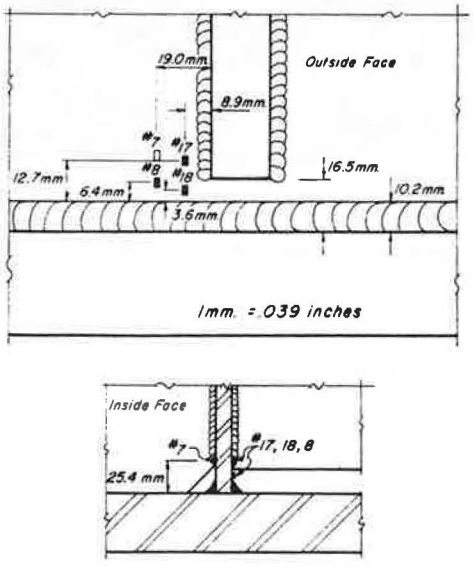

Figure 17. Typical strain response at B-27 NW, B-27 FBI-W.

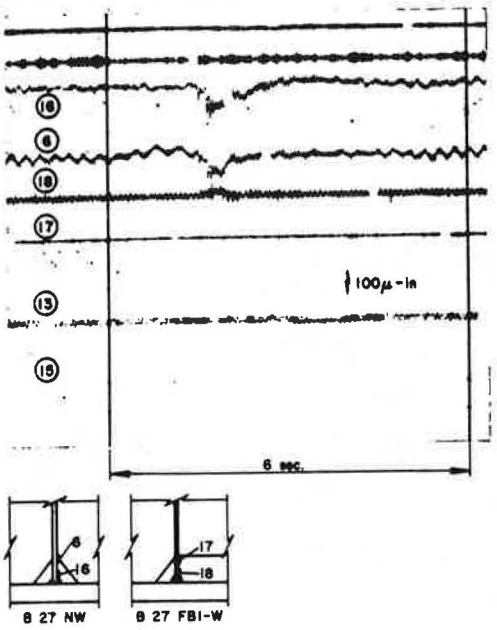

Figure 18. Strain gages near web gap at interior floorbeam B-26 FBI-W.

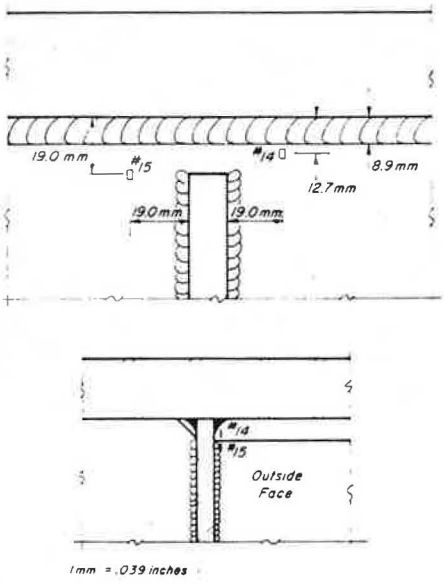

Figure 19. Stress gradient at interior floorbeam B-26 FBI-W.

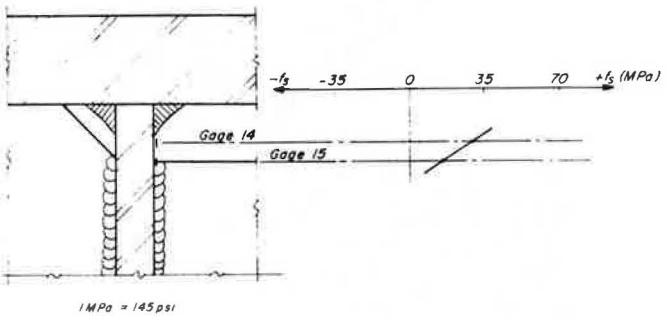

Figure 20. Possible movement at gap region.

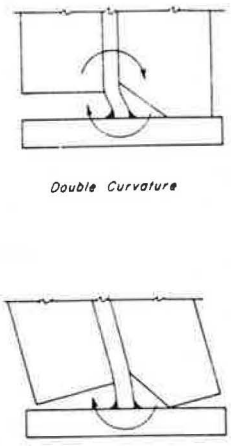

Figure 21. Galling on the surface of the bearing pin (1/3 size model).

Figure 22. Galling on the supporting saddle (1/3 size model).

Figure 23. Specimens after cyclic test.

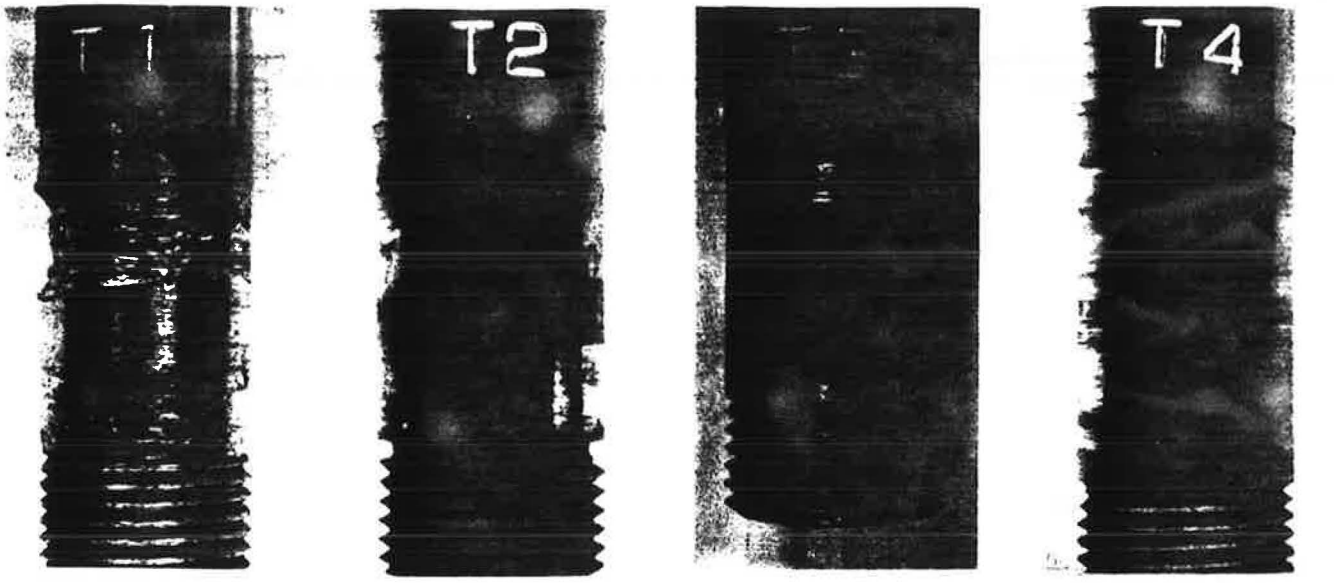

Mild steel only | Mild steel case harden (dry) | Mild steel (greased) | Case harden (dry lube)

Figure 24. Coefficient of friction of dry, mild and case hardened pins.

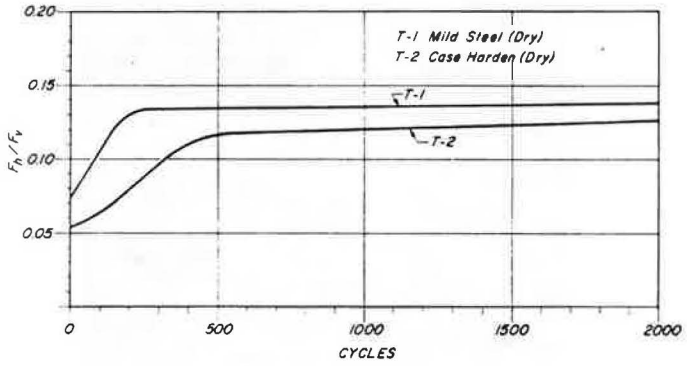

Figure 25. Coefficient of friction of lubricated, mild and case hardened pins.

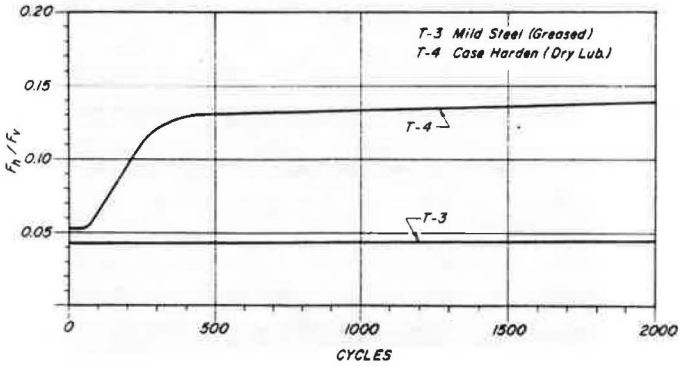

Figure 26. Pin from removed bearing assembly of E. Abut., Ramp B.

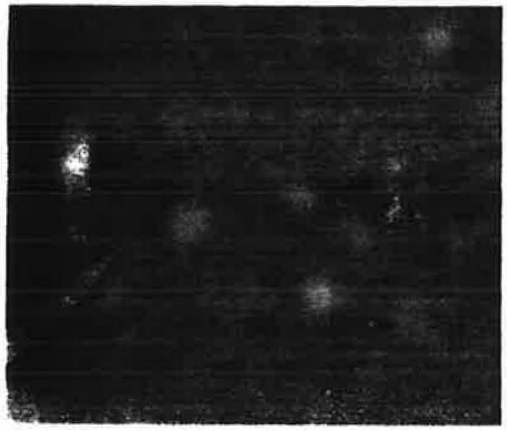

Figure 27. Saddle from removed bearing assembly of E. Abut., Ramp B.

Figure 28. Saddle from removed bearing assembly of E. Abut., Ramp B.

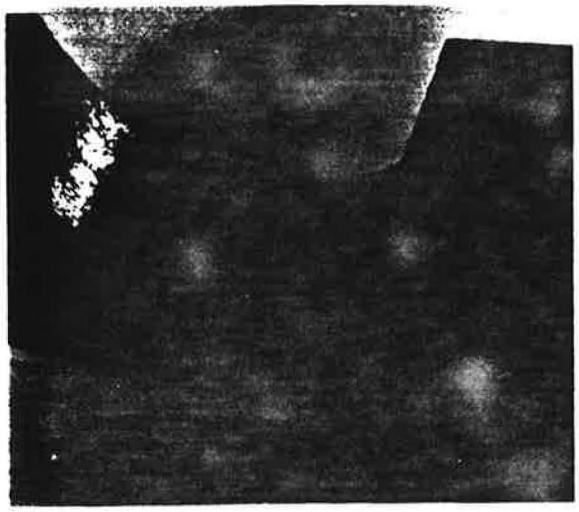

Figure 29. Repair of cracked webs.

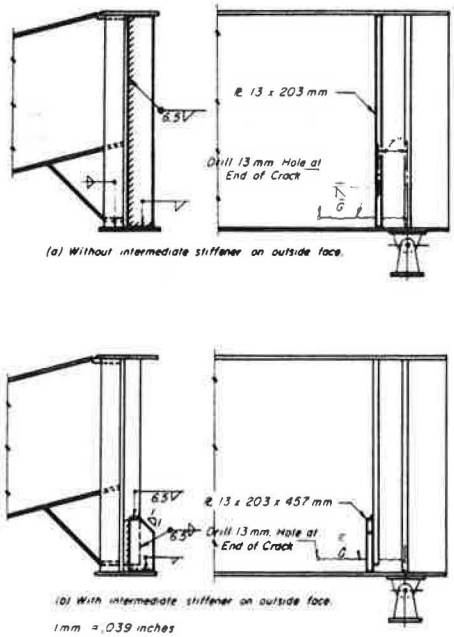

Figure 30. Location of drilled holes to arrest crack.

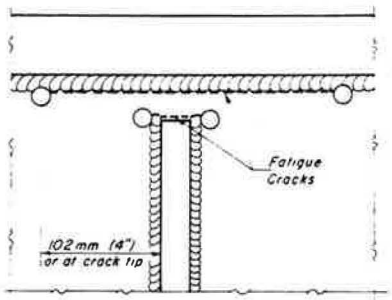

Figure 31. Repair of buckled webs.

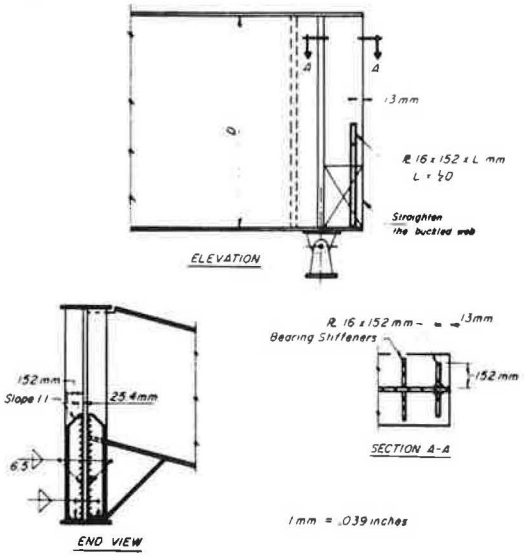

Figure 32. Suggestions for future designs.

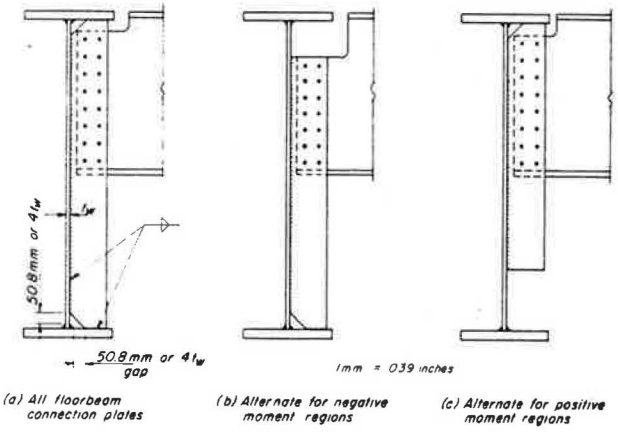

FATIGUE CRACKS OF DEEP THIN-WALLED PLATE GIRDERS

Yukio Maeda, Osaka University, Japan

Recently in Japan, fatigue cracks have been observed in bridges, cranes and tanks. Generally, there is a possibility of two types of fatigue cracks inherent in thin-walled plate girders. A crack which is initiated at the toe of fillet welds of compression flange-to-web, is called Type-1 crack. Then, a crack at the toe of fillet welds of vertical stiffener-to-web, is called Type-2 crack. Type-1 and -2 cracks are governing ones in homogeneous and hybrid plate girders, respectively. For the fatigue design of deep thin-walled stiffened plate girders of bridges, the paper presents an extensive study on fatigue strength based on observations at the tests of initiation and propagation of the above-mentioned two fatigue cracks. The outline of girder tests and of coupon-type model tests for Type-2 cracks, and then the outline of girder tests and of plate-type and bar-type model tests for Type-1 cracks, are described and the results are discussed. The mechanism of initiation of Type-1 cracks at the bar-type model tests is discussed from the point of fracture mechanics in connection with unavoidable inherent initial defects due to welding or fabrication. Although the application of the test results to design is discussed, the problem of Type-1 cracks is a matter of structural details subjected to displacement-induced secondary bending stress ranges, and the need of further studies is stated.

As pointed out by Yen (1, 2, 3), Stallmeyer (4), Toprac (5), and the author (6, p. 287, 7, p. IIIA2.2), there is a possibility of the initiation and propagation of three types of inherent fatigue cracks, as seen in Figure 1, at beams or girders subjected to repeated bending. Type-3 cracks are the most ordinary cracks in a tension flange of any kind of beams or girders. On the other hand, Type-1 cracks which occur at toes on the web side of fillet welds to connect a compression flange to the web, are due to the out-of-plane repeated movement of unavoidable initial deflections under repeated in-plane bending, and are the most governing crack at homogeneous thin-walled stiffened girders. Then, Type-2 cracks which occur at toes on the web side of fillet welds to connect a vertical stiffener to the web, will propagate into a tension flange across the web, and are the most critical one at hybrid thin-walled girders.

Figure 1. Pattern of fatigue cracks of thin-walled plate girder under repeated bending.

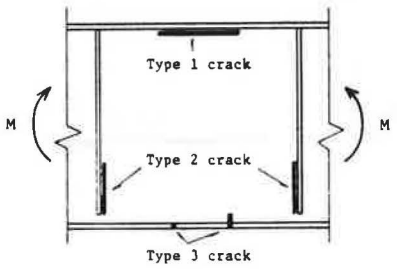

At the present paper, Type-1 and -2 cracks are dealt with, because they are particular to deep thin-walled plate girders. First of all, the fatigue strength against Type-2 cracks is discussed based on girder tests and model specimen tests. Then, the fatigue strength against Type-1 cracks is investigated on the basis of two kinds of model tests together with the results of the author's previous girder tests. Moreover, a matter of structural details subjected to displacement-induced secondary bending stress ranges is discussed for the design of plate girders against Type-1 cracks.

Type-2 Crack

Girder Tests

At the fatigue tests of hybrid girders by Toprac (9), Type-1 cracks were observed. He suggested that it would be effective to use horizontal stiffeners and or limit the web slenderness ratio less than 200 for the prevention of Type-1 cracks. However, all of the test girders by the author(10) failed due to Type-2 cracks. Type-1 and -3 were also observed, but not critical cracks to cause the failure of the girders. Table 1 shows the results of the fatigue tests of six large-sized stiffened hybrid girders

Table 1. Parameters and test results of hybrid girders.

Test Girder	Aspect Ratio	Web Slenderness Ratio β	Longi. Stiff. Rigidity Ratio γ/γ^*	Tens. Flg. Max. Stress (MPa)	Tens. Flg. Stress Range (MPa)	Stress Ratio R	Type of Crack, No.(×10⁴) of Cycles Type 1	Type 2	Type 3	Fatigue Life(×10⁴)	Mode of Failure
B4-L1	1.0	413	1	266	207	0.221	46.5	34.1	-----	67.0	Type 2
B4-L7			7	286	226	0.209	----	24.3	-----	26.0	Type 2
B3-L1		310	1	251	115	0.543	----	218.0[b]	218.0	224.0	Type 2
B3-L6			6	356	207	0.402	----	28.0	-----	33.5	Type 2
B2-L0		206	0[a]	308	172	0.439	----	104.0	-----	116.0	Type 2
B2-L5			5	289	158	0.456	----	116.6	-----	123.5	Type 2

Note: 1 MPa = 145 lbf/in.^{2}

[a]No Longitudinal Stiffener. [b]Max. Stress Increased up to 344 MPa after 2×10^6 Cycles.

carried out by the author (10).

The girders were fabricated of HT80 steel in a tension flange, SM58 steel in a compression flange and SS41 steel in a web. HT80, SM58 and SS41 are respectively, a quenched and tempered high-yield high-strength steel, an ordinary high-strength steel and an ordinary mild steel, and have respectively such mechanical properties as min. yielding point and min. tensile strength as 686.0 MPa (99.5 kipf/in.^{2}), 784.0 MPa (113.8 kipf/in.^{2}); 450.8 MPa (65.4 kipf/in.^{2}), 568.4 MPa (82.5 kipf/in.^{2}); 235.2 MPa (34.1 kipf/in.^{2}), 401.8 MPa (58.3 kipf/in.^{2}). Table 1 summarizes the values of parameters to evaluate the test results, those are, web slenderness ratio, relative rigidity ratio of horizontal stiffeners, tensile stress range and min. to max. stress ratio.

The regression analysis of the test results on the initiation of Type-2 cracks carried out by the author (10) and Toprac (5), gives the fatigue strengths at 2 x 10^6 cycles of 126.4 MPa (18.3 kipf/in.^{2}) in the mean value and of 104.9 MPa (15.2 kipf/in.^{2}) in 95 % confidence limit, both in stress range. Those are 25 % higher than the allowable stress range of 82.3 MPa (11.9 kipf/in.^{2}) in Stress Category C at the AASHTO Specifications (17).

The fatigue strength against Type-2 cracks can be compared to that of a transverse non-load-carrying fillet welded joint (11, 12). Figure 2 shows S-N curves of the results of tests carried out by other investigators on the joint in three kinds of high-strength steels, and of the results of the author's girder tests (10). S-N curves obtained by the former tests do not significantly differ from each other in the grade of steel. Because the scattering of measured values is unavoidable and the difference of stress ratio exists. Moreover, S-N curves of the model specimen tests agree well with S-N curve of the tests of girders with a web in SS41, within the range of fatigue strength of about 100 to 130 Mpa (14.5 to 18.9 kipf/in.^{2}). Consequently, a web in ordinary mild steel is the most economical for Type-2 cracks.

Model Test of Type-2 Crack

The girder tests described above were not sufficient in numbers to warrant the fatigue strength. Also, the model tests (14) referred to did not exactly simulate the behavior of hybrid plate girders, because the tests were done regardless of a possible maximum strain in the corresponding web. Then, fatigue tests were carried out on axially loaded transverse non-load-carrying fillet welded joints under strain control.

Figure 2. S-N curves for Type-2 crack.

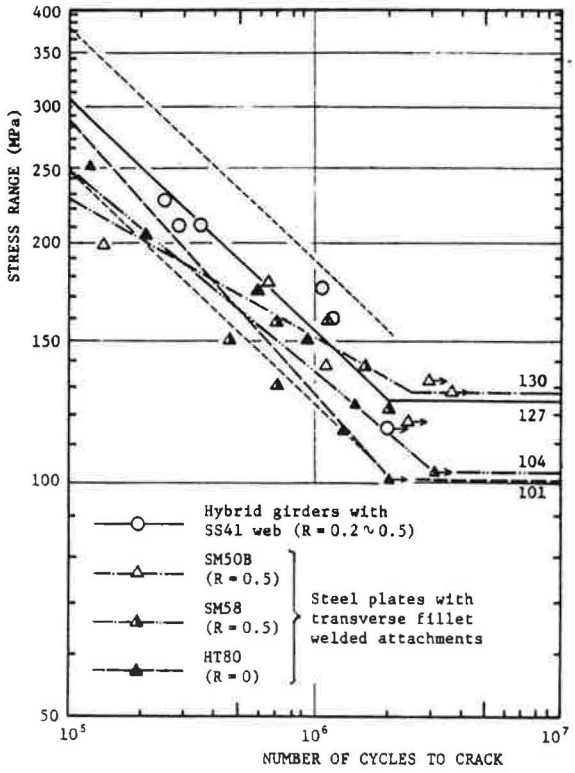

Note: 1 MPa = 145 lbf/in.^{2}

Figure 3. Details of as-welded specimen.

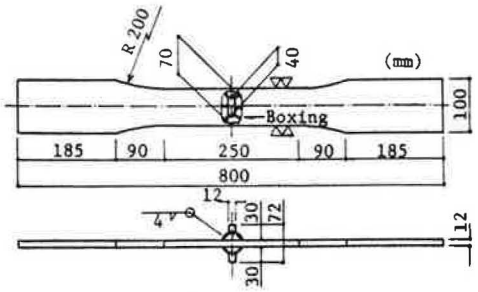

Note: 1 mm = 0.039 in.

Outline of Tests. As shown in Figure 3, the specimens were intended for simulating the boxing part of transverse stiffener-to-web fillet welds in hybrid girders. They were axially loaded under strain control by fixing the out-put of strain gages on the specimen to the maximum strain of 1700 x 10^{-6}, which corresponded to the design working strain of 784.0 MPa (113.8 kipf/in.^{2}) grade high-strength steel in a tension flange of girders.

The specimens were made up of SS41 steel with the specified tensile strength of 401.8 MPa (58.3 kipf/in.2). The tests were divided into two series of as-welded specimens and of specimens lightly ground at the toe of fillet welds to examine the effect of finishing. Such tests were able to simulate the behavior proper to a hybrid girder. Because its web reached a kind of strain-controlled state, after the start of its yielding, due to restraining given by the elastic frame action of the tension flange.

Test Results. S-N diagrams in Figure 4 show the test results in terms of stress range equivalent to strain range at the number of cycles to failure, neglecting the effect of stress ratios. The fatigue strengths of as-welded specimens and of lightly -ground specimens at 2 x 10^6 cycles can be estimated respectively at 93.1 MPa (13.5 kipf/in.^{2}) and 120.9 MPa (14.9 kipf/in.^{2}) as the mean value of stress ranges. The effect of finishing on the fatigue strength is not so remarkable at the present tests. Because the grind operation was not fully performed and consequently some fine notches were not removed.

Figure 4. Fatigue test results.

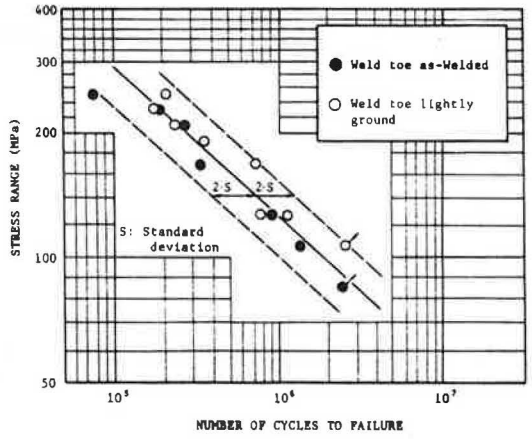

Note: 1 MPa = 145 lbf/in.^{2}

Discussions.

1. Figure 5 shows a comparison of the present test results with the previous fatigue test data on model specimens, under load-controlling, with the same configuration as the present test specimens. Gurney et al. (13, p. 35) gave the latter data as the result of reanalysis of numerous tests. Since the present test results agree well with S-N curves re-analized by Gurney et al., there is no significant difference between load-controlling and strain-controlling.

2. Figure 6 shows another comparison of the present test results for the as-welded specimens in SS41 steel with test results in other steels (15). In Figure 6, SM58 and HT80 are high-strength steels with the specified min. tensile strength of 568.4 MPa

Figure 5. S-N curves for transverse non-load -carrying fillet welded joint.

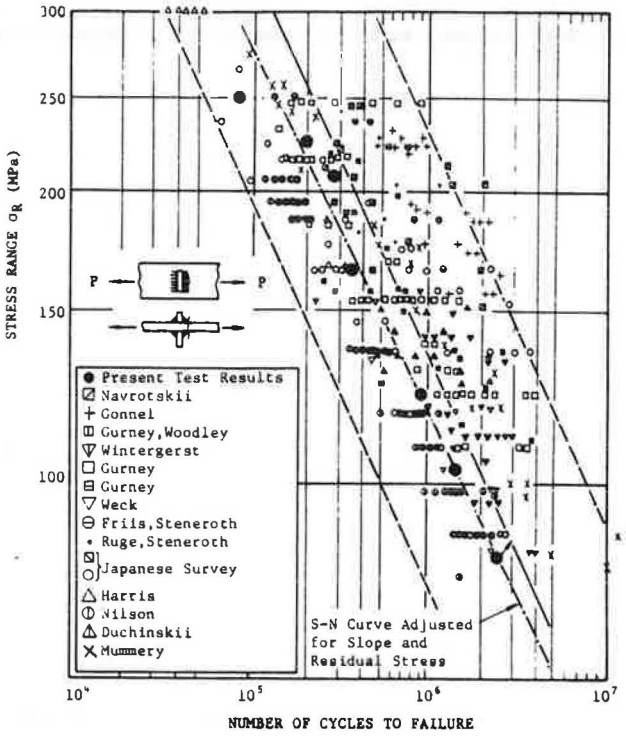

Note: 1 MPa = 145 lbf/in.^{2}

Figure 6. S-N curves for transverse non-load -carrying fillet welded joint in SS41, SM58 and HT80.

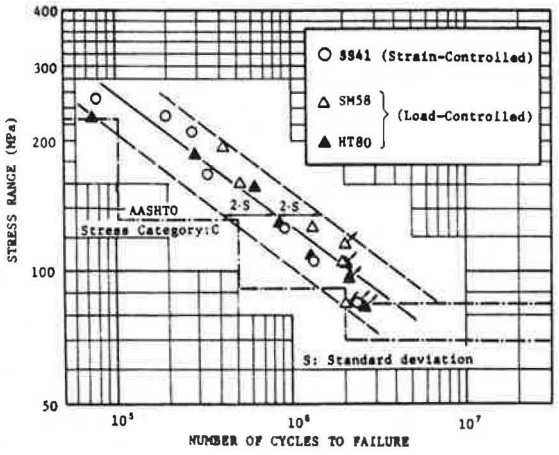

Note: 1 MPa = 145 lbf/in.^{2}

(82.5 kipf/in.^{2}) and 784.0 MPa (113.8 kipf/in.^{2}), respectively. Those specimens were provided with the same configuration as the present test specimens, but their test loads were controlled not by strains, but by loads from zero to tension. Since any significant difference among such results cannot be observed, the fatigue strength of such a welded joint with a large notch effect is almost identical one another, regardless of steel grade, stress ratio and again loading method.

3. Finally, Figure 7 shows the relation between girder tests (8, 10) and some model tests. The model tests results consist of the results of

the present tests and the previous ones in Japan (14. 16) on steel plates with a transverse fillet welded attachment without boxing parts. The present test results under relatively severe loading conditions, can be compared well with lower 95 % confidence limit line of all the quoted results except the present results. This implies that the present test results give conservative fatigue lives for Type-2 cracks in hybrid girders. Also, Figure 6 shows that the allowable fatigue stresses for Stress Category C specified at the AASHTO Specifications (17, p. 87), 1974, are reasonable for Type-2 cracks in hybrid girders.

Figure 7. Comparison of fatigue strength in girder tests with model specimen tests for Type-2 cracks.

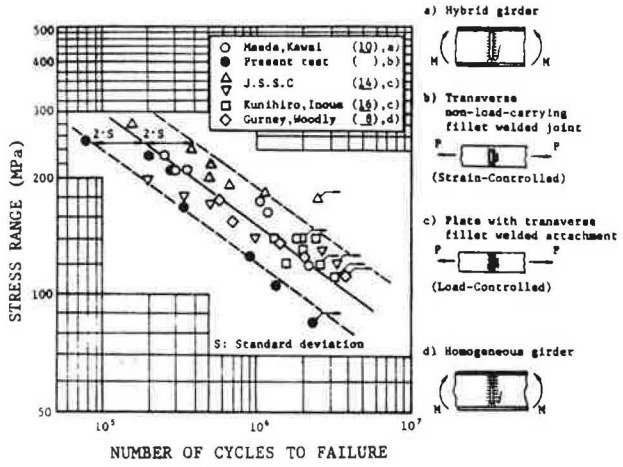

Note: 1 MPa = 145 lbf/in.^{2}

Type-1 Crack

Previous Girder Tests

At the Colloquium of IABSE on "Design of Plate and Box Girders for Ultimate Strength" in 1971, the author published a paper (6). In this paper, the author discussed on the results of flexural fatigue tests of six large-sized welded homogeneous plate girders subjected to repeated bending. The following facts were pointed out:

1. The maximum initial web deflections of 0.3 to 1.6 times the web thickness influenced greatly on the initiation of Type-1 cracks due to secondary bending moment, as seen in Figure 8, caused by lateral web movement under cyclic in-plane loading. Moreover, Type-1 cracks were observed in the case of transversely-stiffened plate girders with a web slenderness ratio larger than 200.
2. The test showed that it would be possible to prevent Type-1 cracks by providing with longitudinal stiffeners and also a smaller web aspect ratio. Rigidities of longitudinal stiffeners of the test girders were selected to 3.83 to 5.30 in terms of the relative flexural rigidity ratio. With a greater rigidity of longitudinal stiffeners, a larger ultimate strength could be achieved and an effective control against Type-1 crack could be expected.
3. In conclusion, the initiation and propagation of Type-1 cracks are influenced by web slenderness ratio, web aspect ratio, initial web deflections and if longitudinal stiffeners are provided with, their rigidity.

Figure 8. Initiation of Type-1 cracks and secondary bending at web boundary.

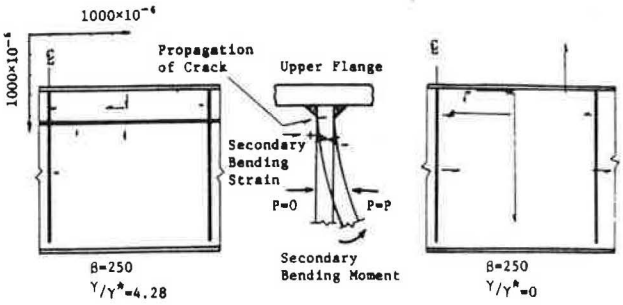

These girder tests, however, did not give sufficient informations of fatigue strength in the moment of initiation of the crack. Even a model specimen test to simulate the initiation and propagation of Type-1 cracks has hardly been reported, because of the complicated condition of cracking, except the values given by girder tests at Lehigh University. The author carried out two kinds of model specimen tests to obtain the fatigue strength against Type-1 cracks. The first plate-type test was intended for the investigation of initiation and propagation of cracks on a web surface along the toe line of fillet welds parallel to girder length. The second bar-type test which is still in progress, is to study on the initiation of cracks propagated through the web thickness.

Plate-Type Specimen Tests (18)

Fatigue tests of two kinds of plate-type specimens in SS41 steel were carried out, as seen in Figure 9, to simulate the fatigue of a web panel enclosed by a compression flange and a horizontal stiffener of a stiffened plate girder. The section of plate specimens was T-shape or I-shape, respectively modelling a less rigid horizontal stiffener or a greatly rigid stiffener. Because at the former specimen, a plate was hinged at the end of web of

Figure 9. Plate-type fatigue test specimens.

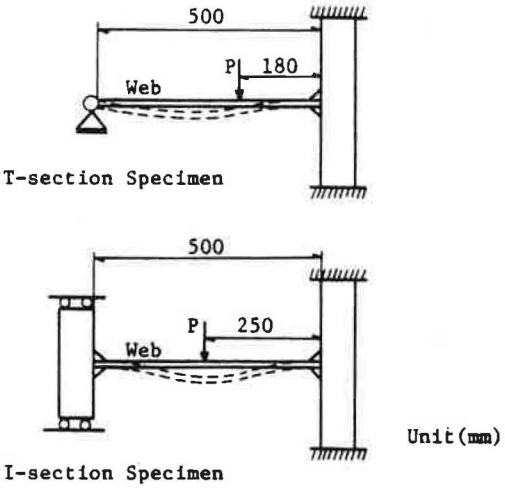

Note: 1 mm = 0.039 in.

Figure 10. Propagation of Type-1 crack.

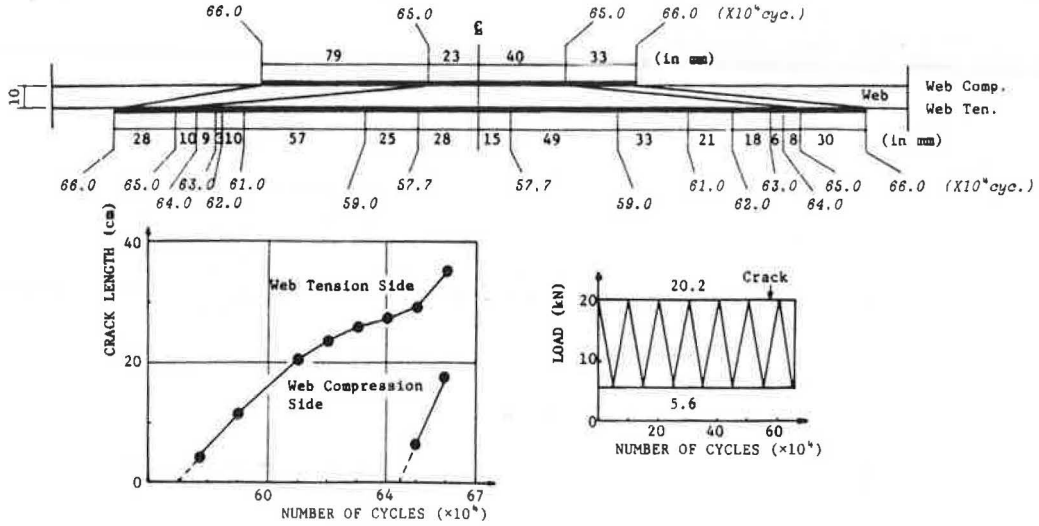

Note: 1 cm = 0.39 in. 1 mm = 0.039 in. 1 kN = 0.255 kip.

T-section and fixed to the flange at the other end, while at the latter specimen, a web plate of I-section is fixed to the both flanges. Deflections of the specimens under an applied concentrated load simulated the web deflections of an actual plate girder. Figure 10 illustrates the initiation and propagation of a fatigue crack observed at a T-section.

Figure 11 shows the test results in terms of the number of cycles at the crack initiation estimated from crack discovery and of the local strain range at the toe of fillet welds estimated by combined finite element analysis and strain measurement. The possibility of about 30 % increase of fatigue strength is expected by machine-finishing at the toe. The regression analysis shows that the fatigue strength at 2 x 10^6 cycles of the fillet weld is 814 x 10^{-6} in strain range or 178.4 MPa (25.9 kipf/in.^{2}) in stress range. Available values from the fatigue test of large-sized plate girders conducted by Yen and then modified by Ostapenko at Lehigh University (19, p. 49) are also given in Figure 11. There is considerable scattering among the test vakues to be attributed to inherent inevitable fine defects at the toe surface of fillet welds.

Figure 11. Test results for Type-1 cracks at Osaka University and Lehigh University.

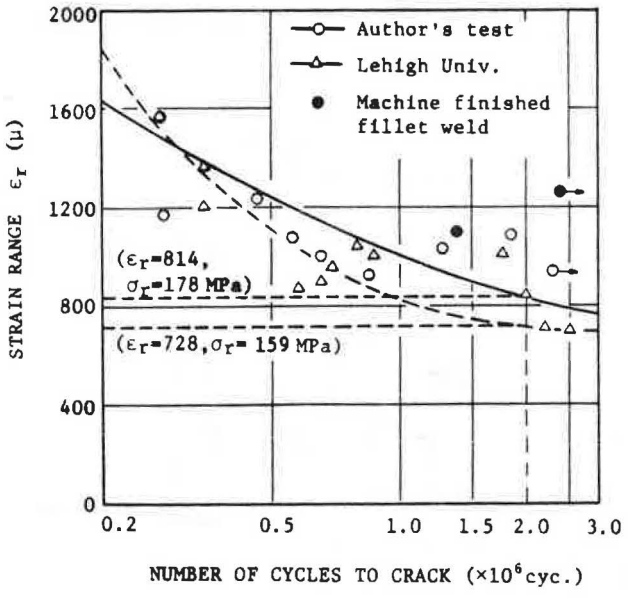

Note: 1 MPa = 145 lbf/in.^{2}

Bar-Type Specimen Tests

To investigate the mechanism of initiation of Type-1 cracks in the direction of web thickness, a series of fatigue tests for specimens of a Tee type fillet welded joint, as seen in Figure 12, was carried out. At the test, the steel of the specimens was 22 mm (0.866 in.) thick in SS41 of the yielding point of 235.2 MPa (34.1 kipf/in.^{2}) and the tensile strength of 401.8 MPa (58.3 kipf/in.^{2}). A repeated load was applied to the web plate of T-joint with 300 cycles per minute, so as to simulate the back and forth movement of the web plate due to its initial deflections of an original plate girder.

Figure 12. Profile of Bar-Type specimen.

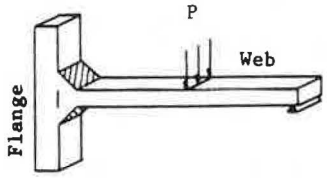

As expected, a crack was initiated at either toe of fillet welds and propagated in the direction of the web thickness. The speed of propagation was measured with crack gauges spaced by 0.2 mm (0.008 in.). Furthermore, to examine how the fatigue strength against Type-1 cracks could be increased by finishing the surface of toes of fillet welds, B-series test, in addition to A-series test of as -welded specimens, was conducted with the test spe-

cimens of Tee type joint, in which the toes were finished with a circle radius of 2.0 mm (0.08 in.). Applied nominal stress ranges in a web section are shown in Table 2.

Table 2. Applied nominal stress ranges (Mpa).

Specimen	A-1	A-2	A-3	A-4	B-1	B-2	B-3	B-4	B-5
Stress Range	297	238	199	189	309	268	284	270	252

Note: 1 MPa = 145 kipf/in.^{2}

It was quite difficult to paste strain gauges on the toe of a fillet weld because of sudden sectional change at the toe. Then, in addition to strain gauges pasted on the web surface of the Tee section at the loading point, strain gauges were pasted on the web surface at a distance of 10 mm (0.4 in.) from the edge of the toe. Strains at the toe edge were estimated from the measured values of strains at those two points.

Figure 13. Strain range versus number of cycles.

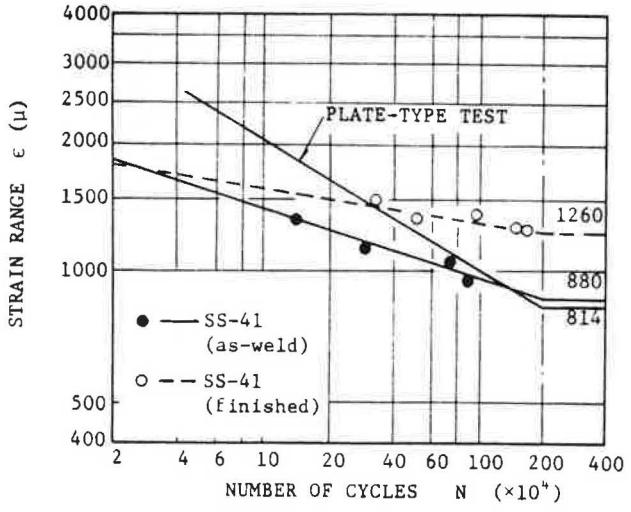

Test Results. Figure 13 shows the test results of fatigue lives expressed in terms of strain range versus number of cycles. Two lines are obtained by the regression analysis of strains observed at the time when a crack propagated over approximately 11 mm (0.433 in.) which was half the web thickness. The fatigue strength at 2 x 10^6 cycles is 168.6 MPa (24.5 kipf/in.^{2}) in stress range or 880 μ (micron) in strain range for as-welded specimens, and is 242.1 MPa (35.1 kipf/in.^{2}) or 1260 μ for finished specimens. A considerable increase of fatigue strength is given by machine-finishing at the toe.

In Figure 13, strain range versus number of cycles for the plate-type tests obtained in Figure 11 is also shown. When a girder is subjected to a certain strain range at its toe of fillet welds in a compression flange-to-web joint, Type-1 crack will start in the direction of web thickness with smaller numbers of cycles than the ones given by Bar-Type tests in Figure 13. Because the curve in Figure 13 was determined by the propagation to about 11 mm (0.43 in.) growth. The growth rate of the crack in this direction is 1 x 10^{-5} to 2 x 10^{-4} mm/cycle (4 x 10^{-6} to 8 x 10^{-6} in./cycle) and is much slower than that of the crack in the direction of the toe line on the web plate.

Before the crack penetrates the web thickness, it will propagate along the toe line on the web surface with the number of cycles on the curve for Bar-type tests. The growth rate of the crack in this direction is 6 x 10^{-4} to 4 x 10^{-3} mm/cycle (2.4 x 10^{-5} to 1.6 x 10^{-4} in./cycle) and much faster than that in the direction of web thickness. Then, after the crack has propagated to a certain length along the toe line, it will penetrate into the back side of the web.

Thus, the crack grows three-dimentionally and Bar-type fatigue curve and Plate-type fatigue curve may not be compared under the same conditions. Further study is required. The initiation and propagation to a certain length do not mean the failure of the girder. As far as the present available informations are concerned, the fatigue curve of Bar-type tests may be considered a design criterion for fatigue. Then, the fatigue strength at 2 x 10^6 cyclea may be regarded about 800 μ in strain range and about 167 MPa (24 kipf/in.^{2}) in stress range.

Application of Fracture Mechanics. The stress intensity factor, K, for single edge-cracked bending in a plate is in general given by

$$K = \sigma_o \sqrt{\pi a} \cdot F(a/W) \qquad (1)$$

where σ_o = the extreme flexural fiber stress, a = the crack length, W = the plate thickness and $F(a/W)$ = the flaw shape parameter. Since the shape of crack tip at the toe of a fillet weld is circular and the shape at the toe point is peculiar, the stress distribution along the crack interface is so complicated that the equation of $F(a/W)$ has not been derived for the present specimens. By applying stress extrapolation with a finite element method to the variation of K value due to the growth of crack length a, the following fourth-order polynomial equation of $F(a/W)$ can be obtained

$$F(a/W) = 2.40 - 7.90(a/W) + 30.10(a/W)^2 - 54.79(a/W)^3 + 46.38(a/W)^4,$$

$$0 \leq a/W < 0.7 .$$

Next, if the measured rate of crack growth is assumed to be expressed as a power of the range of stress intensity, ΔK, as given by Paris (20, p. 70), the crack advance per cycle, da/dN, is shown by

$$da/dN = C \cdot (\Delta K)^m \qquad (2)$$

where C and m are the material constants in crack propagation. By plotting test values of da/dN and calculated values of ΔK for arbitrary load range on da/dN versus ΔK diagram, C and m are obtained as 2.9 x 10^{-11} and 3.2 , respectively as shown in Figure 14. N-equation in Figure 15 shows that the integration of da/dN gives the number, N, of cycles required for the crack growth from a_0 to a_1. N-equation is calculated numerically from a_0 to a_1 with

a_0 = an unknown initial crack length,
a_1 = a certain final crack length within 11 mm (0.43 in.), and
N = the number of cycles corresponding to a

Figure 14. *(da/dN) - K* curve.

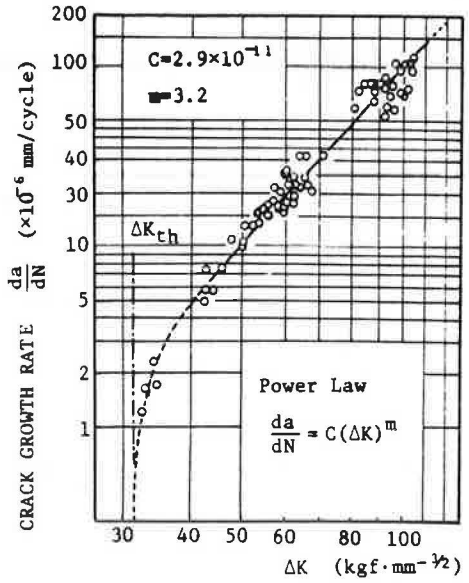

Note: 1 kgf·mm$^{-3/2}$ = 0.2822 kipf·in.$^{-3/2}$

Figure 15. *N* - equation.

$$\frac{da}{dN} = C(\Delta K)^m$$

$$dN = \int_{a_0}^{a_1} \frac{1}{C(\Delta K)^m}\, da$$

$$\Delta K = \frac{6 \cdot M(a/W) \cdot \sqrt{a/W}}{W \cdot \sqrt{W} \cdot B} \cdot F(a/W) \cdot \Delta P$$

$$N = \int_{a_0/W}^{a_1/W} \frac{da}{C[6 \cdot B^1 W^{3/2} \sqrt{a/W} \cdot F(a/W) \cdot M(a/W) \cdot \Delta P]^m}$$

a_0 = initial crack length
a_1 = final crack length
W = web thick
B = web width
M(a/W) = moment

Figure 16. Crack propagation curves (as-welded).

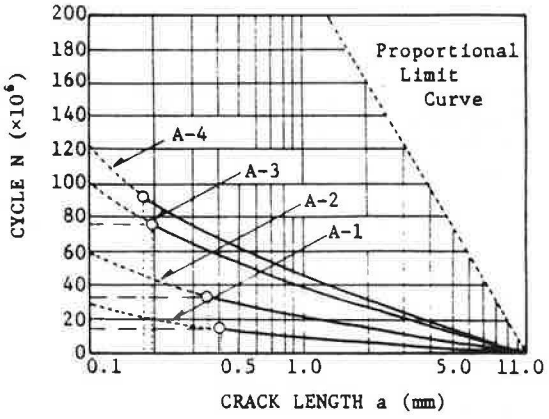

Note: 1 mm = 0.039 in.

Figure 17. Crack propagation curves (finished).

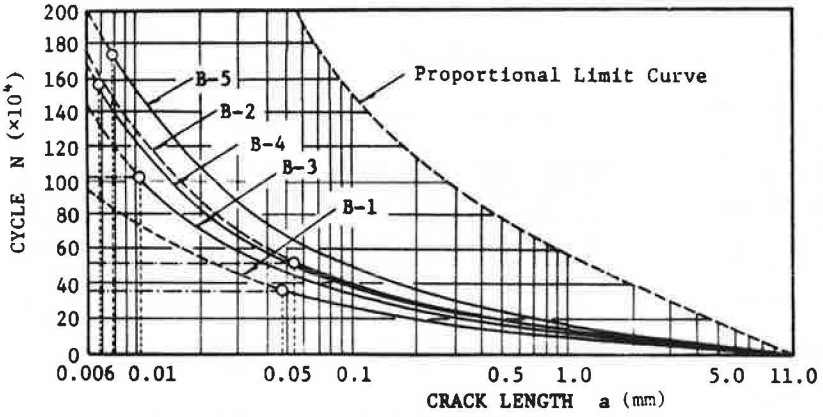

Note: 1 mm = 0.039 in.

certain strain or stress range which is given in Figure 13.

Then, the curves of N versus $a = a_0 - a_1$ are obtained for as-welded specimens A-1 to A-4 and for finished specimens B-1 to B-5, respectively in Figure 16 and Figure 17. The unknown initial crack lengths a_0 are determined as shown by circles in the both figures. Such initial possible cracks are idealized initial cracks equivalent to defects like slug inclusion, undercut, blow hole, notch, etc. In other words, assuming a triger for the initiation of cracks to be such a defect due to welding or fabrication, the fatigue cracking will be interpreted as the propagation of such inherent initial cracks. This is the reason why the test specimens were not provided intentionally with an initial notch. At the application of fracture mechanics, it will be the best way to regard various weld defects as equivalent initial cracks.

In addition to the test of the rate of crack growth, the test to determine the threshold stress intensity factor for fatigue crack propagation, ΔK_{th}, was also conducted. By reducing a load range every crack growth of 0.2 mm (0.008 in.) after a crack had started, the values of ΔK_{th} was obtained

at the time when the crack finally stopped its growth. During the propagation of the crack at the test, the final value of ΔK_{th} was 33 kgf·mm$^{-3/2}$ (9313 lbf·in.$^{-3/2}$) for da/dN of 1.2 x 10^{-6} mm/cycle (0.047 x 10^{-6} in./cycle), as seen in Figure 14, and during the next 1 x 10^6 cycles for ΔK = 28 kgf·mm$^{-3/2}$ (7902 lbf·in.$^{-3/2}$), the crack growth was not observed, and then the test was stopped. Therefore, the value of ΔK_{th} may be approximately 30 kgf·mm$^{-3/2}$ (8466 lbf·in.$^{-3/2}$), below which the Paris equation cannot be applied to any stress range and which will give a limit shown as the proportional limit curve in Figures 16 and 17.

Conclusion.

1. Fatigue strength of Type-1 cracks at 2 x 10^6 cycles will be about 167 MPa (24 kipf/in.^{2}) in stress range in the direction of propagation toward the web thickness.

2. Mechanical-finishing at the toe on the web side of fillet welds will increase the fatigue strength considerably. At the present test, it will be about 40 % higher than the fatigue strength of the as-welded specimens in nominal stresses.

3. The application of fracture mechanics will be enable to evaluate fatigue qualitatively, so that micro initial defects may be evaluated without applying the theory of material science. The application of the Paris equation shows that the initial crack length equivalent to latent defects will be 0.18 to 0.41 mm (0.007 to 0.016 in.) for as-welded specimens (Figure 16) and 0.0068 to 0.053 mm (0.0003 to 0.002 in.) for finished specimens (Figure 17). Such estimation, however, has to be verified by more precise tests.

4. As stated previously, Type-1 cracks will propagate not only in the direction of web thickness, but also in the direction of the toe lines. Furthermore, a study on three-dimensional crack propagation has to be made.

Application to Design

1. As discussed above, the fatigue strength against the initiation of Type-1 cracks along the weld toe line at 2 x 10^6 cycles is 178.4 MPa (25.9 kipf/in.^{2}) and 164.6 MPa (23.9 kipf/in.^{2}), respectively in the plate-type tests for as-welded specimens and in the girder tests at Lehigh University. Also, the fatigue strength against the growth of a crack to half the web thickness is 168.6 MPa (24.5 kipf/in.^{2}) in the bar-type tests for as-welded specimens.

The fatigue strength may be estimated about 167 to 176 MPa (24 to 26 kipf/in.^{2}), but there are some problems to be solved. How much is the fatigue strength for different grade of steel other than SS41 grade steel? Which is the design criterion, the fatigue strength for cracks along the weld line on the web or that for cracks across the web thickness ?

2. The initiation of Type-1 crack is caused by out-of-plane deflections of a web plate due to initial deflections of the web, and the out-of-plane deflections are non-linear with in-plane bending stresses in the web. Therefore, the fatigue strength alone is not sufficient for a practical design purpose. The test results for the plate-type specimens are rearranged in Figure 18 in terms of the maximum web deflection in a compression sub-panel of the web and the fatigue lives. In the figure, the vertical axis on the left side shows the non-dimensional expression of the ratio of out-of-plane deflection range of the web to the web thickness, δ_r/t_w . The vertical axis on the right side gives the ratio, δ_r/h , of δ_r/t_w to the slenderness ratio, $\beta = h/t_w$, where h = the depth of a web sub-panel surrounded by a compression flange, a horizontal stiffener and two vertical stiffeners. From the diagram, the allowable amount of out-of-plane deflection under a live load will be determined for a certain web slenderness ratio.

For example, the value of δ_r/h at 2 x 10^6 cycles can be read as 1/325 as the mean value. Then, if $\beta = h/t_w$ = 50, the out-of-plane web deflection due to live load has to be controlled to about 1/6.5 of the web thickness.

3. In Figure 18, the full-line shows mean values obtained by the regression analysis of the plate-type test values of I-section and of T-section except machine-finished specimens. The most outside broken lines show the range of two times the standard deviation and can be regarded as the upper and lower limits of a scattering band. I-section models equivalent to $\gamma/\gamma^* = \infty$ of horizontal stiffeners, locate near the upper limit of the scattering band, compared with the lower values for T-section models equivalent to $\gamma/\gamma^* = 1.0$. This fact was confirmed at the author's previous girder test.

Figure 18. Out-of-plane deflection of web and fatigue lives of Type-1 crack.

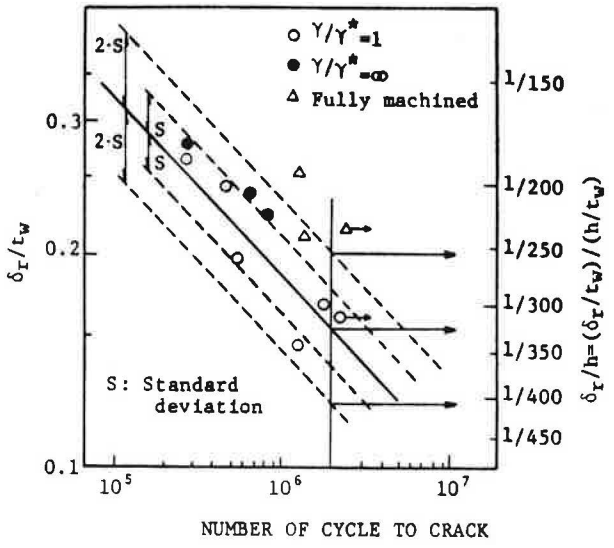

4. Massonnet, Skaloud, Maeda, etc. reported that horizontal stiffeners with a large value of γ/γ^*, for example 3 to 7 recommended by Massonnet, is greatly effective for the increase of ultimate strength of a girder. Even if Type-1 crack was initiated, horizontal stiffeners with large rigidity can delay its propagation. According to Toprac's test (5), Type-1 crack was not observed in girders provided with a horizontal stiffener. Requirement for the number of γ/γ^*, however, has not been clarified. Figure 19 indicates the effect of web slenderness ratio and relative rigidity ratio of horizontal stiffeners on the number of Type-1 cracks observed at the tests at the University of Texas, Lehigh University and Osaka University. Type-5 cracks in the figure is a crack along a vertical stiffener observed for combined bending and shear.

In general, a horizontal stiffener takes great effect on preventing the upper sub-panel of a web from the development of greater web deflections, but

Figure 19. Web slenderness ratio, β , rigidity ratio parameter, γ/γ^*, and number of cracks.

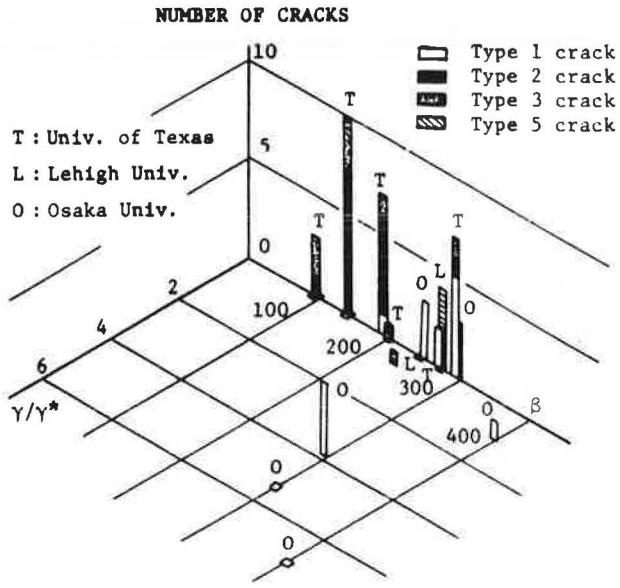

Figure 19 shows that the initiation of Type-1 crack was not observed for $\gamma/\gamma^* < 1.0$ or > 5.0, and also for less than 200 of β . With the intermediate number like $\gamma/\gamma^* = 3.83$ and $\beta = 300$, Type-1 crack was not observed. Since the effect of γ/γ^* has to be discussed in relation to aspect ratio, web slenderness ratio, secondary bending stress at flange - to -web connection and horizontal stiffener-to-web connection, a further study will be needed.

5. The author is carrying out an analytical and experimental studies to establish the relations among the maximum initial deflection, δ_o, the out-of -plane web movement, δ_r, the applied in-plane bending stress, σ and the relative rigidity ratio of horizontal stiffeners, γ/γ^* , with the equation

$$\delta_r/h = f(\sigma, \delta_o, \gamma/\gamma^*).$$

Summary Conclusion

Fatigue cracks of Type-1 and Type-2 proper to deep thin-walled stiffened plate girders were discussed through a number of tests of girders and model specimens.

When a plate girder either homogeneous or hybrid with a web in ordinary mild steel is subjected to repeated bending, the initiation and growth of Type -1 cracks will be prevented by controlling secondary bending stresses at the toe of fillet welds in a compression flange below about 167 to 176 MPa (24 to 26 kipf/in.^{2}). In addition to the stress control, mechanical-finishing at the toe or the control of initial web deflections will be very useful.

On the other hand, Type-2 cracks will be prevented by reducing web tensile stresses during repeated bending below about 93 MPa (13.5 kipf/in.^{2}) or by finishing at the toe of fillet welds in vertical stiffeners.

As far as Type-1 cracks are concerned, in-plane bending stresses of a web are related to secondary bending stresses of the web only by initial web deflections or out-of-plane movements. A survey of actual initial deflections of webs in plate girder bridges will be required.

References

1. B. T. Yen and J. A. Mueller. Fatigue Tests of Large-Size Welded Plate Girders. WRC, Bull. 118, 1966.
2. J. A. Mueller and B. T. Yen. Girder Web Boundary Stresses and Fatigue. WRC, Bull. 127, 1968.
3. Patterson, Corrado, Huang and Yen. Fatigue and Static Tests of Two Welded Plate Girders. WRC, Bull. 155, 1970.
4. D. W. Goodpasture and J. E. Stallmeyer. Fatigue Behavior of Welded Thin-Web Girders as Influenced by Web Distortion and Boundary Rigidity. Univ. of Illinois, C. E. Studies SRS 328, 1967.
5. A. A. Toprac and M. Natarajan. Fatigue Strength of Hybrid Plate Girders. Proc. of ASCE, 97, ST4, 1971, pp. 1203 - 1225.
6. Y. Maeda. Ultimate Static Strength and Fatigue Behavior of Longitudinally Stiffened Plate Girders in Bending. IABSE, Proc. London Colloquium, March 1971, pp. 269 - 282.
7. Y. Maeda. Initiation of Fatigue Cracks in Welded Plate Girders. Japan Welding Society, Proc. 1st International Symposium, Nov. 1971, pp. IIIA2.1 - IIIA2.10.
8. T. R. Gurney and C. C. Woodley. Investigation into the Fatigue Strength of Welded Beams. British Welding J., 9, 9, 1962, pp. 446 - 454.
9. H. S. Lew and A. A. Toprac. Fatigue Tests of Welded Hybrid Girders under Constant Moment. Univ. of Texas, Center for Highway Res., Res. Rept. 77-2F, 1967.
10. Y. Maeda, M. Ishiwata and Y. Kawai. Fatigue Strength of Thin-Walled Hybrid Plate Girders. IIW, Doc. XIII-734-74, 1974.
11. W. H. Munse and J. E. Stallmeyer. The Influence of Weld Details on the Fatigue of Welded Beams and Girders. British Welding J., 77, 3, 1960, pp. 180 - 200.
12. L. R. Hall and J. E. Stallmeyer. Thin Web Girder Fatigue Behavior as Influenced by Boundary Rigidity. Univ. of Illinois, C. E. Studies SRS 278, 1964.
13. T. R. Gurney and S. J. Maddox. A Re-Analysis of Fatigue Data for Welded Joints in Steel. The Welding Institute Res. Rept. E/44/72, 1972.
14. Fatigue Committee. Fatigue Strength of Plates with Transverse Fillet Welded Attachments. Soc. of Steel Construction of Japan (J.S.S.C.), Journal, 7, 72, 1971, pp. 17 - 38 (in Japanese).
15. Y. Tanaka, M. Ishiwata et al. Fatigue of Welded Joints in High-Strength Steel (80 kg/mm^2 Steel). 26th Annual Conference of the Japan Soc. of Civil Engineers, 1971, pp. 63 - 66 (in Japanese).
16. T. Kunihiro and K. Inoue. Fatigue Design of Orthotropic Steel Deck Plates. Tech. Rept. of Public Works Res. Inst., Japan, 14, 2, 1972, pp. 17 - 20 (in Japanese).
17. AASHTO. Interim Specifications for Bridges - Interim 8. 1974, pp. 86 - 90.
18. Y. Maeda, M. Ishiwata and Y. Imamura. Fatigue Strength of Fillet Welds to Connect Compression Flange to Web of Plate Girders. 30th Annual Conference of the Japan Soc. of Civil Engineers, 1975, pp. 226 - 227 (in Japanese).
19. S. Parsanejad and A. Ostapenko. On the Fatigue Strength of Unsymmetrical Steel Plate Girders. WRC, 156, 1970, pp. 48 - 59.
20. P. C. Paris and G. C. Sih. Stress Analysis of Cracks. ASTM, Rept. STP-381, 1965, pp. 30-83.

ACOUSTIC EMISSION AND FATIGUE CHARACTERISTICS OF TYPICAL BRIDGE STEELS

Theodore Hopwood and J. H. Havens, Division of Research, Kentucky Department of Transportation

Acoustic emission monitoring was used during tensile tests of low-carbon structural steels to determine the physical characteristics of the acoustic emission phenomena. Results indicate that acoustic emissions are caused by micro-plastic deformation processes (i.e., dislocation motion).

A series of axial-fatigue tests was performed on several types of structural steels, some of which had extensive service in bridges. There was no apparent relation between specimen load histories and subsequent performance in fatigue tests. Tensile tests of specimens subjected to extensive fatigue testing, at stresses below the yield strength of the material, revealed no major difference in mechanical properties or acoustic emission response due to their fatigue histories.

Further tests revealed that acoustic emission testing in the frequency range of 100-300 kHz has the physical capability of detecting cracks on large structural steel members. This may prove beneficial for the comprehensive nondestructive evaluation of steel bridges.

Summary

Most bridges which have failed have succumbed to brittle failures. However, fatigue failure of bridges is a constant danger. Bridges are being subjected to heavier traffic loads and higher traffic volumes. The increased use of welding in bridge construction has also increased the hazard of fatigue failures.

The Division of Research, Kentucky Bureau of Highways, has been concerned with the problem of bridge fatigue. The Division of Research approached this problem from a statistical viewpoint, attempting to determine bridge fatigue lives from traffic loading patterns. However, a need existed to determine the mechanical behavior of bridge steels which had seen long service in fatigue environments. Acoustic emission, a new nondestructive evaluation tool, showed some potential for providing data about the loading history of a material. A study was initiated to investigate these subjects.

Acoustic emissions (AE) are transient elastic waves generated in a material subject to external stress. In metals, sensitive electronic 'listening' devices must be used detect acoustic emission. A Dunegan Model 3000 acoustic emission detector was used in this study.

A series of tensile and compressive tests was performed on mild steel and aluminum specimens to determine the physical sources of acoustic emission. Steel specimens in both the annealed and cold-rolled states produced acoustic activity which was best explained as being caused by elements of microplasticity (i.e., dislocation motion). The behavior of aluminum tensile and compressive specimens reinforced this view. AE activity was found to be irreversible with increased loading. If a specimen was partially loaded and relieved, no emission was detected until the specimen was stressed to a higher level. This behavior is termed the Kaiser effect.

Tensile specimens were prepared from an old eyebar from the C & O bridge at Covington. The eyebar had lain in a storage yard for a year since the bridge had been demolished. Tests revealed that strain aging had occurred, preventing AE monitoring from detecting the specimens' loading history.

A series of axial-fatigue tests was initiated using eyebar specimens and five specimens from a special batch of replica steel furnished by National Steel Corporation. Twelve specimens each came from two additional types of structural steels. These steels, probably ASTM A 7, came from rivited bridge members that had suffered fatigue failures.

The fatigue tests were performed by Metcut Research Associates of Cincinnati, Ohio, on a Baldwin-Lima-Hamilton, IV-20 fatigue machine. The eyebar and replica specimens were tested at various stress ratios and fractions of fatigue lives at those stress ratios. ASTM A 7 specimens were tested in completely reversed loading to failure or runout which was specified at 12 x 10^6 cycles.

Inspection after the tests were completed revealed that all fractured specimens failed at the transition between the fillet and the gage section. This did not affect the continuity of test results. There was no appreciable difference in the fatigue behavior of the eyebar and replica specimens.

None of the steels tested showed any significant loss in mechanical properties, compared to results of fatigue tests of mild steel performed by others. The two ASTM A 7 steel specimens had lower ratios of fatigue limits to ultimate strengths than values obtained by others. However, this was probably caused by the stress risers at the gage-section fillets.

Tensile AE tests were conducted on unfatigued specimens and those which had survived the specified fatigue run-out. No major differences in mechanical behavior or AE response were noted. The fatigue specimens had undergone strain aging between the time of fatigue testing and the subsequent tensile tests.

Several of these specimens were notched and tensile tested to determine the behavior of specimens with stress concentrations. Each specimen showed high strength and low ductility. AE activity of notched specimens differed from the unnotched ones. The notched specimens showed a slight increase in AE rate prior to failure.

A field test was performed using a large I-beam and an AE simulator. The simulator induced sound waves in the beam similar in frequency content and magnitude to AE waves produced by a growing crack. At high signal resolutions, the AE detection system could detect these excitations at a distance of about 45 feet (14.8 m). This shows the capability of AE testing on large structural members.

Scope

The Division of Research, Kentucky Bureau of Highways, has been concerned with the problem of bridge fatigue for the past 15 years. Most of the Division's past research used statistical models based on the analysis traffic patterns in an attempt to predict the remaining safe life of bridges *(1, 2)*. The utility of this type of analysis is limited by several facts. Bridges subject to fatigue show the cumulative effects of random cyclic loads (sometimes above the fatigue limit). Damage theories postulated by the Division of Research were based on Miner's rule, which assumes that if n_i cycles of stress σ_i are applied to a member, where N_i was the fatigue limit

for the member, failure could occur when

$$(\Sigma\ n_i/N_i) = 1.$$

Miner's rule has not proven conservative and is subject to the same statistical variations encountered in fatigue tests. Also, in its simplest form, it precludes the possibility of a pre-existent crack which can easily occur in a structure as large as a bridge.

It was realized that some information on actual material performance would be required to substantiate assumptions incorporated in earlier statistical models. Little previous research could be found on the mechanical performance of steels subjected to many years service in a fatigue environment. Acoustic emission, a new laboratory and nondestructive evaluation tool, showed some potential for providing data about the loading history of a material. Therefore, a study was initiated to investigate acoustic emission and fatigue.

Acoustic Emission

Acoustic emissions (AE) are transient, elastic waves generated by the rapid release of energy from a material subjected to an external stress. Consider breaking a stick by slowly bending it: when the wood fibers fracture, a noise can be heard. However, most dynamic processes in metal release insufficient energy to be detected audibly. Therefore, sensitive electronic equipment is required to detect these processes.

A schematic diagram of the Dunegan Model 3000 acoustic emission detector used in the study is shown in Figure 1. The essential components are transducers, preamplifiers, and totalizers (counters). Transducers receive weak, high-frequency mechanical vibrations from dynamically stressed specimens and converts them into electrical signals proportional to the rate and the intensity of the impressed vibrations. Preamplifiers amplify the signals, filtering out frequencies below 100 kHz, which are usually extraneous mechanical noises. The totalizers (counting circuitry) measure and count the voltage signals from the preamplifier that exceed a certain threshold level. This data is displayed as 'counts', being proportional to the frequency and intensity of the impressed vibrations. The totalizer can work in conjunction with a Dunegan Model 402 reset clock to provide count rates. Counting is visually displayed on a panel meter and on a strip chart. The amplified signal is heard through a Dunegan Model 702 audio monitor. The couplant used in this study to connect transducers to test specimens was a viscous polyester resin, Dow DV-9.

Initial Acoustic Emission Tests

Several basic questions needed to be answered about the exact physical sources of acoustic emission before any correlation could be made between acoustic emission and fatigue. Ingham, et al., associated the AE phenomena in steel with cracking of cementite *(3)*. They noted that steels with spheriodized peralite produce less total acoustic emission than those with lamellar pearlite. Dunegan and Harris, however, associated AE activity with mobile dislocations *(4)*.

Figure 1. Acoustic Emission Detection System.

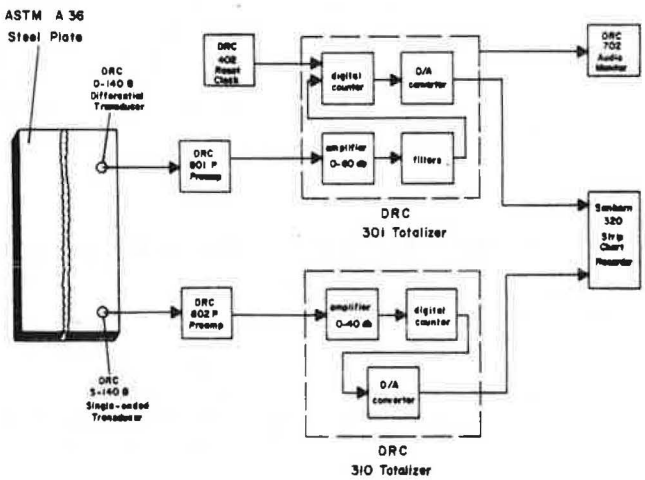

A series of tensile and compressive tests was performed on steel and aluminum specimens. The tests were conducted at the University of Kentucky Department of Metallurgical Engineering and Materials Science using a 20,000-pound (88,960-N) capacity, universal testing machine (Instron). Pin-type grips were required for tensile specimens. A special prestressing device was used to preload pin holes. The preload was higher than fracture load of the specimens. This had two beneficial effects: it work-hardened the specimen pin holes, and it 'silenced' noise from deformation at the pin holes. This minimized AE activity from the grip area during the tests.

The initial tensile tests, shown in Figure 2, were conducted using AISI 1018 steel specimens. The resulting load- and AE rate-versus-strain curve of Figure 3 shows a difference between cold-worked AISI 1018 steel (Test 9) and annealed AISI 1018 steel (Test 10). These tests were run at a crosshead speed of 0.05 in./min (1.3 mm/min). Low-noise (differential) Dunegan D140 transducers were used for the tests. Acoustic emissions were summed over a time interval of two seconds to give a rate indication of AE activity. The Model 301 totalizer was run with a gain of 95 dB. The AE output of the totalizer was plotted on a strip-chart recorder.

Figure 2. Tensile/AE Test of a Steel Specimen.

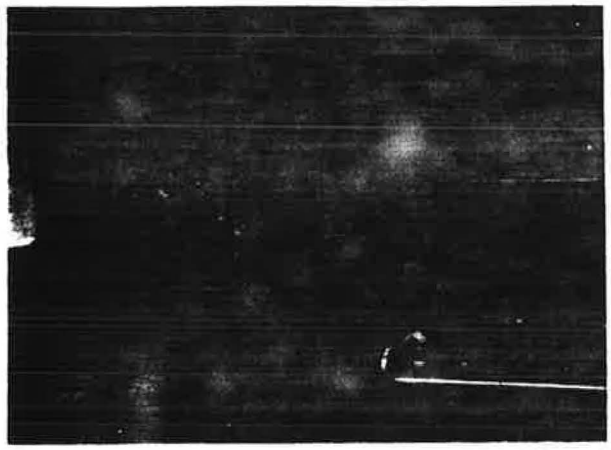

AE activity of cold-worked steel increased rapidly with the rising tensile load and reached a maximum value at the proportional limit. After plastic deformation began, the AE activity decreased. The AE rate for the annealed specimen increased gradually with load, reaching a maximum value at the proportional limit. After plastic deformation began and as it proceeded, the AE rate decreased. Whereas the cold-worked steel had the highest AE rate, the annealed steel had nearly three times as many total AE counts. Most of the potential for AE activity in the cold-worked steel had been dissipated by creating dislocations in the cold-forming process; therefore, less total AE activity was possible.

Figure 4 demonstrates the irreversibility of acoustic emissions with loading, using the fully annealed steel. The summing interval was increased to 10 seconds. The specimen was loaded until discontinuous yielding took place. Then, the load was decreased to a low value. The specimen was reloaded and pulled to failure. The AE rate curve demonstrated the irreversibility of acoustic emission. AE activity ceased on unloading, and no emissions occurred until the previous maximum load was exceeded. This behavior, called the Kaiser effect, was found to exist for both elastic and plastic deformation.

Figure 5 shows the load- and AE rate-vesus-strain for a one-inch (25.4-mm) cube of commercially pure aluminum in compression. The Kaiser effect was also demonstrated in this test. The specimen was strained at a crosshead rate of 0.01 in./minute (0.254 mm/minute). A 2-second summing interval was used for the AE rate. No AE activity was found until the proportional limit was exceeded. The maximum AE rate occurred prior to the onset of gross plastic flow. The AE activity, for most aluminum specimens tested, decreased gradually with increasing plastic flow. The compression test was stopped when the load reached the maximum capacity of the testing machine.

The ductile aluminum specimen shown in Figure 5 had approximately the same volume of material subject to maximum strains as the steel specimens. The rate of AE activity from the aluminum specimen is of the same order of magnitude as the AE rate from the steel specimens. Commercially pure aluminum has no brittle second phase such as cementite.

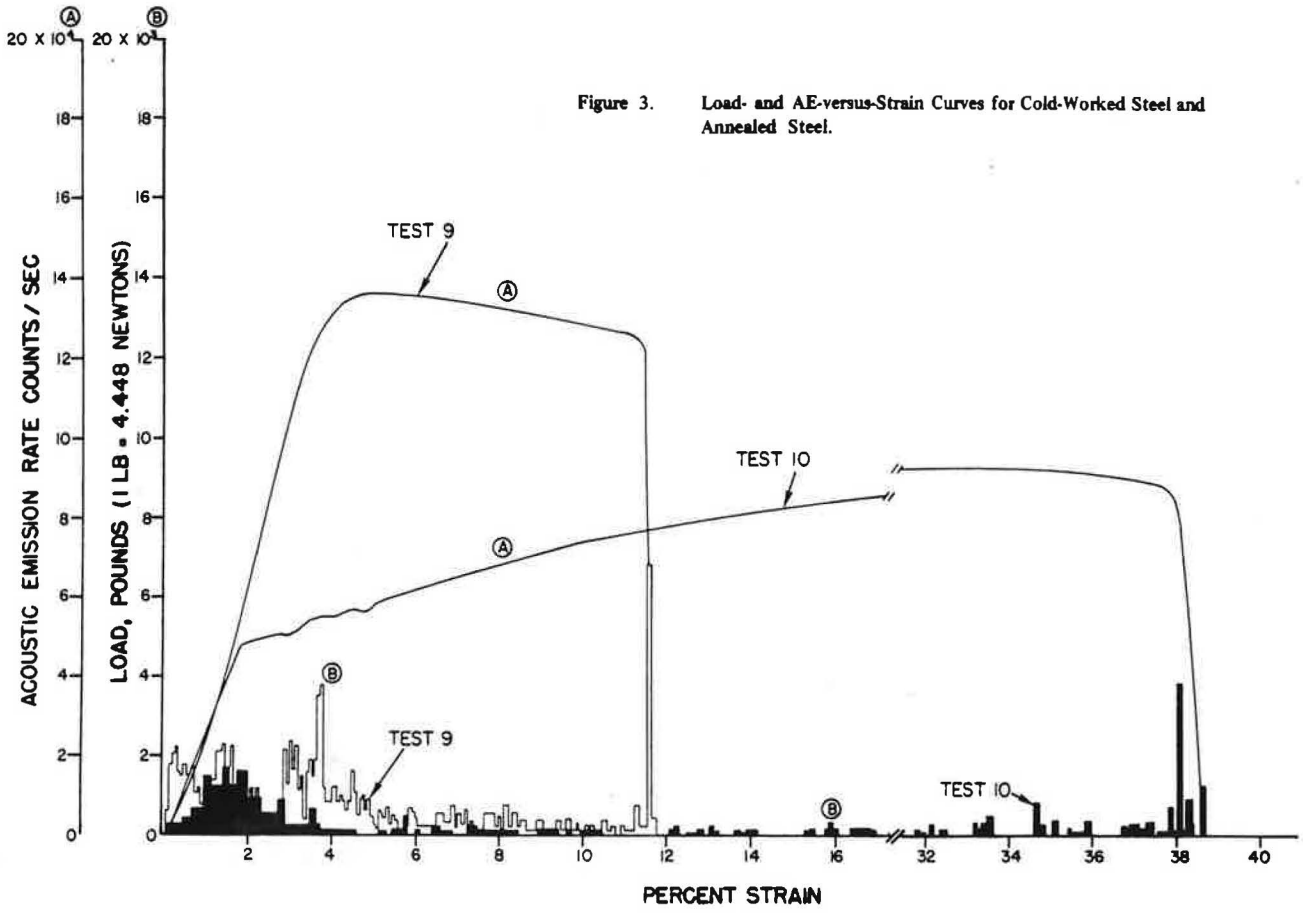

Figure 3. Load- and AE-versus-Strain Curves for Cold-Worked Steel and Annealed Steel.

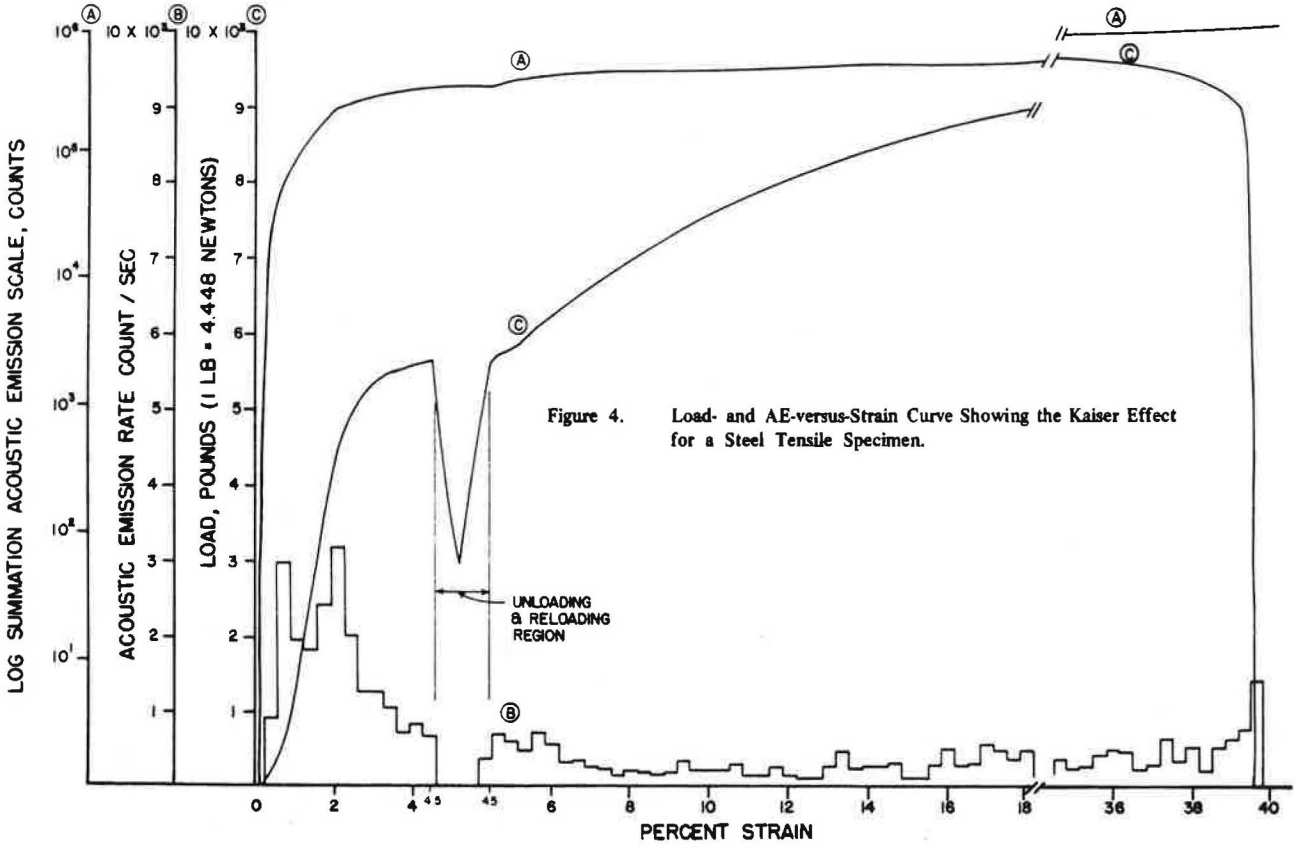

Figure 4. Load- and AE-versus-Strain Curve Showing the Kaiser Effect for a Steel Tensile Specimen.

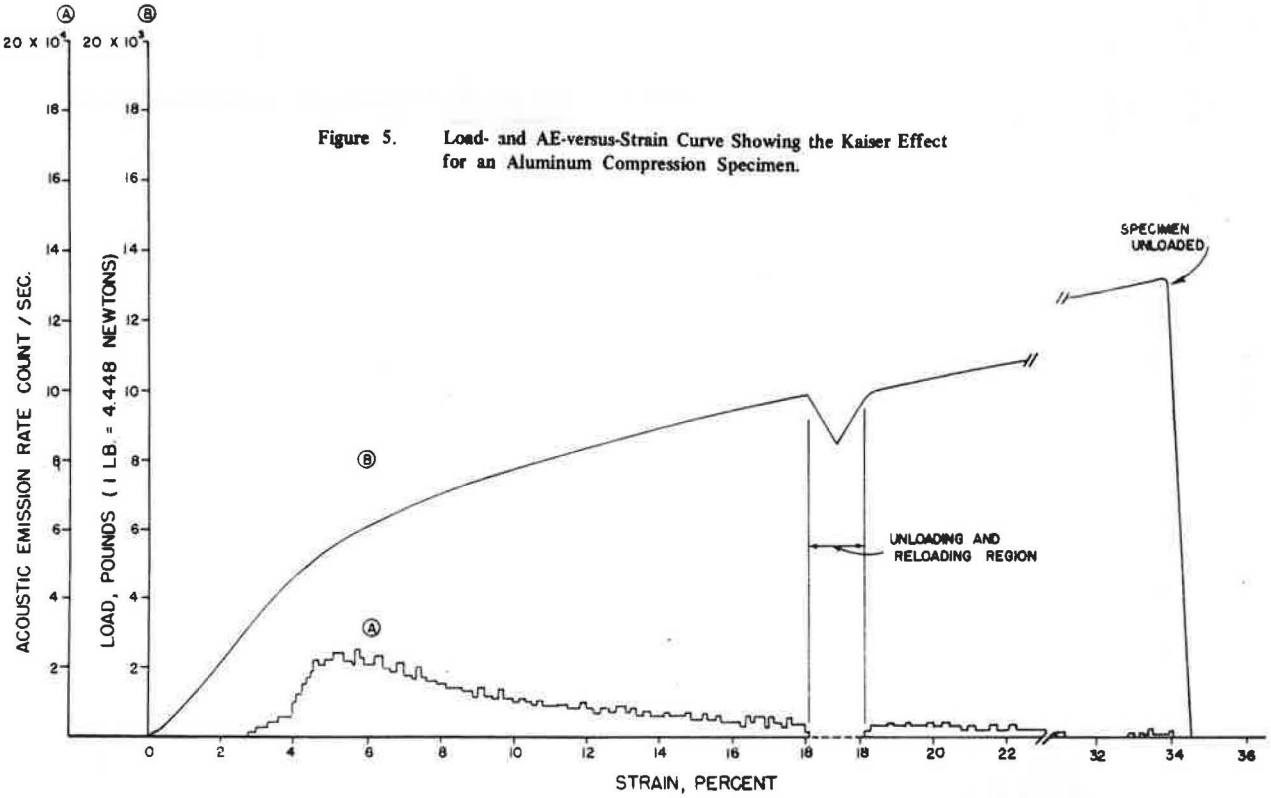

Figure 5. **Load- and AE-versus-Strain Curve Showing the Kaiser Effect for an Aluminum Compression Specimen.**

The source of AE activity in this metal must be attributed to dislocation motion *(5, 6, 7)*. The decrease of mobile dislocations, with the continuation of plastic flow and work-hardening, closely correlates with the AE-rate behavior of aluminum due to the greater ease of dislocation motion in the face-centered cubic metal. A ductile phase of steel, ferrite, must also be capable of producing a significant amount of acoustic emission. The contribution of cementite fracture to the total AE activity in a structural steel must be dependent on the percentage present. In most structural steels, the cementite content is very small.

The difference between AE rates of the cold-worked and annealed AISI 1018 steels is better explained by dislocation motion. The initial dislocation density of the cold-worked steel was from 10^2 to 10^4 times greater than the annealed steel. Immediately on load application, many dislocations became mobile. Dislocations were created in the annealed steel upon loading. Therefore, the annealed steel showed a more gradual increase in AE rate and a greater total amount of AE activity.

Tests at different crosshead speeds showed that AE activity would increase with increased loading rates. AE activity was perceptable at crosshead rates as low as 0.001 in./minute (0.025 mm/minute). The Kaiser effect persisted at crosshead speeds as high as 0.7 in./minute (17.8 mm/minute). Steel specimens cut in the transverse rolling direction and normal specimens cut in the longitudinal rolling direction were tested and compared. Both types of specimens exhibited the same yield and ultimate strengths. However, the transverse-cut specimens showed 5-percent less elongation and about 80-percent less total acoustic emission.

Tensile specimens were cut from an 80-year old bridge eyebar, from the C&O bridge at Covington, which had lain in a storage yard for a year since the bridge was demolished. Specimens were cut from the eyebar stem parallel to the loading direction. It was hoped that the Kaiser effect would give an indication of the maximum service stress. However, tests revealed behavior similar to that of AISI 1018 steel. Strain aging had probably erased the Kaiser effect.

Fatigue Testing

A series of axial-fatigue tests were planned, using four types of steel. Steel from the C & O bridge eyebar was duplicated by National Steel Corporation (see Table 1). The old bridge specification was typical for acid-Bessemer steel. To duplicate the eyebar steel, National Steel Corporation phosphorized an open-hearth steel plate after it was rolled. A 7-in. x 4-in. x 1/2-in. (178-mm x 102-mm x 13-mm) unequal angle and a C9x15 channel member were also incorporated in these tests. Both were from riveted members, about 40 years old, and were presumed to be ASTM A 7. Both of these beams failed by fatigue in bridge service. The tensile strength of the angle specimen was 54.9 ksi (378 MPa), and the tensile strength of the channel specimen was 55.1 ksi (380 MPa). A typical specimen is shown in Figure 6. The specimens were cut in the logitudinal rolling direction of the steels. All natural surfaces were preserved, and all machined surfaces were ground.

The 11 C&O (Series A) specimens and the National Steel (Series B) specimens were fatigued at various stress ratios and fractions of fatigue lives at those stress ratios. Angle (Series C) and channel (Series D) specimens were tested in completely reversed loading to determine their endurance limits. The fatigue tests were run by Metcut Research Associates of Cincinnati, Ohio, on a Baldwin-Lima-Hamilton, IV-20 fatigue machine. Loading alignment was achieved by drilling pin holes, centered along the gage length of a specimen. The specimens were tested in air at room temperatures (70 ± 10 F (21 ± 5.5 C)). The specimen temperature was limited to 200 F (93 C). Loading was applied in a sinusoidal manner at the rate of 1200 cpm. The total dynamic load error was limited to ± 3 percent of the applied stress.

Test results are shown in Table 1. The fatigue limit (also the runout) was 12 x 10^6 cycles. On inspection of the specimens, after machining, some discontinuity was found between the fillet radii and the ground faces of the gage sections. This was not corrected as it was feared that any subsequent grinding would undercut the specimens at the gage root. All failed specimens fractured at this location. However, the continuity of the results suggests that the stress concentration factors which contributed to the failures were almost constant for all specimens. Plastic flow in specimens stressed greater than 30 ksi (207 MPa) led to buckling and caused three Series D tests to be aborted.

Figures 7 and 8 show modified Goodman diagrams for the Series A and B fatigue tests *(8)*. The average lines indicate average fatigue limits of new low-carbon structural steel for fatigue lives of 100,000 and 200,000 cycles. The shaded areas show stress variations between the average and minimum fatigue limits. Imposed on Figure 7 are the points representing test failures which occurred at fatigue lives greater than two million cycles. Figure 8 shows points representing test failures which occurred at fatigue lives between 96,000 and two million cycles. Figure 7 reveals that even though most of these fatigue tests lasted six times longer than values for fatigue lives of two million cycles, their fatigue limits usually equalled or exceeded the established minimum fatigue limits of typical steels for two million cycles. Figure 8 shows that fatigue limits of most specimens having

Table 1. Results of Axial Fatigue Tests

SPECIMEN NUMBER	MAXIMUM STRESS (KSI)	MINIMUM STRESS (KSI)	CYCLE DESIGNATION	CYCLE REQUIRED	CYCLES TO FAILURE (THOUSANDS)	RESULTS
A1	19	-19	NA1	TO FAILURE	12,000	FAILURE
A2	29	-29	NA2	75% OF NA5	86	FAILURE
A3	29	-29	NA3	50% OF NA5	600	REMOVED
A4	29	-29	NA4	TO FAILURE	611	FAILURE
A5	29	-29	NA5	TO FAILURE	1,197	FAILURE
A6	35	0	NA6	TO FAILURE	204	FAILURE
A7	35	0	NA7	75% OF NA6	153	REMOVED
A8	35	0	NA8	50% OF NA6	102	REMOVED
A9	54	0	NA9	TO FAILURE	96	FAILURE
A10	50	25	NA10	TO FAILURE	12,154	RUNOUT
A11	56	28	NA11	TO FAILURE	526	FAILURE
B1	29	-29	NB1	TO FAILURE	181	FAILURE
B2	29	-29	NB2	75% OF NB1	136	REMOVED
B3	35	0	NB3	TO FAILURE	12,057	RUNOUT
B4	35	0	NB4	75% OF NB3	3,985	FAILURE
B5	35	0	NB5	50% OF NB3	6,000	REMOVED
C1	25	-25	NC1	TO FAILURE	108	FAILURE
C2	25	-25	NC2	TO FAILURE	48	FAILURE
C3	30	-30	NC3	TO FAILURE	19	FAILURE
C4	30	-30	NC4	TO FAILURE	20	FAILURE
C5	20	-20	NC5	TO FAILURE	672	FAILURE
C6	20	-20	NC6	TO FAILURE	1,627	FAILURE
C7	10	-10	NC7	TO FAILURE	12,000	RUNOUT
C8	15	-15	NC8	TO FAILURE	12,143	RUNOUT
C9	19	-19	NC9	TO FAILURE	1,550	FAILURE
C10	18	-18	NC10	TO FAILURE	1,762	FAILURE
C11	16	-16	NC11	TO FAILURE	6,998	FAILURE
C12	16	-16	NC12	TO FAILURE	4,712	FAILURE
D1	45	-45	ND1	TO FAILURE		TEST ABORTED
D2	40	-40	ND2	TO FAILURE		TEST ABORTED
D3	30	-30	ND3	TO FAILURE	64	FAILURE
D4	30	-30	ND4	TO FAILURE	99	FAILURE
D5	20	-20	ND5	TO FAILURE	835	FAILURE
D6	20	-20	ND6	TO FAILURE	1,169	FAILURE
D7	10	-10	ND7	TO FAILURE	15,395	RUNOUT
D8	19	-19	ND8	TO FAILURE	1,832	FAILURE
D9	15	-15	ND9	TO FAILURE	12,000	RUNOUT
D10	18	-18	ND10	TO FAILURE	12,000	RUNOUT
D11	19	-19	ND11	TO FAILURE	474	FAILURE
D12	35	-35	ND12	TO FAILURE		TEST ABORTED

NOTES: POSITIVE STRESS DENOTES TENSION
NEGATIVE STRESS DENOTES COMPRESSION
1 KSI = 6.895 MPa

fatigue lives of approximately 100,000 cycles met or exceeded the minimum fatigue limits of typical structural steels. Most specimens with fatigue lives approaching two million cycles had slightly lower fatigue limits than the average values given for typical steels with 100,000-cycle lives. However, these specimens had higher fatigues limits than typical steels with fatigue lives of two million cycles. The Series C and Series D specimens both had fatigue limits of approximately 15 ksi (103 MPa).

The yield and ultimate strengths of the National Steel (Series B) specimens were greater than those of the C&O eyebar (Series A) specimens. Therefore, higher fatigue limits were expected from the National Steel specimens. The maximum ratios of the fatigue limit to the ultimate strengths for the angle and channel specimens were 0.27 and 0.26, respectively. These values are in the lower range of this ratio as compiled by others *(8)*. The low values are attributable to stress risers at the gage-section fillets.

Thirty days after the fatigue tests ended, tensile/AE tests were performed on some untested specimens and specimens which survived the fatigue tests. Prior to each test, the coupling efficiency between a specimen and a transducer was measured using a Trodyne, 'Sim-Cal', spark-gap, AE calibration device. The 'Sim-Cal' duplicates an AE wave source with a signal repeatable within ± 20 percent. The average number of AE counts recorded by the AE detector from ten 'Sim-Cal' excitations was used in a simple ratio between the lowest average (as a reference) and the average of other tests to standardize data. The specimen pin holes were preloaded, and the tests were performed at a crosshead speed of 0.05 in./minute (1.3 mm/minute). The gain was set at 95 dB with high-pass filtration of 0.1 MHz. Thirteen specimens were tested to failure. Three were loaded to their yield points, removed, notched, and tested to failure. The results of these tests are shown in Table 2.

The tests revealed that the specimens had strain aged. The AE rate curves resembled those of earlier tests, and the Kaiser effect was not evident. There was no discernible effect on the mechanical properties of the specimens subjected to low-level cyclic stresses. A C&O eyebar specimen (A 11), fatigued in the range from 56 ksi (386 MPa) to 28 ksi (193 MPa) for 12 million cycles, differed little in ductility and toughness from specimens which had not been fatigued.

It became apparent that no gross changes in mechanical behavior resulted from cyclic loading below the yield region. One C&O eyebar specimen (A3) produced an unusually high AE count. Most of the activity

Figure 6. National Steel (Series B) and Angle (Series D) Fatigue Specimens.

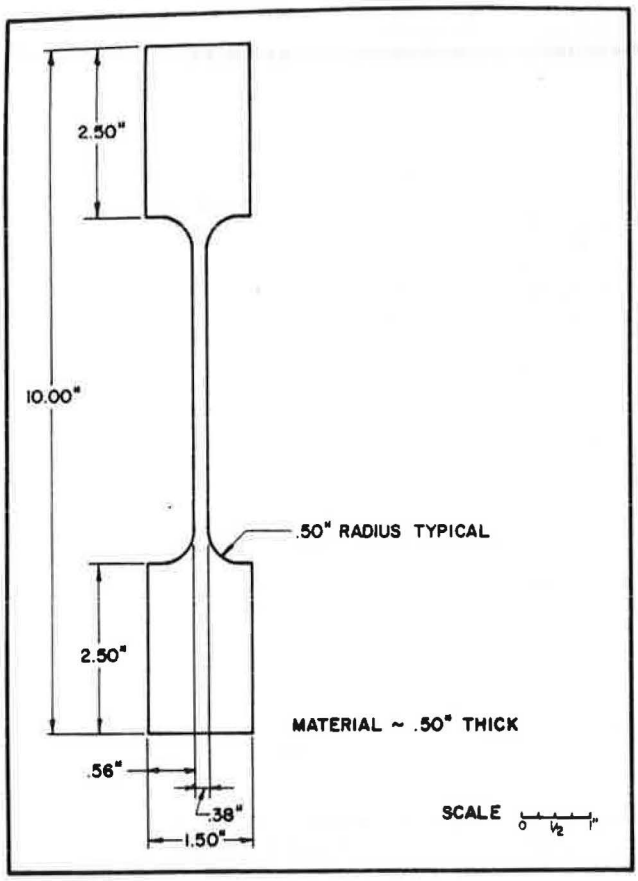

Figure 7. Modified Goodman Diagrms Comparing Fatigue Limits of Bridge Steels with Average Values, for Fatigue Lives Greater than 2,000,000 Cycles *(14)*.

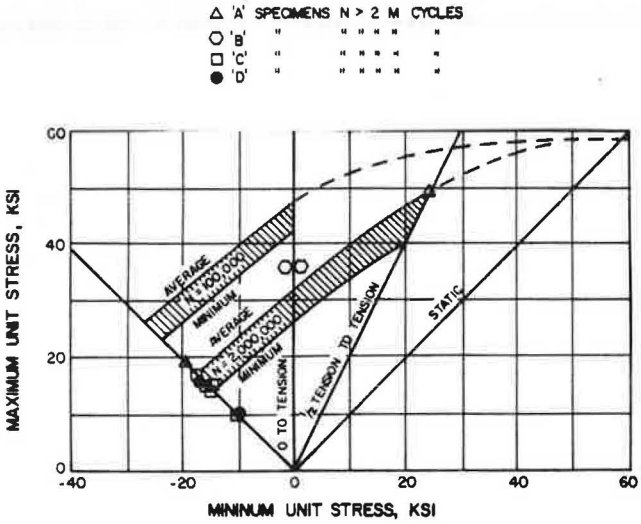

Figure 8. Modified Goodman Diagram Comparing Fatigue Limits for Bridge Steel with Average Values, for Fatigue Lives Less than 2,000,000 Cycles and Greater than 96,000 Cycles.

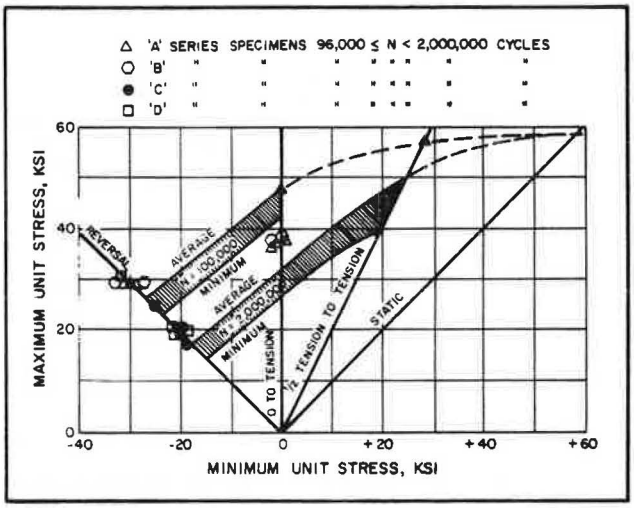

Table 2. Tensile Test Data for Fatigue-Tested Specimens

SPECIMEN NUMBER	FATIGUE LOAD (KSI)	NUMBER OF CYCLES (THOUSANDS)	REDUCTION IN AREA (PERCENT)	ELONGATION (PERCENT)	ULTIMATE STRESS (KSI)	2% YIELD STRESS (KSI)	VOLUME IN TEST ($IN.^3$)	TRODYNE COUNTS (AVERAGE)	TOTAL CORRECTED ACOUSTIC EMISSION COUNTS	TOUGHNESS ($IN.-KIP/IN.^3$)
A1	19 TO -19	12,000	61.4	24.6	55.85	35.10	0.7973	13.5	331.5	30.38
A3	29 TO -29	600	58.4	22.6	57.80	36.99	0.7268	12.6	1,039.6	31.75
A7*	35 TO 0	153	23.0	12.0	64.94	47.58	0.7875	9.5	2,455.6	14.13
A8	35 TO 0	102	60.7	22.0	56.83	36.08	0.7165	9.4	417.3	30.63
A11	56 TO 28	12,150	59.4	21.0	62.15	53.55	0.8019	11.6	290.6	28.88
A12*			62.4	23.0	57.13	36.35	0.6179	15.5	536.0	28.13
B2	29 TO -29	136	57.4	29.3	62.96	38.60	0.8025	7.7	230.4	40.25
B3	35 TO 0	12,050	57.6	27.7	62.43	37.83	0.8014	7.1	78.7	39.38
B5	35 TO 0	6,000	57.3	31.6	64.17	38.77	0.7835	6.2	240.5	42.25
B6*			58.9	31.4	61.37	36.46	0.8118	10.3	191.3	42.38
C7	10 TO -10	12,000	54.2	41.2	62.24	36.36	0.4776	6.6	60.9	58.13
C8	15 TO -15	12,140	50.2	8.1	71.78	52.38	0.4491	5.9	1,913.4	8.50
D6	15 TO -15	12,000	60.4	29.7	57.57	38.90	0.8059	14.0	382.9	37.00
D7	10 TO -10	15,400	80.2	27.2	58.47	40.68	0.8099	16.0	55.5	35.75
D10*	18 TO -18	12,000	22.8	10.8	68.69	52.84	0.7846	11.3	322.5	12.38
D12**	35 TO -35	TEST STOPPED	59.2	21.5	58.69	38.95	0.8047	14.5	57.5	27.38

NOTES: * NOTCHED
** DAMAGED
1 KSI = 6.895 MPa
1 IN. = 163.9 mM
1 $IN.-KIP/IN.^3$ = 2.756 MJ/M^3

occurred in the discontinuous yield region. However, the mechanical properties measured during this test did not markedly differ from values of other specimens. This event represents some presently undetermined variance in properties not measurable by tensile testing.

Three specimens (A7, C8, and D10) were notched with a jeweler's hacksaw after an initial loading. After notching, the specimens were pulled to failure. During the tests, the notches were observed to become blunted, and areas of localized plastic deformation appeared on the faces of the specimens adjacent to the notches. Compared to unnotched specimens, the notched specimens showed higher yield and ultimate strengths but exhibited lower toughness and elongation. The total AE count was greater for unnotched specimens. AE activity of notched specimens began immediately with the load application. It reached a maximum value during discontinuous yielding and decreased with the onset of fully plastic flow. A slight increase in AE rate occurred prior to failure. The increase in strength and loss of ductility are results of the notch effect. The high initial rate of AE activity was caused by the rapid onset of localized plastic flow. The increase of AE rate prior to fracture was probably due to rapid growth of the plastic zone.

As a result of these tests, it became evident that no gross changes in mechanical properties had occurred in steels which had seen extended service. Also, there was no detectable difference in AE activity between any of the fatigued steels or any unfatigued steels.

Tests indicated that field fatigue failures should be viewed as discrete events which were much more difficult to characterize than laboratory-derived values such as the yield strength or even the fatigue limit. This led to the view that material properties were not of prime importance, especially when compared to geometric factors (stress risers).

Field Testing

AE systems have been interfaced with computers to locate defects in pressure vessels for the past 12 years. Much field experience has been accumulated from oil storage tanks, rocket motor cases, and nuclear reactors *(9, 10, 11)*. Several techniques have been developed for AE discrimination in a high noise environment *(12, 13)*. However, few significant trials of AE flaw-locating equipment have been made on bridges *(14)*.

To further explore the listening and probing capabilities of equipment, a large, welded plate girder, approximately 50 feet (16.4 m) long having a web length of 27 inches (690 mm) and a thickness of 3/4 inch (19 mm) was tested using the AE device and the 'Sim-Cal' calibrator. The 'Sim-Cal' produced a repeatable, simulated acoustic pulse of lower magnitude than an AE burst in a notched tensile specimen. Using a gain of 97 dB, with band-pass filtration of 0.1 to 0.3 MHz and a single-ended Dunegan S-140B transducer, the 'Sim-Cal' signal could readily be detected from 45 feet (14.8 m) by the AE device. A decrease in AE intensity occurred with increasing distance between the transducer and the AE calibrator. However, the test showed that AE energy caused by crack blunting or growth can be detected by AE systems over long distances. Recent improvements in AE flaw-locating systems have enabled their use on geometrically complex structures and reduced the amount of electronics required to locate defects over long distances.

References

1. Havens, J. H. and Deen, R. C.; *Bridges: Synthesis of Load Histories and Analysis of Fatigue;* Division of Research, Kentucky Department of Highways, January 1972.
2. Lynch, R. L.; *Analysis of Traffic Loads on Bridges; Report II, Characteristics of Traffic on Ohio River Bridges - 1968;* Division of Research, Kentucky Department of Highways, March 1969.
3. Ingham, T., Scott, A. L. and Cowan, A.; *Acoustic Emission Characterization of Steels, Part 1: Acoustic Emission Measurements from Tensile Tests;* **International Journal of Pressure Vessels and Piping,** Applied Science Publishers, UK, February 1974, pp 31-49.
4. Dunegan, H. L. and Harris, D. O.; *Acoustic Emission - A New Nondestructive Testing Tool;* **Ultrasonics,** IPC Press, Guilford, UK, July 1969, pp 160-166.
5. Frederick, J. R. and Felback, D. K.; *Dislocation Motion as a Source for Acoustic Emission;* **Acoustic Emission,** STP 505, American Society for Testing and Materials, 1972, pp 129-139.
6. Gillis, P. P.; *Dislocation Motions and Acoustic Emissions;* **Acoustic Emission,** STP 505, American Society for Testing and Materials, 1972, pp 20-29.
7. James, D. R. and Carpenter, S. H.; *Relationship between Acoustic Emission and Dislocation Kinetics in Crystalline Solids;* **Journal of Applied Science,** AIP, Menasha, Wis, November 1971, pp 4685-4697.
8. Munse, W. H.; *Fatigue of Welded Steel Structures;* Welding Research Council, 1964, p 36, 37, 74.
9. Tatro, C. A.; *Design Criteria for Acoustic Emission Experimentation;* **Acoustic Emission,** STP 505, American Society for Testing and Materials, 1972, pp 84-99.
10. Cross, N. O., Loushin, L. L., and Thompson, J. L.; *Acoustic Emission Testing of Pressure Vessels for Petroleum Refineries and Chemical Plants;* **Acoustic Emission,** STP 505, American Society for Testing and Materials, 1972; pp 270-296.
11. Harris, D. O. and Dunegan, H. L.; *Acoustic Emission 5 - Application of Acoustic Emission to Industrial Problems;* **Nondestructive Testing,** IPC Press, Guilford, UK, June 1974, pp 137-144.
12. Liptai, R. G., Harris, D. O., Engle, R. B., and Taro, C. A.; *Acoustic Emission Techniques in Materials Research;* **International Journal of Nondestructive Testing,** May 1971, pp 215-175.
13. Nakamura, Y.; *Acoustic Emission Monitoring System for Detection of Cracks in Complex Structures;* **Materials Evaluation,** ASNT, Columbus, OH, January 1971, pp 8-12.
14. Pollock, A. A. and Smith, B.; *Stress Wave-Emission Monitoring of a Military Bridge;* **Nondestructive Testing,** IPC Press, Guilford, UK, December 1972, pp 348-353.

FATIGUE FAILURE MECHANISM OF REINFORCED CONCRETE BRIDGE DECK SLABS

Kiyoshi Okada, Kyoto University
Hirokazu Okamura, Osaka Institute Technology
Keiichiro Sonoda, Osaka City University

The aim of the paper is to clarify the fatigue failure mechanism of reinforced concrete slabs under moving wheel loads. Seven slabs with full scale dimensions were tested under static load, central pulsating loads, and moving pulsating loads. To investigate deflection characteristic and reserve fatigue strength of cracked slabs subjected to actual traffic loads, especially, four test slabs were sawn out from two distressed bridge decks. Experimental findings were mainly as follows: rubbing together of crack faces due to the repeatedly moving loads eventually produced a slit with a narrow opening in the cracked section; the formation of the slit reduced both flexural and shearing rigidities of the slab; if rain water were poured into the cracked section, the reductions of these rigidities were remarkably accelerated and caused the slab surface to collapse prematurely. Three-dimensional stress analysis in the vicinities of cracks predicted their penetration through the entire depth of the slab. It was found that the process of the penetration consisted of two stages: the first stage was a growth of flexural cracks occurring at the bottom surface of the slab, beneath the wheel load, and the second stage was a progression of twisting cracks occurring at the top surface, when the wheel load had moved away.

Introduction

The design code for reinforced concrete bridge deck slabs in Japan follows an allowable stress method based upon the thin elastic plate bending theory, which has been supposed to lead to conservative results. During the past decade, however, many instances of damage or collapse of deck slabs have been reported in Japan. To examine direct or indirect causes for such damage or collapse, some tests of model and prototype slabs have been carried out under both static and pulsating loads, but these test results merely indicated that the slabs had load-carrying capacities several times greater than the design loads (1,2). On the other hand, from field observations on actual damaged deck slabs, the effects of rolling and moving wheel loads on fatigue of deck slabs appear to be highly significant. However, such effects have not been considered in previous tests.

The aim of this study is to clarify both experimentally and theoretically the fatigue strength and the failure mechanism of reinforced concrete deck slabs under moving wheel loads. Seven slabs with full-scale dimensions were tested under static, pulsating and moving pulsating loadings. In order to investigate reserve fatigue strengths and durabilities of cracked slabs under repeatedly moving loads, some of the test specimens were sawn out from two distressed bridge deck slabs which had been subjected to the traffic loads of 20 - 50 thousand cars a day over a period of 8 to 10 years. The other specimens were virgin slabs fabricated to the same specification as for the old slabs.

An analysis based upon three-dimensional elasticity of a model slab with grid-like cracks was made to investigate the distribution of stresses near the cracks due to moving loads and to clarify the process of crack growth through the entire depth of the slab, under the action of alternate transverse and twisting shearing stresses.

Description of Specimens and Tests

Details of the test specimens are given in Table 1. The specimens marked " O " were sawn out from the two distressed bridge decks. The cracking pattern of one of these specimens is illustrated in Fig.1, in which the existence of numerous cracks of widths 0.05 - 0.2 mm at the bottom surface of the slab, some of which penetrate to the top surface are apparent. The specimens marked " N " mean full-scale virgin slabs made for these tests. All specimens also include top reinforcement amounting to about 50 % of the bottom reinforcement indicated in Table 1. The reinforcement consists of round steel bars with diameters 16 mm in the longitudinal direction and 13 mm in the transverse direction. These specimens have standard depth and reinforcement in accordance with the Japanese code.

The test setup is shown in Fig.2. The slabs were supported rigidly along their longer edges and elastically on steel beams with H-sections along their shorter edges so as to obtain variations of

bending moments comparable to those in actual bridge deck slabs which are supported on longitudinal steel girders. To ensure bond strength of reinforcing bars in the sawn-out slabs, ends of the bars were welded to anchorage steel plates placed on edge-sides of the slabs.

Load was applied on a 20 x 50 cm^2 rectangular area corresponding to one rear wheel load specified by the code. Two types of loading procedures were used: static or pulsating loads applied at center of slab, and pulsating loads transferred stepwise and cyclically on several different points as shown in Fig.4. The number of cycles of pulsating load per point was in the range from 0.2 x 10^4 to 1.0 x 10^4. The latter type was regarded as a simulation of moving wheel loads. The movement of loading point was carried out by sliding stepwise the slabs in the longitudinal direction, and by changing in the transverse direction the support-point of the lever arm sustaining a pulsating load from an actuator. The pulsating load was of sinusoidal wave form and frequencies ranged from 4 Hz to 5 Hz. The intensity of the load was varied for different tests in the range between 108 kN corresponding to one rear wheel load including impact load specified by the code and 245 kN of the maximum capacity of the testing machine used. Loading sequences for the various specimens are shown in Fig.3.

Observation of Crack Propagation

In the central pulsating loading test of the virgin slab N_2, radial cracking patterns developed at the bottom surface of the slab, spreading from the loading point. Crack propagation was slow, and nearly ceased after one hundred thousand cycles of a load successively higher than previous maximum load. Initial cracks occurred beneath a loading point and then extended along the principal moment trajectory. In the moving pulsating loading test of the virgin slab N_3, on the other hand, the cracking pattern had a grid-like form similar to that of the old slab as shown in Fig.1. Movement of the loads sequentially changed the principal moment directions, and consequently, the cracking spread over the entire lower surface of the slab. In the slab N_3, the grid-like cracking pattern was essentially completed after 200 x 10^4 cycles of loading and 50 cycles of movement, in which one cycle of movement consisted of the pulsating loadings of five different points aligned as shown in Fig.4.

The relationships between the characteristics of the cracked surface and the number of cycles of the pulsating load obtained in specimen N_3 are indicated in Fig.5. The crack density, which is defined here as the total length of surface cracks per unit area, becomes stationary after a finite number of cycles. Namely, new cracks occur severely only at the initial stage of loading. On the other hand, by the actions of alternate compression and twisting due to sequential and repeated movements of loads, the crack faces are clapped together and rubbed against each other, and consequently the crack faces are worn away and then a slit with a narrow opening is formed in the cracked section. This was confirmed in the test through observation of sequential falling of fine concrete powder from crack openings. This will also be supported by field observations that in actual damaged deck slabs so large plastic deformations did not occur, in spite of the existence of numerous cracks with large residual widths.

The formation of such a slit impairs the continuity of flexural rigidity and also causes a remarkable reduction of shearing strength mainly relying upon interlocking of the aggregate particles. A discontinuity of flexural rigidity is shown in Fig.6, where cracks beneath the load open widely but other cracks in a slightly remote position from the load contrastedly close until widths remaining under no loading vanish, and the behaviours of these cracks greatly differ from the shape of the moment influence line predicted by the homogeneous elastic plate theory. Furthermore, such a discontinuity will produce alternate stresses of compression and tension on the upper side of the cracked section with the movement of the load and then will eventually result in penetration of cracks across the entire depth. In specimen N_3, such a fully penetrating crack was detected in the longitudinal direction after 490 x 10^4 cycles of loading and 190 cycles of movement of the load with 226 kN as a maximum, corresponding to about twice the design load (see crack B in Fig. 6). The cycles of movement of the load were greatly restricted in number because with the loading equipment used the movements were carried out manually. Therefore, more cycles of load movement which would be encounted in actual bridge decks could be assumed to reduce considerably the load intensity causing full penetration cracking. Further discussion on full penetration cracking will be described in a subsequent section.

Stresses of Reinforcing Bars

Table 2 shows a comparison of observed strains and theoretical ones of longitudinal bottom reinforcing bars in cracked sections beneath the load. The theoretical strains are derived from the conventional elastic equation neglecting the strength of tensile concrete under a moment obtained by the elastic plate bending theory. It can be concluded from these results that the stress intensity of reinforcing bars is sufficiently small in the initial stage of cracking and does not exceed, in the state of extensive cracking, the value predicted by the conventional elastic equation.

Deflection Characteristics

Fig.7 shows load-central deflection curves of specimens N_1, O_1, N_2 and O_2. The deflections of the slabs with slight cracks may be estimated, in the ranges below or near the design load, by the isotropic elastic plate theory with consideration of the flexural rigidity of entire slab depth, and those of the impaired slabs with a number of fully penetrating cracks as shown in Fig.1 may be predicted well by the orthotropic elastic plate theory with the rigidities of only compressive concrete and tensile reinforcement. Fig.8 indicates how the central deflection under constant load of 108 kN corresponding to design load grows with the number of cycles of loading. It seems that the increase of deflection under the central loading is very slow but deflection under moving loading gradually increases.

In field observations of actual damaged bridge decks it often has been seen that rain water comes through concrete slabs along cracks in asphalt pavement, and a solution of lime causes precipitation of calcium carbonate at the lower sides of the cracked sections of the slabs. To examine the effect of the water infiltrated into the cracked

sections on slab failure under moving pulsating loading, specimens O_3 and O_4 were tested in a water-saturated state which was obtained by ponding water on the upper surface of the slab. It is clearly shown that water infiltrated into cracks remarkably influences increase of deflection. This is probably due to the fact that water infiltrated into cracks oozes out the fine powder of crushed concrete from the crack openings by virtue of vibrating action of the slab, and the enlargement of crack width consequently induces accelerative reductions of both flexural and shearing rigidities.

Collapse Load and Fatigue Failure Mechanism

It is well known that slabs loaded at the center collapse in punching shear modes. Some specimens in the tests collapsed eventually due to punching shear of concrete after precedence of partial flexural failure. The values of collapse loads of the specimens are shown in Table 3. The collapse load of the virgin slab N_1 under central static-loading agreed well with the value predicted by the punching shear failure formula presented by Kakuta et al. (3). In the old slab O_1 distressed due to travelling of actual traffic loads, the collapse load in the static test seemed to be somewhat reduced by the influence of the existence of extensive cracks, but still it was very large in comparison with the design load. The old slab O_2 under central pulsating loading collapsed due to fatigue fracture of tensile reinforcing bars at the maximum load 245 kN equal to 2.3 times the design load. However, the virgin slab N_2 did not collapse under the same load.

On the other hand, it was clearly recognizable that water infiltrated into the cracked sections caused the premature collapse of the slab. Specimen O_3 collapsed under maximum load of 167 kN and at 530×10^4 cycles of loading, the specimen having been loaded in a wet condition after 475×10^4 cycles in a dry condition. Specimen O_4 which was tested from the start in a wet condition under a constant load of 108 kN corresponding to the design load collapsed at 250×10^4 cycles of loading. The collapse mechanism of a slab saturated with water proceeded as follows: when the deteriorated slab with many fully penetrating cracks was saturated with water, the crushed concrete powder existing in the cracks was changed into a mud-like paste and flowed out from the crack openings by virtue of the pumping effect due to vibration of the slab. Consequently, the crack openings were rapidly enlarged with the repetitions of loading and the shear resistance of the slab was reduced remarkably. After falling of small concrete fragments from the cracked sections followed by peeling off of the concrete covering the bottom reinforcing bars, the upper surface of the slab eventually caved in and collapsed.

Theoretical Consideration

To research further the process of full penetration of cracks into flexural compression side, which was detected in the previous experiment, a three-dimensional stress analysis for the concrete near tip of flexural crack and the reinforcing bars was carried out under the assumptions: concrete and reinforcing bars were of isotropic elastic material; tensile and shearing stresses were not transmitted through the surface of flexural cracks; dowel effects of reinforcing bars were neglected; reinforcing bars were perfectly bonded; the cracking pattern was of a grid-like form and spacing of cracks was about equal to slab depth. Further, to confirm a possibility of the failure of concrete due to such fully penetrating cracks in a bridge deck slab, a two-dimensional bending analysis for a one-way spanning slab was also carried out, and by the combination of results of this and those of three-dimensional analysis the range of principal tensile stress acting in concrete throughout the slab under moving wheel loads was examined.

The method of three-dimensional analysis here belongs to an integral equation method, described fully in the previous papers (4,5), which is developed by superposing the solutions of Mindlin's first and second problems and by using the collocation method. The characteristic of the method is that an objective slab containing a part with variable rigidity due to cracks and reinforcements is cut out from a semi-infinite elastic solid, by replacing the effect of deviation from uniform rigidity by application of equivalent self-equilibrating body forces.

A slab model for numerical investigations by the three-dimensional analysis was simplified, as shown in Fig.9, which had the following properties: all edges of the slab were simply supported; aspect ratio, $b/a=1.5$; depth of cracks, $h_t=0.7h$; spacing of cracks, $e=h$; loaded area, $u \times v = 0.039\, a^2$; Poisson's ratio of concrete, $\nu=1/6$; ratio of elastic moduli of steel and concrete $=10$; ratio of bottom reinforcement $=1.0$ %. The value $h_t=0.7h$ was taken from the assumption that flexural cracks would prematurely proceed from bottom face to the neutral plane determined by the conventional formula derived from neglecting the strength of tensile concrete and using Bernoulli's assumption.

Fig.10 shows distributions of the normal stresses in the compressive domain of the cracked section beneath the applied load. The results are almost the same as those by the conventional formula under moment calculated by the elementary plate bending theory.

Fig.11 shows distributions of the normal stress, σ_x, in concrete along the entire depth of the sections b - f as marked in Fig.9. Remarkable differences in the shapes of stress distributions are seen between cracked and uncracked sections, but the intensities of compressive stresses occurring at the top surface of each section are not different between them. Fig.12 shows variation of the tensile stress, σ_{sx}, acting in a reinforcing bar between cracked sections b - g. In this figure, it should be noted that the intensity of σ_{sx} in the cracked sections becomes large in comparison with that in the uncracked sections, but the maximum intensity is nearly equal to the values predicted by the conventional formula mentioned above.

On the other hand, distributions of transverse shearing stress, τ_{yz}, along the depth of compressive concrete in the cracked sections near the applied load are indicated in Fig.13. As the distributions of τ_{yz} are of nearly triangular shape, the intensities of it may be predicted well by assuming a linear distribution of the resultant shearing force, Q, which can be obtained by the elementary plate bending theory, as shown by the dotted lines in Fig.13.

Then, since the other stress components, except τ_{yz} at the crack tip which is nearly on the neutral plane are sufficiently small in comparison with τ_{yz}, the maximum principal tensile stress, σ_{pl}, due to the above stress concentration will amount to

Table 1. Details of specimens, material properties, and loadings.

Specimens	Sizes (m) (W) (L) (T)	Bottom Reinforcement (%) (Long.) (Trans.)	Strength of Conc. (MN/m^2)	Strength of Reinfct. Yield/ Ultimate (MN/m^2)	Type of Loading
N_1	2.5 x 3.8 x 0.18	1.3 / 0.5	25.0	274.7 / 454.2	Static
N_2	2.5 x 3.8 x 0.18	1.3 / 0.5	29.5	274.7 / 454.2	Central pulsating
N_3	2.5 x 3.8 x 0.18	1.3 / 0.5	31.4	274.7 / 454.2	Moving pulsating
O_1	2.5 x 3.8 x 0.18	1.3 / 0.5	31.7	323.7 / 461.1	Static
O_2	2.5 x 3.8 x 0.18	1.3 / 0.5	31.7	323.7 / 461.1	Central pulsating
O_3	1.8 x 2.7 x 0.17	1.1 / 0.4	40.8	318.8 / 438.3	Moving pulsating
O_4	1.8 x 2.7 x 0.17	1.1 / 0.4	40.8	318.8 / 438.3	Moving pulsating

Table 2. Tensile strains of reinforcing bars under central load 108 kN.

Specimens	Number of Cycles	Measured Values	Theoretical Values
N_1	Static	140×10^{-6}	381×10^{-6}
N_2	100	95×10^{-6}	381×10^{-6}
	4×10^5	115×10^{-6}	381×10^{-6}
N_3	1×10^4	110×10^{-6}	381×10^{-6}
	2×10^5	135×10^{-6}	381×10^{-6}
	5×10^5	175×10^{-6}	381×10^{-6}
	1.5×10^6	180×10^{-6}	381×10^{-6}
O_3	1	320×10^{-6}	441×10^{-6}
	1×10^4	360×10^{-6}	441×10^{-6}
	1×10^5	375×10^{-6}	441×10^{-6}
	5×10^5	420×10^{-6}	441×10^{-6}
	2×10^6	400×10^{-6}	441×10^{-6}

Figure 1. Cracking pattern of a distressed slab sawn out from bridge deck.

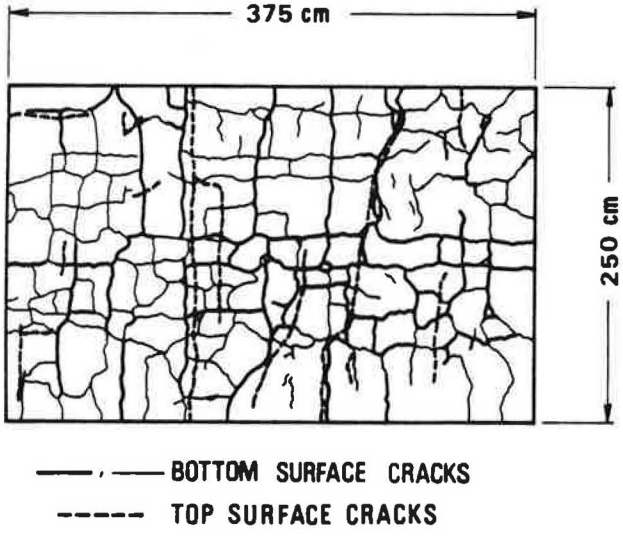

Table 3. Collapse loads.

Specimens	Collapse Loads (kN)	Total Number of Cycles	Remarks
N_1	626	Static	Calculated punching shear load 647 kN
N_2	No collapse	230×10^4	Maximum applied load 245 kN
N_3	No collapse	513×10^4	Maximum applied load 226 kN
O_1	526	Static	Calculated punching shear load 736 kN
O_2	245	275×10^4	Fracture of bottom reinforcing bars
O_3	167	526×10^4	No fracture of reinforcing bars
O_4	108	256×10^4	No fracture of reinforcing bars

Figure 2. Test setup.

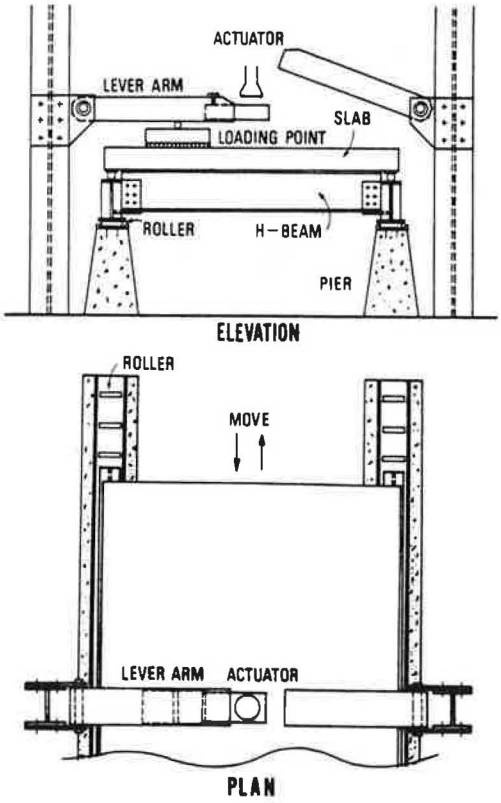

Figure 3. Loading sequences for each specimen.

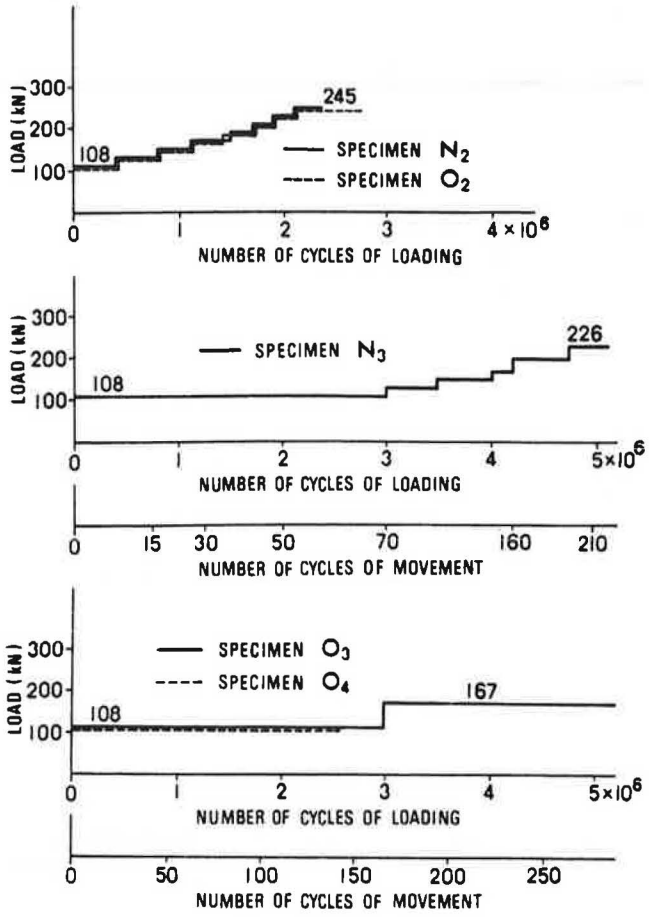

Figure 4. Sequence of movement of load.

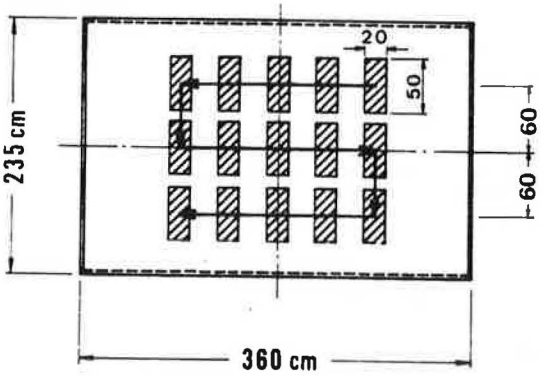

Figure 5. Characteristics of cracked surface of virgin slab related with cycles of moving pulsating loading.

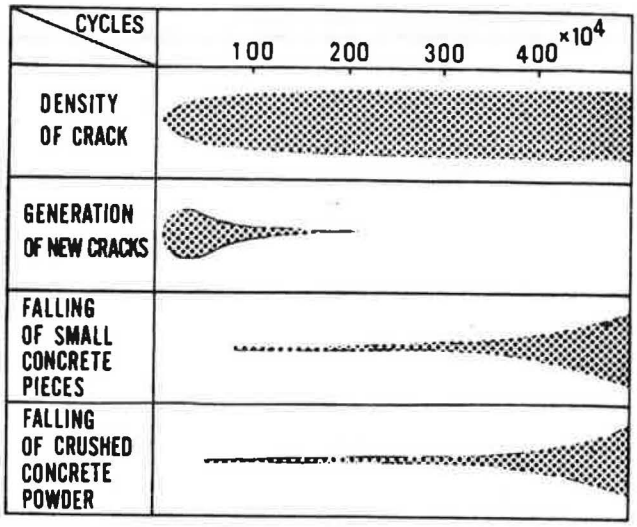

Figure 6. Relation between crack widths and location of loading point along transverse center line, in specimen N_3.

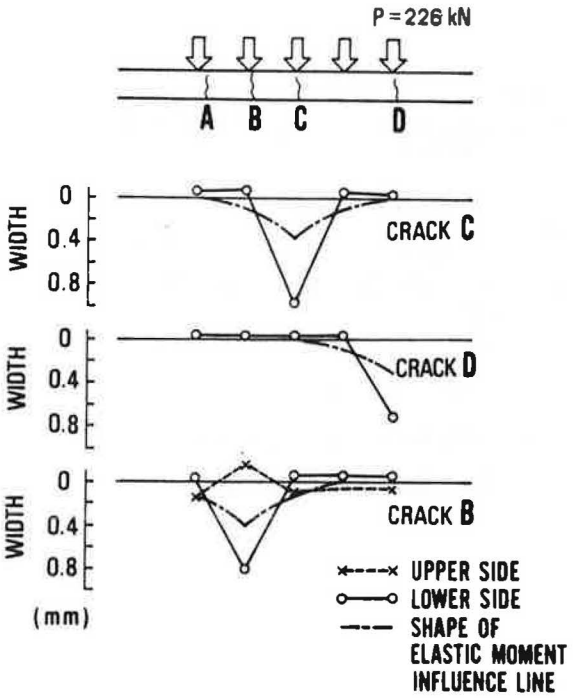

Figure 7. Load-deflection curves under central static or pulsating loadings.

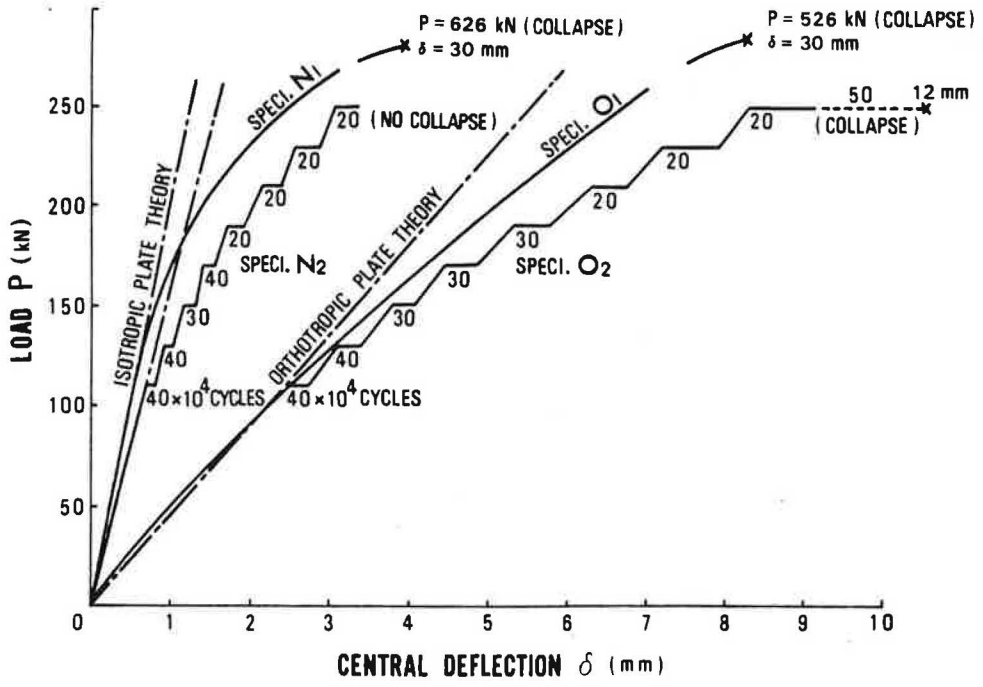

Figure 8. Relationships between growth of central deflection and cycles of loading under 108 kN.

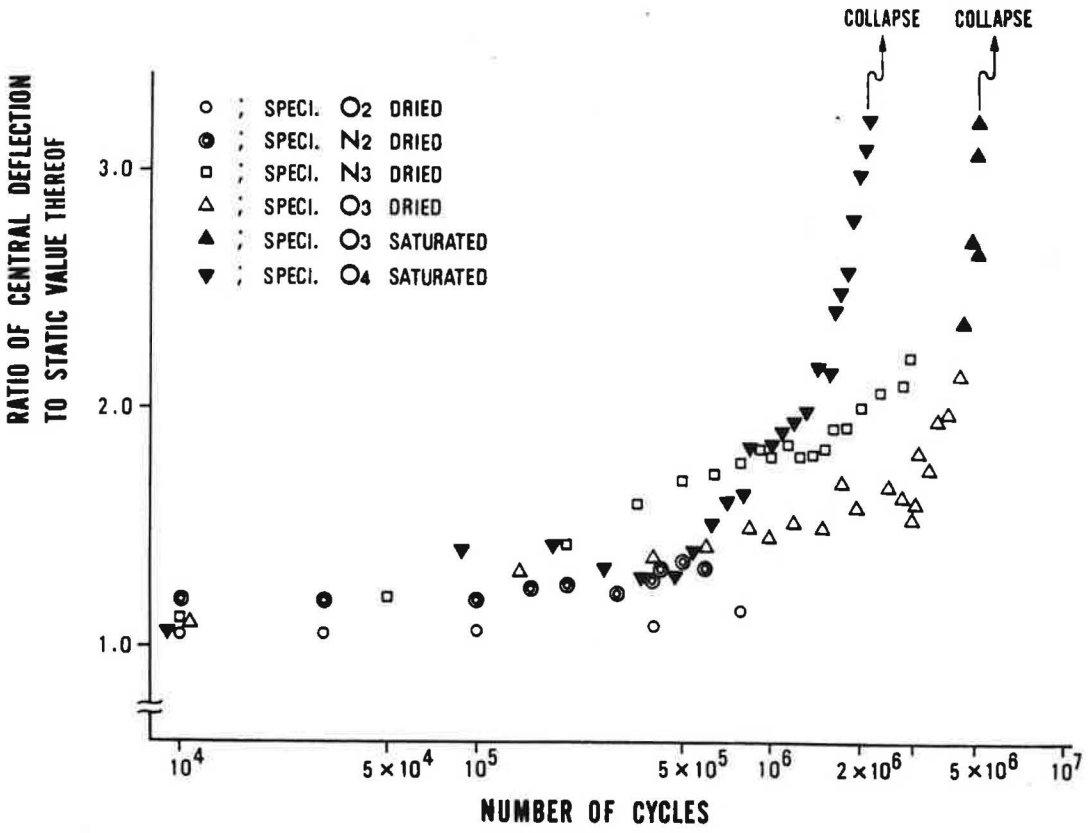

Figure 9. Model slab for numerical investigation.

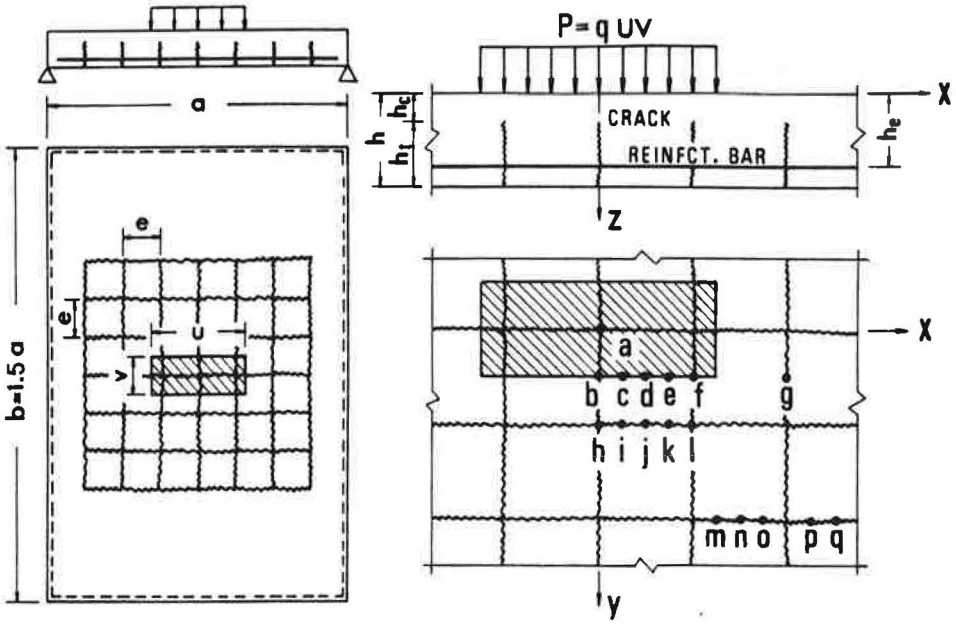

Figure 10. Variations of normal stresses in compressive domain.

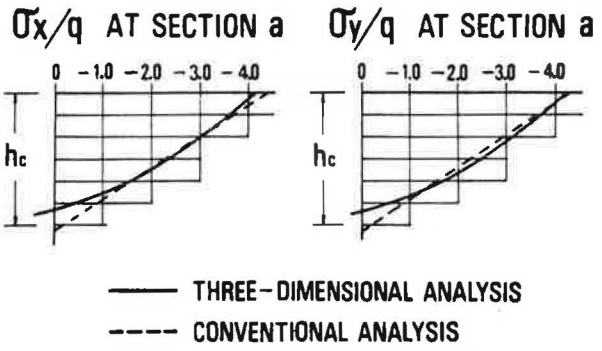

Figure 12. Variation of axial stress σ_{sx}/q in reinforcement.

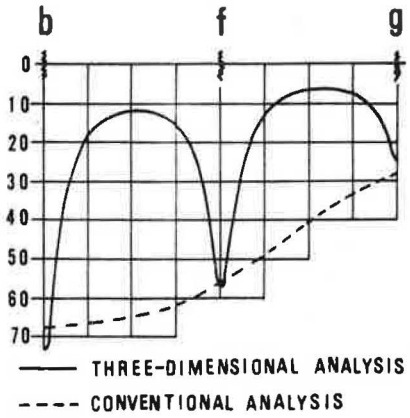

Figure 11. Variations of normal stress σ_x/q in concrete in cracked and uncracked sections.

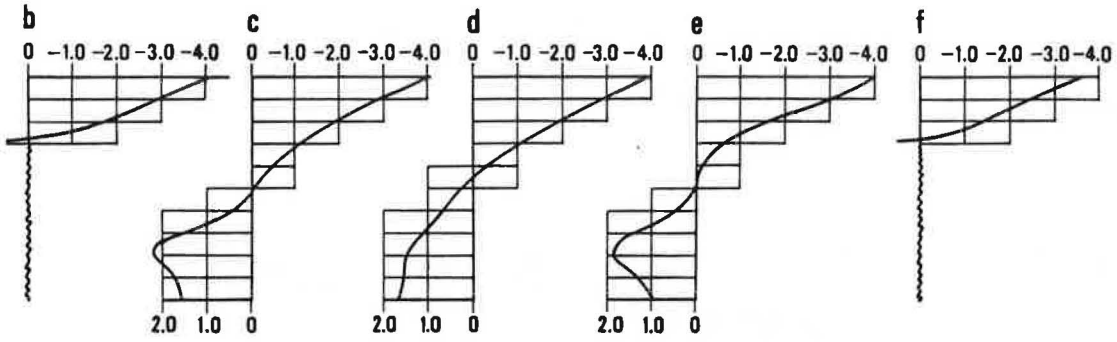

Figure 13. Variations of transverse shearing stress τ_{yz}/q in compressive domain.

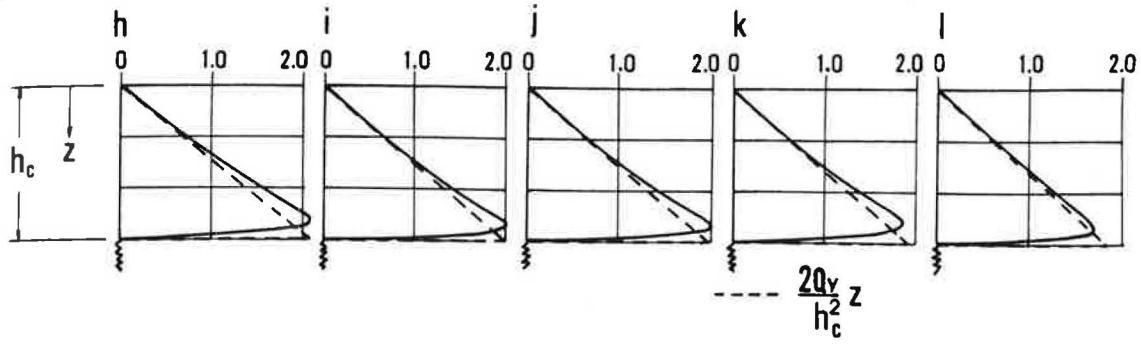

Figure 14. Variations of horizontal shearing stress τ_{xy}/q in compressive domain.

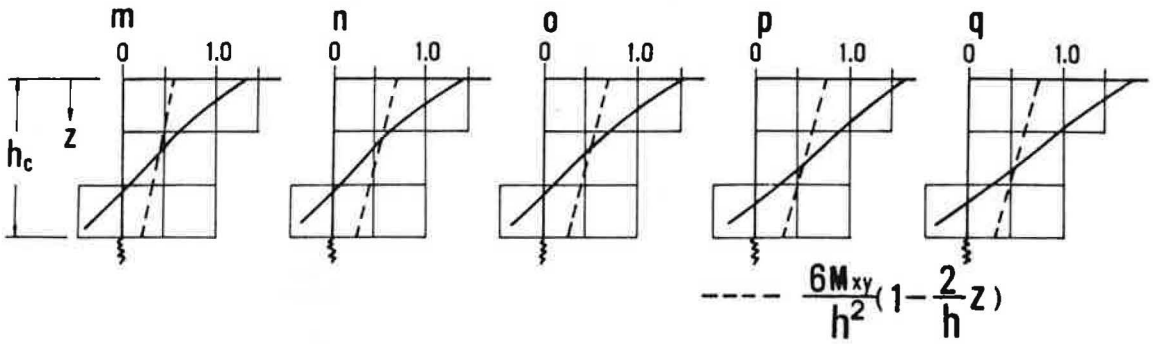

Figure 15. Distribution of transverse shearing forces along periphery of loaded area.

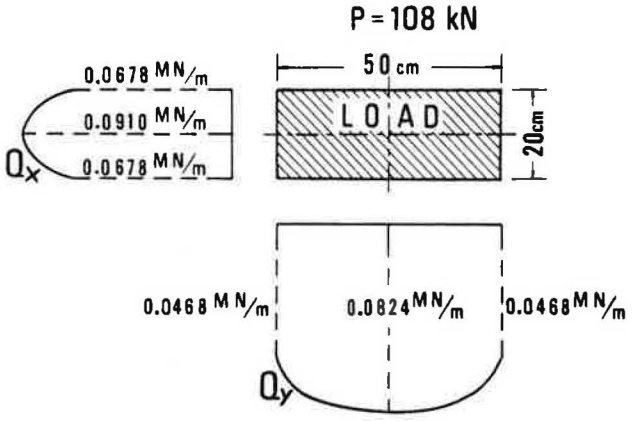

Figure 16. Contour line of twisting moment in a simply supported one-way slab under two rear wheel loads.

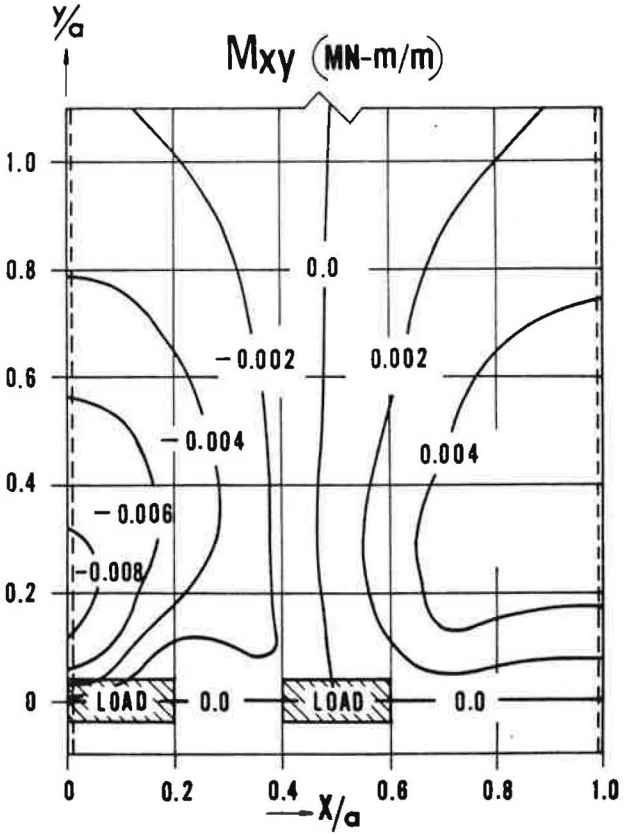

$$\sigma_{p1} \doteqdot 2.0 \frac{Q}{h_c} \quad (1)$$

in which h_c is depth of compressive concrete.

As severe intensity of Q will occur along the periphery of the loaded area, the distribution of Q along that periphery is examined by the plate bending theory, as shown in Fig.15, which is calculated for a one-way slab with the span, 250 cm, considered as an actual bridge deck, under the central load, 108 kN, corresponding to one rear wheel load as specified by the Japanese code. Substituting the maximum value of Q given by Fig.13 into eq.(1) under the assumption, h_c=6 cm, the intensity of tensile stress at the tip of a flexural crack reaches to 3.0 MN/m^2, which is considered to be larger than the tensile fatigue strength of plain concrete. Thus, if shear resistances of the surfaces of flexural cracks produced prematurely in a bridge deck slab are sufficiently reduced due to repeated traffic loads, as the previous experimental observation pointed out, then, a further progression of flexural cracks to the compression side becomes possible, but such cracks can not extend to the top surface of the slab, because large flexural compressive stresses are in existence near the top resulting from application of finite bending moment.

On the other hand, Fig.14 indicates distributions of the horizontal shearing stress, τ_{xy}, in the remote sections from the load indicated in Fig.9. The intensity of τ_{xy} increases toward the top surface of cracked sections, and its maximum value reaches about 2.5 times the value, $6M_{xy}/h^2$, in which M_{xy} is twisting moment, which is derived from the elementary plate bending theory. As the applied load moves away from a relevant cracked section, τ_{xy} related with twisting moment increases gradually but the other stress components except τ_{xy} decrease rapidly. Then, the maximum principal tensile stress, σ_{p2}, at the top surface of the cracked section will be given by

$$\sigma_{p2} \doteqdot 2.5 \frac{6M_{xy}}{h^2} \quad (2)$$

Fig.16 indicates a distribution of M_{xy} in the same one-way slab, as shown in Fig.15, subjected to two rear wheel loads with the intensity, 108 kN, respectively. Using the result from Fig.16 and eq.(2) under the assumption, h=17 cm, the predominant value of σ_{p2} will be in a range from 2.5 MN/m^2 to 3.5 MN/m^2 in an extensive region. Accordingly, this tensile stress may induce a new crack developing from the top surface toward the tip of a precedent flexural crack.

In ordinary bridge deck slabs meeting the Japanese code, such tensile stresses, σ_{p1} and σ_{p2}, possibly exceed the inherent tensile strength of concrete, particularly when considering impaired strength due to fatigue. Hence, the combined action of σ_{p1} and σ_{p2} alternately resulting from repetition of moving wheel loads will eventually induce full penetration of crack extending from the bottom surface of the slab to the top surface.

Finally, it should be mentioned that both compressive stresses in concrete at the top surface and tensile stresses in reinforcing bars almost never become greater than those derived from the conventional formula under moment calculated by the elementary plate bending theory, even if cracking progresses so severely that shear resistances of crack surfaces vanish and some cracks penetrating the entire depth exist. Then, it can be supposed that failure of concrete at the flexural compression side precedes the tensile fracture of reinforcing bars in actual bridge deck slabs.

Conclusion

It was found that deterioration of a reinforced concrete bridge deck slab under repetitions of both pulsating and moving loads proceeded through the following process: cracking patterns at the bottom surface of the slab were of a grid-like form; propagation of surface cracks ceased after a certain finite number of repetitions of the load; crack faces of concrete were rubbed together and were worn down by virtue of repetitions of moving loads, and slits with narrow openings were consequently formed in the cracked sections; the formation of such slits reduced the shearing rigidity of the slab associated with interlocking of the aggregate particles; and if rain water entered the cracked sections, the reductions of both flexural and shearing rigidities were remarkably accelerated making it possible to cause the slab surface to cave in and to collapse under the moderate load estimated in the design code.

On the other hand, three-dimensional stress analysis for the vicinities of cracks revealed the process of full penetration of cracks through the entire depth of the slabs. This process consisted of two stages: the first stage was the growth of flexural cracks occurring at the bottom surface of the slab beneath a wheel load, and the second stage was progression of twisting cracks occurring at the upper side of the cracked section of the first stage when the wheel load had moved away to a remote position.

Acknowledgement

The assistance of the Ministry of Construction of Japan in supplying the distressed deck slabs is gratefully acknowledged.

References

1. Y. Kakuta et al. Experimental Study on Fatigue Punching Shear Strength of Reinforced Concrete Slabs. CAJ Review of 28th General Meeting, held in Tokyo, May, 1974.
2. The Research Committee on Fatigue Design of Reinforced Concrete Slab. Fatigue Modes of Reinforced Concrete Deck Slabs and An Approach to Fatigue Design Thereof. Kansai Branch of the Japan Society of Civil Engineers, Osaka, 1977.
3. Y. Kakuta et al. Experimental Study on Punching Strength of Reinforced Concrete Slabs. Proc. of the Japan Society of Civil Engineers, No.229, 1974, pp.105-115.
4. H. Okamura et al. A Method of Numerical Analysis of Three-Dimensional Elastic Problems with Its Applications. Proc. of the Japan Society of Civil Engneers, No.199, 1972, pp.33-43.
5. H. Okamura et al. A Method of Three-Dimensional Analysis of Solid of Elasto-Plastic Property or of Nonuniform Elasticity. Proc. of the Japan Society of Civil Engineers, No.212, 1974, pp.11-24.

FATIGUE TESTS OF BOLTED CONNECTIONS DESIGNED BY SHEAR-FRICTION

B. G. Rabbat and N. W. Hanson, Portland Cement Association

For the elevated structure of Metropolitan Atlanta Rapid Transit Authority's (MARTA) system, bolted connections were designed to provide composite action between the precast concrete deck slab units and the main longitudinal girders. The connections were designed using the shear-friction procedure described in Section 11.15 of the 1971 ACI Building Code. Pretorqued bolts were used as "reinforcement". The paper describes tests of 16 specimens that simulated the joint between the deck and the girder of the MARTA structure. Controlled variables included use of concrete girder, steel girder, different size bolts and different types of grout between deck and girder. The specimens were subjected to repeated loads of either 2 or 5-million cycles. These tests provided a means for determining the behavior of the bolted connection under repeated loading. The test results are compared with values calculated according to the shear-friction concept. Design recommendations are presented.

Highlights

For the elevated structure of Metropolitan Atlanta Rapid Transit Authority's (MARTA) system, bolted connections were designed to provide composite action between precast concrete deck slab units and the main longitudinal girders. The connections were designed to resist the horizontal shears using the shear-friction procedure described in Section 11.15 of the 1971 ACI Building Code (1). The shear-friction procedure states that shear stresses along an assumed crack may be resisted by frictional stresses. The frictional stresses are calculated as the product of the normal stresses that prevent opening of the crack, and a coefficient of friction characteristic of the materials on each side of the crack. The normal stresses are developed by "reinforcement" across the assumed crack.

The connection detail designed for the MARTA system employed pretorqued high-strength bolts as "reinforcement". Besides practical considerations such as ease of installation, these bolts were expected to produce the following additional benefits:

1. A clamping force was provided to maintain compression in the grout layer between girder and deck slab. This ensured composite action of the girder and deck slab.
2. The pretorquing of the bolts tended to eliminate stress changes and minimize fatigue effects.

Existing experimental data on connections designed by shear-friction cover the cases of static loading to destruction. These appeared adequate for load factor designs of members subjected to relatively low number of loading cycles. However, no data existed concerning the integrity of these connections under repeated loads approaching 5-million repetitions.

This paper describes 16 test specimens that simulated the joint between the precast deck and the girder of the MARTA structure. The specimens were subjected to repeated loads of either 2 or 5-million cycles. The tests provided a means to determine the behavior of the connection under repeated loading.

Conclusions

1. Slip occurred prior to or during repeated loading as a result of breaking of the bond at the joint surface. The amount of slip increased with increasing number of cycles. However, the rate of slip decreased with increasing number of cycles.
2. The load at initial bond slip increased as the precompression of the joint surface increased.
3. The amount of initial bond slip decreased as the precompression increased.
4. All specimens that survived the repeated loading tests also resisted increasing static load up to a maximum slip of about 25-mm (1-in.) without sudden failure. The load versus slip relationship was parabolic with a steady loss of stiffness with increasing load.
5. Load capacity after 5-million cycles was reduced by an average of 5% as compared to specimens subjected to 2-million cycles. The maximum reduction was 14%.

Recommendations

Based on the test results and the conclusions outlined above, it is recommended that:

1. The bolts should be debonded over their entire length prior to torquing to ensure an effective prestress.
2. The coefficient of friction used for shear-friction design of bolted connections should be 0.7 for both precast concrete to precast concrete and precast concrete to rolled steel surfaces. The design yield strength of the bolts should not exceed 414 MPa (60 ksi), even if the yield strength of the bolts is higher.

Experimental Program

This section describes the procedure used to manufacture and test the specimens.

Test Specimens

The test specimens as shown in Figs. 1 and 2 consisted of a portion of concrete deck slab grouted and bolted to a portion of the girder. The girder portion represented either a concrete or structural steel beam. Details of all specimens are listed in Table 1. Test loading consisted of a fatigue test with repetition of specified loads followed by a static test to destruction. All loadings subjected the specimen to a sliding shear along the joint between the deck and girder portions. The minimum and maximum loads were predetermined for the MARTA system and specified by the Sponsor.

Specimens designated as Type C specimens consisted of a deck slab and a concrete girder. Specimens designated as Type S consisted of a deck slab and a steel girder.

In the specimen designation, the number following the C or S indicates bolt diameter in 3.2-mm (1/8-in.) multiples. Each specimen with the designation mark "-2" indicates repeated loading for 2-million cycles. The mark "-5" indicates repeated loading for 5-million cycles. The small letter "e" preceding the dash in the mark indicates specimens in which epoxy grout was used at the interface between the deck and girder portions.

Manufacture of Specimens

Concrete Girder. The reinforced concrete girder portion shown in Fig. 1 was cast with the joint contact surface at the bottom of the form. A stainless steel form-liner on the bottom ensured a smooth joint surface on some girders. The form-liner was later sandblasted to produce a rougher surface on other girders. Table 1 identifies the joint surface condition of the girders.

Bonding of the bolts to adjacent concrete and grout was allowed in some specimens and prevented in others. In the C9 specimens, the bolts were used in the same condition as received from the manufacturer. In the C9e specimens, the portion of bolts outside the girder part was coated with a thin layer of grease. In concrete girders C10, C11 and C12, bond was prevented over the full bolt length by tightly wrapping the bolts with a thin sheet of polyethylene. Rotation of the bolts during assembly was prevented by welding the head of the bolts to the girder steel plate with fillet welds.

Concrete compressive strength of each element was obtained from the average of three 150x300-mm (6x12-in.) concrete cylinders. At test time, the concrete strength ranged between 35.2 and 49.6 MPa (5100 and 7200 psi, respectively).

Steel-Girder. The steel girder is shown in Fig. 2. Prior to assembly, the steel joint contact surface was cleaned following the procedures of SSPC-SP3-63 (2), Power Tool Cleaning. To produce field practice, the cleaning was not carried to perfection.

Bond of the bolts to the adjacent grout was prevented in two ways. In the S12 specimens the bolts were greased. In the S10 and S11 specimens the bolts were covered with a thin sheet of polyethylene.

Concrete Deck Slab. The reinforced concrete deck slab shown in Figs. 1 and 2 was cast with the joint contact surface at the bottom of the form. A stainless steel form-liner on the bottom ensured a smooth joint surface on some deck slabs. The form-liner was later sandblasted to produce a rougher surface. Table 1 identifies the joint surface condition of the deck slabs.

Concrete compressive strength was obtained from the average of three 150x300-mm (6x12-in.) concrete cylinders. At test time the concrete compressive strength ranged between 34.5 and 50.3 MPa (5000 and 7300 psi, respectively).

Assembly of Specimens

Two types of grout were used between deck and girder elements:

1. High strength, non-shrink grout
2. Epoxy grout

The compressive strengths of both grouts were obtained from tests of 51-mm (2-in.) cubes. At test time the cube strength of the non-shrink grout ranged between 48.3 and 57.2 MPa (7000 to 8300 psi, respectively). The cube strength of the epoxy grout ranged between 51.7 and 55.2 MPa (7500 to 8000 psi, respectively).

In the specimens where non-shrink grout was used, the joint surfaces were sprinkled with water 1/2-hour before the grout was mixed. Excess water was brushed away.

When epoxy grout was used, the joint contact surfaces were lightly wire brushed to remove any form oil, laitance, or other material which could prevent bond between the grout and the concrete.

To assemble the specimen, the girder portion was positioned with the joint surface horizontal and upward. The grout was prepared and placed on the contact surface in a layer with a thickness of more than 6.35-mm (1/4-in.). The deck slab was then placed over the bolts and in contact with the plastic grout. Excess grout was squeezed out until the deck rested on 6.35-mm (1/4-in.) spacers. In all specimens the contact area grouted was the full width of the girder portion over a length of 0.915-m (3-ft).

In all specimens, the blockout portion below the steel plate in the deck slab was then filled with non-shrink grout packed thoroughly by means of a compacting rod. The upper bolting plate was placed in position and the nuts finger tightened.

When the grout attained a compressive strength of 27.6 MPa (4000 psi), the bolts were tensioned to

60% of their yield stress of 558 MPa (81 ksi) by applying torque in increments to the nuts.

The calculated torques (3) for a bolt stress of 335 MPa (48.6 ksi) are listed in Table 2. All threads and washers were cleaned and lubricated with grease before torquing.

Testing Procedure

Initial Static Test. The specimen was positioned in the loading frame with the joint contact surface vertical as shown in Fig. 3. The base of the girder portion rested on a high strength plaster leveling course on the bed of the frame. Two 490 kN (50 ton) loading rams located above the specimen and 0.915-m (3-ft) apart, applied the load to the specimen through a rigid steel cross beam.

A dial gage was attached at mid-height of the joint on each side of the specimen to measure joint slip. The average change of the dial readings is reported as slip.

The specified maximum load, P_{max}, shown in Table 1 was applied to each specimen. The relative slip of the deck with respect to the girder was recorded at increments of 44.5 kN (10 kips). Maximum load was sustained for 3 minutes and the slip was again recorded. The applied load was then reduced to the specified minimum repeated load in preparation for the repeated load test.

Repeated Load Test. The applied load was varied from the minimum P_{min}, to the maximum force, P_{max}, specified in Table 1. The loading rate was 500 cycles per minute. The cyclic loading was applied continuously for either 2 or 5-million cycles.

Except for the C9 and S12 specimens in which the slip gages were removed during the repeated loading tests, gages were left attached to the specimen. Slip was recorded at least once a day together with the number of cycles completed.

Static Test to Destruction. Static tests to destruction were performed in a 4.45-MN (1-million-lb) testing machine. The specimen was positioned with the joint contact surface vertical as shown in Fig. 4. The base of the girder portion rested on a thin sheet of plywood on the lower bed of the machine. The movable loading head of the machine contacted the deck slab element through a high strength plaster leveling course. The joint contact area of the specimen was centered with respect to the loading head. The slip gages were reset to make use of their maximum travel.

Load was applied in increments. In the early stages of loading, slip was recorded in increments of 89 kN (20 kips). At higher loads the slips were recorded in increments of 44.5 kN (10 kips). In most of the specimens, the static load was sustained for a short time at two different load levels in order to observe the crack patterns. In such a case, slip was also recorded at the end of the period, together with the length of time the load was sustained. The test was terminated when the total slip space was exhausted. This maximum slip was about 25-mm (1-in.) for the concrete to concrete specimens and about 32-mm (1-1/4-in.) for steel to concrete specimens.

Test Results and Discussion

Specimens C9 and C9e broke prematurely prior to application of the specified maximum repeated loads. Therefore the results of these specimens are excluded from the analyses. All other specimens survived the repeated load test and were loaded to destruction.

Initial Bond Slip at the Joint Surface

Specimen C9-5 was not subjected to the initial static test and the bond broke at the joint surface during application of the repeated loads. Bond broke at the joint surface of Specimens C9-2, C9e-2 and C9e-5 during the initial static test.

For the C9 and C9e specimens, excessive initial bond slip occurred at low loads. The size of the bolts of these specimens was smaller and the torquing of the bolts was probably ineffective because of the bond of the bolts with the adjacent concrete and grout.

In Specimens C10, C11 and C12-2, bond broke at the joint surface during the static test to destruction. In C12-5 it occurred after 1 day of repeated loading.

In all the steel to concrete specimens, the bond broke at the joint surface during the initial static test.

A summary of the loads and stresses at which the bond broke at the joint surface is given in Table 3. Shear stress at failure is calculated as the applied load divided by the joint surface area. The concrete to concrete "C" specimen had a contact area of 0.465 sq.m (720 sq.in.), while the steel to concrete "S" specimens had a contact area of 0.290 sq.m (450 sq.in.).

The load at initial bond slip tends to increase with prestress in each specimen type. However, the relationship cannot be defined precisely with the limited amount of data.

Table 3 summarizes joint slip that occurred during the initial static and repeated load tests. During the initial static test, slip was recorded as the load reached the specified maximum force. Slip was again recorded after the specified maximum load had been sustained for 3 minutes. Slip was also recorded after the specimen had survived 2 or 5-million cycles.

Data in Table 3 shows that generally the "C" specimens exhibited very little slip, while the "S" specimens had a substantial slip. When the bond broke before or during the cyclic test, e.g., all "S" specimens, the slip increased during the repeated loading test.

Slip During the Static Test to Destruction

Load versus slip curves obtained during the static tests to destruction are shown in Figs. 5 and 6 for the "C" and "S" specimens, respectively. The slip plotted in these figures do not include any permanent movement that occurred during the initial static and repeated load tests. Generally, the specimens previously subjected to 5-million cycles of loading indicate reduced load at larger deformations than for companion specimens loaded to only 2-million cycles.

Strength by the Shear-Friction Procedure

According to Section 11.15 of ACI 318-71 (1), the strength of a joint by shear-friction is:

Figure 1. Type "C" specimen.

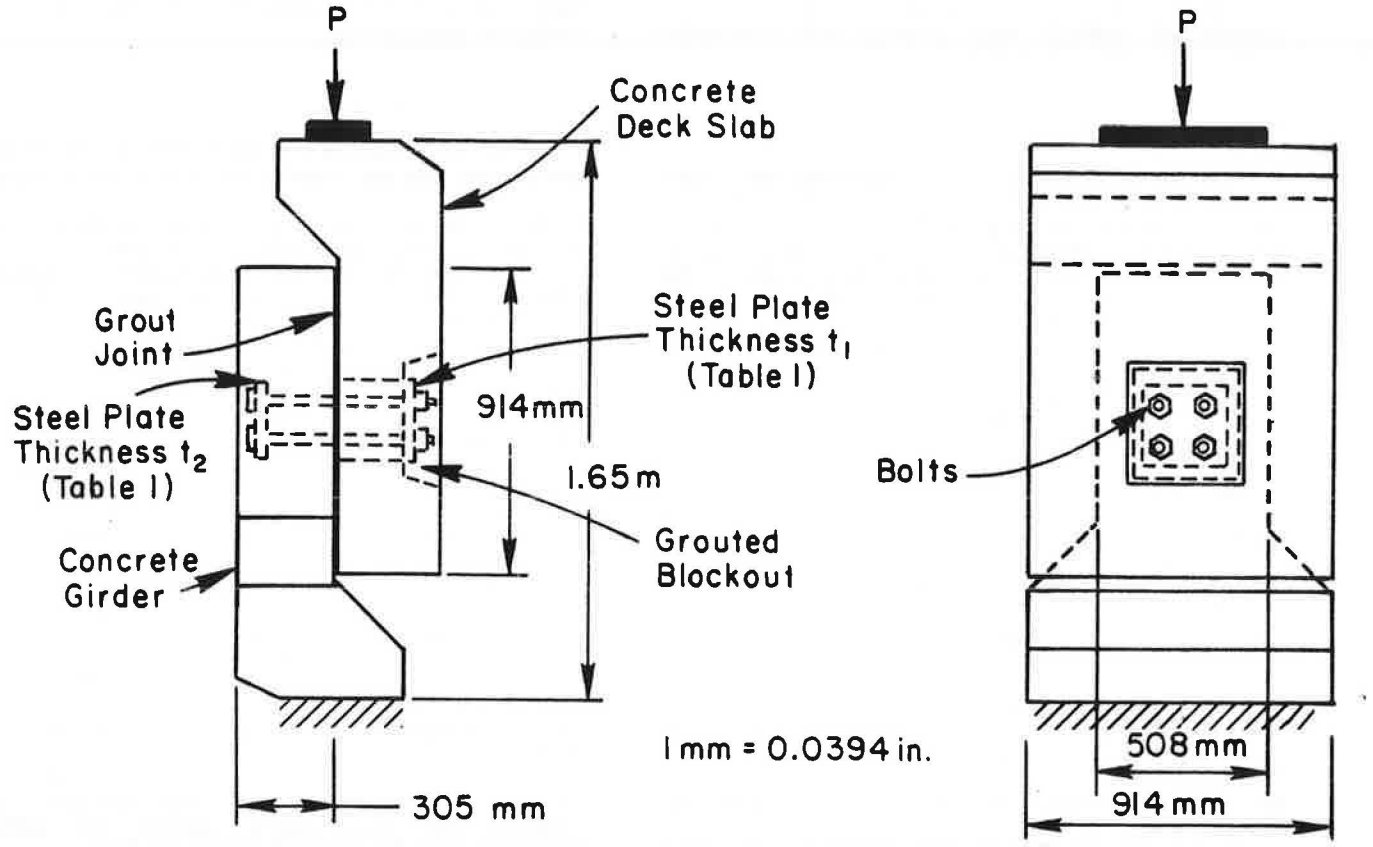

Figure 2. Type "S" specimen.

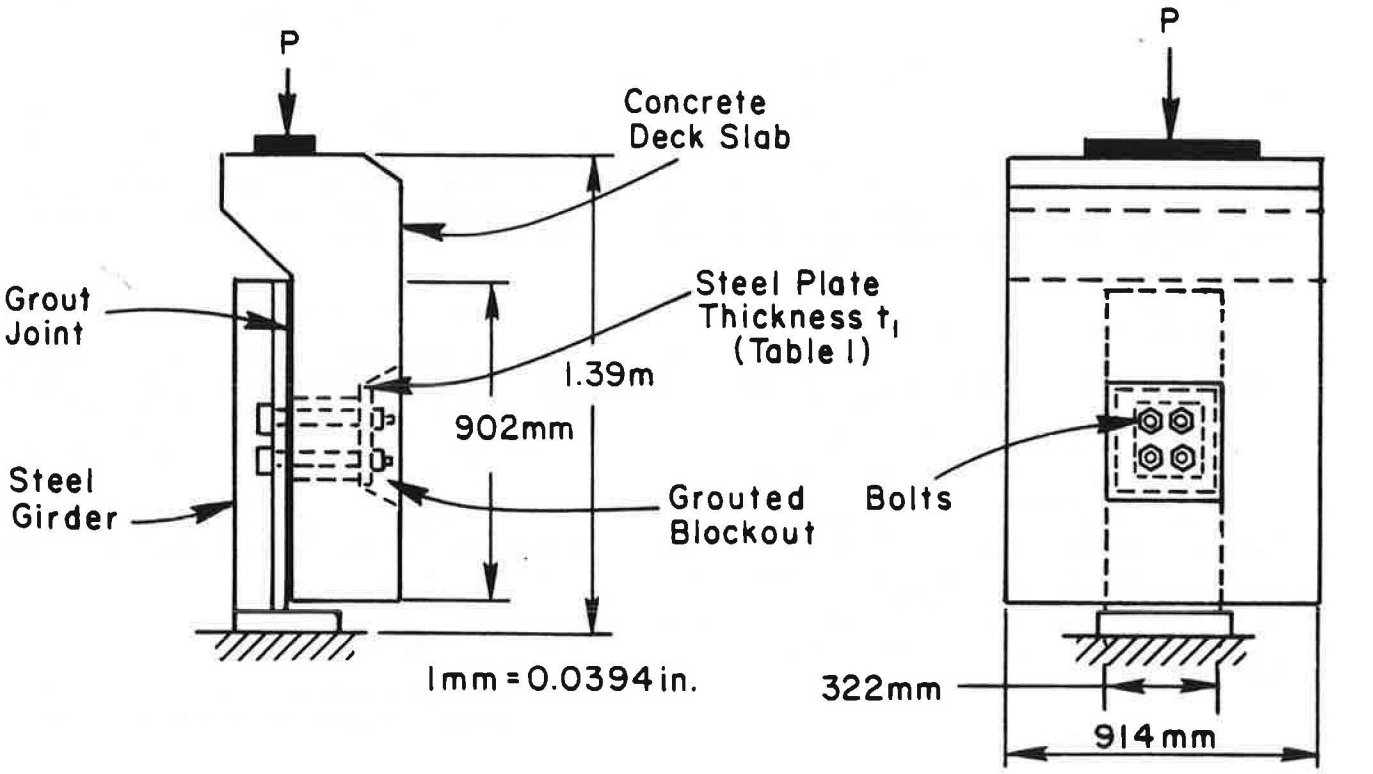

Table 1. Test specimens.

Specimen	Bolt Size (mm)	Plate Thickness (mm)		Repeated Load (kN)		Bolt in Blockout	Concrete Joint Surface
		t_1 (deck)	t_2 (girder)	P_{min}	P_{max}		
C9-2	28.6	31.8	28.6	200	600	bonded	smooth
C9-5	28.6	31.8	28.6	200	600	bonded	smooth
C9e-2	28.6	31.8	28.6	200	600	unbonded*	smooth
C9e-5	28.6	31.8	28.6	200	600	unbonded*	smooth
C10-2	31.8	41.3	38.1	111	400	unbonded	rough
C10-5	31.8	41.3	38.1	111	400	unbonded	rough
C11-2	35.0	47.6	44.5	178	556	unbonded	rough
C11-5	35.0	47.6	44.5	178	556	unbonded	rough
C12-2	38.1	50.8	47.6	200	600	unbonded	rough
C12-5	38.1	50.8	47.6	200	600	unbonded	rough
S10-2	31.8	41.3	-	133	423	unbonded	rough
S10-5	31.8	41.3	-	133	423	unbonded	smooth
S11-2	35.0	47.6	-	178	512	unbonded	rough
S11-5	35.0	47.6	-	178	512	unbonded	smooth
S12-2	38.1	50.8	-	222	645	unbonded*	smooth
S12-5	38.1	50.8	-	222	645	unbonded*	smooth

*Unbonded using grease - All other bolts unbonded using thin polyethylene sheet.

NOTE: 1 mm = 0.0394 in.
1 kN = 0.225 kip

Table 2. Applied torques.

Bolt Size		Torque	
(mm)	(in.)	(N.m)	(ft. lb)
28.6	1-1/8	698	515
31.8	1-1/4	976	720
35.0	1-3/8	1315	970
38.1	1-1/2	1729	1275

Table 3. Joint bond failure and joint slip.

Specimen Mark	Initial Bond Slip		Joint Prestress* (MPa)	Joint Slip (mm)		
	Load (kN)	Shear Stress (MPa)		Initial Static Load	Initial +3 min.	After Repeated Loading
C9-2	436	0.94	1.86**	-	-	-
C9-5	534	1.14	1.86**	-	-	-
C9e-2	578	1.24	1.86**	1.820	2.222	-
C9e-5	445	0.96	1.86**	2.960	3.454	-
C10-2	654	1.41	2.28	0.003	0.005	0.008
C10-5	721	1.55	2.28	0.005	0.008	0.010
C11-2	796	1.71	2.75	0.005	0.005	0.005
C11-5	645	1.39	2.75	0.013	0.013	0.013
C12-2	685	1.47	3.30	0.010	0.010	0.025
C12-5	+	+	3.30	0.010	0.010	1.130
S10-2	365	1.25	3.65	1.200	1.270	1.980
S10-5	374	1.28	3.65	1.450	1.540	1.960
S11-2	+	+	4.40	0.140	0.157	1.140
S11-5	512	1.76	4.40	0.419	0.437	1.820
S12-2	534	1.83	5.85	0.673	0.737	-
S12-5	445	1.53	5.85	1.550	-	-

*Intended bolt force divided by joint surface area.
**Actual value is probably much less since bolts were bonded.
+Bond failure during repeated loading.

NOTE: 1 kN = 0.225 kip
1 MPa = 145 psi
1-mm = 0.0394-in.

Figure 3. Repeated load test setup.

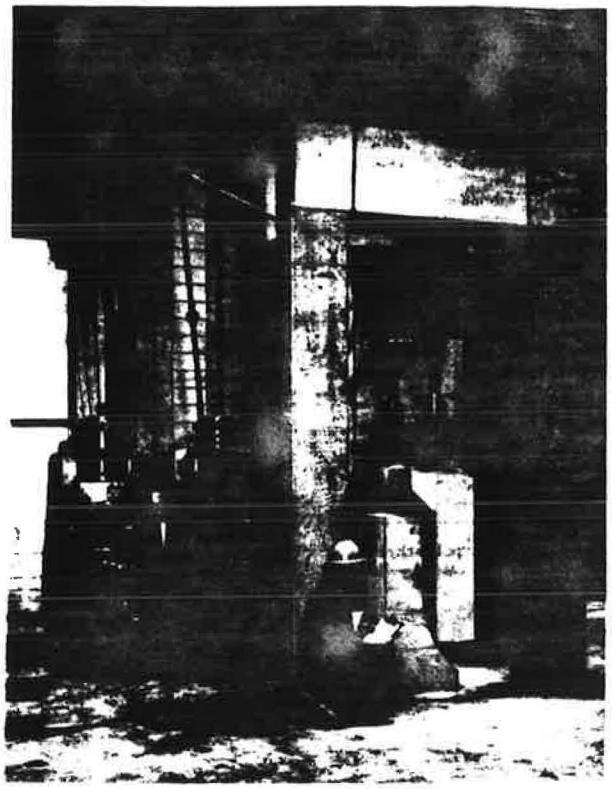

Figure 4. Setup for static loading to destruction.

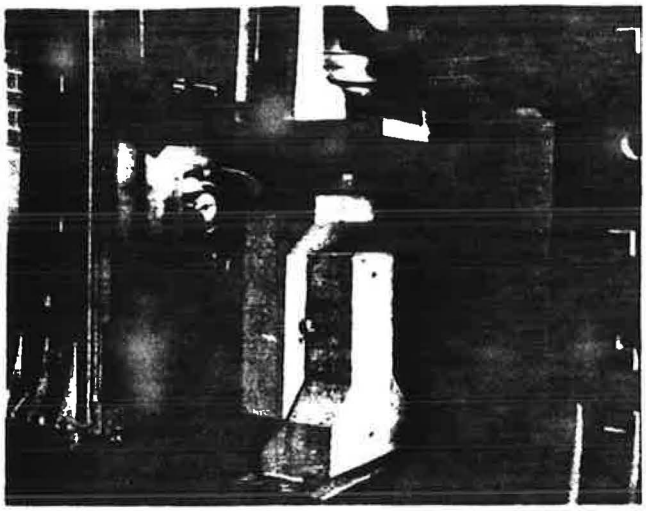

Figure 5. Load versus slip during static test to destruction for the "C" specimens.

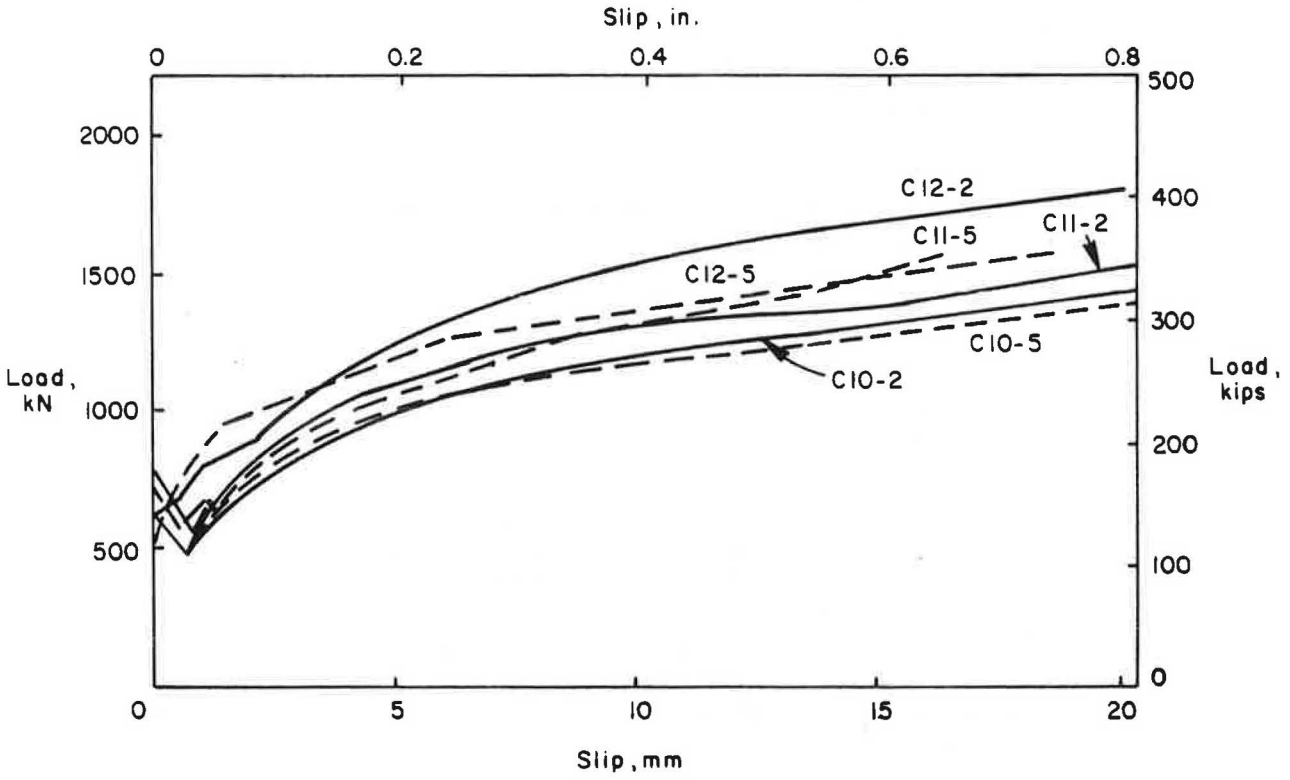

Figure 6. Load versus slip during static test to destruction for the "S" specimens.

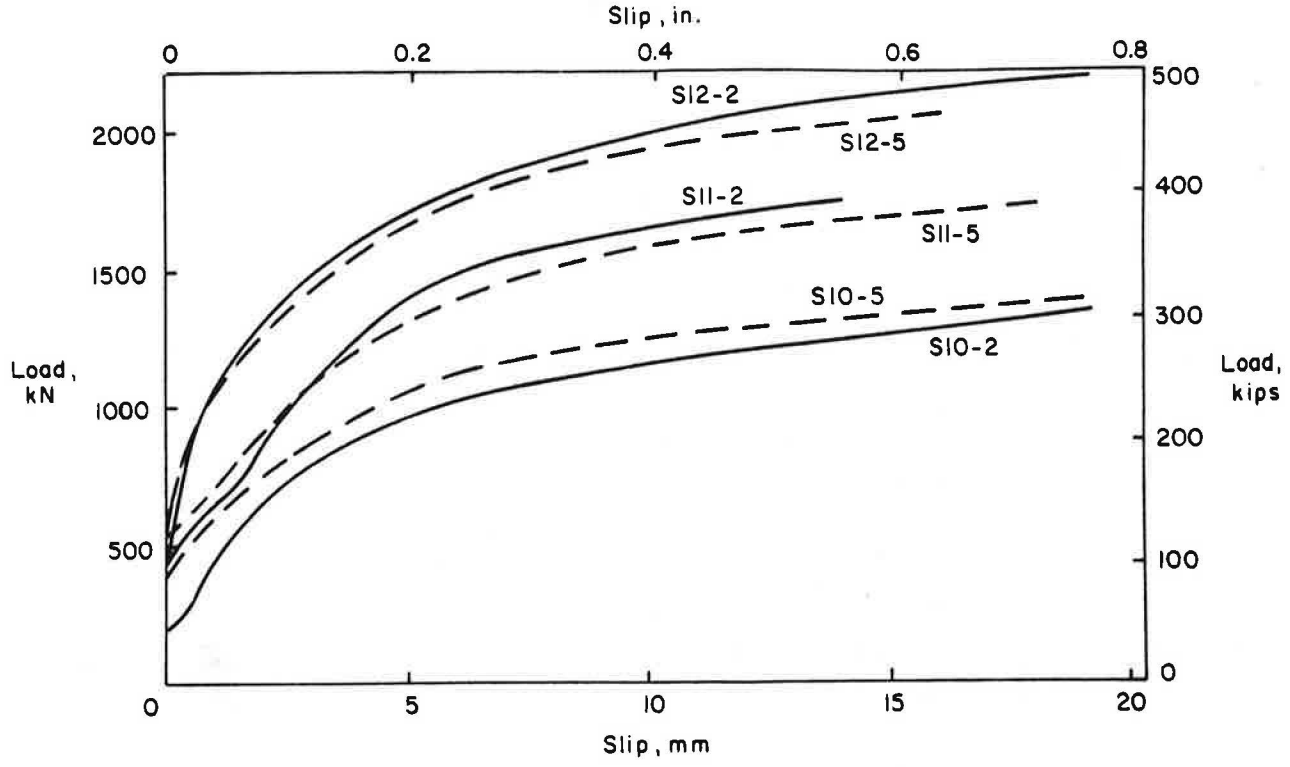

Figure 7. Experimental versus calculated strength.

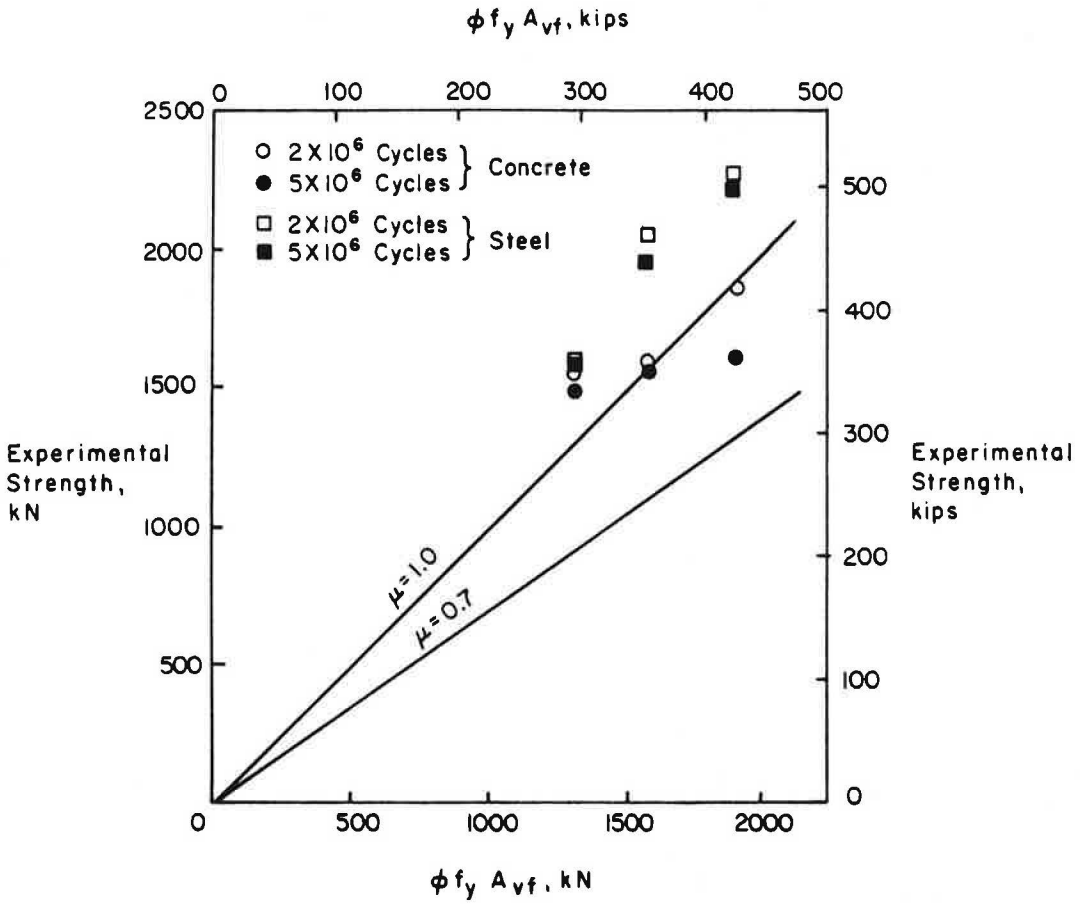

$$V_u = \Phi f_y A_{vf} \mu$$

where

V_u = the total applied design shear force
Φ = a capacity reduction factor
f_y = the specified yield strength of non-prestressed reinforcement
A_{vf} = area of shear-friction reinforcement
μ = the coefficient of friction

In the ACI Code (1), the specified coefficients of shear-friction apply to concrete cast monolithically, to concrete placed against hardened concrete, and to concrete placed against as rolled structural steel. Also, in calculating the area of the shear-friction reinforcement, the shear-friction formula stipulates that the specified yield strength is that of non-prestressed reinforcement and shall not exceed 414 MPa (60 ksi).

In the specimens tested, precast concrete was bolted to either precast concrete or rolled structural steel. Moreover, the bolts (shear-friction reinforcement) were pretorqued.

In spite of the above differences, the experimental maximum static load is plotted versus the yield strength of the bolts in Fig. 7. The yield strength of the bolts is computed assuming that for all specimens $\Phi = 1.0$, and $f_y = 414$ MPa (60 ksi), maximum value allowed by the present code. The shear-friction equation is also plotted in Fig. 7 for the specified coefficients of friction; $\mu = 0.7$ for concrete cast against rolled steel and $\mu = 1.0$ for concrete cast against concrete.

The plot of Fig. 7 indicates that a coefficient of friction of 0.7 for concrete on rolled steel produces a conservative estimate of strength. It will be recalled that the experimental load is defined as the load that corresponds to an arbitrary slip value of about 25-mm (1-in.). Data for concrete on concrete with the coefficient of 1.0 indicates a satisfactory prediction of strength after 2-million cycles. The additional loss in stiffness resulting from 5-million cycles of loading further reduced the strength and in one case resulted in low experimental loads.

With a coefficient of friction of 0.7 for concrete on concrete specimens, the ratio of test to design loads ranged from a maximum of 1.68 to a minimum of 1.21.

Smooth Versus Rough Interface Surfaces

A limited comparison of the effect of the surface roughness at the interface can be made through the S10 and S11 specimens.

Specimens S10-5 and S11-5 had smooth surfaces while Specimens S10-2 and S11-2 had rough surfaces. A comparison of the slip in Table 3 and Fig. 6 reveals that the surface roughness of the specimens used in this investigation did not affect the behavior.

Concluding Remarks

Test specimens representing a bolted connection between concrete and concrete or concrete and steel were subjected to repeated loads for 5-million cycles without failure. Prestress in the joint produced by torquing the nuts to a specified torque enabled the specimens to survive the repeated loading without excessive slip. However, positive treatment is necessary to debond the bolt from surrounding grout so that tension is developed in the full length of the bolt during torquing.

Conclusions and design recommendations based on this investigation appear at the beginning of the paper. Subsequent to this investigation, the steel to concrete design was modified for use in the actual structure.

Acknowledgments

This paper is based on an investigation sponsored by Parsons Brinckerhoff-Tudor-Bechtel, General Engineering Consultants to the Metropolitan Atlanta Rapid Transit Authority (MARTA), D. J. Mansfield, Manager of Engineering, Mike Viarnes, Structural Specialist. The investigation was financed in part through a grant from the U.S. Department of Transportation, Urban Mass Transportation Administration, under the Urban Mass Transportation Act of 1964, as amended, and in part by the taxes of the citizens of Fulton and DeKalb Counties of the State of Georgia. The experimental work was carried out at the Structural Laboratory of the Portland Cement Association under the direction of H. G. Russell, Manager, Structural Development Section and W. G. Corley, Director, Engineering Development Department. Particular credit is due G. B. Barney for getting the program started, and for R. C. O'Neill, Wm. H. Graves, B. Wm. Fullhart and R. K. Richter, for their assistance in the manufacture and testing of the specimens.

Disclaimer

The contents of this report reflect the views of the authors who are responsible for the facts and the accuracy of the data presented herein. The contents do not necessarily reflect the official views or policies of Parsons Brinckerhoff-Tudor-Bechtel or MARTA. This report does not constitute a standard, specification, or regulation.

References

1. "Building Code Requirements for Reinforced Concrete", ACI-318-71, American Concrete Institute, Detroit, November 1970, 78 pp.
2. "Surface Preparation Specifications - No. 3, Power Tool Cleaning", SSPC-SP3-63, Steel Structures Painting Council, October 1963.
3. Marks, L. S., Mechanical Engineers Handbook, Fourth Edition, McGraw-Hill Book Co., New York, 1941, p. 239.

AN INVESTIGATION OF THE FATIGUE STRENGTH OF DECK SLABS OF COMPOSITE STEEL/CONCRETE BRIDGES

Barrington deV. Batchelor, Queen's University, Ontario
Brian E. Hewitt, Public Works Dept., Western Australia
and P. Csagoly, Ontario Ministry of Transportation and Communications

An investigation of the effects of repeated loads on slabs of steel/concrete composite bridges - the most common type in highway construction - was undertaken to supplement static studies conducted under the Ontario Joint Transportation and Communications Research Program No. Q50. The study which involved tests of a number of 1/8th scale direct models of a typical bridge, was aimed at determining endurance limits of the slabs under repeated concentrated loads. Main variables were stress range, and percentage and arrangement of reinforcement. Emphasis was focused on slabs with 0.2 percent top and bottom isotropic reinforcement, this being the amount recommended for use as a result of the static model testing phase of the program. The study showed that the deck slabs of conventionally designed steel/concrete bridges have large reserves of fatigue strength. An endurance limit of 50 percent of the ultimate capacity can be expected in such slabs. In the case of slabs with 0.2 percent isotropic reinforcement, an endurance limit of 40 percent of the ultimate static capacity can be safely adopted for design. These slabs have also performed adequately in static tests; and adoption of their use, where appropriate, would result in considerable reduction of reinforcement requirements in bridge decks.

Background

The experimental study reported in this paper is an integral part of a major program aimed at obtaining a thorough understanding of the behaviour of concrete bridge deck slabs supported by beams or girders. Other parts of the project have included extensive testing of deck slabs of model and prototype bridges, measurement of horizontal membrane forces in circular slab specimens, and an investigation of scale effects in model deck slabs subjected to concentrated loads.

It has been found that, contrary to the classical plate bending theory developed by Nadai and promoted successfully by Westergaard in North America, slabs of practical thicknesses carry concentrated loads primarily by compressive membrane action, often referred to as "internal arching". The development of membrane forces in typical deck slabs is a direct result of lateral confinement of the loaded slab by its supporting members or by adjacent portions of the slab itself. Indications are that while a bending component is still present, it is not significant as far as the load-carrying capacity of the slab is concerned.

The fact that the major part of the load is carried by compressive membrane action permits a substantial reduction of the slab reinforcing steel requirements. It appears that the minimum amount of steel specified by ACI for crack control against volumetric changes, is adequate to carry all present day and probable future live loads. Since this reduction entails the elimination of two-thirds to three-quarters of the current typical reinforcement requirements, it was considered advisable to investigate various aspects other than the ultimate strengths of these slabs. One such aspect reported in this paper is the fatigue life of reinforced concrete slabs, an area of structural engineering, which has received very little attention.

It is shown that typical deck slabs designed with a consideration of the high compressive membrane stresses developed when subjected to concentrated loads, can be expected to give satisfactory fatigue performance, even though their reinforcement requirements are nominal.

Brief Historical Review

Although it is generally recognized that the repeated load that will cause failure of a structure is likely to be significantly less than the static failure load, the behaviour of bridge decks under repeated loads has in the past received scant attention. A review of the available data related to fatigue of reinforced concrete reveals that the past studies were primarily carried out on isolated beams as opposed to slabs. Exceptions are the studies by Graf (reported by Nordby (1) and Loo (2)). It is recognized that substantial differences exist in the structural responses of reinforced concrete beams and slabs, therefore, it appears

questionable whether fatigue behaviour observed in reinforced concrete beams can be reliably extended to slabs. In 1958, Nordby (1) concluded the following in a review of fatigue of reinforced concrete beams:

a) Most failures of reinforced concrete beams were due to the fracture of reinforcing steel. Under-reinforced beams appeared to have a fatigue load limit of 60 to 70 percent of the static ultimate strengths for a life of 1,000,000 cycles of loading.

b) Except for a few cases, compression failures were virtually absent.

c) Failure was often due to diagonal tension, though the real cause of failure was obscured by a combination of bond and shear failures. Beams have failed in shear under repeated loads at levels of 40 percent of static ultimate strength.

d) Accumulation of residual deflections occurred under extensive fatigue loading but some amount of recovery was evident during rest periods.

In an investigation conducted at Queen's University on the slabs of a reinforced concrete double-T beam bridge, Loo (2) reported that different fatigue failure modes occurred in the slabs. At loads close to the static capacity, failure was mainly due to punching after a small number of cycles of loading. At lower levels of loading, failure was caused by fracture of the reinforcing steel after a large number of cycles. Loo found that the fatigue behaviour of slabs subjected to concentrated loads could be predicted from the fatigue properties of the reinforcing steel. Although there was no positive evidence of an endurance limit in the slabs tested, Loo speculated that this may be as low as one-half of their static capacities.

In a model study of composite bridges (3,4) Batchelor and Hewitt concluded that the conventional design of the deck slabs of composite bridges is very conservative. It was shown that the deck reinforcement requirements in such slabs could be safely reduced. However, the study did not include a consideration of the response to repeated loads, of slabs designed by the method proposed which results in a substantial reduction of the reinforcing steel requirements.

Scope of Investigation

The study reported in this paper was, therefore, undertaken to determine the fatigue strength of composite steel/concrete deck slabs and, in particular, the fatigue behaviour of slabs with the reduced amount of reinforcement recommended in the static studies carried out under Project Q50 (3). The fatigue study was considered essential in view of the considerable reduction of reinforcement proposed, and in view of the fact that with the increasing intensity of commercial traffic, bridges are now required to have longer fatigue life than in the past.

The investigation, which was mainly experimental, has shown that deck slabs with either conventional orthotropic reinforcement, or with the recommended reduced reinforcement ratios, have large reserves of strength against fatigue failure, thereby confirming the validity of the design recommendations based on the static tests.

In this report an orthotropic slab is one in which the reinforcement ratios provided in a face, in two orthogonal directions, are unequal. An isotropic slab is one in which the reinforcement ratios in a face are equal in two orthogonal directions.

Model Bridges and Tests

The study was carried out on a total of five 1/8th scale direct models of a 24.4 m (80 ft) simply supported four-beam bridge. The prototype and model bridges are detailed in Figure 1. Dead load stresses appropriate to unshored construction were simulated in one model. The means of inducing dead load stresses, as well as the solutions of problems encountered in modelling material properties, section properties and stud shear connector behaviour, are described in detail elsewhere (4,5).

The investigation started with the fatigue studies by Dixon (6), and, initially slabs with orthotropic reinforcement were investigated. Subsequent studies involved top and bottom isotropic reinforcement which was found suitable in the previous static studies, as well as mid-depth reinforcement which would afford maximum cover.

All panels of a model were tested under concentrated loads. A bridge panel is defined as that portion of the deck bounded by adjacent bridge beams and adjacent diaphragms. The model bridges tested are numbered 1 to 5, and the designation of the bridge panels is shown in Figure 2. To facilitate testing of panels with different percentages of reinforcement, the amount of reinforcement was varied in bridges numbered 3, 4, and 5, since it was concluded from previous static tests that the behaviour of a panel under load is not influenced by the reinforcement of adjacent panels. The slab reinforcement in each bridge is given in Table 1. Dead load compensation was

FIGURE 1: DETAILS OF PROTOTYPE AND MODEL BRIDGES.

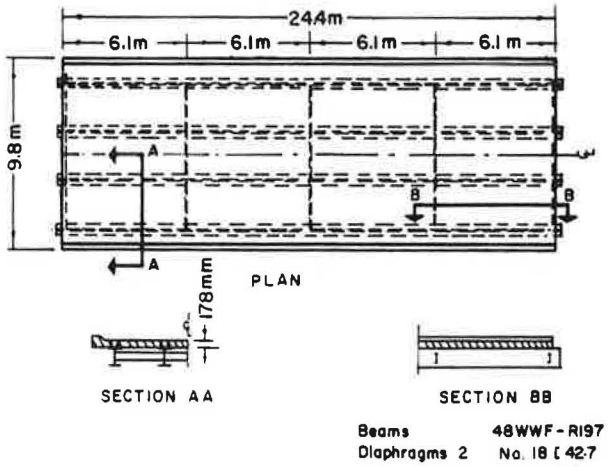

FIGURE 2: DESIGNATION OF BRIDGE PANELS.

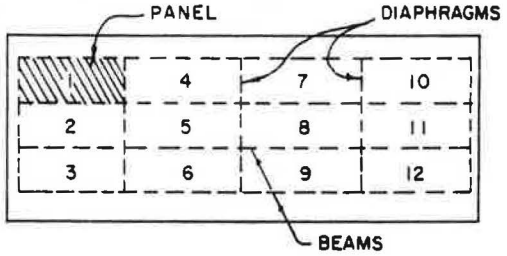

TABLE 1, DETAILS OF MODELS

BRIDGE NO.	REINFORCEMENT			
	PANELS 1, 2, 3,	PANELS 4, 5, 6,	PANELS 7, 8, 9,	PANELS 10, 11, 12,
1	ORT	ORT	ORT	ORT
2	ORT	ORT	ORT	ORT
3	0.4%**	0.2%	ZERO	0.2%
4	0.4%	ZERO	2"***	0.2%
5	51 mm	76 mm	NONE	25 mm

LOGITUDINAL SECTIONS

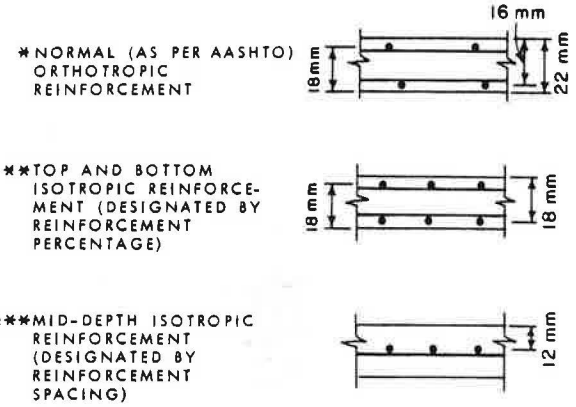

applied to bridge No. 2 and the results of tests on this model indicated that for the scale of the model and with the types of slabs involved, dead load compensation could be eliminated.

In all cases the single concentrated load was applied at the centre of a panel through a steel plate bearing on a neoprene pad. The contact area modelled an ellipse with major and minor axes of 762 mm and 508 mm (30 and 20 in) respectively, which represents the assumed contact area of the pneumatic tires of large trucks. Loading was applied by means of an MTS closed loop electro-hydraulic testing system. A number of panels of each model were tested to failure under static loading. The static failure load was then used to set the maximum load of the fatigue loading function for the corresponding panels of the particular model. The fatigue loading was continued until panel failure, or up to a minimum of 2,000,000 cycles of loading. The AASHTO Standard specifications for Highway Bridges (7) specify 2,000,000 as the number of cycles of maximum stress to be considered in design.

The applied dynamic load was in the form of a sinusoidal wave superimposed on a mean value. The applied load was programmed so that the minimum load was of the order of 890 N (200 lb), and the maximum load was a proportion of the estimated static strength of the panel. The frequency of the applied load was varied for different tests because the response of the dynamic loading system was influenced by the travel of the loading ram and therefore by the bridge deflections. Frequencies as high as 5 Hz could be used for tests in regions near the end supports of the bridge where the deflections were small. On the other hand, in tests towards mid-span of the bridges, frequencies as low as 1 Hz were necessary. Nordby (1) has noted that a rate of testing between 1 and 7 Hz has little or no effect on the fatigue strength of plain concrete, and it is considered that the variation of the testing rate in this investigation did not significantly influence the fatigue behaviour of the deck slabs.

Model Material Properties

Concrete

A special concrete suitable for structural models, and which was developed at Queen's University, was used for the bridge deck slabs. Although a very fine aggregate was used, the ratio of tensile to the compressive strength for this concrete is similar to that of prototype concrete.

The properties of the concrete of the deck slabs of the model bridges are given in Table 2. The tabulated compressive and tensile strengths were determined from 102 mm x 203 mm (4 x 8 in) cylinders which were tested about halfway through the testing program for a particular bridge model. The tests conducted under Project Q50 (3) indicated that the static ultimate load carrying capacity of rectangular slabs of a composite bridge deck is not significantly influenced by the strength of the concrete. It was therefore considered reasonable to assume that the concrete strength had little influence on the fatigue behaviour of the bridge decks.

Reinforcing Steel

The reinforcement used in the models was a 13 gauge wire having a diameter of 2.32 mm (0.0915 in.) and manufactured by the Steel Company of Canada Ltd. The wire was indented and specially annealed so that it had a yield stress conforming to ASTM Standards for intermediate grade steel.

Table 2. Model concrete properties

Bridge No.	Age when tested (days)	Compressive strength f'_c MPa	Splitting tensile strength f_t MPa
1	28	35.54	2.48[a]
2	64	37.65	Not done
3	43	33.37	3.30
4	23	31.30	3.35
5	35	37.54	3.29

[a]Different mix from others

Note: 1 MPa = 0.145 ksi

The fatigue behaviour, in tension, of the model reinforcement was investigated in a series of tests using a Sonntag Universal Testing Machine. This was done to determine whether, as suggested by Loo (2), there was any relationship between the life of the slab and that of the reinforcement. As in the case for the model bridges, the applied dynamic load was in the form of a sinusoidal curve superimposed on a mean value. The minimum load was set near zero and the maximum load was a

proportion of the ultimate strength of the reinforcement. The load function was applied at a frequency of 30 Hz. In Figure 3 the ratio of maximum load to the ultimate load is plotted against the number of cycles to fatigue failure of the reinforcement. There is some scatter, but it is clear that fatigue failure is unlikely in any practical situation at any load ratio less than about 0.6, which can be taken as an approximate value of the endurance limit for the reinforcing steel.

Observations

Failure Mechanism

A total of 37 panels were tested to failure under fatigue loading and all but a few failed by punching. The crack patterns up to failure were much the same as those obtained in punching failures under static loads. Cracking was observed after a few cycles of repeated loading. The cracks then widened and spread as the number of cycles of loading increased, until a relatively stable condition was reached in which crack propagation was much reduced and any change was imperceptible over a period of a few hours of testing. All visible cracking was observed to be confined to the panel under test, and there was no spreading of the cracks into adjacent panels. The punched area after fatigue failure was often larger and less symmetrical than that resulting in failure under static loading, particularly in slabs

FIGURE 3: LOAD RATIO VERSUS NUMBER OF CYCLES TO FAILURE FOR SLAB REINFORCEMENT.

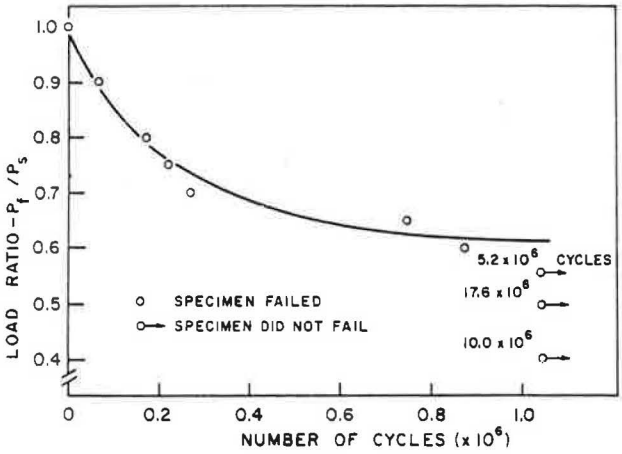

with little or no reinforcement. In some cases, fracture occurred in the bottom slab reinforcement within the loaded area.

Flexural failures resulted in six panels having little or no reinforcement. It cannot be said that such panels always failed in flexure; however, panels with orthotropic reinforcement or with 0.4 or 0.6 percent isotropic reinforcement always failed in punching. Imminent flexural failure was usually indicated by crushing and spalling of the concrete along lines radiating from the loaded area on the upper surface of the slab.

Deflection Behaviour

Typical net slab deflections are plotted in Figure 4. These deflections were measured during static tests carried out before and after fatigue tests in which the panel did not fail. In the fatigue test of the orthotropically reinforced panel, over 3 million cycles of loading were applied with the maximum load being 50 percent of the estimated static strength, whereas over 2 million cycles of loading were applied to the isotropically reinforced panel. It can be seen that in each case there was little loss in stiffness up to the maximum fatigue load. The loss of stiffness occurred in the initial stages of the fatigue tests, and can be attributed only to cracking of the concrete.

The maximum net slab deflection was monitored in all fatigue tests. In slabs that did not fail, the net deflection increased initially and then became constant. In the case of slabs that did fail, the net deflection continued to increase up to failure.

Test of Panels with Orthotropic Reinforcement

The results of the tests of panels with orthotropic reinforcement are given in Table 3.

FIGURE 4: TYPICAL NET DEFLECTION VERSUS LOAD, BEFORE AND AFTER FATIGUE.

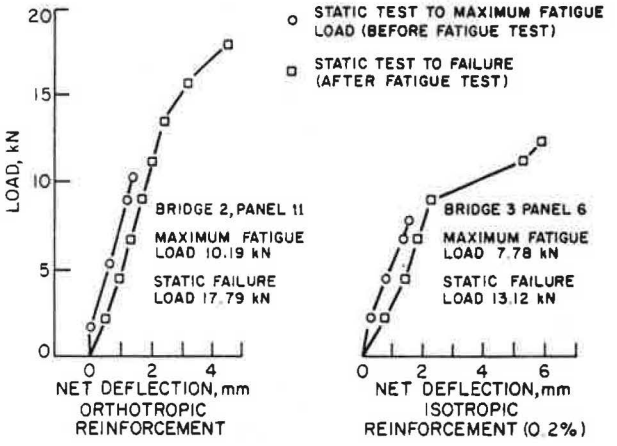

In each test the maximum load P_f of the fatigue load function was set at a proportion of the static failure load, P_s, of the first tested panel of each bridge. It was indicated in the Project Q50 report of the static tests that there was considerable variation in the static punching loads for panels of the same design dimensions and properties, and that this variation was at least partly attributable to variations in the effective depth of the slab. An assumption that the failure load is the same for all panels with the same amount of reinforcement neglects the influence of slab thickness on punching load. Therefore, in assessing the ultimate strength of an orthotropically reinforced panel, use was made of the relationship in Equation 1 which was derived in Project Q50 for the extremely small slab thickness used in the models:

$$P_s' = -1.139 + 1.361\, d \text{ (kN)} \qquad (1)$$

Table 3. Results of tests of panels with orthotropic reinforcement

Bridge no.	Panel no.	Maximum fatigue load P_f (kN)	$\frac{P_f}{P'_s}$	No. of cycles to failure	d (mm)	Estimated static load P'_s (kN)	$\frac{P_f}{P'_s}$
1	2	9.12	0.39	2,052,400	17.6	22.82	0.40
	4	23.36**	1.0	1	17.2	22.24	-
	6	14.41	0.62	756,470	17.4	22.64	0.64
	8	17.93	0.77	1,510	16.5	21.31	0.84
	10	16.77	0.72	91,250	19.1	24.82	0.68
	12	15.52	0.66	103,510	18.1	23.49	0.66
2	1	13.66	0.67	165,000	17.4	22.60	0.60
	2	13.66	0.67	166,900	18.0	23.31	0.59
	3	14.28	0.70	10,940	17.6	22.77	0.63
	4	14.32	0.70	6,010	25.4	21.80	0.66
	5	15.30	0.75	51,040	17.5	22.68	0.67
	6	14.32	0.70	46,190	17.6	22.82	0.63
	7	12.23	0.60	1,143,130	17.2	22.24	0.55
	8	18.37	0.90	35	17.1	22.15	0.83
	9	17.35	0.85	248	17.0	23.04	0.75
	10	20.02	-	1	17.1	22.15	-
	11	10.19	0.50	3,039,000	16.6	21.48	0.47
	12	20.42**	1.0	1	16.9	22.02	-
				Design	17.9	23.17	

Note: 1 mm = 0.039 in
1 kN = 0.225 kip

** Assumed static strength P_s

where P'_s is the punching load, and d is the slab effective depth in mm. The effective depths of panels were determined by averaging the effective depths measured at a number of points in each panel after the completion of testing. Table 3 shows average effective depths, static punching loads obtained from use of the Equation 1, and the resultant ratios P_f/P'_s of maximum fatigue load to the estimated static punching load. Panel No. 2 of bridge No. 1 and Panel No. 11 of bridge No. 2 did not fail under fatigue loading.

In Figure 5 the ratio of the maximum load to the estimated static punching load is plotted against the number of cycles to failure, while Figure 6 is a semi-log plot of the test results. The second order 'line of best fit' shown in Figure 6 was determined using the method of least squares and has the equation:

$$\frac{P_f}{P'_s} = 1.0 - 0.102N + 0.006N^2 \qquad (2)$$

where N is the log. of the number of cycles to failure. The static test point $P_f/P'_s = 1.0$ was weighted in the least squares analysis. The load ratio is equivalent to the stress ratio S, thus Equation 2 also defines the S-N curve for orthotropically reinforced panels.

The results of tests with and without dead load compensation are indicated in Figures 5 and 6. It appears that the panels without dead load compensation gave slightly higher fatigue strength than the others. However, the scatter of the results is no more than is to be expected in fatigue studies of reinforced concrete structures; and it is unlikely that the lack of dead load compensation could have a significant effect on the fatigue behaviour of the slabs.

FIGURE 5: LOAD RATIO VERSUS NUMBER OF CYCLES TO FAILURE FOR ORTHOTROPICALLY REINFORCED PANELS.

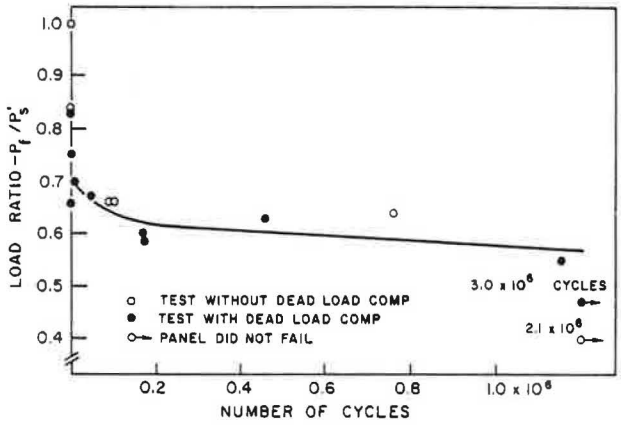

Figures 5 and 6 indicate that the endurance limit of orthotropically reinforced panels is at least 50 percent of the static ultimate load. The static tests suggest that a 1/8th scale model of a panel of design dimensions has a static strength of 23.17 kN (5.21 kips). If an endurance limit of $0.5P'_s$ is adopted, the strength of a panel of design dimensions when subjected to fatigue loading can be assumed to be 11.56 kN (2.60 kips). If a prototype design wheel loads of 71.16 kN (16 kips) is assumed, the corresponding model design wheel load is 1112 N (250 lbs) and so the factor of safety against punching failure in fatigue is approximately 10. If a prototype design wheel load of 71 kN (16 kips) and an impact factor of 0.3 are assumed, the factor of safety is approximately 8. Clearly, conventional orthotropic bridge deck design is very conservative and can be expected to have indefinite life when subjected to repeated loads up to the design wheel

FIGURE 6: LOAD RATIO VERSUS LOG OF NUMBER OF CYCLES TO FAILURE FOR ORTHOTROPICALLY REINFORCED PANELS.

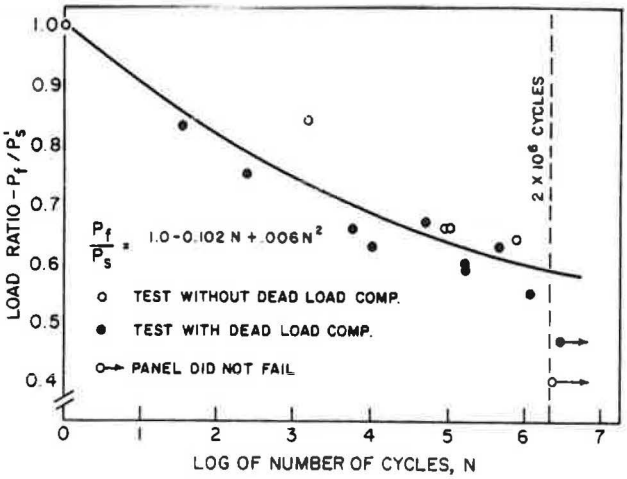

loads.

Tests of Panels with Isotropic Reinforcement

The results of the tests of panels with isotropic reinforcement are given in Tables 4 and 5. Table 4 shows the results of tests of plain concrete panels and of panels with top and bottom reinforcement. Table 5 shows the results of tests of panels with mid-depth reinforcement. In each case, either the effective depth or the thickness of the slab is given, so that the possible errors in the experimental load ratios can be assessed.

There are not sufficient results to permit a reliable correction of load ratios with variation in slab thickness for any slab panels except those with 0.2 percent reinforcement. This is the amount of isotropic reinforcement recommended in Project Q50 (3,4) for the type of bridge slabs under consideration. The following equation was proposed for calculating static ultimate strength (P_s') of panels with 0.2 percent isotropic reinforcement:

$$P_s' = -51.650 + 92.674d \text{ (kN)} \qquad (3)$$

The ratios of maximum fatigue load to the estimated static load P_f/P_s' for panels with 0.2 percent isotropic reinforcement are shown bracketed in Table 4. It can be seen that there was little variation in the effective depths of these panels, therefore correction would not have significantly affected the experimental load ratios.

Table 4 indicates that the endurance limit appears to increase with the reinforcement percentage, and for panels with 0.4 and 0.6 percent reinforcement an endurance limit of 0.5, i.e. the same as that for orthotropically reinforced panels, could be adopted. However, with the very high factors of safety against static punching failure in mind, the tests of the panels with lower reinforcement percentages are of particular interest. Consequently, allowing for the scatter of the test results and errors in the experimental load ratios, it is recommended that an endurance limit of 0.4 be accepted. Thus, a fatigue load factor of 2.5 may be adopted. This value appears adequate for unreinforced panels and for panels with 0.2 percent top and bottom isotropic reinforcement.

On the basis of ultimate strength and shrinkage and temperature reinforcement requirements, 0.2 percent isotropic reinforcement has been recommended (3,4) as the minimum reinforcement for the deck slabs of composite steel/concrete bridges. The static tests of panels with 0.2 percent reinforcement have indicated that a 1/8th scale model of a panel of design dimensions has a static strength of 13.66 kN (3.07 kips). If an endurance limit of 0.4 is adopted, the strength of a panel of design dimensions when subjected to fatigue loading can be assumed to be 5.47 kN (1.23 kips). Thus, if a prototype design wheel load of 71 kN (16 kips) is assumed, the factor of safety against punching failure in fatigue is approximately 5 for a life of at least 2,000,000 cycles. If a design wheel load of 71 kN (16 kips) and an impact factor of 0.3 are assumed, the factor of safety is approximately 4, assuming a load scale factor of 64 for the 1/8th scale models.

Table 5 shows that increase of mid-depth reinforcement did not significantly increase either the static strength or the endurance limit of a panel, although the static strengths of panels with mid-depth reinforcement were higher than those of panels without reinforcement. An endurance limit of 0.4 also appears adequate for panels with mid-depth reinforcement.

Panel 9 of bridge number 5, which has been left unreinforced, was subjected to over 6,000,000 cycles of fatigue loading. The maximum fatigue load was progressively increased until failure occurred. The results of this test are given in Table 6. Noting the maximum fatigue loads expressed as multiples of the scaled design wheel load, and the accumulated cycles of loading, it is clear that in practical situations fatigue failure of composite bridge deck panels of the types studied is extremely unlikely.

Reserve Static Strengths

Any panels that did not fail under fatigue loading were statically tested to determine the panel reserve static strength P_r. Details of the fatigue tests and the reserve strengths of these slabs are given in Table 7. Again the ratios of reserve strength to static strength, i.e. P_r/P_s, can only be considered to be approximate because of probable errors in the assumed static strengths. However, it can be seen that, generally, there was little loss of strength of a panel after it had withstood 2,000,000 or more cycles of fatigue loading. This suggests that if failure under the same load has not occurred in less than 2,000,000 cycles, then fatigue life under the same load function is likely to be infinite. In all cases the maximum fatigue load was well in excess of the scaled design wheel load of 1112 N (250 lb).

Conclusions and Recommendations for Design

Deck slabs of steel/concrete composite bridges have large reserves of strength against fatigue failure. The endurance limit for conventionally reinforced slabs can be assumed to be 0.5. The endurance limit for slabs with less reinforcement than that in conventional slabs can be assumed to be 0.4. This holds for even unreinforced slabs.

On the basis of ultimate strength and shrinkage and temperature requirements, 0.2 percent isotropic reinforcement has been

Table 4. Results of tests of panels with top and bottom isotropic reinforcement

Nominal percentage reinforcement (p)	Bridge no.	Panel no.	Maximum fatigue load P_f (kN)	$\frac{P_f}{P_s}$	No. of cycles to failure	d (mm)	t (mm)	Mode of failure P-Punching F-Flexural
Zero	3	7	6.67	0.51	2,000,000*	-	22.1	-
		8	8.01	0.61	1,326,000	-	22.7	P
		9	13.08**	1.0	1	-	22.8	P
	4	4	11.56**	1.0	1	-	21.4	F
		5	8.10	0.70	17,740	-	22.5	P
		6	6.94	0.60	2,029,240*	-	20.9	-
	5	7	6.09	0.50	682,940	-	21.4	F
		8	12.19**	1.0	1	-	20.9	P
		9	2.67	0.22	2,490,000*	-	21.2	-
0.2	3	5	7.78	0.50 (0.44)	2,000,000*	19.1	-	-
		6	15.57**	1.0	1	19.2	-	P
	4	10	13.92**	1.0	1	18.0	-	F
		11	9.74	0.70 (0.70)	244,580	17.9	-	F
		12	8.36	0.60 (0.60)	235,840	17.9	-	F
0.4	3	1	8.67	0.50	2,155,660*	20.0	-	-
		2	10.41	0.60	3,260	20.6	-	P
		3	17.35**	1.0	1	20.4	-	P
	4	1	8.90	0.50	2,000,000*	17.4	-	-
		2	12.45	0.70	266,000	18.2	-	P
		3	17.75**	1.0	1	18.1	-	P
0.6	3	10	22.24**	1.0	1	20.1	-	P
		11	11.12	0.50	2,000,000*	20.0	-	-
		12	13.34	0.60	425,450	20.0	-	P
					Design	17.9	22.2	

Note: 1 mm = 0.039 in
1 kN = 0.225 kip

* Did not fail under fatigue loading
** Assumed static strength (P_s)

Table 5. Results of tests of panels with mid-depth isotropic reinforcement

Reinforcement spacing (mm)	Bridge no.	Panel no.	Maximum fatigue load P_f (kN)*	$\frac{P_f}{P_s}$	No. of cycles to failure	t (mm)	Mode of failure P-Punching F-Flexure
76	5	4	10.81	0.60	77,020	21.7	P
		5	18.01**	1.0	1	21.4	P
		6	9.03	0.50	822,250	21.9	F
51	4	7	11.83	0.70	45,030	21.6	P
		8	10.14	0.60	453,338	21.7	P
		9	16.90**	1.0	1	22.0	P
25	5	1	9.34	0.50	507,150	21.4	F
		2	18.68**	1.0	1	21.7	P
	5	10	7.12	0.40	2,000,000*	21.9	-
		11	17.79**	1.0	1	21.5	P
		12	8.90	0.50	817,420	21.3	F
					Design	22.2	

Note: 1 mm = 0.039 in
1 kN = 0.225 kip

* Did not fail under fatigue loading
** Assumed static strength P_s

Table 6. Fatigue test of panel no. 9 of bridge no. 5 (zero reinforcement)

Maximum fatigue load P_f (kN)	$\frac{P_f}{P_s}$	Multiples of design wheel load	No. of cycles at load level	Total no. of cycles	Comments
2.67	0.22	2.4	2,490,000	2,490,000	
3.27	0.27	2.9	1,999,940	4,489,940	
3.87	0.32	3.5	550,000	5,039,940	
4.94	0.40	4.4	1,070,000	6,109,940	
6.09	0.50	5.5	240,000	6,349,940	Failure

Table 7. Reserve strengths of slabs

Reinforcement	Bridge no.	Panel no.	$\frac{P_f}{P_s}$	No. of cycles of loading	Reserve static strength P_r (kN)	$\frac{P_r}{P_s}$
Orthotropic						
	1	2	0.39	2,050,000	22.24	0.95
	2	11	0.50	3,040,000	17.79	0.87
Isotropic						
None	3	7	0.51	2,000,000	14.06	1.07
	4	6	0.60	2,030,000	12.85	1.11
0.2%	3	5	0.50	2,000,000	13.12	0.84
0.4%	3	1	0.50	2,160,000	18.33	1.06
	4	1	0.50	2,000,000	12.85	0.72
0.6%	3	11	0.50	2,000,000	21.93	0.99
Mid-Depth						
25.4 mm	5	10	0.40	2,000,000	17.79	1.00

Note: 1 mm = 0.039 in
1 kN = 0.225 kip

recommended as the minimum amount required. The fatigue tests have confirmed that this is adequate and that considerable strength against fatigue failure is ensured by such reinforcement, together with the inherent slab boundary restraint due to the composite bridge substructure of beams, diaphragms and shear connectors. An endurance limit of 0.4, and therefore a fatigue load factor of 2.5, should be adopted in design with this type of reinforcement.

Although mid-depth reinforcement offers the advantage of maximum cover, adoption of this type of reinforcement is not recommended since it does not satisfy the conventional temperature and shrinkage reinforcement requirements. However, if mid-depth reinforcement is used, then, for ultimate strength determination, the slab should be assumed to be unreinforced and an endurance limit of 0.4 and a fatigue load factor of 2.5 can be adopted.

Acknowledgements

The study reported herein was initiated and sponsored under the Ontario Joint Transportation and Communications Research Program by the Ministry of Transportation and Communications.

References

1. G.M. Nordby. Fatigue of Concrete - A Review of Research. Proceedings of the American Concrete Institute, Vol. 55, August 1958, pp. 191-215.
2. C.Y. Loo. The Behaviour of Reinforced Concrete Slabs Subjected to Concentrated Loads Repeated Many Times. M.Sc. Thesis, Queen's University, Kingston, Ontario, 1968.
3. B. deV. Batchelor and B.E. Hewitt. An Investigation of the Ultimate Strength of Deck Slabs of Composite Steel/Concrete Bridges. Research Report Ministry of Transportation and Communications, Downsview, Ontario, Canada,1976.
4. B.E. Hewitt. An Investigation of the Punching Strength of Restrained Slabs with Particular Reference to the Deck Slabs of Composite I-Beam Bridges. Ph.D. Thesis, Queen's University, Kingston, Ontario, 1972.
5. B. deV. Batchelor and B.E. Hewitt. Direct Model Studies of Some Reinforced Concrete Structures. Proceedings of the First Australian Conference on Structural Models, University of Sydney, 1972.
6. E.B. Dixon. Fatigue Behaviour in Slabs of a Composite Steel/Concrete Bridge. M.Sc. Report, Queen's University, Kingston, Ontario, 1970.
7. American Association of State Highway Officials. Standard Specifications for Highway Bridges. (10th edition), 1969.

Notation

d	effective depth of concrete slab, mm
f'_c	concrete compressive strength, MPa
f_t	concrete tensile strength, MPa
P_f	maximum load of fatigue load function, kN
P_r	reserve static strength, kN
P_s	assumed static strength, kN
P'_s	estimated static strength, kN
p	percentage of reinforcement
N	log. of number of cycles
S	stress ratio
t	slab thickness, mm

INVESTIGATION OF THE ULTIMATE STRENGTH OF DECK SLABS OF COMPOSITE STEEL/CONCRETE BRIDGES

Barrington deV. Batchelor, Queen's University, Ontario
Brian E. Hewitt, Public Works Dept., Western Australia
P. Csagoly, and M. Holowka, Ontario Ministry of Transportation and Communications

A theoretical and experimental study of the ultimate strength of the deck slab of composite I-beam bridges is summarized. A theory, based on a mechanical model proposed by Kinnunen and Nylander, for punching failure of simply supported slabs, is developed which permits the calculation of the punching strength of restrained slabs. The theory suggests that a deck slab can be expected to have a high inherent strength due to boundary restraints ensured by the presence of shear connectors, beams, diaphragms and the neighbouring slab areas. One-eighth scale direct models of a 24.4 m (80 ft) span prototype bridge were tested in laboratory studies of both orthotropically and isotropically reinforced slabs. Shear connector behaviour and dead load stresses appropriate to unshored construction were simulated. The results of the tests show that conventionally reinforced deck slabs have very high factors of safety against failure by punching and are wastefully reinforced. From considerations of ultimate strength as well as shrinkage and temperature reinforcement requirements, 0.2 per cent isotropic reinforcement is recommended as being adequate for bridge slabs of the type studied. Although this amounts to approximately 30 per cent of the current reinforcement requirements for such slabs, a high factor of safety can still be expected.

Background

The research described in this paper was undertaken to investigate the ultimate strength of the concrete deck slabs of composite steel/concrete bridges under concentrated loads. It was considered that the inherent restraint of slabs of structures of this form could result in enhancement of load carrying capacity, and if this were considered in design, the reinforcement of the slab could be reduced. This report is a summary of an extensive investigation carried out at Queen's University (1).

It is current practice (2,3) to design the deck slab of a composite bridge by assuming a wheel load to be distributed over transverse slab strips of unit width, that are perpendicular to the direction of the traffic. After approximating the maximum moments to be resisted, the slab strips are designed as if they were concrete beams. It is understood that slabs designed in this manner can be regarded as being safe against shear type failures.

An investigation (1,4) sponsored by the Ontario Ministry of Transportation and Communications, has confirmed that the conventional design of deck slabs of composite bridges is very conservative, and that even with considerable reduction of the slab reinforcement, satisfactory factors of safety against failure by punching can be anticipated. Similar high strengths for restrained slabs have been noted by researchers including Taylor and Hayes (5) and Batchelor and Tong (6).

It is shown in this report that, by considering the mechanism of failure and following an ultimate strength method of design rather than an elastic approach, an adequate and more economical slab design can be achieved.

Outline of Theory

The idealized model of failure proposed by Kinnunen and Nylander (7) has been proven to give a good estimate of the punching strength of simply supported slabs (1). The punching shear strength of restrained slabs has been investigated (1,4) by modifying Kinnunen and Nylander's theory to incorporate a boundary restraining force, F_b, and a boundary restraining moment, M_b. Both F_b and M_b are per unit length of slab, and act at the level of the tensile reinforcement at the boundary. The idealized mechanical model adopted for a restrained slab at punching failure is shown in Figure 1.

In Fig. 1, the outer portion of the slab, which is bounded by the shear crack and by radial cracks, is considered to be loaded through a compressed conical shell that develops from the perimeter of the loaded area to the root of the shear crack. The conical shell is assumed to have the shape shown in Figure 1a, and its thickness is assumed to vary in such a manner that the

compressive stresses at the intersection with the column and at the root of the shear crack are approximately equal.

The sector element shown in Figure 1b is acted upon by the external load $P\beta/2\pi$ and by the following forces which are caused by rotation:

1. The oblique compression force $T\beta/2\pi$ in the compressed conical shell.
2. Horizontal forces in the reinforcement at right angles to the radial cracks, with resultants R_1.
3. Horizontal forces in the reinforcement crossing the shear crack, with resultants R_2.
4. Horizontal tangential compressive forces in the concrete, with resultants R_3.
5. The boundary restraints F_b and M_b acting at the level of the tensile reinforcement at the boundary.

Figure 1. Mechanical model of a slab with boundary restraints at punching failure.

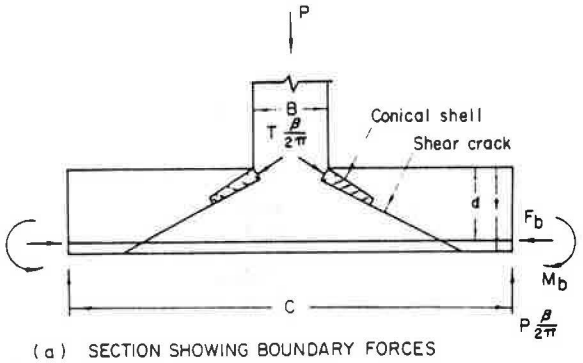

(a) SECTION SHOWING BOUNDARY FORCES

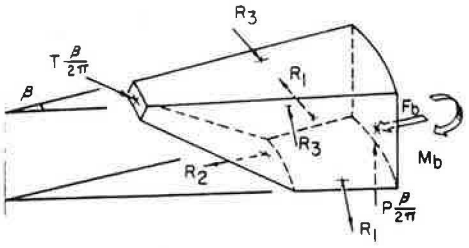

(b) SECTOR ELEMENT SHOWING SLAB FORCES

The criterion of failure is that punching occurs when the tangential strain at the top surface of the slab in the vicinity of the root of the shear crack reaches a critical value. By considering the equilibrium of the sector element and adopting an empirical criterion of failure used by Kinnunen and Nylander, the theoretical punching load, P, can be determined in an iterative process using a computer program (1) developed for this purpose. This theoretical punching load can then be corrected for the dowel effect to give the ultimate punching load, V, of the restrained slab.

During the analysis of reported shear tests, it became apparent that the theory of Kinnunen and Nylander was unreliable for estimating the punching shear strengths of slabs of extreme dimensions and material properties. It was found that, for slabs with any of the parameter functions outside the following limits, the theory generally gave inaccurate estimates of the punching load or because of limited test results, the theory could not be verified. These limits are:

Parameter function	Limits
C/d	4 - 17
q	0.05 - 0.45
E_{steel}	186 - 228 GPa (27×10^6 - 33×10^6 psi)
γ	4 - 20

The equations used in computing the theoretical punching load have been derived and presented in Reference (4).

Influence of Boundary Restraints

A hypothetical slab was analysed in order to demonstrate the influence of variations of the boundary restraint on the punching load of a restrained slab. The assumed dimensions and properties of the slab were as follows:

Slab thickness (t)	178 mm (7 in.)
Slab effective depth (d)	140 mm (5.5 in.)
Diameter of the loaded area (B)	305 mm (12 in.)
Slab diameter (C)	1.83 m (72 in.)
Reinforcement Ratio (p)	1.0 per cent
Yield stress of reinforcement (f_{sy})	310 MPa (45 ksi)
Compressive strength of concrete (f'_c)	34.5 MPa (5.0 ksi)

The boundary force was varied from 0 to 1400 kN/m (0 to 8,000 lb/in.), and the boundary moment from 0 to 53.3 kN.m/m (0 to 12,000 lb.in/in). The theoretical punching load is plotted against the boundary force in Figure 2 for various boundary moments. The theory evidently suggests that considerable increase of the punching shear strength of a slab can result from boundary restraining forces.

Few punching tests of restrained slabs have been reported in which the magnitudes of the restraining forces were known or could be inferred. However, tests of prestressed concrete slabs by Scordelis, Lin and May (8) have permitted a limited investigation of the accuracy of the punching load calculated using the theory proposed for restrained slabs. Seven prestressed concrete slabs were analysed assuming the prestressing cable forces to be boundary restraining forces acting in the plane of the slab. Estimates of the dowel and tensile membrane effects were made for each slab and the influence of the unbonded prestressing cables was considered. The ratio of the test load to the calculated load was found to

Figure 2. Variation of theoretical punching load with edge restraints.

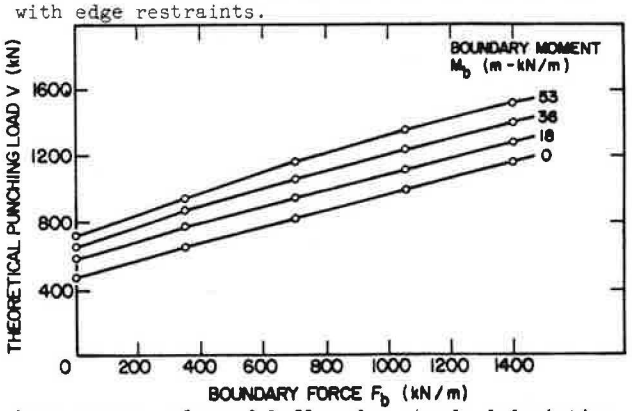

have a mean value of 1.01 and a standard deviation of 0.044. Considering the assumptions made in estimating the dowel and tensile membrane effects

and in assessing the influence of the unbonded prestressing cables, the calculated punching loads were remarkably consistent and accurate. Using an empirical approach, Scordelis, Lin and May obtained ratios with a mean value of 1.02 and a standard deviation of 0.075. A more in-depth comparison is given in Reference (4). Additional comparisons of tests by others are provided in Reference 1.

Restraint Factor

In practical situations the boundary restraining forces on a slab loaded to punching failure are usually not known and would be difficult to calculate or to measure accurately. In a slab such as the deck slab of a composite bridge, the difficulty is further increased by the likelihood of varying support and boundary restraint conditions at adjacent boundaries. For these reasons a single factor, F_r, to be termed the 'restraint factor', is proposed which expresses the slab strength enhancement due to practical boundary conditions. This factor can be used for the calculation of the punching load of restrained slabs by means of the largely rational approach already described, though it must be noted that the factor is itself empirical.

The idealized geometry of displacement of a slab at failure, as used by Brotchie and Holley (9), and the resultant maximum boundary stresses and forces are given in Fig. 3. The maximum force, T_b, per unit length of the boundary in the tensile reinforcement at the boundary is given by:

$$T_b = d\ p\ f_{sy} \qquad (1)$$

Figure 3. Idealised displacement and maximum boundary forces for a restraint slab.

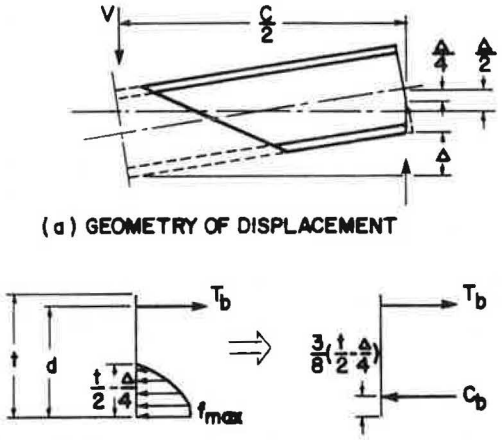

T_b is zero if reinforcement is absent or discontinuous at the boundary. The maximum compressive force, C_b, in the concrete per unit length of the boundary is given by:

$$C_b = k\ f_{max}\ \left(\frac{t}{2} - \frac{\Delta}{4}\right) \qquad (2)$$

in which k is the ratio of the average stress to the maximum stress and depends on the stress distribution.

If a parabolic distribution of stress is assumed, then k is 2/3 and f_{max} is assumed to be 0.85 f'_c. The idealized maximum boundary restraints are then given by:

$$M_{b(max)} = T_b(2d - t) - C_b\left(d - \frac{13}{16}t - \frac{3}{32}\Delta\right) \qquad (3)$$

and

$$F_{b(max)} = C_b - T_b \qquad (4)$$

A value of $F_r \leq 1.0$ was introduced to take account of the fact that the maximum boundary restraints would rarely be attained at failure. The actual boundary restraints at failure by punching are then given by:

$$M_b = F_r\ M_{b(max)} \qquad (5)$$

and

$$F_b = F_r\ F_{b(max)} \qquad (6)$$

It is not implied that the distribution of stress at the boundaries and the actual boundary restraints at the instant of punching are known. It is a fact, however, that F_r varies from zero for the simply supported slabs usually tested in investigations of punching, to unity for slabs with a full edge restraint, therefore, F_r must lie between 0 and 1 for all practical cases of restrained slabs. The restraint factor will depend on the properties of the slab as well as on the confining structure and can be determined empirically for a particular slab system.

After calculation of $M_{b(max)}$ and $F_{b(max)}$, F_r can be determined for any type of restrained slab for which the punching load is known. The lower limit of this factor can then be used in determining punching loads for design purposes. The values of $M_{b(max)}$ and $F_{b(max)}$ are dependent upon the deflection, Δ, and consequently must be calculated iteratively. A computer program has been developed (1) which calculates the punching load of restrained slabs for values of F_r varying from zero to unity in steps of 0.25.

Influence of Restraint Factor

The typical slab previously described was analysed in order to demonstrate the influence of the restraint factor on the punching load of a slab. The calculated punching load is plotted against the restraint factor in Fig. 4. The boundary moment and force for each restraint factor are also given. By varying the restraint factor from 0 to 1, the calculated punching load increases through the full range of feasible punching loads even though actual values of the boundary moment and force are not necessarily used.

If the punching load of a restrained slab is known, the restraint factor can be determined by interpolation after calculating the punching load for given values of the restraint factor. Slabs tested by Taylor and Hayes (5), Aoki and Seki (10) and others have been investigated in this way. It was found that the restraint factor of a slab with no tension reinforcement at the boundary generally decreases as the reinforcement index, q, ($= pf_{sy}/f'_c$) increases. As a rule, with all variables constant except the reinforcing ratio,

Figure 4. Variation of theoretical punching load with restraint factor.

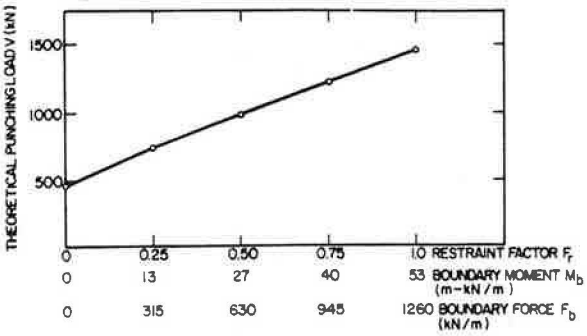

a slab with low reinforcement ratio will have deflected more at failure than one having a high reinforcement ratio. Consequently, the boundary restraining forces, which are dependent upon the slab deflection, are likely to be nearer their maximum values in the restrained slab with the lower reinforcing ratio, and would therefore have the higher restraint factor. Although there were limited available test results, the following can be tentatively suggested to apply to slabs with this form of restraint.

$$\text{For } \frac{C}{B} \leq 6.0 \text{ and } q = 0.1, \; F_r = 0.50,$$

and

$$\text{For } 6.0 \leq \frac{C}{B} \leq 9.0 \text{ and } q = 0.2, \; F_r = 0.25$$

Tests and Observations

The behaviour of I-beam bridge slabs was investigated by testing a total of nine 1/8th scale direct models of 24.4 m (80 ft) span four-beam and three-beam bridges. Apart from the usual difficulties of small scale modelling, particular problems arose in the accurate modelling of all section properties, stud shear connector behaviour and dead load stresses appropriate to unshored construction. The solutions to these problems are described in detail elsewhere (1,11). The four-beam prototype and model bridges are detailed in Figure 5. A view of a four-beam model bridge superstructure is given in Figure 6. The three-beam model was similar to the four-beam model except that the beam spacing

Figure 5. Details of prototype four-girder bridges

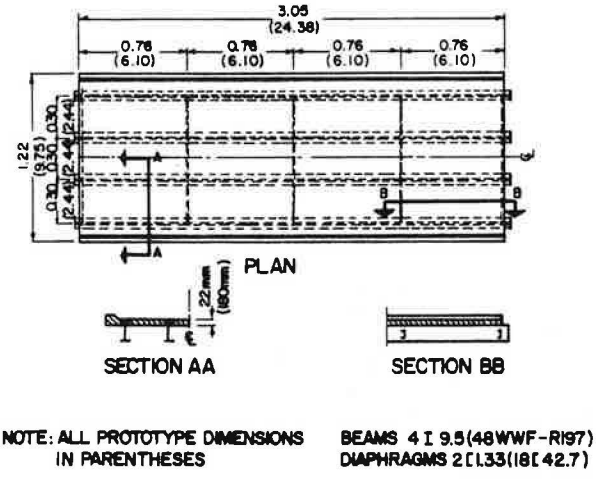

Figure 6. View of four-beam model

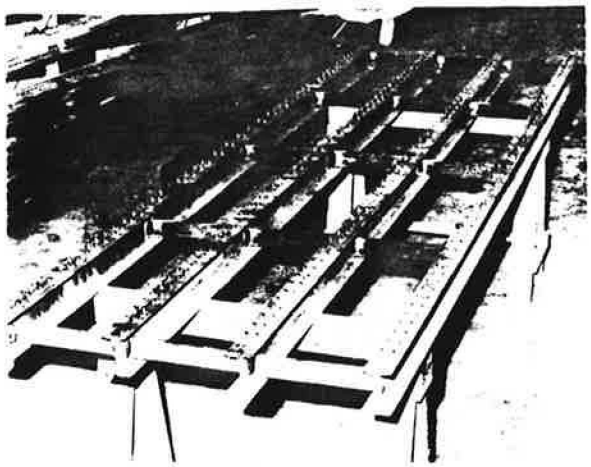

was 460 mm (18 in.) and the beams were supplemented with bottom flange plates.

The deck slabs of the bridges were tested to failure under single concentrated loads applied mid-way between adjacent bridge beams through a steel plate bearing on a neoprene pad. The contact area modelled an ellipse with major and minor axes of 760 mm (30 in.) and 510 mm (20 in.), respectively, which represents the assumed contact area of the pneumatic tires of large earth moving equipment. A view of a model bridge and the testing arrangement is given in Figure 7.

Deck slabs with orthotropic and with isotropic reinforcement, as well as plain concrete slabs, were tested. The orthotropic reinforcement modelled the reinforcement of conventional deck slabs. Slabs with isotropic reinforcement at mid-depth of the slab, and therefore with maximum cover, were also tested. The influences of slab span and thickness, load position, dead load stresses, reinforcement ratio, and concrete strength on the ultimate strength of the deck slabs were studied, together with the punching strength in a hogging moment region.

The model bridges tested are numbered 1 to 9. A bridge panel is defined as that portion of the deck bounded by adjacent bridge beams and adjacent diaphragms, and panels across a bridge are referred to collectively as strips. The bridges and the tests are described generally in Table 1. Bridges numbered 1 to 8 were four-beam bridges, bridge No. 9 was a three-beam bridge.

A total of 68 tests to failure were carried out. All but one of the reinforced panels and some of the unreinforced panels failed by punching. Failure by punching usually left a neat elliptical hole, a little larger than the loaded area, in the top of the slab and a pushed-through plug of concrete in the form of a frustum of a cone with an approximately circular base. The cracking patterns were similar for the slabs of the four-beam and three-beam bridges.

As the load was applied, visible cracking in the form of longitudinal and diagonal cracks was observed on the underside of the slab. This occurred directly beneath the loaded area and usually commenced at a load of between 25 and 50 percent of the failure load. Subsequently, transverse cracks appeared on the upper-side of the slab on either side of the loaded area in the vicinity of the adjacent bridge beams. As failure approached, the underside cracking developed into a complete pattern of cracks radiating from beneath

Figure 7. View of testing arrangement

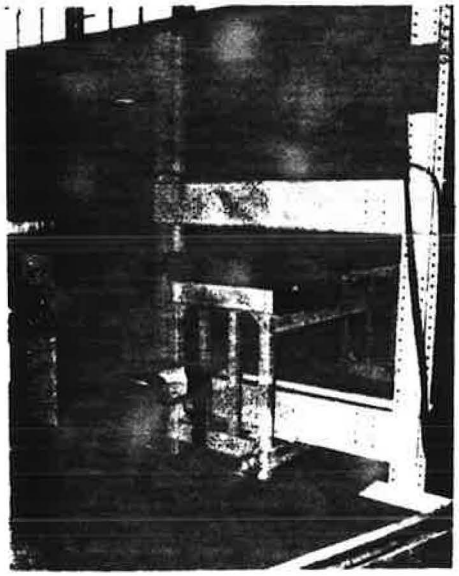

Figure 8. View of cracking pattern at failure of panel with 0.2% reinforcement

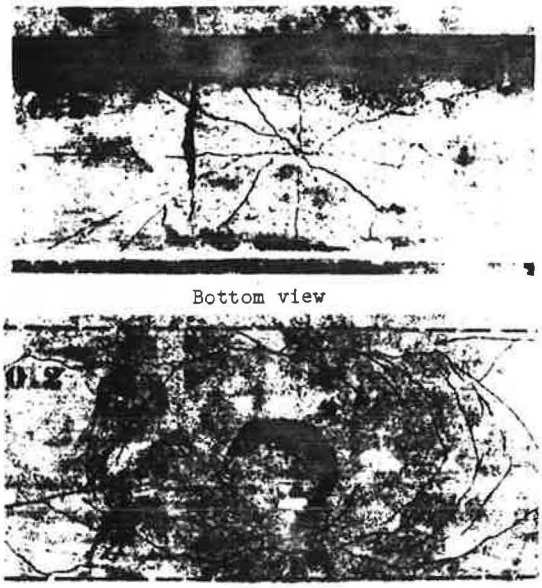

Bottom view

Top view

Table 1. Models constructed

Bridge number	Reinforcement* Strip 1	Strip 2	Strip 3	Strip 4	Special Tests
1	ORT	ORT	ORT	ORT	
2	ORT	ORT	ORT	ORT	Full dead load compensation
3	ORT	ORT	ORT	ORT	Some panels with dead load compensation
4	ORT	ORT	ORT	ORT	Full dead load compensation
5	ORT	zero	0.4%	0.2%	
6	0.6%	0.2%	0.6%	M	Hogging moment in strips 2 and 3
7	0.4%	0.2%	zero	0.6%	
8	0.4%	zero	M	0.2%	
9	0.4%	0.2%	zero	0.6%	

Note: ORT indicates orthotropic reinforcement

0.6, 0.4, 0.2 - is percentage of isotropic reinforcement

M indicates mid-depth isotropic reinforcement

Designation of strips:

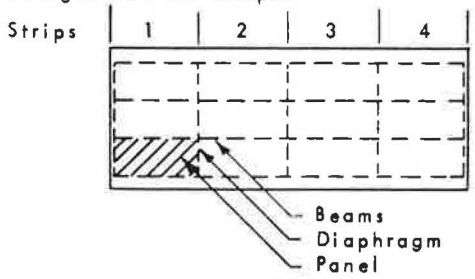

the loaded area, and the upperside longitudinal cracks lengthened and curved around the loaded area. Prior to failure, the cracking pattern indicated imminent flexural failure in an elliptical fan mechanism and never suggested failure by punching. Although accelerated creep usually gave some warning, failure was always explosive. Cracking rarely extended into adjacent panels and, generally, the higher the percentage of reinforcement, the more symmetrical and closely spaced was the cracking. Views of the cracking pattern of a four-beam bridge panel with 0.2 percent isotropic reinforcement after failure by punching, are given in Figure 8.

Some unreinforced panels and one panel with a low percentage of reinforcement failed in flexure in elliptical fan mechanisms. Up to failure the cracking behaviour was similar to that for all other slabs but failure occurred after much creep and with some crushing of the concrete on the upperside of the slabs along lines radiating from the loaded area. The major axis of the fan mechanism was aligned with the major axis of the loaded area, and the cracking pattern was contained within adjacent bridge beams.

Deflection Behaviour

Figure 9 shows typical variations of net slab deflection with load for a four-beam bridge. There was considerable scatter of the net slab deflections for panels of the same design but the tests plotted in Figure 9 were chosen to show the general trend of deflection behaviour. Panels with low percentages of reinforcement failed after relatively large deflections. Panels with 0.6 percent isotropic reinforcement behaved similarly

Figure 9. Typical variations of net slab deflection with load for four beam bridges

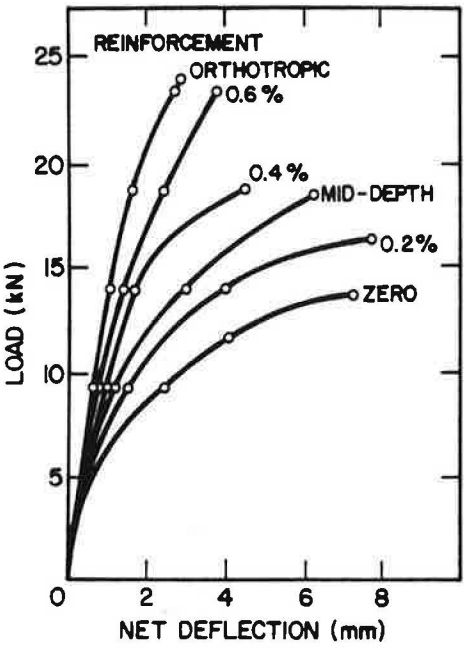

Figure 10. Punching load vs depth to reinforcement-orthotropic reinforcement

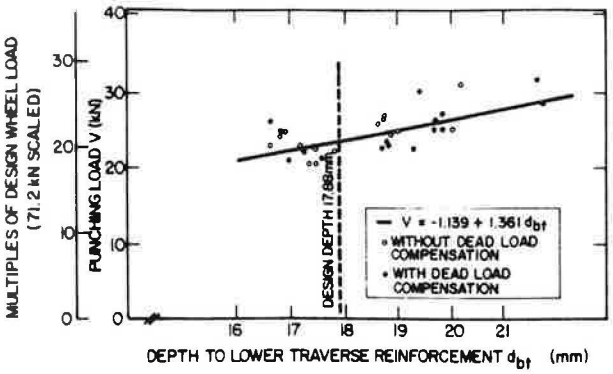

to panels with orthotropic reinforcement and failed after relatively small deflections.

Punching Strength

Slabs with Orthotropic Reinforcement

There was considerable variation of the failure loads for slabs of the same design. A statistical analysis of all the results of tests of orthotropically reinforced panels indicated that the variation of failure load could be attributed to unavoidable variations of the slab dimensions. The analysis showed that the failure load is not significantly influenced by the position of the panel, by previous failures in adjacent panels, and by the strength of the concrete or dead load stresses.

Figure 10 is a plot of test punching load for orthotropically reinforced panels versus effective depth, d_{bt}, to the bottom transverse reinforcement and shows the regression line determined using all results. There was no significant difference between this regression line and those determined using only the results of tests with and without dead load compensation. It should not be inferred that the regression line can necessarily be extrapolated for slabs of properties outside the range of those which have been included in the analysis. The scale of multiples of design wheel load shows that the factor of safety against failure by punching, ignoring impact, was never less than 17.

The punching load for a slab of design dimensions determined using the regression line, is 23.2 kN (5.21 kips). If a design wheel load of 71.2 kN (16 kips) is assumed, the factor of safety against punching is approximately 21. If a design wheel load of 71.2 kN (16 kips) and an impact factor of 0.3 are assumed the factor of safety is approximately 16. The bridge deck design is obviously very conservative.

In a few cases the load was applied at four points simultaneously to simulate a truck with wheels 1.83 m (6 ft) apart on axles 4.3 m (14 ft) apart. By measuring the extreme bottom fibre strains of the bridge beams it was shown that for a conventional I-beam bridge under truck loading, beam failure is to be expected well before slab failure. This is further indication that the bridge deck slab design is conservative.

Slabs with Isotropic Reinforcement

The average test punching loads for each nominal percentage of reinforcement and for panels of both four-beam and three-beam bridges are shown plotted against average reinforcement percentage in Figure 11. The average reinforcement percentages were calculated using the means of all

the measured effective depths of panels with the respective nominal reinforcement. Both flexural and punching failures occurred in four-beam bridge panels with 0.2 percent and with zero reinforcement, and it was assumed that flexural and punching strengths were the same for these panels. Only flexural failures, at an average load of 9.43 kN (2.12 kips), occurred in the unreinforced panels of the three-beam bridge and results of the tests of these panels were excluded from the analysis.

Figure 11 shows that the punching strength increases with increase of reinforcement and with decrease of span to thickness ratio (C/t). The scale of multiples of design wheel loads indicates that the factor of safety is always high, even when the span to depth ratio is unusually large, and that the factor of safety for a panel of a bridge of conventional dimensions would be approximately 13, if impact is ignored. There was some scatter of the test results but the factor of safety for unreinforced panels of four-beam bridges was never less than 10.

In the usual elastic design only the strength due to reinforcement is considered. Only in an ultimate strength design can both the strength due to the reinforcement and the very significant additive inherent strength of the unreinforced panel be utilised.

In tests on a model bridge in which hogging moment was induced, it was shown that such a moment has little, if any, effect on the punching load. It became apparent that extensive transverse cracking can be tolerated before any decrease in the punching strength of the bridge deck is to be anticipated.

The restraint factors for panels of the four-beam and three-beam bridges are given in Table 2. The theory was not considered to be applicable to the unreinforced panels of the three-beam bridges, which all failed in flexure, or to the panels with mid-depth reinforcement. The restraint factors here quantify the actual boundary restraints of the panels in terms of the idealized maximum restraints on the boundaries of the idealized equivalent slabs. It is seen that the restraint factors generally increase with increase of percentage reinforcement. This is contrary to

Figure 11. Load vs reinforcement percentage - isotropic reinforcement

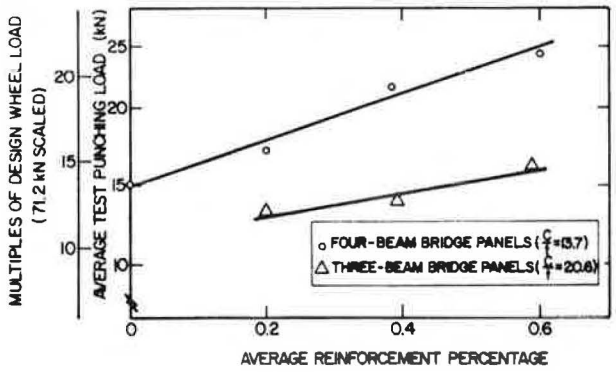

the findings from the analysis of the tests of Taylor and Hayes (5) and Aoki and Seki (10) discussed previously, and is thought to be due largely to the fact that in bridge panels the top reinforcement may also contribute to the boundary restraint.

However, noting the reinforcing indices (q) and the diameter ratios (C/B) given in Table 2, it is seen that the limits of the restraint factor which have been tentatively proposed, also apply here although the increase of restraint factor with increase of reinforcement is not utilised. With the high factors of safety, slabs with very low percentages of reinforcement are of interest, and for design purposes a restraint factor of 0.50 is proposed for use in the calculation of the ultimate punching strength of the deck slabs of composite I-beam bridges. This would be satisfactory for a slab with a span to thickness ratio as high as 20 and with a reinforcement percentage as low as 0.2.

Design Recommendations

In accordance with the philosophy of the ACI Code, the ultimate strength of a structure is expected to exceed about two and a half times the design live load. The factor of safety against failure by punching of an unreinforced panel of a four-beam bridge, assuming a wheel load of 71.2 kN (16 kips) and an impact factor of 0.3, is approximately 10. The study indicated that cracking under working loads is not a problem and that slab failure is highly unlikely, particularly since the bridge beams would probably fail first under truck loading.

Clearly, if only the punching strength is to be considered, reinforcement is theoretically not required in the deck slab of I-beam bridges. However, the AASHTO Standard Specifications for Highway Bridges (2) recommends that 'not less than 125 in.^{2} (81 mm^2) of reinforcement per foot shall be placed in each direction of all concrete surfaces to resist the formation of temperature and shrinkage cracks'. This amounts to approximately 0.2 percent reinforcement for 178 mm (7.0 in.) slab with 38 mm (1.5 in.) cover, and is here recommended as the maximum reinforcement required for the deck slabs of composite I-beam bridges. Using 0.2 percent isotropic reinforcement rather than the conventional orthotropic reinforcement as in the prototype bridge, the reinforcement requirement is reduced by about 66 percent.

The tests of panels with 0.2 percent reinforcement are therefore of particular interest. The test punching loads of the four-beam bridge panel with 0.2 percent reinforcement are plotted against the measured effective depths to the bottom transverse reinforcement in Figure 12. The line of regression of the punching load on the effective depth is shown. The scale of multiples of design wheel load shows that a slab of design dimensions has a factor of safety of approximately 12. Considering a wheel load of 71.2 kN (16 kips) and an impact factor of 0.3, the factor of safety is greater than 9.

Thus the design of the deck slab of I-beam bridges can be made very simple because only the AASHTO requirements regarding the temperature and shrinkage reinforcement need be satisfied. Assuming a restraint factor of 0.50 the ultimate strength of any slab with a span to depth ratio within the range of 14 to 21 of the tested panels can be estimated. Figure 13 shows a design curve, derived using the outlined theory, which relates punching loads and span to depth ratios of panels with 0.2 percent reinforcement. The punching loads were calculated assuming slabs of the following dimensions and properties:

Slab thickness	178 mm (7 in.)
Slab effective depth	127 mm (5 in.)
Diameter of loaded area	650 mm (25.6 in.)
Slab diameter	2.44 to 3.66 m (96 to 144 in.)

Reinforcement	0.2 percent
Yield stress of reinforcement	310 MPa (45 ksi)
Compressive strength of concrete	34 MPa (5000 psi)
Restraint factor	0.50

Table 2. Restraint factors for panels of four-beam and three-beam bridges

Isotropic Reinforcement (%)	Four-beam Bridge Slabs C/B = 3.7 Number of Tests	q (average)	V_{test} (average) (kN)	Restraint Factor	Three-beam Bridge Slabs C/B = 3.6 Number of Tests	q (average)	V_{test} (average) (kN)	Restraint Factor
0.6	7	0.055	23.66	0.74	2	0.054	16.46	0.59
0.4	5	0.036	21.57	0.66	2	0.036	14.14	0.52
0.2	7	0.018	18.01	0.60	2	0.018	13.48	0.55
zero	3	0	16.50	0.57	2[a]	0	-	-

Note: a) Both slabs failed in flexure
1 kN = 0.225 kip

Figure 12. Punching load vs depth to reinforcement-0.2% isotropic reinforcement

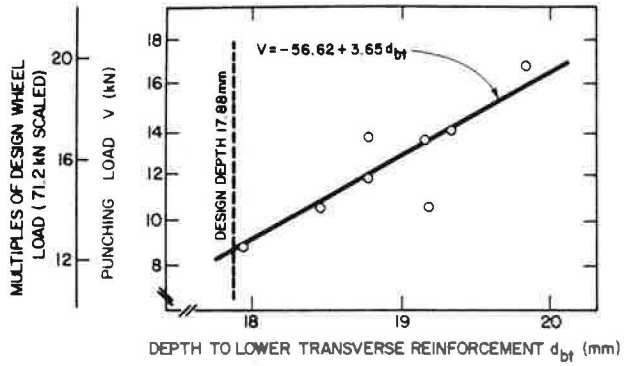

Figure 13. Calculated punching load vs span/thickness ratio with restraint factor of 0.5-0.2% - isotropic reinforcement

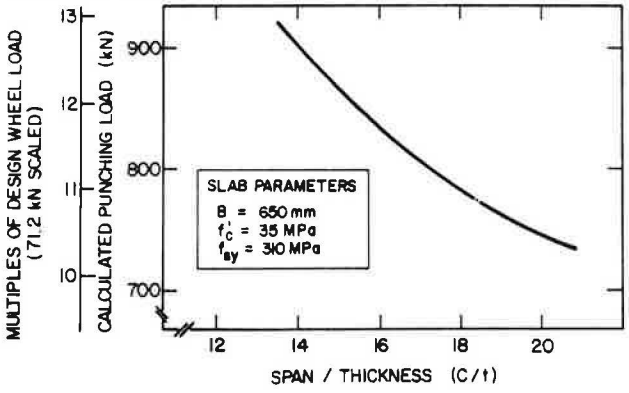

The loaded area was assumed to be circular and of the same perimeter as the assumed elliptical tire contact area. The slab diameter was taken as equal to the bridge beam spacing. The design curve could be used to check the ultimate strength and the factor of safety against failure by punching of any deck slab of comparable dimensions and with the required reinforcement of 0.2 percent.

The preceding discussion does not apply to the exterior cantilevering portions of I-beam bridge deck slabs which should be designed by conventional methods. The discussion applies only to panels with adequate boundary restraint the development of which is ensured by the shear connectors, bridge beams, diaphragms, and by the continuity of the slab itself. According to the AASHTO Specifications, "the maximum pitch of shear connectors shall not exceed 610 mm (24 in.), except over the interior supports of continuous beams where wider spacings may be used to avoid placing connectors at locations of high stresses in the tension flange". The maximum spacing of the shear connectors in the model bridges was 102 mm (4 in.). It follows that theoretically for a prototype bridge, shear connectors at spacings of up to 810 mm (32 in.) provide adequate restraint, and some reduction in the factor of safety for the bridge deck could result from shear connector spacings in excess of 810 mm (32 in.). Diaphragms may need to be provided to prevent spread of the bridge beams due to in-plane forces in the loaded deck slab, and it appears that the AASHTO requirements are adequate. The end edges of the deck slab should always be stiffened.

Mid-depth reinforcement offers the advantage of ensuring maximum reinforcement cover but it does not satisfy the AASHTO requirements regarding temperature and shrinkage reinforcement. If, despite this, mid-depth reinforcement is used to resist the formation of temperature and shrinkage cracks, the ultimate strength of the slab could be conservatively estimated by assuming it to be unreinforced.

Conclusions and Recommendations for Further Research

Conclusions

The mechanical model used by Kinnunen and Nylander (7) can be modified to predict the punching strength of restrained slabs. This factor can be empirically determined for slabs of unknown boundary restraint.

The current method of design of the deck slab of a steel/concrete composite bridge results in the wasteful use of reinforcement. The factor of safety against failure by punching under a single wheel load can be expected to be approximately 16. Under truck loading, beam failure can be anticipated before slab failure. The punching strengths of such slabs vary inversely with span and directly with reinforcement ratio and effective depth.

The punching strength is not influenced significantly by the following factors:

1. The position of the load on the bridge deck slab.
2. Previous failures of the slab in adjacent

panels.

3. A hogging moment.
4. Dead load stresses and deflections.
5. The strength of the concrete of the slab.

It has been shown that, theoretically, no reinforcement is required in the deck slabs of composite I-beam bridges if only the ultimate strength of the designed structure is considered. In view of the AASHTO requirements regarding temperature and shrinkage reinforcement in mind, 0.2 percent isotropic top and bottom reinforcement is recommended as the maximum requirement. This amounts to a reduction of 66 percent of the current reinforcement requirements. For a deck of conventional dimensions with 0.2 percent reinforcement the factor of safety against failure by punching can be expected to be about 9.

A restraint factor of 0.50 should be used for the calculation of the punching strength for design purposes.

References

1. B.E. Hewitt. An Investigation of the Punching Strength of Restrained Slabs with Particular Reference to the Deck Slabs of Composite I-Beam Bridges. Ph.D. thesis, Queen's University, Kingston, Ontario, 1972.
2. American Association of State Highway Officials, Standard Specifications for Highway Bridges, (10th ed.), 1969.
3. Canadian Standards Association. Design of Highway Bridges, CSA Standard S6, 1966.
4. B.E. Hewitt and B. deV. Batchelor. Punching Shear Strength of Restrained Slabs. Journal of the Structural Division, Proceedings of the American Society of Civil Engineers, Vol. 101, No. ST9, 1975.
5. R. Taylor and B. Hayes. Some Tests on the Effect of Edge Restraint on Punching Shear in Reinforced Concrete Slabs. Magazine of Concrete Research, 17, 1965, p. 39.
6. B. deV. Batchelor and P.Y. Tong. An Investigation of the Ultimate Shear Strength of Two-way Continuous Bridge Slabs Subjected to Concentrated Loads. Ontario Ministry of Transportation and Communications, Research Report No. RR167, 1970.
7. S. Kinnunen and H. Nylander. Punching of Concrete Slabs without Shear Reinforcement. Transactions of The Royal Institute of Technology, Stockholm, No. 158, 1960.
8. A.C. Scordelis, T.Y. Lin and H.R. May. Shearing Strength of Prestressed Lift Slabs. Proceedings of the American Concrete Institute, 55, 1958, p. 485.
9. J.F. Brotchie and M.J. Holley. Membrane Action in Slabs. American Concrete Institute Publication SP-30, 1971, pp. 345-377.
10. Y. Aoki and H. Seki. Shearing Strength and Flexural Cracking and Capacity of Two-way Slabs Subjected to Concentrated Load. American Concrete Institute Publication SP-30, 1971, pp. 103-126.
11. B. deV. Batchelor and B.E. Hewitt. Direct Model Studies of Some Reinforced Concrete Structures, Proceedings of the First Australian Conference on Structural Models, University of Sydney, 1972.

THE TRUE BEHAVIOR OF THIN CONCRETE BRIDGE SLABS

P. Csagoly, M. Holowka and R. Dorton, Ontario Ministry of Transportation and Communications

It has been observed that thin concrete deck slabs supported by beams or girders are generally capable of carrying concentrated wheel loads far in excess of design values established by traditional methods of analysis. This capacity appears to be present even if the concrete has considerably deteriorated or a large percentage of the reinforcing steel is lost due to rusting. The usual failure mode is that of punching and not flexure, hence the load-carrying capacity is defined in terms of the former. Under a concentrated wheel load, the present AASHTO Specifications, based on 2-dimensional plate bending theory, overestimate the maximum tensile reinforcing steel stresses by a considerable margin. It has been found that the load-carrying capacity of the slab is governed by internal arching action, rather than by flexural strength. The net result is that a multiple of the absolute minimum reinforcing is being built into thin concrete deck slabs. In the presence of deicing salt, too much steel too close to the wearing surface usually results in extensive spalling of the concrete decks, leading to a marked reduction in service life. This paper covers the results of an extensive prototype investigation. Field testing of existing bridges, both composite and non-composite, deteriorated and not deteriorated, with a 445 kN (1000,000 lb.) simulated wheel load resulted in no permanent damage or upper surface cracking to the slabs. New prototype deck slabs have been built with as little as 0.2% isotropic reinforcement. The test results indicate sufficient capacity for concentrated wheel loads with steel stresses and deflection being at acceptable levels. These research findings are being incorporated into the new Ontario Highway Bridge Design Code.

In the Province of Ontario, as in most North American jurisdictions, the design of thin concrete bridge decks supported by girders and/or beams is based at present on the AASHTO Specifications for Highway Bridges (1). The deck may be designed to act only as the riding surface or, alternatively, it may be considered composite with the supporting components if shear connectors are employed. The beams or girders may be of concrete, prestressed concrete, timber or steel. The geometry of supporting components can be of various types: rectangular, with or without voids, I-shaped, and open or closed box sections.

The fundamental concept behind the AASHTO provisions is that these slabs, subdivided into transverse strips for design convenience, are carrying concentrated wheel loads entirely in flexure. The format of calculations, until 1974, was based on the working stress method. This approach, without altering the fundamental concept, has been recently modified and a load factor method is now used (2). It is also assumed that slabs designed for bending moment in accordance with the AASHTO Specifications can be considered safe regarding bond and shear.

The authors maintain that these concrete slabs are greatly over-designed and that a new design approach should be developed. This type of bridge superstructure is the most common design in Ontario (and also in the United States) and significant savings in construction costs could be anticipated by an improved design method. On the basis of this anticipation, a series of projects sponsored by the Ontario Ministry of Transportation and Communications' Joint Highway Research Program was initiated at Queen's University in Kingston, Ontario, in 1967. The ultimate aim of these projects was to investigate the load-carrying capacity of composite I-beam bridges.

Another recent problem with concrete decks is spalling (3) resulting from reinforcement corrosion due to deicing salts. Corrosion, among other factors, is directly related to the depth of cover over the reinforcement. A more meaningful parameter is the ratio of clear cover to bar diameter (C/D). It is believed that a C/D value of 3.0 can provide reasonably good protection. Reducing the reinforcing steel requirements can mean smaller bar sizes and, consequently, increased concrete cover-to-diameter ratio — thereby improving the durability of exposed concrete bridge decks. A better understanding of their behavior may also lead to increasing the absolute cover without substantially reducing the load-carrying capacity of these slabs.

This paper describes part of the research work conducted by the Ministry to verify and to

implement a revolutionary new method of slab design based on the theoretical model for ultimate load capacity of the slab as developed at Queen's University (4, 5). The physical work included field testing of existing concrete decks and the design and testing of prototype full-scale decks built in accordance with the new theoretical model. In this paper, only the field testing of old, existing bridges is discussed in detail. The effects of using reduced amounts of reinforcement in prototype bridges are reported elsewhere (6, 7). The results confirm the existence of large ultimate capacities of the slabs as predicted by the theoretical model.

Recommendations are given to simplify the design of most concrete decks, to substantially reduce the reinforcing steel requirement and to develop standardization of deck reinforcement.

Background

The initial research conducted at Queen's University indicated that the ultimate strength of concrete deck slabs of composite steel/concrete bridges under concentrated load was about one order higher than predicted by the AASHTO design method. It was also observed that the mode of failure is in punching shear, not flexure, suggesting the presence of considerable membrane forces providing for load-carrying by internal arching.

It was also shown that satisfactory factors of safety against failure by punching can be anticipated even with reduced slab reinforcement as illustrated in Figure 1. It can be seen that the effect of reducing the amount of reinforcement from the customary 1.0 to 0.2% causes a drop of about 20% in the load-carrying capacity at the practical span-to-thickness ratio. It is also evident, that the most important parameter is this ratio. In Appendix A it is shown that stresses, regardless whether related to flexure or internal arching, decrease with the square of the slab thickness.

The ultimate capacity is greatly influenced by the degree of lateral restraints present (Figure 2). These restraints prevent the horizontal movement and rotation of the slab adjacent to the point load by developing forces due to the physical boundary conditions such as massive continuity of slab, bracings, diaphragms, shear connectors and laterally stiff beams. However, this unaccounted-for strength of slabs due to boundary conditions can only be utilized if the designer knows the degree of restraints present.

Since the theoretical model was verified only on small scale models, it was decided to test a number of existing decks in order to determine its applicability for prototypes. Existing decks, generally deteriorated to varying degrees, with variable supporting elements were subsequently load tested.

Objectives

The three main objectives of the field testing of existing decks were as follows:

1. To ensure that no slab failure is caused by a concentrated test load of 445 kN (100 kips). This no-failure criterion for existing deteriorated decks ensures a factor of safety of 5 against the maximum measured wheel loads of 90 kN (20 kips) in Ontario.

2. To determine if different types of slab and girder bridges provide different degrees of confinement or restraint. For example, is there a difference in slab strength, due to restraint factor, between composite and non-composite slabs, or between concrete and steel girders? Consequently, the test bridges chosen were of four categories:

Type	
A	Non-composite steel girder and concrete slab.
B	Composite steel girder and concrete slab.
C	Concrete beam and slab (monolithic).
D	Composite AASHTO girders and concrete slab.

3. To establish the lower bound restraint factors for each category. These factors were to be based on a comparison between the experimental data and the theoretical analysis.

Testing Procedure

Prior to the testing program, a total of 40 bridges were chosen to obtain a wide range of parameters of span, slab thickness, age, deterioration, bridge type and reinforcing. Due to testing difficulties and/or lack of sufficient data regarding the concrete deck and its strength, data from only 32 bridges were examined and included. There were 13 Type A, 9 Type B, 8 Type C, and 2 Type D bridges. These were generally older structures and had deteriorated to varying degrees of disrepair by the time of testing.

The testing apparatus is shown in Figure 3. The test load of 445 kN (100 kips) is hydraulically controlled and applied through the loading apparatus attached to the underside of the trailer. The test vehicle has a weight of 212 kN (47.8 kips) and is loaded with 378 kN (85.0 kips) of concrete blocks for a total load of 490 kN (132.8 kips). The test load is applied, by a hydraulic ram, through two 254 mm (10 in.) square pads with a 76 mm (3 in.) space between them. These loading pads simulate the footprint of a dual tire wheel.

Once the load positions were established, the load was gradually applied and the deflection at the point of load application, as well as the load recorded on an X-Y plotter. The load was monitored by a pressure transducer and the displacement measured by a transducer riding on a 3.7 m (12 ft.) long aluminum bar simply supported at the ends as shown in Figure 3. Accordingly, the measured displacement is based on the assumption that the support points of the bar, being remote from the load position, exhibit insignificant vertical movements. The orientation of the bar was always parallel to the traffic lanes.

Test Results

Figure 4 illustrates a typical test plot of load versus deflection. As can be seen, the test consists of applying the test load in a cyclic manner until the load-vs-deflection plot is repetitive and shows no further progressive permanent deflection upon application of load.

With each test bridge, an attempt was made to obtain concrete cores near the test points. Thereby, the effect of matured strength of the concrete deck due to time could be included in the evaluation of the results. The compressive strength of the various decks varied from 18.6 MPa (2,700 psi) to 75.8 MPa (11,000 psi).

The first objective of ensuring no-failure for loads of 445 kN (100 kips) was accomplished since no failures of any continuous decks were observed. Two failures have occurred, on the same bridge, at loads of 288 kN (65 kips) and 360 kN (81 kips), respectively. In both cases, the concrete was so deteriorated that cores could not be taken and the slab, being at the edge of a cantilever, had no lateral restraint whatsoever.

This ultimate strength theory predicts that, with typical reinforcement level of 0.8% and with zero restraint, the deck failure load is between 445 and 670 kN (100 and 150 kips). For a 20.7 MPa (3,000 psi) concrete and a load of 445 kN (100 kips), the vertical shear stress, computed on the perimeter of the critical section at d/2 from load is 1.45 MPa (210 psi) or $4\sqrt{f'c}$. In other words, vertical shear failure could not be expected even if present code requirements were applied.

No serious structural cracking was noticed in any of the slabs. No visible cracking on the top surface of the slab in the transverse negative moment regions above the longitudinal girders was ever noticed. Directly under the load on the bottom surface of the deck, hairline cracking was observed during the tests, however, the cracks disappeared upon removal of the load.

The presence of boundary restraint was expected to significantly increase the punching shear capacity of bridge decks. Boundary restraint is provided by prohibiting the free movement of the slab, in both rotation and lateral movement. This restraint is provided by the main beams, the lateral bracing and the slab itself. The boundary restraint is difficult to calculate and the difficulty is further complicated by the large variety of bridges that exist and that can be designed. With this situation, the bridges tested were subdivided into the four categories as defined above, to see if a significant difference in boundary restraint exists among them. The value of restraint factor, F_r, is based on the Queen's study by B.deV. Batchelor and B.E. Hewitt (5) and is empirically taken between zero for no restraint and 1.0 for absolute restraint.

The comparison between experimental and theoretical results is based on measured and theoretical deflections. During the testing, plots of load versus deflection (as illustrated in Figure 4) were obtained. These were then compared with theoretical deflections for restraint factors of 0.25, 0.50, 0.75 and 1.00, in order to establish the actual restraint factor for each bridge. The deflection and ultimate load-carrying capacity were provided by the computer program developed at Queen's University (5). These ultimate deflections were then linearly interpreted to correspond to the 445 kN (100 kips) test load in order to estimate the actual restraint factor present. The following factors were considered; slab thickness and span, reinforcement ratio, effective slab thickness, slab span, applied load area and concrete strength. Experimental deflections and deck parameters are provided in Tables 1 to 4.

Table 5 shows the predicted restraint factors present and only tests where actual concrete strengths were available are included. The data indicate the presence of boundary restraint for all four classifications. The non-composite girder/concrete slab bridges exhibit the smallest average F_r of 0.41. A safe lower bound value would appear to be 0.20. The other three types, which are all of composite construction, exhibit average F_r values between 0.78 and 0.93, with a lower bound value of 0.40. There appears to be no significant difference between Types B, C and D. Maximum variation in restraint factor is in Type C while Type B has the highest overall restraint factor.

For the test results, the deflection/span ratios varied between 1/100 to 1/900 for the non-composite and between 1/900 to 1/3500 for composite slabs. Although a large variation is present, the non-composite slabs generally exhibit deflections three times larger than the corresponding composite slabs. This suggests that the composite slab exhibits a greater restraint factor since there is a positive connection to the main load-carrying members.

It should be noted that the above results are based on small deflection results [a maximum of 8.6 mm (0.34 in.)]; consequently, small experimental errors could potentially result in a large percentile error. Experimental errors may have occurred from the following sources: movement of reference points, instability of asphalt wearing surface, calibration of testing equipment, and friction in the hydraulic ram. These factors, and the large variation in the restraint factors obtained from this testing program, therefore, lead to general rather than detailed recommendations.

References 6 and 7 describe extensive prototype testing on bridge decks designed to the provisions of the new theory employing a reduced steel ratio of 0.3%. Although the tests were rather encompassing, no bottom steel exhibited stress in excess of 230 MPa (33 ksi) for bottom reinforcement under the 445 kN (100 kips) test load. This corresponds to a stress level of 46 MPa (6.7 ksi) for the observed maximum half axle weight of 90 kN (20 kips). No stress in excess of 35 MPa (5.0 ksi) was ever measured on negative reinforcement indicating the inadequacy of the AASHTO strip equation.

Appendix A is devoted to a parametric study regarding a simply-supported beam exposed to a single concentrated load with varying lateral displacement and rotational restraints. While it is understood that three-dimensional behavior can differ from this quantitatively, the authors believe that the analogy presented will provide some insight to the subject matter.

Summary and Conclusions

The punching shear testing of existing thin concrete decks indicates that there is a very large capacity against failure that can now be identified. The research at Queen's (4, 5) shows that for typical decks, a punching failure of the slab should occur prior to any flexural failure. The test load of 445 kN (100 kips), representing a dual-tired wheel, is 10 times larger than the allowable legal load and 4 to 5 times larger than the maximum half-axle weight observed. Even under this heavy overload, combined with the deterioration of some decks, no failures of restrained decks were ever observed. Consequently, these slabs can be considered to be greatly overdesigned as they showed no sign of structural damage due to simulated wheel loads.

As a general conclusion for the concrete decks tested, a restraint factor of 0.25 may be assumed for non-composite decks; for composite decks, a factor of 0.50 may be assumed. These lower bound tentative values may be safely used to design more economic slabs. The aspect of crack control must still be investigated however large cracking can be eliminated by providing small bar sizes at close spacing.

For a typical concrete deck, based on the AASHTO working stress design, the theoretical ultimate strengths are presented in Table 6.

Theoretical ultimate strengths for a concrete deck with 0.2% reinforcing steel ratio, which is typically the minimum steel ratio for temperature and shrinkage requirements, are also shown. It can be seen that a typical slab having an AASHTO design load of 93.6 kN (20.8 kips) live load plus impact with a restraint factor of 0.5 has a factor of safety against failure of 14.5. Furthermore, the 80% reduction in steel results in only a 28% reduction in ultimate capacity.

Table 7 shows the factor of safety for the above decks for various restraint factors. Assuming a lower bound restraint factor of 0.5 for composite decks, the minimum factor of safety based on a wheel load of 93.6 kN (20.8 kips) is 10.4.

Substantial savings in construction costs can be obtained by revising the design of concrete decks of this type. The design should be based on the actual collapse mechanism of the decks and not on an elastic approach as outlined in the AASHTO Specifications. The savings, resulting from reducing the reinforcing steel by 80%, are approximately $\$15/m^2$ ($1.40/sq. ft.), or approximately $10,000 for a 2-lane, 61 m (200 ft.) span bridge. Further cost benefits of reduced construction time, reduced maintenance and standardization of reinforcement will also be realized.

Recommendations

It is strongly suggested that the design approach as specified by AASHTO should be discontinued for decks within the parameters outlined. The deck strength developed by restraining boundary conditions should be utilized by basing the design on the theory developed at Queen's University (4,5).

It is recommended that thin concrete decks of composite construction and within the outlined design parameters be designed by assuming a restraint factor (F_r) of 0.5. Consequently, an isotropic reinforcing steel ratio of 0.2 is sufficient for standard decks. For better crack control for live loads, shrinkage and temperature, however, a ratio of 0.3% should be used.

Figure 5 shows a welded wire mesh recommended for use in a standard 200 mm (8 in.) 2-stage construction deck. This is a suggested method of standardization for new concrete thin deck construction. The 150 mm (6 in.) base concrete will have reinforcement as shown. The 50 mm (2 in.) high quality concrete will provide a skid resistant riding surface and ensure proper cover and protection against the rusting of the reinforcing steel. The reinforcement consisting of welded wire mesh with integral supports will provide a sufficiently rigid reinforcing mat. The welded wire mesh of gauge 5/0½ steel at 200 mm (8 in.) centers, for both top and bottom layer would be prefabricated and uniform throughout the entire length of the deck and simply placed on the framework. This welded wire mesh provides a reinforcing steel area of 13 mm^2 (0.2 sq. in.). This type of reinforcement spaced in 200 mm (8 in.) modules could become standard in bridge deck design and construction.

As the AASHTO-recommended large negative moments do not seem to materialize on the bridges tested, it appears that a cover of 76 mm (3 in.) in a 200 mm (8 in.) deck can be safely permitted. For #4 bars, this would give a cover/diameter ratio of 6 which is considered absolute protection against the ingress of salt. The future might see bridge decks built in a single course, with 0.2% reinforcement under 76 mm (3 in.) cover requiring no additional protection.

References

1. Standard Specifications for Highway Bridges. American Association of State Highway and Transportation Officials, 1973.
2. Interim Specifications, Bridges 1974. American Association of State Highway and Transportation Officials, 1974.
3. D.C. Manning and J. Ryell. Durable Bridge Decks. RR203, Ontario Ministry of Transportation and Communications, Downsview, Ontario, Canada, 1976.
4. B. deV. Batchelor, B.E. Hewitt, P.F. Csagoly and M. Holowka. An Investigation of the Ultimate Strength of Deck Slabs of Composite Steel/Concrete Bridges. Proceedings of the Bridge Engineering Conference, TRB, St. Louis, Missouri, 1978.
5. B.E. Hewitt and B. deV. Batchelor. Punching Shear Strength of Restrained Slabs. Journal of the Structural Division, ASCE, Vol. 101, No. St9, September 1975, pp. 1837-1853.
6. R.A. Dorton, M. Holowka and J.P.C. King. The Conestogo River Bridge — Design and Testing. Canadian Journal of Civil Engineering, Vol. 4, No. 1, 1977, pp. 18-39.

Table 1. Steel beam and concrete slab (non-composite).

Bridge Number	Stringer Spacing (m)	Stiffener Spacing (m)	Slab Thickness (mm)	Main Rebars (mm)	Distribution Rebars (mm)	Experimental Deflection (mm)	Concrete Strength (MPa)	Restraint Factor (F_r)
S1	1.83	3.81	180	#5 @ 305 (T) #5 @ 150 (B)	#5 @ 305 (T) #5 @ 150 (B)	3.56 3.81	52.5 62.7	0.25 0.23
S2	1.74	4.78	180	#5 @ 150 (T) #5 @ 150 (B)	#5 @ 455 (T) #5 @ 915 (B)	2.29 5.08 4.57	54.7 54.7 40.8	0.33 0.20 0.21
S14	1.75	7.62 to 4.72	180	#5 @ 150 (T + B)	#5 @ 455 (T + B)	2.29 2.79	53.7 43.5	0.33 0.31
S17	2.84	9.14	215	#5 @ 125 (T + B)	#4 @ 510 (T + B)	1.52	41.5	0.71
S32	3.45	3.56	180	#5 @ 150 (T + B)	#5 @ 150 (T + B)	5.08 4.82	32.5 36.4	0.63 0.61
S34	1.83	6.10 to 7.01	180	#5 @ 150 (T + B)	#4 @ 380 (B)	3.56	52.5	0.24
S35	1.52 to 1.84	6.10 to 7.21	180	#5 @ 150 (T + B)	#5 @ 535 (T) #5 @ 455 (B)	2.79 1.78	26.8 44.3	0.34 0.55
S37	3.51	3.12	215	#6 @ 150 (T + B)	#6 @ 150 (T + B)	3.30	19.3	1.00
S39	1.52	3.05	180	#5 @ 150 (T + B)	#4 @ 380 (T + B)	3.56 2.54	27.49 38.52	0.21 0.25

1 ft. = 0.3048 m 1 in. = 25.4 mm 1 psi = 6.89 x 10^3 MPa 1 psi = 6.89 kPa

Table 2. Steel beam and concrete slab (composite).

Bridge Number	Stringer Spacing (m)	Stiffener Spacing (m)	Slab Thickness (mm)	Main Rebars (mm)	Distribution Rebars (mm)	Experimental Deflection (mm)	Concrete Strength (MPa)	Restraint Factor (F_r)
S23	2.74	5.79 to 8.23	205	#6 @ 230 (T + B)	#4 @ 380 (T) #4 @ 430 (B)	0.71 0.84 1.17	27.6 (design)	1.0 1.0 1.0
S38	2.13	5.49	205	#6 @ 250 (T + B)	#4 @ 305 (T + B)	1.60 1.50 1.02	29.6 27.6 (est) 27.6 (est)	0.75 0.83 1.00
S18	1.93	5.72	180	#5 @ 150 (T + B)	#5 @ 305 (T + B)	1.78	18.9	1.00
S37	3.51	3.15	215	#6 @ 150 (T + B)	#6 @ 150 (T + B)	3.05 2.80	48.6 27.6 (est)	0.80 1.00
B1	1.93	4.46	195	#5 @ 150 (T + B)	#5 @ 380 (T + B)	1.65	27.6	0.96
B2	2.59	7.51	195	#5 @ 150 (T + B)	#5 @ 305 (T + B)	1.78	37.3	0.75
B3	1.83	4.34	190	#6 @ 230 (T + B)	#4 @ 230 (T + B)	1.35	28.5	1.00
B4	1.83	4.57	180	#6 @ 230 (T + B)	#4 @ 230 (T + B)	1.65	25.1	0.98
B5	3.17	6.74	215	#5 @ 150 (T + B)	#5 @ 305 (T + B)	1.78	38.00	0.94

1 ft. = 0.3048 m 1 in. = 25.4 mm 1 psi = 6.89 x 10^3 MPa 1 psi = 6.89 kPa

Table 3. Concrete beam and concrete slab (monolithic).

Bridge Number	Stringer Spacing (m)	Stiffener Spacing (m)	Slab Thickness (mm)	Main Rebars (mm)	Distribution Rebars (mm)	Experimental Deflection (mm)	Concrete Strength (MPa)	Restraint Factor (F_r)
S3	3.15	7.01 & 10.36	200	#5 @ 150 (T + B)	unknown	1.40	42.9	1.0
S5	7.77	2.13	215	#5 @ 280 (T) #5 @ 140 (B)	#4 @ 535	0.58 0.97 0.99 0.71	67.9 60.1 66.0 60.1	0.75 0.50 0.48 0.71
S6	3.20	10.36	255	#5 @ 190 (T + B)	#4 @ 305	0.46 0.48 0.37	76.1 74.2 56.6	0.75 0.75 0.75
S10	2.95	3.74	230	#5 @ 150 (T + B)	#5 @ 455 (T + B)	0.71 0.71 0.38	61.1 71.1 55.9	0.75 0.63 1.00
S15	3.04	5.49 & 7.32	180	#4 @ 125 (T + B)	#4 @ 610 (T + B)	1.27	42.6	1.00
S22	1.83	4.80	200	#4 @ 150 (T + B)	#4 @ 455 (T + B)	1.52	68.3	0.40
S32	3.30	–	200	#5 @ 150 (T + B)	#4 @ 610 (T) #4 @ 510 (B)	2.29 1.45	36.4	0.82 1.00
S42	1.93	–	200	#5 @ 280 (T) #5 @ 140 (B)	#4 @ 510 (B)	0.28 0.25 0.28	27.6 (assumed)	1.00 (all)

1 ft. = 0.3048 m 1 in. = 25.4 mm 1 psi = 6.89 x 10^3 MPa 1 psi = 6.89 kPa

Table 4. AASHTO girders and concrete slab (composite)

Bridge Number	Stringer Spacing (m)	Stiffener Spacing (m)	Slab Thickness (mm)	Main Rebars (mm)	Distribution Rebars (mm)	Experimental Deflection (mm)	Concrete Strength (MPa)	Restraint Factor (F_r)
S16	2.51	6.10	190	#5 @ 125 (T + B)	#5 @ 300 (T) #5 @ 200 (B)	1.78	64.9	0.66
S33	2.21	14.63	190	#6 @ 165 (T + B)	#5 @ 455 (T) #5 @ 180 (B)	1.27	32.5	1.00

1 ft. = 0.3048 m 1 in. = 25.4 mm 1 psi = 6.89×10^3 MPa 1 psi = 6.89 kPa

Table 5. Predicted effective restraints in bridges tested.

Type A: Non-Composite Steel Girder and Concrete Slab		Type B: Composite Steel Girder and Concrete Slab		Type C: Concrete Beam and Slab - Composite		Type D: AASHTO Girder and Concrete Slab - Composite	
Bridge Number	F_r	Bridge Number	F_r	Bridge Number	F_r	Bridge Number	F_r
S1	0.23, 0.25	S18	1.0	S3	1.0	S16	0.66
S2	0.21, 0.33	S23	1.0, 1.0, 1.0	S5	0.48, 0.50	S33	1.0
S14	0.31, 0.33	S37	0.8, 1.0		0.71, 0.75		
S17	0.71	S38	0.75, 0.83, 1.0	S10	0.63, 0.75, 1.0		
S32	0.61, 0.63	B1	0.96	S15	1.0		
S34	0.24	B2	0.75	S22	0.40		
S35	0.34, 0.55	B3	1.0	S32	0.82, 1.0		
S37	1.0	B4	0.98	S42	1.0, 1.0		
S39	0.21, 0.25	B5	0.94	S6	0.75, 0.75, 0.75		
Average Restraint	0.41	Average Restraint	0.93	Average Restraint	0.78	Average Restraint	0.83

Table 6. Ultimate strength of decks.

	Theoretical Ultimate Strength	
Restraint Factor	Reinforcing Steel Ratio = 0.01	Reinforcing Steel Ratio = 0.002
0.0	810 kN (183 kips)	210 kN (47 kips)
0.25	1080 kN (243 kips)	610 kN (137 kips)
0.50	1340 kN (302 kips)	960 kN (216 kips)

Deck Description:

Span = 2.44 m (8 ft.)
Thickness = 200 mm (8 in.)
Effective depth = 165 mm (6.5 in.)
Concrete strength = 27.6 MPa (4000 psi)
Reinforcing steel ratio = 0.009 to 0.002
Yield strength = 413 MPa (60,000 psi)

Table 7. Factor of safety of decks.

Typical Structure with Various Restraint Factors	1% Reinforcement		0.2% Reinforcement	
	f'_c = 27.6 MPa	f'_c = 34.5 MPa	f'_c = 27.6 MPa	f'_c = 34.5 MPa
0.0	8.8	9.2	2.3	2.3
0.25	11.7	12.9	6.6	7.7
0.50	14.5	16.5	10.4	12.4
0.75	17.5	20.3	13.9	16.7
1.00	20.6	24.2	17.1	20.6

1 MPa = 145 psi

Figure 1. Concrete slab load capacity.

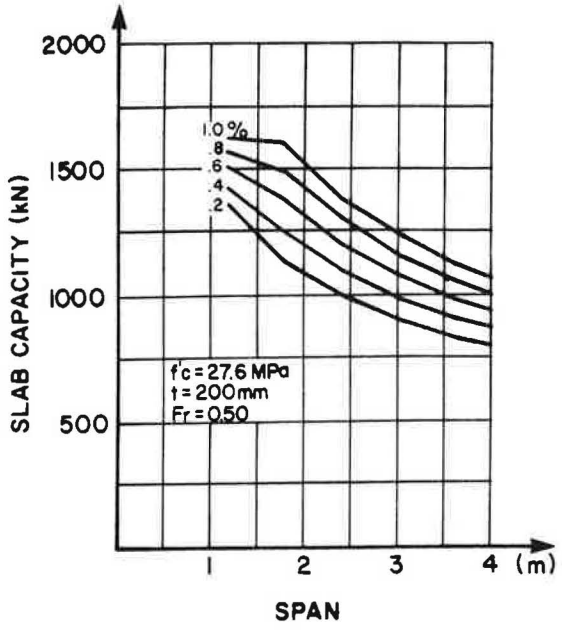

Figure 2. Arching action in deck slabs.

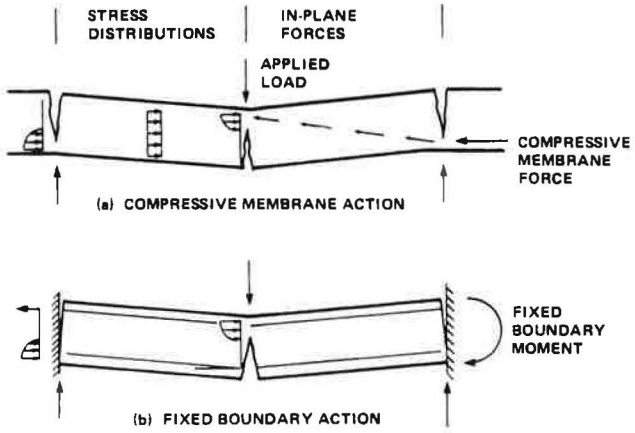

Figure 3. Overall view of typical testing apparatus.

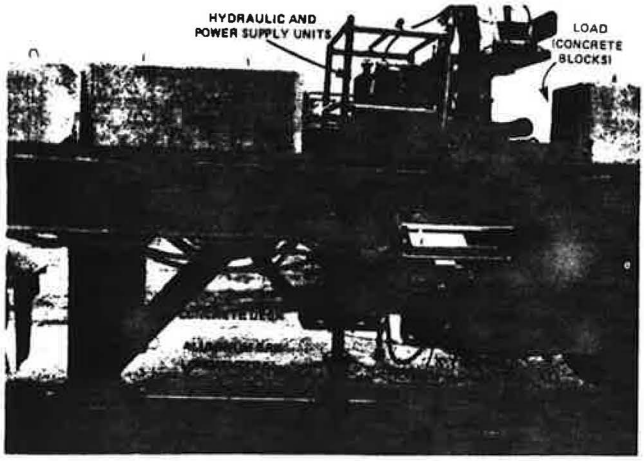

Figure 4. Plot of typical load vs. deflection curve.

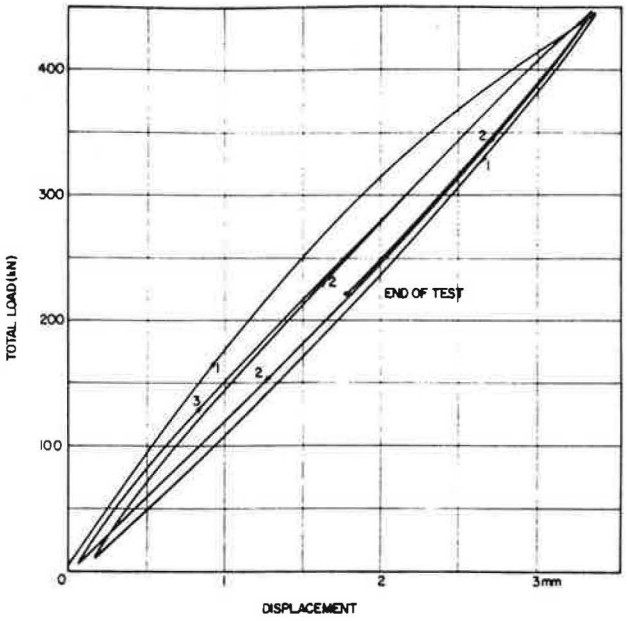

Figure 5. Standard prefabricated steel reinforcement.

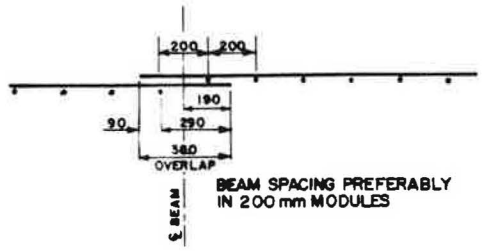

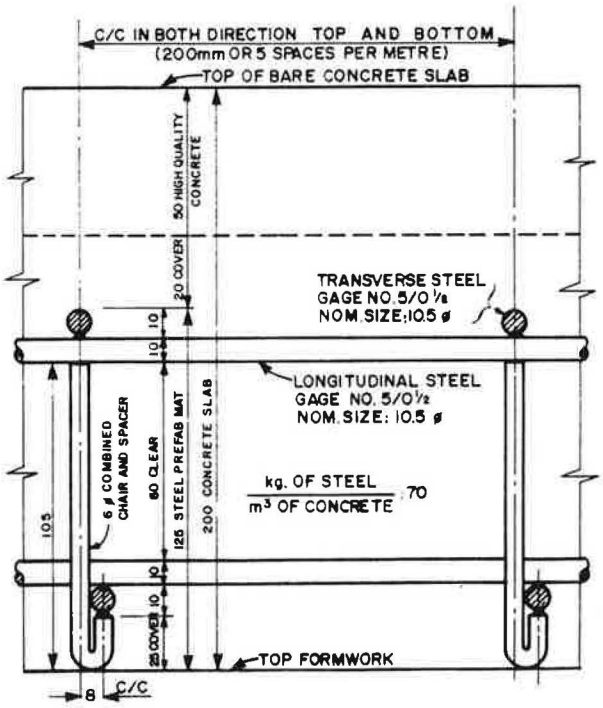

Appendix A, Effect of Boundary Restraints

The effect of boundary restraints and the resulting boundary forces can be qualitatively illustrated by the simple beam model shown in Figure A.1. The beam is loaded by a central point load (P) and the ends are restrained against free movement by a horizontal force (H) and a moment (M) which act at a distance (a) from the bottom surface of the beam. In a reinforced concrete beam, these forces would be assumed to act at the reinforcing steel level. Figure A.1 also shows the moment diagram for all three forces.

Since M and H are the unknown variables, the following equations can be used to solve for M and H in terms of P by equating displacements:

$$\Delta_{HH}\, H + \Delta_{HM}\, M = \Delta_{HP} \qquad (1)$$

$$\Delta_{MH}\, H + \Delta_{MM}\, M = \Delta_{MP} \qquad (2)$$

The magnitude of the horizontal force and moment depends on the rotational and lateral resistance of the boundary. Two additional variables can be defined as:

- F = lateral resistance, defined as the force required to move the boundary by unit length, and
- K = flexural resistance, defined as the moment required to move the boundary by unit rotation.

After resolving equations 1 and 2, and substituting the appropriate parameters, the following expressions are obtained:

$$M = \frac{1.5\, P\ell^2\, Kh^2\, F\ell + 2Eh}{h^2\, [\ell\rho F + 2Eh]\, [12\ell K + 2Eh] - 144e^2\ell^2 FK} \qquad (3)$$

and

$$H = \frac{3P\ell^2\, eEFh^3}{h^2\, [\ell\rho F + 2Eh]\, [12\ell K + 2Eh^3] - 144e^2\ell^2 FK} \qquad (4)$$

where h = overall height
e = 0.5h - a
a = distance from bottom surface to location of force (H)
α = e ÷ h
ρ = 1 + 12α^2
I = $h^3/12$ (assuming a unit width)
A = h (assuming a unit width)
E = modulus of elasticity

If the value of K is taken as a function of the adjacent span then,

$$K = \frac{3EI}{\bar{\ell}} = \frac{Eh^3}{4\bar{\ell}}$$

where $\bar{\ell}$ = the length of adjacent span

If the value of F is taken as a function of the surrounding slab then,

$$F = \frac{EA}{\ell} = \frac{EhN}{\ell}$$

where N = the number of strips of unit width providing lateral confinement for the strip under consideration.

By substituting the above relationships into equations 3 and 4, the following expressions for M and H are obtained:

$$M = \frac{3P\ell}{8}\gamma \qquad (5)$$

where

$$\gamma = \frac{j\,(N+2)}{[\rho N + 2]\,[3_j + 2] - 36\alpha^2 N_j} \qquad (5a)$$

j = the ratio of length of the span under consideration and the adjacent span length.

and

$$H = \frac{3P\ell}{h}\beta \qquad (6)$$

where

$$\beta = \frac{\alpha N}{[\rho N + 2]\,[3_j + 2] - 36\alpha^2 N_j} \qquad (6a)$$

By using Figure A.1, top and bottom surface stresses can be obtained for this beam:

$$f_r = \frac{P\ell}{4}\cdot\frac{6}{h^2} + \frac{3P\ell}{h}\,\beta\cdot\frac{1}{h} - \frac{3P\ell}{h}\,\beta\cdot e\cdot\frac{6}{h^2} - \frac{3P\ell}{8}\cdot\gamma\cdot\frac{6}{h^2}$$

$$f_T = \frac{3P\ell}{h^2}\left[+\frac{1}{2} + \beta - 6\beta\alpha - \frac{3\gamma}{4}\right] \qquad (7)$$

and

$$f_B = \frac{3P\ell}{h^2}\left[-\frac{1}{2} + \beta + 6\beta\alpha + \frac{3\gamma}{4}\right] \qquad (8)$$

It can be seen from equations 7 and 8 that the expression in brackets is a variable depending on the degree of restraint. With M and F equal to zero, equations 7 and 8 give the stress expected for a simply-supported beam.

Where

$$f_T = f_B = \frac{P\ell}{4}\,\frac{6}{h^2} = \frac{1.5\,P\ell}{h^2}$$

equations 7 and 8 indicate that the stress, with or without restraint, increases with the span length and decreases with the square of the beam thickness.

By assuming typical concrete deck slab dimensions, the effect of varying lateral and flexural restraint can be illustrated. For a typical 200 mm (8 in.) beam, e_{min} can be estimated to be 65 mm (2.5 in.). The span length ratio (j) is varied between 0.50 and 2.00, while the ratio (N) is varied between 1 and infinity. Figure A.2 illustrates the effect of the varying restraint.

For the top stresses (Figure A.2a), increasing adjacent slab spans decrease the stress coefficients while the horizontal restraint, irrespective of its effective width, has a very small effect on the top stresses.

Figure A.2b indicates that both lateral and horizontal restraint has an effect on the bottom surface stresses. The stress coefficient decreases with increasing slab span ratio and increasing effective width of lateral restraint width.

Figure A.3 shows the effect on the bottom stress coefficient of a varying lateral restraint with zero rotational restraint. The stress coefficient varies inversely with N and with full restraint, the case where N is infinite, the

limiting value of the stress coefficient is 0.2923. As previously mentioned, this stress coefficient is equal to 0.50 with zero lateral and rotational restraint. For this case, the effect of different e values (where e is the eccentricity between the location of the restraining force and the neutral axis) was also investigated. The above stress coefficient decreases with increasing e as expected. For a 25 mm (1 in.) increase in e, the stress coefficient decreases by 12%.

The parametric study of a simply-supported beam loaded by a single concentrated load with varying lateral displacement and rotational restraints indicates that the extreme fiber stresses are significantly lower (by up to 45%) than extreme fiber stresses with zero restraint.

Figure A.1. Simply-supported beam of rectangular cross section.

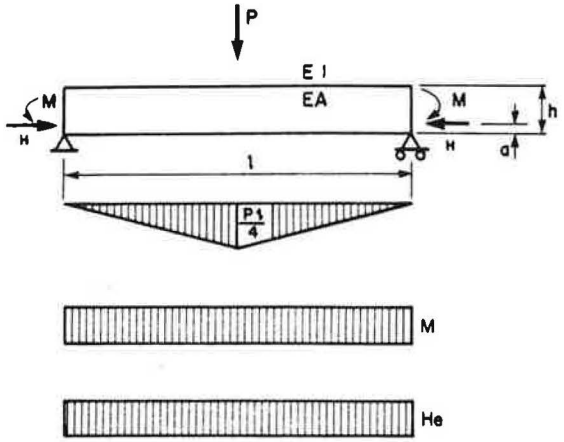

Figure A.2(a). Effect of varying restraint values (top face of slab).

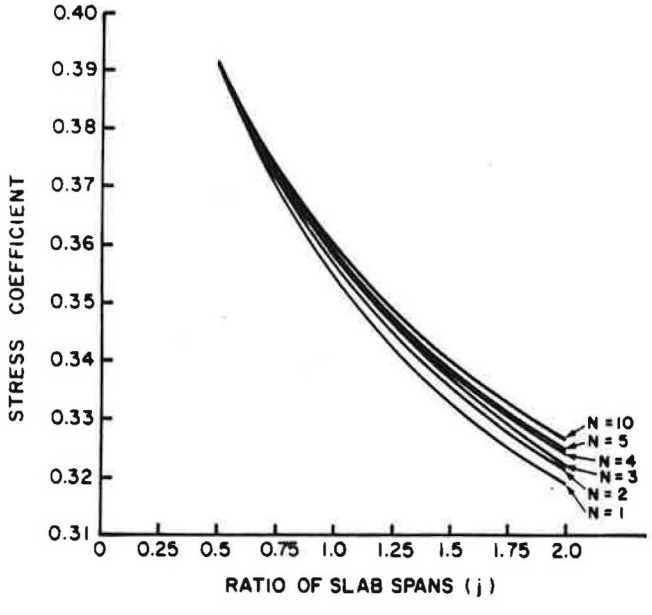

(a) TOP FACE OF SLAB

Figure A.2(b). Effect of varying restraint values (bottom face of slab).

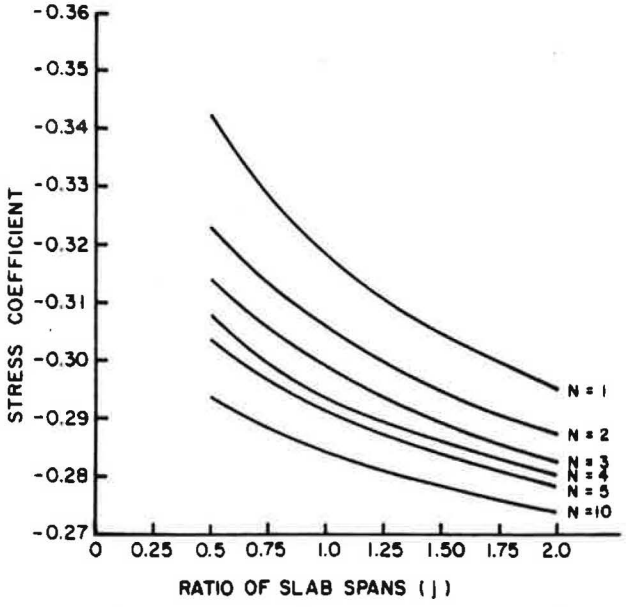

(b) BOTTOM FACE OF SLAB

Figure A.3. Variation of stress coefficient with lateral restraint (assuming zero rotational restraint).

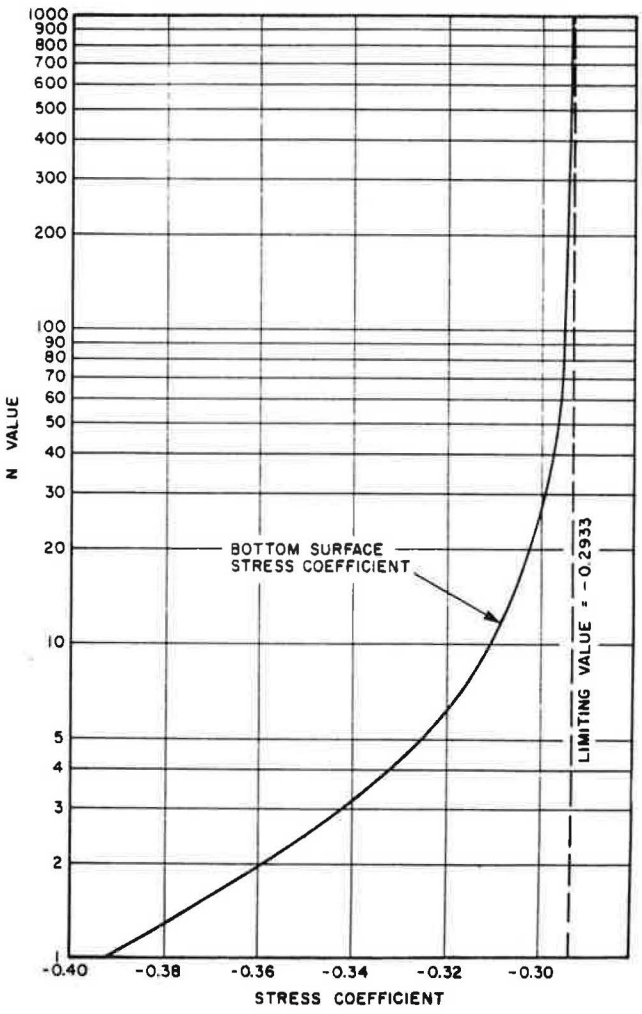

DETECTION OF DELAMINATION IN BRIDGE DECKS WITH INFRARED THERMOGRAPHY

Gerardo G. Clemena and Wallace T. McKeel, Jr.
Virginia Highway & Transportation Research Council

The use of infrared thermography to define very accurately variations in surface temperatures was evaluated as a means of defining delaminated areas caused by corrosion of reinforcing steel in concrete bridge decks. Differences in the temperatures of the deck surface, shown in various shades or colors on a cathode-ray tube, were photographed to provide a permanent graphic record of the location of the warmer, distressed areas. In a comparative study of infrared thermography and conventional deck evaluation techniques, including the sounding of the surface with a hammer and chain drag and the use of a rolling delamination detector, all were found generally satisfactory in locating severe to medium delaminations. However, the infrared thermography procedure had important advantages in disclosing incipient delaminations, those in which the cracking is confined to the close vicinity of the reinforcing steel, and in providing detailed records of the separated areas.

A major problem in the repair of bridge decks is locating the areas of delamination caused by corrosion of the reinforcing steel. None of the available methods of locating delamination are completely satisfactory. The sounding method relies on subjective judgments of the hollow sound produced when the concrete is struck with a hammer or when a chain device is dragged across the deck surface. It is useful only in locating relatively severe delaminations and is subject to interference by traffic noises. A recently introduced rolling delamination detector, the Delamtec, is based on the same "sounding" principle, but it utilizes piezoelectric hydrophones to characterize vibration waves generated by steel tapping wheels striking delaminated areas.(1) Although it is faster than the hammer or chain drag and provides a graphic record of distressed areas, the Delamtec detects only delaminations more than 10 cm (4 in.) in width, and it allows only a relatively narrow coverage of the deck per scan.

There is a need for a more reliable method of delamination detection that is capable of locating not only severe, but also incipient, delaminations with some degree of detail and rapidity. To develop such method, the authors evaluated the use of infrared (IF) thermography.

Rationale in Delamination Detection with Infrared Thermography

The authors conceptualized that the cracks, or physical separations, in delaminated concrete are occupied by trapped air. Considering the large difference between the volumetric heats of solid concrete and air, which are 30.0 and 0.19 Btu/(yd.^{3})(^{o}F), respectively, a severely delaminated concrete area would have a volumetric heat lower than that of surrounding solid concrete and consequently would be warmer, given the same amount of solar heating. Conversely, when the solar heating disappears, the delaminated concrete would be cooler than the solid concrete. It logically follows that the more delaminated a spot is, the warmer it would be compared to adjacent sound concrete. This temperature difference could serve to define delaminated areas in concrete if one had a technique, such as infrared thermography, for rapidly mapping an accurate temperature profile of a bridge deck.

Principle of Infrared Thermography

Any object whose temperature is above absolute zero (-273^{o}C or 0^{o}K) emits IR radiation generated by the vibration and rotation of its atoms and molecules. The IR radiation emited by most objects falls within a band of wavelengths from about 2 to 15 microns (μ), and is proportional to the object's absolute temperature. Thus, the temperature can be indirectly determined by measuring the intensity of the emitted IR radiation.

In IR thermography, a camera (or scanner) that incorporates a sensitive and fast-response IR detector is used to automatically scan an object and produce a thermal image of it on a cathode-ray tube. The two types of detectors most commonly used are the Indium-Antimonide (InSb) photovoltaic detector and the Mercury-Cadmium-Telluride (HgCdTe) photoconductive detector, both of which can detect a fraction of a degree temperature difference at 300^{o}K. Indium-Antimonide has a spectral response of 2 μ to 5.6 μ, while Mercury-Cadmium-Telluride re-

sponds over a range of from 8 μ to 14 μ. These spectral ranges are different from that detectable by IR photographic film which is 0.7 μ-0.9 μ.

The thermal image, or thermogram, obtained with the scanner represents the surface temperature profile of the object under examination. In a black and white picture, which looks something like an ordinary photographic negative, the warm areas are light and cold areas are dark. In some thermal imaging systems, the picture comes out in brilliant colors, with the various tones representing different temperatures.

Study Methodology

In the study, several deck areas, mostly 180 x 360 cm (6 x 12 ft.) in size were tested for delamination with an infrared scanner. For comparison, the areas were also evaluated by sounding with a hammer and chain drag, and a delamination detector. Cores were obtained from selected spots in the test areas to verify the degree of delamination shown on the thermograms.

The scanner system used, the Thermovision Model 750 manufactured by the AGA Corporation of Secaucus, NJ, consisted of a camera unit, a display unit, a power supply, and a color monitor.

The camera unit was equipped with a liquid nitrogen cooled InSb detector and an infrared lens with a 20° x 20° field of view. With the camera set at a comfortable working height of 150 cm (5.0 ft.) above a bridge deck, the deck area covered was slightly larger than 45 x 45 cm (1.5 x 1.5 ft.); and the individual profiles of the 45 cm (1.5 ft.) square areas had to be made into mosaics to obtain composite thermograms of the larger deck areas. For the mosaic to be useable, the camera must be aimed at a right angle to the deck, since any other angle gives rise to problems due to perspective, but it was not possible to point the camera straight down without spilling the liquid nitrogen. To eliminate the perspective problem, the camera was aimed parallel to the surface of the deck and a surface reflective mirror, about 10.2 x 11.4 cm (4.0 x 4.5 in.) in size, was mounted at 45° with its reflective surface directly facing the camera lens to allow focusing of the infrared camera indirectly downright at the deck. The thermogram obtained in this manner is an inverted image, but this presents no problem.

It was also found that solar radiation reflected from the deck surface interfered with the thermogram, and a filter which transmitted only wavelengths longer than 3.5 μ was needed to eliminate the reflection.

To enhance the interpretability of the thermogram, a color monitor was used so that different temperatures were represented by various colors. Specifically, a selected temperature range was divided into 10 isotherm units presented in white, yellow, orange, red, pink, violet, aquamarine, green, light blue, and dark blue, corresponding to the decreasing order of temperature level. Type 108 color Polaroid film was used to record the individual thermograms.

Discussion of Results

Optimum Time for Using Infrared Thermography

A preliminary survey of the test areas confirmed that under direct solar heating a delaminated concrete area is warmer than the surrounding solid concrete. It also revealed that for the best compromise between the maximum detectability of delaminations (i.e., the best definition of severe and even incipient delaminations by thermography) and the stability of the temperature profile of a deck area, the period from 12:00 noon to 2:00 p.m. would be the ideal time for the use of thermography. (This period may vary in length depending on the time of year and geographic location.)

A Typical Thermogram of the Test Areas and Its Interpretation

In obtaining a thermogram of a deck area, the temperature level setting of the infrared scanner was adjusted so that a severely delaminated spot would show up as the "warmest", or white, in the color monitor. This allowed interpolation between the warmest and coldest colors so that a mediumly delaminated spot might appear one or two isotherm units below white, i.e., as yellow or orange; and an incipient delamination would appear either two or three isotherm units below white, i.e., as orange or red. The remaining cooler colors of pink, violet, etc. would represent the solid concrete. It must be emphasized that the classification of different stages of delamination is relative.

One of the typical thermograms taken in the above manner is shown in Figure 1. This mosaic thermogram, covering part of a test area, was made from individual thermograms of 45 cm (1.5 ft.) squares. In terms of pattern, the thermograms are exact duplications of the original photographs of color thermograms. However, because of the high expense of color reproductions, the warmer colors of white, yellow, orange, and red, in order of decreasing intensity; while the relatively cooler colors are left unshaded because of their relative inconsequentiality.

Figure 1 shows few delaminations in the medium stages; mainly the narrow band of intense shade around a spalled area that has been patched with asphaltic concrete (dark area) which overlaps squares 2-5 and 3-5, and the similarly shaded spots in squares 2-3 and 3-2. In addition, the thermogram shows semi-regular patterns, the lightly shaded areas that run approximately 50° with respect to the X-axis of the thermogram. Since this angle is similar to the skew angle of the reinforcing steel and to the direction that the two medium delaminations in squares 2-3 and 3-2 run with respect to each other, these lightly shaded areas must be incipient delaminations occurring around some of the reinforcing steel. Cores obtained from such areas confirmed this assumption.

In order to preclude misinterpretations, infrared thermography must be supplemented with visual examinations. It has been found that spots of asphalt and tire marks appeared warmer than the concrete because they have a relatively higher infrared emissivity, and they can be mistaken for delaminations in the thermograms.

Comparison of Techniques

For comparison, the same deck areas were also evaluated with the conventional deck evaluation techniques of sounding with a hammer and a chain drag and the use of a rolling Delamtec. A chain drag device, made of five 75-cm (2.5-ft.) steel chains connected to and evenly spaced on a metal rod by ropes, was used to make a rapid initial survey of each area. Then, for more precise outlining of any delaminated spots, a hammer was used. In addition to listening for the hollow sound indicating a delamination, the surveyor placed one hand on the deck to feel for vibrations. This practice is be-

Figure 1. Typical thermogram with delamination shaded. (Delaminations located by sounding and Delamtec are superimposed.)

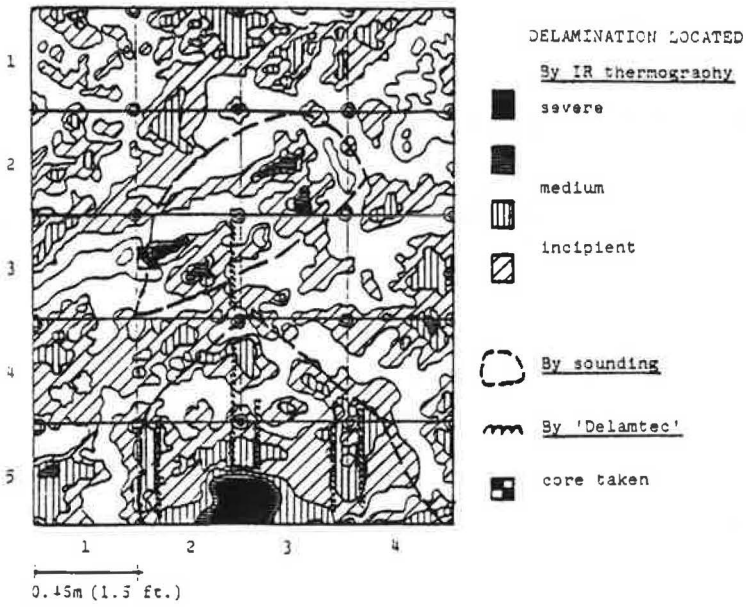

Figure 2. Delaminated areas located by different techniques.

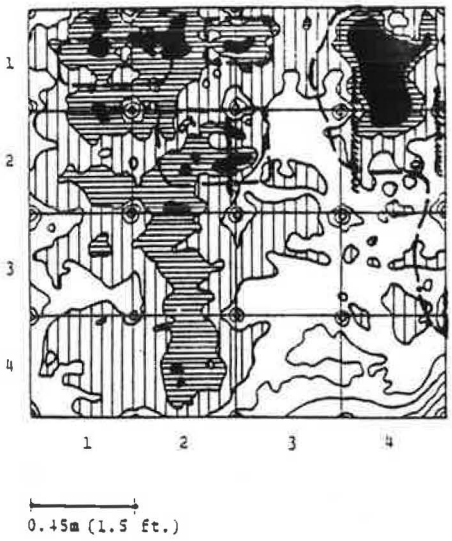

lieved to enhance the reliability of the hammer sounding. The rolling detector was rolled longitudinally over each of the test areas at 46-cm (1.5-ft.) intervals.

In terms of the number of delaminations detected in the test areas, it was found that approximately 95% of those in the medium and severe stages that were identified by thermography were also detected by sounding, while only approximately 85% were detected by the Delamtec. The delaminations missed by sounding with the chain drag and hammer were in the medium stage; such as that extending from square 2-2 down to square 2-4 of Figure 2. However, with the Delamtec, some severely delaminated areas were not detected for unknown reasons. An example is shown in Figure 2, where a few neighboring severe delaminations in squares 1-1 to 3-1 were not located by the Delamtec.

An inherent inadequacy of sounding and the delamination detector is their inability to provide detail, which made it difficult to delineate delaminations accurately. A typical example is again shown in Figure 2, wherein the severe delaminations that extended across the top of squares 1-1 and 2-1 were detected but not properly located by sounding. A similar inadequacy of the Delamtec is shown in Figure 1 where, according to thermography, two medium delaminations, each about 15 cm (3 in.) across, existed in square 2-3. The Delamtec did not detect these completely, as indicated by the presence of the detector signal on only the right side of the square, but a core taken from the left side of the square confirmed the extent of delamination indicated by thermography. A more important advantage of thermography is its ability to locate incipient delaminations. Cores from incipiently delaminated spots had cracks that had not yet completely extended across the core to separate the concrete into at least two layers, as was the case for the cores from severe and medium delaminations.

It must be pointed out, however, the occasional inconsistencies were observed in the correlation between warmness of a deck area and the severity of delaminations. In those cases the cores showed slightly more advanced delamination than the incipient delamination indicated by the thermogram. It is uncertain whether the observed inconsistency is real, or was caused by slight changes of colors in the thermograms that were occasionally observed when scattered clouds interfered with incoming solar radiation. If the inconsistency results from this cause, it can be minimized or probably eliminated by a setup incorporating videotape for rapid recording of the thermogram.

Applicability of Results

The subject research has indicated the suitability of infrared thermography in providing graphic records of delaminated areas in concrete bridge decks. The ability of the technique to disclose incipient delamination is considered particularly promising as this would provide an early warning of oncoming distress. While some degree of experience is necessary for proper interpretation of the thermograms, the problem of training operators is manageable. However, additional research is required for implementation.

With an estimated equipment cost of from $30,000 to over $40,000, infrared thermography, as used in this study, is not cost-effective compared to conventional survey techniques. The additional detail provided by the thermograms, while desirable, would not support the high cost differential, and it appears that the application of thermographic techniques to rapidly survey a large number of bridges must be developed for cost-effectiveness. The authors feel that this might be accomplished through the use of videotape recordings, a subject proposed for future research.

Reference

1. Moore, W. M., G. Wift, and L. J. Milberger, "An Instrument for Detecting Delamination in Concrete Bridge Decks", Report 130-4, Texas Trans. Inst., Texas A & M Univ., March 1970.

Acknowledgment

The research was financed by HPR funds administered through the Federal Highway Administration.

DEEP IMPREGNATION OF CONCRETE BRIDGE DECKS WITH LINSEED OIL

Philip D. Cady, Donald E. Kline, Paul R. Blankenhorn,
The Pennsylvania State University

The overall objective of the research described in this paper was to evaluate the feasibility of deep (> 5 cm) impregnation of concrete bridge decks with boiled linseed oil/diluent mixtures. Impregnation is one of the techniques that is currently receiving considerable attention as a means of improving the longevity of bridge decks by reducing or preventing spalling problems associated with corrosion of reinforcing steel. The choice of linseed oil was based on safety (low volatility and high flash point), cost considerations, and the elimination of the polymerization step required for other polymers. Also, many highway agencies are already familiar with linseed oil, since it is commonly sprayed on bridge deck surfaces periodically to retard surface scaling. The latter procedure results in penetration depths of less than 3 mm and has little or no effect on preventing spalling. Deep impregnation requires a drying step to remove water, followed by sufficient contact with the impregnant to permit penetration to the desired depth. Following a period of preliminary laboratory studies, demonstration impregnations were carried out on 5.6 m^2 areas on two bridge decks. One of the bridges had been subject to 3 winters of deicer salt application. The other had received no salt. Four days soaking time with a 50-50 mixture of boiled linseed oil/mineral spirits mixture was used in the impregnation step. Examination of cores subsequently removed from the test areas revealed that penetration depths ranging from about 5 to 10 cm were obtained.

The Problem

Spalling of concrete bridge decks is currently one of the most serious problems facing highway agencies in the snow belt states. There has been a dramatic increase in the incidence and severity of bridge deck deterioration during the past twenty years. Two factors largely account for this. First, the increased volume of highway construction associated with the building of the interstate highway system produced a significant increase in the number of highway structures. Second, the "bare pavement" policy, stressing safe, all-weather driving conditions, was adopted by highway agencies in response to public pressure. The latter factor has involved the use of deicing chemicals which permeate concrete bridge decks causing corrosion of reinforcing steel and resultant spalling of the overlying concrete.

A formidable body of data exists to indict corrosion of the reinforcing steel, caused by presence of chloride deicer salts, as the major cause of bridge deck deterioration (1-4). There has been a phenomenal increase in the use of deicing salts in recent years. In 1947 less than one-half million metric tons were used in the entire country. By the winter of 1966-67, this figure had risen to about 6 million metric tons, and by the winter of 1975-76 it was estimated to be between 10 and 11 million metric tons (5). At the application rates currently in use, a typical bridge deck in a snow belt state receives about 1.2 Kg of salt per M^2 (about 1/4 pound per square foot) during an average winter season. The increased use of deicers is reflected in the accelerated pace of bridge deck deterioration observed. New bridges should last thirty years or more, but many now show signs of significant deterioration in five years or less (6). In 1973, the Federal Highway Administration estimated the annual cost for bridge deck repairs in the U.S. to be $70 million (7). By 1975, that figure had increased to $200 million per year (8). Even so, as a measure of damage being incurred, these figures are probably deceptively low since they likely represent the bounds of limited maintenance budgets. The Road Information Program (TRIP) estimates that during the winter of 1976-77 alone, 1626 bridges were rendered unusable due to record low temperatures and heavy salt applications (9). Most of the damage involved deck spalling, according to TRIP, and replacement or repair costs were estimated at $1 Billion.

Bridge Deck Impregnation

Deep impregnation with sealants to immobilize chlorides present and to prevent the ingress of water, oxygen, and deicer salts is one of only two techniques that presently seem to offer promise for protection of existing chloride contaminated, but sound, concrete bridge decks.

Methyl methacrylate monomer (MMA) has been the principal impregnant used in field studies prior to the research described here. Proper drying, impregnation, and polymerization procedures using methyl methacrylate will produce concrete with essentially zero permeability to water and will immobilize deleterious contaminants already contained in the concrete pore system (viz, chlorides). Also, the mechanical and durability properties of the concrete, per se, are significantly enhanced. However, the use of methyl methacrylate has serious drawbacks. The monomer is expensive, highly volatile, extremely flammable, and must be subjected to a separate polymerization step. Assuming that the improvement in mechanical and other properties afforded through the use of methyl methacrylate is not a necessary prerequisite, other materials may be used as impregnants whose function is merely that of blocking the pores and immobilizing salts contained therein. Furthermore, these impregnants could be selected to countermand the disadvantages of methyl methacrylate cited above.

A logical candidate as an impregnant is linseed oil. For years, highway agencies have been using mixtures of boiled linseed oil and diluents to seal the surfaces of concrete bridge decks to retard surface scaling. However, these applications penetrate the concrete surface to depths of only about 3 mm (1/8 inch) and have little or no effect in reducing spalling. Impregnation with linseed oil, or similar materials, to the level of the top reinforcing steel (5 to 10 cm or 2 to 4 in.) should, however, effectively block the continuous capillary system and immobilize chloride ions in the vicinity of the rebars.

Purpose of the Research

The purpose of the research described in this paper was to develop in the laboratory and demonstrate in the field the methodology for deep penetration of concrete bridge decks with boiled linseed oil to prevent the ingress of deicer salts and water and to immobilize deleterious ions already present. This goal was pursued by addressing the following specific objectives:

1. Determination of the time, temperature, and impregnant conditions to optimally impregnate suitably dry concrete to a depth of about 6.4 cm (2 1/2 in.)
2. Evaluation of the protection against corrosion of the reinforcement by water and deicer salts afforded by the selected impregnant.
3. Demonstration of the feasibility of the technique involved on a chloride-contaminated and a non-contaminated bridge deck in the field.

Laboratory Tests

Impregnant

A series of laboratory experiments was conducted to examine boiled and raw linseed oil, straight and diluted with various amounts of mineral spirits, as candidate impregnants. In experiments where the ease of penetration of the impregnant was determined by the uptake of impregnant in dried concrete by capillary action, it was found that both raw and boiled linseed oil in various combinations with 25 percent by weight or more of mineral spirits gave penetrations of 5 cm (2 in.) or more. At high mineral spirits contents (50 to 70 percent), the raw linseed oil gave deeper penetrations than the boiled linseed oil, but not on a specimen weight gain basis. These tests also revealed that impregnant uptake is approximately 75 percent complete in four days at room temperature. In general, increasing temperatures, up to 60°C (140°F), slightly increased the percent completion of impregnant uptake at any specified time.

Loss of impregnant by evaporation from concrete specimens stored in the laboratory for six months, as measured by weight loss, was negligible. However, mortar specimens obtained from the impregnated concrete that were vacuum dried at 110°C (230°F) for 24 hours showed increases in porosity with increasing mineral spirits content in mercury porosimetry tests. This indicates that when the mineral spirits are removed, penetrable porosity may be obtained. However, this was under very severe conditions, and it is believed that the negligible losses observed on the specimens in laboratory air storage are indicative of good retention of the impregnant in the field.

On the basis of these tests, it was decided to use a 50-50 boiled linseed oil-mineral spirits mixture and a four-day soak impregnation period to obtain impregnation depths of at least 5 cm (2 in.).

Large Scale Slabs

The drying and impregnation procedures developed in the bench-scale laboratory experiments were tested on full-scale depth, reinforced concrete slab specimens in the laboratory to perfect techniques before going into the field. Two 1.83 m by 1.83 m by 20.3 cm thick (6 ft. x 6 ft. by 8 in.) slabs were constructed. Reinforcement consisted of two layers of reinforcing bars with 5 cm (2 in.) of clear concrete cover from the top and bottom faces of the slab. Each layer of reinforcement consisted of 1.59 cm diameter (no. 5) bars on 20.3 cm (8 in.) centers in one direction over 1.27 cm diameter (no. 4) bars on 15.2 cm (6 in.) centers in the other direction. The concrete used in these slabs was produced in one batch having a cement factor of 350 kg/m^3 (590 lb/yd^3), water/cement ratio of 0.53 by weight, 11.4 cm (4.5 in.) slump, 7.5 percent air content, and had a 28-day compressive strength of 25.304 mPa (3670 lbf/$in.^2$).

The temperature attained at a depth in the concrete during drying can be used as the criterion to gage the sufficiency of drying relative to securing a selected depth of impregnation. Therefore, it is important to know to what extent the manner of obtaining temperatures within the concrete affects the temperature readings. It was suspected by the researchers that temperature measurements obtained from thermocouples inserted in holes drilled in the top surface of the slabs would be falsely high due to conduction of heat through the thermocouple wires and to direct exposure of the hot junction to IR radiation. To evaluate this problem, temperature measurements were made at depths of 1.3, 2.5, 6.4, and 10.2 cm (1/2, 1, 2 1/2, and 4 in.) from the top surface of the slab using type T (copper-constantan) thermocouples inserted in 0.64 cm (1/4 in.) diameter holes drilled in the slab from both the top side and the bottom side. Temperature measurements for all eight thermocouples, plus one located on the top surface, were continuously recorded while drying was carried out using a propane fired, infrared heater. It was found that thermocouples inserted through the top surface give readings that may be falsely high by as much as 111°C (200°F) at the surface to 28°C (50°F) at

10.2 cm (4 in.) deep. However, it was determined that a 100 MJ/hr/m^2 (9000 BTU/hr/sq ft) propane-fired catalytic IR heater set about 28 cm (11 in), from the concrete surface will produce sufficient drying in three to four hours to provide 5 cm (2 in.) or more penetration of 50-50 by weight boiled linseed oil-mineral spirits after four days of soaking.

One of the large slab specimens was salt contaminated by ponding brine solution for 90 days. Sixteen corrosion potential determinations (10) gave an average of -0.53 volts relative to the copper-copper sulfate half-cell, well in excess of the -0.35 volts considered to be indicative of active corrosion. Impregnation of this slab with 50-50 boiled linseed oil-mineral spirits by weight resulted in a reduction of the corrosion potential by 40 percent (-0.32 volts CSE), putting it in the "uncertain" range. It is concluded from this that deep impregnation by linseed oil will significantly reduce the probability of active rebar corrosion in chloride-contaminated concrete. The question may arise as to whether the reduction in corrosion potential resulted from drying or the presence of the linseed oil. It should be pointed out that the area of the slab that was dried and impregnated was only 0.30 m x 0.61 m (1 ft. x 2 ft.) of the 1.83 m x 1.83 m (6 ft. x 6 ft.) slab. Furthermore, drying was carried out to a depth of only 10.2 cm (4 in.) maximum of the 20.3 cm (8 in.) slab thickness. Therefore, the slab was by no means totally dried and by the time that impregnation was completed (4 days) moisture equilibrium was undoubtedly re-established in the slab.

Long-term corrosion potentials after salt contamination and impregnation with linseed oil mixtures were not investigated. However, Clear and Hay (11) found that a surface treatment of linseed oil retarded the ingress of chlorides into their test slabs. Deep impregnations would not be worn off by traffic as surface treatments would.

Test Sites

Evaluation of the selected impregnant and methodology that resulted from the laboratory work was carried out in the field on two selected bridge decks. One of the bridge decks had been subjected to deicer salt application and the other had not. The bridge that had received deicer applications was constructed in 1972. It is a four-span, steel I-beam and multigirder structure on the eastbound lanes of traffic route 322 at the Oak Hall interchange in central Pennsylvania. Steel stay-in-place forms had been used for deck placement. The bridge was placed in service in November 1973, and therefore, it had been subjected to three winter seasons of deicer salt applications at the time of test. The 1.52 m x 3.66 m (5 ft. x 12 ft.) test area was selected in the acceleration lane of the west end span, the lowest area of the deck. This area of the deck was selected because it was felt that the deck drainage would tend to concentrate the deicer salts in this area. Chloride determinations (using the Berman titration technique) (12) gave values that ranged from 2.43 kg Cl^-/m^3 (4.1 lb Cl^-/cu yd) at the surface to 0.18 kg Cl^-/m^3 (0.3 lb Cl^-/cu yd) at a depth of 3.8 to 5.1 cm (1 1/2 to 2 in.) adjacent to the test site and 1.42 to 0.95 kg Cl^-/m^3 (2.4 to 1.6 lb Cl^-/cu yd) at 1.3 to 3.8 cm (1/2 to 1 1/2 in.) in the water table area at the actual low point of the deck.

Although the second bridge was constructed in 1971, it had not yet been placed in service (as of impregnation) and had received no deicer applications. It is a three-span, prestressed spread box beam structure on the eastbound lanes of traffic route U.S. 322 over the Bellefonte Central Railroad right-of-way near Toftrees, Pennsylvania. Conventional wood forms had been used for deck placement. The 1.52 x 3.66 m (5 ft x 12 ft) test area was selected in the traffic lane of the west end span.

Procedure

In order to permit impregnation depths of at least 5.1 to 6.4 cm (2 to 2 1/2 in.), the drying criterion adopted for the field tests was the attainment of a temperature of 110°C at 10.2 cm (230°F at 4 in.). This was accomplished using propane-fired, catalytic infrared heaters in much the same manner as drying was carried out on the large test slabs in the laboratory. Drying of each of the two 1.52 m x 3.66 m (5 ft x 12 ft) test areas was done in two 1.52 m x 1.83 m (5 ft x 6 ft) sections using a trailer mounted unit in combination with a smaller portable unit. The drying operation is illustrated in Figure 1.

Figure 1. Drying the test area with gas fired IR heaters.

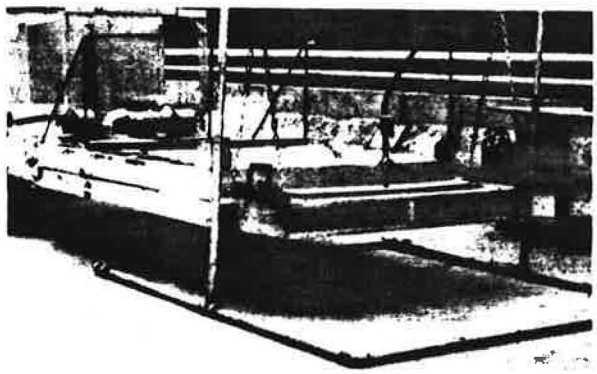

In order to monitor the heating process relative to the drying criteria presented above, copper-constantan (Type T) thermocouples were installed at the surface and at a depth of 10.2 cm (4 in.) in 0.64 cm (1/4 in.) diameter holes drilled from the top surface. The thermocouple outputs were continuously recorded. Spot temperature checks were also made with a handheld thermocouple indicator. The time-temperature curves for the two test sections are shown in Figure 2. In both cases, these are the data for the first of the two equipment set-ups needed to cover the designated test areas, and the temperatures have been corrected for top insertion. The second set-ups in each case produced similar results. It is noteworthy that the drying process on the non-contaminated (Toftrees) deck was carried out during a light, but steady, rain. To prevent rewetting of the dried areas, timber dams sealed with caulking were placed around the periphery to divert surface drainage, and the areas were covered with galvanized sheet metal.

Figure 2. Typical temperature vs. time during drying on bridge decks.

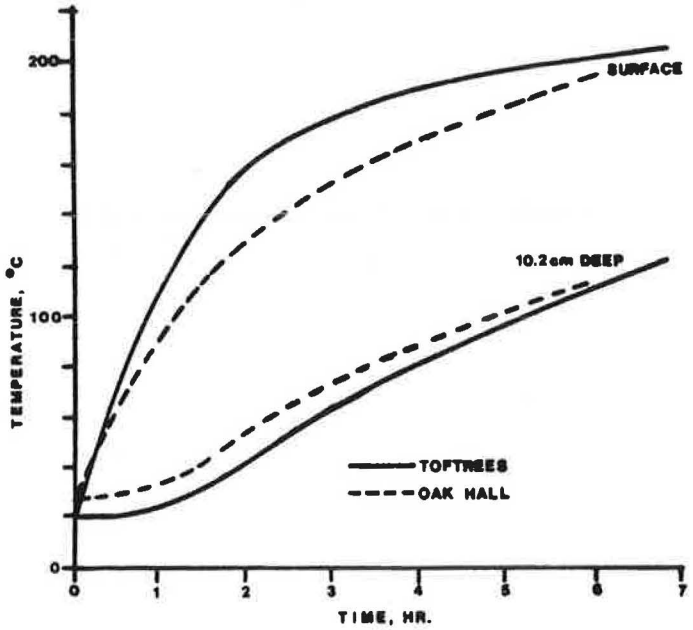

As shown in Figure 2, the time required to meet the stated drying criterion, 110°C at 10.2 cm (230°F at 4 in.), was about six hours in both instances. This is somewhat longer than encountered in the laboratory, but not unexpected in view of the effects of wind and heat conductivity. Since the propane consumption rate was approximately 2.44 kg/m^2/hr (0.5 lb/sq ft/hour) with the heating devices employed, the unit fuel consumption for drying to 4 in. was about 12.2 kg/m^2 (2 1/2 lb/sq/ft). Larger unit heaters required for practical full-scale field application (units up to 3.66 m x 12.19 m (12 ft x 40 ft) have been built) would undoubtedly have lower fuel consumption because of reduced heat loss due to the smaller perimeter to heating area ratio. Also, shallower depths of drying will require less fuel, the quantity required being approximately proportional to the depth of drying in the range of 2.5-10.2 cm (1-4 in.).

After the test areas had cooled for about two hours, impoundment dams for containing the impregnant were constructed with building brick and mortar, sealed with epoxy resin. For practical, full-scale bridge work, it is envisioned that portable, reusable dam sections might be used in conjunction with a suitable sealing or gasket material. For the purpose of this study, however, the brick and mortar technique was quick, efficient, and provided reliable impoundment.

After the surface temperature dropped into the range 45°-50°C (113-122°F), the impregnant, a 50-50 mixture by weight of boiled linseed oil and mineral spirits, was introduced into the impoundment. The temperature range cited above optimizes the opposing effects of temperature and evaporation of diluent (mineral spirits) on the viscosity, and hence, the penetration rate, of the impregnant. After ponding the area with the impregnant, it was covered with plywood sheathing and a tarpaulin for weather protection.

Based on the results of the laboratory studies, reported earlier, the ponding process at each site was carried on for four days in an effort to obtain at least 6.4 cm (2 1/2 in.) of penetration.

After completion of the required period of ponding, 10.2 cm (4 in.) diameter cores were removed from the two test areas to ascertain the depth of penetration. In all, three cores were removed from the Oak Hall and two from the Toftrees deck. The appearance of the cores shortly after removal are shown in Figures 3 and 4. The depth of heavy penetration of the impregnant is clearly evident in these photographs. However, as will be shown below, the depth of sealing extends considerably deeper than this zone.

Figure 3. Cores removed from Oak Hall deck.

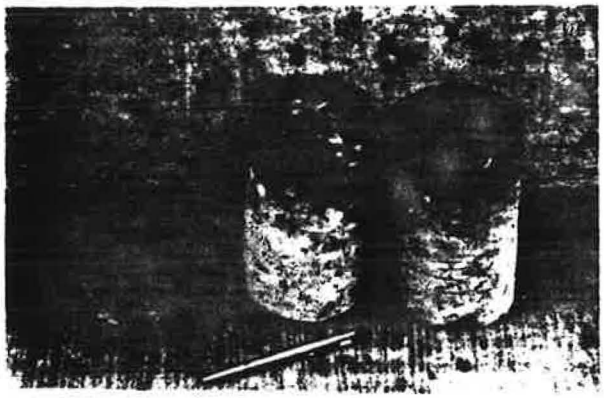

Figure 4. Cores removed from Toftrees deck.

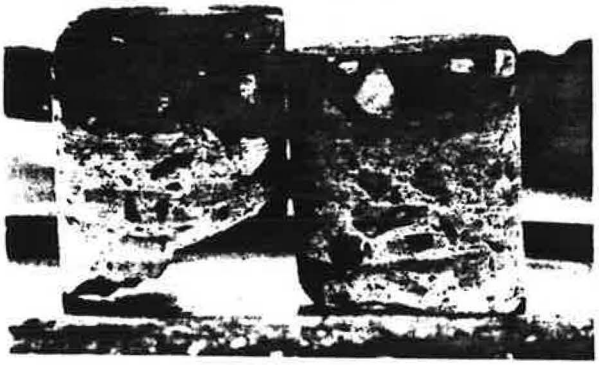

Each of the cores was sectioned longitudinally with a diamond saw. One half-section of each core was then polished in successive grinding steps on a lap to 1900 fineness. The other half of each core was etched with concentrated hydrochloric acid for about 10 minutes. The results are shown in Figures 5 through 8. The polished sections clearly show depths of penetration of 5.7 to 6.4 cm (2.25 to 2.5 in.) for the Oak Hall Cores and 2.5 to 5.1 cm (1 to 2 in.) for the Toftrees cores. However, acid etching reveals that the actual depth of sealing ranges up to 10.8 cm (4.25 in.) and 7.0 cm (2.75 in.), respectively. The rather significant difference in penetration between the two decks is believed to be due to the fact that the drying and initiation of the impregnation step were carried out on the Toftrees deck during a steady rain storm. It would definitely not appear to be related to the presence of deicer salts

because the Toftrees deck, the deck with the lesser penetration, was the deck which had not been subjected to deicer application. In any event, it is clear that the goal of sealing the concrete to a depth of approximately 6.4 cm (2 1/2 in.) was attained.

Figure 5. Oak Hall core specimens (polished).

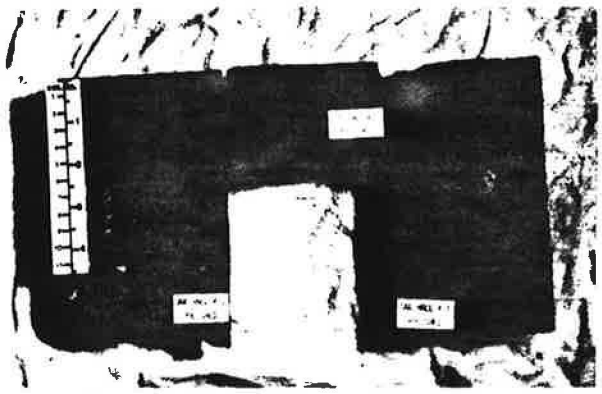

Figure 6. Oak Hall core specimens (acid etched).

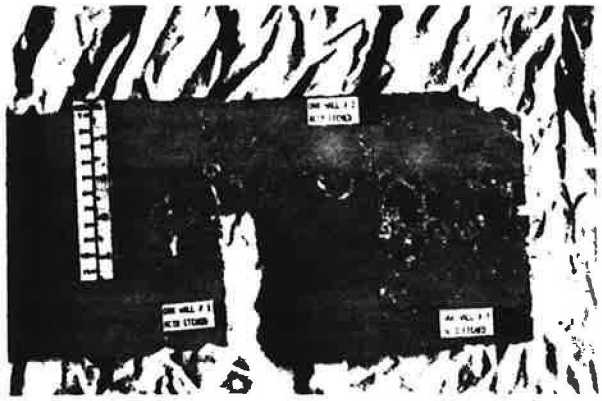

Figure 7. Toftrees core specimens (polished).

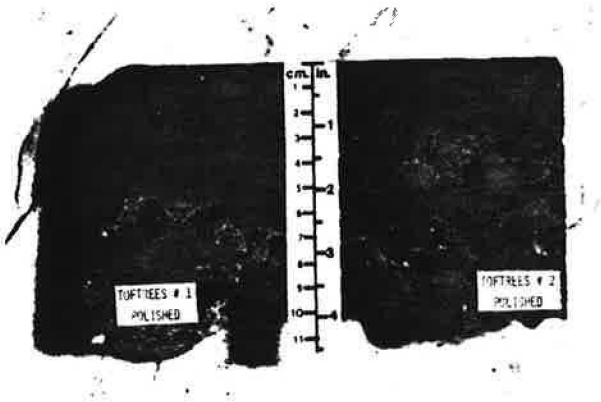

Figure 8. Toftrees core specimens (acid etched)

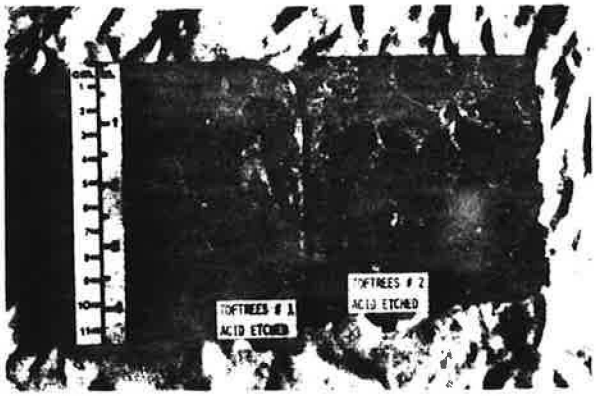

Applicability of Results

While the equipment used in this research is not of sufficient size to be practical for commercial application, it is readily amenable to scale-up. Based on the work reported here, it is estimated that with equipment of appropriate size, a 12 m wide by 60 m long (40 ft x 200 ft) bridge deck could be impregnated in less than two weeks. If it is assumed that 15 bridge decks of this size were done per year and the capital equipment is amortized at 6 percent, has zero salvage value, and a 10-year life, it is estimated that the unit cost, excluding contractors' profit, for commercial impregnation will be about $\$23.35/m^2$ ($2.17 per sq ft). This is based on summer 1976 costs. Of this estimated cost, 41 percent is for the impregnant, 29 percent for labor, 18 percent for fuel, and 12 percent for capital recovery and maintenance of equipment.

Conclusions

The following conclusions appear to be warranted relative to the research described in this paper:

1. Concrete that has been suitably dried to temperatures of at least 110°C (230°F) can be impregnated to depths of 5 to 10 cm (2 to 4 in.) by ponding a mixture consisting of equal parts by weight of boiled linseed oil and mineral spirits for a period of 4 days.
2. Corrosion potentials of actively corroding reinforcing steel in salt contaminated concrete slabs are significantly reduced by impregnation with 50-50 boiled linseed oil-mineral spirits mixtures.
3. The techniques developed were demonstrated to be applicable in the field and, with appropriate scale-up, should be commercially feasible.

However, the long-term benefits of deep impregnation with linseed oil in the field remain to be demonstrated.

Acknowledgments and Disclaimer

This work was sponsored by the Pennsylvania Department of Transportation and the U.S. Department of Transportation, Federal Highway Administration. The contents of this paper reflect the views of the authors who are responsible for the

facts and the accuracy of the data presented herein. The contents do not necessarily reflect the official views or policies of the Pennsylvania Department of Transportation or the Federal Highway Administration.

References

1. Concrete Bridge Deck Durability. NCHRP Synthesis of Highway Practice--4, Highway Research Board, 1970, 28 pp.

2. R. E. Carrier and P. D. Cady. Factors Affecting the Durability of Concrete Bridge Decks. Special Publication SP-47, American Concrete Institute, 1975, pp. 121-168.

3. Durability of Concrete Bridge Decks. Report 5, Portland Cement Association and U.S. Bureau of Public Roads in Cooperation with Ten State Highway Agencies, 1969, 46 pp.

4. Durability of Concrete Bridge Decks. Final Report, Portland Cement Association and U.S. Bureau of Public Roads in Cooperation with Ten State Highway Agencies, 1970, 35 pp.

5. Environmental Impact of Highway Deicing. Water Pollution Control Research Series 11040 GKK 06/71, Environmental Protection Agency, June 1971, 120 pp.

6. L. D. Sandvig. PennDOT Attacks Bridge Deck Durability Problem. Highway Builder, Nov. 1974, pp. 16-17, 42.

7. G. Dallaire. Designing Bridge Decks That Won't Deteriorate. Civil Engineering, Vol. 43, No. 8, Aug. 1973, pp. 43-48.

8. K. A. Godfrey, Jr. Bridge Decks. Civil Engineering, Vol. 45, No. 8, Aug. 1975, pp. 60-65.

9. One in Six U.S. Highway Bridges is Deficient, Engineering New Record, March 10, 1977, pp. 18-21.

10. R. F. Stratfull. Half-Cell Potentials and the Corrosion of Steel in Concrete. Highway Research Record No. 433, Highway Research Board, 1973, pp. 12-21.

11. K. C. Clear, and R. E. Hay. Time to Corrosion of Reinforcing Steel in Concrete Slabs: Vol. 1. Effect of Mix Design and Construction Parameters. Report No. FHWA-RD-73-32, Federal Highway Administration, Interim Report, April 1973, 103 pp.

12. K. C. Clear, Evaluation of Portland Cement Concrete for Permanent Bridge Deck Repair. Report No. FHWA-RD-74-5, Federal Highway Administration, Feb. 1974, 48 pp.

A DEMONSTRATION PROJECT FOR DEICING OF BRIDGE DECKS

Charles H. Wilson, David H. Pope, Wyoming Highway Department
Vic A. Cundy, John E. Nydahl, and Kynric M. Pell, University of Wyoming

An experimental facility to study the use of gravity operated heat pipes to couple earth heat to a bridge deck for snow and ice control has been developed at a site in southeastern Wyoming. Fifteen heat pipes of three different designs were incorporated in the design and construction of a composite bridge deck. Nine standard heat pipes 24.4 m (80 ft.) long and 2.5 cm (1 in.) outside diameter were installed transverse to the direction of traffic flow 5 cm (2 in.) below the deck surface on 15 cm (6 in.) centers. These pipes extend from depths of 15 m (50 ft.) in the earth up through the earth surface and through the edge of the deck to the bridge centerline. The performance of the heat pipe system has been monitored and recorded continuously at one minute intervals for over one year using a variety of instrumentation transducers and a digital data acquisition system. In addition the surface conditions on the deck and the adjacent roadway were recorded photographically at five minute intervals during daylight hours. The results obtained demonstrate that heat pipes can be an effective means of snow and ice control on bridge decks.

Heat pipes are a relatively recent invention (1) and have proven extremely efficient for transferring thermal energy. They have been widely used for thermal control of spacecraft and are being incorporated in an increasing variety of earth bound applications. Bienert and Pravda, et al. (2) proposed that gravity operated heat pipes be used to transfer low grade energy from the earth below highway structures to the road surface for control of ice and snow. The concept was investigated experimentally using several concrete slabs incorporating heat pipes in a study conducted at the Fairbank Highway Research Station (3,4). Results of this study were used in the design of a heat pipe system installed in a 366 m (1200 ft.) long interchange ramp in Oak Hill, WV (5). This system has operated successfully for the past two years. The use of heat pipes for control of preferential icing of bridge decks was investigated by Ferrara and Yenetchi in a study undertaken in 1975 (6). Somewhat earlier, work had been initiated at the University of Wyoming on modification of a heat transfer simulation for highway structures (7) to treat the case of heat transfer from the ground to a bridge deck via heat pipes (8). The simulation was used to investigate the performance of a heat pipe system at a site located in southeastern Wyoming. It was shown that heat pipes could be effective for the control of preferential icing; however, uncertainties in the thermal modeling of the coupling between the heat pipes and the earth imposed a requirement for field testing prior to incorporation of heat pipes in a major structure located in a severe environment. In the Spring of 1976, the Wyoming Highway Department and the University of Wyoming entered into an agreement to conduct a rather extensive research program on the thermal control of bridge decks using gravity operated heat pipes. In particular, a limited number of heat pipes and requisite instrumentation were to be incorporated in the construction of a new bridge. The overall objective of the research program was to generate an empirical data base on the insitu performance of gravity operated heat pipes. Specific goals of the program included:

1. Measurement of the power and energy delivered to the deck by a heat pipe.
2. Characterization of the thermal coupling between the earth, the heat pipe and the bridge deck.
3. Investigation of the thermal recovery of the earth surrounding the heat pipe during periods when the heat pipes were not functioning.
4. Characterization of the relative surface condition of the unheated portion of the bridge deck, the heated section of the deck and the adjacent roadway during an entire winter season.
5. A variety of minor studies, such as, the use of unconventional heat pipes.

This paper describes the design, fabrication and installation of the heat pipes and instrumentation at the experimental site which is located at a bridge over Sybille Creek on State Highway No. 34 in southeastern Wyoming.

Heat Pipes

Conventional Heat Pipes

A conventional gravity operated heat pipe is a closed chamber, generally constructed of metal, containing a volatile working fluid. Figure 1(a)

Figure 1. Configurations of three types of heat pipes.

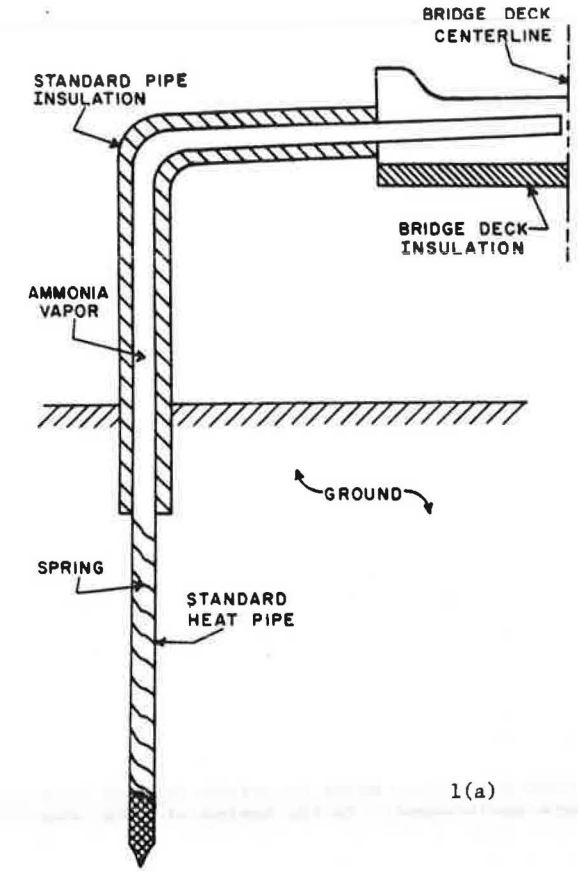

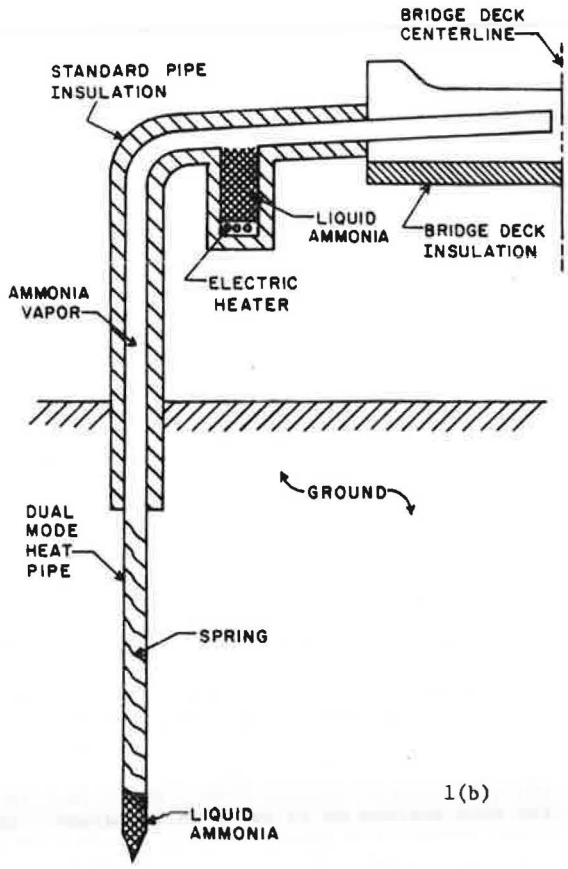

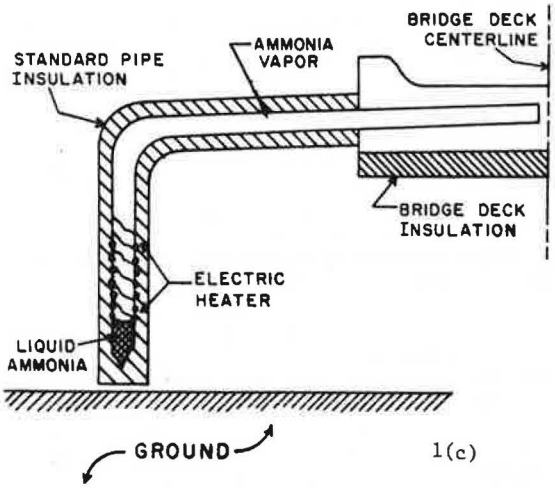

illustrates the standard heat pipes used in this study. The heat pipes were fabricated from seamless, cold rolled, low carbon steel tubing with an outside diameter of 2.5 cm (1 in.) and a 0.3 cm (1/8 in.) wall thickness into 24.4 m (80 ft.) lenghts. These tubes were evacuated and filled with 0.2 kg (0.45 lbm) of ammonia which was also the condensable fluid that was used in the other two demonstration projects. Over the temperature range that a heat pipe was exposed to, part of the ammonia resided as a liquid in a pool at the bottom of the tube while the remaining ammonia was in the vapor phase filling the rest of the tube. Anytime the deck temperature fell below the temperature of the ground in contact with a heat pipe, the vapor in the deck section condensed and flowed towards the bottom of the tube. At the same time, energy was conducted from the ground to the colder heat pipe where it evaporated part of the liquid ammonia. The spring in the evaporator section was used to increase the area that was wetted by returning condensate. The heat pipe is essentially an isothermal device since the energy is transferred in the form of latent heat of evaporation instead of sensible heat. It was therefore ideally suited for this application where low grade energy was extracted from the ground. Besides its apparent constructional simplicity, this device is self-regulating, should have a long lifetime, and could possibly be incorporated as part of the rebar structure.

Dual Mode Heat Pipes

Three experimental heat pipes were also used in the project. Their design termed here, dual mode, is illustrated schematically in Figure 1(b). As the name implies this heat pipe has two means of energy input. In addition to the standard evaporator in the ground there was an additional evaporator provided at a convenient location above ground. The purpose of this design was to allow additional energy to be transferred to the bridge surface when necessary by heating the secondary evaporator with an alternate energy source. Electrical resistance heaters were mounted in good thermal contact with the bottom of the secondary evaporator. These heat pipes operated as conventional heat pipes when the secondary evaporator was full of liquid ammonia and no power was applied to the heaters. When additional

power was required and the heaters were activated some of the ammonia vapor from the secondary reservoir condensed in the lower part of the pipe as well as in the condenser and eventually the liquid ammonia in the secondary evaporator was depleted. The secondary evaporator was then recharged through a period of operation as a conventional heat pipe.

Electric Heat Pipes

Figure 1(c) is typical of three electrically operated heat pipes which were installed at the site. The evaporator sections of these pipes protruded from the side of the deck and were equipped with external heaters to provide the energy input. These pipes were included for two reasons. First, they could be heated using a controller to provide an accurate measurement of the power being provided by the standard heat pipes. Secondly, this design appears to be a viable approach to coupling renewable energy sources such as wind energy to a bridge deck and therefore merits further study.

Fabrication and Installation of Heat Pipes

Fabrication

Fabrication of the heat pipes involved the following seven steps regardless of the particular type of pipe being fabricated:

1. Cleaning of the tubing.
2. Installation of the springs.
3. Welding of the tubing sections.
4. Evacuation of the pipe.
5. Loading of the ammonia.
6. Crimping and welding of the fill nipple.
7. Testing.

Cleaning of the tubing was initiated with a solvent rinse using unleaded gasoline which was followed with a mechanical abrasive cleaning using SOS pads and alcohol. Following an acetone rinse, a clean dry rag was pulled through the tubes.

The inside wall of each of the evaporator sections was lined with a spring to cause the condensate to spiral down the pipe rather than run down one side in the form of a rivulet. This wets the wall more effectively allowing more efficient and uniform vaporization. There was a mechanical problem due to the fact that the springs must be tight against the inside wall of the pipe. Piano wire was wound on a mandrel in a lathe and placed inside the heat pipe where it was released to uncoil against the inside of the pipe.

Welding of the 6 m (20 ft.) lengths of seamless tubing to form the 24 m (80 ft.) heat pipes was accomplished using a TIG arc welder and an end cap was welded on one end and a workable steel nipple was welded to the opposite end. The pipes were evacuated using conventional vacuum techniques and then filled with 0.2 kg (0.5 lb) of ammonia. Finally, the nipples were crimped and welded. Testing of the pipes included resistive heating of the evaporators to cause the heat pipes to operate for a period of one month. The pipes were situated on an incline of approximately 5° for this test. Each weld was also tested chemically using a technique developed by NASA to insure that the leak rate was less than 3.3×10^{-7} std cc sec^{-1} (9). Fabrication of the dual mode and electrically operated heat pipes was similar to the conventional heat pipes.

Installation

After all of the footings had been poured at the bridge site, but prior to construction of any above ground formwork, a drilling crew from the geology division of the state highway department drilled 12 holes 15 cm (6 in.) in diameter and 18.3 m (60 ft.) deep at the locations indicated in Figure 2. The holes were cased with 10 cm (4 in.) PVC. Three men assisted in guiding each pipe into its particular hole and all twelve pipes were installed, using a crane, in two hours. In order to make the heat pipes as unobtrusive as possible during the subsequent construction, they were left standing vertical and the 6 m (20 ft.) to 9 m (30 ft.) of pipe extending beyond the surface of the ground was guyed off as shown in Figure 3. The pipes were installed in late October 1976 and remained in the vertical position until early in December when they were bent into position on top of the rebar. The bending operation may be seen in Figure 4. and the position of the pipes in the deck is shown in Figure 5. A manual tubing bender commonly used by electricians was used to bend the pipes. All of the heat pipes were tied to the rebar at a depth of 5 cm (2 in.) below the surface on 15 cm (6 in.) centers. The 2 percent slope from the centerline to the curb was adequate to insure that the condensate would flow back to the evaporator.

Wooden dowels were attached to the formwork under and in the vicinity of the heat pipes as shown in Figure 5. After the deck was poured, the PVC casing was removed from the holes surrounding the heat pipes with the exception of a 3 m (10 ft.) long section which was left extending from the surface down into the earth. The holes were backfilled with bentonite up to the PVC and then the region where the casing remained was insulated with strips of rigid, closed cell, insulation. The exposed portion of the pipe between the earth and the bridge deck was insulated with standard fiberglass pipe sections which were in turn wrapped with a thin plastic cover.

Instrumentation

Temperature Sensors

Previous investigations involving measurement of temperature in bridge decks and the earth have shown that thermistors can be a cost effective approach to temperature measurement; however, care must be taken to protect the small leads from vibration and to protect the thermistor and its associated circuitry from moisture (10). The technique used to instrument the deck involved attaching a thermistor and its precision resistor to each of ten pairs of shielded, twisted, conductors in an eleven pair cable. A single precision resistor was connected across the eleventh pair of conductors in the cable. The termistors and resistors were then potted in high thermal conductivity epoxy in one of the configurations shown in Figure 6.

The approach used on fabrication of the ground sensors was somewhat different and was intended to provide more assurance that moisture would not penetrate the cable or sensor. A short section of the outer jacket of the cable was peeled back and a single twisted pair of conductors was cut to install the thermistor and associated resistor. A cylindrical mold incorporating a reduced diameter on each end was used to cast an epoxy housing for the sensor. The cylinder was concentric with the cable. Silicone rubber sealant was then applied to the exposed shielded conductors and the shoulder of the epoxy

Figure 2. Schematic arrangement of experimental site.

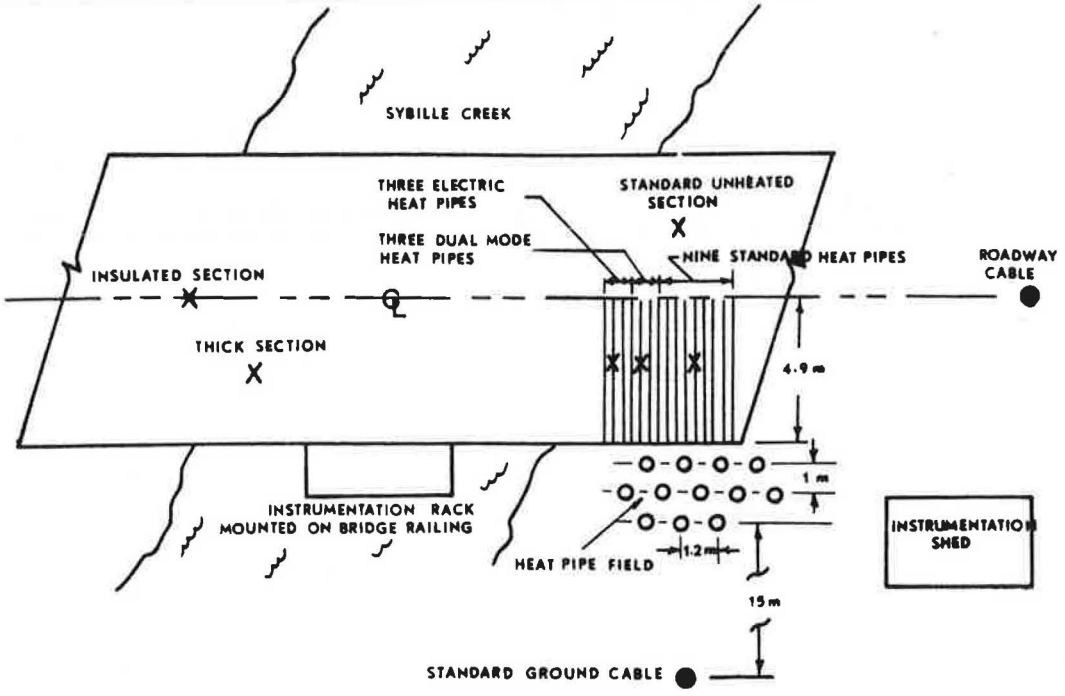

Figure 3. Heat pipes installed in the ground.

Figure 4. Heat pipes bent into the bridge deck.

Figure 5. Heat pipes and instrumentation dowels in the bridge deck.

step. The outer jacket of the cable was pulled over the shoulder of the epoxy and a fine wire was used to clamp the outer jacket to the epoxy. A small amount of silicon rubber sealant was applied to the outside of the cable jacket at the epoxy interface. A second mold was used to form a complete epoxy cylinder by filling in the region of the step. This sequence is illustrated photographically in Figure 7.

The technique used to instrument the heat pipes in the ground was similar to those described previously; however, each cable included only a single pair of conductors. An epoxy cylinder housing the thermistor and its resistor was cast concentrically on the heat pipe at various axial locations. The cylinders were 4.5 cm (1.7 in.) in diameter and 2.5 cm (1 in.) in length.

The wooden dowels installed prior to pouring the deck were drilled out to allow installation of the temperature sensors from the bottom of the deck as shown in Figure 8. Sensors were installed to mea-

Figure 6. Typical temperature sensor design and placement.

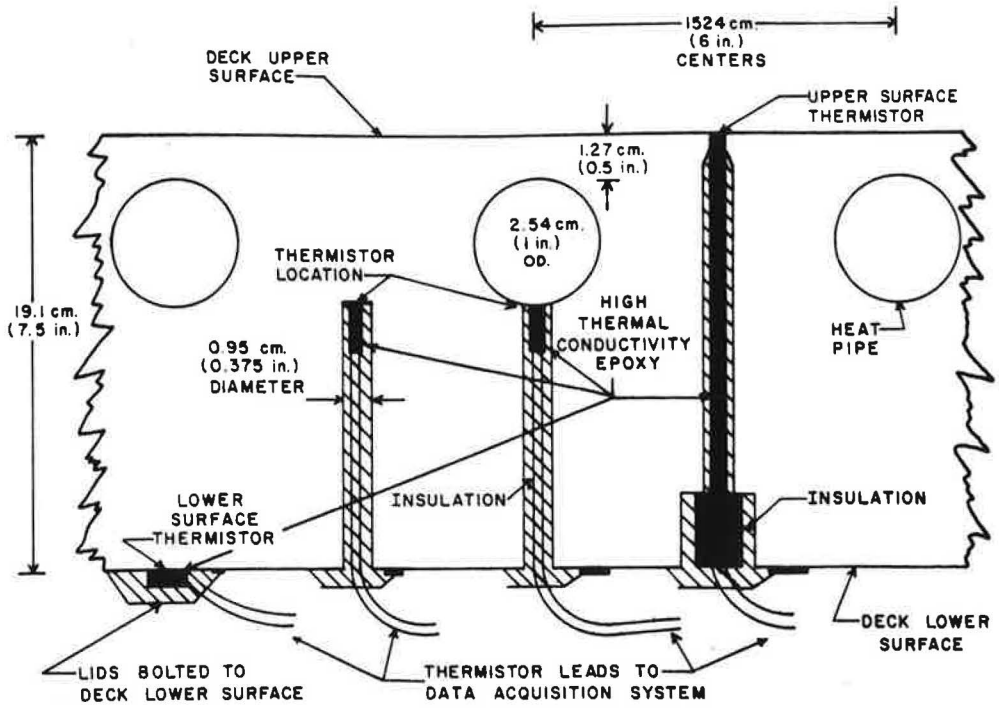

Figure 7. Sequence of fabrication steps for temperature sensors.

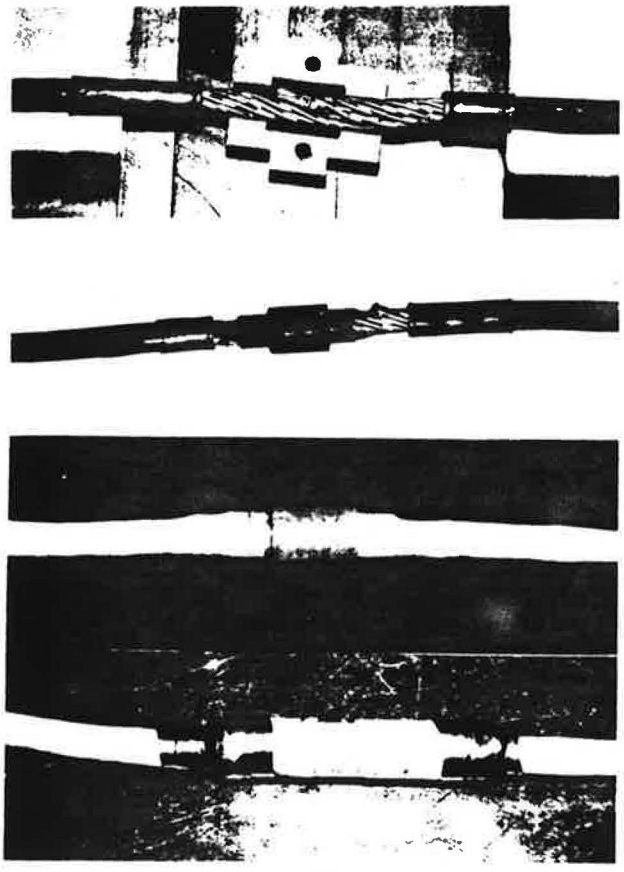

Figure 8. Instrumentation as viewed from the bottom of the bridge deck.

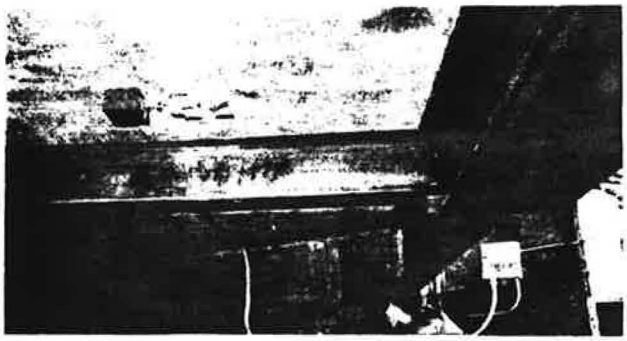

sure vertical temperature distributions in the deck at the locations indicated in Figure 2. In addition, one of each of the different heat pipes was instrumented with a symmetrical array of temperature sensors approximately at the midpoint of the condenser. Temperature sensors were also located on the surface of each heat pipe approximately 0.6 m (2 ft.) from the centerline of the bridge. The dual mode heat pipes each had a thermistor on the secondary reservoir approximately 2.5 cm (1 in.) above the bottom and an additional thermistor about 0.3 m (1 ft.) from the secondary evaporator on the surface of the condenser.

Two ground temperature instrumentation cables were fabricated with temperature sensors located at 1.5 m (5 ft.) intervals over a distance of 12 m (40 ft.). These cables were installed in 15 cm (6 in.) diameter holes indicated in Figure 2. which were then back filled with sand.

Table 1. Meteorological Instrumentation.

Parameter	Sensor	Sensor Range	Sensor Accuracy	System Accuracy
Relative Humidity	General Eastern Model 400-C	0-100%	±0.5%	±0.5% Humidity
Solar Radiation	Eppley Labs Model 8-48	0-2 cal.cm^{-2}min^{-1}	±1%	±.02cal.cm^{-2}min^{-1}
Reflected Radiation	Eppley Labs Model 8-48	0-2cal.cm^{-2}min^{-1}	±1%	±.02cal.cm^{-2}min^{-1}
Wind Speed	Electric Speed Indicator Model 420CR	0-100 Knots	±1%	±1 Knot
Wind Direction	Electric Speed Indicator Model 420CR	0-360 Degrees	±1%	±4 Degrees
Barometric Pressure	H.E. Sostman Co. 2014	19.2-25.7" Hg	±0.1%	±0.065" Hg
Precipitation	Science Associates Model 598-2	Yes-No	----	----------
Temperature	Yellow Springs Inst. Thermilinear Thermistors	-50°C→+150°C	±0.15%	±0.32°C

Meteorological Sensors and Data System

The meteorological sensors and the data acquisition system were moved from the site of a previous experimental program and installed at the Sybille Canyon project after refurbishment and calibration in the laboratory. A list of the transducers installed at the site is provided in Table I. The data acquisition system is housed in the concrete shed illustrated in Figure 2. This system was designed and fabricated at the University of Wyoming and is capable of sequentially sampling, digitizing, and recording 100 channels of analog input in less than four seconds. The entire system consisting of a line voltage regulator, digital system and digital recorder is mounted in one instrumentation rack. The digital system includes an electronic multiplexer, amplifier, A/D converter, digital clock, and a logic module. These components are mounted in functional arrays on printed circuit boards. A rack mounting unit with appropriate card guides and terminal strips houses the complete digital system. In order to isolate the data acquisition system from transients introduced by the various heaters and the air conditioner in the instrumentation shed, a separate power line, operating off its own step down transformer, was provided.

Precipitation data was obtained from the Wyoming Game and Fish Commission Sybille Canyon Experiment Station, which is 0.8 km (0.5 mi.) west of the bridge site.

Other Instrumentation and Cabling

Surface conditions on the bridge deck and the adjacent roadway were monitored using a time lapse camera which was mounted on the instrumentation rack. The camera is a modified super eight movie camera which can be driven electronically by a variable timer which was set to provide a photograph every 5 minutes during daylight hours.

Power delivered by the standard heat pipes was measured indirectly by heating the electric heat pipes so that their condenser temperature matched the condenser temperature of the standard heat pipes and recording the amount of power delivered to the electric heat pipes. A simple binary controller was found to be suitable for maintaining the temperature of the electric heat pipes within 1 C° (1.8 F°) of the standard pipes.

Two 10 cm (4 in.) diameter PVC conduit were run underground from the shed to the bridge. All of the data cables installed on the bridge were run in steel conduit to a box at the bridge end of the PVC conduit and then through the PVC back to the instrumentation shed. The AC power lines for the various heaters and a utility outlet installed under the bridge were routed through the other PVC conduit in an attempt to isolate noise from the data lines. Cabling for the heat pipe instrumentation installed in the ground was gathered in a metal box located just below the earth surface in the heat pipe field and run through an underground conduit to the instrumentation shed. The roadway instrumentation cable and the ground cable were also installed in metal conduit.

Testing and Calibration

The fixed value precision resistors on the instrumentation cables provided a means of correcting the temperatures read by the data system for systematic errors. Several different values of resistance were used so that any nonlinearity in the system response could also be detected and taken into account. Based on twelve months of data from these resistors a systematic correction of 0.4 C° (0.7 F°) was applied to all temperature readings. Thermistors also exhibit a systematic nonlinearity which was almost completely compensated for using a sinusoidal response correction. With both of these corrections taken into account the absolute accuracy of the temperature measurements is ± 0.3 C° (0.5 F°).

Calibration of the radiometers was accomplished by direct comparison of their outputs with a super radiometer which was periodically taken to the field site. The anemometer and humidity detection system

were calibrated in the laboratory periodically. Wind direction and barometric pressure transducers were not calibrated on a routine basis but were periodically checked for consistency.

Results and Conclusions

The data acquisition system has been recording data continuously at one minute intervals since March 1977. During this period two of the sixty thermistors installed at the site have failed. A power supply in the digital system failed causing the loss of two days data, an instance of improper mounting of the magnetic tape caused the loss of six days data, and a power disruption due to a severe storm accounted for the loss of three days data. A decrease in the brush contact force on the anemometer resulted in invalid readings of wind speed during a thirty-day interval.

A detailed study of the accuracy of the temperature measurements indicated that the design of the temperature sensors was not only effective in providing protection from the environment but also led to accurate readings. With the exception of the anemometer the meteorological transducers and the time lapse camera proved extremely reliable.

In summary, of 487 days when data could have been recorded there were eleven days during which all data was lost. In addition there were 36 days when the wind speed data was in error.

The heaters for the dual mode and electric heat pipes utilized nichrome wire resistance heaters which were originally designed to provide 600 w (2050 Btu/hr) each. The high power requirement and compact design led to repeated heater failures. In January of 1978 the heaters for the electric heat pipes were replaced utilizing a design which incorporated shielded nichorme wire and provided 300 w (1025 Btu/hr). Although some noise problems were originally encountered in the operation of the electric heat pipe controllers they were found to be very effective in tracking the temperature of the standard heat pipes. The dual mode heat pipes were operated on numerous occasions with manual control of the heaters on the secondary evaporators. The period for which the heaters could operate prior to depletion of the ammonia in the secondary evaporators was found to be a linear function of the power applied.

A detailed description of the performance of the heat pipe system has been given elsewhere (11) but in the interest of completeness those results will be summarized here. In response to a rather severe environment where the yearly mean temperature was 6.7°C(44°F) and the monthly average temperature for January was -5.3°C (22.5°F) the heat pipes functioned intermittently from September to May. Typically, they provided energy to the deck during the night and in the daylight hours if precipitation occurred. However, even in severely cold weather the solar heating of the deck which occurred during the day was generally sufficient to heat the deck above the earth temperature at depth thereby shutting off the heat pipes. During an eight month period each pipe delivered in excess of 1×10^9 joules (1×10^6Btu) at an average rate of 125 w/m^2 (40 Btu/hr-ft^2). A monthly summary of the energy flux is given in Figure 9 where it may be noted that the maximum flux occurred in November. The earth surrounding the heat pipes was cooled a maximum of 7C° (13F°) below the undisturbed earth in January; however, the temperature at the surface of the heat pipes recovered to the undisturbed earth temperature by July.

The heated portion of the deck was below freezing 30% of the time that the standard deck was below

Figure 9. Energy flux for a single heat pipe.

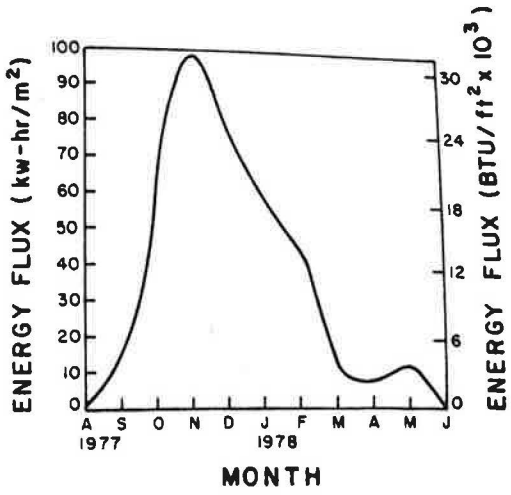

Figure 10. Typical early morning snow pack.

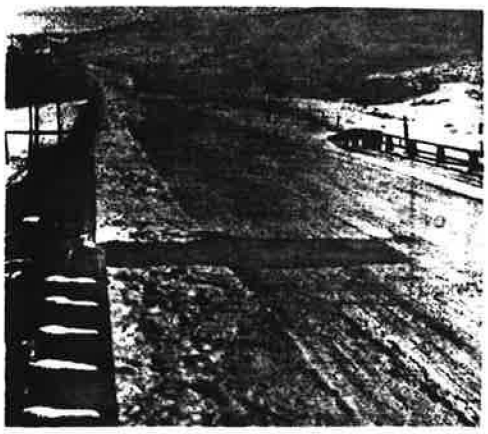

Figure 11. Typical snow pack situation as day progresses.

freezing. Although the surface of the standard (unheated) bridge deck was colder than the surface of the adjacent roadway it was, on the average, only two degrees colder and as a result the roadway had only 7% less time below freezing than the standard deck. The roadway, however, experienced twice as many freeze-thaw cycles as the standard deck.

Although the heat pipes were not capable of melting all of the snow as fast as it fell, they were completely successful in eliminating all instances of preferential icing. Figures 10 and 11 are typical of

Figure 12. Typical 28 hour period exhibiting diurnal cycling of heat pipes.

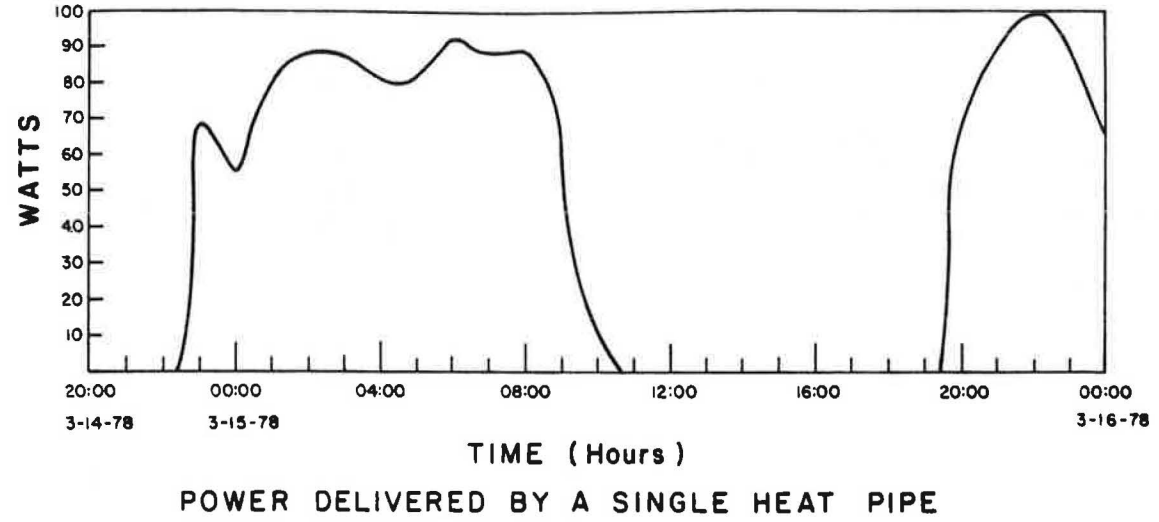

POWER DELIVERED BY A SINGLE HEAT PIPE

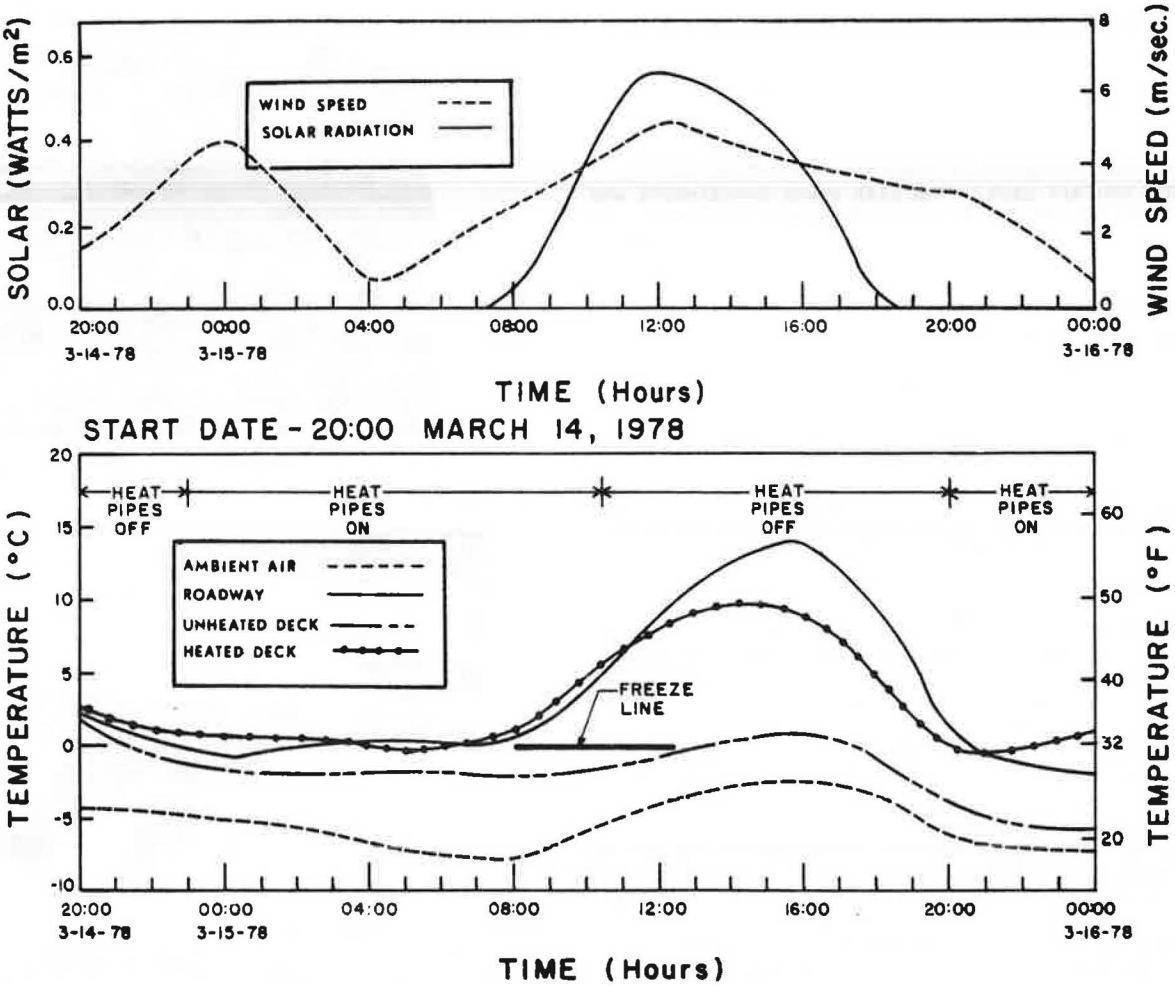

the two most common situations involving accumulated precipitation. The case where the heat pipes were melting the snow and both the roadway and unheated deck were snow covered is shown in Figure 10. Generally, as the day progressed the roadway would clear and the situation shown in Figure 11 would develop.

Figure 12 depicts some of the most significant environmental variables and the corresponding surface temperature for the standard deck, heated deck and the adjacent raodway. Also shown in the figure is the power delivered by a heat pipe. The diurnal cycling of the heat pipes in response to the thermal coupling of the environmental parameters to the deck is evident. For the period of heating shown the average power is 80w (273 Btu/hr) and the peak power is 100w (342 Btu/hr). It may be seen that the heated portion of the deck remained above freezing, corresponding closely to the temperature of the adjacent roadway, whereas the unheated deck was below freezing a significant amount amount of time and experienced a freeze-thaw cycle.

Heat pipes utilizing energy from the upper 15m (50 ft.) of the earth have been demonstrated to be effective in eliminating preferential icing of a section of bridge deck in a quite severe environment. The location of the heat pipes in the bridge and the manner of installation were selected to minimize problems associated with construction of the bridge and interfacing of the bridge and heat pipes. It would not only be difficult to use a similar approach on an entire bridge of any size, but also rather expensive. There are two avenues for future study which could significantly reduce the cost of a heat pipe system and also reduce the potential construction problems. Techniques for manifolding several heat pipes from a single header pipe should be investigated. In addition, techniques for field assembly of a heat pipe composed of two or more segments would compliment the manifolding study.

Acknowledgments

The data acquisition system and heat pipe controllers were designed and fabricated under the direction of George Twitchell, Electronics Engineer, Department of Mechanical Engineering. A number of students in the Mechanical Engineering Department have been involved in the project. John Niethammer and Mark Weber assisted in the construction of the heat pipes. Doug Stephen assisted all of the above personnel with the installation of the heat pipes. Data reduction has occupied Doug Stephen, Tom Munro, Bruce Wise, Steven Ownbey and Victor Dlugoszewski.

References

1. S.W. Chi, Heat Pipe Theory and Practice. McGraw-Hill Book Comapny, New York, 1976.
2. W.B. Bienert, M.F. Pravda, et al., Nuclear Wastes in Comparison with Other Heat Sources for Deicing, Bridges, Ramps and Pavements, FHWA-DTM-70-6, 1970.
3. W.B. Bienert, M.F. Pravda, H.J. Suelau, and D.A. Wolf. Snow and Ice Removal from Pavement Using Stored Earth Energy. FHWA_RD_75-6, 1974.
4. C.P. Brinkman, Space-Age Technology for Deicing Hazardous Highway Locations. Public Roads, V39, pp. 89-95.
5. Don Long and John S. Baldwin, Earth Heat-the answer to highway ice?, Construction News, December 1977, pp. 8-12.
6. A.A. Ferrara and G. Yenetchi, Prevention of Preferential Bridge Icing Using Heat Pipes, Final Report, FHWA RD-76-167, September 1976.
7. K.M. Pell, J.E. Nydahl et al., Thermal Response of Bridges, Transportation Research Record, No. 576, 1976.
8. E. Faccini, Heat Transfer Simulation of the Geothermal Heating of Bridge Decks Using Heat Pipes, Thesis, University of Wyoming, 1976.
9. R. McIntosh, National Aeronautics and space Administration, Goddard Spaceflight Center, Greenbelt, Maryland (Private Communication).
10. K.M. Pell, J.E. Nydahl, and V.A. Cundy, Thermodynamics of Bridges, Roadways and Runways. DOT-TST-75-41, November 1974.
11. V.A. Cundy, J.E. Nydahl and K.M. Pell, Geothermal Heating of Bridge Decks, Proceedings of the Second International Snow Removal and Ice Control Research Symposium, Hanover, N.H., May 1978.

RELIABILITY APPROACHES TO BRIDGE SAFETY AND TRUCK LOADING UNCERTAINTIES

Fred Moses, Case Western Reserve University

Design decisions for highway structures can utilize probability and statistics to express uncertainties in vehicle loading, analysis, strength and construction control. Structural reliability research is described to provide design codes with consistent risk levels and optimal designs. A detailed reliability approach is presented for deriving load and performance factors for steel element fatigue design. The uncertainties in truck weight, volume, headway, strength distribution (analysis), impact and fatigue life are included. The fatigue load model is extended to strength design by considering two behavior levels. The first level utilizes a limit state format with element-oriented load and performance factors derived for components with failure criteria such as maximum moment. Ultimate strength is recognized in a second level check with system coefficients based on the ratio of the load causing significant bridge distress to the limit state load. Code oriented research is described to derive system coefficients for various types of bridge structures using nonlinear and ultimate load analysis. The goal is to utilize the load margin between an element limit state and major bridge damage to contain load uncertainties in future load growth and overweight vehicle operations. The sparce load data available has inhibited introduction of reliability oriented specifications. A project is described for undetected weighing of vehicles in motion using instrumented highway bridge girders. The field results show its feasibility and opportunities for filling in missing data on load history and overweight vehicles.

The design decisions for highway structures involve uncertainties in loading, analysis, strength and construction control. Historical experience is an excellent guide for evaluating proposed design changes which affect the safety margin. This experience should also be supplemented by probabilistic and statistical analysis which quantifies these uncertainties.

The codified variables for controlling designs are the prescribed safety factors. These factors should reflect the degree of uncertainty in predicting behavior and the risk and consequences of not meeting performance criteria. Recent research in structural reliability theory has shown how load, analysis and strength uncertainties can be quantified to determine their impact on rational safety factors (1). In these studies, uncertainties are described as random variables and through probabilistic analysis the risk of damage or unserviceability is computed. This computation is often approximate to reflect the limited data base in most structural situations. Design factors can still be derived, however, to achieve structures with more uniform risk levels based on the corresponding uncertainties.

Code developments using structural reliability theories have been studied for adoption in steel buildings, concrete structures and offshore platforms (2,3,4). These reliability changes can also affect the economy of the structure. For example, savings in bridge structures would result by reducing design uncertainties through more load-data collection, accurate behavior analyses or improved construction quality control.

There are some important differences between highway bridges and buildings in applying structural reliability principles. Buildings are affected primarily by environmental (wind and seismic) loads which can be analyzed statistically from historical data. In bridges, especially short and medium span structures, the major loading is due to heavy trucks. Its statistical description is not precisely known due to limited and possible biased data and furthermore, evolves over time after the bridge is constructed. In addition, truck loads are repeated by millions of passages during a bridge lifetime so the statistical problem of estimating maximum loads (which also include multiple presence of more than one vehicle on the bridge) is quite formidable.

A reliability oriented strategy requires load statistics and design factors to provide safe structures, i.e., meet strength and serviceability limits and also be economical over long periods of time. An example of a code "strategy" is the AASHTO specification of its design vehicle (5). This vehicle weighs less than the legal load limit and is also considerably lighter than vehicles known to use the roadways, either by permit or illegal passage. Safety is maintained, however, by conservative distribution and material safety factors which are more than adequate based on load tests and examples of

bridge performance (6,7,8).

A number of studies have investigated the problem of bridge live loads and safety (9,10,11). A recent Symposium brought to light practices from different countries (12). The need for a rational methodology to derive design loads also became apparent in research for a limit state oriented bridge code (13). Similar problems in assessing load and bridge behavior uncertainties affect the normal operation of authorizing permit vehicles and establishing procedures for rating of existing bridges (14).

This paper presents a reliability-based framework for bridge design and analysis, especially the rational determination of truck loadings. The intent is not to present detailed code recommendations but rather to explore a general methodology for deriving reliability oriented bridge codes. The first problem described is a loading model to predict fatigue behavior. The uncertainties in truck weight, headway, volume, stringer distribution (analysis), impact and fatigue life are presented. A design calibration is described to produce uniform but small probabilities of premature cracks. An extension of this loading model is described for strength design and a strategy is described for achieving a uniform reliability by also considering the ultimate behavior of the bridge. A major factor in a bridge analysis is accurate load data because of the frequency of overloaded vehicles on our various highway systems. The paper describes a current project at Case to obtain such data by using highway bridges as load scales to weigh, undetected, vehicles in motion. Possible applications of the system are described

Reliability Theory

The fundamental problem of structural reliability is illustrated in Figure 1. A single element with strength, R, is subjected to a load, S. R and S represent the random variables associated with strength capacity and loading including analysis uncertainties. These random variables may be described by frequency distributions. The overlapped portions of the curves in Figure 1 indicated regions of risk where load (S) exceeds capacity (R). The probability of failure (P_f) or risk may be calculated from these frequency distributions ($f_R(r)$ and $f_S(s)$) as

$$\text{Risk, } P_f = \text{Probability } [R < S]$$

$$= \int_S [\int_o^s f_R(r)dr]\, f_S(s)ds \qquad (1)$$

Risk decreases with increasing safety factor (initial cost). We can express the total cost (C_T) as illustrated in Figure 2 as

$$C_T = C_I + (P_f)C_f \qquad (2)$$

where: C_T = total cost

C_I = initial cost

C_f = cost of failure

An optimum or minimum cost occurs when the slope of initial cost (C_I) equals the negative slope of equivalent failure or insurance cost ($P_f \times C_f$).

The calculations in equations 1 and 2 can be used with precision only if there is high confidence in the load and resistance statistical data. Otherwise, relative measures of risk have been proposed which contain the important reliability parameters and can be used in deriving code safety factors (15,16,17). One simple approach is to define a safety margin (Z).

$$Z = R - S \qquad (3)$$

Failure occurs if Z is negative. The most important statistical parameters of Z are its mean ($\bar{Z}$) and variance (σ_Z^2) expressed as

$$\bar{Z} = \bar{R} - \bar{S} \qquad (4)$$

$$\text{and } \sigma_Z^2 = \sigma_R^2 + \sigma_S^2 \qquad (5)$$

A measure of risk is the safety index (β) or the number of positive standard deviations contained in the safety margin. (If R and S are normal variables, entering β in the standard normal distribution table gives the risk.) To arrange a design format, note that (17)

$$\beta = \frac{\bar{Z}}{\sigma_Z} = \frac{\bar{R} - \bar{S}}{\sqrt{\sigma_R^2+\sigma_S^2}} \qquad (6)$$

$$\text{and } \sqrt{\sigma_R^2+\sigma_S^2} \simeq 0.7\ (\sigma_R + \sigma_S) \qquad (7)$$

Making the latter substitution in equation 6 and rearranging terms gives a safety check as

$$(1 - 0.7\beta V_R)\ \bar{R} \geq (1 + 0.7\beta V_S)\ \bar{S} \qquad (8)$$

where V_R and V_S are the nondimensional coefficients of variation (standard deviation divided by the mean) of strength and load respectively. Load (γ) and (ϕ) factors are, therefore, dependent on the safety index and their respective coefficients of variation, i.e.

$$\phi = 1 - 0.7\beta V_R \qquad (9)$$

$$\gamma = 1 + 0.7\beta V_S \qquad (10)$$

Extensions of these basic equations have been reported for load combinations, nominal rather than mean values of variables and a lognormal (R/S) form of equation 3 rather than the normal (R - S) (1,16). Equations 1 - 10 give a theoretical basis for deriving safety factors based on probability theory and corresponding statistical parameters. These equations have already been used when introducing limit state formats which separate load and performance safety factors (2,4,13). Past experience must be incorporated through a code calibration process (18). This calibration cannot be overemphasized as the introduction of reliability formats must proceed with caution especially for "fleet" type systems such as highway bridges.

Loading for Fatigue Design

The uncertainties in repetitive vehicle loading include truck dimensions, weight histograms and volume, possible changes during bridge lifetime of weight and volume and the likliehood of multiple presence of trucks on the bridge causing load superposition. For example, highway trucks vary in their number of axles and axle spacing, truck type, distribution of load to axles and gross weight. The frequency of different vehicle combinations depends on location (urban, suburban, rural and industrial, etc.), time, season and other economic factors.

Several studies of the different truck types (7,19) have concluded that reasonable accuracy in loading histories can be obtained if all the truck types are lumped into a few specific categories. This is because axle weights and total gross weights are the major factors affecting girder stresses while axle spacing and load distribution are of secondary importance. The fatigue behavior is also an averaging process depending on the load spectra rather than the specific occurrence of a relatively few load cycles. It has been suggested that even two truck types would be sufficient for a fatigue model lumping all vehicles as either tractor trailers or single unit trucks (19). As a justification, note that five axle tractor trailers often comprise on an interstate highway over half of the truck traffic stream.

Stress ranges at critical locations may be calculated as a function of bridge dimensions and the bending moments derived from the truck configurations. Uncertainty in stress analysis includes the distribution of total static bending moment to individual girders and also the dynamic response.

Fatigue properties of steel highway bridge components may be estimated from the considerable amount of experimental work done over the last few years (20). The tests show that fatigue life is dependent on stress range amplitude with different weld or attachment details behaving like stress concentrations. The results may be expressed as:

$$N S^3 = c \tag{11}$$

where: N - number of cycles to failure
S - stress range in constant amplitude sinusoidal loading
c - a constant depending on weld or attachment category

c may be expressed in terms of the stress range at 2 million cycles (any point on the fatigue curve could be used since a plot of log S vs. log N for the test data often exhibits no apparent fatigue life limit). This gives:

$$c = 2 \times 10^6 [S_{(2 \times 10^6)}]^3 \tag{12}$$

or substituting in equation 11 for the number of cycles to failure, N,

$$N = \frac{2 \times 10^6 [S_{2 \times 10^6)}]^3}{S^3} \tag{13}$$

Where: $S_{(2 \times 10^6)}$ - is the stress range amplitude for failure at two million cycles.

Laboratory tests also suggest that damage under random amplitude cycles can be estimated from the Miner linear cumulative damage theory. Fatigue failure occurs when the damage sum equal one, or:

$$\text{Damage, } D = V \sum \frac{f(S_i)}{N(S_i)} = 1 \tag{14}$$

Where: $f(S_i)$ - fraction of stress cycles at amplitude S_i.

$N(S_i)$ - number of constant stress (S_i) cycles to failure (See equation 13).

V - total number of load cycles taken as the truck volume. This means each truck passage causes one cycle of load.

To further simplify calculations we assume that stress is proportional to vehicle weight (this is accurate for fixed truck dimensions). In order to normalize the data we designate a fixed dimension design truck, say of 72 kips, which causes a stress range, S_r (see Figure 3). These assumptions imply a fixed relationship between stress range (S) and truck weight (W).

$$S = W \frac{S_r}{72} \tag{15}$$

Substituting in equation 14 the expression for N from equation 13, and replacing S from equation 15 gives:

$$D = \frac{V}{2 \times 10^6 [S_{(2 \times 10^6)}]^3} \sum f(W) \left(\frac{W S_r}{72}\right)^3 \tag{16}$$

Replacing the volume by the daily truck traffic (ADTT) and a 50 year life and rearranging terms gives for the damage, D:

$$D = \frac{50(365)ADTT}{2 \times 10^6} \left[\frac{S_r}{S_{(2 \times 10^6)}}\right]^3 \sum \left(\frac{W_i}{72}\right)^3 f(W_i)$$

$$= .0091 \left[\frac{S_r}{S_{(2 \times 10^6)}}\right]^3 L \tag{17}$$

Where: $L = \sum \left(\frac{W_i}{72}\right)^3 f(W_i)$

The summation, L, is denoted as the loadometer survey value and is a weighted average of truck loads using the cubic factor from the fatigue life data. Several state loadometer surveys were studied by Pavia giving loadometer values ranging from .28 to .52 with a value of .4 being slightly above average (21). This study showed the increase over time of both the load histogram and the truck volume. One disconcerting result was the inconsistencies between loadometer survey values in similar regions of the country or interstate highways passing through adjacent states. Also, there were differences in the high weight portion of the histograms between data taken from weigh station enforcement and data for load survey purposes (no penalties for violations). This is because overweight vehicles bypass enforcement stations. There is a need for more reliable data for bridge design purposes and this is discussed further below.

Solving equation 17 for the allowable stress range, S_r, for a damage, D = 1, gives

$$S_r = S_{(2 \times 10^6)} \left[\frac{110}{L(ADTT)}\right]^{1/3} \tag{18}$$

The allowable stress range, S_r in equation 18 is the stress range which for the weighted truck histogram given by L and volume ADTT just reaches the fatigue damage criteria at the end of 50 years. A safety check means that at each critical weld location the allowable stress range, S_r, should be compared to the design stress, S_g. The conventional approach is used here in which the gross bending moment is computed from the design vehicle increased by the impact factor. The girder moment is found by multiplying by the distribution factor. The design stress range, S_g, may therefore be written as:

$$S_g = \frac{M_R}{S_x} g\ h\ I \tag{19}$$

Where: M_R - moment range calculated with a specified fixed wheelbase design truck weighing 72 kips and having average tractor-trailer dimensions as shown in Figure 3.
S_x - girder section modulus
g - stringer distribution factor depending on stringer spacing and deck configuration
h - average headway or multiple presence factor
I - impact factor

The factor (h) is used to incorporate the multiple presence of trucks on the bridge causing superposition. In a reliability format, the safety checks mean the comparison of design stress (equation 19) caused by the load with allowable stress (equation 18) based on the strength after determining suitable probability-based load and performance safety factors. These factors must be found by treating as random variables the strength terms, $S_{2 \times 10^6}$, L and ADTT and the load term, M_R, g, h, I and S_x. In this general reliability model the uncertainties, therefore, include load, highway bridge analysis and strength. Walker (22) has discussed the probability distribution of some of these parameters in computing the probability distribution of the bridge life. Knab, et al (23), have applied such distributions to the design of military bridges. For civilian highway bridges, the uncertainties in load and the limited data base require an approximate safety index code format to control the risk of premature fatigue during the expected bridge lifetime. Following the reliability theory described in equations 1 - 10, a margin of safety ratio, Z, is defined as

$$Z = \frac{\text{STRENGTH}}{\text{LOAD}} = \frac{S_r}{S_g} \tag{20}$$

The safety index (β) for this case has been defined from a lognormal format and leads to the following expression (1):

$$\beta = \frac{\text{Ln}\ \bar{S}_r - \text{Ln}\ \bar{S}_g}{\sqrt{V_{S_r}^2 + V_{S_g}^2}} \tag{21}$$

Where: $\bar{S}_r$ - mean allowable stress range
$\bar{S}_g$ - mean design stress range
V_{S_r} - coefficient of variation of S_r
V_{S_g} - coefficient of variation of S_g

The safety index (β) has a similar interpretation as in equation 6 except that it gives a precise probability value if the variables are lognormal rather than normal. [Since S_r and S_g are made up of the products of random variables a lognormal rather than a normal format is preferred.] Eliminating the square root term as in equation 7 and rearranging terms gives as a safety criteria:

$$\bar{S}_r e^{-0.7\beta V_{S_r}} \geq \bar{S}_g e^{+0.7\beta V_{S_g}} \tag{22}$$

Both S_r and S_g in equations 18 and 19 are related to the same 72 kip design vehicle. Equation 22 can be used as a safety check to derive respective load and performance factors.

Using equation 19, the mean girder design stress (load) is:

$$\bar{S}_g = \frac{\bar{M}_r \bar{g}\ \bar{h}\ \bar{I}}{\bar{S}_x} \tag{23}$$

and Load Coefficient of Variation

$$V_{S_g} = \sqrt{V_{M_f}^2 + V_g^2 + V_h^2 + V_I^2 + V_{S_x}^2} \tag{24}$$

From equation 18, the mean allowable Stress (strength) is:

$$\bar{S}_r = \bar{S}_{2 \times 10^6} \left[\frac{110}{\bar{L}\ (\overline{ADTT})}\right]^{1/3} \tag{25}$$

and strength coefficient of variation:

$$V_{S_r}^2 = \sqrt{V_{S_{2 \times 10^6}}^2 + \left(\frac{1}{3} V_V\right)^2 + \left(\frac{1}{3} V_L\right)^2} \tag{26}$$

Where $\bar{M}_R\left(V_{M_R}\right)$, $\bar{g}\left(V_g\right)$, $\bar{h}\left(V_h\right)$, $\bar{I}$, $\left(V_I\right)$ and $\bar{S}_x\left(V_{S_x}\right)$ are mean (coefficient of variation) of moment range, girder distribution, headway superposition, impact and section modulus respectively. $\bar{S}_{2 \times 10^6}$ $\left(V_{S_{2 \times 10^6}}\right)$, $\bar{L}\left(V_L\right)$, $\bar{V}\left(V_V\right)$ are mean (coefficient of variation) of constant amplitude fatigue stress at 2 million cycles, loadometer survey and volume respectively. Each of these statistical parameters must be estimated for the specified bridge traffic and section being checked.

From a practical code viewpoint, the means and coefficients of variation can be combined into discrete load and performance factors for various categories of roadway and weld attachments. Statistical data for carrying out the codification can be found from loadometer surveys, field measurements of stress histories and laboratory fatigue data. This information has been reported to code committees in a format which leads to more uniform safety levels (24).

In general, proposed changes in design specifications should not lead to drastic differences in design section values. This involves examining current structures which are believed to have good performance and computing their implied safety index. If these structures are generally considered not to be excessively over-designed, then some representative average of their safety indices becomes the target goal in a new, balanced risk code format (1,2).

For the fatigue design model the calibration of the reliability format uses equation 21 to calculate β for a number of different bridge configurations, traffic and weld combinations. This was done to determine the safety index, (β) implied in current design (21,25). A weighted value of the β's becomes the risk level in the code format with each load and resistance parameter calculated from equations 22 - 26. Typical β values using current design are found in the range of 1.5 to 3.0. An advantage in using equations 21 - 26 to derive code design factors is to achieve a more uniform safety level. This has been studied and the specific

results published but its presentation herein is beyond the present scope of this paper (21,25).

Reliability Model for Strength Design

Many of the uncertainties in modelling fatigue loading are also found in describing strength behavior. For example, analytical and simulation studies have found the distribution of maximum bending moments using weight histograms, truck characteristics and multiple presence frequencies (10,19). These studies highlight the influence of these uncertainties on the peak distribution. Several important differences, however, should be considered between fatigue loading and a model for strength design.

1. The number of repeated loadings on a typical short or medium span bridge can easily exceed fifty million during its lifetime (i.e., ADTT > 2700 for a projected 50 year life). This causes formidable statistical problems to estimate the maximum loading distributions which are sensitive to the distribution tails used for multiple presence, truck weight, truck characteristics, impact, etc. The confidence in such distribution tails is small and casts doubt on the validity of these maximum load predictions.
2. A strength failure is often more severe than a fatigue crack so the safety index or risk level must be more conservative. This further limits the usefulness of simulation based on the current load data.
3. Predictions based on truck load "data" use measured or available information which may not correspond to maximum loads. The latter may, in fact, arise due to illegally overweight vehicles operating on the highway system.
4. The specified design load may also have political implications. If the specified design loads are the maximum expected loads, then these values may be cited to justify legislative increases in the legal load limits. For example, one load data study has shown, at least for axles, that the percent of illegal values remains almost constant and independent of the legal specified value (26). Marketing practices may encourage illegal loads so judgement and control must be exercised in raising design loads.
5. Despite the difficulty of predicting maximum loading the fact remains that few bridges exhibit failure due to a negative margin of safety (R - S) as illustrated in Figure 1. One explanation is the overload capacity contained in conservative analysis and design practices. Tests on recently constructed bridges show reserve strength several times in excess of the design load without encountering distress (8). For example, failure of steel beam-slab bridges is a progressive development under increasing load with large deformations, cracks and local buckling preceding collapse.

The uncertainty of load data coupled with the problems cited above make it difficult to derive appropriate safety factors for these solutions. Figure 4 shows three typical structural responses for bridge behavior. Damage vs. load is plotted in Figure 4a for a statically determinate or brittle structure which exhibits little reserve strength beyond a serviceability limit and failure is quite sudden. Figure 4b illustrates a response for a structure with moderate reserve strength which exhibits progressive damage as the load increases. Figure 4c shows a structure with large reserve strength capabilities and small amounts of damage until the load has exceeded several times the initial serviceability limit.

Figure 5 illustrates the load and response uncertainty superimposed on these damage vs. load curves. The expected damage cost (D) may be calculated by integrating over the load distribution ($f(\ell)$) as:

$$\text{Damage Cost,} \quad D = \int \left[\int f_D\left(d \middle| _{L=\ell}\right) dd \right] f_L(\ell) d\ell \quad (28)$$

where $f_D\left(d \middle| _{L=\ell}\right)$ is the conditional damage frequency given a load ℓ. The difficulties in finding precise distributions for the damage cost are apparent from the previous discussions of the load and strength uncertainties. This points, however, to designing for the whole range of responses from serviceability damages through collapse and even maintenance and rehabilitation. Some general conclusions are, however, obvious. Bridges, with behavior as in Figure 4a, show few signs of distress prior to high damage levels being encountered. These bridges are less likely to exhibit any warning signs under loads less than the vehicle loading causing significant damage. A bridge, as in Figure 4c would show signs of distress at loads significantly below the ultimate load. It would provide the safe options of strengthening the bridge or tightening the enforcement of load limits.

The following design approach is a general guideline. It is not intended that each bridge be studied this way. Rather, it suggests tools for code writers and researchers to classify groups of structures and provide more uniform reliability levels than currently exist.

1. Develop a safety index analysis (β) using a strength limit criteria. This would be used to derive element oriented load and performance factors as in the current AASHTO and other codes. Rather than categorizing this member design as the strength limit we should recognize that it is only another control on performance. It does not recognize the potential of the bridge to resist collapse or even large damage under major overloads. This would only be predicted by an ultimate load analysis to derive a damage curve as in Figure 4. It also implies that the definition of element strength is not critical and could either be elastic stress, plastic moment capacity, maximum strain, etc. Since the "damage" levels in this level of element strength or serviceability limit state are not severe, the safety index (β) need not be as high as for a true strength limit state.
2. Research on behalf of code writing agencies should perform ultimate nonlinear behavior analysis of various types of bridge structures. These analyses, supplemented by test data should lead to damage vs. load curves. The results should also show the distribution of reserve strengths beyond the serviceability limit state.
3. One possible additional input to codified design is a computed ratio of ultimate (U) to serviceability load (S). This should be incorporated in the strength performance factor as a system coefficient. This system performance coefficient should be in addition to the element strength factor derived from the conventional reliability theory described above. If the ratio (U/S) is close to one, as say, in a structure with important non-redundant elements, the system coefficient would be large, say at least 2.0. If the ratio of U/S is large, as in the slab-beam bridge where it may exceed 4 or 5, then the partial system factor may be much smaller, say 1.2.
4. These proposals contained herein are only preliminary conclusions, as further study is needed of full-scale bridge performance. In addition,

accurate load statistics must also be made available.

Load Data

A major obstacle to a probability oriented specification for bridge strength is the relatively sparce load data available. The load history studies which accumulated data for fatigue design primarily measured stresses at critical attachment locations (6,7). Generally, these studies could not relate to the vehicle configurations, headways and axle loads causing the stresses being measured. While such detailed information is unnecessary for predicting repetitive fatigue loads, they are important for establishing design loads. The extensive strain-history study performed at Case Western Reserve University in Ohio measured some 20,000 trucks crossing on ten bridges and considered headway and truck type in the automated data acquisition and processing (27). Random gross vehicle weights, axle spacing and axle weights were not recorded.

The loadometer survey data has obvious inconsistencies since overweight vehicles avoid the survey stations because of penalties. This truncates the significant part of the load distribution. To improve the situation, a current project at Case has instrumented longitudinal girders of beam-slab bridges as load scales. The system obtains undetected weight information to produce an unbiased load data base.

During the last decade there have been several systems developed to weigh vehicles in motion (WIM). These WIM systems have utilized pavement scales or a section of roadway cut out and replaced with a slab held by instrumented supports. One difficulty with the WIM pavement scales is that the wheels are in contact with the scale for a very short time, say 5 - 10 milliseconds. The contact forces between tire and roadway undergo significant oscillations especially for typical roadway roughnesses encountered. Since the oscillation period is large compared to the time on the scale, the latter records a discrete value at some point on the oscillation which can be above or below the true static value. In a typical vehicle moving at high speeds, the tire force oscillations can easily exceed 50% or more of the static value. Hence, pavement scales require extremely smooth surfaces some distance in front of the scale and this surface must be periodically restored to maintain smoothness. If this is not done, then the best scale application would be low velocity operations, say at a busy survey station to segregate heavy vehicles for testing on the static scales. This does not solve the problem, however, of obtaining accurate data for vehicle load prediction.

The approach described here uses strain records of instrumented girders. A major requirement for accurate weight prediction is a description of the vehicle's dimensions. This is obtained by roadway sensors such as pneumatic tubes. A schematic of the operation is shown in Figure 6. The sensors provide the vehicle description while the analog strain data is digitized and stored in the computer for processing. To date, the processing is not carried out in the field but the data is stored on magnetic tape for subsequent computer processing.

Weight prediction is done as follows: The measured strain record (M*(t)) is compared to a predicted signal (M(t)) based on the vehicle's configuration, axle spacing and bridge influence line (I(t)) (the latter can be obtained analytically or more accurately from calibrating with a vehicle of known axle spacing and weights). Thus the predicted signal is

$$M(t) = \sum_i A_i I_i(t), \quad i = 1, \text{number of axles} \qquad (29)$$

where A_i are the unknown axle weights as shown in Figure 6. An error difference function, E, may be calculated as

$$E = \int_{\text{time}} [M^*(t) - M(t)]^2 dt \qquad (30)$$

where the integration is over the time taken by the truck to cross the bridge. Substituting equation 30 for the predicted signal M(t) gives:

$$E = \int [M^*(t) - \sum A_i I_i(t)]^2 dt \qquad (31)$$

Minimizing the error (i.e., least square fit) gives a linear set of equations to solve for A_i.

This procedure has been tried in the Case Weigh in Motion system with promising results for weighing trucks in an undetected manner. The actual cost per bridge-scale is quite small and can utilize reuseable strain transducers. The investment is primarily in the electronic recording and processing equipment which can be transported to several sites. Further effort is underway to improve the accuracy of the system and to expand its usefulness.

Some examples of the results are shown in Tables 1 and 2. These show the weight obtained at a survey station and the values predicted by the Case WIM system. Table 2 shows predicted weight histograms compared to data from a load survey station and a state loadometer report. These were not taken at the same time so only relative comparisons can be made. The loadometer report which did not involve enforcement showed 11% of the five axle vehicles in excess of the legal limit while the Case WIM showed 15%. The load survey station which involved enforcement reported no overweight vehicles for the period observed. A field system to perform such weigh in motion measurements has been assembled at Case and delivered to FHWA in March, 1978.

Conclusions

Structural reliability theory has been used as an analysis and design aid for incorporating probability and statistics in characterizing uncertainties in bridge load, behavior and capacity. Safety and performance factors can be derived to provide a uniform level of risk against unserviceability. Coupled with past experience and judgement, reliability methods can be used by code writers to introduce more rational and optimal code formats such as limit state design.

A detailed presentation of the fatigue design load indicates that uncertainties in vehicle weights, volume, multiple presence, impact, girder distribution, fatigue life and section properties can be incorporated in safety factors to achieve more uniform risk against premature fatigue cracks. An extension of the load prediction model to strength design presents difficulties because ultimate strength behavior is quite complex. A proposal is made to consider safety checks for strength on a serviceability basis with a system safety coefficient established to represent ultimate behavior. System coefficients would be prepared by code researchers for various types of bridges to represent the reserve capacity existing before significant damage occurence.

Uncertainty in load data is a major limitation in introducing reliability-based design. A project is described for undetected weighing of vehicles in motion by using instrumented highway bridge girders as load scales to predict axle and gross weights. Preliminary data reported shows the feasibility of this approach.

Acknowledgements

The author wishes to acknowledge contributions of his colleagues in carrying out various phases of this work and the support of sponsoring organizations. The development of the fatigue model and study was helped by R. Garson and A. Pavia in projects supported by Ohio Department of Transportation (ODOT) and the Federal Highway Administration (FHWA). Data for the fatigue study was obtained in a field measurement project supported by ODOT and FHWA and assisted by Professor George Goble. The Case Weigh-in-Motion study was supported by FHWA.

The contents of this report reflect the views of the author, who is responsible for the facts and accuracy of the data presented. The contents do not necessarily reflect the official views or policy of the State or the Federal Highway Administration. This report does not constitute a standard, specification or regulation.

Figure 1. Fundamental reliability model - weaving of load and strength distributions to obtain risk (P_f).

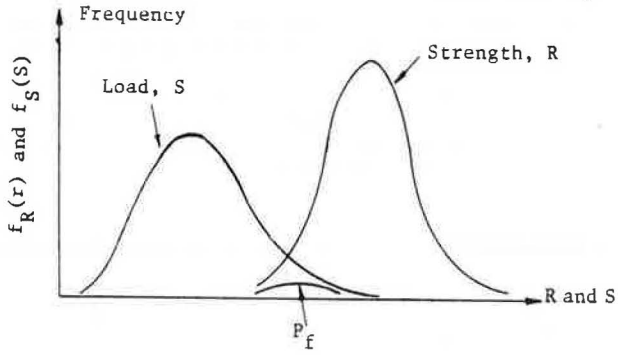

Figure 2. Illustration of total cost, initial cost and failure cost versus risk.

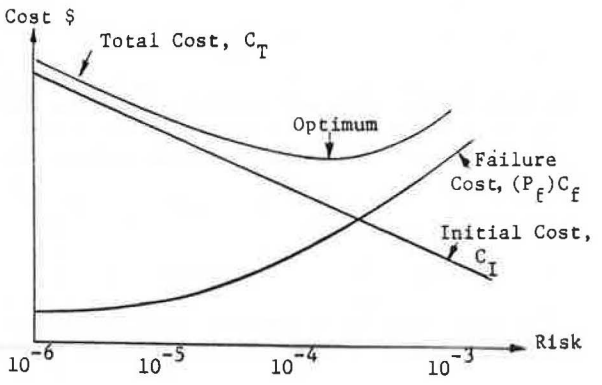

Figure 3. 72 kip tractor trailer with average dimensions and load distribution.

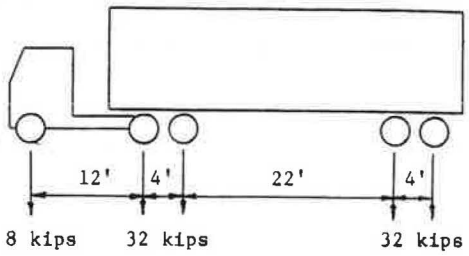

Figure 4. Illustrations of bridge damage versus load response curves.
(a) "Statically determinate or brittle" behavior.
(b) Moderate reserve strength.
(c) Large reserve strength.

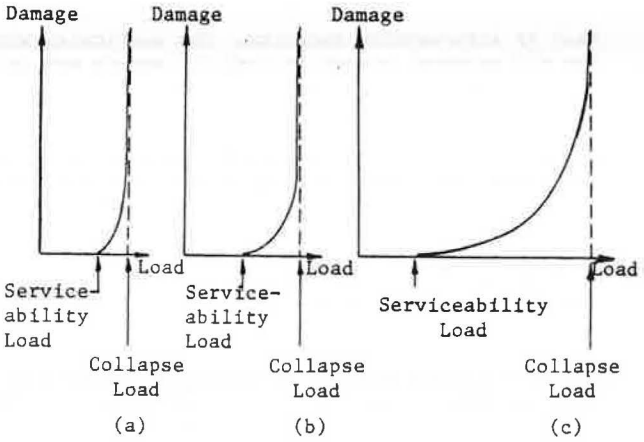

Figure 5. Illustration of bridge damage versus load with damage and load frequency distributions.

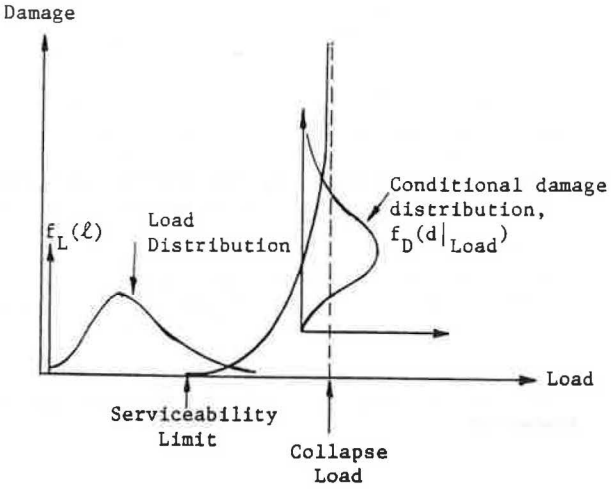

Figure 6. Schematic layout of weigh in motion system using instrumented bridge girders.

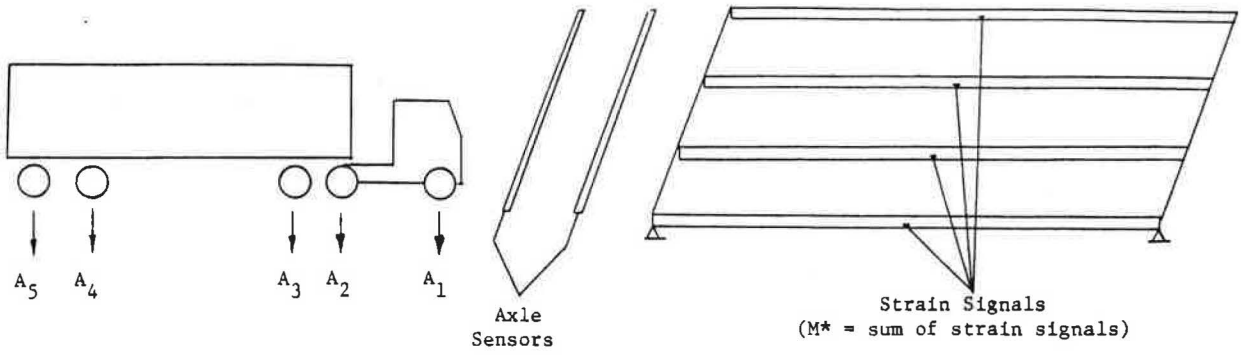

Table 1. Examples of WIM predictions and survey station weights.

Case	Description	WIM Prediction		Survey Station	
		Gross Weight (kips)	Rear Tandem (kips)	Gross Weight (kips)	Rear Tandem (kips)
1	4-axle delivery truck	40.2	16.5	40.3	15.6
2	5-axle tractor trailer	75.5	33.5	67.7	30.4
3	3-axle car carrier	49.1	17.2	50.3	18.2
4	5-axle open trailer	26.7	7.8	29.5	8.9

Table 2. Comparison of WIM predictions and survey station gross weights for tractor trailers.

Gross Weight (kips)	Cumulative Percent		
	State Loadometer Survey* (Percent)	Nearby Survey Station** (Percent)	WIM Prediction*** (Percent)
< 20	-	-	1
30	8	13	20
40	35	31	47
50	43	48	53
60	54	64	62
70	70	80	76
80	89	100	86
Legal Limit			
90	97		93
100	100		98
> 100	100		100

*Data from variety of state roads.
**Data taken in proximity to but not precisely correlated to WIM data.
***132 vehicle samples.

References

1. A. Ang and C.A. Cornell, Eds. Modern Concepts of Structural Safety and Design. Journal of the Structural Division, ASCE, Sept. 1974.
2. T.V. Galambos. Proposed Criteria for Load and Resistance Factor Design of Steel Buildings. Report 45, Civil Engineering Department, Washington University, St. Louis, May, 1976.
3. Probabilistic Design of Reinforced Concrete Buildings. Publ. SP-31, ACI, Detroit, 1972.
4. S. Fjeld. Reliability of Offshore Structures. Paper OTC 3027, Offshore Technology Conference. Houston, Texas, 1977.

5. Standard Specifications for Highway Bridges. AASHTO, American Association State Higway Officials, 1969.
6. R.F. Varney and C.F. Galambos. Field Dynamic Loading Studies of Highway Bridges in the United States, 1948-1965. Highway Research Record 76, Highway Research Board, 1965.
7. C. Heins and C.F. Galambos. Highway Bridge Fatigue Tests in the United States, 1948-1970. Public Roads, Feb. 1972.
8. D.W. Goodpasture and E.G. Burdette. Comparison of Bridge Stress History Results with Design-Related Analyses. Highway Research Board 428, Washington, D.C., 1973.
9. H. Bissell, D. Cramer and R. Eckert. Forecasting of Heavy Loading Patterns on Highway Bridges. Contract FH-11-7314, Kelly Scientific Corp., Washington, D.C., June 1970.
10. D. Harman and A.G. Davenport. The Formulation of Vehicular Loading for the Design of Highway Bridges in Ontario. U. of Western Ontario, London, Dec., 1976.
11. H.K. Stephenson. Highway Bridge Live Loads Based on Laws of Chance. Proceedings, ASCE, Vol. 83, July 1957.
12. Colloquium on Highway Bridge Loading. International Association of Bridge and Structural Engineers, Cambridge, England, April 1975.
13. R.A. Dorton and P. Csagoly. The Development of the Ontario Bridge Code. Ontario Ministry of Transportation and Communication, Downsview, Oct. 1977.
14. C.W. Peterson. Bridge Rating by Limit State. Report prepared for CSA S6, Province of Alberta, Bridge Branch, Dec. 1976.
15. C.A. Cornell. A First Order Reliability Theory of Structural Design. Structural Reliability and Codified Design, Ed. N. Lind, SM3, U. of Waterloo Press, 1970.
16. L. Esteva and E. Rosenbleuth. Use of Reliability Theory in Building Codes. First Intl. Conf. on App. of Stat. and Prob. to Soil and Struct. Engineering., U. of Hong Kong, Sept. 1971.
17. M.K. Ravindra, N.C. Lind and W.C. Siu. Illustration of Reliability Based Design. Journal of the Structural Division, ASCE, Sept. 1974.
18. W.C. Siu, S.R. Parimi and N.C. Lind. Practical Approach to Code Calibration. Journal of the Structural Division, ASCE, July 1975.
19. F. Moses and R.C. Garson. New Procedure for Fatigue Design of Highway Bridges. TRB Research Record 507, 1974.
20. J.W. Fisher, K.H. Frank, M.A. Hirt and B.M. McNamee. Effect of Weldment on the Fatigue Strength of Steel Beams. NCHRP Report 102, HRB, 1970.
21. F. Moses and A. Pavia. Probability Theory for Highway Bridge Fatigue Stresses-Phase II. Final Report, Case Western Reserve University, Ohio, Department of Transportation, Aug. 1976.
22. W.H. Walker, Loading Histories. ASCE Specialty Conference on Metal Bridges, St. Louis, Nov. 1974.
23. L.I. Knab, A.H.-S. Ang and W.H. Munse. Reliability Based Fatigue Design Code for Military Bridges. ASCE Specialty Conference on Metal Bridges, St. Louis, Nov. 1974.
24. F. Moses. Comprehensive Fatigue Design Procedures. Presentation for AASHTO Bridge Committee Meeting, 1975.
25. F. Moses. Bridge Loading Spectra and Fatigue Design. Presented at ASCE National Meeting, New Orleans, April 1975.
26. R. Winfrey and others. Manual of Procedures for Conducting Studies of the Desirable Limit of Dimensions and Weights of Motor Vehicles. Report No. FHWA-RD-73-68, July 1970.
27. F. Moses, G.G. Goble and A. Pavia. Applications of a Bridge Measurement System. Transportation Research Record 579, 1976.

OVERLOADING OF HIGHWAY BRIDGES - INITIATION OF DECK DAMAGE

Celal N. Kostem, Lehigh University

Various surveys have indicated that highway bridges are subjected to vehicular load levels and combinations far in excess of those for which they were designed. The prediction of the effects of the overloading as well as the overload permit operations do not reflect the sophistication scientific or technical fields have attained. The paper presents the findings of a parametric investigation employing Program BOVA (Bridge OVerload Analysis), that encompasses 45 case studies. Five different commonly encountered overload vehicles and nine different bridge configurations are considered. The bridge superstructures are simple span beam-slab bridges with prestressed concrete I-beams and reinforced concrete deck, and having no skew. The results of the findings are presented in tabular form for the bridges and the overload vehicles. For given bridges and vehicles the gross vehicular weights, axle weights and "equivalent area loads" are defined that will induce cracking in the concrete that will reach the reinforcing bars. It has been found that if a small amount of damage to the bridge deck is permitted, the load levels which the superstructure can carry are usually in excess of the commonly reported permissible overload weights. Recommendations have been made for the use of the tabulated results in overload permit operations. It has been suggested that the findings can be applied to overload permit operations in the absence of reliable methods of predicting the overload response of bridges. It is also indicated that the suggested guidelines are useful for infrequent traverses of vehicles until the completion of research programs that will delineate the permissible and impermissible overloadings that will be based on limited damage criteria.

Various surveys have indicated that a substantial percentage of existing bridges is in some state of structural distress. Furthermore, it has been found that a noticeable number of overload vehicles traverse these bridges, with or without overload permits (1,2). Permit operations, as well as the assessment of the strength of bridge superstructures when subjected to a given overload vehicle, still are not fully based on rational methods (2,5). To the extent that the vehicular configuration differs from the standard design truck (5), the use of distribution factors and similar design aids will lead to increasingly incorrect results. Any analysis scheme based on linear elastic behavior will also lead to conservative results since this approach will ignore the ever present material nonlinearities and the redistribution of stresses in the superstructure (2). Similarly, the ultimate strength approach will not yield much useful information. There may be a substantial difference between the collapse load level and the load level which will induce limited damage to the structure.

Program BOVA

To predict the overload response of simple span beam-slab bridge superstructures with reinforced or prestressed concrete I-beams and reinforced concrete deck, a research program was undertaken. A computer based simulation technique using a finite element method was developed which predicts the behavior of a given superstructure for a given vehicle, including the initiation and spread of damage, if any, damage characteristics, and collapse (2,3). The research has resulted in Program BOVA (Bridge OVerload Analysis) which simulates the full range elastic and inelastic behavior of the superstructure (3). A comparison of the results obtained in field testing of bridges and prediction of their behavior via Program BOVA has indicated that the maximum discrepancy between the results is 5%. This is far more accurate than the current "methods" employed in permit and rating operations.

Research has indicated that superstructures have enough reserve strength to carry substantially heavy overload vehicles, if a limited amount of damage is permitted to the superstructure (1,2,3). The damage to the superstructure has invariably started as flexural cracking of the deck slab. If the "permissible damage," e.g. crack depth, is related to the "serviceability limits," which may be imposed by transportation authorities, and if a minimal amount of cracking is permitted to take place, then it will be possible to determine vehicular load levels that can be realistically permitted to traverse the bridges infrequently. The basic premise in permitting a minimal amount of cracking is the fact that the deck slab is already cracking due to such factors as construction,

freeze-thaw, and overloading. Thus, to allow limited cracking will not lead to an uncontrolled increase in vehicular weights; on the contrary, it will impose maximum limits which are based on scientific findings.

Parametric Study

Research has indicated that the identification of the common factors that can be employed in conjunction with the assessment of the strength of superstructures and overload permit operations requires a major parametric study. After such a study, it will be possible to simplify the permit operations for a majority of the cases encountered into a "table look-up," rather than executing Program BOVA for each case. A limited parametric investigation to fulfill this purpose has been carried out. Extensive details of the findings of this study in the form of Overload Directories have been reported elsewhere (1). These Overload Directories can be used for permit operations with great ease, even by unskilled personnel (1). Due to space limitations, this paper will present only the information dealing with the initiation of the deck slab cracking. Within the framework of this paper the loads that cause "deck cracking" are defined as the loads which will induce cracks through the full depth of the concrete cover of the reinforcing bars at the top and/or bottom of the slab.

The parametric investigation included nine bridges with various span lengths designed in accordance with the recent design guidelines (1,4). Beam spacing was taken as 2.29 m (7'-6") for all bridges. The pertinent dimensions of the bridges can be seen in Figures 1-3. Five different overload vehicle configurations have been considered; they approximate a vast majority of the vehicles encountered in the traffic stream in and between metropolitan areas. Figures 4 through 8 show the plan and elevation of these vehicles, and axle weights. The parametric study, excluding the additional pilot cases, contained 45 case studies (1).

Deck Damage

For given bridges and vehicular configurations, as indicated in Figures 1-8, the gross vehicular weights that result in the cracking of the deck are seen in Table 1. It should be noted that gross weights are not the same as those indicated in the figures. For example, Vehicle 2 has a gross weight of 427 kN (96 kips). If this vehicle is on Bridge 1 or 4 the tabulated weights are 476 kN (107 kips) and 325 kN (73 kips) respectively. Therefore, it can be concluded that if this vehicle traverses the bridges, Bridge No. 1 will not sustain significant damage, whereas Bridge No. 4 will have excessive deck cracking. Since the threshold limit is 325 kN (73 kips), it is expected that substantial damage to the deck may take place. In order to cause "deck cracking" in Bridge No. 1 the axle weight of the vehicle can be increased up to 159 kN (36 kips), which is in excess of the original vehicle, which has an axle weight of 142 kN (32 kips).

Inspection of Table 1 indicates that it is hard to draw any conclusions by studying the gross vehicular weight, which varies from 325 kN (73 kips) to 587 kN (132 kips). Table 1 also contains the axle weights for the case studies presented herein. There still exists a wide variation among the axle weights that induce deck cracking, with the spread from 88 kN (20 kips) to 185 kN (42 kips). It can be concluded that overload permit operations and the assessment of the strength of the superstructures should not be solely related to the axle weights. In Table 2 average axle loads for different bridge span lengths have been presented. Even though there is a large standard deviation, the average axle weights are in the vicinity of 125 kN (28 kips). Therefore, for the lack of any other information, the maximum axle weights should not exceed this value, if only a limited amount of cracking is to be permitted.

Another guideline in the determination of the vehicular loading is the use of equivalent area load. The equivalent area is defined as that enveloping the extremities of tire prints. It should, however, be noted that the accuracy of this approach depends on the use of multiple axles and multiple wheels per axle. The equivalent pressure is obtained by dividing the gross vehicular weight by the equivalent area. In Table 1 the pressure varies from 30 kPa (1.44 ksf) to 70 kPa (3.35 ksf). Again, inspection of Table 2 indicates that, as it is for the average axle weights, the average equivalent pressure is relatively constant with a small standard error in the mean, but with a large standard deviation. Consequently, due to the absence of more reliable guidelines, it is recommended that for limited cracking in the deck slab the equivalent area load should not exceed 47 kPa (2.25 ksf). The above guidelines are rather crude benchmarks. A more accurate prediction of the vehicular weights, permitting limited deck cracking, can be obtained on a case by case basis by using Table 1. One of the bridges, presented herein, that is similar to the actual bridge, and one of the vehicles, presented herein, that is similar to the actual vehicle can be used to enter Table 1. Depending upon the listed weight versus actual weight, a decision can be reached for the issuance of the overload permit. It is possible to interpolate between different bridges and vehicles included in the paper; however, this leads to a gradual loss of accuracy of the prediction of the threshold value. Detailed application of Overload Directories to permit operations is presented in Reference 1. For permit and rating operations the use of this reference is strongly recommended.

Additional research is currently underway ("Implementation of Program BOVA"). At the completion of this research more information in the form of Overload Directories will be available, which will also include information on the overloading of deteriorated bridge decks.

Conclusions

Rating and permit operations for highway bridges (1) should not be based on "reverse design" process and (2) preferably should not be based on an elastic analysis. These will lead to either erroneous or conservative results. In the overloading of bridges, the damage initiates through the flexural cracking of the deck slab. If a limited amount of cracking of the slab concrete is permitted, there may be substantial increases in the permissible gross weight of overload vehicles, provided that they will traverse the bridge infrequently and that they have a large number of axles and wheels per axle. If these conditions are met, the axle weights (125 kN; 28 kips) or equivalent pressure (47 kPa; 2.25 ksf) can be used for rough estimation of the permissible vehicular weights. Through the use of the table provided, it is possible to predict with greater accuracy the effects

of overload vehicles on the deck.

Acknowledgments and Disclaimer

The reported research was conducted under the sponsorship of the Pennsylvania Department of Transportation and the Federal Highway Administration. Their support is gratefully acknowledged. The contents of the paper reflect the view of the author. The contents do not necessarily reflect the official views or policies of the sponsors.

References

1. Kostem, C. N. Overloading of Highway Bridges - A Parametric Study. Fritz Engineering Laboratory Report No. 378B.7, Lehigh University, Bethlehem, Pennsylvania, August 1976.
2. Peterson, W. S. and Kostem, C. N. The Inelastic Analysis of Beam-Slab Highway Bridge Superstructures. Fritz Engineering Laboratory Report No. 378B.5, Lehigh University, Bethlehem, Pennsylvania, March 1975.
3. Peterson, W. S. and Kostem, C. N. User's Manual for Program BOVA. Fritz Engineering Laboratory Report No. 378B.6A, Lehigh University, Bethlehem, Pennsylvania, March 1975.
4. Standards for Bridge Design (Prestressed Concrete Structures) BD-201. Bureau of Design, Department of Transportation, Commonwealth of Pennsylvania, Harrisburg, Pennsylvania, March 1973.
5. Standard Specifications for Highway Bridges (1973) and Interim Specifications - Bridges (1974, 1975, 1976). The American Association of State Highway and Transportation Officials, Washington, D. C.

Table 1. Vehicular load levels causing deck cracking

Vehicle No.	Bridge No.	Gross Weight (kN)	Axle Weight (kN)	Equiv. Pressure (kPa)
1	1	538	119	64
1	2	574	128	69
1	3	587	130	70
1	4	405	90	48
1	5	445	99	53
1	6	552	123	66
1	7	405	90	48
1	8	445	99	53
1	9	552	123	66
2	1	476	159	68
2	2	471	157	68
2	3	396	132	57
2	4	325	108	47
2	5	342	114	49
2	6	356	119	51
2	7	325	108	47
2	8	342	114	49
2	9	356	119	51
3	1	507	127	52
3	2	485	121	50
3	3	414	104	42
3	4	351	88	36
3	5	365	91	37
3	6	369	92	38
3	7	351	88	36
3	8	369	92	38
3	9	369	92	38
4	1	512	171	55
4	2	556	185	60
4	3	454	151	49
4	4	516	172	55
4	5	494	165	53
4	6	467	156	50
4	7	512	171	55
4	8	489	163	53
4	9	498	166	54
5	1	534	134	34
5	2	543	136	35
5	3	471	118	30
5	4	552	138	35
5	5	534	134	34
5	6	525	131	34
5	7	547	137	35
5	8	520	130	33
5	9	480	120	31

Table 2. Statistical averaging of load levels causing deck cracking.

Span Length (m)	30.5	21.35	12.2
Average Axle Weight (kN)	126.7	128.5	125
St. Deviation (kN)	31.3	28.7	21
St. Error in the Mean (kN)	8	7	5.4
Average Eqv. Pressure (kPa)	47.7	48.9	48.5
St. Deviation (kPa)	10.5	11.6	12.8
St. Error in the Mean (kPa)	2.8	3	3.3

Figure 1. Plan and cross-section of Bridges 1, 2 and 3 (subscripts indicate bridge numbers; 1 in. = 25.4 mm, 1 ft. = 0.305 m)

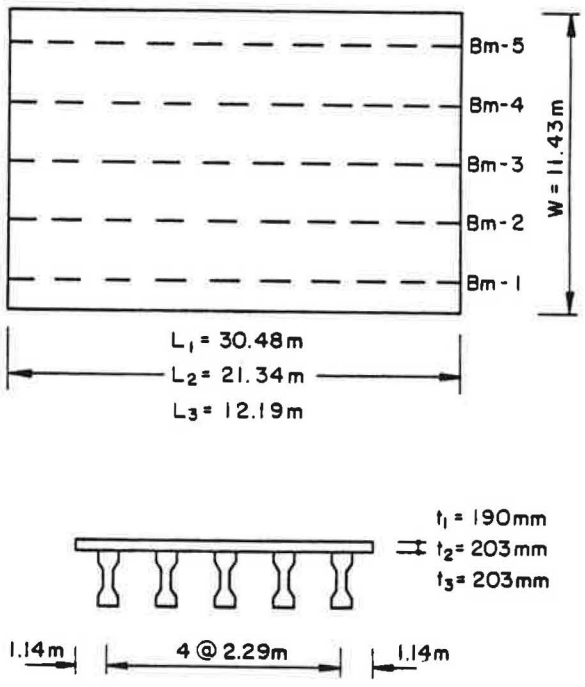

Figure 2. Plan and cross-section of Bridges 4, 5 and 6 (subscripts indicate bridge numbers; 1 in. = 25.4 mm, 1 ft. = 0.305 m)

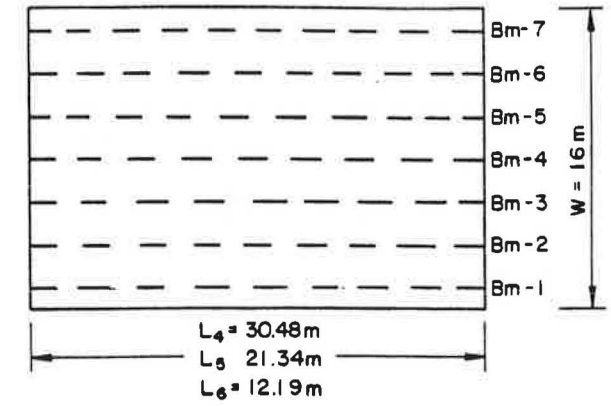

Figure 3. Plan and cross section of Bridges 7, 8 and 9 (subscripts indicate bridge numbers; 1 in. = 25.4 mm, 1 ft. = 0.305 m)

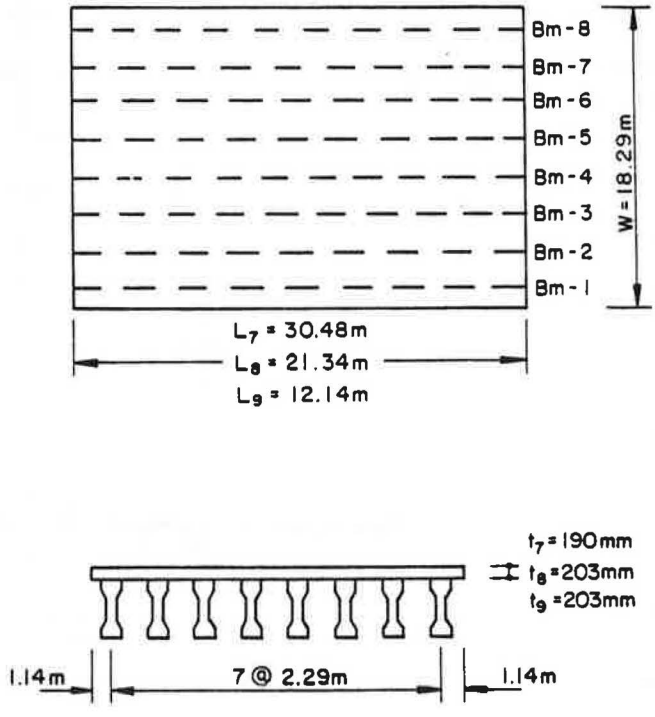

Figure 4. Overload Vehicle No. 1 (1 k = 0.225 kN, 1 in. = 25.4 mm, 1 ft. = 0.305 m)

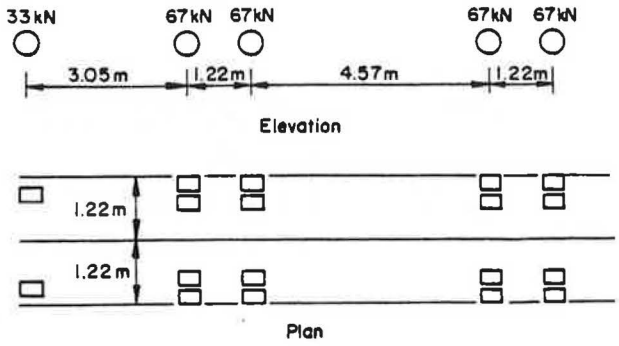

Figure 5. Overload Vehicle No. 2 (1 k = 0.225 kN, 1 in. = 25.4 mm, 1 ft. = 0.305 m)

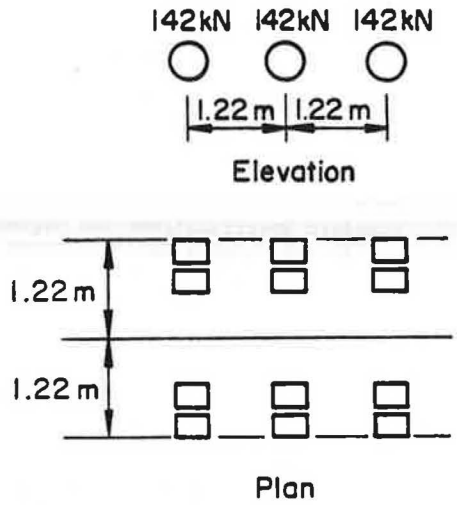

Figure 6. Overload Vehicle No. 3 (1 k = 0.225 kN, 1 in. = 25.4 mm, 1 ft. = 0.305 m)

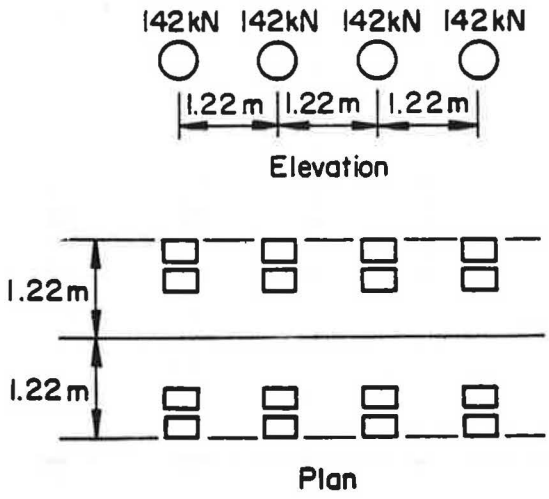

Figure 7. Overload Vehicle No. 4 (1 k = 0.225 kN, 1 in. = 25.4 mm, 1 ft. = 0.305 m)

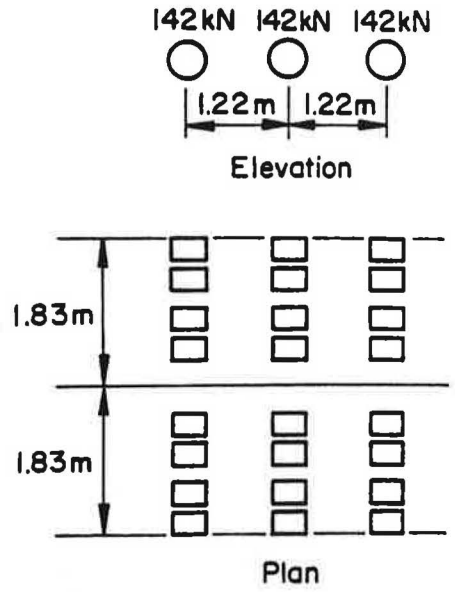

Figure 8. Overload Vehicle No. 5 (1 k = 0.225 kN, 1 in. = 25.4 mm, 1 ft. = 0.305 m)

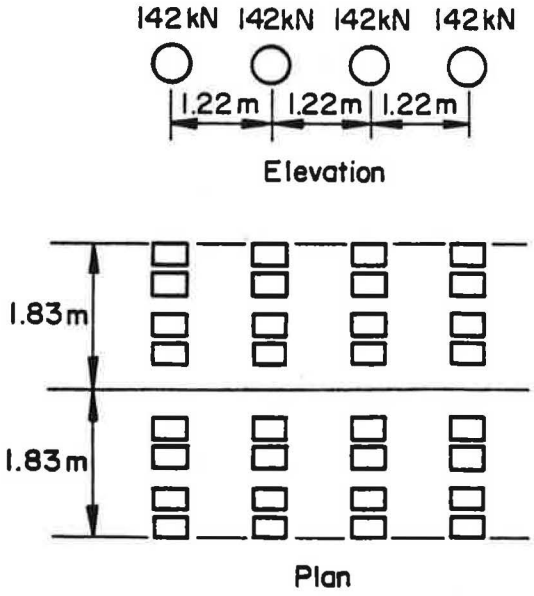

METHOD OF ASSESSING HIGHWAY BRIDGES FOR SUPERLOADS

Michael A.G. Duncan and Stuart G. Davis, National Institute for Transport and Road Research, Republic of South Africa.

Technological progress has made it economically beneficial to use larger and heavier industrial components termed "Superloads". These generally involve equipment for electric power and very heavy chemical plants located on coal fields. Because of the absence of inland waterways and the limited capacity of railways in Southern Africa, these loads must travel along the highway network. A current project involves the movement of payloads of up to 400,000 kg (440 tons) over some 500 km (310 miles) of road. In this instance a total of 60 under-bridges of various sizes must be crossed. In order to meet pavement loading restrictions, the transporters carrying these loads may have as many as 288 wheels distributed on 5 m (16 ft) wide axles. The four haulers used to draw these vehicles may give total combination masses of up to 800,000 kg (880 tons) and overall lengths of about 120 m (385 ft). Accurate analytical techniques are required to optimize the effects of these load trains on bridges so that every reserve of strength may be utilised. The multiplicity of structural configurations, construction materials, and original design specifications requires that each structure be assessed individually. Moreover, the variety of vehicle combinations is practically endless. For these reasons the method adopted to make such assessments relies on a load independent computerized influence surface technique involving stresses at critical points. A research program to develop a system termed "Generate-Simulate-Compare" (GSC) is now well advanced and initial analytical results show good correlation with parallel studies on monitoring techniques in the field. The paper describes the package of analytical programs and field observation methods.

In many parts of the world modern technology is making increasing demands for the use of larger and heavier industrial components. These generally comprise equipment for electric power stations and chemical plants and their movement presents transport operators and public authorities with tremendous problems. Although demand for these components is economically justified because the savings over a quarter of a century are vast, the associated repercussions and hidden costs of moving these loads are so extensive that the wisdom of permitting them to increase indefinitely is questionable.

Whereas many countries possess inland waterways, the absence of these in Southern Africa, coupled with a limited railroad carrying capacity, requires that they move along highways. Such loads are therefore of paramount interest to highway officials responsible for preserving the road network and minimizing traffic congestion.

Superload movements are limited by the height and width of the loads as well as by the forces they exert on pavements and bridges. In order to satisfy pavement loading regulations they are often supported on hundreds of wheels and are therefore very long and wide.

Although new bridges in South Africa will be designed to carry Superload transporters with a gross mass of 610,000 kg (670 tons), it is possible that many existing structures could support or be strengthened to carry these or lesser loads. As a result, the safety and stability of components in highway structures, such as bridge decks, must be carefully investigated.

National Policy

The Committee of State Road Authorities is responsible for general policy on Abnormal Loads and Superloads in South Africa. Its responsibilities include:

(a) preparation of regulations governing load movements
(b) selection of special routes
(c) preparation of design standards for highway structures.

Load categories

The four load categories shown in Table 1 have been tentatively adopted for the purpose of issuing permits and checking highway structures (1).

Abnormal loads. Since this category is intended to provide blanket coverage for all structures, including the weakest, with minimum structural investigation, the allowable loads are of necessity conservative. It applies to two bogie transporters drawn

Figure 1. Class B Superload of 495,000 kg (544 tons) gross mass comprising two Nicolas hydraulic suspension trailers and four haulers.

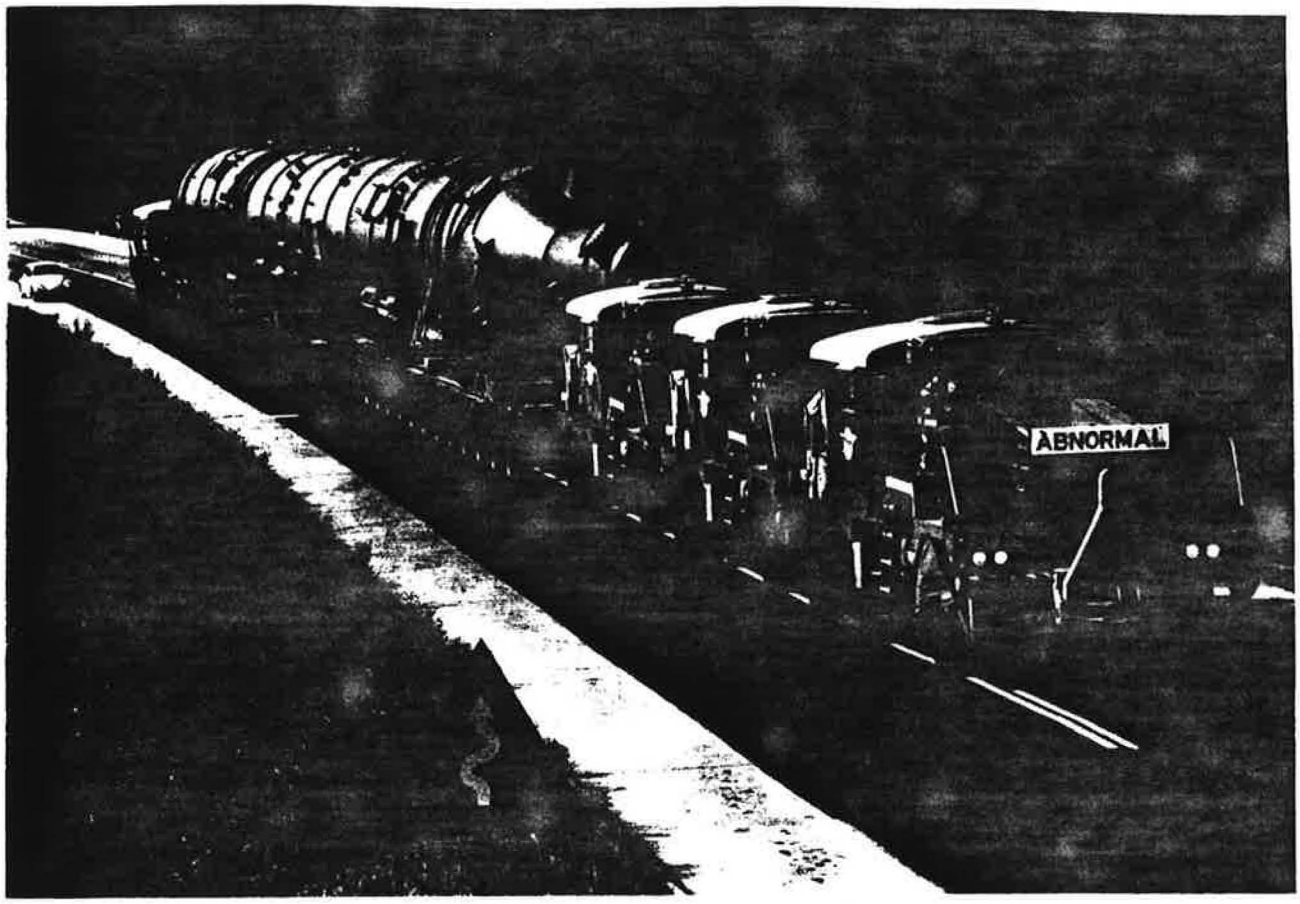

by one hauler. The permissible load is also governed by the width and inter-axle distance of two-, three- and four-axle bogies. Restrictions are also placed on the minimum distances between hauler and leading bogie and the centers of bogies. The allowable loads have been approximated by comparing bending moments and shear forces produced by 80 per cent of British Standard 153 HA loading (2) and axle group loadings on both simple and continuous decks. Overstress amounting to 25 per cent is permitted. The 125,000 kg (140 tons) gross load limitation may be revised upwards once the computerized system described in this paper becomes fully operational.

Broadly speaking, vehicles in this category may travel anywhere on bridges unless the payload exceeds 100,000 kg (110 tons).

Table 1. Load classification.

CATEGORY	GROSS VEHICLE COMBINATION MASS kg*	TRANSPORTER AND PAYLOAD MASS kg*
Abnormal loads	above legal but less than 125,000	less than 100,000
Class A Superloads	126,000 - 250,000	101,000 - 200,000
Class B Superloads	251,000 - 800,000	201,000 - 610,000
Class C Superloads	over 800,000	---

*1,000 kg = 1.102 tons

Class A Superloads. Permits for this category are issued after all structures on the proposed route have been individually checked. Transporters are generally escorted and restrictions are placed on the speed at which they traverse bridges as well as their location on the structure. Although structural investigations have hitherto relied on approximate analytical techniques (3,4), it is generally accepted that the system given below will find its greatest application to this load category.

Class B Superloads. This category is exemplified by the Nicolas trailer shown in Figure 1. Each of the two bogies of the transporter has a mass of 55,000 kg (60 tons) which bears on twelve 12-wheel axles. The 4.34 m (14 ft) wide transporter is drawn by four 40,000 kg (44 tons) haulers. With the 225,000 kg (248 tons) self-supporting payload the combined mass is 495,000 kg (544 tons). The overall length of the 36-axle load train is approximately 117 m (375 ft).

Such vehicles may only travel after each structure to be crossed has been rigorously analysed and thoroughly inspected. Structures are temporarily closed to other traffic and speeds reduced below 10 km per hour (6 mph). No braking or acceleration is permitted whilst the vehicle is on the structure and crossings may only occur in the presence of a professional engineer. Structural deflections are frequently monitored before, during and after the passage of these loads.

Precise knowledge of the masses, geometrics and position on the structure enable reductions in load

factors to be made; these may be further reduced depending on the accuracy of the analysis. Typical load factors are given later in this paper. In extreme cases the haulers may be disconnected and the transporter winched across the structure.

Class C Superloads. It is anticipated that these will only be required to move short distances along coastal roads.

Routes

The majority of Superloads originate from ocean terminals and travel to destinations located within industrial complexes or mining areas near the interior of the subcontinent. Less frequent movements also originate from inland complexes.

Routes connecting major cities are usually dictated by factors such as load width and height, highway geometrics, pavement strength and the carrying capacity of bridges. Whilst each province within the Republic is responsible for the selection of routes within its area of jurisdiction, it is necessary that these routes connect with neighbouring provinces. With this in mind, the tentative route map shown in Figure 2 has been prepared. Structures along these routes will be strengthened, where necessary, to support Class A Superloads. In some instances they will also be capable of carrying Class B Superloads. Many of these routes are intended for use in the future and the requirements in terms of numbers and frequency of Superload movements along them is not known at present.

An example of a designated Class B Superload route in operation is that between Richards Bay Harbour, on the Natal coast, and Trichardt in the important industrial and coal mining area of the Eastern Transvaal. This route is approximately 500 km (310 miles) in length and includes around 60 under-bridges. It has been carrying loads in excess of 250,000 kg (275 tons) gross since September 1977 and is expected to do so for some years to come. Over the next two years alone, a total of 700 loads in the category of Abnormal Loads and Class A and B Superloads is scheduled to be moved along this route. Of these, approximately 100 will exceed 250,000 kg (275 tons) gross, and 12 will be heavier than 600,000 kg (660 tons) gross.

Design loads

Specifications are at present being prepared for the design of future bridges in South Africa. Figure 3 shows two proposed classes of design loading: type NB and type NC.

Figure 2. Provisional Superload routes in the Republic of South Africa.

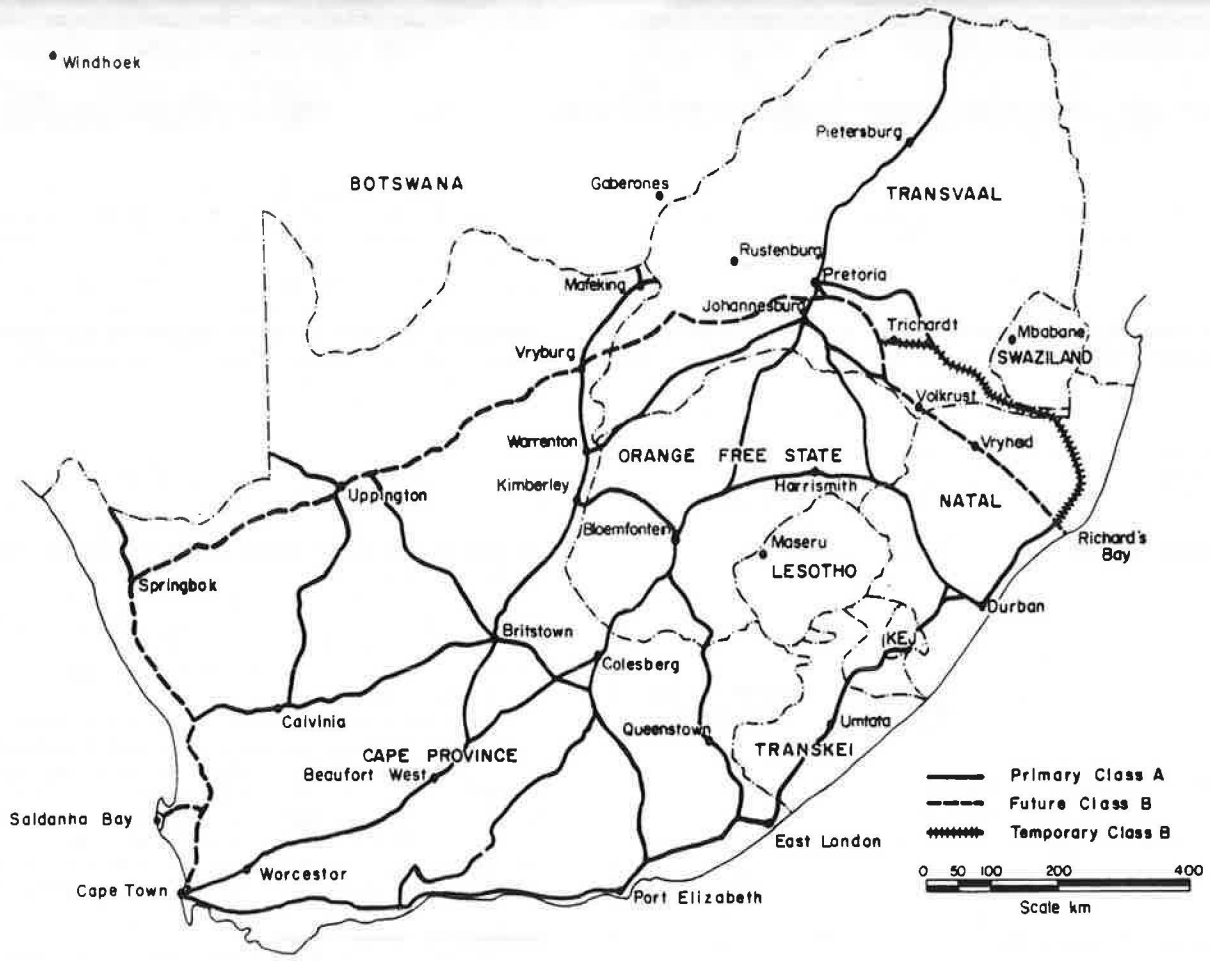

Figure 3. Design loads for structures on Superload routes.

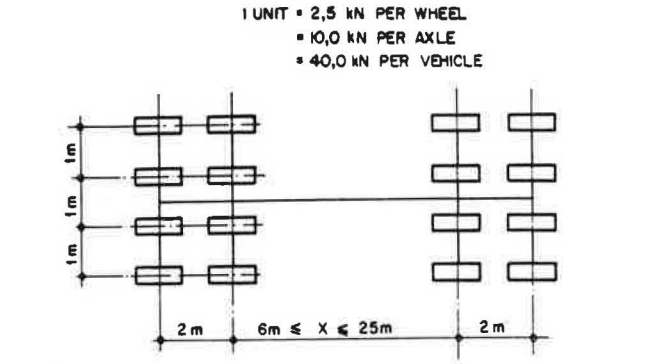

Type NB loading. This comprises an abnormal vehicle with a heavy load concentration on two bogies each having two 4-wheeled axles. Although this does not represent a realistic vehicle it is intended to ensure the adequate design of structures against possible rogue overloads of up to 150,000 kg (165 tons) gross. In order to provide for continuous spans the distance between the innermost axles varies from 6 to 25 m (19 to 82 ft).

Type NC loading. This is a special vehicle loading representative of multi-wheeled transporters with controlled hydraulic suspension and steering or self-propelled multi-wheeled vehicles with a gross mass of 610,000 kg (670 tons). Depending on whether or not the load is self-supporting, these vehicles can carry payloads of between 320,000 and 400,000 kg (350 and 440 tons). It is based on a wheel configuration typical of existing Class B Superloads. Although the haulers, which may each have a mass of 45,000 kg (50 tons), have been omitted for simplicity, these should be included where the load effects on a structure become critical. It is intended that all bridges on Class B Superload routes will be capable of supporting this load whilst closed to other traffic.

Safety factors for Superload analysis

The calculations involved in checking the capacity of bridge decks to carry Superloads are based on limit state theories. At present, the values ascribed to the various partial safety factors are similar, with certain modifications, to those proposed in the draft British limit state code for bridges, B/116 (5). Equivalent South African codes are being prepared, and research is being directed towards deriving the values for the partial safety factors most suited to local conditions.

From the point of view of the safety factors employed, the major difference between designing a bridge deck for everyday traffic loading and checking for a Superload is that the loading imposed by a Superload is known with a much higher reliability than in the case of normal traffic. A major advantage of the limit state philosophy is that it allows the adjustment of the values of individual partial safety factors to provide for such differing situations.

In the case of one important Superload route, in use at present, the Road Authorities concerned have agreed upon a system of partial safety factors for checking purposes, in which a value of 1.10 has been ascribed to the factor γ_{f1}* for the ultimate limit state. The value of the factor γ_{f2}* has been set at 1.00 since no other vehicles are allowed on a bridge during the crossing of a Superload. The values ascribed to the factor γ_{f3}* vary between 1.10 and 1.20, depending on the method of analysis employed.

Implicit in the above system is the assumption that the actual mass of each Superload is checked before departure (by means of individual axle "weigh-bridges") to ensure that both overall mass and individual axle masses do not exceed certain predetermined limits.

Capacity of existing bridges

The load capacity of bridges reflects the traffic of their time. Whereas the oldest local bridges were designed to support a laden wagen and 16 oxen, some future structures will be designed to carry 800,000 kg (880 tons) gross.

Evolutionary changes in design loads as well as increases in permissible working stresses prevent generalized attempts to assess the effects of Superloads on highway structures. The situation is aggravated by past use of inconsistent design standards within the subcontinent (7).

An earlier study (8) suggested that typical two-lane rural road bridges designed for BS 153 HA loading (2) could support Nicolas type transporters with a gross vehicle combination mass of 430,000 kg (475 tons) providing some overstress was allowed. However, it was evident that problems would be encountered with the 610,000 kg (670 tons) transporter on spans exceeding 15 m (48 ft). Although the situation improves as the number of lanes increases, the capacity of a bridge inevitably depends on its ability to distribute loads laterally.

Unfortunately, before the introduction of rational analytical techniques (9,10) in the late 30's, short and medium span bridge decks were designed as a series of independent components supporting a portion of the imposed lane load. The nominal cross beams that were provided frequently have inherent strength deficiencies which now render many older structures inadequate because of poor transverse stiffness.

---

*In the limit state nomenclature (6):
γ_{f1} is a factor to allow for possible unusual increases in load.
γ_{f2} is a factor to allow for the reduced probability of load combinations.
γ_{f3} is a factor to allow for inaccurate assessment of load effects.

Assessment factors

A number of factors are involved in the assessment of the load capacity of a bridge.

Structural and materials variations

Forms of construction commonly encountered in Southern Africa include simply supported, continuous, and articulated spans as well as frames and filled spandrel arches. About 250 box girders are located on primary routes, a figure which is increasing annually by 8.0 per cent. Trusses and cable systems are rare.

Decking arrangements include solid slabs, voided slabs, and beam and slab systems. Orthotropic steel plates and battle decks seldom occur.

Whereas steel and timber are scarcely used, reinforced concrete, prestressed concrete and steel-concrete composite construction appear regularly.

Such a multiplicity of configurations and materials frustrate generalized methods of assessing the Superload capacity of bridges. Assessment techniques have to compromise between precise analyses of the majority of structural types, with a view to reducing the margin of safety, and approximate methods, entailing more conservative safety margins. The latter will temporarily suffice for the minority of bridges, such as frames and arches.

Load configuration

The practically endless number of combinations of axle loads and spacings encountered in Class A Superload vehicles again thwarts attempts to generalize.

Lateral distribution

The ability of a bridge deck to distribute loads across its width depends on the relative flexural and torsional stiffnesses in the longitudinal and transverse directions. The load position is also important and optimum distribution generally occurs when the load is symmetrical about the longitudinal center-line. However, as transverse systems are never infinitely stiff, longitudinal members located directly beneath the vehicle carry a greater proportion of the load than edge members. In this context, local bridge engineers follow European practice and analyse decks as integral units in preference to North American practice where distribution factors are used (11).

Assessment technique

The primary reason for analysing an existing structure under passage of a live load is to predict the maximum forces in its component parts and ascertain if such movement will be safe. Investigations of serviceability, fatigue life and deflections may be equally important. It is usual, but not necessarily reliable, to assume that the capacity of structural components reflects the information shown on completion drawings and contained in the original specification.

The assessment technique should enable highway authorities to process permit application rapidly. Besides being accurate, to allow use of reduced load factors, it should also be simple, economical, and sufficiently flexible to handle any practical load configuration. Some compromise is necessary to meet these differing requirements.

As it would be impractical to assess every bridge element, investigations are restricted to critical sections where the combined dead- and live-load forces tend to maximize. The strength over the remainder of the member should be consistent with that at the critical section. Theoretical strengths at critical sections are reduced proportionally where weaknesses are detected. The more important critical forces encountered in common structures are listed in Table 2(8).

Engineers recognise that bridges may be analysed by any of the following methods: plastic, nonlinear elastic and elastic.

Plastic analysis

Collapse methods based on Johansen's yield line theory depend on the load configuration, its position on the structure and the arrangement of reinforcement. Although computer programs have been developed to determine which of several possible collapse patterns is the most critical, this method is not ideally suited to routine assessments since a complete analysis must be performed for each load position.

Nonlinear elastic analysis

Although the true behavior of most bridge materials is nonlinear, an elasto-plastic method is not favored because of the lengthy analytical process. The technique is relatively new and a computer is essential. The load is applied incrementally beginning at the

Table 2. Critical forces associated with various materials and forms of bridge construction.

CONSTRUCTION	COMPONENT	MATERIAL	CRITICAL FORCES
Multiple beam and slab	Main beams	All	Midspan bending, support shear, reactions
		Reinforced concrete	Steel-concrete bond
		Prestressed concrete	Principal stresses
		Steel	Bearing stiffeners
		Composite	Interface shear
	Cross beams	All	Bending and possibly shear
	Deck slabs	All	Bending, shear, and punching shear
	Bearings	All	Crushing and longitudinal forces
Slab decks	Slab	All	Midspan bending as well as compound moments in skew decks
	Bearings		Uplift at corners of skew decks
Continuous	Main beams	All	Besides those listed above, hogging moments in spans straddled by bogies
	Bearings	All	Uplift at discontinuous ends

fully elastic condition. At each stage the tangent modulus is used to describe the behavior of individual elements. However, because this is only an approximation, the system must be equilibriated by a series of iterations each of which involves a complete elastic analysis. Despite the development of techniques for increasing the rate of convergence, the method remains excessively expensive for routine assessments.

Elastic analysis

Elastic methods may be efficiently employed to obtain information under service conditions. Stresses, cracking, deflections and fatigue life may be readily investigated and the capacity of a structure determined using established margins of strength. Since the law of superposition applies, influence coefficients may be employed with considerable advantage for routine assessments.

Influence coefficients

Influence coefficients describe the variation of structural actions, such as moment, shear, reaction, and deflection, at a particular point for unit load applied anywhere on a structure.

Influence lines

Coefficients are grouped together as influence lines in the case of one- or two-dimensional structures, such as beams or frames. Although engineers have long used these lines to investigate the behavior of bridges, they are unsuitable for accurate assessments because of assumptions regarding transverse distribution.

Influence surfaces

Influence surfaces relate to coefficients extending in two directions across an area, such as a flat plate or bridge deck. They may take the form of either contour diagrams or digital models. Whereas the former are suitable for manual usage, the latter are almost mandatory for computerized load simulations. They are able to handle endless variations in wheel load, inter-axle distance, transverse wheel spacing and vehicle path.

Mesh size

The selection of mesh* size and mesh points is important and a network comprising continuous straight lines with a variable inter-nodal distance is ideal. Nodes located on primary members are supplemented by intermediate points which are closely spaced in the vicinity of the critical point or center-of-interest but more widely spaced at locations remote from it. Although the original intention was to develop programs for generating influence surfaces for points located within the central loading strip, this has been rejected in favor of a more general approach which permits the evaluation of coefficients for centers-of-interest anywhere on the deck. Besides allowing for skew tracking the resulting programs provide a useful design aid.

* A grid or network of application points

The GSC system

Since 1945 the number and frequency of requests for Superload permits has increased steadily. Time limitations have forced engineers to use various shortcuts and approximations. Unfortunately, these methods are no longer satisfactory since, in the case of Class B Superloads, large numbers of axles are involved and more precise analyses are required to justify the use of higher working stresses. It is therefore necessary to adopt a method that will be consistent, accurate and rapid.

The computerized approach described below fulfils these requirements. It involves three basic steps: "Generate", "Simulate", and "Compare" (GSC). An intermediate "Synthesizer" is required between the last two where compound stresses are involved. The system was originally conceived by the Ministry of Roads and Road Traffic, Rhodesia, for investigating Class A Superloads. It is currently being improved and extended for general use in South Africa.

Generate

Initially, the characteristics of a given structure or series of identical structures are established by means of influence surfaces for moments, shears, reactions, and deflections at preselected critical points. Whereas influence lines will be temporarily used for arches, frames and related structures, influence surfaces will be used for slab and multibeam bridges. These data are generated by a suite of computer programs. It is also necessary at this stage to determine the dead-load forces, thermal effects, member strengths, load factors and permissible working stresses. This information need only be evaluated once for permanent storage within a computer installation.

It is anticipated that this aspect will be undertaken by consultants appointed by the provincial authorities and that the results will be stored in computers owned by the provinces for the subsequent processing of loads, using the programs described below.

Simulate

Movements of load trains are simulated to evaluate critical forces. Such simulations are ideally suited to digital computers.

Load train descriptions involve wheel loads, longitudinal axle spacing, and inter-wheel distances as well as the location of the travel path on a given structure. The simulation program seeks the worst sum of the products of wheel loads and coefficients at their point of application. A second order interpolation formula is used to evaluate coefficients at points located between influence surface or influence line nodes.

Optimization efficiency is frustrated by variations in the shapes of influence surfaces or lines as well as by the relative location and magnitude of wheel loads. In order to overcome this difficulty, the load train is advanced across the structure in suitably small increments. Studies have shown that the error involved in using point loads rather than patch (tire contact areas) loads is insignificant where large numbers of wheels are involved.

Compare

Following simulation, the dead-, thermal-, and live-load forces are multiplied by their respective

load factors and the resulting stresses at critical points combined and compared with the allowable stresses. Comparisons with the ultimate moment are also used. The computer prints out a message stating whether the proposed movement is SAFE or UNSAFE along with the stress data upon which this conclusion is based.

Synthesize

In some instances, such as prestressed construction and slab decks, principal stresses and compound moments are required. When this is necessary the computer will complete the simulation process for each force involved and store the results for successive load positions. It will then return to combine these forces, and if necessary, determine their direction prior to evaluating stresses and establishing the optimum value.

Computer programs

Programs are being developed on an in-house CDC Cyber 174. They are written in standard FORTRAN and will eventually be tested on several leading computers.

The "simulate" programs have been completed. The "generate" programs listed below will produce influence surfaces for right angled and skew decks that may be either simply supported or continuous. Types of construction will include beam and slab, solid slab and some voided slabs. An influence line program capable of handling 11 spans of variable section has also been prepared.

1. Grillage beam elements for beam and slab decks.
2. Variable mesh finite differences for either isotropic slabs or "substitute" orthotropic slabs.
3. Quadrilateral plate, membrane and beam elements for beam and slab decks.
4. Hybrid stress plate, membrane and beam elements for beam and slab decks.
5. Hybrid stress plate elements for either isotropic slabs or "substitute" orthotropic slabs.

The apparent duplication is deliberate and is intended to enable users to verify results using another method prior to placing them in permanent storage. The quadrilateral plate in the third program uses a previously developed SAP element (12) which, although generally satisfactory, yields neither shear forces in the plates nor an influence coefficient at the center-of-interest should this lie within the plate. This version will therefore be superseded by the hybrid stress plate and membrane elements (13) mentioned in the fourth program. However, the matrix solution subroutine, USOL (12), has been retained in all the finite element programs. Eventually the finite element programs will be extended to evaluate thermal effects.

The time required to generate influence surfaces has been greatly reduced through use of the Muller-Breslau principle reported by Newmark (14). Descriptions of this technique and the method of handling non-prismatic sections have been given elsewhere (15,16). Running times are very short. For example, it cost about $6.00 to generate five deflection influence surfaces for a simply supported span with eight main beams which reduced to 99 nodes having 114 beam elements and 80 plate elements. The simulation of a 21-axle Class A Superload across these five surfaces cost only 55 cents on the CDC Cyber 174.

Inspection and monitoring of bridges

Inspection prior to load movements

Before a route can be designated as suitable for Superloads, each structure on it is subjected to a detailed visual inspection. Any factor which may affect the structural performance of a bridge is noted, particular attention being paid to such aspects as deterioration of concrete, rusting of reinforcement, cracking of concrete in both super- and sub-structures and settlement or deterioration of bearings.

Evidently, such inspections must go hand in hand with the structural analysis carried out for each bridge to assess its ability to carry the required loads, and it is vital that the present condition of the structure is reflected in the data used in the analysis. For example, if extensive cracking is observed in a reinforced concrete cross-beam, the transverse stiffness of the deck will be adversely affected, and the analysis must be adjusted accordingly. Again, especially with multi-span, continuous structures, the effect of any settlement of the bearings must be taken into account.

This stage of inspection and structural checking is carried out some months before a route is scheduled to carry Superloads, in order to allow time for any remedial or strengthening work which may be necessary.

Strengthening methods are dictated by the structural configuration, material, location and ground-soffit clearance. Methods used in South Africa have included the reinforcement of longitudinal members by coverplating or prestress, increasing the prestress of transverse members and propping from the ground. This last method is generally considered undesirable. Other methods which have received consideration include the insertion of additional longitudinal or transverse beams, the provision of outrider beams or trusses, and the use of towers and stayed cables.

Inspection and monitoring during load movements

The frequency of inspection of the structures on a Superload route over the period of use of the route is greater than that applicable to bridges which have only to carry normal traffic. In addition, the performance of selected bridges during the passage of certain loads is monitored in some detail. Such monitoring is conducted for two reasons. Firstly, the performance of suspect bridges on a route is observed, in order to obtain advance warning of any deterioration or damage caused by the loads, and to generally confirm any assumptions which may have been made in the structural checks. Observations consist primarily of recording maximum vertical deflections in decks, and monitoring the width of cracks in concrete members, together with the development of cracks under load.

Secondly, the National Institute for Transport and Road Research is making use of Superload movements over bridges to further its research in the field of bridge deck analysis. A number of structurally sound bridges have been selected for observation along the Superloads route from Richards Bay to Trichardt*. The observations are at present restricted to monitoring the vertical deflection of the decks, at a number of positions, during the passage of a load. The results will be of use in checking deck analysis programs currently being developed and generally in establishing criteria regarding the behavior of such structures under loads of this magnitude.

An apparatus has been developed specifically for these observations which produces a continuous trace of the deflection at any number of chosen points on

---

*The following consulting engineers have been appointed to check the safety of structures along this route:
Drennan, Maud and Partners; D.L. Webb and Associates; Van Niekerk, Kleyn and Edwards.

Figure 4. Deflection trace from Bridge 2783.

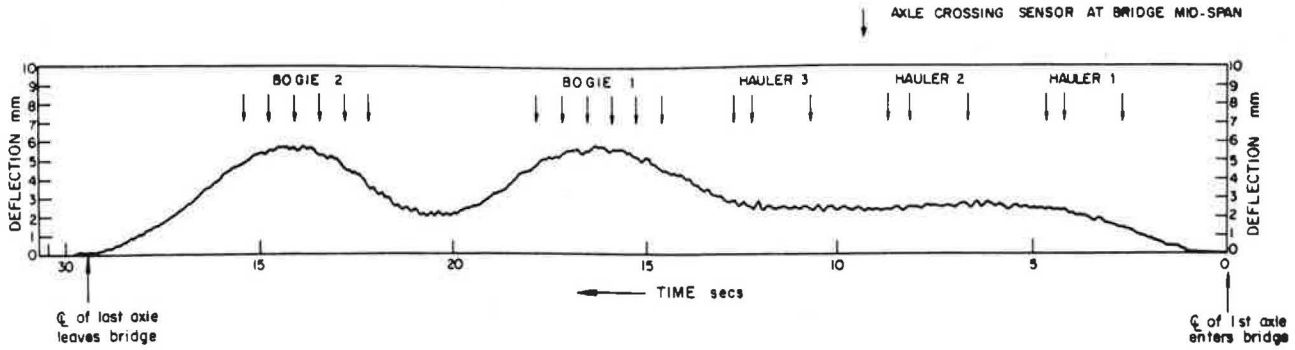

the soffit of the deck, as the load crosses the bridge (17). The deflection is measured by recording the movement of a weight suspended, at ground level, by a wire attached to the deck at the required point. The weight forms part of a mechanism, termed a deflectometer, in which its vertical movement is detected by an LVDT and recorded on a UV recorder. The number of LVDT channels, and hence measurement points, is at present limited to ten. A switch sensor, placed on the deck surface near mid-span, registers a mark on the UV recorder trace as each axle in the load train passes over it.

Despite, or perhaps because of, its simplicity, this system has performed well in the field, producing accurate traces of deflection at relatively low capital and running cost. Traces obtained during tests conducted on two bridges are shown in Figures 4 and 5. Figure 4 shows the mid-span deflection (at the bridge centerline) of a prestressed concrete deck of 21 m (67 ft) span. The total mass of the payload and transporter (excluding haulers) was 174,000 kg (192 tons). In the test shown in Figure 5 the deflection was monitored at five points on the deck. The bridge consisted of a prestressed concrete deck, of 31 m (100 ft) span, and the total mass of the payload and transporter (excluding haulers) was 190,000 kg (210 tons).

So far, the level of agreement between the observed deflections and those predicted by the analysis programs being developed has been encouraging. It is considered that, in the future, monitoring the performance of bridge decks by such methods will play an important part in the assessment of these structures for carrying Superloads.

Summary

Following recognition of the fact that the movement of essential Superloads is necessary for the industrial development of South Africa, national policy has been directed towards the development of systems and techniques required to assess the effects of these loads.

This policy includes the coordination of interprovincial routes, the development of design load specifications for future bridges, load classification, analytical techniques, and methods of inspecting structures and monitoring their behavior during the passage of Superloads.

Attempts to produce generalized methods of assessing the strength of various bridges are frustrated by the multiplicity of materials, decking systems, and architectural styles as well as a variety of axle and wheel load configurations.

Figure 5. Deflection trace from Bridge 1168.

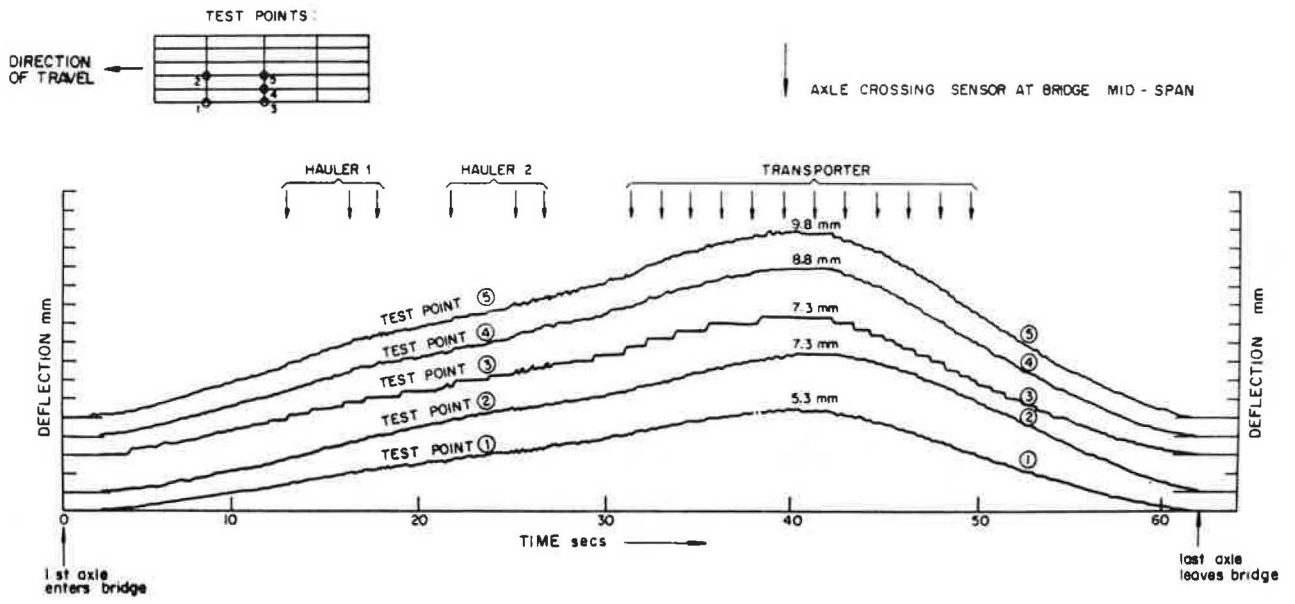

Since structures cannot be completely analysed for every heavy vehicle movement, critical points are selected where forces tend to maximize. The computerized GSC system, which assumes elastic behavior, is being extended to process the large number of Superload movements rapidly, consistently and accurately.

Bridge characteristics, in the form of influence coefficients, sectional properties, load factors, and permissible working stresses, are evaluated once and permanently stored within a computer system. Subsequent load simulations and stress comparisons may then be undertaken quickly and at short notice. This system should enable 80 per cent of the structures located on primary rural routes to be readily investigated.

Importance is attached to the inspection of structures before, during and after the movement of the heavier Superloads. This aspect includes the preparation of an inspection manual and the development of simple equipment for monitoring the deflections of structures during transient loads. Observed deflections are used to check analytical assumptions and verify the GSC system. The results to date show satisfactory agreement.

Acknowledgements

This paper is published by permission of the Director of the National Institute for Transport and Road Research, Council for Scientific and Industrial Research, South Africa.

References

1. Committee on Abnormal Loads. Conveyance of Abnormal Loads. TRH 11, National Institute for Transport and Road Research, Council for Scientific and Industrial Research, Pretoria, South Africa. (Under revision.)
2. British Standards Institution. British Standard 153 : Girder Bridges, Part 3: Loads and Stresses, Section A: Loads. British Standards Institution, London, England, 1954.
3. Hendry, A.W. and Jaeger, L.G. The Analysis of Grid Frameworks and Related Structures. 1st ed., Chatto and Windus, London, England, 1958.
4. Rowe, R.E. Concrete Bridge Design. 1st ed., John Wiley and Sons, London, England, 1962.
5. British Standards Institution. Draft British Standard Specification for the Design of Steel, Concrete and Composite Bridges. London, April 1976, Reference B/116.
6. Construction Industry Research and Information Association. Rationalisation of Safety and Serviceability factors in Structural Codes. London, CIRIA, July 1977, Report 63.
7. Liebenberg, A.C. and Stander, R. Proposals for a Uniform Specification on Live Loading due to Traffic on National Road Bridges. Confidential Report to the National Transport Commission of the Republic of South Africa, Pretoria, South Africa, March 1974.
8. Duncan, M.A.G. Superloads on Highway Bridges in Southern Africa. Journal of the Structural Division, ASCE, Vol. 103, No. ST 11, Proc. Paper 13347. November 1977. pp 2165-2179.
9. Pippard, A.J.S. and De Waale, J.P.A. The Loading of Interconnected Girders. Journal of the Institution of Civil Engineers, London, England, 1938. pp 97-114.
10. Leonhardt, F. Die Vereinfachte Berechnung Zweizeitig Gelagerter Trägerroste. Die Bautechnik, Germany, September 1938.
11. American Association of State Highway and Transport Officials. Standard Specifications for Highway Bridges. 11th ed., 341 National Press Building, Washington, DC 20004, 1973.
12. Wilson, E.L. Solid SAP - A Static Analysis Program for Three Dimensional Solid Structures. University of California Structural Engineering Laboratory Report No: UCSESM 71-19, September 1971.
13. Severn, R.T. and Taylor, P.R. The Finite Element Method for Flexure of Slabs when Stress Distributions are Assumed. Paper No. 6909, Proc. of the Institution of Civil Engineers, Vol. 34, June 1966. pp 153-170.
14. Newmark, N.M. Note on Calculation of Influence Surfaces in Plates by use of Difference Equations. Journal of Applied Mechanics, Vol. 8, No. 2, June 1941. p 92.
15. Davis, S.G. and Williams, R.D. A Proposed Method for Generating Influence Surfaces for Bridge Decks. Technical Note TSL/22, National Institute for Transport and Road Research, Council for Scientific and Industrial Research, Pretoria, South Africa, March 1977.
16. Davis, S.G. and Williams, R.D. Derivation of the Stiffness Matrix for a straight, non-uniform Beam. Technical Note TSL/23, National Institute for Transport and Road Research, Council for Scientific and Industrial Research, Pretoria, South Africa, March 1977.
17. Davis, S.G. and Spurr, W.A. An Apparatus to Monitor the Deflection of Bridge Decks under Moving Loads. Technical Note TSL/35, National Institute for Transport and Road Research, Council for Scientific and Industrial Research, Pretoria, South Africa, November 1977.

EVALUATION AND POSTING OF BRIDGES IN ONTARIO

A.C. Agarwal and P.F. Csagoly, Ontario Ministry of Transportation and Communications

The present system of posting substandard bridges in Ontario with a single load limit serves only as a vague warning to a driver that the bridge is somewhat deficient. Truck drivers generally disregard the posting sign, because they know they can carry heavier loads across without causing any apparent damage to the bridge. The quantitative definition of the posted value is based upon a design load reflecting vehicles in common use three decades ago, and herein lies the problem. Diverse modern traffic cannot be effectively represented by any single value posting which is generally too restrictive on short span bridges, especially for the long vehicles. Specified loads for the purpose of bridge design can be determined through statistically based load surveys to a significant degree of reliability. The procedure employs the concept of the 'Equivalent Base Length' to transform actual vehicles into uniformly distributed loads for mathematic manipulations leading to a single truck model which efficiently represents the wide variation in vehicle types. This report describes the development of live loads and a new triple posting system. Both have been adopted as the basis of capacity rating of existing bridges in the new Ontario Highway Bridge Design Code. The system employs the philosophy of ultimate limit states in evaluation of three levels of posting using an appropriate loading model for each level. Adjustments to the calculated load-carrying capacity are made to account for the operational overloads beyond legal limits, inherent to human nature, and the unusual distribution of loads on various axles in a partially loaded vehicle.

Permissible weights for commercial highway vehicles are regulated by the relevant provisions of the Highway Traffic Act in the Province of Ontario. In order to withstand these legal loads, a bridge must meet standards set in design specifications currently in use in the province. Where a bridge fails to meet these standards, certain restrictions are being applied. A restriction for maximum gross vehicle weight is presently displayed at the bridge by a sign that reads:

MAXIMUM WEIGHT X TONS

The quantitative definition of value X is based on design loads (1) that have not reflected specific Ontario conditions for the last three decades. Consequently, the value X bears little technical relationship to the load-carrying capacity of a bridge with respect to the modern commercial vehicles. The posted value has served only as an administrative tool and a vague warning for a truck driver that the bridge ahead is somewhat less than capable to carry legal highway loads.

Drivers have difficulty in properly interpreting the posting sign. Truckers consider the posting signs too restrictive and tend to believe from their experience that they can carry much heavier loads across without causing any apparent damage to the bridge. Some incorrectly think that the posted limit represents payload on the truck. The combination of these factors has rendered the posting signs useless because the truckers usually disregard them. The success of enforcement of a posted weight limit almost entirely depends upon the proper education and goodwill of a truck driver and his faith in the accuracy of the system.

As a first attempt to update the evaluation procedure to reflect modern highway traffic, a method was proposed by Csagoly (2). This method, still leading to a single velue posting, uses a design load based upon the 1971/72 vehicle survey conducted in the province, and the Ontario Bridge Formula which is the basis for the present vehicle weight regulations in Ontario (3). The background material and details of the design equation and various parameters involved are outlined by Csagoly and Dorton in their report on the Proposed Ontario Bridge Design Load (4).

This method incorporates modern highway loads; however, it produces a weight limit which is too liberal for short trucks which could seriously endanger the safety of the structure. It was later realized that the single value posting load had certain inherent problems irrespective of the design model to be used. A single value based upon a short truck model would be too restrictive for longer trucks and the single value based upon a long truck model would be too liberal for short trucks. Also,

on a short span bridge, the single value obtained by any method would be too restrictive for long vehicles because the procedures fail to recognize that only part of a long vehicle may be accommodated over a short bridge.

A new rating system based on multiple value posting was developed by the Ontario Ministry of Transportation and Communications and, in principle, has been adopted for the new Ontario Highway Bridge Design Code. This report describes the proposed new system and the procedure of evaluating the load-carrying capacity of a substandard bridge using this system.

Classification of Modern Highway Vehicles

To collect more recent data for commercial vehicles, a vehicle survey was conducted in 1975. The sample was statistically distributed across the province and the data for each vehicle included vehicle type and configuration, interaxle spacings, empty vehicle weight and the axle weights of loaded vehicles. Vehicle configurations observed during the survey are shown in Figure 1. Configurations seen most frequently were 1, 15, 19, 20, 24, 25, 26, 29 and 34.

Categorizing the vehicles by the total number of axles appeared to be a simple approach initially, but led to complications. When considering the range of permissible legal loads, a large number of vehicle categories resulted. A more viable classification is based upon the number of vehicle units in a vehicle combination. All commercial vehicles can be grouped into the following three categories.

Vehicle Category I

All single unit vehicles of configurations 1, 15 and 34 fall into this category. Five axle single unit vehicles, without trailer, although rare, are also included. The most common vehicles are of configuration 15 with a single steering axle in front and a dual tandem axle at the rear. The legal weight limit on such a vehicle is about 215 to 250 kN (48,320 to 56,180 lb.).

Vehicle Category II

All two unit vehicles consisting of a tractor unit and one trailer or semi-trailer are included in this category. Common configurations are 19, 20, 24 and 29 with five or six axles. Seven axle combinations of configurations 33 and 36 are also present but in very small numbers. Almost 75% of all vehicles in this category are of configuration 24 with a single steering axle in front and two dual tandems, one on the tractor and one on the trailer. The legal weight limit for most five axle vehicles is 380 to 430 kN (85,400 to 96,630 lb.).

Vehicle Category III

All vehicle trains consisting of a tractor unit and more than one trailer are included here. The most common types of configurations are 25 and 26. The legal weight limit for a seven axle vehicle train is about 530 to 580 kN (119,110 to 130,340 lb.) whereas eight axle trains may carry up to 600 kN (134,840 lb.).

The Rating System

The new system consists of three posting levels illustrated by the typical posting sign given in Figure 2. Levels 1, 2 and 3 control vehicle weights in Categories I, II and III, respectively. The sign may appear to provide too much information to read while travelling at high speed but once the system is operational, it is believed a truck driver will quickly learn to read the value applicable to his own vehicle.

Evaluation Methodology

Evaluation of a bridge with low complexity and well known behaviour is usually done by analysis. Where doubt exists regarding the actual behaviour, a full-scale load testing may be required to establish the proper mathematical model of the bridge structure for analysis. In some cases, a proof load testing may also be conducted to ascertain the accuracy of analytical findings and to verify assumptions regarding material properties and strength. However, bridge testing is beyond the scope of this report and details of only the analytical system are given here.

The three levels of posting are determined by analytical evaluation of the bridge structure using a different live load model for each level. Each model is representative of actual vehicles in the corresponding vehicle category and includes an operational overload allowance beyond the legal limits for all operations other than special permits.

Characteristic Evaluation Equation

Substandard bridges are generally posted for a short period of time before remedial measures of strengthening or replacement are taken. For such a short term evaluation, only ultimate limit states are considered.

The characteristic evaluation equation for the ultimate limit states can be written as:

$$(1-\mu)\,\phi\,R_n \geq \text{Effect of}\left[\sum_{i=1}^{4} \alpha_{D_i} \cdot D_i + F(\alpha_L L_L + \alpha_I L_I)\right] \qquad (1)$$

where
- μ = degree of deterioration
- ϕ = performance factor
- R_n = nominal resistance of structural components
- α = load factor
- F = scale down factor
- D_1 = dead load of factory produced structural components, excluding wood components
- D_2 = dead load of cast-in-place structural concrete components, structural wood components, and all non-structural components other than a superimposed wearing surface
- D_3 = dead load of superimposed wearing surface
- D_4 = dead load of earth fill
- L_L = live load
- L_I = dynamic load allowance

The degree of deterioration is established by a thorough inspection and is governed by the net

Figure 1. Vehicle configurations observed during the 1975 survey.

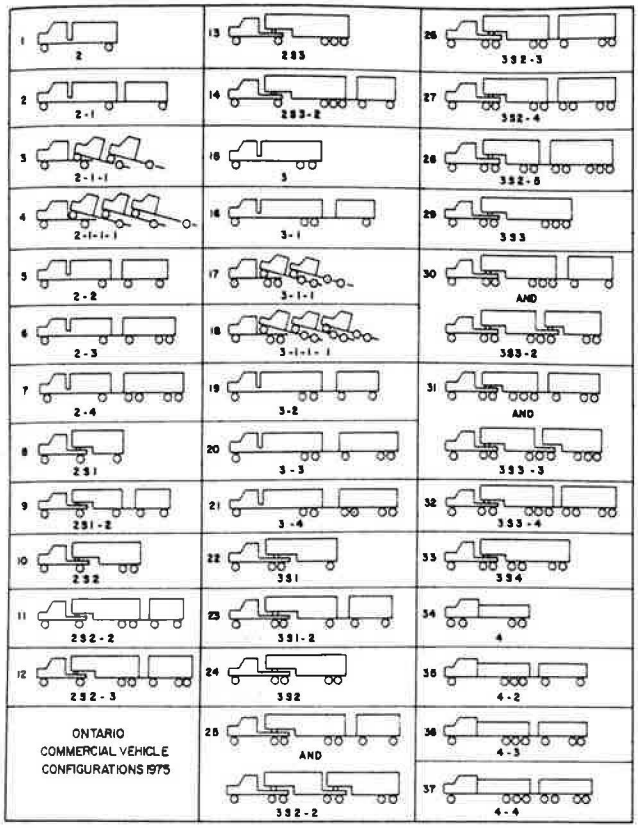

Figure 2. Posting sign.

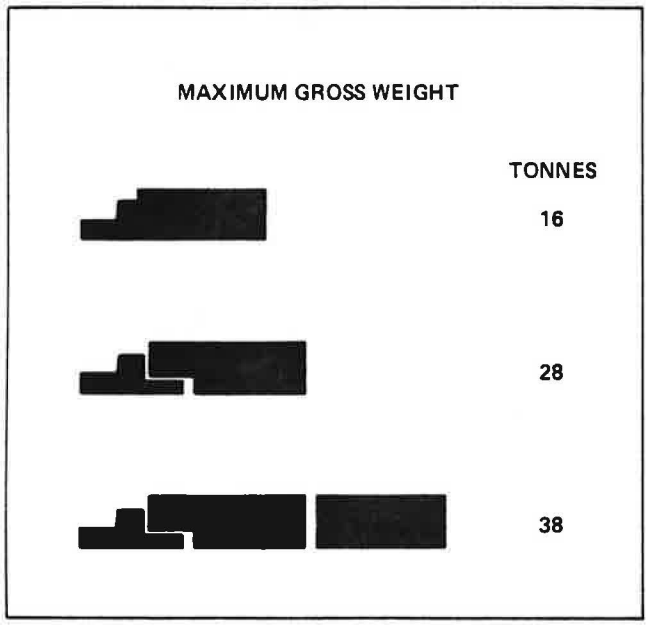

Figure 3. Equivalent base length concept.

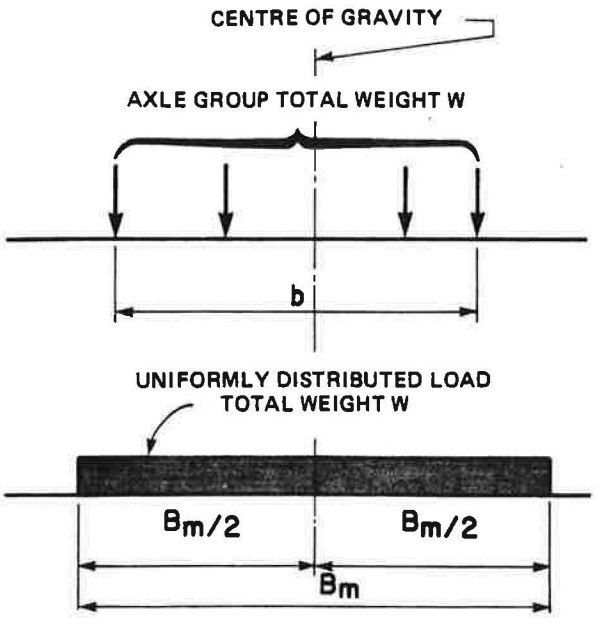

Figure 4. Acceptance test diagram.

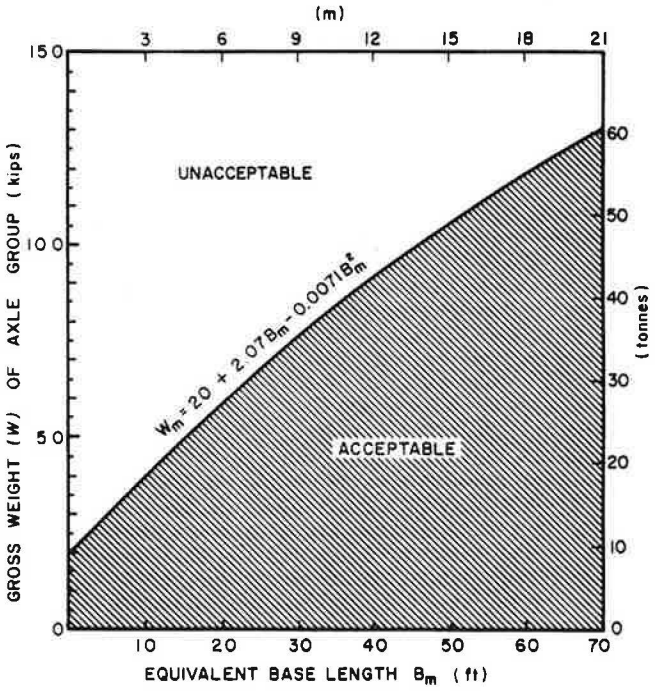

cross-sectional area of the reliable material. For deteriorated compression members, strength will be affected not only by the reduced area directly, but also by any change in effective buckling capacity.

The variability factors ϕ and α have been derived for the design of new bridges (5). They may be subject to change for short-term bridge evaluation, particularly for posting purposes. The performance factor may be modified depending upon age, condition, type and past service of the structural component but any change must not exceed 0.10. The live load factor, α_L, may be reduced to a minimum value of 1.20 for short-term evaluation. Dead load factor, α_{D_3}, for the superimposed wearing surface may be reduced to $(1 + t)/t$ where t is the average measure of asphalt thickness in inches. The above modifications of load factors apply only where the load increases the maximum response.

Structural components which are critical to the strength or stability of the entire bridge and whose individual loss would cause a catastrophic failure may be assigned a reduction in the performance factor by 10%.

The scale down factor, F, defines the fraction of the representative vehicle model that can safely be carried across the bridge. This factor can be determined from the characteristic evaluation equation 1.

There is a possibility that the above modifications in ϕ and α may lead to an unsuitably low overall safety against failure. To guard against this possibility, a minimum overall safety factor of 1.25 must be maintained. Hence the scale down factor, F, should not be greater than the value given by the following equation:

$$F \leq \frac{\frac{(1-\mu)\,\phi\,R_n}{1.25} - \text{Effect of } (D_1 + D_2 + D_3 + D_4)}{\text{Effect of } (L_L + L_I)} \qquad (2)$$

Development of Representative Vehicle Models

Modern highway traffic consists of several variations in vehicle types ranging from short two axle trucks to long truck trains. There exists an infinite number of combinations of interaxle spacings and axle weights. The discontinuous nature of highway loads does not lend itself to a simple mathematical manipulation. However, the concept of 'Equivalent Base Length' permits a simple transformation of highway loads into a continuous mathematical function. Equivalent base length, B_m, illustrated in Figure 3, is defined as the length over which the total weight of a group of axles can be uniformly distributed to cause force effects in a bridge structure similar to those caused by the group of axles itself. This transformation makes it easier to determine the force effects caused by a vehicle or a part thereof.

In 1967 data were collected on the axle weights and interaxle spacings for 6,763 vehicles in Ontario. Analysis of these data, using the equivalent base length concept (6), led to the development of the Ontario Bridge Formula. This formula became the basis for heavy vehicle weight control in the Province of Ontario in 1970. The Ontario Bridge Formula is given as:

$$W_m = 88.96 + 30.21B_m - 0.34B_m^2 \qquad (3)$$

where W_m = permissible total weight on a group of axles in kilonewtons

B_m = equivalent base length for the group of axles in metres

$$\left[W_m = 20.0 + 2.07B_m - 0.0071B_m^2\right.$$

where W_m is in kips and B_m is in feet.$\left.\right]$

The Ontario Bridge Formula is displayed as a curve in Figure 4. Such a diagram is commonly known as an 'Acceptance Test Diagram' and serves as an excellent tool to check a loaded vehicle for violation of legal limits and to compare the force effect of different vehicles on bridge structures. An example truck is displayed on the acceptance test diagram in Figure 5. The full truck or any of its subconfigurations is represented by a single point. If the point lies below the Bridge Formula curve, the subconfiguration is considered to be within the legal limits.

Maximum Observed Load Level

Through various load surveys in Ontario, it has been established that a certain relationship does exist between the legal and actual loads. Based on a commercial vehicle weight survey in 1971/72, in Ontario, a level of maximum observed load (MOL) was established. This level was found to be about 100 kN (22.5 kips) higher than the Ontario Bridge Formula and was further verified by the vehicle survey in 1975 (7).

Modified OBF and MOL Levels

The Highway Traffic Act for heavy vehicle weight control in Ontario was amended in 1978 (8). The new legal limits are based on a modified Ontario Bridge Formula given as:

$$W_m = 9.806\,(10.0 + 3.0B_m - 0.0325B_m^2)$$

The modified MOL level is given as:

$$W_{MOL} = 9.806\,(20.0 + 3.0B_m - 0.0325B_m^2)$$

The modified MOL level has been adopted as the level of specified live load models for the Ontario Bridge Design Code.

Representative Truck Models

During the early stages of writing the Ontario Bridge Code, truck models for the design and evaluation of bridges were developed independently. The reason for this is that evaluation trucks need represent only the corresponding vehicle category whereas the design truck model must represent the entire truck population. A few important observations were made from the 1975 vehicle survey:

1. For vehicles in Category I, the maximum single axle weight was less than 140 kN (31.47 kips) and violation of legal gross weights was within 90 kN (20.23 kips). The most common spacing for a dual tandem was about 1.22 m (4 ft.). Loads as high as 270 kN (60.70 kips) were observed on these axle units.
2. For vehicles in Category II and III, single axle weights as high as 184 kN (41.5 kips) were observed. Violations on axle units and axle groups reached up to 107 kN (24.05 kips). The largest single axle weight in the 1971 survey was 202 kN (45.5 kips).

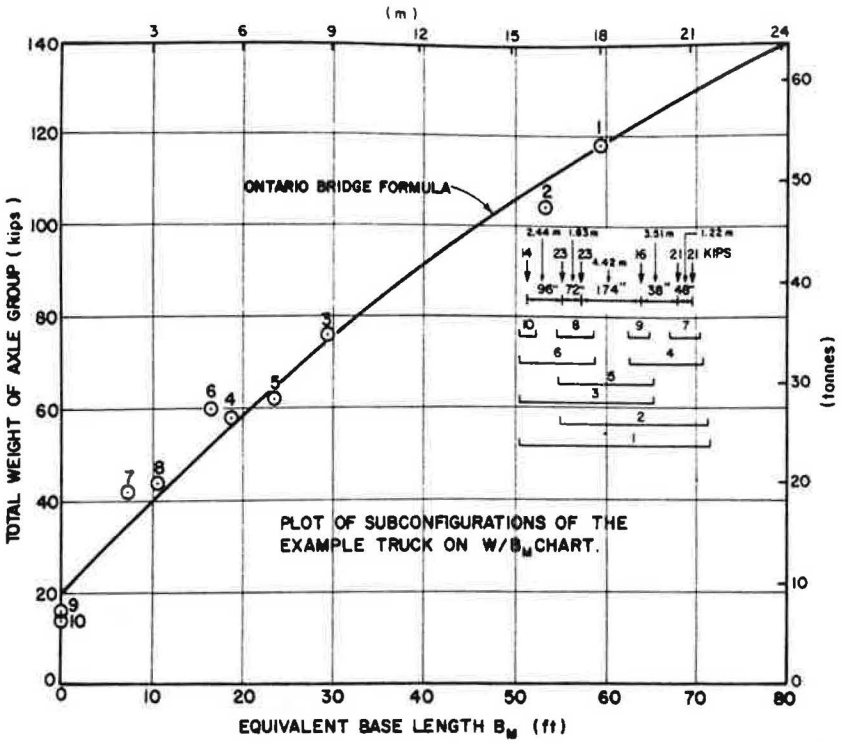

Figure 5. Equivalent base length B_m (ft.)

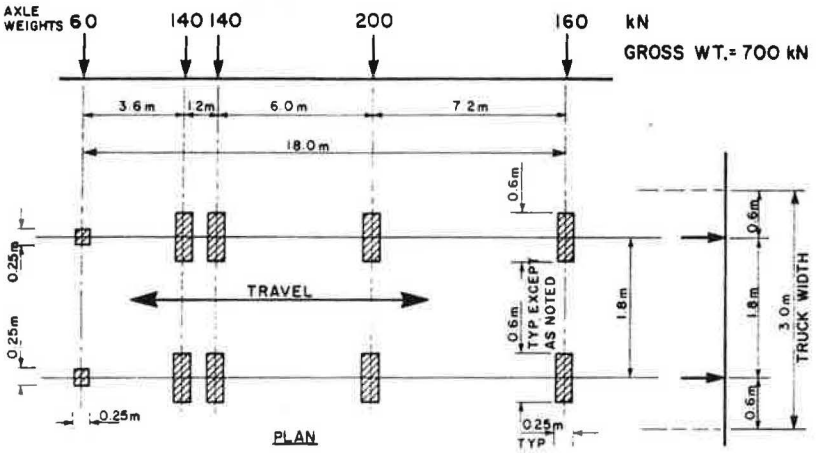

Figure 6. Ontario Highway Bridge Design Truck (OHBD Truck).

Figure 7. Comparison of OHBD Truck with the maximum observed load level.

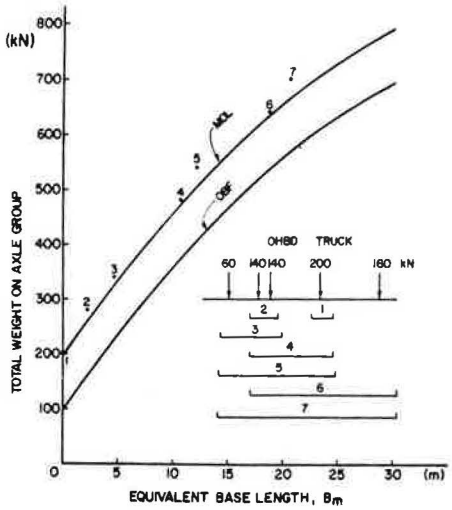

Figure 8. Trucks for rating of bridges.

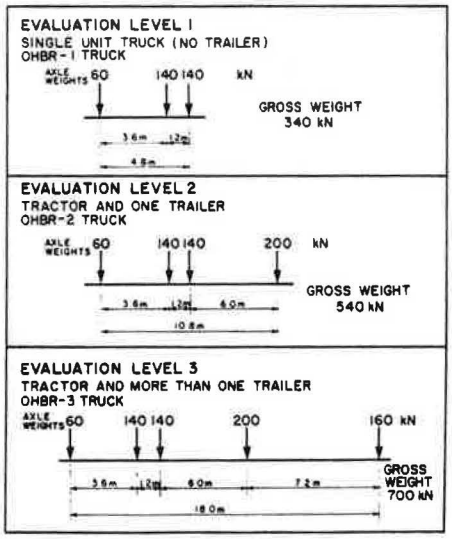

The truck models which would be used frequently in future design and evaluation should be simple and spacings and axle weights should be easy to remember. The requirements for the design truck model and the Level 3 evaluation truck model are essentially similar. The model should have:

1. At least one single axle weight of 200 kN (44.96 kips).
2. A light front axle typical of most highway vehicles. The common front axle weights were found to be close to 53 kN (12 kips).
3. A dual tandem axle at about 1.22 m (4 ft.) spacing, carrying close to 270 kN (60.70 kips).
4. A total length of about 18.3 m (60 ft.) which is the commonly observed distance between the extreme axles in truck trains.

For the truck model for Level 1 evaluation, the heavy single axle of 200 kN (44.96 kips) was not required, but the heavy dual tandem axle unit had to be retained.

Finally, it was possible to develop a truck model which, in its entirety, can be adopted for design and Level 3 evaluation, and whose subconfigurations can be utilized for Level 1 and 2 evaluation. This model, designated as the Ontario Highway Bridge Design Truck (OHBD Truck), is shown in Figure 6. Its subconfigurations are compared to the MOL level in Figure 7. The three truck models for evaluation are shown in Figure 8 and designated as OHBR-1, OHBR-2 and OHBR-3 Truck. The fact that OHBR-1 Truck is a part of the OHBR-2 Truck, which in turn is a part of the OHBR-3 Truck, makes the computation for three-level evaluation reasonably simple. It may also be noted that the OHBR-3 Truck is identical to the OHBD Truck. Although not essential, this is convenient for the Code. Gross weights of the three models are 340, 540 and 700 kN (76.44, 121.40 and 157.37 kips), respectively.

Multiple Presence of Vehicles

The live load model previously described represents a population of single trucks. In the evaluation of bridge capacity, the total live load effect is determined by considering the simultaneous presence of a number of trucks on the bridge. These trucks may belong to one or several vehicle categories. It can be proven that the load limitation determined by the exclusive use of a particular truck model for each level is valid for any mixture of truck types.

Consider a situation where two trucks are placed on the bridge for evaluation of bridge capacity for the three levels. The bridge is analyzed by placing two OHBR-1 Trucks and a posting load of 150 kN (33.72 kips) is obtained for Level 1. Similarly, a posting load of 250 kN (56.20 kips) for Level 2 is obtained by using two OHBR-2 Trucks. The bridge will be able to safely carry either two trucks from Category I, each loaded to 150 kN (33.72 kips), or two trucks from Category II, each loaded to 250 kN (56.20 kips). The governing effect would be due to either the gross weight of the trucks, or the weight on the axles, particularly for short span bridges and in the event a secondary member is most critical.

Now let us examine the effect of placing one truck from Category I, loaded to 150 kN (33.72 kips), and another from Category II, loaded to 250 kN (56.20 kips). If axle weights govern the bridge capacity, the effect of a truck from Category I would be similar to the effect of a truck from Category II, and the mixed truck case will have the same effect as with two trucks from either category. If the gross vehicle weight is the governing item, the mixed truck case would be less severe than the case using two trucks from Category II. Thus, mixing trucks from various categories need not be considered for the evaluation.

Highway Classification

The number of trucks to be placed simultaneously on a bridge depends largely on the type of road and the traffic volume using the bridge. For the design and evaluation of bridges, all roads and highways in Ontario are categorized into the following three classes:

Class A - includes all freeways and arterial roads. These roads carry high volumes of commercial traffic.

Class B - includes all collector roads. These carry a medium volume of commercial traffic.

Class C - includes all local roads carrying a light volume of commercial traffic. Roads with no commercial traffic also are included in this class. Roads in this class are limited to two traffic lanes.

Multiple Truck Arrangement

For all simple span bridges with span lengths up to 100 m (330 ft.) and continuous bridges where the sum of two adjacent spans does not exceed 122 m (400 ft.), no more than two trucks need to be considered in a traffic lane. Based upon his probabilistic study of multiple presences (9), Agarwal suggested to use a maximum of 4, 3 and 2 trucks simultaneously on a bridge in highway Classes A, B, and C, respectively. For the negative moments near, and the reaction at the intermediate supports in a continuous structure, up to 5 trucks are suggested for Class A highway bridges. Some truck arrangements for the three classes are displayed in Figure 9.

Representation by Uniformly Distributed Load

The multiple truck arrangement described above, although looks physically simple, may lead to some difficulties in positioning trucks on longer spans. Furthermore, it is considered to be a less efficient way to represent a wide variety of traffic mix which may also include a large number of light and/or non-commercial vehicles. It was found that such a diverse traffic mix can be more effectively represented by a complementary, uniformly distributed load in each traffic lane together with a fraction of the basic truck model.

Figure 10 shows Lane Load models for the three levels of evaluation. To determine the critical force effects on a structural component, one or more traffic lanes may be loaded. Each lane is loaded by one OHBR Truck or the corresponding Lane Load, whichever gives the larger effect. Total force effect is then multiplied by a reduction factor given in Table 1, to account for reduced probability of having simultaneous loads in more than one traffic lane.

Figure 9. General load patterns under the proposed multiple presence of a number of the trucks.

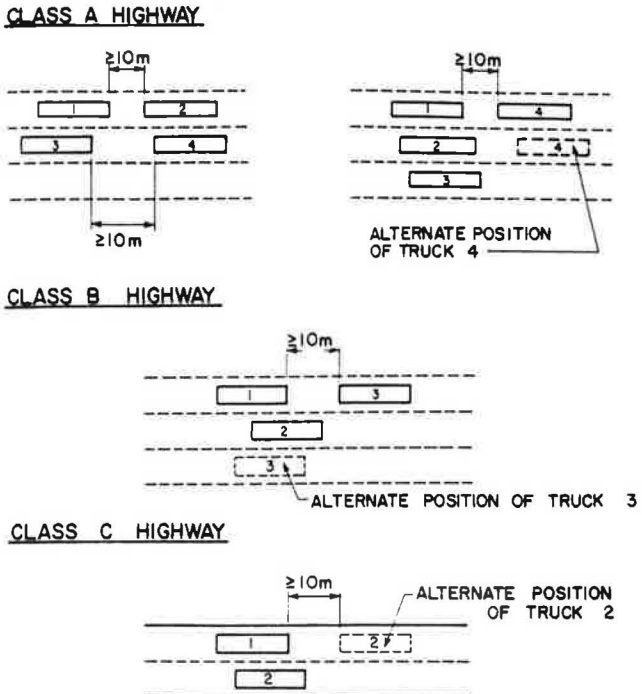

Figure 10. Lane loads.

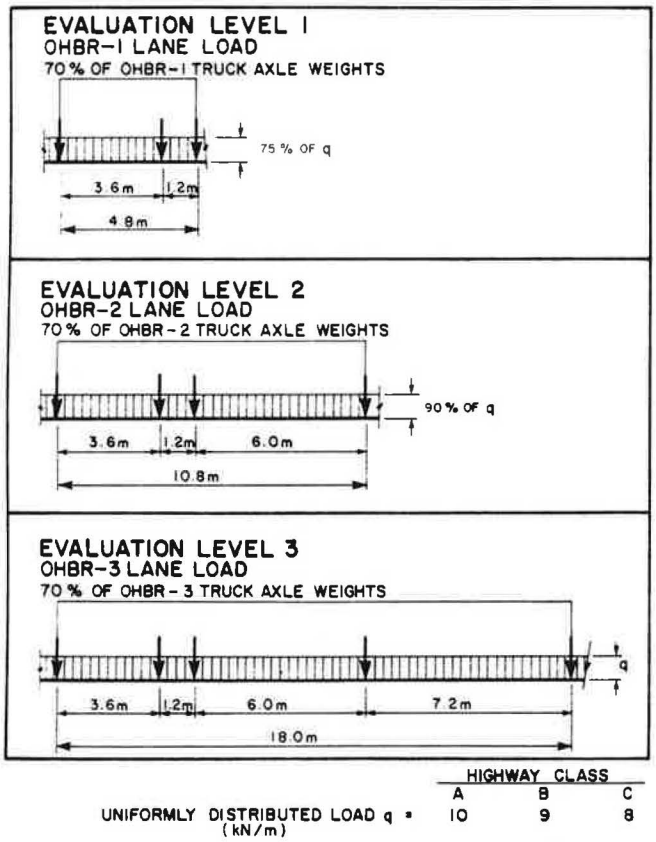

UNIFORMLY DISTRIBUTED LOAD q = (kN/m)	HIGHWAY CLASS A	B	C
	10	9	8

Figure 11. Partial loads on OHBR-2 Trucks.

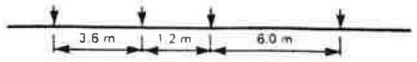

Full Load	60	140	140	200	= 540 kN
Partial Loads	59	138	138	185	= 520
	58	136	136	170	= 500
	57	134	134	155	= 480
	56	132	132	140	= 460
	55	130	130	125	= 440
	54	128	128	110	= 420
	53	126	126	95	= 400
	52	124	124	80	= 380
	50	120	120	70	= 360
	48	116	116	60	= 340
	44	110	110	56	= 320
	40	104	104	52	= 300
	36	98	98	48	= 280
	32	92	92	44	= 260
	28	86	86	40	= 240
	24	78	78	40	= 220
	20	70	70	40	= 200
	20	60	60	40	= 180

Figure 12. Load shift factors for shear and moments.

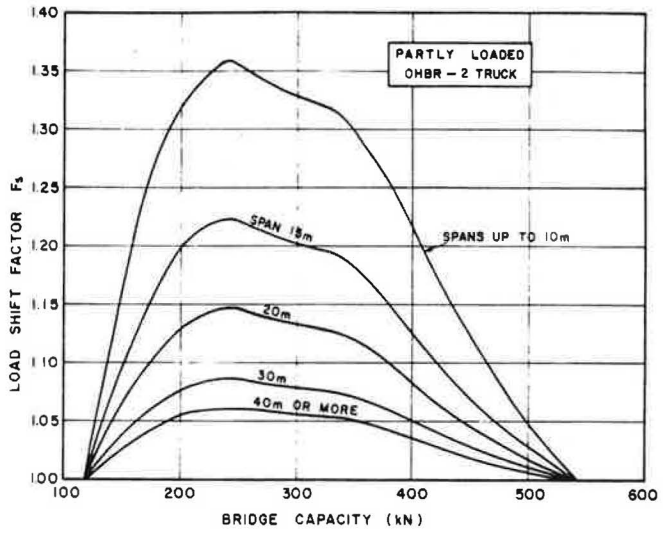

Figure 13. Posting load for first level.

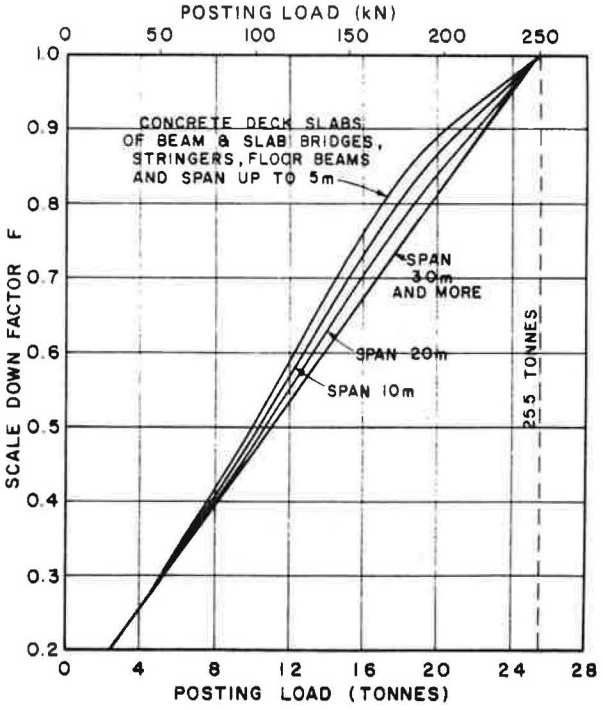

Table 1. Reduction factors for multi-lane loading.

Number of Loaded Lanes	Reduction Factor
1	1.00
2	0.95
3	0.85
4	0.75
5	0.67
6 or more	0.60

Partially Loaded Vehicles

An empty vehicle, or a vehicle loaded close to its legal limits in accordance with the Highway Traffic Act, would generally have an even distribution of load on various axles. The force effect per unit gross weight of the vehicle would be close to the force effect per unit gross weight of the truck models. Vehicles with partial loads may have an uneven distribution on various axles due to the unloading procedures. For instance, a truck train may travel with an empty second trailer but the first trailer may be fully loaded in the legal sense or even overloaded. Such a vehicle may cause much larger force effects per unit gross weight. Allowance, therefore, should be made in the bridge capacity rating for such odd distributions.

Load shift factor, F_s, defines the ratio of the force effect per unit gross weight of a partially loaded vehicle, and the force effect per unit gross weight of the truck model for the level of evaluation under consideration. The largest load shift factors are determined by using various unusual distributions of partial loads. Generally, force effects are found to be larger if the load is concentrated over the middle axles of a vehicle. Figure 11 shows an example of unloading an OHBR-2 Truck to obtain large load shift factors. For each loading level, the force effect per unit gross weight is determined for simple spans and compared to the force effect per unit gross weight due to a full OHBR-2 Truck. The results are shown in Figure 12. Load shift factors are found to be larger for shorter spans or secondary members and approach unity as the load level approaches empty vehicles or fully loaded vehicles.

Overload Allowance

From the commercial vehicle surveys in 1971/72 and 1975, it has been established that a considerable number of trucks do violate the legal limits. The degree of violation depends upon the clarity of vehicle weight regulations, its enforceability, the degree of enforcement and, to a great extent, on the penalty structure for overloads beyond legal limits. The truckers would like to carry maximum loads without endangering vehicle safety and receiving heavy penalties. Some may find it more economical to pay the fines for small overloads. In Ontario, the fines increase exponentially with the amount of overloads in order to discourage the truckers from carrying large overloads.

Using vehicle surveys, maximum overloads have been established for normal operation on routes where full Bridge Formula loads were permitted. The overload could be on the full vehicle or its subconfigurations. The maximum overload for Category I trucks was found to be about 90 kN (20.23 kips), while for other categories it could be as high as 107 kN (24.05 kips). For bridges which are not capable of carrying full legal loads, permissible weights would be less than those permitted by the Bridge Formula.

Unfortunately, no information is available regarding the degree of violation when only part of the full legal loads is permitted but, it is believed that these overloads will be somewhat smaller than the values given above. Prediction of such overloads is at present a matter of judgement. However, a minimum overload allowance of 50 kN (11.24 kips) for permissible load levels corresponding to empty vehicles seems to be justified. The overload allowances for the three levels of posting are given by the following equations:

First Level:

$$L_o = 35.0 + \frac{C}{6} \leq 90.0 \qquad (4)$$

Second Level:

$$L_o = 30.0 + \frac{C}{7} \leq 107.0 \qquad (5)$$

Third Level:

$$L_o = 30.0 + \frac{C}{9} \leq 107.0 \qquad (6)$$

where L_o = overload allowance in kN

C = bridge capacity rating in kN after adjustment for odd distribution of load for partially loaded vehicles

Posting Load Charts

The scale-down factor, F, defines the bridge capacity before any adjustment is made for partially loaded vehicles and overloads beyond permissible limits. Two steps of adjustments are made before arriving at the posting load. First, an adjustment is made for load shift in partially loaded vehicles to obtain the adjusted bridge capacity, C:

$$C = \frac{F}{F_s} \text{ (Gross Weight of Truck Model)} \qquad (7)$$

Second, using equations 4 to 6, overload allowance, L_o, is determined. Posting load is then given by:

$$P = C - L_o \qquad (8)$$

Posting load charts have been developed which give the posting load, P, directly as a function of the scale-down factor, F. The above two adjustments are implicit in the charts. Figures 13, 14 and 15 give the three Posting Load charts for Levels 1, 2 and 3, respectively.

The following steps summarize the analytical evaluation procedure.

1. Select critical members and sections in the bridge and determine the force effect for various dead loads and live load placing an appropriate OHBR Truck or corresponding Lane Load in each of the traffic lanes.
2. Select appropriate variability factors.
3. Using equation 1, determine the scale-down factor, F, for each level of evaluation.
4. Check to assure that equation 2 is satisfied.

5. Read the posting load for three levels from the appropriate posting load chart for corresponding scale-down factor.

Figure 14. Posting load for second level.

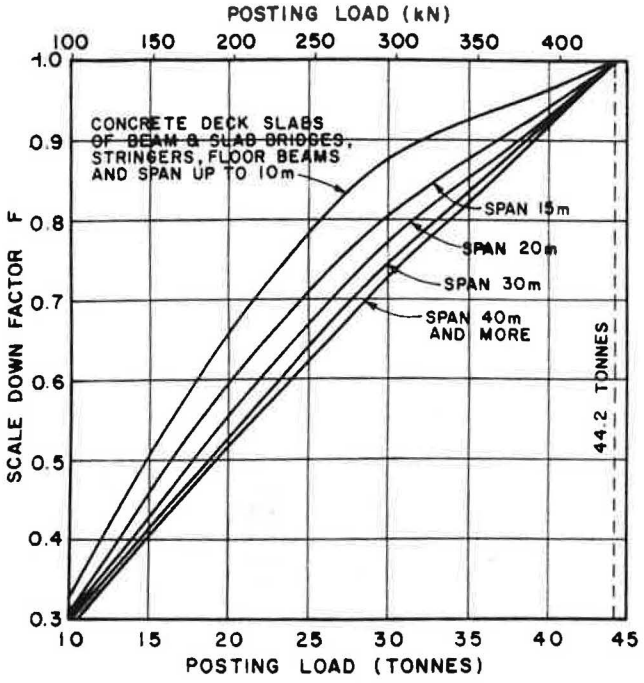

Figure 15. Posting load for third level.

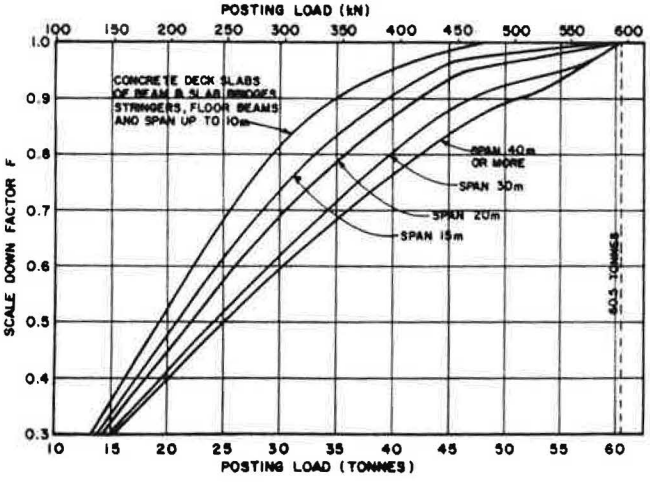

Conclusions

1. It has been shown that a posting system that relates to a 20-ton AASHTO Truck weight is not compatible with modern commercial highway traffic.

2. Using statistically based load surveys and the principle of the Equivalent Base Length, vehicle models can be built for design and evaluation purposes to represent the total vehicle population.

3. The limit states design philosophy, which is the basis of the Ontario Highway Bridge Design Code, is readily adoptable for the evaluation and rating of existing bridges.

4. The three-level posting system appears to be reasonably accurate and operationally practical for controlling modern highway traffic.

5. The posting is to be considered as a temporary measure to assure the safety of the travelling public.

References

1. AASHTO. Standard Specifications for Highway Bridges. American Association of State Highway and Transportation Officials, 1973.
2. P.F. Csagoly. Posting Bridges: A Proposed New Method. Research and Development Division, Ministry of Transportation and Communications, Ontario, 1974.
3. MTC. Axle Weight Legislation made under the Highway Traffic Act and Regulations. Ministry of Transportation and Communications, Ontario, 1971.
4. P.F. Csagoly and R.A. Dorton. Proposed Ontario Bridge Design Load. RR186, Research and Development Division, Ministry of Transportation and Communications, Ontario, 1973.
5. A.S. Nowak and A.C. Agarwal. Calibration of the Ontario Highway Bridge Design Code. (to be published), Ministry of Transportation and Communications, Ontario, 1978.
6. F.W. Jung and A.A. Witecki. Determining the Maximum Permissible Weights of Vehicles on Bridges. RR175, Research and Development Division, Ministry of Transportation and Communications, Ontario, 1971.
7. A.C. Agarwal and M. Wolkowicz. Ontario Commercial Vehicle Survey 1975. Interim Report, Research and Development Division, Ministry of Transportation and Communications, Ontario, 1976.
8. MTC. An Act to Amend the Highway Traffic Act: Bill 23. Ministry of Transportation and Communications, Ontario, 1978.
9. A.C. Agarwal. Probabilistic Study of Multiple Presence of Heavily Loaded Trucks on a Bridge in Ontario. (to be published), Research and Development Division, Ministry of Transportation and Communications, Ontario, 1978.

CORRELATING BRIDGE DESIGN PRACTICE WITH OVERLOAD PERMIT POLICY

Robert C. Cassano and Richard J. LeBeau, California Department of Transportation

Bridge engineers in many states have been designing bridges using working stress methods and AASHTO HS20 live load vehicles for the past 35 years. Recently, the AASHTO Specifications have permitted the use of load factor design for common structure types. During this same period there has been a significant increase in the number of vehicles that greatly exceed legal loads operating with special permits, as well as a marked increase in the weight of legal vehicles. To accommodate these loads, higher stress levels, defined as "operating stresses" in the AASHTO Manual of Maintenance Inspection of Bridges, are allowed at the discretion of the responsible agency. The practice of designing new structures by one set of rules and computing overload capacities by another results in a peculiar situation. The overload capacity of new structures varies widely depending upon construction materials and span length. It is inefficient to have the load capacity of a route segment limited by one or two structures while others have far greater capacity than can possibly be utilized. The purpose of this paper is twofold. First, to alert bridge engineers that they will reduce the usability of their highways by adopting load factor design without a corresponding increase in design live loads. Second, to relate how the California Department of Transportation assures uniform overload capacity at "operating stress" levels in new structures by routinely including a family of standard permit vehicles as one of the loading conditions in a load factor design method.

This paper will cause state bridge engineers to question the adequacy of their present design procedures. It will particularly throw doubt on the prudence of following the Load Factor Design (LFD) method prescribed in the American Association of State Highway and Transportation Officials (AASHTO) Standard Specifications for Highway Bridges using HS20 loads only.

We hope to cause the bridge engineer to consider some serious questions:

- Are the bridges under construction in his state adequate to carry the extra-legal loads that are currently operating there under permits?
- Will they be adequate to accommodate both legal and extra-legal loads anticipated 10 or 15 years from now?
- Is the capacity for overload in his bridges fairly uniform regardless of structure type and span length or is the usability of a particular route segment controlled by a single structure, or structure type?
- Will he make matters better or worse by adopting LFD?

These questions are timely because the nation is about to embark on an accelerated federally funded bridge replacement program. Since this provides an opportunity to upgrade a significant number of structures, it is reasonable that the bridge engineer give serious thought to the load capacity required in these replacement structures.

There is another reason for reviewing design loads for states that have adopted, or are thinking of adopting, LFD as standard office procedure. This design method produces structures with lower initial cost than those designed by the Working Stress Design (WSD) method, but the capacity for overload, although more uniform, is lower. Building these lighter structures may be a poor investment.

We, in California, asked ourselves the above questions a few years ago before adopting LFD. We found little correlation between loads and stresses assumed in design and those that occur in operating the structure after it is built. We found a wide variation in overload capacity from bridge to bridge. Most importantly, we found that if we adopted LFD using only an HS20 design load, our newest structures would not be able to carry permit vehicles that had become fairly common on our highways.

Definition of Loads

This paper will be more readily understood if agreement is reached on loading terminology.

The H and HS hypothetical loads are defined in the AASHTO Standard Specifications for Highway Bridges and are illustrated in Figure 1. The HS20 load is routinely used by all but a few states in the design of new bridges on major routes.

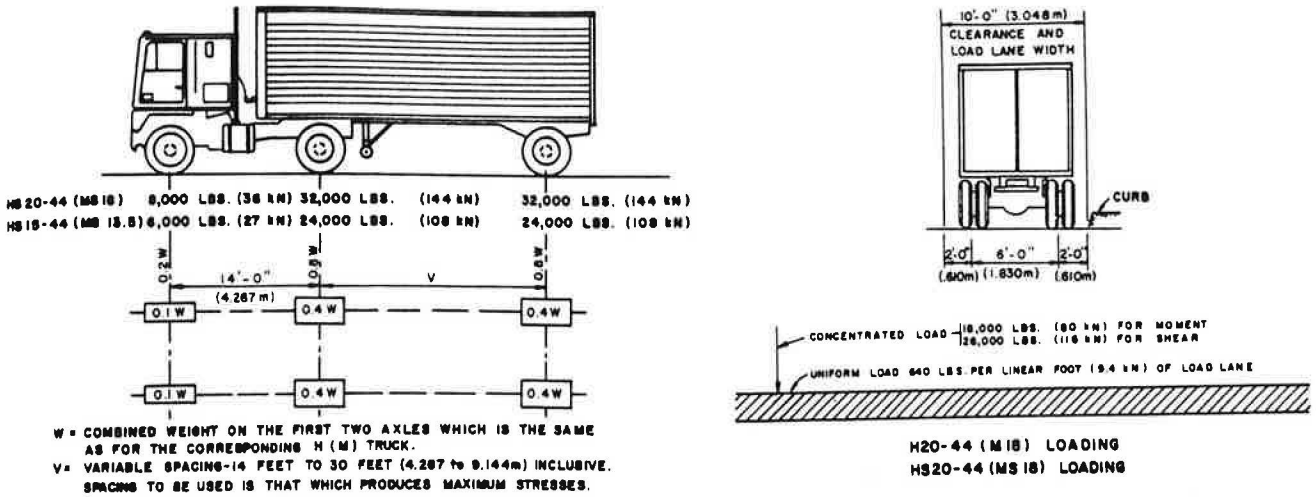

HS LOADINGS

Figure 1

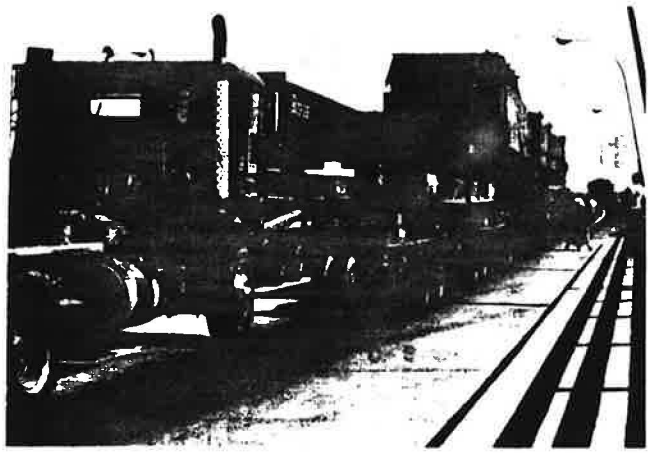

Figure 2

Legal loads are those maximum weights and dimensions of motor vehicles that can operate on highways without special approval from authorities. Federal Aid Amendments of 1974 increased the permissible weight of vehicles operating on the Interstate Highway System to the following levels:

Single Axle Wt	9,060 kg (20,000 pounds)
Tandem Axle Wt	15,400 kg (34,000 pounds)
Gross Wt	36,240 kg (80,000 pounds)

Legal loads vary somewhat from state to state in total weight, weight control on internal axle spacings, and overall truck dimensions. However, in most states they are quite similar to those shown above, which are allowed by the Federal Highway Administration on the Interstate Highway System.

Permit loads are those loads that exceed legal limits (extra-legal) but are allowed to operate on the highway under a permit issued by a regulatory agency. There is a wide variation in extra-legal load permit policy from state to state and the details of these policies are not accurately documented at this time. A National Cooperative Highway Research Program Synthesis, now in progress, entitled "Motor Vehicle Size and Weight Regulation, Enforcement, and Permit Operations", will soon provide information on current practice.

In California maximum axle weights allowed under routine permits are about 50% greater than legal loads. We have devised a family of overload vehicles called "P-loads" which are used in rating structures. (See Figure 6) A cursory review of information prepared commercially for the trucking industry by Heavy-Specialized Carriers Conference indicates that California's permit loads rank with the heaviest in the country.

Permit Policy

California's existing highway system is typical in that it includes bridges of many vintages in diverse states of repair. The structures were designed by various working stress design rules to carry several different AASHTO loadings. Since about 1941 we have used AASHTO HS20, but earlier structures were designed for H15 or even lighter loads.

In addition to legal loads, it has long been California's policy to allow vehicles that exceed legal weight limits to use its highway with controlled permits. To simplify the administration of the permit program, all of the existing structures on the state highway system are being rated using axle configurations and weights that resemble actual permit vehicles. This rating process involves a detailed structural analysis of every bridge.

In each highway district, a permit engineer has data, organized by route and post mile, that relates the live load capacity of each bridge to standardized loads. Using these data and other information concerning limitations on truck dimensions, axle spacings, and truck suspension systems, he can issue permits for extra-legal loads routinely, i.e., without further stress analysis of structures on the route. Last year approximately 200,000 trips were made in California using routine permits. These included loads of up to 110,500 kg (244,000 pounds) carried on vehicles with nine axles.

Besides these routine permits, special permits for even heavier loads are issued. This kind of permit requires a detailed analysis of each structure on the planned route for the specific load and vehicle under consideration. Frequently, certain operating conditions such as driving at reduced

speed and limiting other traffic on critical structures, are imposed to reduce stress levels. A load of this type is shown in Figure 2.

Operating Stresses

To fully utilize the mix of existing bridges for permit loads, stresses much higher than design working stresses may be used to determine maximum load capacities. AASHTO has sanctioned the use of these higher stress levels and has defined them as "allowable operating stresses" in the Manual for Maintenance and Inspection of Bridges. A recent review of federal inventory data showed that 27 states use the maximum operating stress levels in rating existing structures, i.e., determining safe load capacities. Other states rate their bridges at lower stress levels, ranging from design working stresses to the maximum operating stress levels.

The rationale for permitting higher stresses for permit loads is based partly on the fact that these loadings are known, whereas during design, future increases in loads must be anticipated. Also, heavy permit loads are thought to be applied infrequently so that fatigue damage is not a major concern.

The relationship between design stresses and operating stresses can be shown by considering the tension flange of a girder constructed of ASTM A-36 steel. For this material, the allowable design working stress is 0.55 F_y or 138,000 kN/m^2 (20,000 psi). The maximum allowable operating stress on this same material is 0.75 Fy or 186,000 kN/m^2 (27,000 psi).

For a concrete structure the spread in reinforcing steel stresses is even greater. For ASTM A-615, Grade 60 bars, the allowable working stress is 230,400 kN/m^2 (24,000 psi) and the operating stress is 345,600 kN/m^2 (36,000 psi).

The practice of designing a structure using one stress level, then rating it for overloads using a higher stress level results in a wide array of overload capacities for newly designed structures. This happens because the reserve capacity in a structure proportioned for one stress level and then reviewed at a higher stress level is derived from lowering the factor of safety for both dead and live loads. Therefore the additional capacity that can be made available for increased live load depends on the ratio of dead load to live load. Typically, for bridges designed by WSD and then reexamined at operating stress levels, concrete structures have a much greater capacity than steel structures.

AASHTO also allows rating of bridges with a load factor method. This method, which bases the safe load capacity on ultimate strength with a safety factor of 1.3, allows even greater load increases at the operating level. The basic load factor relationship for ratings is:

$$\phi\, Mu = 1.3 \left[M_{DL} + M_{(LL+I)}\right] \quad (1)$$

Solving for $M_{(LL+I)}$ gives the live load capacity:

$$M_{(LL+I)} = \frac{\phi\, Mu}{1.3} - M_{DL} \quad (2)$$

This variation in capacity is illustrated in Figure 4 by comparing a steel girder bridge with a reinforced

GIRDER SECTIONS

Structural Steel

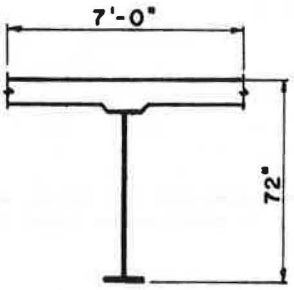

Reinforced Concrete

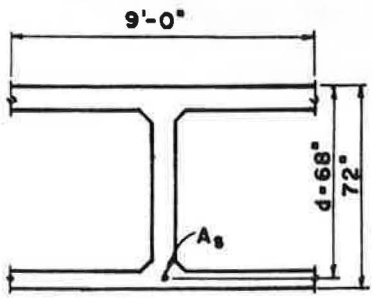

ASSUMPTIONS

100 ft (30.48 m) simple span	100 ft (30.48 m) simple span
Composite welded plate girder	Reinforced concrete box girder
Girder spacing s = 7'-0" (2.13 m)	Girder spacing s = 9'-0" (2.74 m)
LL distribution $\frac{s}{5.5}$	LL distribution $\frac{s}{7.}$
A-36 structural steel	Grade 60 reinforcement
F_s = 20 ksi (137.9 MPa)	f_s = 24 ksi (165.5 MPa)
F_y = 36 ksi (248.2 MPa)	f_y = 60 ksi (413.7 MPa)
$F_{s(oper)}$ = 27 ksi (186.2 MPa)	$f_{s(oper)}$ = 36 ksi (248.2 MPa)
Concrete: f'_c = 3250 psi (22.41 MPa)	Concrete: f'_c = 3250 psi (22.41 MPa)

Design controlled by maximum positive moments

These assumptions are used in the design examples in Figures 4, 5, and 7

Figure 3

concrete box girder bridge, both having 30.5 meters (100-foot) simple spans. For this example the two structures shown in Figure 3 were selected to have approximately equal LL+I capacity at WSD allowable stresses. At the operating stress level (WSD), however, the concrete structure has nearly 40% more capacity for live load than the steel structure. When compared using the load factor rating method the concrete bridge has nearly twice the live load capacity of the steel bridge.

Load Factor Design

The AASHTO Specifications have allowed the use of LFD as an alternative design method for steel bridges since 1970. Similar provisions were included for reinforced concrete and prestressed concrete soon after that.

There are three fundamental loading conditions used in applying LFD. These are shown in Table 1.

The LFD method, which includes an overload check, produces structures with a more uniform overload capacity. Unfortunately, structures designed by this method using HS20 loads are often not able to accom-

WORKING STRESS

This example represents bridges designed by working stress and demonstrates the method of rating these structures at operating level for both WSD and LFD. (Both are permitted by AASHTO)

GIRDER SECTIONS

Structural Steel

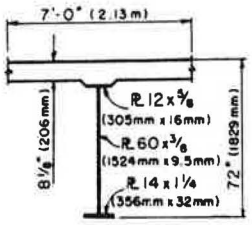

Reinforced Concrete

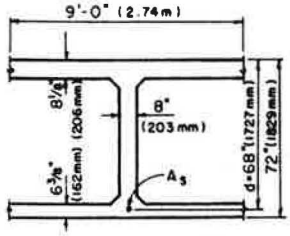

Working Stress Design

0.712 K/ft 10.39 kN/m	Dead Load	2.145 K/ft 31.30 kN/m
890 Kft 1207 kNm	M_{DL}	2681 Kft 3635 kNm
1185 Kft 1607 kNm	$M_{(LL+I)}$	1197 Kft 1623 kNm
2075 Kft 2814 kNm	Design M	3878 Kft 5259 kNm

$\frac{M_{DL}}{S_s} + \frac{M_{(LL+I)}}{S_{comp}} = .55\ F_y$

$9.4 + 8.9 = 18.3 < 20$ ksi (137.9 MPa)

$M = A_s f_s Jd$

$A_s = \frac{3878 \times 12}{24(.922)70} = 30\ in^2\ (193.5\ cm^2)$

Live Load Capacity at Operating Level (WSD)

$F_{s\text{-}oper} = .75\ F_y = 27$ ksi (186.2 MPa)

$F_{s\text{-}oper} - F_{s\text{-}DL} = F_{s\text{-}(LL+I)oper}$

$27 - 9.4 = F_{s\text{-}(LL+I)oper} = 17.6$ ksi (121.4 MPa)

$M_{(LL+I)oper} = \frac{F_{s(LL+I)oper}}{S_{comp}} = \underline{2335}$ Kft (3166 kNm)

$f_{s\text{-}oper} = 36$ ksi (248.2 MPa)

$M_{oper} = (A_s) f_{s\text{-}oper} (J)d = M_{DL} + M_{(LL+I)oper}$

$= \frac{30(36).922(70)}{12} = 5809$ Kft (7877 kNm)

$M_{(LL+I)oper} = M_{oper} - M_{DL}$

$= 5809 - 2681 = \underline{3128}$ Kft (4242 kNm)

Live Load Capacity at Operating Level (LFD)

$F_y = 36$ ksi (248.2 MPa) = M/S

$\frac{M_{oper}}{S} = 1.3\left[\frac{M_{DL}}{S_s} + \frac{M_{(LL+I)oper}}{S_{comp}}\right] = 36$ ksi (248.2 MPa)

$\frac{36}{1.3} - 9.4 = 18.3$ ksi (126.2 MPa) $= \frac{M_{(LL+I)oper}}{S_{comp}}$

$M_{(LL+I)oper} = 18.3(S_{comp}) = \underline{2450}$ Kft (3322 kNm)

$f_y = 60$ ksi (413.7 MPa)

$M_{oper} = \phi A_s f_y (d - \frac{a}{2}) = 1.3\left[M_{DL} + M_{(LL+I)oper}\right]$

$= \frac{0.9(30)60(66)}{12} = 8910$ Kft (12,082 kNm)

$M_{(LL+I)} = \frac{M_{oper}}{1.3} - M_{DL}$

$= \frac{8910}{1.3} - 2681 = \underline{4173}$ Kft (5656 kNm)

Figure 4

Table 1

AASHTO
LOAD FACTOR DESIGN

	LOADING	PERFORMANCE CONDITION	LIMITING CRITERION	
			Structural Steel	Reinforced Concrete
1.	Service Load D+(LL+I)	LL Deflection	L/Factor	L/Factor
		Fatigue	Controls on stress range same as for WSD	Controls on stress range in reinforcement. Concrete- $0.5f'_c$ (Reversal Areas)
		Concrete Crack Control	None	Limits on stress in reinforcement based on cover and spacing
2.	Overload D+5/3(LL+I)	Prevent excessive permanent distortion under an occasional overload	Noncomposite: $F_s = 0.8\ F_yS$	None
			Composite: $F_s = 0.95\ F_yS$	
3.	Max Design Load $1.3\left[D+5/3(LL+I)\right]$	Provide a reasonable factor of safety against collapse	Noncompact section $M_u = F_yS$	All compression in flange $M = \phi A_s f_y(d-a/2)$
			Compact Section $M_u = F_yZ$	Compression in flange & web $M = \phi(A_s-A_{sf})f_y(d-a/2) + A_{sf}f_y(d-0.5h_f)$

AASHTO LOAD FACTOR

These girders have been designed and rated using Load Factor Design procedures shown in AASHTO.

Structural Steel

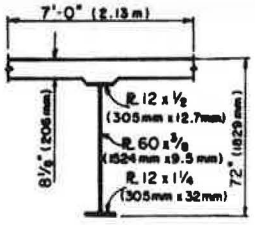

Reinforced Concrete

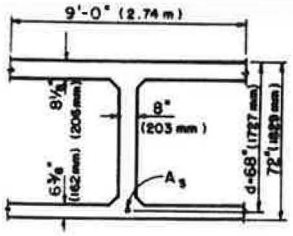

Load Factor Design

890 Kft 1207 kNm	M_{DL}	2681 Kft 3635 kNm
1185 Kft 1607 kNm	$M_{(LL+I)}$	1197 Kft 1623 kNm
3725 Kft 5051 kNm	$M_u = 1.3\left[M_{DL} + 5/3\ M_{(LL+I)}\right] = F_yS$	6079 Kft 8247 kNm
	Overload (M_o)	
2865 Kft 3885 kNm (77% of M_u)	$M_o = M_{DL} + 5/3\ M_{(LL+I)} = 0.8\ F_yS$	4676 Kft 6341 kNm (77% of M_u)

By inspection Overload does not control

Live Load Capacity at Operating Level

3725 Kft 5051 kNm	$M_u = 1.3\left[M_{DL} + M_{(LL+I)oper}\right]$	6079 Kft 8247 kNm
	$M_{(LL+I)oper} = \frac{M_u}{1.3} - M_{DL}$	
$M_{(LL+I)oper} = \frac{3725}{1.3} - 890$ $= \underline{1974}$ Kft (2677 kNm)		$M_{(LL+I)oper} = \frac{6079}{1.3} - 2681$ $= \underline{1995}$ Kft (2705 kNm)

Figure 5

modate permit loads that have been carried safely on older structures designed by WSD.

This can be illustrated by going back to the bridge used in the earlier example. Figure 5 shows a comparison of the capacity for live load at operating stress level for a similar steel and concrete structure designed by LFD using HS20 live loads.

With this design method the capacities for live load using the load factor rating system are nearly equal, i.e., both structures have the same capacity for permit loads. The problem is that this capacity is significantly reduced under those for structures designed by WSD. Randomly located bridges designed by these criteria can severely limit the usability of a highway network.

Need for New Criteria

Perhaps it was good fortune that specifications for LFD and the federal requirements for inventorying and rating existing structures occurred at about the same time. This forced us to consider bridge design methods in relation to the way we intended to utilize the completed structures. It became apparent that when our Maintenance Engineer added a new structure

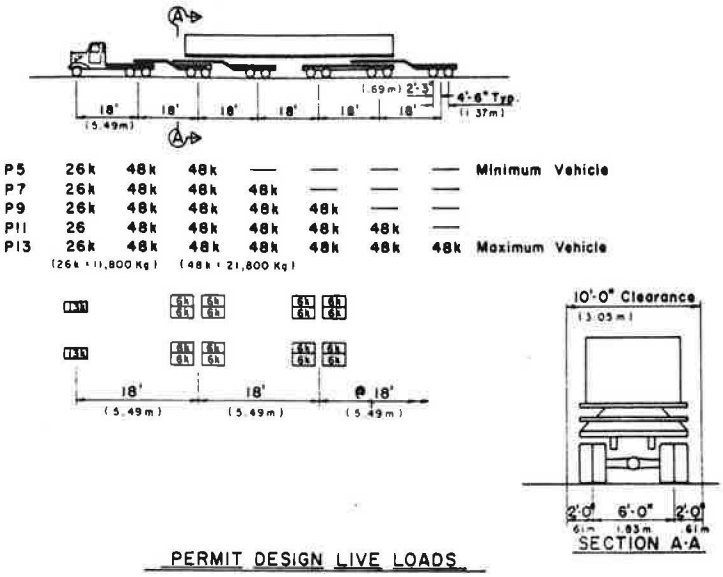

PERMIT DESIGN LIVE LOADS

Figure 6

Table 2

CALIFORNIA CURRENT PRACTICE

	LOADING	PERFORMANCE CONDITION	LIMITING CRITERION	
			Structural Steel	Reinforced Concrete
1.	Service Loads $D+(LL+I)_H$	LL Deflection	L/Factor	L/Factor
		Fatigue	Load repetitions and stress ranges defined by AASHTO	Controls on stress range in reinforcement. Concrete-$0.5f'_c$ (Reversal Areas)
		Concrete Crack Control	None	Limits on stress in reinforcement based on cover and spacing
	$D+(LL+I)_P$	Fatigue	100,000 cycles - Stress ranges defined by AASHTO	None
2.	Max Design Load $1.3\left[D+5/3(LL+I)_H\right]$	Provide a reasonable factor of safety against collapse using HS20 loads[a]	Noncomposite section $M_u = F_yS$	All compression in flange $M = \phi A_s f_y(d-a/2)$
			Compact section $M_u = F_yZ$	Compression in flange & web $M = \phi\,(A_s-A_{sf})f_y(d-a/2) + A_{sf}f_y(d-0.5h_f)$
3.	Max Design Load $1.3\left[D+(LL+I)_P\right]$	Provide a reasonable factor of safety against collapse using the permit vehicle (P-Truck)[a]	Noncomposite section $M_u = F_yS$	All compression in flange $M = \phi A_s f_y(d-a/2)$
			Compact section $M_u = F_yZ$	Compression in flange & web $M = \phi\,(A_s-A_{sf})f_y(d-a/2) + A_{sf}f_y(d-0.5h_f)$

a - Values from the envelope of the maximum effects of the HS or P loadings, whichever controls at a given section, are used to proportion members.

to his inventory, he immediately reanalyzed it to rate it for extra-legal loads. Under fresh scrutiny, the practice of designing new bridges by one criteria and rating them by another seemed a little absurd.

We saw that the continued use of WSD, which results in a haphazard array of capacities at the operating stress level had some obvious disadvantages. A few structures with low overload capacities limited the usability of entire routes. Other structures on the same route had far greater overload capacity than we could reasonably expect to use.

The adoption of LFD with only HS20 loadings was out of the question for us. We could not bear the cries of anguish that would be forthcoming from the truckers if the level of permit loads was suddenly lowered. Besides, it seemed foolish to knowingly downgrade our highway system in the face of continuing pressure to increase both legal and permit loads.

We gave serious consideration to adopting LFD with a larger HS vehicle, perhaps an HS25 or HS30. This was rejected in favor of designing each new structure for both a standard permit vehicle and HS20 loadings. We eventually realized that there was only one way to directly correlate design practice with permit policy: Design the structure for the load you expect to put on it using operating stress levels. In other words attaining the desired permit load capacity is made one of the performance conditions in the design procedure.

Permit Vehicle

To provide a systematic method of rating bridges for permit purposes, California bridge maintenance engineers devised a loading system that has axle weights approximately 1.5 times legal loads. As shown in Figure 6, this family of overload vehicles, which we call "P-loads", is a set of five trucks. Each of the five is composed of a steering axle and from two to six pairs of tandem axles at 5.49 meters (18-foot) centers. The total length ranges from 10.98 meters (36 feet) to 32.94 meters (108 feet). The width is 2.44 meters (8 feet) with the wheel lines 1.83 meters (6 feet) apart. The heaviest of the series, the P-13 loading, has a gross weight of

CALTRANS LOAD FACTOR

These girders have been designed according to Caltrans' LFD procedures and rated using AASHTO LFD criteria.

Structural Steel

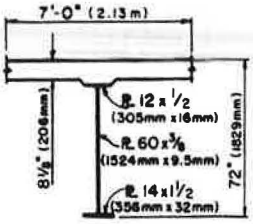

Reinforced Concrete

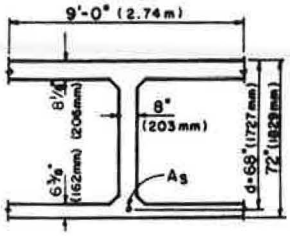

Load Factor Design
(Caltrans)

890 Kft 1207 kNm	M_{DL}	2681 Kft 3635 kNm
1185 Kft 1607 kNm	$M_{(LL+I)H}$	1197 Kft 1623 kNm
2652 Kft 3596 kNm	$M_{(LL+I)P}$	2679 Kft 3633 kNm
3724 Kft 5050 kNm	$M_u = 1.3\left[M_{DL} + 5/3\ M_{(LL+I)H}\right]$	6079 Kft 8247 kNm
	or	
4605 Kft 6244 kNm	$1.3\left[M_{DL} + M_{(LL+I)P}\right]$	6968 Kft 9449 kNm

Live Load Capacity at Operating Level

4605 Kft 6244 kNm	$M_{oper} = 1.3\left[M_{DL} + M_{(LL+I)oper}\right] = M_u$	6968 Kft 9449 kNm

$$M_{(LL+I)oper} = \frac{M_{oper}}{1.3} - M_{DL}$$

$$M_{(LL+I)oper} = \frac{4605}{1.3} - 890 \qquad M_{(LL+I)oper} = \frac{6968}{1.3} - 2681$$

$$= \underline{2652}\ \text{Kft} \qquad = \underline{2679}\ \text{Kft}$$

(3596 kNm) (3633 kNm)

Figure 7

142,242 kg (314,000 pounds).

On many routes, routine permits are issued for vehicles closely resembling the P-9 truck. The P-13 truck, which is larger than anything that has actually travelled California's highways with a routine permit, was chosen as an upper limit to allow a reasonable margin for growth. While this load seems immense compared with an HS20 vehicle, existing structures with a high D/(LL+I) ratio that were designed by WSD can carry the P-13 truck without exceeding operating stresses.

Current Practice

Our current design practice is an adaptation of the AASHTO LFD specifications using P-loads in addition to HS20 loads. All loading combinations except Group 1 come directly from AASHTO and are applied using HS20 loading. Group 1 has been expanded by adding another loading condition using the family of P-loads. The AASHTO overload check with an HS20 truck is not made because it never controls. The loading and limiting criteria are illustrated in Table 2.

For narrow girder spacings California uses AASHTO "S-over" factors for distributing P loads to individual girders. For wider girder spacings one P vehicle and one HS vehicle are placed in adjacent lanes and the distribution to individual girders is found by assuming simple beam action on the slab. This method of distribution is conservative, and we hope eventually that better distribution factors will be developed.

Figure 7 shows the results of a redesign of the same two structures using California's current

LIVE LOAD CAPACITY
(Operating Level)

Reinforced Concrete

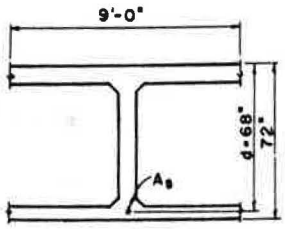

Structural Steel

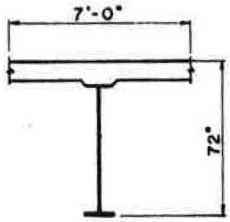

Design Load	LL Capacity	Criteria	LL Capacity
HS20	2335 Kft 3166 kNm	W. S. Design W. S. Rating	3128 Kft 4242 kNm
HS20	2450 Kft 3322 kNm	W. S. Design L. F. Rating	4173 Kft 5656 kNm
HS20	1974 Kft 2677 kNm	L. F. Design (HS) L. F. Rating (HS)	1995 Kft 2705 kNm
HS20 & P-Loads	2652 Kft 3596 kNm	L. F. Design L. F. Rating	2679 Kft 3633 kNm

(HS) - AASHTO Live Load
(P) - Caltrans Permit Live Loads

Figure 8

DEFINITIONS AND NOTATIONS

a	Depth of equivalent rectangular stress block for balanced strain conditions
A_s	Area of reinforcing steel
A_{sf}	Area of reinforcement to develop compressive strength of overhanging flanges
f'_c	Specified 28 day compressive strength of concrete
f_s	Allowable stress in reinforcing steel
F_s	Allowable stress in structural steel
f_y	Specified yield strength of reinforcement
F_y	Specified minimum yield strength of structural steel
h_f	Compression flange thickness of I and T sections
L	Span length
LFD	Load Factor Design
$(LL+I)_H$	Live Load effects of H (M) loads
$(LL+I)_P$	Live Load effects of P loads
M_{DL}	Moment due to dead load
$M_{(LL+I)}$	Moment due to live load + impact
M_o	Overload Moment
M_u	Maximum moment capacity
P-Loads	Family of truck loads used in California Permit Policy
S	Section modulus
S_{comp}	Section Modulus of composite structural steel
S_s	Section Modulus of structural steel only
Ø	Strength Reduction Factor
WSD	Working Stress Design
Z	Plastic Section Modulus

practice. This procedure produces structures of equal capacity for permit loads, and this capacity is greatly increased over that obtained using LFD and HS20 loads.

Live load capacities for permit loads obtained using the three design methods under consideration are summarized in Figure 8. The notable general characteristics of bridges designed using California's current practice are:

- Live load capacity for permit loads is essentially equal for all structure types.
- This capacity is higher than that which would result from using LFD with HS20 loads only.
- This capacity may be more or less than the wide array of values obtained using WSD methods.

While the criteria listed in Table 2 are simple and straightforward, implementing this change in procedure has not been easy. Computer programs that were based on HS20 loads had to be modified to generate moments and shears for P-loads. Designers had to be indoctrinated in LFD concepts and learn many complex rules included in the AASHTO Specifications. A forty-year collection of charts, design aids and short-cuts based on WSD became obsolete instantaneously. Training, developing new computer software, and general wheel-spinning raised engineering costs and slowed production temporarily.

Effect on Structure Types

Using LFD and our permit vehicle, we have found that reinforced concrete bridges require as much as 20% less reinforcing steel than those designed by WSD. For prestressed concrete structures we have found it necessary to either add significant amounts of mild steel to satisfy the ultimate moments caused by the overload vehicle in the common span ranges or use a higher prestress force. For structural steel bridges, slightly heavier steel sections are usually needed to accommodate our overload vehicle. In some cases, the steel section is controlled by fatigue considerations rather than the ultimate load capacity.

Based on our typical mix of structures, the total cost of our bridges has not changed significantly as a result of this design procedure.

Conclusions

The correlation of design method with permit policy was long overdue in California. It was slow in coming because nobody looked at the big picture. The designer followed AASHTO WSD rules using HS20 loads, which is common practice in the majority of states. The maintenance engineer was apparently content to live with these new designs even though his evaluations showed a wide disparity in their capacity for loads at operating stress levels.

It took consideration of implementing LFD to start a meaningful dialogue between the designer and the maintenance engineer. Both agreed that a general decrease in load capacity was unreasonable. Both thought that providing a uniform load capacity at the operating stress level was a desirable goal. It was out of these discussions that California's current design practice evolved. The advantage is considerable. For no increase in cost we are building new bridges that have a uniform, planned capacity to carry standard permit loads at the operating stress level. Being able to fully utilize every structure along a route provides maximum usability at least cost.

Before starting on an accelerated bridge replacement program, bridge engineers should review their design methods as they relate to policies concerning routine permit loads. They must decide on the stress level at which they want uniform capacity in their bridges. Particularly, they should take a hard look at the kind of structures they will get using LFD with HS20 loads only. The decisions that are made concerning design criteria will have a significant impact on the usability of the transportation network. The importance of studying this issue carefully cannot be overemphasized.

UTILIZATION OF STRESS HISTORY DATA IN BRIDGE DESIGN

David W. Goodpasture, Department of Civil Engineering, University of Tennessee, Knoxville

A method for checking the adequacy of steel stringer highway bridges for fatigue is presented. Truck types and weights are utilized with stress analyses to predict the fatigue life of bridges. The distributions of truck weights, axle weights and truck types were based on recent field measurements. A simplified method of establishing stress ranges due to typical trucks is summarized and an example is presented. However, any method may be used to obtain the stress ranges and the procedure outlined in the paper may be used. The method may be used in design or in checking existing bridges.

1. Background

The fatigue behavior of highway bridges has been the subject of numerous research projects in the past ten years (1,2,3,4,5,6,7,8,9). This increase in interest was caused in part by the failure of the Point Pleasant bridge in which forty-six persons were killed. As a result much has been learned about material behavior and traffic characteristics, but this knowledge requires time to be disseminated and to be converted into an easily utilized format. This paper presents a method of utilization of data generally known to the bridge designer and which enables him to be as sophisticated as desired in his analysis. It is presumed that the bridge design is dictated by factors other than fatigue and that the proposed method is used as a checking procedure to establish the expected life of a bridge.

The proposed method was developed as a part of a stress history research project conducted by the Department of Civil Engineering of The University of Tennessee and sponsored by the Bureau of Planning and Programming of the Tennessee Department of Transportation and the Federal Highway Administration. The contents of this paper reflect the views of the author who is responsible for the facts and the accuracy of the data presented herein. The contents do not necessarily reflect the official views or policies of the State of Tennessee or the Federal Highway Administration.

2. Fatigue Design

The four distinct phases of the design procedure are summarized below and described in detail in the remainder of the paper.

Step 1. Determine the traffic characteristics for the proposed bridge such as average daily traffic, type of truck mix, etc.

Step 2. Compute the range of stresses due to the loads of step 1. The analysis may be as simple or complex as desired. A simple method is described herein.

Step 3. A factor of safety must be established, probably in two parts. One part should account for the uncertainty in weight and volume increases during the life of the structure. The second part should reflect the uncertainties in the analysis method chosen or the variations in material properties.

Step 4. The expected life of the bridge is computed and compared to the design life. If the computed life is not sufficient then alterations in the design are in order.

3. Detailed Procedure

3.1 Truck Traffic Characteristics. The designer must establish the number of each type of truck using the bridge. This is accomplished by obtaining the average daily traffic (ADT) plus the percentage of trucks present or by obtaining the average daily truck traffic (ADTT). After the total number of trucks per day is known, the different types present and their percentage may be determined. Table I contains the usual nomenclature used to identify truck types. Reference 7 contains a table which presents the various truck type percentages based on whether the bridge is located in a metropolitan, urban or rural setting. Surveys of present traffic in the vicinity of the bridge and projections of future traffic may suffice to furnish the number of each type of truck to be expected. Overloads may be accounted for if the number is known or can be approximated.

3.2 Calculations of Stress Range. A simplified method is proposed herein to compute the stress ranges caused by the various types of truck traffic. The method was developed and compared to a STRUDL finite element analysis. Reference 10 describes the method in detail and presents an example for its use. The weight and axle spacing data shown in Table I are very similar to the average values from four other states and presented in Reference 7. Two stress ranges are determined for each truck type based on a graph constructed as described below. A 3S2 truck with:

(a) front axle weight = 8.75 kips (38.92 KN)
(b) front axle spacing = 12.75 feet (3.89 m)
(c) gross vehicle weight - 50.0 kips (222.4 KN)

is placed on the bridge to produce maximum moment at the bridge centerline for four cases. The four loading variations are shown in Figure 1. The bridge may be idealized as a wide beam in order to obtain a summation value for plotting. The four stress sums are plotted as shown in Figure 2. The slopes of the two lines (B and C) and the vertical axis intercept (A) must be determined. Also the rate of change in the slopes of change in the slopes (D) is computed by dividing the difference in the two slopes by 38.0. These values are used in the following equation.

$$\Sigma\sigma = \{A - [\, B - D\,(X - 31.0)\,]\; Y\,\} \frac{Z}{50.0} \qquad (1)$$

where:

X = percent of gross vehicle weight (GVW) on middle group for tractor-trailer trucks or the percent of GVW to rear axle group for single unit trucks,
Y = rear axle spacing in feet,
Z = gross vehicle weight,
$\Sigma\sigma$ = summation of stress ranges on all girders.

An impact factor to account for the dynamic nature of the loading could be introduced into the equation above if desired by the designer. A Monte Carlo simulation was used to obtain a typical truck type and weight distribution. Stresses computed from this procedure are plotted in Figure 3 as the simplified method and compare very well with the results of a STRUDL finite element analysis also shown on the figure. There is general agreement with the values obtained by field measurements reported in Reference 9.

3.3 Factor of Safety. The determination of the factor of safety is beyond the scope of this paper; however, a brief discussion of the subject is in order. It was suggested earlier that the factor of safety should be separated into two parts. The first part, used to account for growth in traffic volume and in truck weights, is very difficult to estimate. There has been a significant increase in the number of 3S2 trucks on the highways in the past several years. The gasoline shortage in 1974 led to a substantial decrease in traffic volume and, therefore, the trend to higher volumes of traffic each year has altered. The long term effects are even harder to define. Recently, increases in maximum truck weights have been sought both nationally and in Tennessee. It seems prudent to include a factor in the design of the bridge that reflects these possible increases. Reference 8 includes a factor of 1.5 to account for future truck weight and volume growth.

The second part of the factor of safety is for the uncertainty in material properties and methods of analysis. For steel structures designed on the basis of elastic behavior this factor is taken to be 1.8 (AASHTO). For fatigue this factor should be altered depending on the confidence limit of the allowable stress values for a given welded or bolted detail. If mean values are used in establishing the allowable stress range, then the safety factor should be higher than when the mean is reduced by two standard deviations as suggested in Reference 3.

3.4 Determination of Fatigue Life. There are a number of methods for determining the fatigue life of steel structures. Most design specifications utilize an allowable stress range based on laboratory fatigue test data. This method works very well if the design stress range occurs with great frequency relative to lower stress ranges. However, this is not the case for highway bridges where the loading varies from automobiles to trucks weighing in excess of 100,000 lbs. (444.8 KN). Recently a research project (NCHRP 12-12) was conducted to study the effects of variable cycle fatigue loadings on welded steel bridge members. The results of this research indicated that the vast amount of laboratory fatigue test data conducted at constant stress range magnitude could be used in estimating the life of structures loaded by variable stress ranges (11).

There are at least three methods for estimating fatigue life of a structure. Two of these methods, Miner's theory and root-mean-square method (RMS) are widely known, whereas the third method, root-mean-cube method (RMC), was recently proposed by Yamada and Albrecht in Reference 12. Miner's theory assumes that a fraction of the total fatigue life is expended with each loading cycle. If the stress ranges can be grouped together in a reasonable number of intervals, then the fractional life expended at each stress level may be computed by using the number of cycles to failure obtained from a S-N curve and the actual number of stress range cycles experienced. The usual procedure is to compute the sum of these fractional parts for a year. The reciprocal of this fraction is then the number of years to failure provided that the loading history for future years is the same as that assumed in the computation. The RMS and RMC methods allow the designer to compute one equivalent stress range that has the same effect as the variable stress ranges. The total number of variable cycles is used with the equivalent stress range to determine the amount of damage experienced based on the S-N curve of the particular steel and structural detail.

4. Example

The preceding steps may be clarified by the use of an example problem. Therefore, the fatigue life of a bridge used in the tests reported in Reference 9 will be presented.

The truck traffic at the bridge site is approximately 11% of the ADT based on data obtained during continuous sampling periods and the estimated 1974 ADT of 40,000 vehicles for the bridge.

The percentages of the various truck types are given below.

Type	Percentage
2D	32.4
3	7.8
2S1	2.2
2S2	10.2
3S2	45.6
Other	1.8

Based on the percentages above and 11% of 40,000 vehicles, the following number of trucks can be expected each day.

2D - 1426
3 - 343
2S1 - 97
2S2 - 449
3S2 - 2006
others - 79 (neglected)

Next the stress ranges caused by these trucks will be estimated. This step may be as simple or as precise as the designer wishes. A simple method that agrees with measured values for steel girder bridges with composite concrete decks was developed and is summarized herein.

Reference 13 gives details about the derivation of an equation for the summation of the girder stresses for the example bridge. For illustration a 3S2 truck is chosen with a front axle weight of 8.75 kips (38.9 KN), a front axle spacing of 12.75 feet (3.89 m), and a gross vehicle weight of 50.0 kips (222.4 KN). The weights on the tractor drive axles and on the trailer axles are distributed in a 31% to 69% ratio for two rear axle spacings of 14 feet (4.3 m) and 30 feet (9.1 m) as shown in Figure 1. These four loading arrangements were used to compute the maximum moment in the bridge and, therefore, the resulting average stress across the cross-section. The average stress was then multiplied by the number of girders present to obtain the summation of girder stresses. It was determined that GVW correlates very well with the sum of the girder stresses (13). These four stress values were plotted on the graph shown in Figure 2. The slopes of the two lines were determined and used to obtain the equation shown below.

$$\Sigma\sigma = \{8.333 - [0.14575 - (0.00138322)\ (X - 31)]\ Y\} = \frac{Z}{50} \qquad (2)$$

where X, Y, and Z were defined in section 3.2.

Distributions of gross vehicle weights indicate that the majority of trucks are either heavily loaded or essentially empty with smaller percentage with weights between these two extremes (9). Therefore, one half of the trucks of a given type were considered to have a weight equal to the mean value less one standard deviation and the other half were considered to have a weight equal to the mean value plus one standard deviation as indicated in Table I. The weights of the various types of trucks are summarized in Table II. These weights were then used with the tabulated distribution percentages and axle spacings shown in Table I to obtain maximum and minimum loading configurations given in Table II as columns A and B, respectively. The sum of the girder stresses was then divided by the number of girders and multiplied by a lateral load distribution factor. The lateral load distribution factor may be obtained theoretically or the AASHTO factor may be used. In this example, there were seven girders and the lateral load distribution factor of 2.80 was obtained experimentally (9). These stress ranges were then used to estimate the fatigue life of the bridge using Miner's theory, RMS and RMC methods. The stresses shown in Table II were for the center of the span, but the critical locations for fatigue on this bridge were at the end of the cover plates. Experimental results (9) indicate that the stress range at the end of a cover plate was from 0.6 to 1.11 times that at the center of the span for this bridge. The computed stress ranges at the cover plate ends and the number of cycles to failure from S-N curves in Reference 11 are shown in Table III. This information and the number of trucks causing these stress ranges are sufficient for the calculation of the expected life in fatigue. If the present traffic volume and weight limits are assumed to continue for the lift of the bridge, then fatigue cracks at the cover plate end-welds would be expected to occur after 107, 113, or 82 years when predicted using Miner's theory, the RMS method or the RMC method, respectively. It is also assumed that all of these trucks are using the same lane which is very conservative.

Sample calculations illustrating each of the three methods are shown below.

(A) Miner's theory: damage in one year

$$365\left\{\frac{713}{7.33\times10^{8}}+\frac{713}{1.33\times10^{10}}+\frac{171.5}{8.39\times10^{7}}+\frac{171.5}{1.11\times10^{9}}+\frac{48.5}{7.32\times10^{9}}+\frac{48.5}{1.48\times10^{9}}+\frac{224.5}{1.39\times10^{8}}+\frac{224.5}{1.12\times10^{9}}+\frac{1003}{3.94\times10^{7}}+\frac{1003}{5.49\times10^{8}}\right\}=0.00929$$

and the expected life is the reciprocal of the damage

$$\frac{1}{0.00929} = 107 \text{ years}$$

(B) Root-mean-square (RMS)

$$\left\{\frac{[713\ (0.979)^2 + 713\ (0.358)^2 + 171.5\ (2.08)^2 + 171.5\ (0.847)^2 + 48.5\ (0.98)^2 + 48.5\ (0.768)^2 + 224.5\ (1.745)^2 + 224.5\ (0.845)^2 + 1003\ (2.705)^2 + 1003\ (1.083)^2]}{4321}\right\}^{\frac{1}{2}}$$

$$= 1.601 \text{ ksi}$$

$$\text{Log } N = 8.839 - 2.877 \text{ Log } (1.601)$$

$$N = 178{,}255{,}294 \text{ cycles to failure}$$

$$\text{life} = \frac{N}{4321 \times 365} = 113 \text{ years}$$

(C) Root-mean-cube (RMC)

$$\left\{\frac{[713\ (0.979)^3 + 713\ (0.358)^3 + 171.5\ (2.08)^3 + 171.5\ (0.847)^3 + 48.5\ (0.98)^3 + 48.5\ (0.768)^3 + 224.5\ (1.745)^3 + 224.5\ (0.845)^3 + 1003\ (2.705)^3 + 1003\ (1.083)^3]}{4321}\right\}^{1/3}$$

$$= 1.792 \text{ ksi}$$

$$\text{Log } N = 8.839 - 2.877 \text{ Log } (1.792)$$

$$N = 128{,}840{,}409 \text{ cycles to failure}$$

$$\text{life} = \frac{N}{4321 \times 365} = 82 \text{ years}$$

It might be more realistic to expect that the traffic volume may increase and the number of trucks using the bridge would also increase. If a 4% growth rate is assumed, the the expected life decreases to approximately 40 years. Increases in the allowable loads on trucks would also decrease this life. An increase of 10% of present truck weights would result in an expected life of approximately 60 years even if there were no increase in truck traffic volume.

5. Conclusions

This paper described a method of fatigue design that incorporates significant data obtained from field measurements of truck weights and girder stresses in highway bridges. The method allows the designer with the flexibility of obtaining girder stresses with as much accuracy as deemed necessary.

References

1. Cudney, G. R., "Stress Histories of Highway Bridges", Journal of the Structural Division, ASCE, Vol. 94, No. ST12, December 1968.
2. Fisher, J. W., K. H. Frank, M. A. Hirt, and B. M. McNamee, "Effect of Weldments on the Fatigue Strength of Steel Beams", NCHRP Report 102, Highway Research Board, 1970.
3. Goodpasture, D. W., "Final Report on Stress History of Highway Bridges", University of Tennessee, December 31, 1972.
4. Walker, W. H. and J. A. Ruhl, "Investigation of Dynamic Stresses in Highway Bridges - An Interim Report", Civil Engineering Studies Structural Research Series No. 404, University of Illinois at Urbana - Champaign, October 1973.
5. Bowers, D. G., "Loading History, Span No. 10, Yellow Mill Pond Bridge I-95, Bridgeport, Connecticut", Department of Transportation, State of Connecticut, Research project HRP 175-332, May 1972.
6. Fisher, J. W., P. A. Albrecht, B. T. Yen, D. J. Klingerman, and B. M. McNamee, "Fatigue Strength of Steel Beams with Welded Stiffness and Attachments, NCHRP Report 147, Transportation Research Board, 1974.
7. Heins, C. P. Jr., and C. F. Galambos, "Bridge Fatigue due to Daily Traffic", Transportation Research Board Record No. 507, 1974.
8. Moses, Fred and Robert Garson, "New Procedure for Fatigue Desing of Highway Bridge Girders", Transportation Research Board Record No. 507, 1974.
9. Goodpasture, D. W., "Final Report on Stress History of Highway Bridges - II", University of Tennessee, June 30, 1976.
10. Bolt, Charles R., "A Simplified Approach for Determining Stresses on Highway Bridges", Master's thesis, The University of Tennessee, Knoxville, March 1976.
11. "Fatigue of Welded Steel Bridge Members Under Variable - Amplitude Loadings", Research Results Digest 60, National Cooperative Highway Research Program, April 1974.
12. Yamada, K. and P. Albrecht, "Fatigue Design of Welded Bridge Details for Service Stresses", A paper presented at the 54th Annual Transportation Board Meeting, January 1975.
13. Patrick, Perry C., Jr., "Comparison of Measured and Theoretical Stresses in a Simple Span Bridge", Master's thesis, The University of Tennessee, Knoxville, June 1975.

TABLE I

CHARACTERISTICS OF EACH TRUCK TYPE

Truck Type	Configuration	Axles Spacing and Standard Deviation (feet)	Gross Weight and Standard Deviation (Kips)	Present Weight to Middle Axle and Standard Deviaiton
3S2	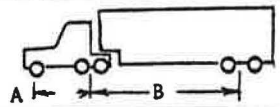	A = 12.75 ± 1.0 (constant) B = 30.75 ± 3.3	50.1 ± 16.9 Fix front axle weight = 8.75	52.6 ± 6.6
2D	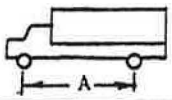	A = 15.0 ± 2.25	14.5 ± 5.9	37.0 ± 6.5
2S2	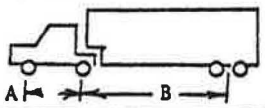	A = 11.10 ± 0.9 (constant) B = 28.5 ± 2.5	35.2 ± 10.6 Fix front axle weight = 8.0	48.6 ± 6.4
2S1	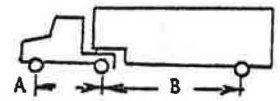	A = 11.0 ± 1.0 (constant) B = 29.5 ± 3.5	29.7 ± 6.7 Fix front axle weight = 8.0	52.6 ± 7.5
3	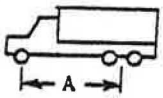	A = 17.25 ± 2.4	26.8 ± 9.5	38.0 ± 6.0

1 kip = 4.448 KN 1 ft = 0.3048 meter

TABLE II

TRUCK LOADINGS AND RESULTING STRESS RANGES

Truck Type	Z Weight (kips) A	Z Weight (kips) B	Y Rear Axle Spacing (ft.) A	Y Rear Axle Spacing (ft.) B	X Weight Distribution (percent) A	X Weight Distribution (percent) B	Girder Stress (ksi) A	Girder Stress (ksi) B
2D	20.4	8.6	12.75	17.25	43.5	30.5	1.093	0.400
3	36.3	17.3	14.85	19.65	44.0	32.0	1.869	0.761
2S1	36.4	23.0	26.0	33.0	60.1	45.1	1.628	0.768
2S2	45.8	24.6	26.0	31.0	55.0	42.2	1.981	0.845
3S2	67.0	33.2	27.45	34.05	59.2	46.0	2.896	1.083

1 kip = 4.448KN

1 ft = 0.3048M

A = maximum loading configuration

B = minimum loading configuration

TABLE III

FATIGUE CHARACTERISTICS FOR EXAMPLE BRIDGE

Truck Type	Stress at Coverplate end (ksi) A	B	Number of Cycles to Failure Log N = 8.839 - 2.877 Log Sr. A	B
2D	0.979	0.358	7.33×10^8	1.33×10^{10}
3	2.080	0.847	8.39×10^7	1.11×10^9
2S1	0.980	0.768	7.32×10^8	1.48×10^9
2S2	1.745	0.845	1.39×10^8	1.12×10^9
3S2	2.705	1.083	3.94×10^7	5.49×10^8

1 ksi = 6900 $KN/_M2$

A = maximum loading configuration

B = minimum loading configuration

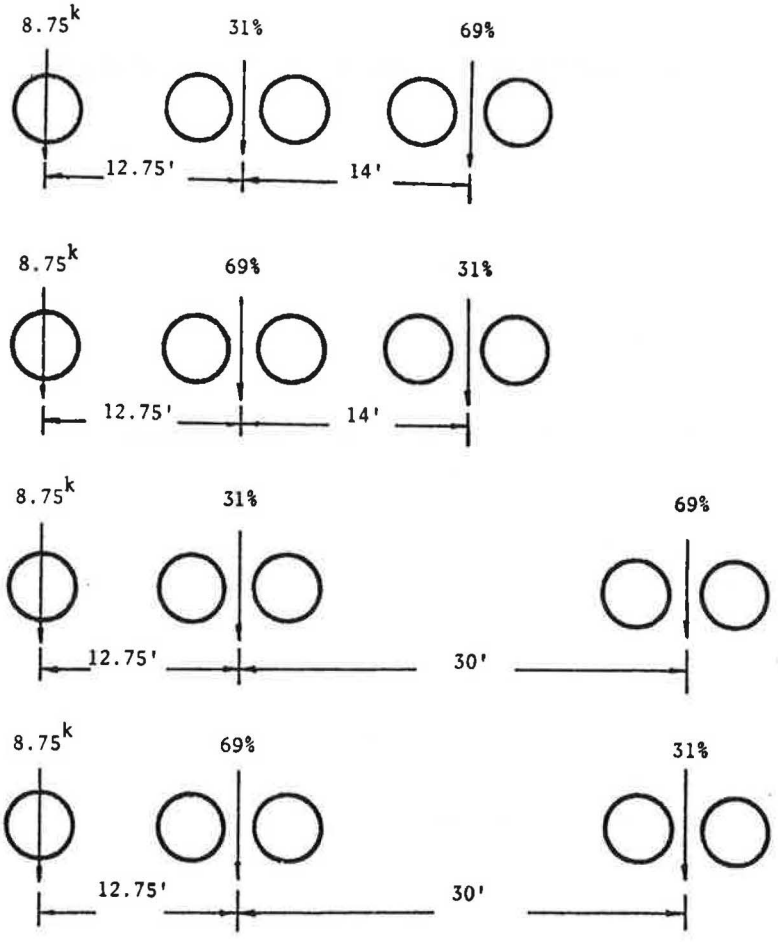

Figure 1 3S2 Truck Loading Variation

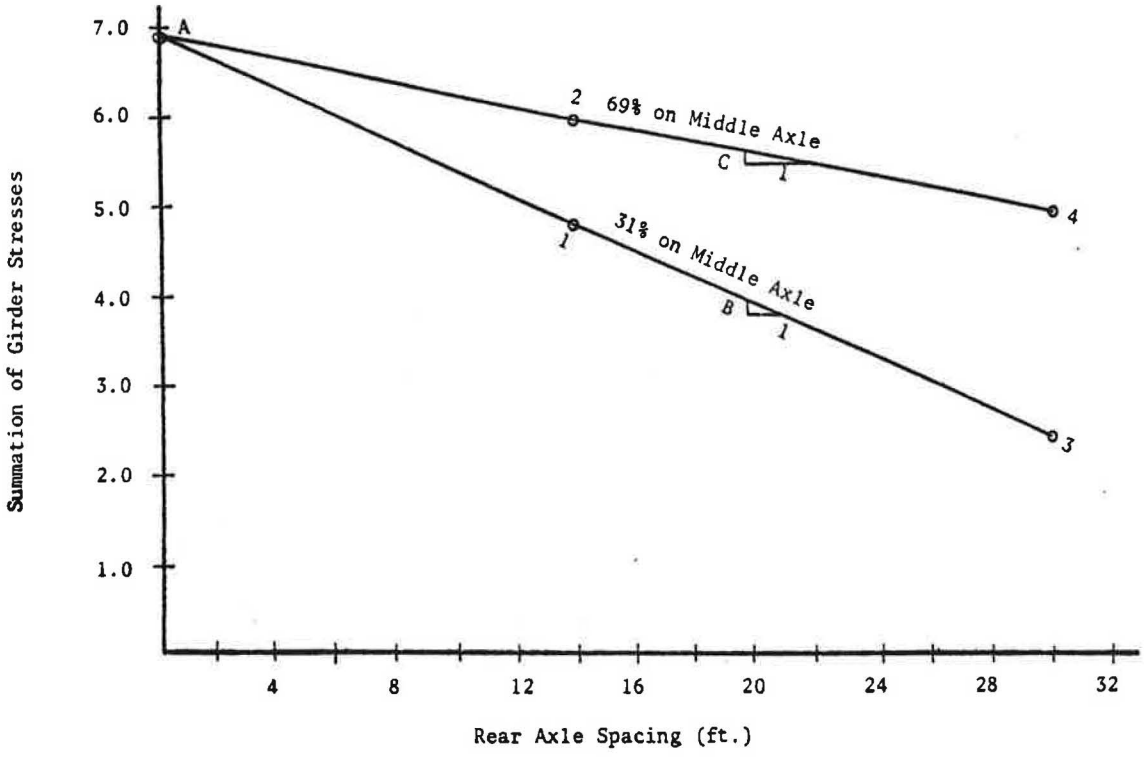

Figure 2 Summation of Stresses Versus Rear Axle Spacing

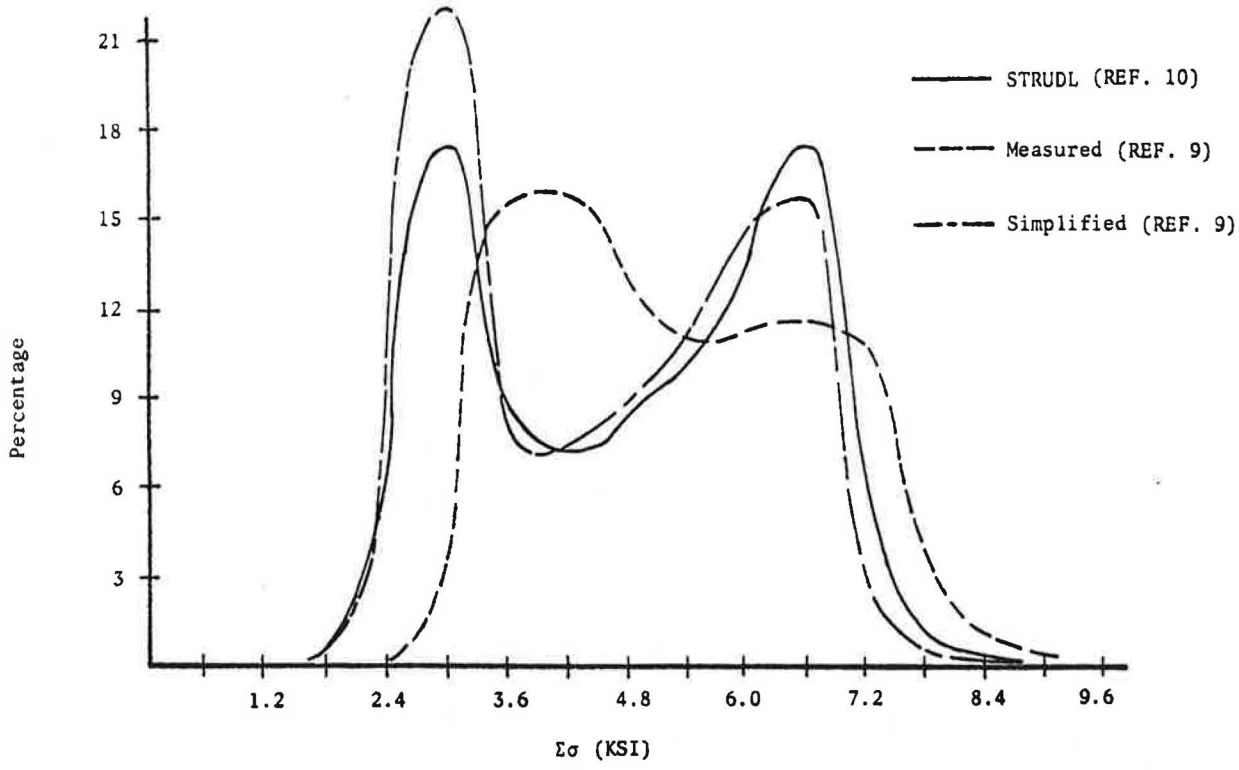

Figure 3 Comparison of Measured, Theoretical and Simplified Summation of Stresses - 3S2 Trucks.

IN-PLANE AND OUT-OF-PLANE INSTABILITY OF A 297 M SPAN STEEL ARCH BRIDGE

Yukio Maeda and Masa Hayashi, Osaka University, Japan

Ohmishima Bridge, which is now under construction in Japan, is a steel highway bridge spanning 297 m (974.4ft.) of a half-through two-hinged solid rib arch stiffened by side ties. The two main arch ribs of box section are stiffened respectively, by two side ties. One end of each tie is fixed to the top of an abutment in both side spans. Bending moments and stresses due to live loads or wind loads in the arch ribs can be reduced by the stiffening ties more than those of ordinary two-hinged arches, and the steel weight of the ribs decreases considerably. Therefore, this new type arch is more economical than an ordinary two-hinged or fixed solid rib arch. Since the arch ribs become more slender, geometrical nonlinearity of the arch may be more remarkable. To investigate the geometrical and material nonlinearities of such a long-span and unusual type of steel arch bridge including overall inelastic instability, extensive experimental and analytical studies were carried out. In this paper, the results of the analytical study with discussions are reported. The combined nonlinear analyses are performed by a matrix method based on finite displacement theory for in-plane and out-of-plane instability. It was confirmed that the side ties for stiffening a two-hinged arch bridge are very effective for the reduction of stresses and geometrical nonlinearities and for an increase of overall ultimate strength in-plane or out-of-plane of the arch.

Ohmishima Bridge is now under construction in Japan as the first bridge of long-span bridge projects to connect the Mainland to Shikoku Island crossing the Seto Inland Sea. It is a half-through highway bridge spanning 297 m (974.4 ft.) of a two-hinged steel arch stiffened by side ties, which may be called a new type of arch bridge not experienced in the world.

The first design proposed for *Ohmishima Bridge* was a fixed steel arch bridge(1), but it was changed into the present final design of a new type of two-hinged arch. Since smaller box sections can be used for its arch ribs due to reduced bending moments, this type of bridge gives a more economical and rational design than a fixed arch bridge or an ordinary two-hinged arch bridge. However, its more slender arch ribs may cause greater nonlinear structural behaviors.

In this paper, a theoretical study on this new type of arch bridge modelling *Ohmishima Bridge* will be presented(2). The geometrical nonlinear behaviors under design loads and the ultimate strength are investigated in terms of in-plane and out-of-plane instability. First of all, the outline of analytical method by a matrix method based on finite displacement theory will be shown. Then, the calculation results will be discussed on the characteristics of structural behaviors.

The three-dimensional nonlinear analysis of framed structures considering finite rotations of displacement components has not been reported. Also, the elasto-plastic space analysis taking account of the effects of finite rotations and spread of plastic region in the whole members has not been applied to an actual bridge. Therefore, these effects are considered as accurately as possible in numerical calculations by means of theoretical analysis and numerical computation.

Summary of Nonlinear Analysis

Nonlinear analyses of the arch are carried out by a matrix method based on finite displacement theory. An outline of analytical methods for space frames is given as follows, except the planer analysis.

Assumptions

The following assumptions are imposed in the combined nonlinear analysis of space frames:

1. Members are straight thin-walled beams of a doubly symmetrical uniform cross-section.
2. The longitudinal dimension of a beam is much larger than its lateral dimension.
3. The middle line of thin walls in a cross section does not distort after the deformation of the beam.
4. Thin walls deform under the Kirchhoff-Love hypothesis for thin shells.
5. Warping of cross sections, shear distortion, overall buckling of members and local buckling of thin walls are ignored.
6. The Mises yield condition and the Prandtl-Reuss equation are employed in plastic regions of walls.
7. The stress-strain diagram of material is assumed to be linearly elastic-perfectly plastic.

Finite Displacement of Beam

Finite rotations in a three-dimensional space do not satisfy a commutative law, nevertheless they have been treated as a vector in most studies(3, 4). In space analysis, only Oran(5) pointed out the above-mentioned misunderstanding and used a rotation matrix which was called a joint orientation matrix in his paper. However, the rotation matrix shown in his paper is one for a small rotation.

A rotation matrix of a nodal point was formularized(6) with a coordinate transformation matrix of a member taking account of finite rotations as well as finite translations. These matrices are mathematically exact ones.

Figure 1. Local coordinate systems of a member.

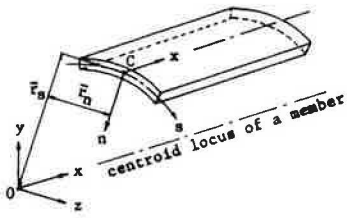

By the use of this rotation matrix, the finite displacements $\bar{u}$, $\bar{v}$ and $\bar{w}$ of an arbitrary point C on the middle surface of a thin wall are obtained under the assumption 3. They are expressed by omitting nonlinear terms higher than the third order as follows:

$$\bar{u} = u_0 - v_0'\bar{y} - w_0'\bar{z} - \frac{1}{2}\phi_0(w_0'\bar{y} - v_0'\bar{z}), \tag{1}$$

$$\bar{v} = v_0 - \phi_0\bar{z} - \frac{1}{2}[\phi_0^2\bar{y} + (v_0')^2\bar{y} + v_0'w_0'\bar{z}], \tag{2}$$

$$\bar{w} = w_0 + \phi_0\bar{y} - \frac{1}{2}[\phi_0^2\bar{z} + (w_0')^2\bar{z} + v_0'w_0'\bar{y}] \tag{3}$$

where u_0, v_0, w_0 are the displacement components and ϕ_0 the torsional angle at the centroid O of a cross section having the coordinates $(x, 0, 0)$ in a rectangular Cartesian coordinate system (x, y, z). $\bar{y}$ and $\bar{z}$ are the coordinates of the point C, and the prime superscript indicates differentiation with respect to x.

Strains of Thin Wall

The strains and the stresses of a thin wall are expressed in a local system of orthogonal curvilinear coordinates (x, s, n) at the point C.

Strain components are obtained by using the displacements of equations 1, 2 and 3 on the middle surface of the wall under the Kirchhoff-Love hypothesis(7).

The Lagrangian strain components of e_{ss}, e_{nn}, e_{xn} and e_{sn} may be ignored due to the assumptions 3 and 4:

$$e_{ss} = e_{nn} = e_{xn} = e_{sn} = 0. \tag{4}$$

The other components can be written in terms of the displacement components at the centroid O as follows:

$$e_{xx} = u_0' - (v_0''\bar{y} + w_0''\bar{z}) + \frac{1}{2}[(u_0')^2 + (v_0')^2 + (w_0')^2]$$
$$- \frac{1}{2}(\phi_0 w_0'' - \phi_0' w_0' + 2u_0' v_0'')\bar{y} + \frac{1}{2}(v_0''\bar{y} + w_0''\bar{z})^2$$
$$+ \frac{1}{2}(\phi_0 v_0'' - \phi_0' v_0' - 2u_0' w_0'')\bar{z} + \frac{1}{2}(\phi_0')^2(\bar{y}^2 + \bar{z}^2)$$
$$+ [(v_0''\sin\beta - w_0''\cos\beta) - \phi_0''\bar{r}_n]n \tag{5}$$

$$2e_{xs} = [\phi_0'\bar{r}_s + \frac{1}{2}(v_0''w_0' - v_0'w_0'')\bar{r}_s + \frac{1}{2}\phi_0(w_0'\cos\beta$$
$$- v_0'\sin\beta) - u_0'(v_0'\cos\beta + w_0'\sin\beta)](1 - n/R)^{-1}$$
$$- 2\phi_0'n \tag{6}$$

where β is the angle between y-axis and t-axis which is the tangent at C to the curvilinear coordinates s; R is the radius of curvature of the wall in the direction n; and $\bar{r}_s$ and $\bar{r}_n$ are given by the following expressions:

$$\bar{r}_s = \bar{y}\sin\beta - \bar{z}\cos\beta, \quad \bar{r}_n = \bar{y}\cos\beta + \bar{z}\sin\beta. \tag{7}$$

According to the assumption of thinness of a wall, the nonlinear terms with respect to the n-axis are ignored in equations 5 and 6.

Stresses of Thin Wall

By virtue of the assumptions 3 and 4 about beam theory and thin-shell theory, respectively, only two strain components of equations 5 and 6 will be considered in the nonlinear analysis of a thin-walled member and are expressed by the notations ε and γ, respectively.

Let the stress components corresponding to the above strains be σ and τ, the incremental stress-strain relations are expressed as follows:

$$\begin{Bmatrix} \Delta\sigma \\ \Delta\tau \end{Bmatrix} = \begin{bmatrix} D_1 & D_3 \\ D_3 & D_2 \end{bmatrix} \begin{Bmatrix} \Delta\varepsilon \\ \Delta\gamma \end{Bmatrix} \tag{8}$$

where the notation Δ indicates the increments and D_1, D_2 and D_3 are given for elastic materials with Young's modulus E and shear modulus G

$$D_1 = E, \quad D_2 = G, \quad D_3 = 0, \tag{9}$$

and for plastic materials under the assumptions 6 and 7(8)

$$\left.\begin{aligned} D_1 &= 9EG\tau^2/D_0, \quad D_2 = EG\sigma^2/D_0, \\ D_3 &= -3EG\sigma\tau/D_0, \quad D_0 = E\sigma^2 + 9G\tau^2. \end{aligned}\right\} \tag{10}$$

To take into account the spreading of plastic region in a member in the directions x and s in the elasto-plastic analysis of framed structures, a thin-walled member is divided into many small elements as shown in Figure 2.

Figure 2. Elements of box beam.

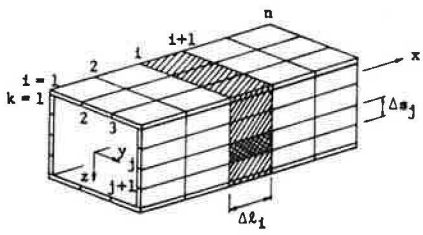

The incremental strain components in plastic regions have a combined effect as expressed by equations 8 and 10. For a thin-walled beam of closed cross section, the incremental shearing stress is obtained by using the shear flow theory which assumes a constant shear flow q in the closed cross section.

The nonlinear terms of the incremental shearing strain may be negligible and a thin-walled beam is assumed to have a box section. Then, the following expression is given by substituting the increments of strain components into equation 8 and by applying linear integration along the closed middle line of the cross section of an elasto-plastic member:

$$\oint \Delta\tau \, ds = \Delta\phi_0' \oint D_2 \bar{r}_s ds + \int_p D_3 \Delta\varepsilon ds \qquad (11)$$

where $\int_p$ implies the integration with respect to plastic regions in the closed cross section.

Let the thickness of a thin wall be t, the incremental shear flow Δq is given by

$$\Delta q = t\Delta\tau , \qquad (12)$$

so that the incremental stress $\Delta\tau_j$ of the j-th element can be obtained by rewriting equation 11 as follows:

$$\Delta\tau_j = \frac{\sum_k (D_2 \bar{r}_s \Delta s)_k}{\sum_k (\Delta s/t)_k} \frac{\Delta\phi_0'}{t_j} + \frac{\sum_p (D_3 \Delta\varepsilon \Delta s)_p}{\sum_k (\Delta s/t)_k} \frac{1}{t_j} \qquad (13)$$

where $\sum_k$ and $\sum_p$ indicate the summation over all elements and over plastic elements alone in a cross section, respectively.

Equilibrium Equations

Equilibrium equations of an elastic or an elasto-plastic member are formularized by the usual matrix method based on the principle of virtual work.

The equations are expressed in terms of matrices as follows:

$$\Delta k \cdot \Delta d = \Delta p - (f - p) \qquad (14)$$

where Δk, Δd, Δp, p and f are the tangential stiffness martix, the incremental displacement vector, the incremental load vector, the total load vector and the internal force vector, respectively.

The matrix Δk and the vector f can be divided into two parts as shown in the following expressions, respectively:

$$\Delta k = k^* - \sum_i k_i^p , \quad f = f^* - \sum_i f_i^p \qquad (15)$$

where the matrix k^* and the vector f^* are defined for an elastic member or for an elasto-plastic member, of which all elements are assumed to be elastic, and k_i^p and f_i^p are defined for the i-th plastic or unloaded element and respectively equal to a zero matrix and a zero vector for an elastic element.

k^* and f^* are formularized and also k_i^p and f_i^p are calculated not by a numerical integration but by an analytical procedure, so that the computation may be very quick and the numerical solutions may be accurate.

Numerical Procedure

In the numerical analysis, the mixed method of combined Newton-Raphson method with an incremental load or displacement method is used in an elastic range. The increments of external loads or of a component of displacements at a nodal point to control the numerical calculation, are decided automatically in the program so that a few elastic elements in the whole members may yield. Since these increments will be very small quantities, modified incremental method with equilibrium check is used instead of the mixed method in an elasto-plastic range.

The maximum load of a structure is defined by the condition that a structure becomes unstable when the tangential stiffness matrix of the system turns to a negative definite matrix.

Structural Models

Dimensions

Ohmishima Bridge is a stiffening two-hinged solid rib arch as shown in Figure 3, and its overall rigidity is increased by fixing both side ties to each abutment at both side spans. Namely, the arch ribs may be considered to be elastically supported at about one-sixth points of the arch span by triangular frames consisting of an arch rib, a side tie and an abutment. Therefore, the bending moments in the arch ribs can be reduced and improved structural behaviors may be expected at this modified two-hinged arch bridge as if the span length were shortened to two-thirds.

Sectional dimensions of the arch ribs and the other members are shown in Figure 4.

Figure 3. General pictures of Ohmishima Bridge.

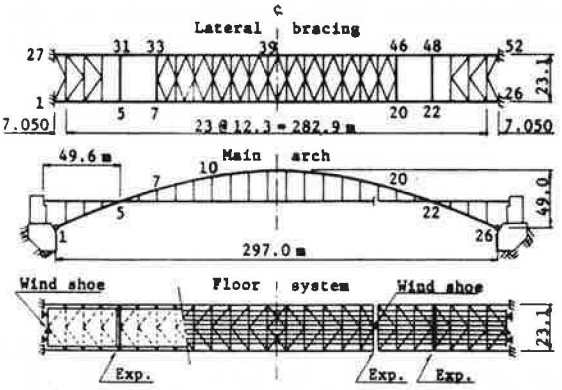

Note: 1 m = 3.28 ft.

Figure 4. Sectional dimensions of members.

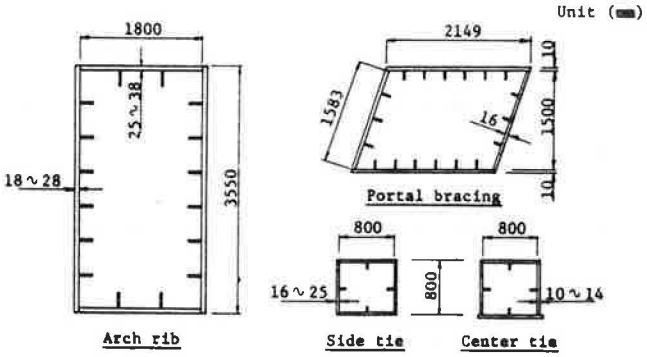

Note: 1 mm = 0.0394 in.

Analytical Models

For a model arch used for in-plane and out-of-plane analyses and elastic and elasto-plastic analyses, the same dimensions as the design of Ohmishima Bridge are used including the condition of supports, the arrangement of expansion joints, the rigidities of members, etc.. To make the calculation simpler, the rigidity of concrete-encased steel grating floor is neglected, eight stringers are replaced by one equivalent stringer, and the arrangement of lateral bracing members between two arch ribs is partly changed. As the result, the model is provided with 139 nodal points and 340 members and is constrainted with 52 degrees of freedom.

In addition to this Model-1, Model-2 is investigated, too, in which either of two side ties is not fixed to the abutment, but supported by a sliding shoe so that the tie is not subjected to any axial force. Moreover, Model-3 with an assumed initial imperfection due to the error of shape in Model-1 is employed in the in-plane ultimate strength analysis.

Applied Loads

In the in-plane analysis, the dead load(D), the live load(L) consisting of uniform load(p) and trailer truck load(TT), both including impact, and the earthquake load(EQ) with the horizontal seismic coefficient of 0.2, are applied at numerical analyses. In the out-of-plane analysis, the dead load, the horizontal earthquake load and wind load(W) are employed.

The intensities of the specific loads like elastic buckling load or ultimate strength load are expressed by a load multiple, α, considering design loads as standard loads, of which the intensities are given in Table 1(2).

Table 1. Intensities of design loads.

Design load	Intensity (kN/m)	Loaded member
Dead load (D)	43.5	arch rib
	94.8	center or side tie
	84.8	stringer
Live load (p)	20.9	stringer
(L) (TT)	765.0(kN)	stringer
Earthquake load (EQ)	8.7	arch rib
	19.0	center or side tie
	17.0	stringer
Wind load (W)	19.9	arch rib
	13.0	center or side tie
	3.2	post

Note: 1 kN = 0.225 kip. 1 kN/m = 68.5 lbf/ft.

Geometrical Nonlinearity due to In-Plane Loads

Influence Values

To examine the nonlinearity due to live loads, the following five kinds of influence values are considered:

1. An ordinary linear influence value for a unit concentrated load.
2. A linearized influence value for a concentrated live load(TT-Load) obtained by a tangential stiffness matrix at the loading of dead loads.
3. A nonlinear influence value of the exact solution for the value of 2.
4. A linearized influence value for TT-Load obtained by a tangential stiffness matrix at the loading of dead and half-span uniform live loads.
5. A nonlinear influence value of the exact solution for the value of 4.

At the computation of the values of 2 to 5, the exact equilibrium state is obtained for dead loads or plus a uniform live load with the intensities of the design loads. Then, these influence values are calculated not for a unit load, but for TT-Load as a moving concentrated load. At this time, the removal of the linearized errors is tried for bending moments or stresses with the values of 2 and 4.

Nonlinearity due to TT-Load

Figure 5 shows the maximum values of deflections due to a trailer truck load(TT-Load) for Model-1. Figure 6 shows the minimum values of fiber stresses due to TT-Load at the upper and lower flanges for Model-1. Since the linearized influence values of 2 and 4 agree with the values of 3 and 5, respectively, they are not shown in the figures. Those figures indicate clearly the favourable effect of the side ties on the deflections and stresses.

Figure 5. Maximum deflections due to TT-Load.

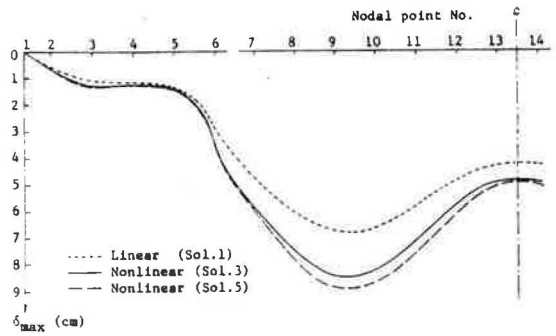

Note: 1 cm = 0.394 in.

Figure 6. Minimum fiber stresses at upper and lower flanges due to TT-Load.

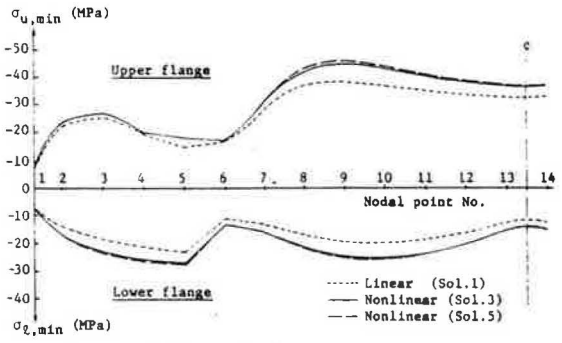

Note: 1MPa = 145 lbf/in^2.

For the maximum or minimum values of deflection δ, bending moment M and fiber stresses σ_u and σ_ℓ in the upper and lower flanges respectively, due to a concentrated TT-Load, the increase ratios of the linearized or the nonlinear values of 2 - 5 to the linear value of 1 are shown in percent on the uppermost column in Table 2.

Table 2. Geometrical nonlinearities of various influence values.

Solution	max δ	max M	min M	min σ_u	min σ_ℓ
Nonlinearity due to TT-Load					(%)
2	25.4	18.8	22.8	17.3	17.0
3	26.4	19.2	22.5	17.8	18.7
4	30.1	21.3	26.3	19.5	19.6
5	31.3	21.7	25.8	20.0	21.4
Nonlinearity due to dead and live loads					(%)
2	6.6	13.4	10.6	4.1	2.2
3	6.9	13.7	10.4	4.3	2.4
4	13.5	22.5	18.9	8.8	5.8
5	13.7	22.7	18.8	8.8	6.0

Since each value shows about 20 - 30% nonlinearity, the linear values cannot be applied to the analysis of the arch. But it may not be required to perform the exact nonlinear calculation for the concentrated live load, as far as the linearized values with 1 - 2% errors are used. When the nonlinear effect due to a uniform live load is taken into account, too, the increase of nonlinearity due to *TT*-Load is about 5% in deflections and about 2- 3% in stresses in comparison of the values of 2 with 4 or the values of 3 with 5.

Nonlinearity due to Dead and Live Loads

Large stresses due to dead loads are observed at a solid rib arch and more than 50% of the stresses are almost axial stresses without nonlinearity. Therefore, nonlinearities due to the dead load plus the live load are indicated on the 2nd column in Table 2, in which the values of 5 give the exact nonlinear effects due to the dead and live loads at Ohmishima Bridge.

Influence Line Analysis

In case that geometrical nonlinearity due to live loads appears at a structure subjected to dead load, an influence line analysis based on the law of superposition cannot be strictly applied to its analysis. Then, an influence line analysis with the above-mentioned influence values of 2 or 3 is applied to the analysis of Model-1.

Table 3. Errors of influence line analysis.

Solution	max δ	max M	min M	min σ_u	min σ_ℓ
Error due to superposition					(%)
2	-2.2	-2.0	-1.2	-1.8	-2.2
3	-1.3	-1.3	-1.2	-1.1	-0.9
Error of influence line analysis					(%)
2	-1.6	-2.0	-1.3	-0.9	-0.9
3	-1.1	-1.5	-1.4	-0.6	-0.5

The value of the uppermost column in Table 3 indicate errors due to the application of the superposition law to the influence analyses of the arch subjected to a uniform live load(p), in terms of the relative errors against the exact values due to the uniform live load.

Furthermore, the errors for the values due to the dead and the uniform live loads are shown on the 2nd column in the table.

The negative signs on the both columns mean unfavorable values.

Effect of Side Ties on Elastic Stability

Load versus displacement curves obtained by a buckling analysis and by an exact finite displacement analysis are given in Figure 7 for the in-plane elastic stability of Model-1 and Model-2 in which the stiffening effect of one of the side ties is neglected. The vertical axis shows load multiples for dead plus live loads and the horizontal axis shows the maximum deflections, both at the nodal point No. 10.

As illustrated in Figure 7, a dynamic jump does not occur at the both models owing to the stiffening effect of the side ties. The comparison between Model-1 and Model-2 shows that the ties have an effect on the constraint of geometrical nonlinearity of the arch. Particularly, the side ties are effective against a seismic load, because the nonlinearity of bending moments due to the dead load plus the seismic load is only 15 - 17% at Model-1, while 60 - 70% at Model-2.

Figure 8 indicates the first mode of buckling due to dead load for Model-1 and -2, in which the left side tie alone is fixed to the abutment. In the figure, the vertical and horizontal axes show relative displacements and nodal point Nos., respectively.

Figure 7. Load versus displacement curves for dead and live loads α (D + L).

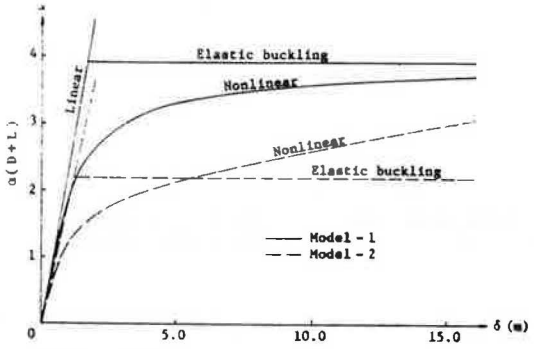

Note: 1 m = 3.28 ft.

Figure 8. Buckling modes due to dead load (α D).

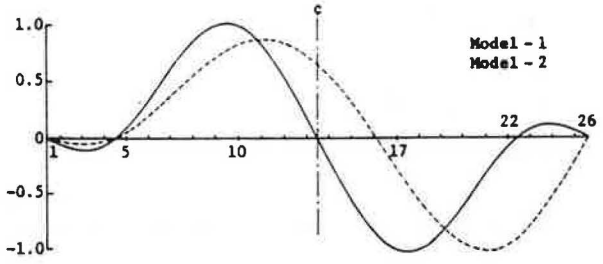

Geometrical Nonlinearity due to Out-of-Plane Loads

Geometrical Nonlinearity

There have been few study reports on the nonlinear behavior of an arch bridge subjected to an out-of-plane load. In Table 4, the geometrical nonlinearities in displacements and internal forces in arch ribs due to design loads calculated by a three-dimensional finite displacement analysis for Model-1 of Ohmishima Bridge, are shown in percent of the linear values. Model-1* in the table is a model arch taking into account the in-plane and out-of-plane rigidities of slab. V and W are respectively vertical and horizontal displacements, N is axial force, and M_t, M_y, M_z are respectively torsional, in-plane, out-of-plane bending moments. It can be seen in Table 4, that the nonlinearities appear even at the design loads, particularly remarkably in the in-plane moments.

Table 4. Geometrical nonlinearities due to out-of-plane loads. (%)

Model	Load	max V	max W	max N	max|M_t|	max|M_y|	max|M_z|
1	EQ	5.7	8.2	3.0	8.6	17.8	10.4
	D + EQ	5.6	3.2	1.1	4.8	16.0	9.9
	W	4.9	8.7	3.2	7.2	16.1	6.9
	D + W	4.9	3.4	1.1	4.5	8.8	6.9
1*	EQ	4.9	6.3	2.6	5.2	15.7	1.2
	D + EQ	4.8	2.7	0.8	3.0	8.2	1.2
	W	4.3	7.5	3.0	4.5	14.5	5.8
	D + W	4.3	2.9	0.9	2.8	7.7	5.9

The comparison between the values for Model-1 and Model-1* shows that, if the rigidity of the slab is considered at the calculations, the nonlinearities will be reduced considerably, but the axial force in side ties will increase about 50%.

Elastic Buckling

To examine the out-of-plane stability of Model-1 and -2, a three-dimensional buckling analysis is carried out. The results are summarized in Table 5 in terms of α_{cr} values which are load multiples based on the intensity of design dead load. Model-1* and -2* denote the cases that the slab rigidities are taken into account, respectively for Model-1 and -2. In Table 5, the third mode of buckling of Model-1 and -1* alone is related to the out-of-plane buckling, and all of the other modes are to the in-plane buckling. Since, at ordinary rib arches, the first mode appears at the in-plane buckling and the second mode appears at the out-of-plane buckling, a solid-rib arch with side ties shows different behavior from the ordinary solid-rib arch at the higher order of buckling mode.

Table 5. Load multiples for out-of-plane buckling.

Model	1st mode	2nd mode	3rd mode
1	4.833	7.664	9.580
1*	5.215	8.243	9.914
2	2.677	5.097	8.153
2*	2.899	5.511	8.692

Ultimate Strength in In-Plane Loading

Ultimate Strength Analysis

By an elasto-plastic finite displacement analysis with a matrix method, the ultimate strength is calculated for the models of which an arch rib is divided into 832 elements. To discuss the characteristics in the ultimate state, six combined loads are applied as shown in Table 6. The inelastic behaviors are pursued in the numerical calculation until the unstable state. The yielding loads and the maximum loads obtained by the calculation are summarized in Table 6 in terms of load multiples α_y and α_{max}, respectively.

Table 6. Load multiples for yielding and maximum loads.

Model	α D		α (D + L)		D + α L	
	α_y	α_{max}	α_y	α_{max}	α_y	α_{max}
1	2.964	3.012	1.787	1.929	3.261	4.354
2	2.118	2.118	1.434	1.487	2.222	2.764
3 (10^{-4})	2.869	2.923	1.760	1.903	3.215	4.307
3 (10^{-3})	2.359	2.424	1.560	1.714	2.821	3.901

Model	α (D + EQ)		D + α EQ		1.3 D + α EQ	
	α_y	α_{max}	α_y	α_{max}	α_y	α_{max}
1	2.328	2.656	2.378	4.609	2.372	4.364
2	1.412	1.528	2.161	2.432	1.618	2.135
1*	2.690	2.723	4.199	6.050	4.120	4.737
2*	1.412	1.528	2.217	2.970	1.618	2.192

The values in the parentheses of Model-3 with an assumed initial imperfection, indicate the ratio of the maximum initial imperfection to the span length. The initial imperfections are determined from the buckling mode shown in Figure 8, which may be the most unfavorable mode under a uniform load. Model-1* and -2* are modification of Model-1 and -2, respectively, in which the same steel of *SM58* as the arch rib is used for ties, while at the actual bridge, *SM50Y* and *SS41* are used for the ties. *SM58*, *SM50Y* and *SS41* are structural steels specified at the Japanese Industrial Standards, respectively with the specified yielding point of 451, 353, 235 MPa (65.4, 51.2, 34.1 kipf/in^2), and the specified minimum tensile strength of 569, 490, 402 MPa (82.5, 71.1, 58.3 kipf/in^2).

Characteristic in Ultimate State

The comparison between the values for Model-1 and those for Model-2 in Table 6 proves the effectiveness of the side ties. If the arch is not provided with the both side ties, the arch will fail due to its elastic instability at a little greater load than the design dead load. The maximum values of initial imperfections used for the calculations are 1/1000 and 1/10000 of the span length corresponding to the amount of actual deflections of about 30 cm and 3 cm, respectively. Ohmishima Bridge will exhibit the amount of unavoidable initial imperfection between the both values. Table 6 shows that the reduction of ultimate strength due to the initial imperfections will be 2 to 3% for the case of 1/10000 and 10 to 11%

for the case of 1/1000, and also it will be 20% for the dead load alone. Therefore, the effect of initial imperfections on the ultimate strength of the actual bridge would be several percent and is much smaller than the one for an ordinary two-hinged solid-rib arch without side ties.

The typical relations between maximum deflections and various loadings are shown in Figures 9 and 10 at the nodal point No. 10. Elastic displacement curves by a finite displacement analysis and by a linear analysis as well as load versus displacement curves obtained by an elasto-plastic analysis, are presented in the figures. The figures show that any sudden instability after the maximum load does not occur for any Models. When the Models are subjected to a seismic load as well as the dead load, the first yielding is observed at ties. Therefore, at Model-1* and -2* which have ties in a steel of higher yielding point, the ultimate strength may be relatively larger depending on the loading, as proved in Table 6 and Figure 10.

Figure 9. Dead and live loads versus displacements (D + α L).

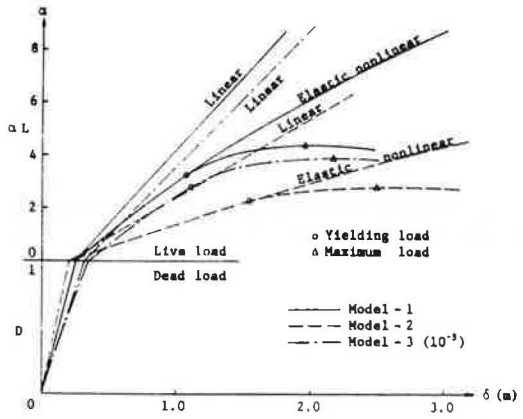

Figure 10. Dead and seismic loads versus displacements (D + α EQ).

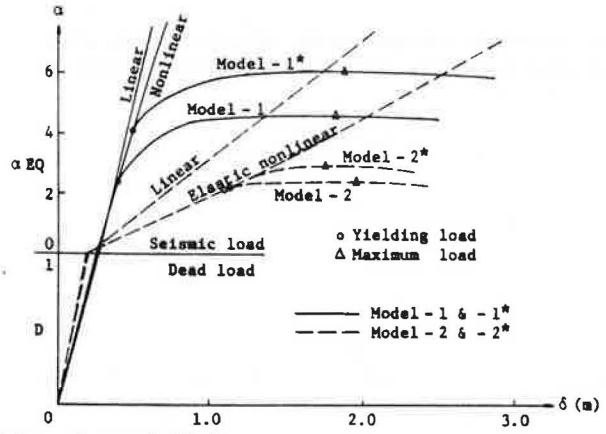

Note: 1 m = 3.28 ft.

Figures 11 and 12 present the spreading of plastic zone at the maximum load, but the members in which a plastic zone does not appear are omitted in the figures. In all of the loading cases, the arch rib fails due to its partial plastification, and particularly at Model-2, the arch rib fails without spreading of plastic zone after the yielding load has been reached.

Figure 11. Plastification due to dead load only (αD).

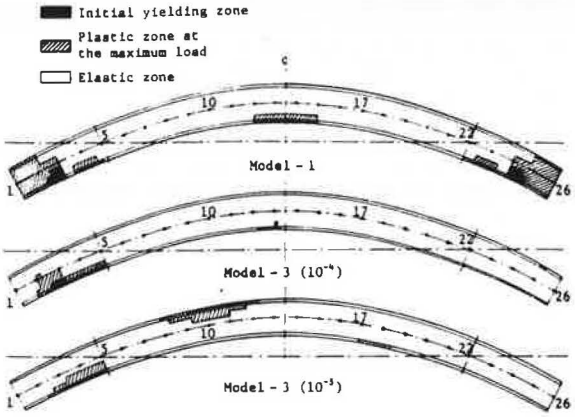

Figure 12. Plastification due to dead load plus seismic load (D + α EQ).

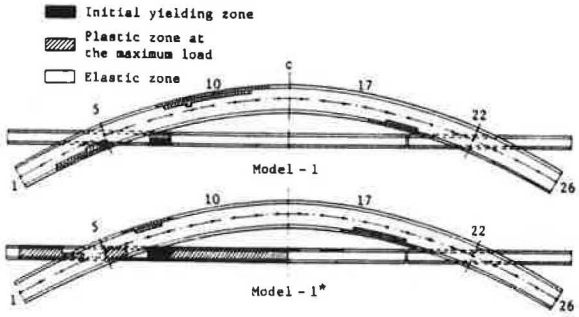

Ultimate Strength in Out-of-Plane Loading

At an elasto-plastic spatial analysis, the arch of Model-1 is divided into about 6000 elements and in addition to the dead load, wind load is applied to the arch rib, because it is dominant among possible out-of-plane loads.

Two kinds of ultimate strength are calculated, as shown in Table 7, in terms of the load multiple, α, for the maximum wind load. The comparison of Case-1 with Case-2 shows that 30% increase of the dead load, D, reduces slightly the strength for the wind load, W, because the model arch has a great in-plane strength for the dead load as shown in Table 6.

Table 7. Out-of-plane ultimate strength.

Loading	Case - 1 (1.0 D + α W)	Case - 2 (1.3 D + α W)
α_{max}	3.240	3.110

The relations between loads and out-of-plane displacements are given in Figure 13, in which the Nos. on the curves denote the nodal points of the leeward rib. The out-of-plane displacements at the nodal points of 31 and 33 differ about 2.5 times, although an interval between the both points is only two panel length. This difference is proper to an arch with side ties, because they constraint the out-of-plane displacements of arch ribs in side spans. Figure 15 which shows the out-of-plane displacements of arch ribs and ties, too, demonstrates clearly the effectiveness of the side ties.

Figure 13. Load versus displacement curves.

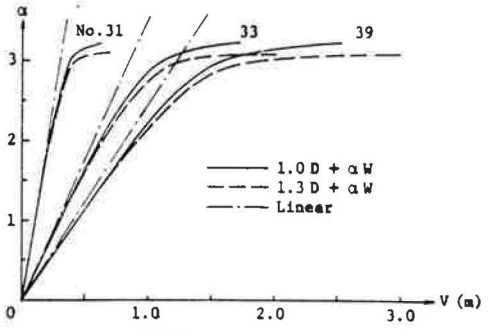

Note: 1 m = 3.28 ft.

Figure 14. Load versus out-of-plane moment curves.

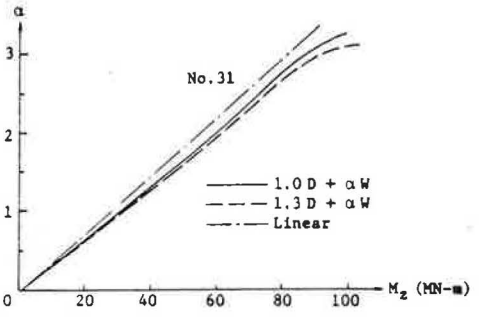

Note: 1 MN-m = 738 kip-ft.

Figure 14 indicates the relations of loads versus out-of-plane bending moments, M_z, at nodal point No. 31, at which the arch rib takes the maximum bending moment. The curves of out-of-plane bending moments in the rib do not show any remarkable nonlinearity as seen in Figure 14. Also, the nonlinearities in bending moments at the other sections are much smaller than those in displacements. The reason for these small nonlinearities in bending momments may be that, when the wind load reaches about 2.8 times as large as the design value, lateral braces between the arch ribs in the neighbourhood of the portal frames will yield and then the rapid displacements of the ribs will occur. Also, at the loading of $\alpha \simeq 3.0$, all of the sections of a great part of the side ties, too, yield, but at this time the greater parts of the ribs remain to be elastic.

Figure 15. Out-of-plane displacement distribution in arch rib and tie.

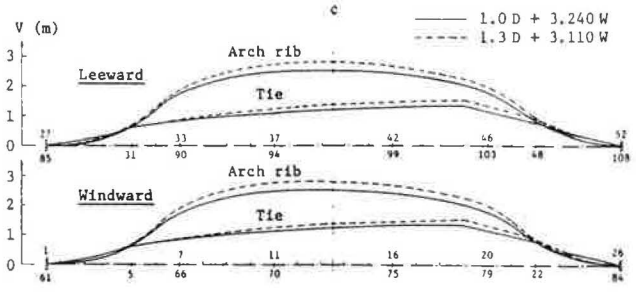

Note: 1 m = 3.28 ft.

Figure 16. Axial force distribution in arch rib for $(D + \alpha W)$.

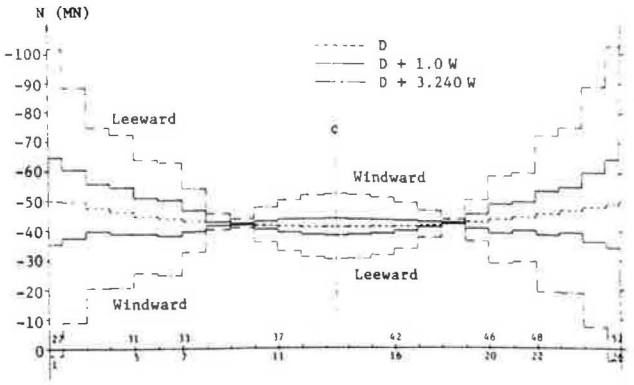

Note: 1 MN = 225 kip.

Figure 17. In-plane moment distribution in arch rib for $(D + \alpha W)$.

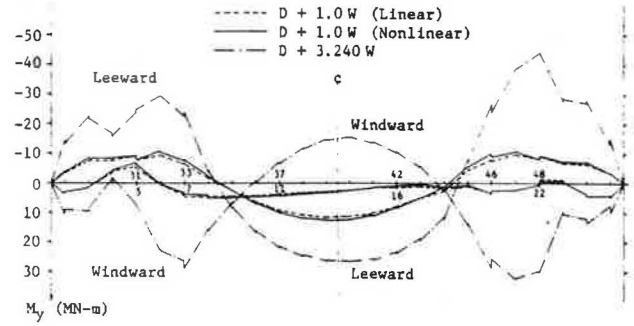

Figure 18. Out-of-plane moment distribution in arch rib for $(D + \alpha W)$.

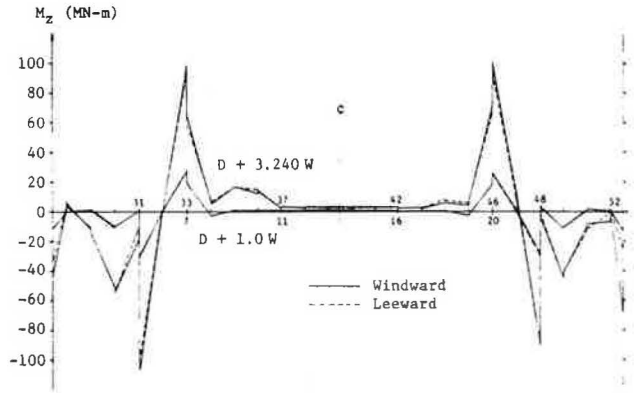

Note: 1 MN-m = 738 kip-ft.

At the model arch with the dimensions of Ohmishima Bridge, the structure reaches its unstable state due to the yielding of side ties and lateral braces around the portal frames. The plastification of the members at the maximum load is illustrated in Figure 19, but considerable portions of the members still remain to be elastic. All of the braces in the both side spans at floor systems not shown in Figure 19 will yield. If the plastic buckling of lateral braces between the ribs around the portal frames is taken into consideration in the numerical calculations, the values of α_{max} in Table 7 will be reduced to about 2.5.

Figure 19. Plastification of members at maximum load for (D + α W).

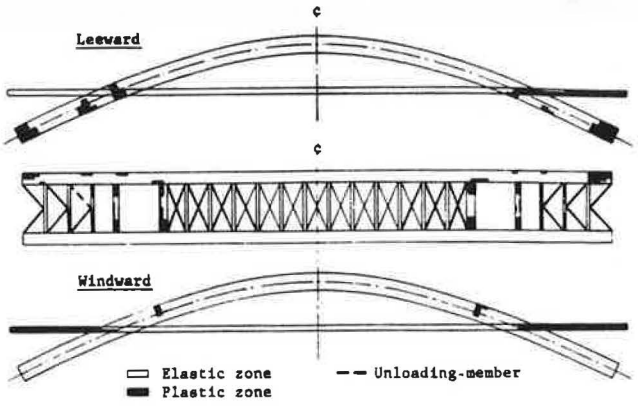

Finally, it should be added that experimental studies were carried out at Osaka University(2), and that six models in steel of a reduced scale of 1/49.5 for Ohmishima Bridge were tested to examine the in-plane and out-of-plane elasto-plastic behaviors and the ultimate strength. As the result, the ultimate strengths of the models by the theoretical analysis presented in this paper were verified quite well with 1 - 4% errors in comparison with the experimental values.

Conclusions

The theoretical and experimental analyses of two-hinged solid-rib steel arches stiffened by side ties modelling Ohmishima Bridge with the span length of 297 m, reveal the following structural characteristics:

1. The stiffening effects of side ties under in-plane loads are so remarkable that they can reduce the bending moments in arch ribs and also can constraint the geometrical nonlinearities of the arch, resulting in an increase of the load-carrying capacity of the overall structure.
2. Since the side ties can constraint the out-of-plane displacements of the arch ribs, they can increase the overall ultimate strength under out-of-plane loads.
3. Since it results that the span length of the arch rib has been shortened in appearance by the help of side ties, this new type of two-hinged arch will be more suitable for long-span arch bridges.

References

1. Honshu-Shikoku Bridge Authority. The Forth Working Design of Ohmishima Bridge, 1974 (in Japanese).
2. Y. Maeda, M. Hayashi and S. Matui. Study Report of Ohmishima Bridge - 1975 and 1976. Bridge Engineering Institute, Osaka University (in Japanese).
3. S.S. Tezcan and B.C. Mahapatra. Tangent Stiffness Matrix for Space Frame Members. ASCE, Vol. 95, No. ST 6, 1969, pp. 1257-1270.
4. K.H. Chu and R.H. Rampetsreiter. Large Deflection Buckling of Space Frames. ASCE, Vol.98, No. ST 12, 1972, pp. 2701-2722.
5. C. Oran. Tangent Stiffness in Space Frames. ASCE, Vol.99, No. ST 6, 1973, pp.987-1001.
6. Y. Maeda and M. Hayashi. Finite Displacement Analysis of Space-Framed Structures. Proc. of Japan Soc. of Civil Eng.(JSCE), 253, 1976, pp. 25-39 (in Japanese).
7. K. Washizu. Variational Methods in Elasticity and Plasticity. Pergamon Press, 1968, pp. 182-204.
8. Y. Yamada. Incremental Formulation for Problems with Geometric and Material Nonlinearities. Advances in Computational Methods in Structural Mechanics and Design. UAH Press, 1972, pp. 325-355.

BRIDGE DESIGN BY THE AUTOSTRESS METHOD

Phillip S. Carskaddan and Geerhard Haaijer, United States Steel Corporation

The Autostress method has been evolving as an extension to the AASHTO Load-Factor method for rolled-beam and plate-girder steel highway bridges. The Autostress method uses the same three load levels as the Load-Factor method: Service Load, Overload, and Maximum Load. However, to satisfy the structural performance requirements, the Autostress method injects two new concepts into bridge design: mechanism formation at Maximum Load and shakedown at Overload. When a structure forms a mechanism, there are sufficient plastic hinges to cause failure. When a structure shakes down, residual stresses and residual moments are automatically developed and assure elastic behavior under subsequent loading—hence the term Autostress. Although results of both methods for a simple span are the same, the Autostress method provides economies in continuous-span bridges; it utilizes the same safety factor against mechanism formation in both simple-span and continuous-span bridges. In contrast, the Load-Factor method uses a higher safety factor in continuous-span bridges than in simple-span bridges. As part of an AISI-sponsored project, nine Load-Factor bridges were redesigned according to the Autostress method; the average cost saving was 10.7 percent. The objective of the AISI project is to suggest that the Autostress method be incorporated into the AASHTO specification after experimental verification.

During the initial few passages of a sufficiently heavy load, a structure designed according to the Autostress-Design method will develop autostresses and automoments caused by local plastic deformations. During subsequent passages of a similar load, these automoments will assure elastic behavior. Automoments are analogous to the moments induced in a concrete beam by prestressing operations; the main difference from concrete prestressing is that a continuous steel beam requires no tendons and develops the required automoments automatically—hence the name Autostress Design.

The Autostress-Design (ASD) method was initially conceived(1) to utilize the ability of a redundant steel structure to shake down—that is, to develop automoments, which permit subsequent elastic behavior. In applying the shakedown principle to bridge design, a related principle—mechanism formation—was also introduced into the ASD method. Today, the ASD method is an extension of the Load-Factor-Design (LFD) method. The American Iron and Steel Institute (AISI), believing that ASD could be fruitfully applied to highway-bridge design, sponsored Project 188, "Autostress Design of Highway Bridges." This paper will review the progress of AISI Project 188: the loadings, the limit-state criteria, some sample designs, and the proposed future work. These topics are more completely discussed in two available reports.(2,3)

Loadings and Limit States

Loadings

The current AASHTO specification(4) permits use of the LFD method. The LFD method approximates the actual behavior of bridges more closely than the Working-Stress-Design method that was previously used for all bridges. As the name suggests, LFD applies factors to the loadings; the two main bridge-load types are dead load, D, and service live load plus impact, L+I. By applying factors individually to dead and live loads, a more uniform safety margin for live loads is achieved among different span lengths because the ratio of D/(L+I) varies with span length.

The LFD method specifies three levels of loading—Service Load, Overload, and Maximum Load—and each load level is associated with appropriate load factors. The second column of Table 1 lists these three load levels in order of increasing load. The third column of Table 1 lists for each load level a structural performance requirement, which is a brief verbal description of the performance required of a bridge at that load level.

Standard vehicles plus nominal dead load are applied at Service Load; for this condition a bridge should have adequate fatigue life, controlled elastic response to live loads, and limited concrete-deck cracking. Occasional permit vehicles, specified by AASHTO as having 5/3 times the weight of a Service-Load vehicle weight, plus nominal dead load are applied at Overload; a bridge should have a riding quality not rendered objectionable due to permanent deformations caused by yielding. A few emergency passages of exceptionally heavy vehicles, specified by AASHTO as having 1.3 times the weight of an Overload vehicle, plus a 30 percent increase in dead load are applied at Maximum Load; a bridge must support these loads although significant permanent damage may result.

The ASD method is applicable to the same three load levels as those specified by AASHTO in the LFD method. However, the ASD method may also be used for different load-level magnitudes that more closely represent the loadings of a particular situation, such as on a restricted route subjected to heavier-than-normal loadings.

Limit States

A limit-state criterion is a constraint that assures a desired structural performance. In Table 1 are listed, for each associated load level, the LFD and ASD limit-state criteria. The criteria for both methods are intended to satisfy the same structural performance requirements; these criteria are discussed and compared below for each load level. Although only certain criteria will govern a design, all criteria must be checked because the governing criteria may not be predictable. Thus, an acceptable design must satisfy all the limit-state criteria associated with the design method.

Service Load. The same limit-state criteria are used for LFD and ASD to satisfy fatigue and live-load response requirements; for fatigue the stress ranges cannot exceed values based on loading cycles and type of detail, and for live-load response the elastic live-load deflection is usually limited to some fraction of the span length. Automoments do not affect live-load stress ranges or elastic deflections. The structural-performance requirement for limited concrete-deck cracking is shown parenthetically in Table 1 to indicate that such a requirement is not explicitly required in the LFD method. However, as will be discussed under Overload, a control on maximum crack width is desired in the ASD method. Thus, AASHTO Equation 6-30, which is under the concrete LFD portion of the specification,(4) is invoked. This equation ensures a limit on the maximum crack width by setting the allowable rebar stress as a function of the rebar distribution; generally, many small bars permit a higher allowable rebar stress than do a few large bars.

Overload. The Overload structural-performance requirement—control of permanent deformations—deals only with serviceability; safety is not considered. The LFD method controls permanent deformations by limiting a flange stress due to negative moment to 0.80FY, where FY is the flange yield strength, and by limiting a flange stress due to positive moment to 0.95FY for composite sections and 0.80FY for noncomposite sections. If certain compactness requirements are met in a continuous-span bridge, the LFD method permits ten percent of the negative pier moment to be redistributed prior to making the stress calculations; the actual moments are generally below the yield moment.

The ASD method controls permanent deformations by permitting a continuous-span bridge to shake down—that is, to undergo small plastic deformations at a pier that will stabilize after a few cycles. These plastic deformations normally occur only in the flange outer fibers—they do not create a plastic hinge. After a bridge has shaken down, it will respond elastically to all subsequent loads not exceeding the Overload. In contrast, a structure that is repeatedly loaded above the shakedown load will fail by incremental collapse: ever increasing deflections caused by increments of plastic deformation in the same direction.(5) However, the greatest load at which a bridge will shake down—the shakedown load—would create deformations objectionable to riding quality. A bridge will shake down at any load less than the shakedown load, and the permanent deformation increases as the load approaches the shakedown load. Thus, the ASD method imposes additional limit states that keep the maximum Overload below the shakedown load. As a result, the interior-pier negative moment is usually above the yield moment but below the plastic moment—although this is not a limit-state criterion.

In the process of shaking down, a continuous structure develops a set of residual forces and moments, as shown in Figure 1, which are in equilibrium when the structure is unloaded. These moments, termed automoments because they are automatically developed, ensure that the structure remains elastic when subjected to Overload and may be considered as a modification of the dead-load moments; for a two-span bridge the automoment reduces the pier dead-load moment. Automoments are determined as the difference between the yielded moment distribution and the elastic unloading Overload moment.(3) The AASHTO Specification provisions for hybrid beams implicitly recognize the beneficial effect of autostresses in assuring elastic behavior after initial local plastic deformations caused by

Table 1. Comparison of Load Factor Design and Autostress Design
(Rolled-beam and plate-girder bridges supporting HS20 or H20 loading)

Load Factor Design Limit-State Criteria (Compact Section)	Load Level	Structural Performance Requirement	Autostress Design Limit-State Criteria
Stress ranges shall be less than categorized limits. Live-load deflection shall be less than a rational amount.	Service Load [D + (L+I)] (standard vehicles)	Provide adequate fatigue life, control elastic live-load deflections, (and limit concrete cracking).	Stress ranges shall be less than categorized limits. Live-load deflection shall be less than a rational amount. Rebar allowable stress shall be based on the rebar distribution within the slab.
Stresses due to positive and negative moments shall be less than a percentage of the yield stress; a 10% redistribution of elastic moments in continuous spans is permitted.	Overload [D + 5/3(L+I)] (occasional permit vehicles)	Control permanent deformations that otherwise could create objectionable riding quality.	A bridge shall shake down, that is, reach a condition in which further loadings cause no further yielding. Automoments may develop. Inelastic rotation at an interior support due to an automoment shall be less than a certain angle. Stresses due to positive moment—applied moment plus automoment—shall be less than a percentage of the yield stress. Rebar yielding at interior supports shall be minimized by using 414 MPa (60 ksi) rebars and unshored construction.
The moment at any cross section shall not exceed the plastic moment capacity; a 10% redistribution of elastic moments in continuous spans is permitted. Criteria related to the following parameters shall be used to assure that the plastic moment can be reached. a. compression-flange width/thickness b. compression-flange slenderness c. web depth/thickness d. shearing force	Maximum Load 1.3[D + 5/3(L+I)] (few emergency passages of exceptionally heavy vehicles plus additional dead load)	Resist loads that may cause significant permanent damage.	A mechanism shall not form; consider uplift. At plastic hinges, except the last to form, the following shall be limited: a. compression-flange width/thickness b. compression-flange slenderness c. web depth/thickness d. shearing force e. cross-section distortion (add a stiffener) Away from plastic hinges, the members shall be able to transmit the moments and shears. No additional load shall be permitted when a hinge forms in positive bending.

Figure 1. Typical automoment diagram for a two-span bridge.

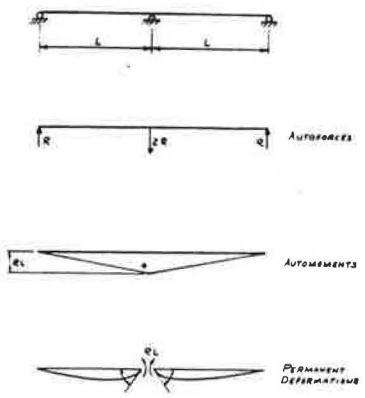

local web yielding. Although the ASD method may consider automoments to meet the Overload performance requirements, the bridge may never experience automoments unless the loading is sufficiently heavy; such behavior is acceptable.

To control permanent deformation at a pier due to the automoment, inelastic rotation, shown in Figure 1, shall not exceed the tolerance to which the slab is constructed: about 3 mm (1/8 in.) in 3 m (10 ft). The angle caused by inelastic rotation is easily computed; for a two-span bridge, as shown in Figure 1, the inelastic-rotation angle equals the end rotation of a simple beam with the indicated end moment of RL. If this were a composite bridge, the composite steel-concrete moment of inertia should be used since the automoment is positive along the entire span. The deflection in the span due to this inelastic rotation is small and may be included in the dead-load camber.

Permanent deformation caused by yielding in regions of positive bending is not directly controlled. Instead, stresses are controlled by the same limit state as that used in the LFD method for two reasons: one is that a better criterion is not known because small amounts of yielding in positive bending may create significant deformations; the other is that the same Overload limit state governs for both methods in a simple-span bridge.

During the development of an automoment, maximum crack width in the concrete deck is better controlled if the rebars remain elastic. This may be achieved if 414 MPa (60 ksi) yield-strength rebars and unshored construction are used. In unshored construction, the dead-load stresses in the steel section are higher than those in the rebars because the steel section is subjected to the full dead load and the rebars are subjected to only the composite dead load. Thus, any yielding necessary to create the automoment will desirably occur entirely within the steel section and the rebars will remain elastic. If this occurs, the rebar dead-load tensile stress will be reduced by the automoment.

Maximum Load. The Maximum-Load structural performance requirement—load resistance—deals only with safety; serviceability is not considered. The LFD method requires the Maximum-Load moment at any section in a bridge to be below either the yield or the plastic moment. These moments are elastic moments with the same possible ten-percent redistribution as mentioned above for Overload. In the LFD method, a simple-span bridge with a compact section reaches its maximum carrying capacity when a plastic hinge forms near midspan. This hinge, together with the two true hinges at the supports, forms a mechanism and prevents additional loading. Plastic design is therefore permitted in LFD for simple spans.

The plastic-design concept of mechanism formation permitted by the LFD method for simple-span bridges is extended to continuous-span bridges in the ASD method. In a two-span continuous beam a plastic hinge usually develops first at an interior pier, but this hinge is not sufficient to form a mechanism. Additional loading is required to cause a second plastic hinge at about midspan. The two plastic hinges, together with the true hinge at the exterior support, form a mechanism and prevent additional loading. During the formation of the second hinge, the interior-support plastic hinge must rotate inelastically at the plastic moment. To ensure that this inelastic rotation can occur while maintaining the plastic moment, the special limit-state criteria indicated in Table 1 are required. In general, these criteria are necessary at all plastic hinges except the last to form; at the last plastic hinge no inelastic rotation is required because the mechanism-formation limit state has been reached. The AISC specification(6) contains such plastic-hinge criteria, but since the amount of inelastic rotation required in a highway bridge is less than that required in a building, new, less restrictive plastic-hinge criteria are being developed for bridges.

A designer must ensure that uplift of an end reaction does not occur during mechanism formation. A downward reaction may be required to satisfy equilibrium and to prevent the ends of the bridge from lifting off their supports. Field testing of a bridge showed that uplift may occur prior to ultimate load.(7)

Away from the plastic hinges, the moments and shears from Maximum Load must not exceed those permitted by the LFD method. Since the inelastic-rotation capacity of a composite section is not accurately known (because of possible concrete crushing),(8) an additional limit-state criterion is imposed: additional load shall not be permitted when a plastic hinge has formed in positive bending. This criterion will not govern the usual bridge.

Design Study

Ten bridges designed by the LFD method were redesigned according to the ASD method to determine the relative weights and costs. The study(2) included rolled beams of constant and variable sections, a cover-plated rolled beam, plate girders, and composite and noncomposite bridges. Relative to the LFD method, the ASD method produced an average weight saving of 12.4 percent and an average cost saving of 10.7 percent. The relative cost savings are plotted versus span length in Figure 2. All bridges were two-span continuous designs except for Case D, which was a simple-span design, and Case F, which was a four-span continuous design. The three designs discussed below illustrate how a LFD bridge compares with an ASD bridge.

Case A

Figure 3 shows both the LFD and ASD bridges. The LFD bridge is a constant-section rolled beam with top and bottom cover plates at the pier. The ASD bridge uses the same section but the cover plates are eliminated. For comparison, the LFD bridge at the pier was designed as an unbraced section. The ten-percent moment redistribution could not therefore be used and the beam size plus cover plates was governed by the Maximum-Load limit state. The ASD bridge at the pier is governed by the limit states of the inelastic rotation at Overload; the rebar stress range for fatigue at Service Load; and the

Figure 2. Autostress-design cost reductions.

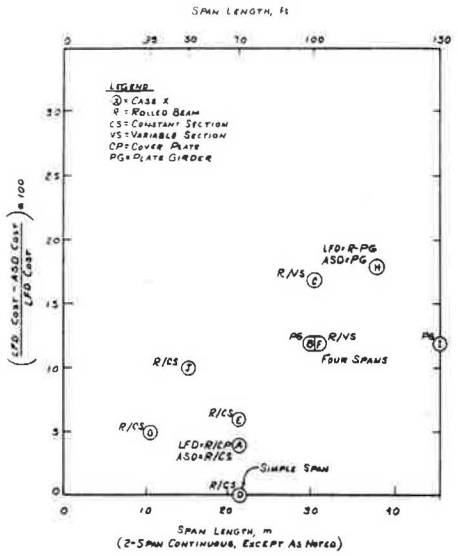

Figure 3. Case A.

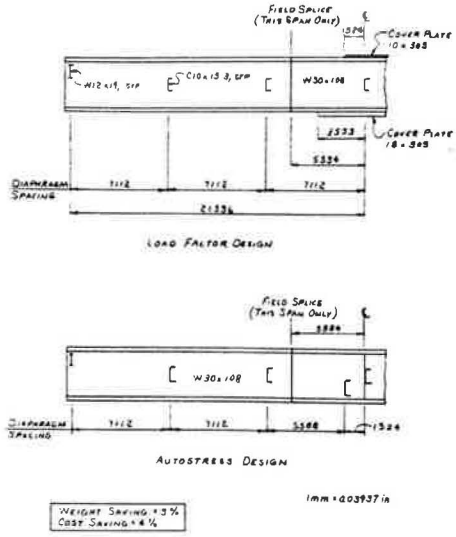

addition of lateral braces and a web stiffener because a plastic hinge occurs at Maximum Load. The automoment of +108 kN-m (+80 kip-ft) causes a permanent downward deflection in the span of 4 mm (0.15 in.).

Case B

LFD and ASD plate girders with unstiffened webs are shown in Figure 4. The ASD-bridge depth is about 5 percent below the LFD depth and requires a thicker web over the interior pier. Termination of this web plate was selected to keep the web splice outside of the short unbraced length and to keep the shearing stress in the thinner web below the allowable stress. The three cross frames in the positive-bending region of the LFD bridge were replaced by diaphragms in the ASD bridge to satisfy the fatigue criterion. Cross frames are used near the interior pier to brace the bottom flange in compression; fatigue does not govern there. The ASD bridge was governed in positive bending by the Overload criteria; at the pier the bottom-flange size was dictated by local and lateral buckling requirements at Maximum Load and the top-flange area was dictated by rebar fatigue requirements at Service Load.

Case C

LFD and ASD variable-section rolled-beam designs are shown in Figure 5. The ASD bridge requires an additional brace on either side of

Figure 4. Case B.

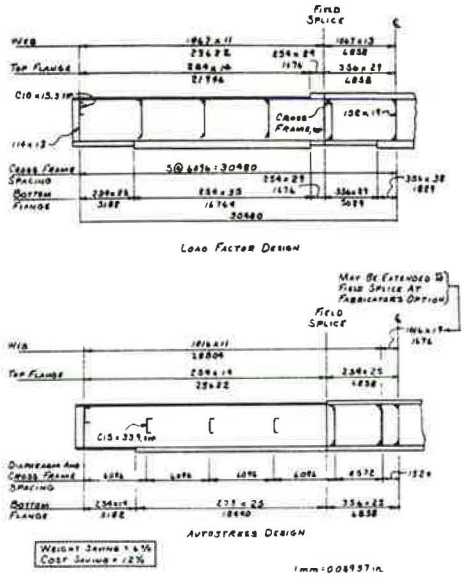

Figure 5. Case C.

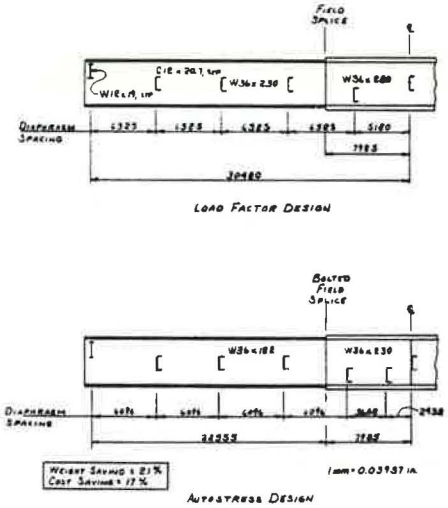

the interior pier and a web stiffener at the interior pier. The ASD is mainly governed by the 0.95FY criterion at Overload in positive bending, although the inelastic pier rotation at Overload also exerts an effect on the design. The structural behavior is influenced by the relative size of the two beam sections because of the effect of stiffness on the moment distribution and because of the automoments. It was better to add material over the pier because the negative-bending region is shorter than the positive-bending region. The large cost saving for the ASD bridge is partly due to the available rolled shapes; the W36 x 230 beam is the smallest section in that series and the next smaller beam, W36 x 194, is too small. The ASD bridge does not encounter this discontinuity in the range of beam sizes.

Reason for ASD Benefits

Although any bridge has peculiar aspects, certain generalizations indicate why an ASD bridge is usually more economical than a LFD bridge. The main reason is that by using the principles of plastic design to compute the resistance at Maximum Load by mechanism formation, the size of the stringers is usually governed by Overload rather than Maximum-Load criteria; Maximum-Load criteria may however dictate flange and web proportions at a hinge location. Thus, serviceability (Overload criteria) rather than safety (Maximum-Load criteria) governs many aspects of a design. Certain details may be controlled by fatigue. The Overload criteria for ASD provide benefits in the negative-bending region by eliminating the 0.80FY limitation used in LFD to control deformations. Instead, the deformations due to negative bending are limited directly in terms of the permissible inelastic rotation. In LFD the ten-percent redistribution in moment at Overload and Maximum Load is permitted if certain compactness criteria are met. This provision, however, does not provide the same benefits as ASD because the stresses due to negative bending after redistribution are limited to 0.80FY.

In the positive-bending region of an ASD composite plate girder, the Maximum-Load positive moment is checked against the composite plastic moment in positive bending (MPP). Since this section is usually the last hinge to form, it is not necessary for the section to have the ability of rotating at MPP. However, no criteria are available for a section to just reach MPP. The LFD compactness criteria are overconservative and uneconomical in this region because they provide the ability to rotate at MPP. The current LFD criteria for noncompact sections were used in this region because the neutral axis at MPP is near or within the deck slab. The entire steel section is thus in tension so that buckling due to the bending stresses is not a consideration. The web was considered capable of resisting the relatively low shear without buckling in this region.

Future Work

Before the ASD method can be suggested to AASHTO for incorporation into their specification, certain assumptions must be subjected to additional investigation. Phase 3 of AISI Project 188 will therefore investigate, both theoretically and experimentally, the number of load cycles required for shakedown, the distribution of the inelastic rotation and concrete cracking at Overload, compactness requirements, and lateral bracing for Maximum Load (the latter two requirements, although contained in the AASHTO specification, may require modification for plastic design). Beyond Phase 3, a full-scale test subjected to actual truck loading is being planned. Development of criteria to assure that a composite plate girder can just reach MPP—particularly the limits on web slenderness—will require additional study and possibly testing.

Conclusions

The ASD method is an extension of the LFD method for steel rolled-beam and plate-girder bridges. The intention of the ASD method is to permit a more rational design of a continuous-span bridge than the LFD method; the ASD limit-state criteria are more directly related to the structural performance requirements at the three factored load levels. An additional benefit of ASD is that the resistance to Maximum Load is computed the same for simple and continuous spans—that is, by mechanism formation. Thus, the inherent strength of a continuous-span bridge can be based on the principles now used in LFD for a simple-span bridge. This is consistent with a goal of LFD to provide a uniform safety margin for live load among different bridges. ASD extends the principles of LFD toward this goal and results in weight and cost savings in the design of typical bridges.

Acknowledgments

The development of the Autostress Design method is sponsored by the American Iron and Steel Institute. The project supervisor is J. A. Gilligan and the AISI staff representative is A. C. Kuentz. The present members of the AISI Project 188 Advisory Task Force are R. S. Fountain (Chairperson), R. J. Behling, R. C. Cassano, D. C. Frederickson, T. V. Galambos, E. V. Hourigan, J. T. Kratzer, R. W. Lautensleger, W. A. Milek, Jr., C. Pestotnik, F. D. Sears, W. M. Smith, L. M. Temple, and C. E. Thunman, Jr. During the initial phase of the project, S. A. Engdahl was also a member of the task force.

R. E. Leffler of U. S. Steel Research assisted in preparing the design examples. W. J. Rowles and R. F. Gasperich of American Bridge Division, U. S. Steel Corporation, prepared the cost estimates.

References

1. G. Haaijer, "Autostress Design of Steel Structures," ASCE National Structural Engineering Meeting, Preprint No. 1930, April 1973.

2. P. S. Carskaddan, "Autostress Design of Highway Bridges, Phase 1: Design Procedure and Example Design (AISI Project 188)," Research Laboratory Report 97-H-045(019-1), March 8, 1976.

3. P. S. Carskaddan, "Autostress Design of Highway Bridges, Phase 2B: Design Studies (AISI Project 188)," Research Laboratory Report 97-H-045(019-3), June 8, 1977.

4. Standard Specifications for Highway Bridges, The American Association of State Highway and Transportation Officials, 12th edition, 1977.

5. Plastic Design in Steel, American Society of Civil Engineers, 2nd edition, 1971.

6. "Specification for the Design, Fabrication, and Erection of Structural Steel for Buildings," American Institute of Steel Construction, February 19, 1969.

7. E. G. Burdette and D. W. Goodpasture, "Full-Scale Bridge Testing, An Evaluation of Bridge Design Criteria," University of Tennessee, December 31, 1971.

8. P. R. Barnard and R. P. Johnson, "Plastic Behavior of Continuous Composite Beams," Institution of Civil Engineers, Proceedings Paper 6836, 1965.

ENVIRONMENTAL STRESSES IN FLEXIBLY SUPPORTED BRIDGES

J. Leroy Hulsey, Assistant Professor of Civil Engineering,
North Carolina State University
Jack H. Emanuel, Professor of Civil Engineering, University of Missouri-Rolla

At present, no rational design method is available to account for movements and stresses in composite-girder bridges supported by flexible stub abutments. Because flexible stub abutments are frequently used, the objectives of this study were to: 1) develop a method for calculating environmentally induced movements and stresses and 2) compare the magnitude of these stresses induced in three types of construction for a 11-26-26-11-m (35-86-86-35-ft) four span six stringer composite-girder highway bridge located in mid-Missouri. Three types of support connections were investigated; 1) frictionless bearings, 2) non-integral end bents, and 3) integral end bents. Twenty years of recorded weather data were used for selection of upper and lower bound environmental loadings. Using these loadings as boundary conditions to the general heat flow equation, a finite element method was used to calculate resultant temperature distributions within a typical interior girder. These temperature distributions were then used as input to a slab-beam type element for calculation of the thermally induced stresses within the girder. Restraints imposed by the substructure, i.e. the bridge piers and earth embankments were modeled by linear springs. The results show that thermally induced stresses are significant for all three types of construction. Maximum beam stresses for the three supports were approximately 35%, 35%, and 52% of the allowable for frictionless bearings, non-integral abutments, integral abutments, respectively.

Bridge structures experience longitudinal movements and induced stresses which change continuously with time. The magnitude of movements and stresses induced by weather exposures is a function of the temperature distribution within the structure, the temperature at time of erection, material properties, geometry, support conditions, and structure flexibility (12, 15).

In conventional bridge design, expansive-contractive movements are generally assumed to be provided for by frictionless expansion bearings and by bridge deck expansion devices. Field observations show that bearings and expansion devices seldom function as anticipated. For example, Emanuel and Ekberg (5) reported numerous bridges with bearings that were tilted in the wrong direction, or frozen due to a build-up of grime, grit, and corrosion. They also reported a variety of problems associated with bridge deck expansion devices. When a conventional composite-girder bridge superstructure is supported by a massive or very stiff substructure, frozen bearings and/or inoperative expansion devices can cause excessive induced stresses. These stresses increase maintenance costs and lower the service life of the structure.

To reduce maintenance costs, some engineers have suggested connecting the superstructure to a flexible substructure. An 84 percent response to a survey of 50 state highway departments and 5 governmental agencies (6) showed that 28 respondents had used or were using this type of construction. The survey also showed that engineers are interested in using this type of construction, if rational design criteria are available to account for induced stresses.

Essentially, three types of superstructure to substructure connection details are being used by highway departments. Some states support the stringers on fixed rotational bearings which are attached to flexible piles at the abutments. This connection, commonly referred to as a "non-integral abutment," transfers shear forces to the piles. Other states encase the stringers in a monothlic pile cap which is referred to as an "integral abutment." This detail resists rotation and is assumed to transfer both shear and moment to the piles. Still other states use a detail that lies between the above two and is called a "semi-integral abutment." If the substructure is flexible enough, induced stresses may be provided for in the original design.

Although the composite-girder bridge superstructure supported by a flexible substructure appears to be a reasonable solution to the problem of a so-called maintenance free bridge, induced thermal stresses can present additional problems depending on structure length and substructure stiffness. Thus, the bridge engineer is faced with uncertainty as to the magnitude of stress induced by this type of construction and the behavior of the bridge over a period of time.

Previous studies of thermal and shrinkage

stresses in composite-girder bridge decks have been limited to bridges resting on frictionless bearings (4, 7, 19).

Zederbaum in 1966 (17) and 1969 (18) reviewed the factors affecting bridge deck movements in concrete bridges and presented a method for finding the location of the point of zero movement (stagnation point) on a bridge deck supported by elastic bearings. Witecki and Raina (16), 1969, presented a similar method to account for the effect of elastic and friction bearings on the point of zero movement and discussed the distribution of substructure forces and their application to the superstructure.

Bridge engineers are reluctant to use bridges supported by flexible substructures because design criteria are not currently available, observed data is limited, and guidelines relating substructure flexibility, bridge length, and induced stresses have not been developed.

As a first step towards the development of simple rational design criteria, the authors developed an analytical method as a basis for parametric studies. The procedure involved: a) evaluation of the factors affecting thermal properties of concrete; b) development of equations to estimate hourly weather extremes for Columbia, Missouri; c) formulation of a finite element method to solve the heat transfer equation which was used to find the temperature distribution through the bridge superstructure; d) development of a finite element method to find resultant thermal stresses; and e) a computerized solution of the magnitudes of thermally induced strains and stresses. Because of a space limitation and the complexity of the formulation, it is the objective of this paper to present results which show the potential magnitude of the maximum stresses induced by environmental loading extremes in an interior girder of a composite-girder bridge supported by a flexible substructure. Where necessary, for the benefit of the reader, an outline of the method is presented. No attempt was made to investigate the potential magnitude of stresses under combinations of dead, live, and environmental loads. The lengthy details of the initial development of these analytical procedures can be found in prior publications (7, 8, 9, 10, 12, 13).

Heat Flow

Generally, a bridge structure warms up during daylight hours due to the heat flux or energy received from the sun's rays. At night the structure cools down due to energy losses by convection and thermal radiation.

Physical Model

Consider a typical interior girder of the multi span composite-girder highway bridge of Fig. 1a. The heat flow through the superstructure produced by an environmental exposure fluctuates with time as a result of changes in air temperature, air velocity, and the solar radiation incident upon the structure.

Dividing the superstructure into long elements or members, m, each having constant sectional properties over the length, ℓ, assuming the concrete deck to be homogenous and isotropic and that the thermal properties are constant over the length of each member, the flow of heat through the member cross-section of Fig. 1b at some distance from the ends is essentially two-dimensional and is given by (12)

$$k\left(\frac{\partial^2 T}{\partial x^2} + \frac{\partial^2 T}{\partial y^2}\right) = c\rho \frac{\partial T}{\partial t} \qquad (1)$$

in which T is the temperature; x and y are cartesian coordinates; k is the thermal conductivity; c and ρ are the specific heat and density, respectively; and t is a point in time.

Figure 1. Heat flow model for a composite-girder bridge

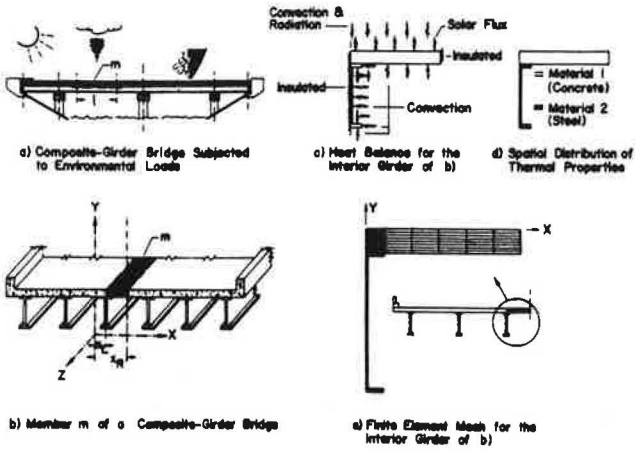

The initial condition, i.e. the temperature of the bridge structure at time of erection, is assumed to be at a steady state condition and is given by the mean daily temperature, T_a, for the day of the year when composite action is assumed to begin. Thus,

$$T(x, y, 0) = T_a \qquad (2)$$

At the air-deck (top) interface (Fig. 1c) energy is transferred by the solar flux absorbed by the bridge deck, $q_s(t)$, convection, $q_c(b,t)$, and thermal radiation, $q_r(b,t)$, such that

$$k\frac{\partial T}{\partial x}\ell_x + k\frac{\partial T}{\partial y}\ell_y + q_s(t) + q_c(b,t) + q_r(b,t) = 0 \qquad (3)$$

in which ℓ_x and ℓ_y are the direction cosines of the outward normal to the bridge deck and b represents the x, y coordinates on the boundary surface. At all other external boundary surfaces, such as the deck-air (bottom) interface and the girder-air interface, energy is assumed to be transferred by convection, and Eq. 3 reduces to

$$k\frac{\partial T}{\partial x}\ell_x + k\frac{\partial T}{\partial y}\ell_y + q_c(b,t) = 0 \qquad (4)$$

Physical Boundary Conditions

The solar radiation (heat gain) received by the deck can be expressed by $q_s(t) = \alpha I_n(t)$, in which α is the absorption coefficient and $I_n(t)$ is the sum of direct and diffuse radiation incident upon the surface.

Heat transfer by convection is given by Newton's Law of cooling

$$q_c(b,t) = h_c\{T(b,t) - T_\infty(t)\} \qquad (5)$$

in which h_c is a film coefficient, T(b,t) is the temperature of the bridge element at the surface-air temperature interface, and $T_\infty(t)$ is the air temperature at time t.

Heat transfer between the structure and the surrounding atmosphere due to thermal radiation (long) wave) produces a nonlinear heat flow boundary which can be modeled by (2, 14)

$$q_r(b,t) = \sigma\varepsilon\,[\theta(b,t)^4 - \varepsilon_{as}\theta_\infty(t)^4] \qquad (6)$$

where σ is the Stephan-Boltzman constant, ε is the emissivity, θ is the temperature in degrees absolute, and ε_{as} is the atmospheric emittance expressed in terms of air temperature as

$$\varepsilon_{as} = 1 - 0.261\,\exp\{-7.776 \times 10^{-4}\theta_\infty(t)^2\} \qquad (7)$$

in which $\theta_\infty(t)$ is in degrees centigrade.

Numerical Solution

The distribution of temperature through the cross section is obtained by solving the heat flow equation, Eq. 1, for the initial conditions of Eq. 2 and the boundary conditions of Eqs. 3 and 4. The geometric complexity and spatial distribution of the thermal properties, Figs. 1b and 1d, imply a need for a numerical method. A finite element method was developed, in which a typical interior slab-stringer was discretized as shown in Fig. 1e and the distribution of temperature was calculated at a given point in time. The formulation and details of the computional procedure are presented elsewhere (10, 12, 13)

Bridge Forces and Displacements

Forces induced by environmental exposures, shrinkage strains, and vehicular loads in an interior slab-stringer of a composite-girder bridge may be approximated by dividing the slab-stringer into prismatic elements connected by nodes; replacing the soil substrata, bearings and supporting structure with springs of equivalent stiffness; and using the stiffness method to solve for unknown displacements and forces.

Superstructure

Assuming an effective slab width, b_{ef}, consistent with present AASHO (now AASHTO) specifications (1), the slab-stringer shown in Fig. 2a is divided into composite-material slab-beam type elements, e, each having constant prismatic properties of length ℓ and defined by nodes i and j located at the neutral surface of the element. For the sign convention of Fig. 2c, the element stiffness matrix, $[k^e]$, is found by standard methods.

The total superstructure structural stiffness matrix, [K], i.e. without restraints imposed by the backfill and supporting structure, is obtained by assembling the element stiffness matrices.

The thermal fixed end forces for each element, $\{F_o^e\}$, at each nodal point and any superimposed nodal point loads, $\{P^L\}$, are assembled to give

$$\{P\} = \{P^L\} - \sum_{e=1}^{N_e} \{F_o^e\} \qquad (8)$$

where {P}, the vector of nodal point forces, is

$$\{P\} = [\,K\,]\,\{\Delta\} \qquad (9)$$

and {Δ} is the vector of unknown nodal point displacements.

Figure 2. Mathematical model for a restrained composite-girder bridge structure

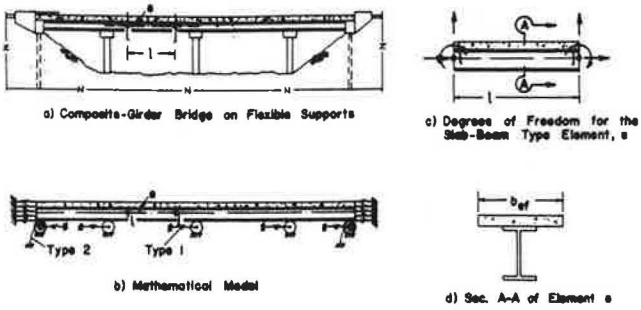

Substructure and Backfill

Restraint of longitudinal movements of a bridge deck induces both forces and moments in the bridge superstructure. For example, in bearing type supports a horizontal force is transferred through the bearing at some distance from the neutral surface, which induces a moment equal to the product of the force and its distance to the neutral surface. Integral or semi-integral abutments induce additional moment. Furthermore, both the approach slab and the fill material adjacent to the bridge deck will resist longitudinal movements. The magnitudes of the axial forces and the moments induced varies with the magnitude and distribution of the passive soil pressure resisting movement and the joint detail between the approach slab and the bridge deck.

Thus, two types of springs, shown in Fig. 2b, were used for analytically modeling the resistance of approach slabs, fills, abutment connections, and pier supports to superstructure movement.

The type 1 springs (one degree of freedom) were used to model bearing-pier supports, non-integral abutments, approach slabs, and fills adjacent to the bridge deck. The passive resistance of the fill material adjacent to the bridge deck is accounted for by applying multiple type 1 springs (winkler spring approximation), (see Fig. 2b). The type 2 springs are used to model the combined shear and moment resistance imposed by either the integral or semi-integral abutments.

Substructure and Backfill--Type 1 Springs

The spring force $^1F_{si,m}$ in spring m, attached to node i at $^1d_{si,m}$ from the neutral surface of the beam element, e, is given by

$$^1F_{si,m} = {}^1k_{si,m}\;{}^1\delta_{si,m} \qquad (10)$$

in which $^1k_{si,m}$ is the spring stiffness and $^1\delta_{si,m}$ is the spring displacement. Nodal point loads at node i of element e resulting from these spring forces are obtained by

$$\{^1P_{si,m}\} = \{^1H_{si,m}\}\;{}^1k_{si,m}\;{}^1\delta_{si,m} \qquad (11)$$

where $\{^1H_{si,m}\}$ is the force transformation matrix and $\{^1H_{si,m}\}^T$ is expressed by

$$\{^1H_{si,m}\}^T = \{\ 1 \quad 0 \quad -d_{si,m}\ \}$$

and $^1d_{si,m}$ is the distance from node i to spring m and is positive for springs located below the neutral surface.

The total nodal point forces, $\{Q_i\}$, at node i, which are located at the neutral surface of the slab-stringer element, are the sum of the nodal point loads, $\{P_i\}$, are the induced spring forces. This gives

$$\{Q_i\} = \{P_i\} + \sum_{m=1}^{^1S_i} \{^1P_{si,m}\}$$

in which $\{P_i\}$ is the summation of nodal point loads at node i; ^1S_i is the number of type 1 springs attached to node i; and $\{^1P_{si,m}\}$ is given by Eq. 11. Recognizing that the total nodal point forces, $\{Q_i\}$, at node i must be equal to the product of the assembled stiffness matrix at node i and the nodal point displacements at node i, it can be seen that

$$\{Q_i\} = [k_{ii}]\{\Delta_i\} = \{P_i\} - \sum_{m=1}^{^1S_i} \{^1H_{si,m}\}\ ^1k_{si,m}\ \ ^1\delta_{si,m}$$

Rewriting and transforming spring displacements, $^1\delta_{si,m}$ to the neutral surface of the slab-stringer element at each node gives

$$\{P\} = [\tilde{k}]\{\Delta\} \tag{12}$$

where

$$[\tilde{k}] = [k] + \sum_{i=1}^{^1N_s} \sum_{m=1}^{^1S_i} (\{^1H_{si,m}\}\ ^1k_{si,m}\ \{^1H_{si,m}\}^T) \tag{13}$$

Substructure--Type 2 Springs

The spring forces at node i are given by

$$\{^2F_{si}\} = [^2k_{si}]\{^2\delta_{si}\} \tag{14}$$

Transforming the spring forces from the spring to node i gives

$$\{^2P_{si}\} = [^2H_{si}]\ [^2k_{si}]\ \{^2\delta_{si}\} \tag{15}$$

where $[^2H_{si}]$ is the force transformation matrix and $[^2H_{si}]^T$ is expressed by

$$[^2H_{si}]^T = \begin{bmatrix} 1 & 0 & -^2d_{si} \\ 0 & 0 & 1 \end{bmatrix}$$

Similarly, as for the type 1 springs, the spring displacements are transformed to the neutral surface at each node and assembled to give

$$\{P\} = [\tilde{k}]\{\Delta\} \tag{16}$$

where

$$[\tilde{k}] = [\tilde{k}] + \sum_{i=1}^{^2N_s} ([^2H_{s_i}]\ [^2k_{s_i}]\ [^2H_{s_i}]^T)$$

After applying boundary conditions to Eq. 16, and rearranging, the nodal point displacements are obtained by

$$\{\Delta\} = [\tilde{k}]^{-1}\{P\} \tag{17}$$

Substructure Forces and Displacements

The pertinent displacements in the fill, approach slab and bearing supports are given by

$$^1\delta_{si,m} = [^1H_{si,m}]^T\ \{\Delta_i\} \tag{18}$$

Similarly, integral or semi-integral end bent displacements are given by

$$\{^2\delta_{si}\} = [^2H_{si}]^T\ \{\Delta_i\} \tag{19}$$

and the corresponding forces in each of the two types of springs are calculated by Eqs. 10 and 14 for types 1 and 2, respectively.

Substructure Stiffness Determination

Bearings

Three basic types of bearings are shown in Fig. 3: a fixed rotational bearing, a friction bearing, and an elastic bearing.

Figure 3. Flexibility coefficients for a bridge supporting structure

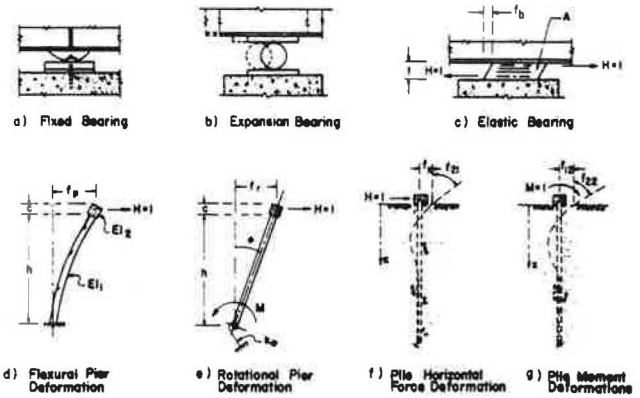

Fixed bearings, such as the curved steel plate of Fig. 3a, do not translate. Thus, the entire superstructure movement is transferred through the bearing to the support and the bearing flexibility, f_b, is

zero.

Friction bearings (Fig. 3b) perform like fixed bearings until a horizontal force equal to $\mu_s R$ produces impending motion. The coefficient of static friction, μ_s, for dry steel on steel varies from 0.15 to 0.8 (3, 11); R is the vertical reaction. After motion impends the resistance to movement (kinetic friction) is approximately three-fourths the static friction and the bearing resistance becomes $0.75\ \mu_s R$.

Elastic bearings, unlike the other two types, restrain movement and deform at the same time. From Fig. 3c, if a unit load is applied at the top of the bearing and the pier is restrained against movement, the resulting flexibility coefficient, f_b, becomes

$$f_b = \frac{t}{AG} \tag{20}$$

Piers

The pier flexibility (Fig. 3d), assuming elastic action, is found by applying a lateral unit load at the top of the pier. The resulting horizontal deflection or flexibility, f_p, is

$$f_p = \left(\frac{h^3}{3EI_1} + \frac{h^2 c}{2EI_2}\right) + \frac{c^3}{3EI_2} \tag{21}$$

From Fig. 3e, the rotation of the pier base may be accounted for by applying a lateral unit load at the top of a rigid pier. The resulting rotational deflection at the top of the pier, f_r, becomes

$$f_r = \frac{(h+c)^2}{k_\theta} \tag{22}$$

where k_θ may be found from the foundation type and the modulus of the soil.

Summing the individual flexibilities, $f = f_b + f_p + f_r$, for the total deflection at the top of the pier, and inverting gives the final effective pier stiffness (type 1 Spring) which is

$$k_s = \frac{1}{f} \tag{23}$$

where

1. For a fixed bearing pier, the total flexibility becomes

$$f = f_p + f_r = \left(\frac{h^3}{3EI_1} + \frac{h^2 c}{2EI_2}\right) + \frac{c^3}{3EI_2} + \frac{(h+c)^2}{k_\theta}$$

2. For a friction bearing, the flexibility is that of a fixed bearing when the horizontal thrust is equal to or less than $\mu_s R$, which gives

$$f = f_p + f_r = \left(\frac{h^3}{3EI_1} + \frac{h^2 c}{2EI_2}\right) + \frac{c^3}{3EI_2} + \frac{(h+c)^2}{k_\theta}$$

After motion impends the total flexibility of the pier is

$$f = \infty$$

3. For an elastic bearing the pier flexibility becomes

$$f = f_b + f_p + f_r = \frac{t}{AG} + \left(\frac{h^3}{3EI_1} + \frac{h^2 c}{2EI_1}\right) + \frac{c^3}{3EI_2} + \frac{(h+c)^2}{k_\theta}$$

Abutments

The governing differential equation for interaction between the surrounding soil and embedded piles subjected to lateral loads is

$$\frac{d^4 y}{dx^4} + \frac{ky}{EI} = 0 \tag{24}$$

where y is the lateral pile deflection, x is the depth below the top of pile, EI is the flexural pile stiffness, and k is the subgrade modulus in force/length^2.

For an assumed constant elastic soil modulus, classical solutions to Eq. 24 are readily available. For design conditions, the modulus may vary and numerical techniques are needed. Assuming an initial soil tangent modulus, i.e., small deformations, the flexibility of the pile supports may be evaluated by applying a unit lateral force and a unit moment at the top of the abutment pile as shown in Fig. 3f and 3g. Thus, taking into account the bearing type and applying the principles used for piers, the effective abutment stiffness can be found by inverting the flexibility matrix.

Superstructure Stress Analysis

Consider an interior composite slab-stringer to be subjected to thermal strains. In the composite section, a biaxial stress state exists at the interface between the slab and the beam flange. The state of stress depends on the imposed strain distribution, shear connector spacing, diaphragm and stringer spacing and support restraints. Previous analytical methods for the analysis of interior girders acting compositely with the slab are limited to frictionless bearing supports and have neglected transverse strain compatibility at the slab stringer interface (4, 6, 19).

In the method described herein, the bridge is first divided into composite-material slab-beam type elements, e, each having constant prismatic properties and a length of ℓ (see Fig. 4). Within each element, e, the assumptions made are: 1) the (one-way) slab and the beam are continuously connected by shear connectors; 2) the materials are homogenous and isotropic; 3) the temperature is constant over the length, ℓ, but may vary through the cross-section; 4) each girder is straight with a symmetrical cross-section; 5) elastic small deflection theory is valid; 6) torsional forces and transverse strain compatibility between separated slab sections are neglected; and 7) vertical strain compatibility is neglected.

Initially, the slab, upper beam flange and the top of the beam web are assumed separated and free to deform independently under the imposed temperature distribution and the resultant thermal strains are determined. Unrestrained thermal stresses within each separated section, n, are given by

$$\sigma'x_n = \frac{\alpha_n E_n}{\gamma}\left[-T(y_n) + \frac{1}{A_n}\int w_n\, T(y_n)\, dy_n + \frac{y_n}{I_n}\int w_n\, T(y_n)\, y_n\, dy_n\right] \tag{25a}$$

$$\sigma'y_n = 0 \quad ; \quad \sigma'z_n = \psi\sigma'x_n \tag{25b, 25c}$$

in which subscript n implies the appropriate separated section (Fig. 4), α_n is the coefficient of thermal expansion, E_n is the elastic modulus, T_n is the change in temperature, w_n is the width, A_n is the area, and I_n is the moment of inertia of each separated section. For plate action in the slab and top flange, $\gamma=1-\mu_n$ and $\psi=1$. Assuming the web and lower flange to be in place stress, $\gamma=1$ and $\psi=0$. The resulting unrestrained thermal strains are obtained from the general elasticity equations. For composite action, the slab and beam must deform with equal strains and curvatures at the interface. If one way slab action is valid, then the interface force system of unknown shears and couples of Fig. 4 must be superimposed. The eight unknown forces F_1 to F_8 are obtained by writing eight strain or curvature interface compatibility equations to yield eight simultaneous equations in eight unknowns. The details for this development have been presented in a separate publication (12).

Figure 4. Compatibility forces for superstructure components in a composite-girder bridge.

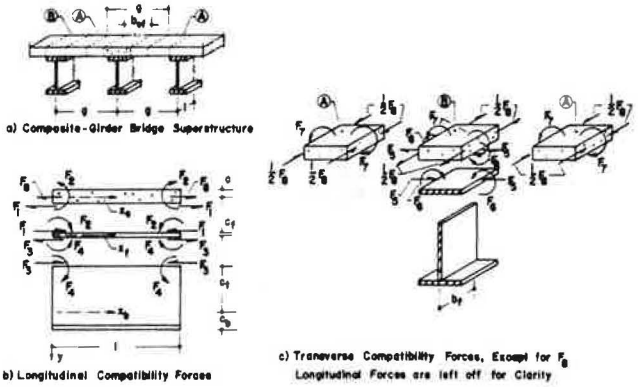

Final Stresses

Final stresses, forces and deformations for the interior slab-stringers of multi-span composite girder bridges subjected to thermal, shrinkage, or initial strains are obtained by superimposing the elastic stresses and the compatibility stresses.

Elastic stresses due to element forces are evaluated by a) dividing the slab-stringer into elements, b) introducing rigid boundaries at the nodal points, c) finding the fixed forces due to the deformations resulting from the thermal stresses of Eq. 25 and the stresses produced by F_1 to F_8, d) formulating the stiffness matrix, e) solving the resulting system of equations for nodal point displacements, and f) obtaining the element end forces and the resulting elastic stresses within the element.

Compatibility stresses are obtained by superimposing thermal stresses within the unrestrained and separated slab, beam flange, beam web and lower flange with the stresses produced by the compatibility forces, F_1 to F_8. Compatibility stresses within a determinate element are final stresses.

Point of Zero Movement

As expansive-contractive movements occur, a unique point on the bridge deck does not move. This point, when located, provides the engineer a rational means for determination of potential movement and placement of expansion joints, if used. Longitudinal displacements at the top surface of the bridge deck are obtained by transferring element nodal point displacements at the neutral surface to the top surface. Top surface strains at intermediate points along the element length can be calculated and used to numerically integrate and obtain axial deformations within each element. These deformations will change sign adjacent to the point of zero movement.

Bridge Study

A typical interior slab-stringer of a 11-26-26-11-m (35-86-86-35-ft) four span composite-girder six stringer highway bridge located in mid-Missouri was investigated for stresses induced by concrete shrinkage strains of 0.0002 and thermal strains resulting from air temperature extremes during the twenty year period of 1946-1965. An air entrained limestone aggregate concrete, for which the coefficient of thermal expansion is approximately 7.2×10^{-6}/°C (4.0×10^{-6}/°F), was assumed for the deck (8). The stringers are supported by flexibile stub abutments (semi-integral), a fixed bearing at the center pier and expansion bearings at intermediate piers. Pertinent superstructure properties are shown in Table 1.

Table 1. Bridge Properties

Type	Value
a) Superstructure	
Concrete compressive strength, kN/m² (psi)	27,600 (4000)
Effective slab width, mm[a] (in.)	1981 (78)
Slab thickness, mm (in.)	191 (7.5)
Depth of girder web, mm (in.)	1067 (42)
Section 1:	
Flange width and thickness, mm (in.)	203, 16 (8, 0.625)
Web thickness, mm (in.)	11 (0.4375)
Section 2:	
Top flange width and thickness, mm (in.)	203, 16 (8, 0.625)
Web thickness, mm (in.)	10 (0.375)
Bottom flange width and thickness, mm (in.)	254, 22 (10, 0.875)
Section 3:	
Flange width and thickness, mm (in.)	330, 25 (13, 1)
Web thickness, mm (in.)	11 (0.4375)
b) Substructure	
Concrete compressive strength, kN/m² (psi)	20,700 (3000)
Three-Column Expansion Piers:	
Pier cap width and height, m (ft)	0.84, 0.97 (2.75, 3.19)
Column diameter, mm (in.)	762 (30)
Column height, m (ft)	5.5 (18.1)
Bearing height, mm (in.)	241 (9.5)
Three-Column Fixed Pier:	
Pier cap width and height, m (ft)	0.84, 1.1 (2.75, 3.62)
Column diameter, mm (in.)	762 (30)
Column height, m (ft)	5.48 (17.96)
Bearing height, mm (in.)	102 (4)

[a]Neglects the top 25.4 mm (1 in.) of the slab.

The abutments are each supported by 5 HP 10 x 42 steel H-piles oriented with the major axis resisting longitudinal bridge movements. The abutment fills are approximately 5.8m (19 ft) deep as measured from the top of the pile cap. The soil boring data indicated the underlying soil strata to be a very stiff clay. Limited soil data were available and the fills were assumed to be a stiff clay. The average pile length is 14.3m (47 ft) at the down station abutment and is 13.9m (45.5 ft) at the other abutment. Pertinent substructure properties are shown in Table 1.

A computerized reduction of weather data at Columbia, Missouri, for the period 1946 to 1965 yielded equations for both diurnal and hourly vari-

Table 2. Maximum Principal Stresses for Superstructure with Frictionless Bearings

h_c[a]	Mo.	Day	Slab								Beam							
			Hr	Vert[b]	Sta[c]	σ[d]	Hr	Vert[b]	Sta[c]	σ[d]	Hr	Vert[b]	Sta[c]	σ[d]	Hr	Vert[b]	Sta[c]	σ[d]
5.68	Jan.	17	4	t	33.60	3328	6	b	30.33	-6291	4	b	15.24	46884	2	b	0.0	-12135
5.68		18	4	t	1.52	3335	6	b	30.33	-6258	2	b	15.24	48401	2	b	0.0	-12273
28.38		17	2	t	30.33	3488	4	b	30.33	-6429	2	b	15.24	47160	2	b	0.0	-12204
28.38		18	2	t	36.88	3418	4	b	30.33	-6452	2	b	15.24	46333	2	b	0.0	-11997
5.68	July	19	16	b	30.33	5008	12	t	0.0	-4528	8	b	0.0	4413	18	t	30.33	-30751
5.68		20	16	b	30.33	5015	12	t	15.24	-4517	8	b	0.0	4275	18	t	30.33	-30268
28.38		19	16	b	30.33	4318	12	t	0.0	-3503	8	b	0.0	5171	18	t	0.0	-25166
28.38		20	16	b	30.33	4319	12	t	0.0	-3487	8	b	0.0	5033	18	t	0.0	-25235

Note: 1 W/m^2-°C = 0.17615 Btu/hr-ft^2-°F ; 1 m = 3.2808 ft ; 1 kN/m^2 = 0.14504 psi

[a] W/m^2-°C ; [b] t = top, b = bottom ; [c] m ; [d] kN/m^2

Table 3. Maximum Principal Stresses for Superstructure with Non-Integral Abutments

h_c[a]	Mo.	Day	Slab								Beam							
			Hr	Vert[b]	Sta[c]	σ[d]	Hr	Vert[b]	Sta[c]	σ[d]	Hr	Vert[b]	Sta[c]	σ[d]	Hr	Vert[b]	Sta[c]	σ[d]
5.68	Jan.	17	4	t	36.98	3328	6	b	30.33	-6291	4	b	15.24	48125	2	b	-0.15	-12135
5.68		18	4	t	0.00	3332	6	b	30.33	-6258	2	b	15.24	49573	2	b	-0.15	-12273
28.38		17	2	t	30.33	3488	4	b	30.33	-6429	2	b	15.24	48401	2	b	-0.15	-12204
28.38		18	2	t	31.96	3418	4	b	30.33	-6452	2	b	15.24	47643	2	b	-0.15	-11997
5.68	July	19	16	b	30.33	5008	12	t	-0.15	-4528	8	127.94	0.0	0	20	t	15.24	-33026
5.68		20	16	b	30.33	5015	12	t	15.24	-4517	8	127.94	0.0	0	18	t	15.24	-33715
28.38		19	16	b	30.33	4317	12	t	-0.15	-3503	8	130.18	-0.15	414	18	t	30.33	-26890
28.38		20	16	b	30.33	4319	12	t	-0.15	-3487	8	130.18	-0.15	276	18	t	30.33	-26890

Note: 1 W/m^2-°C = 0.17615 Btu/hr-ft^2-°F ; 1 cm = 0.3937 in. ; 1 m = 3.2808 ft ; 1 kN/m^2 = 0.14504 psi

[a] W/m^2-°C ; [b] t = top, b = bottom, distance in cm ; [c] m ; [d] kN/m^2

Table 4. Maximum Principal Stresses for Superstructure with Integral Abutments

h_c[a]	Mo.	Day	Slab								Beam							
			Hr	Vert[b]	Sta[c]	σ[d]	Hr.	Vert[b]	Sta[c]	σ[d]	Hr	Vert[b]	Sta[c]	σ[d]	Hr	Vert[b]	Sta[c]	σ[d]
5.68	Jan.	17	4	t	30.33	3328	4	b	30.33	-6210	4	b	30.33	46608	2	b	-0.15	-12135
5.68		18	4	t	0.00	3334	6	b	30.33	-6258	2	b	30.33	47850	2	b	-0.15	-12273
28.38		17	2	t	30.33	3488	4	b	30.33	-6429	2	b	30.33	46884	2	b	-0.15	-12204
28.38		18	2	t	33.60	3418	4	b	30.33	-6452	4	b	0.0	47091	2	b	-0.15	-11997
5.68	July	19	16	b	30.33	5008	12	t	-0.15	-4528	16	b	10.67	3172	16	b	0.0	-71706
5.68		20	16	b	30.33	5015	12	t	18.27	-4517	16	b	10.67	3240	16	b	0.0	-71706
28.38		19	16	b	30.33	4318	12	t	-0.15	-3503	8	b	-0.15	827	16	b	0.0	-61570
28.38		20	16	b	30.33	4319	12	t	-0.15	-3487	6	b	-0.15	620	16	b	0.0	-61570

Note: 1 W/m^2-°C = 0.17615 Btu/hr-ft^2-°F ; 1 m = 3.2808 ft ; 1 kN/m^2 = 0.14504 psi

[a] W/m^2-°C ; [b] t = top, b = bottom ; [c] m ; [d] kN/m^2

ations in ambient air temperature and the sum of direct and diffuse solar radiation incident upon a horizontal surface. From these equations, the maximum air temperature of 41°C (106°F) occurred on July 20 and the minimum air temperature of -23°C (-10°F) occurred on January 18. These temperatures can be expected to recur every 11 and 4.5 years for the maximum and minimum temperatures, respectively. The details of this study have been presented elsewhere (12).

Using the values obtained from the above weather equations as boundary conditions to the differential heat flow equation, a two-dimensional finite element analysis with the grid of Fig. 1e was used to calculate the distribution of temperature through the cross section of an interior composite-girder at two hour intervals over a two day period. These temperatures were then used to calculate the thermal stresses and horizontal forces induced in the structure.

The reference temperature at time of erection was assumed to be 7°C (45°F) for the temperature variations of July 19-20 and 32°C (90°F) for the temperature variations of January 17-18 (12).

For simplicity, it was assumed that soil deformations would be small and that the soil would behave as a linearily elastic material. The approach fill was considered to resist expansive movements only.

Partial Results

Reactions, deflections, slopes, strains, and stresses induced in a typical interior girder by environmental temperature extremes for the twenty year period, 1946-1965, were investigated for support conditions of a) frictionless bearings, b) non-integral abutments and c) integral abutments. To allow for a build up of dirt, a coefficient of static friction of 0.6 was assumed at the pier expansion bearings for cases b) and c). Thus, the force required to produce impending motion at the pier expansion bearings was 19,570 kg (43.2 kips). Both a nominal wind speed, h_c = 28.4 W/m^2 - °C (5 Btu/hr-ft^2 - °F) and no wind, h_c = 5.7 W/m^2-°C (1 Btu/hr-ft^2-°F) were combined with the hot days (July 19-20) and the cold days (January 17-18) weather exposures.

The interior girder was modeled with a composite-material slab-beam type element the formulation of which is presented elsewhere (12). The temperature on each horizontal plane was calculated by averaging the nodal point temperatures found from the finite element analysis. The slab temperatures over the width of the girder flange were assumed constant but different from that of the slab between girders.

The induced stresses for the three support conditions are shown in Tables 2, 3, and 4. Although the results clearly show that environmentally induced stresses are significant, the stresses induced by non-integral abutment type supports are approximately the same as that for frictionless bearings.

Table 5, the horizontal thrust results, shows that impending motion never occured at the expansion bearings.

Table 5. Maximum Horizontal Forces

h_c[a]	Mo.	Day	Hr.	Non-Integral		Integral	
				Abut.[b]	Pier[b]	Abut.[b]	Pier[b]
5.68	Jan.	17	6	23647	3171	22741	3216
5.68	Jan.	18	6	23556	3171	22695	3216
28.38	Jan.	17	4	24100	3216	23148	3262
28.38	Jan.	18	4	24145	3216	23194	3262
5.68	July	19	16	7112	2627	28403	2627
5.68	July	20	16	7067	2627	28403	2627
28.38	July	19	16	6206	2220	25368	2220
28.38	July	20	16	6161	2220	25368	2220

Note: 1 W/m^2-°C = 0.17615 Btu/hr-ft^2-°F ;

1 kg = 2.2075 lbs ; [a] W/m^2-°C ; [b] kg

Discussion of Results and Conclusions

A rational method is presented for placement of expansion bearings and bridge deck devices and for calculation of forces induced in bridge superstructures supported by flexible substructures.

For the composite-girder bridge structure located near Columbia, Missouri, even the most severe climatic conditions will not produce impending motion at the expansion bearings.

As the substructure stiffness increases and/or the bridge length increases, significant horizontal forces can develop in both non-integral and integral types of bridge structures. These forces can be reduced by orienting the abutment piling so that the minor axis (rather than the major) resists longitudinal movements. The calculated thrusts would also be less if nonlinear soil behavior were considered.

Abutment thrusts approached 7112 kg (15.7 kips) compression and 24,145 kg (53.3 kips) tension for the non-integral abutment and 28,403 kg (62.7 kips) compression and 23,194 kg (51.2 kips) tension for the integral abutment.

The maximum induced beam stresses are approximately 48,401 kN/m^2 (7.0 ksi), 49,573 kN/m^2 (7.2 ksi) and 71,706 kN/m^2 (10.4 ksi) for supports of frictionless bearings, non-integral abutments, and integral abutments, respectively. Slab stresses were significant and are approximately the same for each support condition. Based on this data, it can be seen that frictionless bearings and non-integral abutments yield beam stresses which are approximately 35 percent of the allowable whereas integral abutments yield beam stresses of 52 percent the allowable.

References

1. American Association of State Highway Officials, Standard Specifications for Highway Bridges, 11th ed., Washington, D. C., author, 1973.
2. Armaly, B. F., and Leeper, S. P., "Diurnal Stratification of Deep Water Impoundments," Paper No. 75-HT-35, presented at the AICHE-ASME Heat Transfer Conference, San Francisco, Calif., Aug. 11-13, 1975, American Society of Mechanical Engineers.
3. Beer, F. P., and Johnston, Jr., E. R., Mechanics for Engineers, Statics, and Dynamics, McGraw-Hill Book Company, Inc., New York, N. Y. 1957.
4. Berwanger, C., "Thermal Stresses in Composite Bridges," Proceedings, American Society of Civil Engineers, Specialty Conference on Steel Structures, Engineering Extension Series, No. 15, University of Missouri-Columbia, Mo., June 1970, pp. 27-36.
5. Emanuel, J. H., and Ekberg, C. E., Jr., "Problems of Bridge Supporting and Expansion Devices and an Experimental Comparison of the Dynamic Behavior of Rigid and Elastomeric Bearings, "Special Report," Project 547-S, Iowa State University, Iowa Engineering Experiment Station, Sept. 1965.
6. Emanuel, J. H., et al., "An Investigation of Design Criteria for Stresses Induced by Semi-Integral End Bents: Phase I--Feasibility Study," Missouri Cooperative Highway Research Program Final Report 72-9, University of Missouri-Rolla, 1973.
7. Emanuel, J. H., and Hulsey, J. L., "Thermal Stresses and Deformations in Nonprismatic Indeterminate Composite Bridges," Transportation Research Record 607, Transportation Research Board, Washington D. C., January 1976.
8. Emanuel, J. H., and Hulsey, J. L., "Prediction of the Thermal Coefficient of Expansion of Concrete," Journal of the American Concrete Institute, Proceedings, Vol. 74, No. 4, April 1977, pp. 149-155.
9. Emanuel, J. H. and Hulsey, J. L., "Temperature Distribution in Composite Bridges," Journal of the Structural Division, American Society of Civil Engineers, Vol. 104, No. ST1, Jan. 1978, pp. 65-78.
10. Emanuel, J. H. and Hulsey, J. L., "Estimation of Air Temperature Extremes," American Society of Heating Refrigerating and Air-Conditioning Engineers, Inc., ASHRAE Transactions, Vol. 84, Part 2, Albuquerque Meeting, Paper No. 999, June, 1978.
11. Higdon, A., and Stiles, W. B., Engineering Mechanics, Vector Edition, Volume 1: Statics, Prentice-Hall, Inc., Englewood Cliffs, N. J., 1962.
12. Hulsey, J. L., "Environmental Effects on Composite-Girder Bridge Structures," Unpublished Ph.D.

Thesis, Library, University of Missouri-Rolla, Rolla, Mo., 1976.

13. Hulsey, J. L., and Emanuel, J. H., "Finite Element Modeling of Climatically Induced Heat Flow," IMACS Int. Symposium on Simulation Software and Numerical Methods for Differential Equations, VPI & SU, Blacksburg, Virginia, March 9-11, 1977.
14. Idso, S. B., and Jackson, R. D., "Thermal Radiation From the Atmosphere," Journal of Geophysical Research, Vol. 74, No. 23, 1969.
15. Reynolds, J. C., and Emanuel, J. H., "Thermal Stresses and Movements in Bridges," Journal of the Structural Division, American Society of Civil Engineers, Vol. 100, No. ST1, Proc. Paper 10275, Jan., 1974, pp. 63-78.
16. Witecki, A. A., and Raina, V. K., "Distribution of Longitudinal Horizontal Forces Among Bridge Supports," 1st International Symposium on Concrete Bridge Design, American Concrete Institute, Publication Sp-23, 1969, pp. 803-815.
17. Zederbaum, J., "The Frame Action of A Bridge Deck Supported on Elastic Bearings," Civil Engineering and Public Works Review, London, Vol. 61, No. 714, Jan. 1966, pp. 67-69, 71-72.
18. Zederbaum, J., "Factors Influencing the Longitudinal Movement of a Concrete Bridge System with Special Reference to Deck Contraction," 1st International Symposium on Concrete Bridge Design, American Concrete Institute, Publication Sp-23, 1969, pp. 75-95.
19. Zuk, W., "Thermal Behavior of Composite Bridges--Insulated and Uninsulated," Highway Research Record No. 76, Highway Research Board, 1965, pp. 231-253.

Analytical Models

For a model arch used for in-plane and out-of-plane analyses and elastic and elasto-plastic analyses, the same dimensions as the design of Ohmishima Bridge are used including the condition of supports, the arrangement of expansion joints, the rigidities of members, etc.. To make the calculation simpler, the rigidity of concrete-encased steel grating floor is neglected, eight stringers are replaced by one equivalent stringer, and the arrangement of lateral bracing members between two arch ribs is partly changed. As the result, the model is provided with 139 nodal points and 340 members and is constrainted with 52 degrees of freedom.

In addition to this Model-1, Model-2 is investigated, too, in which either of two side ties is not fixed to the abutment, but supported by a sliding shoe so that the tie is not subjected to any axial force. Moreover, Model-3 with an assumed initial imperfection due to the error of shape in Model-1 is employed in the in-plane ultimate strength analysis.

Applied Loads

In the in-plane analysis, the dead load(D), the live load(L) consisting of uniform load(p) and trailer truck load(TT), both including impact, and the earthquake load(EQ) with the horizontal seismic coefficient of 0.2, are applied at numerical analyses. In the out-of-plane analysis, the dead load, the horizontal earthquake load and wind load(W) are employed.

The intensities of the specific loads like elastic buckling load or ultimate strength load are expressed by a load multiple, α, considering design loads as standard loads, of which the intensities are given in Table 1(2).

Table 1. Intensities of design loads.

Design load	Intensity (kN/m)	Loaded member
Dead load (D)	43.5	arch rib
	94.8	center or side tie
	84.8	stringer
Live load (p)	20.9	stringer
(L) (TT)	765.0(kN)	stringer
Earthquake load (EQ)	8.7	arch rib
	19.0	center or side tie
	17.0	stringer
Wind load (W)	19.9	arch rib
	13.0	center or side tie
	3.2	post

Note: 1 kN = 0.225 kip. 1 kN/m = 68.5 lbf/ft.

Geometrical Nonlinearity due to In-Plane Loads

Influence Values

To examine the nonlinearity due to live loads, the following five kinds of influence values are considered:

1. An ordinary linear influence value for a unit concentrated load.
2. A linearized influence value for a concentrated live load(TT-Load) obtained by a tangential stiffness matrix at the loading of dead loads.
3. A nonlinear influence value of the exact solution for the value of 2.
4. A linearized influence value for TT-Load obtained by a tangential stiffness matrix at the loading of dead and half-span uniform live loads.
5. A nonlinear influence value of the exact solution for the value of 4.

At the computation of the values of 2 to 5, the exact equilibrium state is obtained for dead loads or plus a uniform live load with the intensities of the design loads. Then, these influence values are calculated not for a unit load, but for TT-Load as a moving concentrated load. At this time, the removal of the linearized errors is tried for bending moments or stresses with the values of 2 and 4.

Nonlinearity due to TT-Load

Figure 5 shows the maximum values of deflections due to a trailer truck load(TT-Load) for Model-1. Figure 6 shows the minimum values of fiber stresses due to TT-Load at the upper and lower flanges for Model-1. Since the linearized influence values of 2 and 4 agree with the values of 3 and 5, respectively, they are not shown in the figures. Those figures indicate clearly the favourable effect of the side ties on the deflections and stresses.

Figure 5. Maximum deflections due to TT-Load.

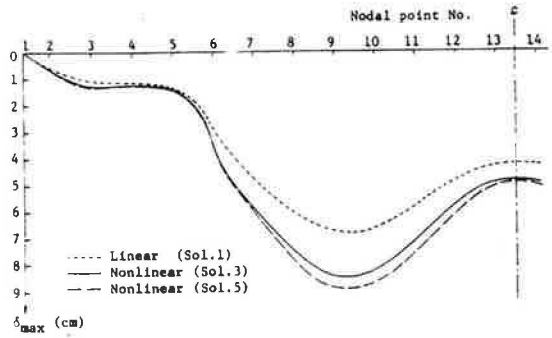

Note: 1 cm = 0.394 in.

Figure 6. Minimum fiber stresses at upper and lower flanges due to TT-Load.

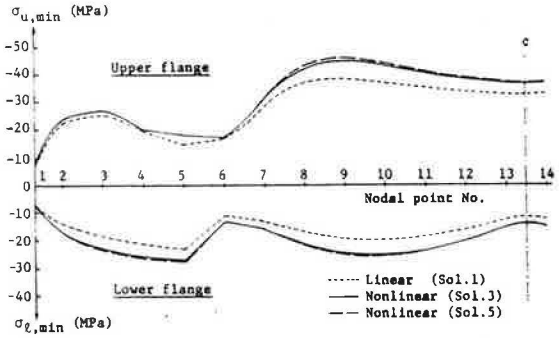

Note: 1MPa = 145 lbf/in^2.

For the maximum or minimum values of deflection δ, bending moment M and fiber stresses σ_u and σ_ℓ in the upper and lower flanges respectively, due to a concentrated TT-Load, the increase ratios of the linearized or the nonlinear values of 2 - 5 to the linear value of 1 are shown in percent on the uppermost column in Table 2.

Table 2. Geometrical nonlinearities of various influence values.

Solution	max δ	max M	min M	min σ_u	min σ_ℓ
Nonlinearity due to TT-Load					(%)
2	25.4	18.8	22.8	17.3	17.0
3	26.4	19.2	22.5	17.8	18.7
4	30.1	21.3	26.3	19.5	19.6
5	31.3	21.7	25.8	20.0	21.4
Nonlinearity due to dead and live loads					(%)
2	6.6	13.4	10.6	4.1	2.2
3	6.9	13.7	10.4	4.3	2.4
4	13.5	22.5	18.9	8.8	5.8
5	13.7	22.7	18.8	8.8	6.0

Since each value shows about 20 - 30% nonlinearity, the linear values cannot be applied to the analysis of the arch. But it may not be required to perform the exact nonlinear calculation for the concentrated live load, as far as the linearized values with 1 - 2% errors are used. When the nonlinear effect due to a uniform live load is taken into account, too, the increase of nonlinearity due to *TT*-Load is about 5% in deflections and about 2- 3% in stresses in comparison of the values of 2 with 4 or the values of 3 with 5.

Nonlinearity due to Dead and Live Loads

Large stresses due to dead loads are observed at a solid rib arch and more than 50% of the stresses are almost axial stresses without nonlinearity. Therefore, nonlinearities due to the dead load plus the live load are indicated on the 2nd column in Table 2, in which the values of 5 give the exact nonlinear effects due to the dead and live loads at Ohmishima Bridge.

Influence Line Analysis

In case that geometrical nonlinearity due to live loads appears at a structure subjected to dead load, an influence line analysis based on the law of superposition cannot be strictly applied to its analysis. Then, an influence line analysis with the above-mentioned influence values of 2 or 3 is applied to the analysis of Model-1.

Table 3. Errors of influence line analysis.

Solution	max δ	max M	min M	min σ_u	min σ_ℓ
Error due to superposition					(%)
2	-2.2	-2.0	-1.2	-1.8	-2.2
3	-1.3	-1.3	-1.2	-1.1	-0.9
Error of influence line analysis					(%)
2	-1.6	-2.0	-1.3	-0.9	-0.9
3	-1.1	-1.5	-1.4	-0.6	-0.5

The value of the uppermost column in Table 3 indicate errors due to the application of the superposition law to the influence analyses of the arch subjected to a uniform live load(p), in terms of the relative errors against the exact values due to the uniform live load.

Furthermore, the errors for the values due to the dead and the uniform live loads are shown on the 2nd column in the table.

The negative signs on the both columns mean unfavorable values.

Effect of Side Ties on Elastic Stability

Load versus displacement curves obtained by a buckling analysis and by an exact finite displacement analysis are given in Figure 7 for the in-plane elastic stability of Model-1 and Model-2 in which the stiffening effect of one of the side ties is neglected. The vertical axis shows load multiples for dead plus live loads and the horizontal axis shows the maximum deflections, both at the nodal point No. 10.

As illustrated in Figure 7, a dynamic jump does not occur at the both models owing to the stiffening effect of the side ties. The comparison between Model-1 and Model-2 shows that the ties have an effect on the constraint of geometrical nonlinearity of the arch. Particularly, the side ties are effective against a seismic load, because the nonlinearity of bending moments due to the dead load plus the seismic load is only 15 - 17% at Model-1, while 60 - 70% at Model-2.

Figure 8 indicates the first mode of buckling due to dead load for Model-1 and -2, in which the left side tie alone is fixed to the abutment. In the figure, the vertical and horizontal axes show relative displacements and nodal point Nos., respectively.

Figure 7. Load versus displacement curves for dead and live loads α (D + L).

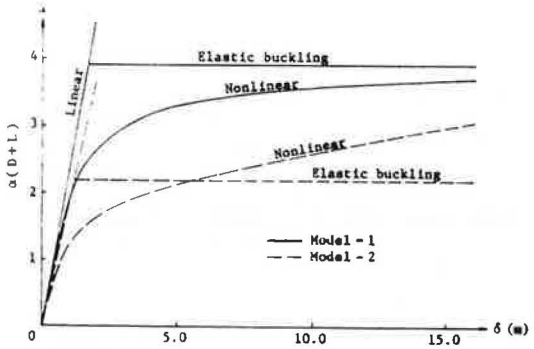

Note: 1 m = 3.28 ft.

Figure 8. Buckling modes due to dead load (α D).

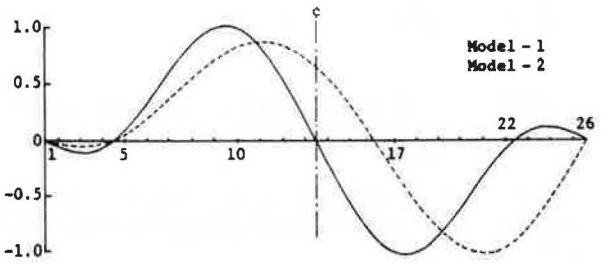

Geometrical Nonlinearity due to Out-of-Plane Loads

Geometrical Nonlinearity

There have been few study reports on the nonlinear behavior of an arch bridge subjected to an out-of-plane load. In Table 4, the geometrical nonlinearities in displacements and internal forces in arch ribs due to design loads calculated by a three-dimensional finite displacement analysis for Model-1 of Ohmishima Bridge, are shown in percent of the linear values. Model-1* in the table is a model arch taking into account the in-plane and out-of-plane rigidities of slab. V and W are respectively vertical and horizontal displacements, N is axial force, and M_t, M_y, M_z are respectively torsional, in-plane, out-of-plane bending moments. It can be seen in Table 4, that the nonlinearities appear even at the design loads, particularly remarkably in the in-plane moments.

Table 4. Geometrical nonlinearities due to out-of-plane loads. (%)

Model	Load	max V	max W	max N	max|M_t|	max|M_y|	max|M_z|
1	EQ	5.7	8.2	3.0	8.6	17.8	10.4
	D + EQ	5.6	3.2	1.1	4.8	16.0	9.9
	W	4.9	8.7	3.2	7.2	16.1	6.9
	D + W	4.9	3.4	1.1	4.5	8.8	6.9
1*	EQ	4.9	6.3	2.6	5.2	15.7	1.2
	D + EQ	4.8	2.7	0.8	3.0	8.2	1.2
	W	4.3	7.5	3.0	4.5	14.5	5.8
	D + W	4.3	2.9	0.9	2.8	7.7	5.9

The comparison between the values for Model-1 and Model-1* shows that, if the rigidity of the slab is considered at the calculations, the nonlinearities will be reduced considerably, but the axial force in side ties will increase about 50%.

Elastic Buckling

To examine the out-of-plane stability of Model-1 and -2, a three-dimensional buckling analysis is carried out. The results are summarized in Table 5 in terms of α_{cr} values which are load multiples based on the intensity of design dead load. Model-1* and -2* denote the cases that the slab rigidities are taken into account, respectively for Model-1 and -2. In Table 5, the third mode of buckling of Model-1 and -1* alone is related to the out-of-plane buckling, and all of the other modes are to the in-plane buckling. Since, at ordinary rib arches, the first mode appears at the in-plane buckling and the second mode appears at the out-of-plane buckling, a solid-rib arch with side ties shows different behavior from the ordinary solid-rib arch at the higher order of buckling mode.

Table 5. Load multiples for out-of-plane buckling.

Model	1st mode	2nd mode	3rd mode
1	4.833	7.664	9.580
1*	5.215	8.243	9.914
2	2.677	5.097	8.153
2*	2.899	5.511	8.692

Ultimate Strength in In-Plane Loading

Ultimate Strength Analysis

By an elasto-plastic finite displacement analysis with a matrix method, the ultimate strength is calculated for the models of which an arch rib is divided into 832 elements. To discuss the characteristics in the ultimate state, six combined loads are applied as shown in Table 6. The inelastic behaviors are pursued in the numerical calculation until the unstable state. The yielding loads and the maximum loads obtained by the calculation are summarized in Table 6 in terms of load multiples α_y and α_{max}, respectively.

Table 6. Load multiples for yielding and maximum loads.

Model	α D		α (D + L)		D + α L	
	α_y	α_{max}	α_y	α_{max}	α_y	α_{max}
1	2.964	3.012	1.787	1.929	3.261	4.354
2	2.118	2.118	1.434	1.487	2.222	2.764
3 (10^{-4})	2.869	2.923	1.760	1.903	3.215	4.307
3 (10^{-3})	2.359	2.424	1.560	1.714	2.821	3.901

Model	α (D + EQ)		D + α EQ		1.3 D + α EQ	
	α_y	α_{max}	α_y	α_{max}	α_y	α_{max}
1	2.328	2.656	2.378	4.609	2.372	4.364
2	1.412	1.528	2.161	2.432	1.618	2.135
1*	2.690	2.723	4.199	6.050	4.120	4.737
2*	1.412	1.528	2.217	2.970	1.618	2.192

The values in the parentheses of Model-3 with an assumed initial imperfection, indicate the ratio of the maximum initial imperfection to the span length. The initial imperfections are determined from the buckling mode shown in Figure 8, which may be the most unfavorable mode under a uniform load. Model-1* and -2* are modification of Model-1 and -2, respectively, in which the same steel of *SM58* as the arch rib is used for ties, while at the actual bridge, *SM50Y* and *SS41* are used for the ties. *SM58*, *SM50Y* and *SS41* are structural steels specified at the Japanese Industrial Standards, respectively with the specified yielding point of 451, 353, 235 MPa (65.4, 51.2, 34.1 kipf/in^2), and the specified minimum tensile strength of 569, 490, 402 MPa (82.5, 71.1, 58.3 kipf/in^2).

Characteristic in Ultimate State

The comparison between the values for Model-1 and those for Model-2 in Table 6 proves the effectiveness of the side ties. If the arch is not provided with the both side ties, the arch will fail due to its elastic instability at a little greater load than the design dead load. The maximum values of initial imperfections used for the calculations are 1/1000 and 1/10000 of the span length corresponding to the amount of actual deflections of about 30 cm and 3 cm, respectively. Ohmishima Bridge will exhibit the amount of unavoidable initial imperfection between the both values. Table 6 shows that the reduction of ultimate strength due to the initial imperfections will be 2 to 3% for the case of 1/10000 and 10 to 11%

for the case of 1/1000, and also it will be 20% for the dead load alone. Therefore, the effect of initial imperfections on the ultimate strength of the actual bridge would be several percent and is much smaller than the one for an ordinary two-hinged solid-rib arch without side ties.

The typical relations between maximum deflections and various loadings are shown in Figures 9 and 10 at the nodal point No. 10. Elastic displacement curves by a finite displacement analysis and by a linear analysis as well as load versus displacement curves obtained by an elasto-plastic analysis, are presented in the figures. The figures show that any sudden instability after the maximum load does not occur for any Models. When the Models are subjected to a seismic load as well as the dead load, the first yielding is observed at ties. Therefore, at Model-1* and -2* which have ties in a steel of higher yielding point, the ultimate strength may be relatively larger depending on the loading, as proved in Table 6 and Figure 10.

Figure 9. Dead and live loads versus displacements (D + α L).

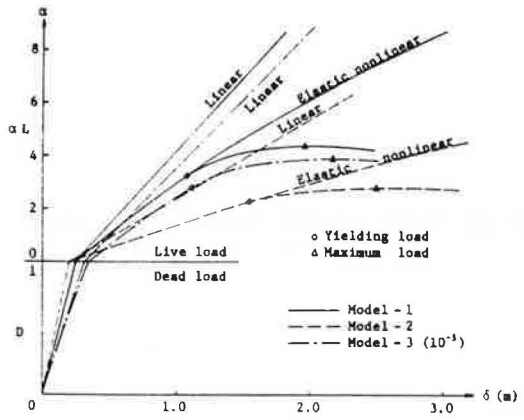

Figure 10. Dead and seismic loads versus displacements (D + α EQ).

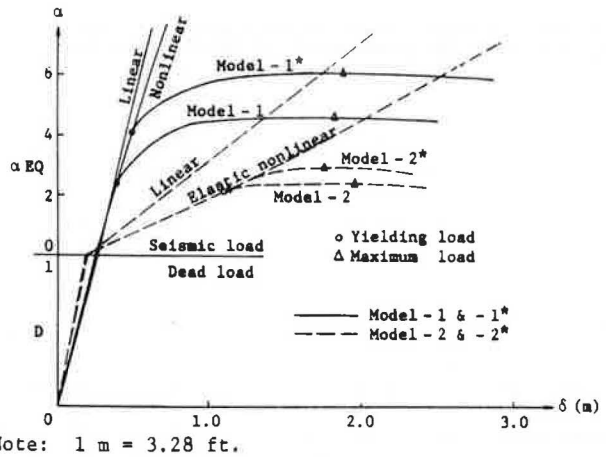

Note: 1 m = 3.28 ft.

Figures 11 and 12 present the spreading of plastic zone at the maximum load, but the members in which a plastic zone does not appear are omitted in the figures. In all of the loading cases, the arch rib fails due to its partial plastification, and particularly at Model-2, the arch rib fails without spreading of plastic zone after the yielding load has been reached.

Figure 11. Plastification due to dead load only (αD).

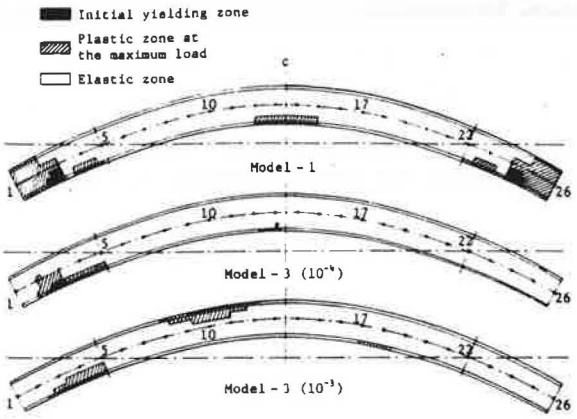

Figure 12. Plastification due to dead load plus seismic load (D + α EQ).

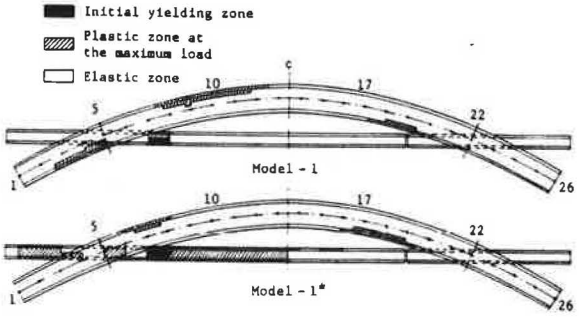

Ultimate Strength in Out-of-Plane Loading

At an elasto-plastic spatial analysis, the arch of Model-1 is divided into about 6000 elements and in addition to the dead load, wind load is applied to the arch rib, because it is dominant among possible out-of-plane loads.

Two kinds of ultimate strength are calculated, as shown in Table 7, in terms of the load multiple, α, for the maximum wind load. The comparison of Case-1 with Case-2 shows that 30% increase of the dead load, D, reduces slightly the strength for the wind load, W, because the model arch has a great in-plane strength for the dead load as shown in Table 6.

Table 7. Out-of-plane ultimate strength.

Loading	Case - 1 (1.0 D + α W)	Case - 2 (1.3 D + α W)
α_{max}	3.240	3.110

The relations between loads and out-of-plane displacements are given in Figure 13, in which the Nos. on the curves denote the nodal points of the leeward rib. The out-of-plane displacements at the nodal points of 31 and 33 differ about 2.5 times, although an interval between the both points is only two panel length. This difference is proper to an arch with side ties, because they constraint the out-of-plane displacements of arch ribs in side spans. Figure 15 which shows the out-of-plane displacements of arch ribs and ties, too, demonstrates clearly the effectiveness of the side ties.

Figure 13. Load versus displacement curves.

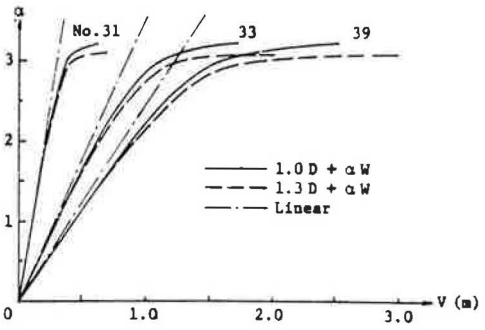

Note: 1 m = 3.28 ft.

Figure 14. Load versus out-of-plane moment curves.

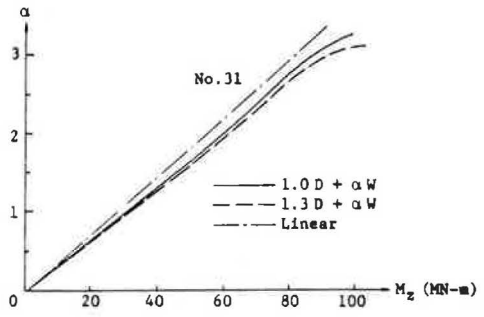

Note: 1 MN-m = 738 kip-ft.

Figure 14 indicates the relations of loads versus out-of-plane bending moments, M_z, at nodal point No. 31, at which the arch rib takes the maximum bending moment. The curves of out-of-plane bending moments in the rib do not show any remarkable nonlinearity as seen in Figure 14. Also, the nonlinearities in bending moments at the other sections are much smaller than those in displacements. The reason for these small nonlinearities in bending momments may be that, when the wind load reaches about 2.8 times as large as the design value, lateral braces between the arch ribs in the neighbourhood of the portal frames will yield and then the rapid displacements of the ribs will occur. Also, at the loading of $\alpha \simeq 3.0$, all of the sections of a great part of the side ties, too, yield, but at this time the greater parts of the ribs remain to be elastic.

Figure 15. Out-of-plane displacement distribution in arch rib and tie.

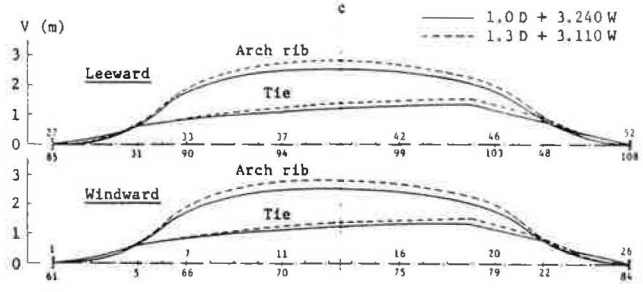

Note: 1 m = 3.28 ft.

Figure 16. Axial force distribution in arch rib for $(D + \alpha W)$.

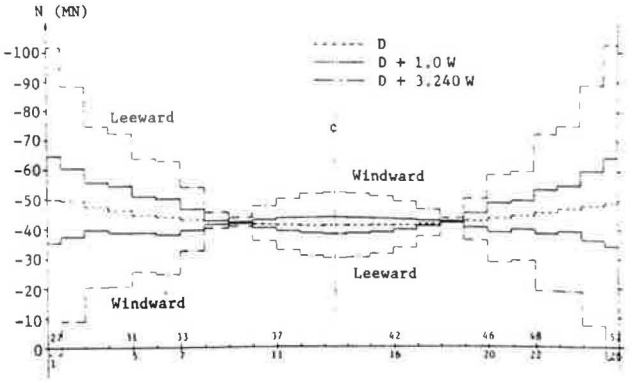

Note: 1 MN = 225 kip.

Figure 17. In-plane moment distribution in arch rib for $(D + \alpha W)$.

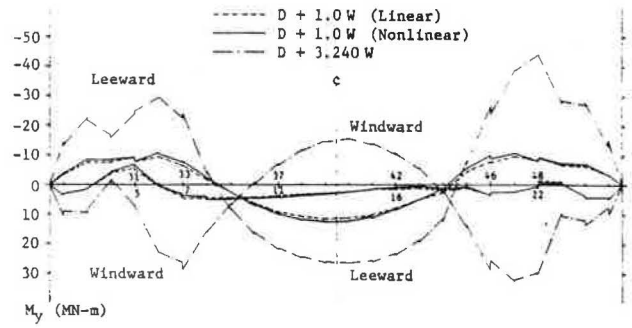

Figure 18. Out-of-plane moment distribution in arch rib for $(D + \alpha W)$.

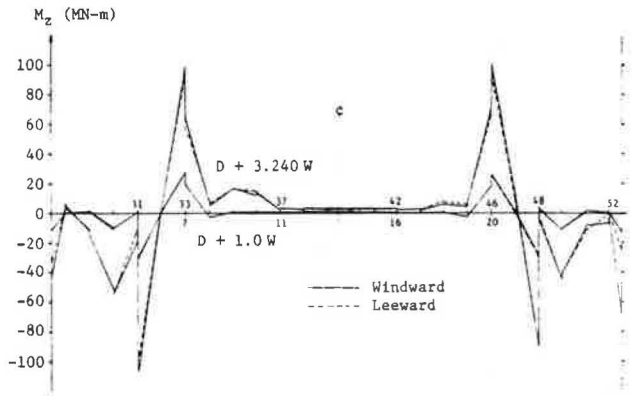

Note: 1 MN-m = 738 kip-ft.

At the model arch with the dimensions of Ohmishima Bridge, the structure reaches its unstable state due to the yielding of side ties and lateral braces around the portal frames. The plastification of the members at the maximum load is illustrated in Figure 19, but considerable portions of the members still remain to be elastic. All of the braces in the both side spans at floor systems not shown in Figure 19 will yield. If the plastic buckling of lateral braces between the ribs around the portal frames is taken into consideration in the numerical calculations, the values of α_{max} in Table 7 will be reduced to about 2.5.

Figure 19. Plastification of members at maximum load for (D + α W).

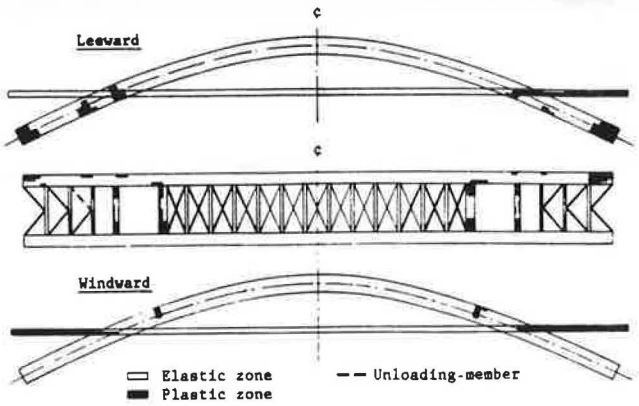

Finally, it should be added that experimental studies were carried out at Osaka University(2), and that six models in steel of a reduced scale of 1/49.5 for Ohmishima Bridge were tested to examine the in-plane and out-of-plane elasto-plastic behaviors and the ultimate strength. As the result, the ultimate strengths of the models by the theoretical analysis presented in this paper were verified quite well with 1 - 4% errors in comparison with the experimental values.

Conclusions

The theoretical and experimental analyses of two-hinged solid-rib steel arches stiffened by side ties modelling Ohmishima Bridge with the span length of 297 m, reveal the following structural characteristics:

1. The stiffening effects of side ties under in-plane loads are so remarkable that they can reduce the bending moments in arch ribs and also can constraint the geometrical nonlinearities of the arch, resulting in an increase of the load-carrying capacity of the overall structure.
2. Since the side ties can constraint the out-of-plane displacements of the arch ribs, they can increase the overall ultimate strength under out-of-plane loads.
3. Since it results that the span length of the arch rib has been shortened in appearance by the help of side ties, this new type of two-hinged arch will be more suitable for long-span arch bridges.

References

1. Honshu-Shikoku Bridge Authority. The Forth Working Design of Ohmishima Bridge, 1974 (in Japanese).
2. Y. Maeda, M. Hayashi and S. Matui. Study Report of Ohmishima Bridge - 1975 and 1976. Bridge Engineering Institute, Osaka University (in Japanese).
3. S.S. Tezcan and B.C. Mahapatra. Tangent Stiffness Matrix for Space Frame Members. ASCE, Vol. 95, No. ST 6, 1969, pp. 1257-1270.
4. K.H. Chu and R.H. Rampetsreiter. Large Deflection Buckling of Space Frames. ASCE, Vol.98, No. ST 12, 1972, pp. 2701-2722.
5. C. Oran. Tangent Stiffness in Space Frames. ASCE, Vol.99, No. ST 6, 1973, pp.987-1001.
6. Y. Maeda and M. Hayashi. Finite Displacement Analysis of Space-Framed Structures. Proc. of Japan Soc. of Civil Eng.(JSCE), 253, 1976, pp. 25-39 (in Japanese).
7. K. Washizu. Variational Methods in Elasticity and Plasticity. Pergamon Press, 1968, pp. 182-204.
8. Y. Yamada. Incremental Formulation for Problems with Geometric and Material Nonlinearities. Advances in Computational Methods in Structural Mechanics and Design. UAH Press, 1972, pp. 325-355.